NCAT Report 24-01

May 2024

National Center for Asphalt Technology
NCAT
AT AUBURN UNIVERSITY

Phase VIII (2021-2024) NCAT Test Track Findings

Randy West, Raymond (Buzz) Powell, David Timm, Nam Tran, Fan Yin, Nathan Moore, Thomas Harman, Benjamin Bowers, Adriana Vargas, Carolina Rodezno, Raquel Moraes Puchalski, Chen Chen, Surendra Chowdari (Suri) Gatiganti, Jason Nelson, Grant Julian, Jason Moore, Adam Taylor, Pamela Turner, Matthew Kmetz, Elizabeth Turochy

NCAT Report 24-01

Phase VIII (2021-2024) NCAT Test Track Findings

By

Randy West, Ph.D., P.E., Director and Research Professor
Raymond (Buzz) Powell, Ph.D., P.E., Former Associate Director and Research Professor
David Timm, Ph.D., P.E., Brasfield & Gorrie Professor
Nam Tran, Ph.D., P.E., Associate Director and Research Professor
Fan Yin, Ph.D., P.E., Assistant Director and Associate Research Professor
Nathan Moore, P.E., Assistant Director for Test Track Research
Thomas Harman, Ph.D., P.E., Senior Research Engineer
Benjamin Bowers, Ph.D., P.E., Assistant Professor
Adriana Vargas, Ph.D., Associate Research Professor
Carolina Rodezno, Ph.D., Associate Research Professor and Lead Researcher
Raquel Moraes Puchalski, Ph.D., Assistant Research Professor
Chen Chen, Ph.D., Assistant Research Professor
Surendra Chowdari (Suri) Gatiganti, Ph.D., E.I.T., Assistant Research Professor
Jason Nelson, Test Track Manager
Grant Julian, Assistant Research Engineer
Jason Moore, P.E., Laboratory Manager
Adam Taylor, P.E., Assistant Research Engineer
Pamela Turner, Assistant Research Engineer
Matthew Kmetz, Ph.D. Candidate
Elizabeth Turochy, Ph.D. Candidate

May 2024

DISCLAIMER

The contents of this report reflect the views of the authors, who are responsible for the facts and accuracy of the data presented herein. The contents do not necessarily reflect the official views or policies of Test Track sponsors, the National Center for Asphalt Technology, or Auburn University. This report does not constitute a standard, specification, or regulation. Comments in this paper related to specific testing equipment and materials should not be considered an endorsement of any commercial product or service; no such endorsement is intended or implied.

ACKNOWLEDGMENTS

This project was sponsored by the Alabama Department of Transportation (DOT), Federal Highway Administration, Florida DOT, Georgia DOT, Kentucky Transportation Cabinet, MnRoad, Michigan DOT, Mississippi DOT, New York State DOT, North Carolina DOT, Oklahoma DOT, South Carolina DOT, Tennessee DOT, Texas DOT, and Virginia DOT.

Private sector sponsors and support included: Astec, Roadtec, Asphalt Plus LLC, ADFORS GlasGrid®, Aztec Asphalt, BASF, Cargill, Caterpillar, Colorbiotics® a Sika Company, East Alabama Paving Company, Entech, Ergon Asphalt and Emulsions, GeoSolutions PETROMAT®, Hi-Tech Asphalt Solutions, Ingevity, Liberty SmartMix™, Martin Marietta, Troxler Electronic Laboratories, U.S. Polyco™, Vulcan Materials, Wiregrass Construction, and the Wirtgen Group.

The authors gratefully acknowledge Pete Capon and the following members of the NCAT Applications Steering Committee for their review of this technical report: Chris Abadie, James Anderson, Tim Aschenbrener, Shane Buchanan, Abdul Dahhan, Stacey Diefenderfer, Ervin Dukatz, Heather Dylla, Katherine Erwin, Gary Fitts, Jean-Paul Fort, Lorena Garcia, Parnian Ghasemi, Stacy Glidden, Elie Hajj, Andrew Hanz, Khaled Hasiba, Chad Hawkins, Mark Homer, Gerald Huber, Steve Jackson, Carl Johnson, Tim Kowalski, Mike Law, Cheng Ling, Chris Lubbers, Joe Mahoney, Todd Mansell, Bob McGennis, Marty McNamara, Brandon Milar, Chuck Mills, Mel Monk, Nathan Morian, Tim Murphy, Derek Nener-Plante, Tanya Nash, Elizabeth Patuszka, Bill Pine, Heather Purdy, Scott Quire, Robert Rea, Greg Renegar, Russell Ross, Kim Schofield, Debbie Schwerman, Todd Thomas, Jason Wielinski, Brett Williams, Tyler Wollmuth, Trey Wurst, and Jack Youtcheff.

TABLE OF CONTENTS

Preface: The Journey to the Track

Two visionary engineers once had a dream that would shape the future of pavement research and technology. Dr. Ray Brown from the National Center for Asphalt Technology (NCAT) and Dr. J. Don Brock from Astec Industries believed a cooperative pavement research facility would yield benefits for all. Through their unwavering perseverance and the forming of many partnerships, this dream materialized into a tangible marvel: the NCAT Test Track.

Their ambitious journey traces back to the late 1980s, when Auburn University proposed the concept of an innovative accelerated loading facility to the Alabama Department of Transportation (ALDOT). In 1991, when Mack Roberts assumed the role of director, that vision reignited, setting the stage for a groundbreaking endeavor. He envisioned the test track as a safe haven for experimentation and discovery, far removed from the bustling roads traveled by the general public.

Drs. Brown and Brock traversed the United States alongside their dedicated colleagues, rallying support from over a dozen state departments of transportation (DOTs). Their path was not without its hurdles— decisions loomed large, spirited debates ensued, and a temporary stall was caused by the shadow of a federal research initiative known as WesTrack. However, the team's resolve never wavered. As Dr. Brown often reflects, their pursuit was about forging a legacy of innovation, which propelled them ever forward.

From left: Bill Muse, Bill Walker, Paul Parks, John Spangler, Ray Bass, Mike McCartney, Don Gallagher, Dale Decker, Tim Docter, and Ray Brown at the NCAT Test Track Groundbreaking ceremony on September 29, 1998.

"Reflecting on that rainy day in 1998, I'm humbled by the foundation Dr. Brock and Dr. Brown forged for NCAT and research impacting pavement technology globally. Our commitment to our partners has never been stronger."

-Dr. Randy West, NCAT Director

Many people contributed to transforming over 300 acres of rugged terrain into a cutting-edge research and testing facility. Fueled by tenacity, engineering prowess, and unwavering collaboration, ALDOT Chief Engineer Ray Bass and NCAT board member Paul Parks were instrumental in the remarkable achievement of constructing the track. It symbolized the culmination of years of meticulous planning, tireless advocacy, and marked the dawn of a new era in asphalt pavement research.

Through its rigorous testing cycles, the track has emerged as a beacon of innovation, helping to increase performance and extend pavement life across the country. In the words of Dr. Brown, "It allows states and private industries to provide real-world answers to questions that otherwise couldn't be researched safely. State DOTs can quickly adopt changes to their specifications and procedures, resulting in better roads at lower costs."

Today, the NCAT Test Track stands as a living testament to the vision and perseverance of Dr. Brown, Dr. Brock, and their dedicated colleagues. It consistently garners support from an ever-expanding consortium that includes state DOTs, the Federal Highway Administration, the National Cooperative Highway Research Program, and numerous private enterprises. It transcends mere facility status; it is a legacy that continues to inspire and propel the future of pavement technology. Their journey—from vision to reality—not only paved the way for safer and more durable roads but also illuminated the path for collaborative innovation. It serves as a powerful reminder that when minds unite for a common goal, the possibilities are limitless.

1. INTRODUCTION

Dr. Thomas Harman

1.1 NCAT Test Track Background

The National Center for Asphalt Technology (NCAT) Test Track, inaugurated in the late 1990s, epitomizes a pioneering approach to asphalt pavement testing. Constructed over two years, from 1998 to 2000, this facility features a 1.7-mile oval track designed for the accelerated evaluation of asphalt materials and pavement technologies. It distinguishes itself by leveraging full-scale test sections and simulating real-world traffic conditions at highway speeds to gauge asphalt pavement performance swiftly. This methodology enables the assessment of innovative technologies and supports the adoption of new materials and design practices to enhance the safety, durability, and sustainability of asphalt pavements.

FIGURE 1 Aerial photograph of the NCAT Test Track.

During the eighth research phase (2021 to 2024), the Test Track sponsorship included fourteen highway agencies, the Federal Highway Administration (FHWA), and dozens of private sector entities, undertaking a range of experiments across individual and grouped test sections. Findings of these experiments were well supported by the test sections' field performance, which empowers highway agencies to refine their specifications for materials, construction techniques, and pavement design, thereby elevating roadway quality. Similarly, industry

sponsors are afforded a credible platform to validate and promote their innovations to the pavement engineering community.

The facility houses forty-six (46) primary test sections, each extending 200 feet (62 meters) in length, though some are further subdivided into shorter segments. Strategically placed, twenty-six of these sections lie along the track's straightaways, with the remaining sections distributed evenly among the two curves.

Research experiments at the Test Track are structured into three-year phases, each comprising three stages. Initially, the stage commences with the construction or renovation of test sections, which includes material selection, mix design, and pavement layout, typically spanning six months. The subsequent stage focuses on the application of traffic loads, data collection regarding field performance and pavement response, and laboratory analysis of materials collected during construction. This stage uses five heavily loaded tractor-trailers that simulate approximately ten million 18,000-pound equivalent single-axle loads (ESALs) over two years, using legal axle weights to mimic actual traffic conditions. The final stage is dedicated to forensic analysis, where experts dissect the reasons behind any observed damages in the test sections, thus identifying key factors influencing pavement distress and longevity.

FIGURE 2 The five tractor-trailers of the NCAT Test Track.

This dynamic and comprehensive approach ensures the NCAT Test Track remains at the forefront of asphalt pavement research, offering invaluable insights into the materials and methods that pave the way for more resilient and sustainable road infrastructure.

1.2 Previous Research Phases

The NCAT Test Track embarked on its pioneering journey in 2000, initiating a series of research phases that have progressively deepened the understanding of asphalt pavement performance under varied conditions. The inaugural phase laid the groundwork with an exclusive focus on surface mixes, incorporating stone matrix asphalt (SMA), Superpave, and Hveem mixes using a wide variety of aggregate types, gradations, and asphalt binders. These mixes were constructed over a robust pavement structure, twenty inches (51 cm) thick, designed to isolate pavement damage to the surface, ensuring a clear assessment of each mix's resilience.

The second research phase began in 2003 and included the continued evaluation of twenty-four of the original test sections. New experiments included fourteen test sections with new surface layers and eight sections that were completely rebuilt from the subgrade up. These were the first "structural experiments" designed and built to analyze the pavement structure, not just the surface layers. Construction of the structural experimental sections began by removing the original thick pavement structure down to the subgrade material, then rebuilding the subgrade, aggregate base, and asphalt layers to result in test sections with asphalt pavement thicknesses of 5, 7, and 9 inches (127, 178, and 229 mm). Strain gauges, pressure plates, and temperature probes were included in the structural sections to monitor how the different thicknesses and mix designs responded to traffic and temperature changes.

Table 1 summarizes the Test Track section construction/reconstruction over each research phase. For the year constructed column, the first number horizontally shows the number of new sections (e.g. in 2003, 22 new sections were constructed) and the subsequent numbers show how many sections remained in place for each research cycle. Each succeeding phase included sections from prior phases to extend trafficking and evaluations. Two of the original sections are still in service after over eighty million ESALs. Table 2 summarizes the number of total in-service pavement preservation sections by location and year linked to the Test Track.

TABLE 1 Summary of Test Track Section Construction by Research Phase

Year Constructed	NCAT Test Track Research Phase								
	I	II	III	IV	V	VI	VII	VIII	IX
	2000	2003	2006	2009	2012	2015	2018	2021	2024
	10	20	30	40	50	60	70	80	Million ESALs
2000	46	24	8	3	2	2	2	2	
2003		22	16	9	3	2	2	1	
2006			22	9	6	3	0	0	
2009				25	14	7	1	2	
2012					21	12	9	6	
2015						20	14	4	
2018							18	14	
2021								16	
2024									
MnROAD (*Cracking Group Experiment*)						8			

Million ESALs - Cumulative Traffic Loading in million 18,000-lbs Equivalent Single Axle Loads.
Approximately 10 Million ESALs/research phase.

TABLE 2 Summary of Pavement Preservation Group Study In-service Sections linked to Test Track

Pavement Preservation Sections/In-serve Sections	2012	2015	2019	2021
Alabama, Lee County Rd 159, Low Volume Roadway	25	25	25	25
Alabama, US H-280, Higher Volume Roadway		46	46	46
Minnesota, CSAH 8, Low Volume Roadway		30	30	30
Minnesota, U.S. Route 169, High Volume Roadway		29	29	29
Minnesota, 70th Street, Low Volume Roadway			16	16

CSAH-County State Aid Highway

More information on the *Pavement Preservation Group Study* can be found here: https://eng.auburn.edu/research/centers/ncat/testtrack/preservation/index.html.

Or by scanning the QR code.

The third research phase, the 2006 Test Track, was designed to perpetuate many of the same research objectives as the 2003 Test Track. Its main purpose was to evaluate the field performance of experimental asphalt mixes and pavement structures in the field. The structural test sections were designed to validate and calibrate new transfer functions for M-E design, develop recommendations for mechanistic-based material characterization, characterize pavement responses in rehabilitated flexible pavement structures, and determine field-based fatigue thresholds for perpetual pavements.

The fourth research phase, the 2009 Test Track, included a group experiment, where six agencies worked together to establish a group of experimental test sections with a common cross-section to assess the performance and structural response of pavements constructed with warm-mix asphalt (WMA) technologies, high RAP contents, the combination of high RAP content and WMA, and a porous friction course containing 15% RAP.

The fifth research phase, the 2012 Test Track, featured a more complex range of experiments than any of the previous cycles, but primarily focused on the use of recycled materials in pavements. This included the continued evaluation of the 2009 Group Experiment, the new Green Group Experiment, new test sections using 100% stabilized RAP, several sections containing ground tire rubber (GTR), and sections containing recycled asphalt shingles (RAS). The second primary focus of the 2012 cycle was on PFC mixes. Eight new PFC test sections and one section with a PFC surface built in the previous cycle were analyzed. The third primary focus of the 2012 cycle was on pavement preservation. These test sections were constructed on the Test Track and a local county road, Lee County Road 159.

In 2015, **the sixth research phase** began a new chapter in full-scale pavement research through a partnership with the Minnesota Department of Transportation's MnROAD facility. The NCAT-MnROAD partnership features a collaboration to address two national research needs. The first

research need is to validate asphalt mix cracking tests suitable for routine use in mix design and quality assurance testing. The experiment for the validation of cracking tests is called the Cracking Group Experiment and includes seven new test sections on the NCAT Test Track and eight rebuilt test sections on MnROAD's main-line test road. The second national research need addressed by the partnership is to objectively quantify the life-extending benefits of pavement preservation treatments. This research significantly expanded the 2012 pavement preservation experiment on Lee County Road 159 by installing thirty-four additional pavement preservation treatment sections on U.S. Highway 280 near the Test Track. To complement the pavement preservation treatments on Lee County Road 159 and US 280, the same treatments were applied to Minnesota's low-traffic volume and high-traffic volume routes. The sixth phase of the Test Track also includes 11 new surface mix sections, two new structural sections, and 17 sections left in place from previous phases for continued evaluation.

The seventh research phase began in 2018 with a continued focus on pavement preservation and cracking tests in collaboration with MnROAD and additional experiments focused on balanced mix design (BMD) and rejuvenators. The goal of the Preservation Group study was to discretely quantify the life-extending and condition-improving benefits of different preservation treatments applied at various stages of pavement life on low- and high-volume roadways in both southern and northern climates. The field performance data is supporting the development of specifications and quality assurance guidelines for preservation treatments. The continued Cracking Group experiment aimed to validate laboratory cracking tests by correlating lab results with field cracking performance. This will aid agencies in selecting appropriate cracking test methods and preliminary performance criteria and making implementation decisions based on practicality, sensitivity to mix design variables, and test variability, among others. Another focus in the 2018 cycle was on BMD. One state conducted a field performance comparison of BMD versus Superpave volumetric mix design, while another state sought to establish performance-based test criteria for BMD implementation. The field performance of various rejuvenators for both hot mix recycling and spray-on applications was also evaluated. A total of 18 sections were resurfaced or rebuilt for new experiments. In comparison, 28 sections remained in place for continued evaluation, including two sections that have been in service since the original construction of the Test Track in 2000.

Complete access to all the Test Track Reports can be found here:
https://eng.auburn.edu/research/centers/ncat/testtrack/reports.html

Or by scanning the QR Code: 

1.3 Eighth Research Phase

During the eighth research phase (2021 to 2024), the Test Track sponsorship included fourteen highway agencies, FHWA, and dozens of private sector entities, undertaking a range of experiments across individual and grouped test sections. Figure 3 depicts the Test Track layout for this research phase, denoted when each test section was constructed/reconstructed.

VIII Research Phase: 32 sponsored sections—

- 16 traffic continuation and monitoring,
- seven mill/inlay sections, and
- nine structural sections.

The mill/inlay and structural sections constitute sixteen repaved/rebuilt sections, which is approximately one-third of the Test Track. This amount of reconstruction is consistent with previous research phases.

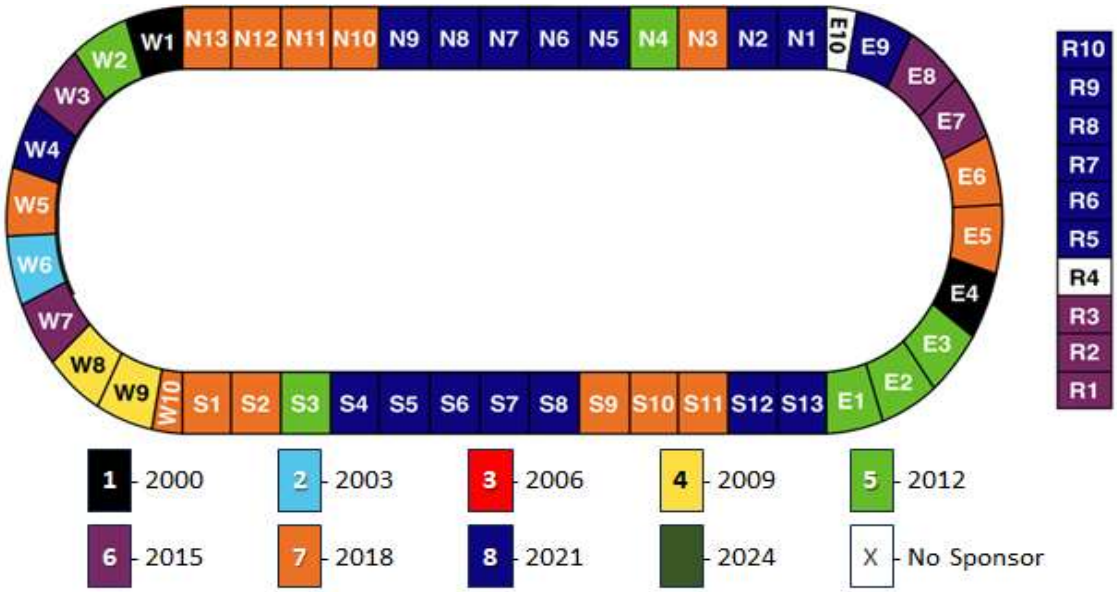

FIGURE 3 NCAT Test Track Phase VIII layout by year of construction.

The 2021 Additive Group Experiment contains six test sections (Figure 4) that are co-sponsored by the Departments of Transportation for Alabama, Florida, Mississippi, New York State, Tennessee, Texas, and FHWA.

FIGURE 4 Additive Group sponsors and six Test Track sections.

The Additive Group experiment focused on exploring the impact of various additives on the performance of asphalt mixes in a balanced mix design framework. The group experiment included recycled tire rubber, both wet and dry processes, recycled plastics, wet and dry processes, high-strength aramid fibers, and a control mix with a PG 76-22 polymer-modified asphalt binder.

Additive Group Test Section Breakdown—

- N1- Dry Recycled Tire Rubber (Smart Mix) with PG67-22 binder,
- N2- Wet Recycled Tire Rubber (Entech) with PG67-22 binder,
- N5- High Strength Aramid Fibers (Surface Tech ACE XP) with PG76-22 binder,
- N7- Control Section with PG76-22 binder,
- S5- Dry Recycled Low-Density Plastic (Pellets) with PG76-22 binder, and
- S6- Wet Recycled Low-Density Plastic (Dow) with Elvaloy PG76-22 binder.

Note: “Dry” and “Wet” are relative terms to explain how the additives are introduced into the mix.

Sponsors of individual experiments for the 2021 Test Track are listed below in alphabetical order.

1.3.1 Alabama Department of Transportation (ALDOT)

ALDOT co-sponsored the Additive Group experiment and sponsored individual traffic continuation on sections N10 and N11. These sections assess high-performance thinlays using dense-graded Superpave and SMA mixes. In addition, ALDOT sponsored the mill/inlay of E9 to assess high-performance OGFC mix design.

1.3.2 Federal Highway Administration (FHWA)

The FHWA provided funding to support the Additive Group experiment.

1.3.3 Florida Department of Transportation (FDOT)

FDOT co-sponsored the Additive Group experiment and sponsored individual traffic continuation on sections E5 and E6. These sections are each divided into two subsections assessing the impact of in-place density on pavement performance.

1.3.4 Georgia Department of Transportation (GDOT)

GDOT sponsored individual traffic continuation on sections N12 and N13. These sections are each divided into three subsections exploring the performance of different crack prevention interlayer strategies.

1.3.5 Kentucky Transportation Cabinet (KYTC)

KYTC sponsored individual section S7, which was subdivided into two subsections. The section was milled and inlaid with two BMD mixes to explore friction under traffic loading. One subsection was designed with a high terminal friction mix and the other with a moderate terminal friction mix.

1.3.6 Michigan Department of Transportation (MDOT)

MDOT sponsored the PG study.

1.3.7 Mississippi Department of Transportation (MDOT)

MDOT co-sponsored the Additive Group experiment and sponsored individual traffic continuation on sections S2 and S3. S2 is assessing lime-modified subgrade and cement-stabilized base in the context of M-E Design. S3 is assessing low-cost mixes for low-volume roads with a surface rejuvenation applied in 2018.

1.3.8 North Carolina Department of Transportation (NCDOT)

NCDOT sponsored individual section W4, which was milled and inlaid to explore bond strength with different tack products and rates.

1.3.9 New York State Department of Transportation (NYSDOT)

NYSDOT provided funding to support the Additive Group experiment.

1.3.10 Oklahoma Department of Transportation (ODOT)

ODOT sponsored individual traffic continuation on section S1 and mill/inlay of sections N8 and N9. S1 is exploring the performance of a 12% RAP surface mix on a 30% RAP base mix with a rejuvenator. Sections N8 and N9 mixes were developed with a BMD approach, including 30% RAP with a rejuvenator and a dry rubber additive, respectively.

1.3.11 South Carolina Department of Transportation (SCDOT)

SCDOT sponsored individual traffic continuation on section S9, which assesses full-depth rapid rebuild in a single paver pass.

1.3.12 Tennessee Department of Transportation (TDOT)

TDOT co-sponsored the Additive Group experiment and sponsored individual mill/inlay of section S4, which assesses gyratory BMD with Marshall specimens for BMD quality control testing.

1.3.13 Texas Department of Transportation (TxDOT)

TxDOT co-sponsored the Additive Group experiment, sponsored individual traffic continuation on sections S10 and S11, and sponsored mill/inlay of section N6. Sections S10, S11, and N6 seek to quantify the life-extending benefits of BMD versus dense-graded Superpave mixes for asphalt overlay applications.

1.3.14 Virginia Department of Transportation (VDOT)

VDOT sponsored individual traffic continuation on section N4 (2014), which assesses a thinner overlay for a 100% recycled base. In addition, VDOT sponsored a mill/inlay of section S12 to explore a thinner overlay on 100% re-recycle base mix via a foaming process.

Private sector sponsors funding a Test Track section are shown in Figure 5a, and industry contributors for the 2021 Test Track are depicted in Figure 5b.

(a) Private sector sponsors

(b) Industry contributors

FIGURE 5 Private sector sponsors and industry contributors for the 2021 research cycle.

The following provides a quick summary of the 2021 Test Track experiments:

Traffic Continuations (16 Sections)

- BMD / Higher RAP with recycling agents – Collaborative Aggregate, CA N3
- Thinner Overlay on Foamed cold recycle (CCPR) base – VA N4
- High-performance thinlays (DGA, SMA) – AL N10, N11
- Crack prevention interlayer strategies – GA N12, N13
- Soybean based polymer modified asphalt – SB W10
- BMD via recycling agents, gradation, etc. – OK S1, TX S10, S11
- Impact of base stabilization, subgrade modification – MS S2
- Long-term benefit of surface rejuvenators – MS S3
- Full-depth rapid rebuilds (grinding vs. thinlays, HiMA) – SC S9
- Open-graded friction surface rejuvenation (Astec) – SR E1
- Impact of density on performance – FL E5, E6

Milled/Inlayed Sections (7 Sections)

- BMD via additives, gradation, etc. – OK N8, N9, TX N6
- BMD with SGC for design and Marshall for QC – TN S4
- Bond strength with different tack products and rates – NC W4
- Friction performance mix optimization – KY S7
- High-performance open-graded friction course surface – AL E9

Structural Sections (9 Sections)

- Minimum HMA thickness over cold (re)recycling – VA S12
- Additive Group (AG) study for impact on pavement life
- "AG+" New polymer from old, recycled tire rubber – Sigmabond HP S8
- "AG+" High polymer performance with reduced viscosity – BASF S13

1.4 Eighth Research Phase Donations

Numerous companies provided generous donations of equipment, materials, and human resources to help build test sections. This support helps minimize costs and ensures the highest quality research is achieved. As before, Astec Industries provided personnel and equipment to assist in producing experimental mixes and constructing test sections. Roadtec, East Alabama Paving and Trucking, and Wirtgen Group provided construction equipment. Materials were donated by Ergon Asphalt and Emulsions, Hi-Tech Asphalt Solutions, Ingevity, Martin Marietta, Vulcan Materials, and Wiregrass Construction. Caterpillar and Troxler Electronic Laboratories made other significant donations.

1.5 Construction

New test sections were milled to the appropriate depth by Roadtec Inc., who generously provided milling machines and highly skilled operators at no cost. The Test Track manager coordinated milling locations and depths, while NCAT personnel operated dump trucks to collect and haul millings.

The instrumentation system developed through previous phases of the NCAT Test Track was again used to measure pavement responses. The instrumentation plan and analysis routines key to gathering data for mechanistic pavement analyses are fully described in NCAT Report 09-01.

East Alabama Paving Company was awarded contracts to produce the asphalt mixes and construct the test sections through a competitive bidding process through Auburn University. Due to space limitations in the contractor's yard, some materials were temporarily stored on paved surfaces on the Test Track property before being moved to the plant site for mix production.

A special production sequence was used for each mix. The plant's cold feed bins were calibrated for each unique stockpile. Production began with running the aggregate through the dryer and mixer without the addition of asphalt binder to achieve a consistent gradation and temperature. This uncoated material was discharged and wasted. Liquid asphalt was then turned on, and the mix was discharged at the slat conveyor bypass chute until the aggregates were well coated. The bypass chute was then closed, and the mix was conveyed into the storage silo until the plant controls indicated that approximately one truckload had accumulated. This mix was loaded into a truck and dumped into a stockpile for future recycling.

At this point, the plant was assumed to have reached steady-state conditions, and that subsequent mix run into the silo would be uniform in terms of aggregate gradation, asphalt content, and temperature. After the desired quantity of mix had been produced, the aggregate and asphalt flows were stopped, the remaining materials in the dryer and mixer were discharged at the bypass chute, and the plant was shut down. The cold feed bins were unloaded, and the plant was readied for the next test mix.

Before the placement of mixes on each test section, at least one trial mix was produced to evaluate the quality control requirements of the sponsor. The trial mixes were hauled to the Test Track and sampled by NCAT personnel for laboratory testing and evaluation. Test results of the trial mixes were presented to each sponsor to determine appropriate plant settings adjustments for the subsequent mix production for placement.

FIGURE 6 Paving test section N6 for the 2021-2024 research phase.

The mix produced for placement on the test sections followed the same production sequence described above. Mix production continued until enough material was available for placement. The contractor was responsible for hauling mixes to the Test Track, and the paving equipment and crew were staged at the Test Track.

Before placing mixes on the test sections, the contractor tacked the underlying asphalt pavement with a PG 67-22 binder, NTSS-1HM emulsion, or other tack material, depending on the sponsor's preference. Unless otherwise directed, the target application rates were generally between 0.04 and 0.07 gallons per square yard (residual for emulsion).

Mixes were dumped from end-dump haul trucks into a Roadtec SB2500 material transfer machine operated from the Test Track's inside lane. Only the paving machine operated on the actual test sections. Compaction was accomplished by at least three passes of a steel-wheeled roller. The roller could vibrate during compaction; however, this technique was not used in every test section. After removing the steel-wheeled roller from the pavement mat, the contractor continued rolling the mat with a rubber tire roller until the desired density was achieved. A finish roller was then used to eliminate any marks the rubber tire roller left.

1.6 Trafficking Operations

Trafficking for the 2021 Test Track was applied in the same manner as with previous phases. Two shifts of professional drivers operated four trucks pulling triple flatbed trailers (Figure 7) and one truck pulling a triple box trailer from 5 a.m. until approximately 10:40 p.m. Tuesday through Saturday. Trafficking began on November 10, 2021, and ended in April 5, 2024. The total traffic applied to the test sections during this phase was 10,052,142 ESALs.

FIGURE 7 Heavily loaded triple-trailer used for accelerated loading on the Test Track.

Axle weights for each of the five trucks are shown in Table 3. Trailers were removed from the operation on some occasions, either due to a specialized study or mechanical malfunction. This left the truck pulling either a single flatbed trailer or a combination of double flatbeds.

TABLE 3 Axle Weights (lbs.) for the 2015 Truck Fleet

Truck ID	Steer	Tandem		Single				
	Axle 1	Axle 2	Axle 3	Axle 4	Axle 5	Axle 6	Axle 7	Axle 8
1	10,150	19,200	18,550	21,650	20,300	21,850	21,100	19,966
2	11,000	20,950	20,400	20,950	21,200	21,000	20,900	20,900
3	10,550	20,550	21,050	21,000	21,150	21,150	21,350	20,850
4	10,550	21,050	20,700	21,100	21,050	21,050	20,900	21,050
5	11,200	19,850	20,750	20,350	20,100	21,500	19,500	20300
Avg.	10,680	20,320	20,290	20,760	20,760	21,310	20,550	20,613
COV, %	3.9	3.9	4.9	2.2	2.5	1.7	3.6	2.2

1.7 Performance Monitoring

The performance of the test sections was evaluated with a comprehensive range of surface measurements. Additionally, the structural health and response of the structural sections were routinely evaluated using embedded stress and strain gauges and falling weight deflectometer (FWD) testing. Table 4 summarizes the performance monitoring plan. The Test Track website reported rut depths, International Roughness Index (IRI), mean texture depth, and cracking results.

TABLE 4 NCAT Test Track Performance Monitoring Plan

Activity	Sections	Frequency	Method
Rut depth	all	weekly	ARAN van, AASHTO R 48
Mean texture depth	all	weekly	ARAN van, ASTM E1845
Mean texture depth	select	quarterly	CTM, ASTM E2157-09
International Roughness Index	all	weekly	ASTM E950, AASHTO R 43
Crack mapping	sponsored	weekly	Jason 3000
FWD	structural	Three times/mo.	AASHTO T 256-01
Stress/strain response to live traffic	structural	weekly	NCAT method
Pavement temperature at four depths	all	hourly	Campbell Sci. 108 thermistors
Pavement reflectivity/albedo	sponsored	quarterly	ASTM E 1918-06
Field permeability	OGFC/PFCs	quarterly	NCAT method
Core density	sponsored	quarterly	ASTM D979, AASHTO T 166
Friction	all	monthly	ASTM E274, AASHTO T 242
Friction	select	quarterly	DFT, ASTM E1911
Tire-pavement noise	all	quarterly	OBSI, AASHTO TP 76-11, CPX, ISO 11819-2, Absorption, ASTM E1050-10

1.8 Laboratory Testing

Mix samples for quality assurance (QA) testing were obtained from the beds of the haul trucks using a sampling stand at the track. Typical quality assurance tests (listed in Table 5) were conducted immediately on the hot samples, and the results were reviewed by the respective section sponsor for acceptance. In cases where the QA results did not meet sponsor approval, the mix placed on the section was removed, adjustments were made at the plant, and another production run was made until the mix properties were satisfactory. Results of the QA tests and the mix designs for each layer for all test sections were reported on the Test Track website.

TABLE 5 Tests Used for Quality Assurance of Mixes

Test Description	Test Method	Replicates
Splitting samples	AASHTO T 328-05	as needed
Asphalt content	AASHTO T 308-10	2
Gradation of recovered aggregate	AASHTO T 30-10	2
Laboratory compaction of samples	AASHTO T 312-12	2
Maximum theoretical specific gravity	AASHTO T 209-12	2
Bulk specific gravity of compacted specimens	AASHTO T 166-12	2
Mix moisture content	AASHTO T 329-15	1

NCAT staff obtained large representative samples of each experimental mix placed on the track for additional testing by diverting the mix from the conveyor of the material transfer machine connecting the paver into the bucket of a front-end loader. The front-end loader then brought the mix to the Test Track laboratory, where it was shoveled into five-gallon buckets and labeled. In total, nearly 1300 buckets of mix were sampled for additional testing. Samples of the asphalt binders were also obtained at the plant for Superpave PG characterization.

A testing plan for advanced characterization of the 22 unique mixes was established to meet section-specific and general Test Track research objectives. Table 6 summarizes the tests and materials/layers typically evaluated. Test results are maintained in a database at NCAT.

TABLE 6 Summary of Testing for Advanced Materials Characterization

Test Description	Test Method	Material or Layer
PG grade	AASHTO R 29-08	Tank binders and recovered binders from mixes containing RAP, RAS, and WMA (No GTR modified binders were recovered)
Multiple stress creep recovery	AASHTO TP 70-09	Same as above
Cantabro	AASHTO TP 108-14	ALDOT and ODOT OGFCs, NCAT Cracking Group surface mixes, KTC mixes
Moisture susceptibility	AASHTO T 283-14	KYTC mixes
Hamburg wheel tracking	AASHTO T 324-14	FDOT surface cracking study, KYTC mixes, Collaborative Aggregates mix
Dynamic modulus	AASHTO TP 79-13	FDOT surface cracking study, TDOT Thinlay mix
Energy ratio	Univ. of Florida	Surface mixes from NCAT Cracking Group and FDOT cracking experiments
SCB-Jc (Louisiana)	LADOTD TR 330-14	Surface mixes from NCAT Cracking Group and FDOT cracking experiments
Overlay tester (Texas)	Tex-248-F	Surface mixes from NCAT Cracking Group, FDOT cracking, and KYTC mix design experiments
Overlay tester (NCAT modified)	NCAT	Surface mixes from NCAT Cracking Group and FDOT cracking experiments
Illinois Flexibility Index Test	IL TP 405	Surface mixes from NCAT Cracking Group, Collaborative Aggregates mix, and FDOT cracking experiment mixes.
IDEAL Cracking Test	Texas A&M Trans. Inst.	Surface mixes from the NCAT Cracking Group experiment.
NCAT TWPD, Dynamic Friction Test, and Circular Track Meter	ASTM E1911, ASTM E2157	TDOT Thinlay mix

1.9 References

1. Timm, D., R. West, A. Priest, B. Powell, I. Selvaraj, J. Zhang, and R. Brown. *Phase II NCAT Test Track Results*. NCAT Report 06-05. National Center for Asphalt Technology at Auburn University, Auburn, Ala., 2006.
2. Prowell, B., and E. R. Brown. *NCHRP Report 573: Superpave Mix Design: Verifying Gyration Levels in the Ndesign Table*. Transportation Research Board of the National Academies, Washington, D.C., 2009.
3. Leiva-Villacorta, F. and R. West. Analysis of Field Compactability Using Accumulated Compaction Pressure Concept. *Transportation Research Record: Journal of the Transportation Research Board, No. 2057*, Transportation Research Board of the National Academies, Washington, D.C., 2008, pp 89-98.
4. Yin, F. and R. West. *Performance and Life Cycle Cost Benefits of Stone Matrix Asphalt*. NCAT Report 18-03. National Center for Asphalt Technology at Auburn University, Auburn, Ala., 2018.
5. West, R., D. Timm, R. Willis, B. Powell, N. Tran, M. Sakhaeifar, R. Brown, M. Robbins, A. Vargas-Nordcbeck, F. Leiva Villacorta, X. Guo, and J. Nelson. *Phase IV NCAT Pavement Test Track Findings*. NCAT Report 12-10. National Center for Asphalt Technology at Auburn University, Auburn, Ala., 2012.
6. West, R., D. Timm, B. Powell, M. Heitzman, N. Tran, C. Rodezno, D. Watson, F. Leiva, A. Vargas, R. Willis, M. Vrtis, and M. Diaz. *Phase V (2012-2014) NCAT Test Track Findings*. NCAT Report 16-04. National Center for Asphalt Technology at Auburn University, Auburn, Ala., 2018.
7. Williams, B. A., A. Copeland, and T. C. Ross. *Asphalt Pavement Industry Survey on Recycled Materials and Warm-Mix Asphalt Usage-2017*. NAPA Information Series 138, 8th Ed., National Asphalt Pavement Association, Lanham, Md., 2018.
8. Brown, E. R., L. A. Cooley, Jr., D. Hanson, C. Lynn, B. Powell, B. Prowell, and D. Watson. *NCAT Test Track Design, Construction, and Performance*. NCAT Report 02-12. National Center for Asphalt Technology at Auburn University, Auburn, Ala., 2002.
9. Merine, G. *VDOT MEPDG Implementation*. Presentation at the 2018 Virginia Concrete Conference, 2018.
10. Peters-Davis, K., and D. Timm. *Recalibration of the Asphalt Layer Coefficient*. NCAT Report 09-03. National Center for Asphalt Technology at Auburn University, Auburn, Ala., 2009.
11. Timm, D., and K. Davis. Are We Underestimating the Strength of Asphalt? *Hot Mix Asphalt Technology*, Vol. 15, No. 1, National Asphalt Pavement Association, 2010.
12. Willis, R., D. Timm, R. West, B. Powell, M. Robbins, A. Taylor, A. Smit, N. Tran, M. Heitzman, and A. Bianchini. *Phase III NCAT Test Track Findings*. NCAT Report 09-08. National Center for Asphalt Technology at Auburn University, Auburn, Ala., 2009.

13. Sakhaeifar, M., R. Brown, N. Tran, and J. Dean. Evaluation of Long-Lasting Perpetual Asphalt Pavement with Life-Cycle Cost Analysis. *Transportation Research Record: Journal of the Transportation Research Board, No. 2368*, Transportation Research Board of the National Academies, Washington, D.C., 2013, pp. 3-11.
14. Guo, X. *Local Calibration of the MEPDG Using Test Track Data*. MS thesis. Auburn University, Auburn, Ala., 2013.
15. Guo, X., and D. Timm. Local Calibration of MEPDG Using National Center for Asphalt Technology Test Track Data. *TRB 94th Annual Meeting Compendium of Papers*, Paper 15-1032, Transportation Research Board 94th Annual Meeting, Washington, D.C., 2015.

2. ADDITIVE GROUP EXPERIMENT (PHASE II)

2.1 Background

Suppliers of new asphalt mixture additives often ask highway agencies to consider their product, asserting economic, environmental, and/or performance benefits for asphalt pavements. However, the absence of widely accepted standards for evaluating mixtures with and without these additives often complicates the assessment process. Typically, state Departments of Transportation (DOTs) use various laboratory tests (either internally or through independent labs or asphalt research organizations) to characterize additives and their effects on asphalt mixtures. In many cases, these results often fail to clearly indicate the potential benefits of an additive, especially regarding any impact on the lifespan of asphalt overlays or pavements. Consequently, for additives showing promising lab results, state DOTs may require the construction of field test sections to better assess real-world performance. Unfortunately, gathering meaningful field performance data may require over a decade of service for pavement test sections with and without the additive.

The Additive Group (AG) Experiment aims to comprehensively evaluate a limited set of asphalt mixture additives, chosen by highway agency sponsors, through laboratory testing, pavement modeling, environmental assessments, and accelerated field performance testing. Recognizing the inherent challenges in constructing and evaluating test sections, whether using an accelerated loading facility or an open highway, a significant secondary objective of this experiment is to establish and validate a framework for predicting long-term performance. This involves characterizing critical stresses and accumulated damage within a pavement structure through laboratory analysis and modeling.

Establishing a reliable process to predict the performance of pavements with new additives is critical, as it will enable pavement engineers to confidently conduct life-cycle cost analyses and assessments based on realistic projections of extended pavement life. This project will determine how well predictions from laboratory tests and models compare to field performance in pavement test sections on the NCAT Test Track, a well-documented environment largely free of confounding factors that could cloud or obscure effects of the additives.

The additives evaluated in this experiment include ground tire rubber (GTR), recycled plastics, and aramid fiber. Each was added to the same dense-graded asphalt mixture without changing the asphalt binder content or aggregate gradation of the mixture. The control mixture was simply the same mixture without any of these additives. Additive dosages were based on recommendations from their respective suppliers using wet and dry processes. The following sections provide additional information about these materials.

2.2 Materials

2.2.1 Rubber Technologies

Ground tire rubber (GTR), also referred to as recycled tire rubber (RTR), is primarily manufactured from scrap tires. The main components of tires include elastomeric compounds of natural and synthetic rubber, carbon black steel, and other components such as fabrics and fillers. The recoverable rubber includes the elastomeric compound and the carbon black steel. GTR can be incorporated into an asphalt mixture through either a wet or dry process. In the wet process, RTR is blended with asphalt binder before mixing with the aggregate. In the dry process, RTR is added to the heated aggregate inside the mixing drum before the introduction of any asphalt binder. Mixture performance improvements when using RTR are influenced by factors such as the amount, size, and chemical composition of the rubber, as well as the blending method.

This experiment used both wet and dry processes to incorporate rubber into the asphalt mixtures. The wet process involved a terminal blended rubber-modified binder that used a PG 64-22 virgin binder modified with 10% (by weight of binder) of a -30 mesh RTR supplied by Entech, Inc. The dosage of the rubber was selected to match the Superpave performance grade (PG) of the PG 76-22 SBS binder. The dry process used a pre-reacted rubber provided by Liberty Tire Recycling, marketed under the name SmartMIX. This process entailed combining a fine-grind rubber with extender oil and heating to approximately 275°F for 30 minutes. After heating, swelling, and saturation, the reacted rubber was moved into a cooling system and mixed with a flow agent to prevent particle sticking. SmartMIX was added to the mix alongside a PG 67-22 binder using a separate feed system to proportion the rubber at a rate of 12% by weight of the total binder. Figure 1 shows the two types of rubber technologies used in the AG experiment.

FIGURE 1 Entech (left) and SmartMIX (right) ground tire rubber.

2.2.2 Fiber Technology

The fiber used in this experiment was an aramid fiber supplied by Surface Tech™, produced in the form of strands, each consisting of over 10,000 individual fibers and pre-treated with wax for ease of dosing. Each strand was comprised of 63% aramid fiber and 37% wax binder by weight. The recommended dosage rate for this fiber is 3.4 ounces per ton of asphalt mixture, of

which 2.1 ounces constitute aramid fiber per ASTM D 8395-2023, Standard Specification for Aramid Fiber for Asphalt Mixtures. The fiber strands were weighed using dosing equipment (Figure 2a), dosed onto the RAP belt (Figure 2b), and then conveyed to the asphalt mixing drum. Once inside, the wax melted, allowing the fibers to disperse into the asphalt mixture. The fiber did not alter the volumetric properties, workability, or compactability of the asphalt mixture. However, it could affect stiffness of the mixture and its resistance to cracking and rutting (Surface Tech, 2024).

(a) (b) (c)

FIGURE 2 Synthetic fiber used in the AG experiment: (a) Fiber stands in dosing equipment, (b) Fiber strands dosed on RAP belt to mixing drum, (c) Individual fibers dispersed into the mix.

2.2.3 Plastic Technologies

The plastic additive used was post-consumer recycled (PCR). As shown in Figure 3, the additive was in pellet form, with 97% passing the 3/8-inch sieve and 3% passing the No. 4 sieve. It contained approximately 95% linear low-density polyethylene (LLDPE), had a specific gravity of 0.91 to 0.92, a melt flow rate of 1.8 to 2.8 g/10 min., and contained less than 1.0% ash. The plastic additive was evaluated for asphalt modification using both the wet process and the dry process. For the wet process, a PG 67-22 virgin binder was modified with 1.0% plastic pellets, 1.5% reactive elastomeric terpolymer (RET) to stabilize the plastic, and 0.32% polyphosphoric acid (PPA)to act as a co-reactant to the RET. The dosages of the plastic, RET, and PPA (approximately 70% at 64°C) were selected to match the Superpave PG and MSCR percent recovery of the PG 76-22 SBS control binder. For the dry process, the plastic pellets were dropped into the SBS control mixture at a dosage of 0.5% by weight of the total aggregate while all other mixture components and proportions remained unchanged.

FIGURE 3 Post-consumer recycled (PCR) plastic additive.

2.3 Phase I Overview

2.3.1 Experimental Plan

Phase I of the experiment entailed a comprehensive assessment of various asphalt additive technologies. This involved laboratory characterization of a dense-graded asphalt mixture with and without additives. Balanced mix design (BMD) tests were used to assess mix quality, while advanced mixture characterization tests were used for structural analysis to predict pavement performance.

Based on these results, agency sponsors selected five additives for full-scale construction, trafficking, and field performance evaluation at the Test Track. In addition, a control section without additives served as a reference for drawing conclusions regarding the effectiveness of the different additives. This section documents the results of these five additives, as shown in Table 1. The technologies chosen for further evaluation include wet and dry process recycled GTR, wet and dry process PCR plastic, and dry process aramid fibers. The control section included an SBS-modified binder.

The mixtures were compared using the Hamburg Wheel Tracking Test (HWTT) and IDEAL-CT for balanced mix design, and theoretical structural pavement analysis in terms of fatigue performance used dynamic modulus (E*) and cyclic fatigue as inputs for WESLEA and FlexPAVE^{TM} programs to predict equivalent pavement section thicknesses relative to the control mix and provisional structural coefficients. The experimental plan of Phase I is presented in Figure 4.

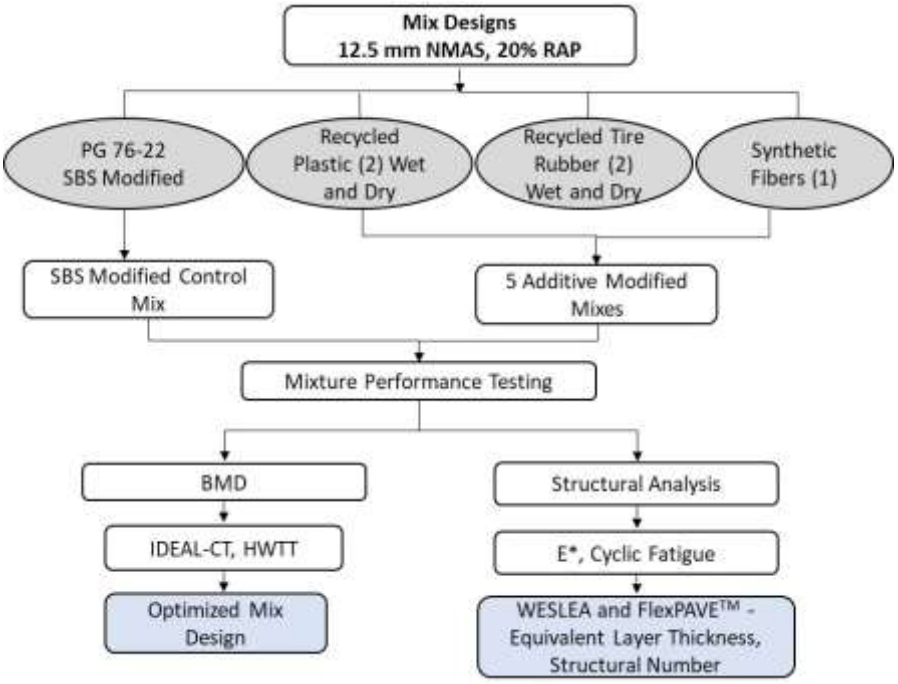

FIGURE 4 AG Phase I experimental plan.

2.3.2 Mix Design

The asphalt mixture design used in this study was a 60-gyration 12.5 mm nominal maximum aggregate size (NMAS) dense-graded mix. The mix contained a blend of granite and manufactured sand and 20% RAP. The gradation and volumetric targets for Phase I, along with the Phase II quality control (QC) values for the plant-produced mixtures, are detailed in Table 2. Baghouse fines were added at 1.0% by weight of aggregate to mitigate potential aggregate breakdown during production. The RAP had a binder content of 5.7%, and the extracted RAP binder had a high-temperature PG of 100.9°C. The five additive technologies (plus the SBS-modified control) selected for evaluation in Phase II of the experiment are detailed in Table 1. The table includes specific additive formulations or product names, additive dosage rates for both wet and dry processes, and binder performance grades before and after wet process. All dosage rates are expressed as a percentage by weight of asphalt binder unless otherwise specified.

TABLE 1 Additive Formulations, Dosage Rates, and Binder Performance Grades

Mixture ID	Wet Modifier	Wet Modifier Dosage Rate	Virgin Binder PG Before Wet Modification	Modified Binder PG	Dry Modifier	Dry Modifier Dosage Rate
N1 (GTR Dry)	None	N/A	67-22	67-22	SmartMIX™ (Liberty Tire Recycling)	12%
N2 (GTR Wet)	Terminal blended (TB) rubber binder (Entech, Inc.)	10%	67-22	76-22	None	N/A

N5 (Aramid)	SBS	3%	67-22	76-22	ACE XP™ (Surface Tech™)	3.4 oz/ton
N7 (Control)	SBS	3%	67-22	76-22	None	N/A
S5 (Dry Plastic)	SBS	3%	67-22	76-22	LLDPE	0.5% (by weight of aggregate)
S6 (Wet Plastic)	LLDPE + ELVALOY™ RET (Dow®) + PPA	1% LLDPE + 1.5% ELVALOY™ RET (Dow®) + 0.32% PPA	67-22	76-22	None	N/A

TABLE 2 Phase I Mix Design and Phase II Plant-Produced Mixture Quality Control Properties

	N1 GTRDry		N2 GTRWet		N5 Aramid		N7 Ctrl		S5 DryPlastic		S6 WetPlastic	
	Target	QC	Target	QC	Target	QC	Target	QC	Target	QC	Target	QC
19 mm (3/4")	100	100	100	100	100	100	100	100	100	100	100	100
12.5 mm (1/2")	98	97	98	97	98	98	98	97	98	97	98	97
9.5 mm (3/8")	89	87	89	86	89	84	89	84	89	87	89	86
4.75 mm (#4)	55	59	55	57	55	54	55	54	55	56	55	56
2.36 mm (#8)	41	44	41	42	41	40	41	41	41	43	41	42
1.18 mm (#16)	33	34	33	32	33	31	33	32	33	33	33	32
0.60 mm (#30)	22	20	22	19	22	18	22	20	22	20	22	20
0.30 mm (#50)	12	10	12	10	12	9	12	10	12	9	12	10
0.15 mm (#100)	7	7	7	6	7	6	7	6	7	6	7	6
0.075 mm (#200)	4.5	4.3	4.5	4.1	4.5	3.8	4.5	4.0	4.5	3.8	4.5	4.0
Binder Content (P_b)	5.6	5.6	5.6	5.8	5.6	5.5	5.6	5.7	5.6	5.8	5.6	5.7
Eff. Binder Content (P_{be})	5.0	5.0	4.9	5.2	5.0	4.9	5.0	5.0	5.0	5.1	5.0	5.0
Dust-to-Eff. Binder Ratio	0.9	0.9	0.9	0.8	0.9	0.8	0.9	0.8	0.9	0.7	0.9	0.8
RAP Binder Replacement (%)	21	20	21	19	21	20	21	20	21	19	21	20
Rice Gravity (G_{mm})	2.453	2.449	2.457	2.453	2.453	2.465	2.453	2.455	2.453	2.439	2.453	2.463
Bulk Gravity (G_{mb})	2.344	2.328	2.314	2.351	2.344	2.350	2.344	2.369	2.344	2.359	2.344	2.333
Air Voids (V_a)	4.4	4.9	5.8	4.2	4.4	4.7	4.4	3.5	4.4	3.3	4.4	5.3
Aggregate Sp. Gravity (G_{sb})	2.627	2.622	2.627	2.636	2.627	2.639	2.627	2.632	2.627	2.616	2.627	2.641
VMA (based on G_{sb})	15.8	16.2	16.8	16.0	15.8	15.8	15.8	15.1	15.8	15.0	15.8	16.7
VFA	72	69	65	74	72	71	72	77	72	78	72	68
Avg. Mat Density (% G_{mm})	94.0	93.7	94.0	94.1	94.0	94.2	94.0	95.9	94.0	93.5	94.0	93.9

2.3.3 BMD Testing

The AG mixture design was optimized to meet the BMD criteria based on the IDEAL-CT per ASTM D8225 and the HWTT per AASHTO T 324. For IDEAL-CT, a cracking tolerance index (CT_{Index}) of 50 was selected for good cracking resistance based on research conducted at the NCAT Test Track (West et al., 2021). The mix design was initially established with a PG 76-22 SBS modified binder. The performance optimum binder content (OBC) of the mix was 5.6% with an average CT_{Index} of 54.1 and an average rut depth of 2.5 mm at 20,000 passes with no sign of stripping. IDEAL-CT and HWTT were conducted on short-term specimens aged for 4 hours at 135°C per AASHTO R 30. IDEAL-CT was conducted at 25°C to evaluate intermediate-temperature cracking resistance and HWTT was conducted at 50°C for rutting evaluation.

2.3.4 AMPT Testing for Structural Evaluation

E* testing was conducted to characterize the stiffness and viscoelastic characteristics of asphalt mixtures containing different additives at multiple temperatures and loading frequencies. The test was conducted on small-size cylindrical specimens using an Asphalt Mixture Performance Tester (AMPT) per AASHTO TP 132-19. Triplicate specimens were prepared in accordance with AASHTO PP 99-19. Each specimen measured 38 mm in diameter and 110 mm in height with 7.0 ± 0.5 percent air voids after coring and saw trimming. Each specimen was tested with nine temperature-loading frequency combinations, which included three test temperatures (4, 20, and 40°C) and three loading frequencies (10, 1, and 0.1 Hz).

In addition to E*, the Cyclic Fatigue test was conducted to evaluate fatigue damage resistance. The test was conducted using small-size cylindrical specimens in an AMPT, which were prepared in the same manner as for the E* test discussed above. The Cyclic Fatigue test was conducted following AASHTO TP 133-19. In this evaluation, a test temperature of 21°C was used based on the climate's high temperature grade requirement of the mix design. The test was conducted with a constant frequency of 10 Hz.

2.3.5 WESLEA and FlexPAVETM Analysis

Provisional structural coefficients were calculated to determine the relative structural capacity of the AG mixtures. Two methods were deployed to generate structural coefficients. However, both yielded nearly identical results. Consequently, this chapter only presents FlexPAVE™ percent damage simulations. Further detail regarding the provisional structural coefficient determination as a part of Phase I has been previously published (Timm et al., 2022).

FlexPAVE™ employs viscoelastic continuum damage theory to account for the effects of loading rate and temperature on asphalt pavement response and distress mechanisms. The program utilizes three-dimensional finite element analysis with moving loads to compute the mechanical response under various traffic loads. It incorporates the Enhanced Integrated Climatic Model (EICM) to provide realistic climatic conditions for pavement response calculations and

performance predictions. Although FlexPAVE™ can predict both rutting and cracking performance, the structural analysis conducted in this study focused only on fatigue cracking because it was the expected mode of pavement distress. Inputs used for the FlexPAVE™ analysis were selected to closely simulate traffic, climate, and subgrade conditions of the NCAT Test Track as well as the anticipated pavement structure of the AG experiment.

A design life of 2 years was used for the FlexPAVE™ analysis (consistent with the paved sections at the NCAT Test Track), and each section was modeled as 5.5 in of AC (initially) over a 6-inch granular base to simulate cross-sections of the sections. E* and Cyclic Fatigue FlexMAT™ outputs were used to characterize each asphalt mixture. The moduli of the unbound materials (granular base and subgrade) were based on representative values obtained through backcalculation of falling weight deflectometer (FWD) data from previous research cycles at the Test Track, and Poisson ratios were assumed based on typical values for these material types (Taylor and Timm, 2009). The simulated loadings were based on the single axles of Test Track vehicles (18,000 lbs). Design speeds of 45 mph and daily equivalent single axle load (ESAL) counts of 13,699 with no traffic growth were chosen to approximate Test Track conditions.

The simulated percentage of damage at the end of pavement design life was used as the primary analysis parameter to compare predicted fatigue performance. To determine the equivalent layer thicknesses and subsequent provisional structural coefficients, iterative FlexPAVE™ simulations were conducted with varying asphalt layer thicknesses. The process was repeated for each additive-modified experimental mix until an equivalent pavement section was found, having approximately identical percentages of simulated damage as the control section with 5.5 in of asphalt layer using the PG 76-22 SBS-modified mixture. The corresponding asphalt layer thickness of the equivalent pavement section was defined as the equivalent layer thickness. The provisional structural coefficient was computed using the methodology described below using Equation 1.

The equivalent thicknesses resulting from FlexPAVE™ simulations were used to estimate the corresponding structural coefficients in the AASHTO 1993 Design Guide of Pavement Structures. This computation assumed a structural coefficient of 0.54 for the mix in the PG 76-22 control section, which is the current value used for this material by the Alabama Department of Transportation. This value, multiplied by the asphalt layer thickness (5 in), produced a structural number (SN) of 2.7 for the asphalt layer. Since the other two sections were designed as structurally equivalent (i.e., SN = 2.7) with different thicknesses, structural coefficients were determined by dividing 2.7 by the corresponding estimated thicknesses from WESLEA simulations according to Equation 1.

$$a_{1e} = \frac{D_c}{D_e} a_{1c} \qquad \text{Equation 1}$$

where

a_{1e} = asphalt structural layer coefficient for experimental mix,
a_{1c} = asphalt structural layer coefficient for PG 76-22 control mix = 0.54 (assumed),
D_c = asphalt layer thickness of PG 76-22 control pavement section = 5 inches (fixed), and
D_e = equivalent layer thickness of additive-modified experimental pavement section.

2.3.6 LMLC BMD Results

IDEAL-CT results (Figure 5) and HWTT results (Figure 6) from Phase I testing are summarized below. The error bars in Figure 5 represent one standard deviation. For the rubber and plastic mixes, the evaluation was conducted on lab-mixed lab-compacted (LMLC) specimens. For the aramid fiber mix, the evaluation was conducted on plant-mixed lab-compacted (PMLC) specimens. A control PMLC and fiber-modified PMLC were produced at a local asphalt plant and sampled for laboratory evaluation. All the LMLC mixes were produced in the lab with design total AC content of 5.6% total asphalt. The control mix with PG 76-22 was designed to have an average CT_{Index} above 50 at the optimum AC content while also passing HWTT rutting criteria.

None of the LMLC mixes in Phase I (rubber, plastic, or control) showed any rutting or stripping potential in the HWTT. All the mixes exceeded the IDEAL-CT design threshold of CT_{Index} = 50, except the dry plastic mix with an average CT_{Index} of 44.1. The dry rubber mix produced the highest CT_{Index} of the LMLC mixes. The remaining LMLC CT_{Index} sets had an average in a narrow range (between 44 and 54).

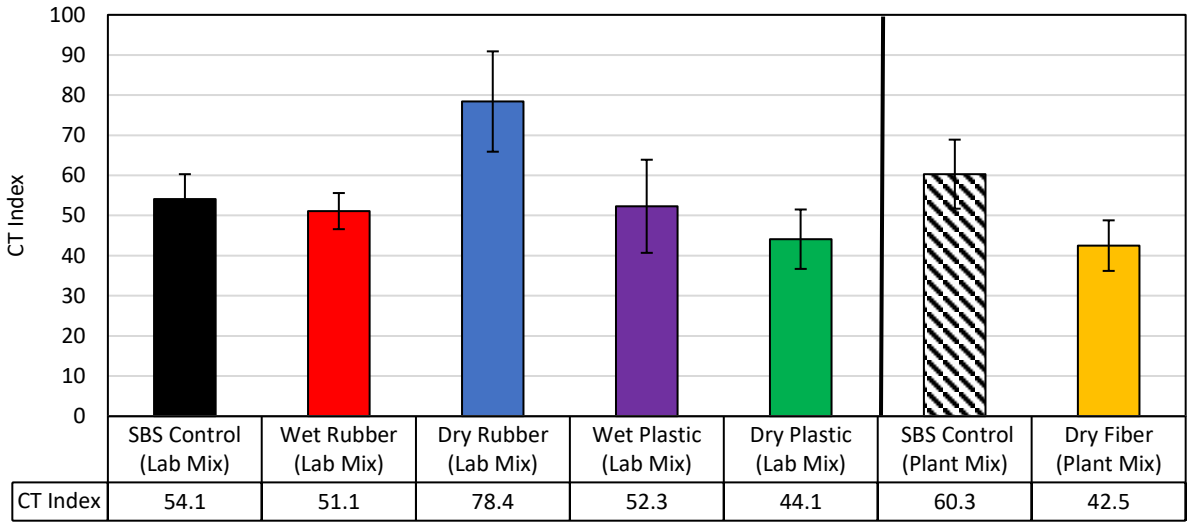

FIGURE 5 Phase I IDEAL-CT results.

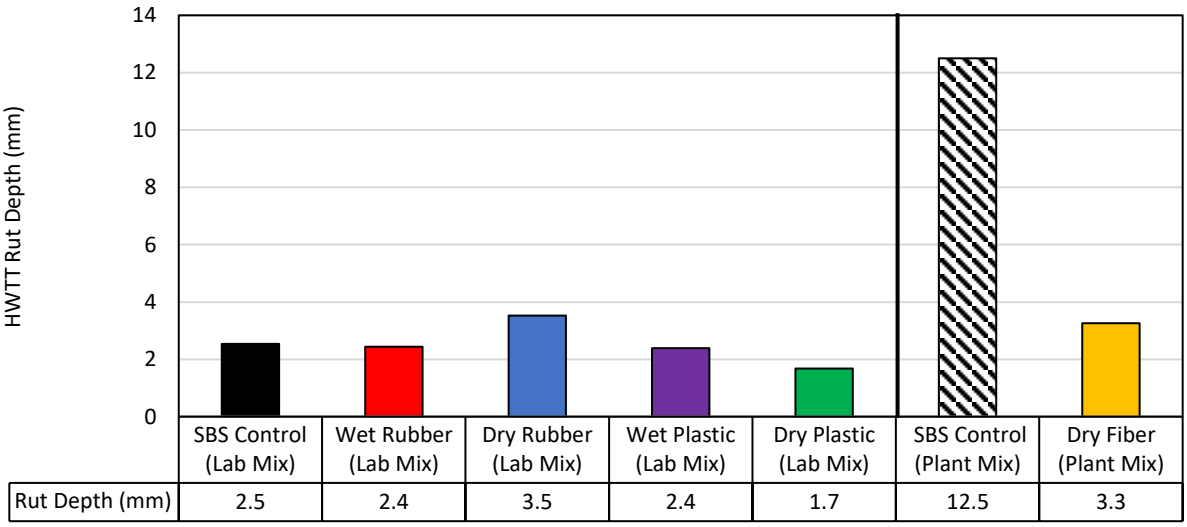

FIGURE 6 Phase I HWTT results.

2.3.7 LMLC AMPT Results

Table 3 summarizes the |E*| master curve coefficients of the control and additive-modified mixes from the Phase I study. The rubber-modified and plastic-modified mixes were prepared in the laboratory, while the fiber-modified mix was produced at an asphalt plant. Figure 7 presents the average |E*| values at 20°C and 10Hz. Among the laboratory-prepared mixes, the wet rubber and wet plastic mixes had comparable |E*| to the SBS control mix, which was expected since they used virgin binders with similar PG. The dry plastic mix had a notably higher |E*| value than the SBS control mix, indicating a mixture stiffening impact from adding dry plastics. Conversely, the dry rubber mix was softer than the SBS control mix, as indicated by a lower |E*| value. The two plant-produced mixes had comparable |E*| values at 20°C and 10Hz, suggesting that adding aramid fibers did not significantly affect the stiffness of the SBS control mix.

TABLE 3 |E*| Phase I Master Curve Fitting Coefficients

Mixture ID	Max E* (ksi)	Delta (δ)	Beta (β)	Gamma (γ)	ΔE_a	R^2
SBS Control (Lab Mix)	3,127.6	1.2	-1.295	-0.435	209,472	0.999
Wet Rubber (Lab Mix)	3,166.4	2.4	-1.245	-0.424	211,137	0.999
Dry Rubber (Lab Mix)	3,112.9	1.3	-1.156	-0.410	210,310	1.000
Wet Plastic (Lab Mix)	3,170.6	2.9	-1.196	-0.458	206,956	0.999
Dry Plastic (Lab Mix)	3,137.6	1.2	-1.421	-0.406	208,010	0.999
SBS Control (Plant Mix)	3,105.6	5.3	-1.207	-0.479	206,812	0.998
Dry Fiber (Plant Mix)	3,087.6	5.5	-1.199	-0.474	208,189	0.997

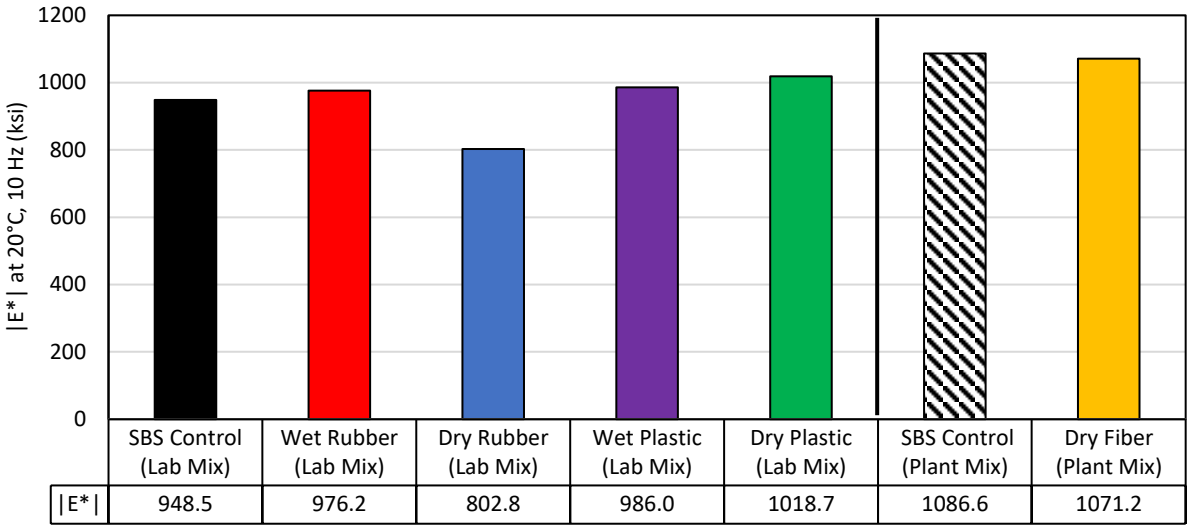

FIGURE 7 Phase I |E*| at 20°C and 10 Hz.

Figure 8 presents the representative S_{app} results from the Cyclic Fatigue test, where a higher S_{app} is desired for better fatigue damage resistance. Among the laboratory-prepared mixes, the wet rubber mix had the highest S_{app}, followed by the wet plastic and SBS control mixes, the dry rubber mix, and the dry plastic mix, respectively. This suggests wet process modification with rubber and plastic can improve or maintain the fatigue damage resistance of the SBS control mix. The dry process modification with rubber and plastic was not as effective as the wet process modification with SBS. When comparing the two plant-produced mixes, the dry fiber mix outperformed the SBS control mix with a notably higher S_{app}, highlighting improved fatigue damage resistance from adding aramid fibers via the dry process.

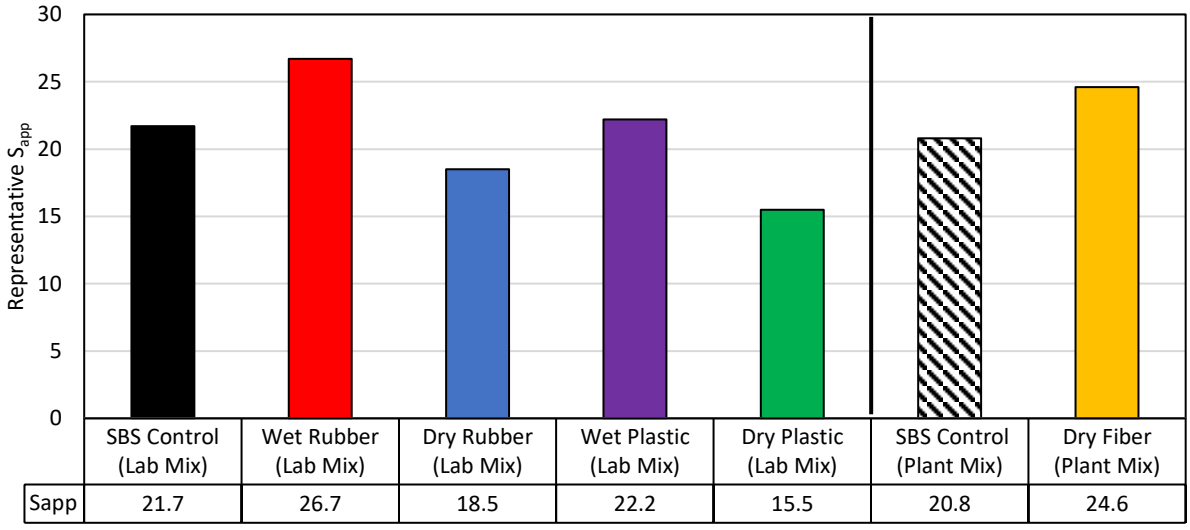

FIGURE 8 Phase I cyclic fatigue S_{app} results.

2.3.8 WESLEA and FlexPAVETM Analysis

Figure 9 presents FlexPAVE™ simulation results regarding the structural layer coefficients. The wet rubber, wet plastic, and dry fiber sections outperformed their corresponding SBS control sections, as indicated by lower equivalent asphalt thicknesses and higher structural layer coefficients. Therefore, these additive technologies can improve the structural capability of asphalt pavements due to improved resistance to fatigue cracking. Conversely, the dry rubber and dry plastic sections did not perform as well as the SBS control section in WESLEA and FlexPAVE™ simulations. They both required a thicker asphalt pavement structure to maintain the predicted fatigue cracking performance as the SBS control section and, thus, had a structural layer coefficient lower than 0.54.

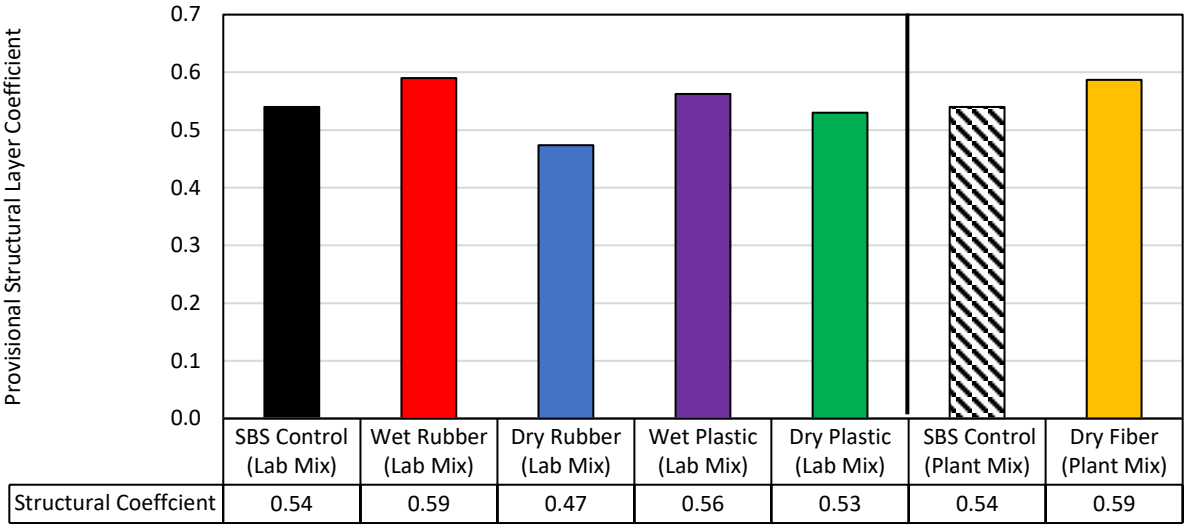

FIGURE 9 Phase I FlexPAVE™ provisional structural coefficients.

2.4 Phase II Experimental Plan

Phase II involved plant production, construction, and instrumentation of the full-scale test sections followed by structural and performance evaluation consisting of applying accelerated traffic, monitoring, and evaluating performance. Plant mix was sampled from each test section to conduct the same battery of tests for BMD and structural analysis evaluation as in Phase I (Figure 4). Bending beam fatigue was added to the test matrix to characterize fatigue performance of the mixtures.

2.5 Phase II Mixture Design

Six test sections were constructed for the AG experiment at the NCAT Test Track. Five of these included some form of additive technology, and an SBS-modified section acted as control. For reference, specific additive formulations and product names, wet and dry process additive dosage rates, and binder performance grades before and after wet process modification are shown in Table 1. N5 (Aramid) and S5 (Dry Plastic) received wet process SBS modification in addition to the dry process additive technologies. Section N1 (GTR Dry) was the only section

without wet process modification, reflected by its unchanged binder PG of 67-22. For reference, gradation and volumetric targets along with quality control (QC) values are presented in Table 2. An identical 12.5-mm NMAS dense-graded mixture design was used for each test section. Each mixture design incorporated 20% reclaimed asphalt pavement (RAP) with a design asphalt binder content of 5.6%. See previously published documentation for further details regarding mixture production, mixture designs and properties, sampling procedures, and laboratory test specimen production (Foshee, 2022 and Kmetz, 2023).

2.6 Phase II Laboratory Testing

2.6.1 Plant-Mixed Lab-Compacted (PMLC) BMD Results

The IDEAL-CT test was conducted per ASTM D8225-19 on specimens conditioned at 25°C (consistent with the BMD testing performed in Phase I). IDEAL-CT data are summarized in Figure 10. The data are shown at three aging conditions: production PMLC, re-heated (RH) PMLC, and critically aged (CA) PMLC. Each data set represents a minimum of four replicates, and all specimens were compacted to 7.0 ± 0.5 percent air voids at a height of 62 mm in the Superpave Gyratory Compactor (SGC). The production specimens were compacted while the mix was being produced and paved at the Track and were not re-heated after production. The re-heated (RH) PMLC specimens were prepared by re-heating 5-gallon buckets of loose mix that were sampled during paving. The critically aged (CA) specimens were compacted from loose mix aged for 8 hours at 135°C to approximate over 5 years of surface field aging at the NCAT Test Track (Chen et al., 2020; Yin et al., 2023).

In general, the average CT_{Index} for production specimens was greater than the re-heated samples, and the average CT_{Index} for the re-heated specimens was greater than the critically aged specimens. The only exception to this trend was the RH CT_{Index} of the wet rubber mixes, which exhibited a slightly higher value compared to the production CT_{Index}. This was due to significant specimen expansion of the mixture, or rebound, during laboratory compaction. These specimens required prolonged cooling in the mold to mitigate expansion, causing the remaining specimens to stay in the oven longer while waiting. Both rubber-modified mixtures displayed lower average CT_{Index} values relative to the control mixture at each of the three aging conditions, with the wet process rubber mixture displaying the lowest average CT_{Index} value of the three mixtures. The control mixture had a greater average CT_{Index} value at the RH and CA conditions relative to the mixture modified with aramid fibers. However, the average CT_{Index} value at the production aging condition was statistically similar between the two mixtures. Both plastic-modified mixtures displayed lower average CT_{Index} values relative to the control mixture at each of the three aging conditions (except the wet plastic and control mixtures at the RH condition, which were statistically similar), with the dry process rubber mixture displaying the lowest average CT_{Index} value of the three mixtures.

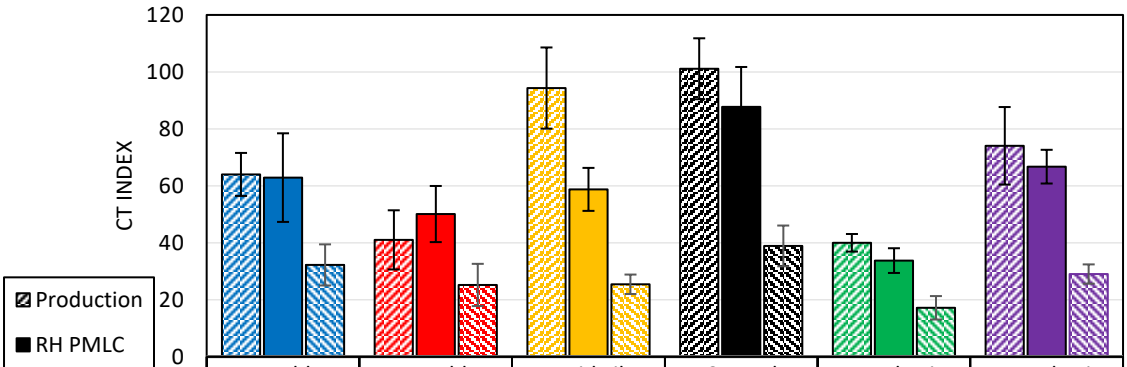

	Dry Rubber N1-1	Wet Rubber N2-1	Aramid Fiber N5-1	Control N7-1	Dry Plastic S5-1	Wet Plastic S6-1
Production	64.0	41.0	94.3	101.1	40.0	74.1
RH PMLC	62.9	50.1	58.8	87.7	33.8	66.7
CA PMLC	32.2	25.2	25.4	38.9	17.2	29.0

FIGURE 10 IDEAL-CT results for PMLC mixtures at multiple aging conditions

Rutting was characterized by the Hamburg Wheel-Tracking Test (HWTT) conducted per AASHTO T 324-22, the high-temperature indirect tension test (HT-IDT) conducted per ALDOT 458, and the IDEAL-RT test conducted per ASTM D8360-22. As part of another study, the HT-IDT and IDEAL-RT tests are being evaluated for use during mix production as faster alternatives to longer-duration wheel-tracking tests (Chen et al., 2023). The rapid rutting tests were performed for the AG mixes as part of that evaluation during the 2021 Test Track research cycle. The tests were conducted on re-heated plant-produced mix (RH PMLC) specimens compacted to 7.0 ± 0.5% air voids. The HWTT was conducted on four specimens per mix (two-wheel tracks with 2 specimens per track) and the HT-IDT and IDEAL-RT were each conducted on three replicate specimens. All rutting tests were conducted on specimens conditioned in water at 50°C.

The RH PMLC HWTT results are shown in Figure 11. No stripping was observed in the HWTT for any of the mixes, and all the final test rut depths after 20,000 passes were very low. A common failure criterion in the HWTT for polymer-modified mixes is less than 12.5 mm rut depth after 20,000 passes (NAPA, 2024). The maximum rutting exhibited by any of the additive group mixes after 20,000 passes was 3.1 mm (wet process rubber and control mixtures). The mixture with the lowest rutting potential in the HWTT was the dry process plastic mix with 1.8 mm of rutting.

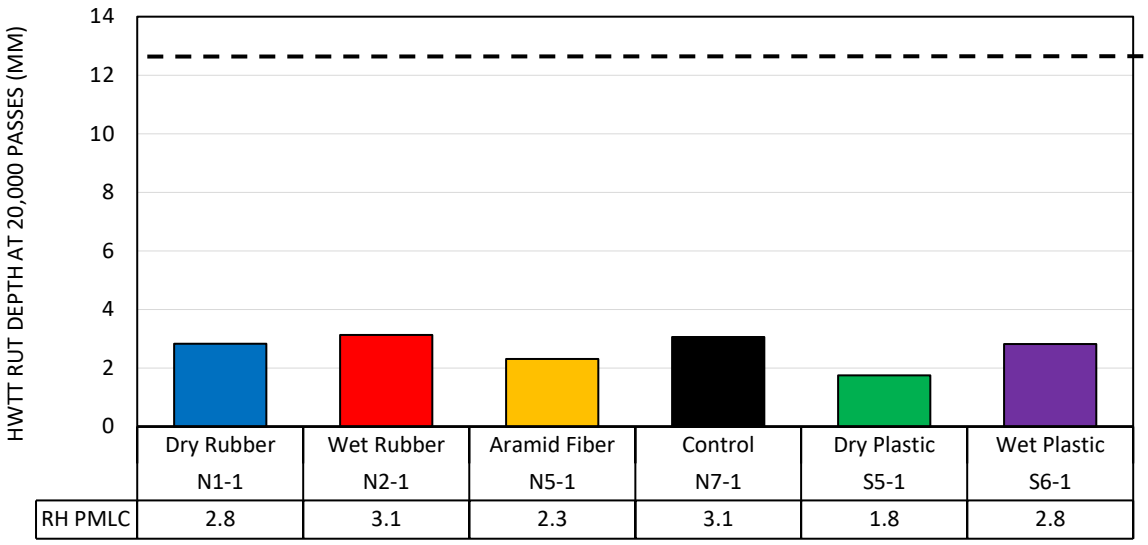

FIGURE 11 HWTT results for PMLC RH mixtures.

The RH PMLC HT-IDT and IDEAL-RT results are shown in Figures 12 and 13, respectively. For the HT-IDT test, ALDOT recommends a minimum ITS of 20 psi for their BMD special provision for local roads (NAPA, 2024). For the IDEAL-RT, Zhou et al. (2021) recommended a preliminary minimum RT Index criteria of 75 for mixtures with a PG 76-XX base binder or higher. All mixes exceeded these recommended preliminary criteria. The dry plastic mix exhibited the greatest rutting resistance while the wet plastic mix exhibited the least rutting resistance for both tests. Figure 14 shows a strong linear correlation between the HT-IDT and IDEAL-RT test results for the RH PMLC AG mixes. This is consistent with findings regarding the relationship between HT-IDT and IDEAL-RT from the larger evaluation of all 2021 Test Track mixes (Chen et al., 2023).

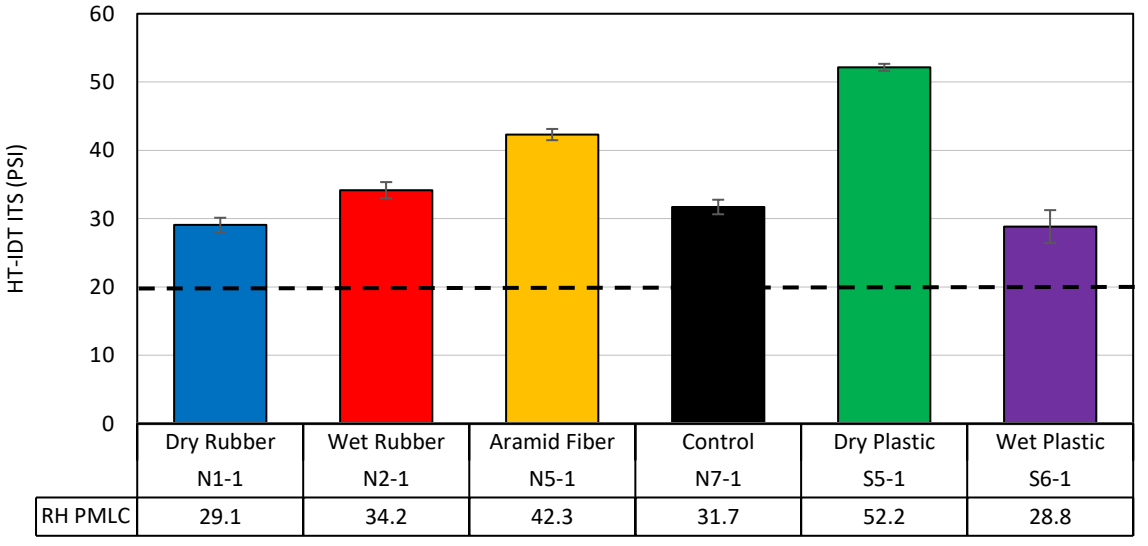

FIGURE 12 HT-IDT results for PMLC RH mixtures.

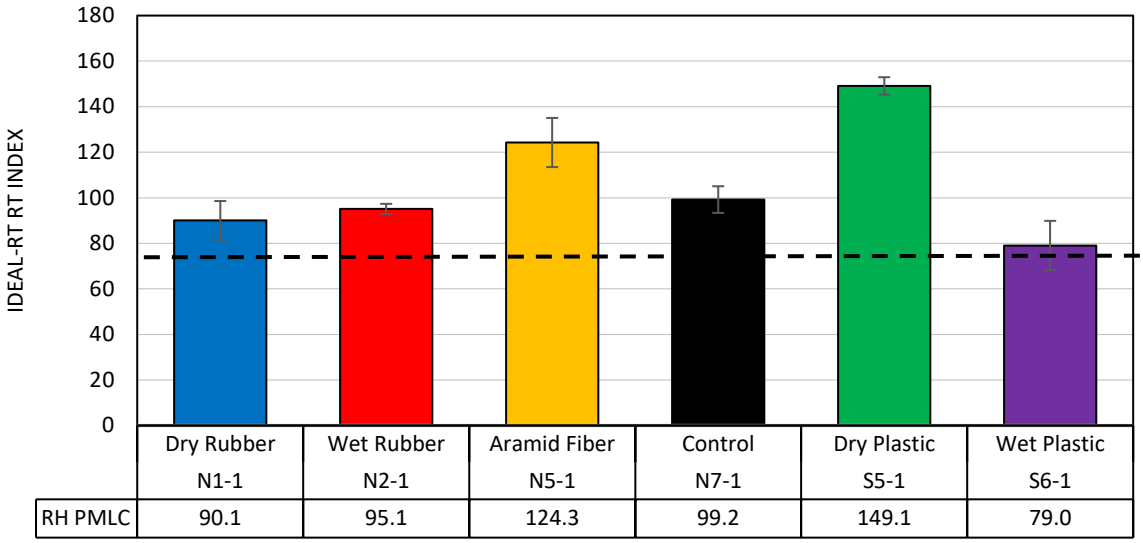

FIGURE 13 IDEAL-RT results for PMLC RH mixtures.

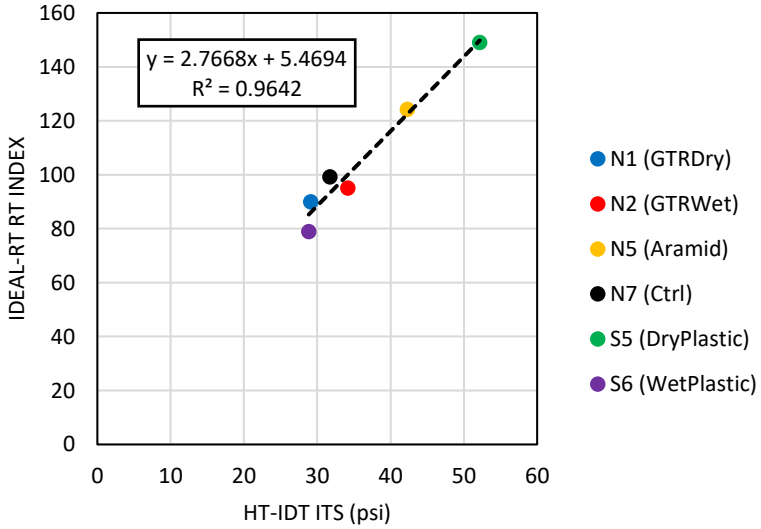

FIGURE 14 HT-IDT versus IDEAL-RT results for PMLC RH mixtures.

2.6.2 PMLC complex dynamic modulus (E) results*

The complex dynamic modulus (E*) test was performed per AASHTO TP 132-19, and E* master curves were developed for each AG mixture using Master Solver for Excel© Version 2.3 per AASHTO R 84. An IPC Global© Asphalt Mixture Performance Tester (AMPT) was used to conduct the tests. Testing temperatures of 4, 20, and 40°C, and loading frequencies of 0.1, 1, and 10 Hz were used. Three test replicates were performed for each mixture. The E* master curve for each mixture was developed at a reference temperature of 20°C. Figures 15, 16, and 17 display

E* master curves developed for the rubber-modified, aramid-modified, and plastic-modified mixtures, respectively. The E* master curve of the control mixture is included on each plot for comparison.

The dynamic modulus of the rubber-modified mixtures, N1 (GTR Dry) and N2 (GTR Wet), was numerically lower at most frequencies and temperatures compared to N7 (Control). At a testing temperature of 4°C, the E* of N1 (GTR Dry) and N2 (GTR Wet) were statistically lower than N7 (Control), as well as the other AG mixtures. The master curves of N1 (GTR Dry) and N2 (GTR Wet) reflect a reduced E* relative to N7 (Control) across most of the reduced frequency range. The Phase I AG investigation evaluated the same N1 (GTR Dry) and N2 (GTR Wet) mixtures against an unmodified control (Timm et al., 2022). In that case, the E* of both rubber-modified mixtures was lower than that of the unmodified control. Discrepancies between results of previous studies and Phase I of the AG experiment are likely due to using a combination of different mixture designs, as well as different rubber additive technologies and dosage rates.

The fiber-modified mixture, N5 (Aramid), and the wet process plastic-modified mixture, S6 (Wet Plastic), both displayed no statistical difference in their average E* relative to N7 (Control) at any testing temperature or frequency. This is reflected by the E* master curves of each, which appear nearly identical. The dynamic moduli of the wet and dry process plastic-modified mixtures were drastically different. The E* of S5 (Dry Plastic) was statistically greater than N7 (Control) at most testing temperatures and frequencies, which is displayed by their master curves relative to one another. The E* of S6 (Wet Plastic) was statistically identical to N7 (Control) at every testing temperature and frequency. This is reflected by their two E* master curves overlayed on top of one another.

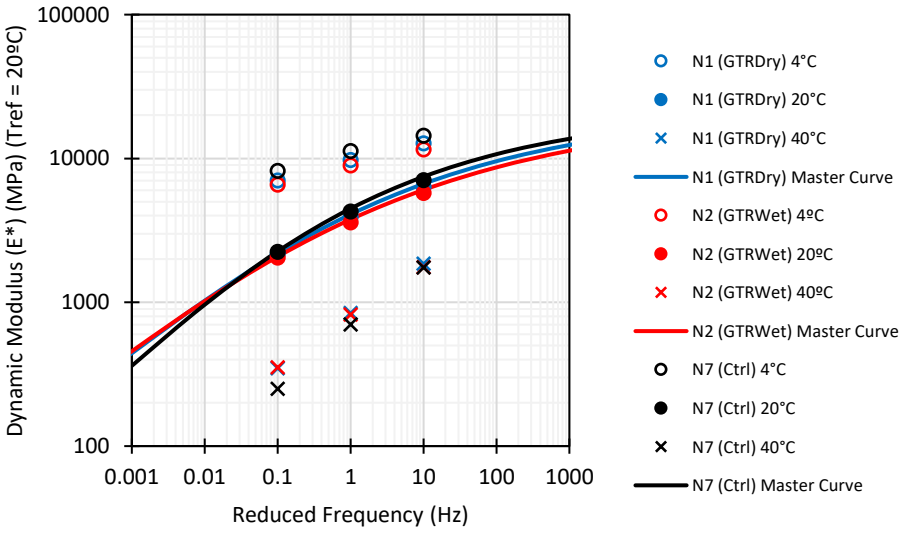

FIGURE 15 E* master curves (rubber-modified and control).

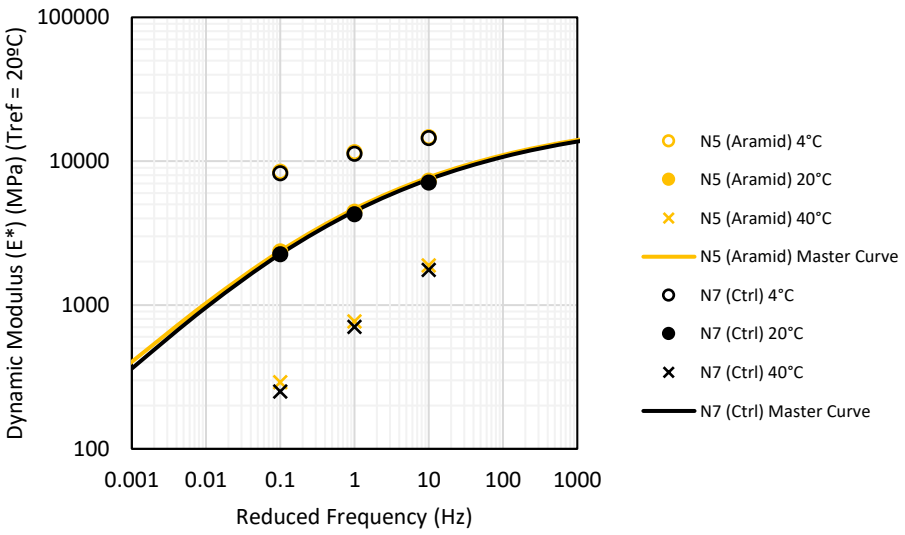

FIGURE 16 E* master curves (fiber-modified and control).

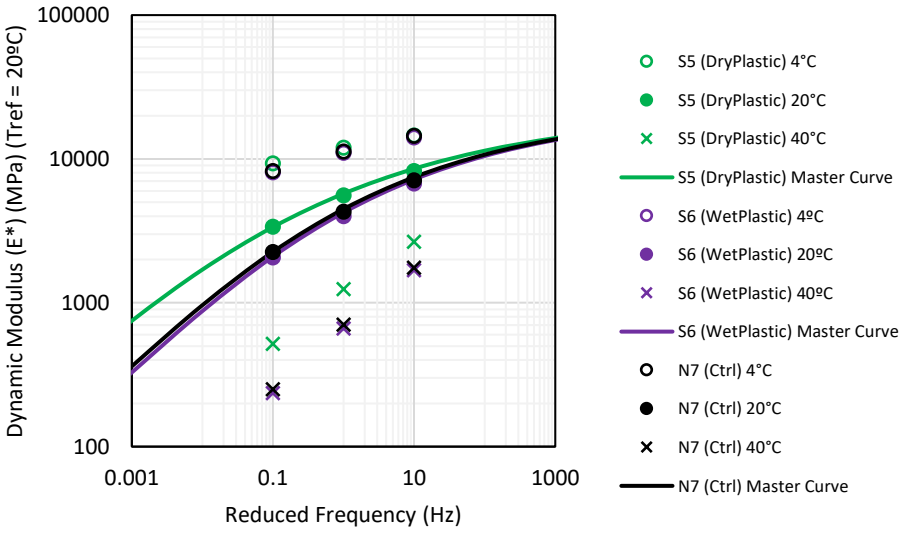

FIGURE 17 E* master curves (plastic-modified and control).

2.6.3 PMLC Direct Tension Cyclic Fatigue Results

Direct tension cyclic fatigue tests were conducted per AASHTO TP 133-22 at 21°C. Initial strain values varied between 450 and 550 microstrain, depending on the stiffness of each mixture. An IPC Global© Asphalt Mixture Performance Tester (AMPT) Pro was used for testing, and FlexMAT^{TM} Cracking v2.1.1 was used for data processing and analysis. For each AG mixture, a fitted pseudo stiffness (C) versus damage (S) curve, or "damage characteristic curve", was developed from three or more successful test replicates. Fitted D^R failure criterion values and S_{app} parameters were calculated for each AG mixture.

Figure 18 displays the fitted S_{app} parameters for each AG mixture, ranked best to worst for laboratory fatigue performance. N2 (GTR Wet) displayed the highest S_{app} parameter value (highest laboratory fatigue performance prediction) of all the mixtures, followed by N1 (GTR Dry). N7 (Control) fell within the middle of the pack, followed closely by N5 (Aramid) and S6 (Wet Plastic). This is an expected result given that these mixtures have statistically identical average E* values and all presented similar damage characteristic curves. S5 (Dry Plastic) displayed the lowest S_{app} parameter, indicating the worst laboratory-evaluated fatigue performance prediction of the mixes.

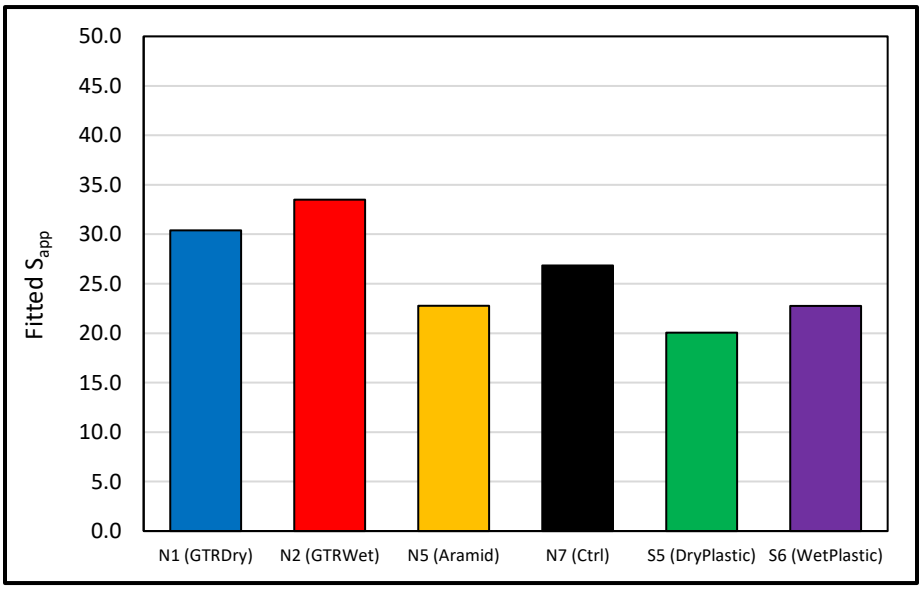

FIGURE 18 Fitted S_{app} parameters.

2.6.4 PMLC Bending Beam Fatigue Results

The bending beam fatigue test (BBFT) was performed following AASHTO T321-22. An IPC Global© BBFT machine was used for testing. Specimens were tested in a controlled strain configuration at 68°F with a loading frequency of 10 Hz. Three strain levels (low, medium, and high) were tested for each mixture, with three test replicates performed at each strain level. For most mixtures, the low strain value was 400 με, the medium was 600 με, and the high was 800 με. However, for N2 (GTR Wet), the low strain value was 600 με, the medium was 400 με, and the high was 1000 με. The IPC Global© BBFT data monitoring and recording software produced a raw Excel© output that included the loading cycle, maximum peak-to-peak tensile stress, maximum peak-to-peak tensile strain, specimen flexural stiffness, and flexural stiffness x cycles. This output was used to evaluate the fatigue life and initial stiffness of each AG mixture. The fatigue failure point was defined as the cycle at which the stiffness x cycles curve reached its peak value.

Fatigue life transfer functions describing the relationship between the applied flexural strain level and the number of cycles to failure (N_f) were developed for each AG mixture. Figures 19, 20, and 21 display N_f versus strain for the rubber-modified mixtures, fiber-modified mixture, and plastic-modified mixtures, respectively. Also shown are the fitted power regression functions for each mixture in the form of Equation 2. An ANOVA and subsequent Tukey-Kramer analysis were performed (using an α of 0.05) to identify mixtures with statistically similar average N_f values at each strain level. Section N2 (GTR Wet) was not tested at 400 με because the number of cycles far exceeded the practical limit for testing detailed by AASHTO T321-22.

$$N_f = k_1 \frac{1}{\epsilon}^{k_2}$$ Equation 2

where

N_f = number of cycles to failure,
ε = flexural strain,
k1 = fitting coefficient 1, and
k2 = fitting coefficient 2.

N2 (GTR Wet) was the only mixture to display statistically different average N_f values relative to N7 (Control). As shown in Figure 19, at 600 με and 800 με, the N_f values of N2 (GTR Wet) were nearly a full magnitude higher than the control or any other AG mixture. The transfer function of N2 (GTR Wet) displays its significantly increased strain-tolerance. The average N_f values of N1 (GTR Dry), N5 (Aramid), and S6 (Wet Plastic) were statistically similar to N7 (Control) at all the flexural strain levels tested. This is reflected by the transfer functions of each of these mixtures, which are overlayed on top of the control.

S5 (Dry Plastic) also had statistically similar average N_f values relative to N7 (Control) and the other AG mixtures, excluding N2 (GTR Wet). However, its fatigue life transfer function was noticeably lower at the 600 με and 800 με levels, though still statistically similar. Due to the high variability inherent to laboratory beam fatigue testing and a practical limit of three test replicates at each strain level, the nuanced material differences brought about by the different additives in this experiment may not have been represented through a pure statistical analysis of averages. If it is assumed the N_f values of S5 (Dry Plastic) were, in fact, lower at 600 με and 800 με, this behavior would correspond with what's commonly understood about the effects of dry process plastic additives.

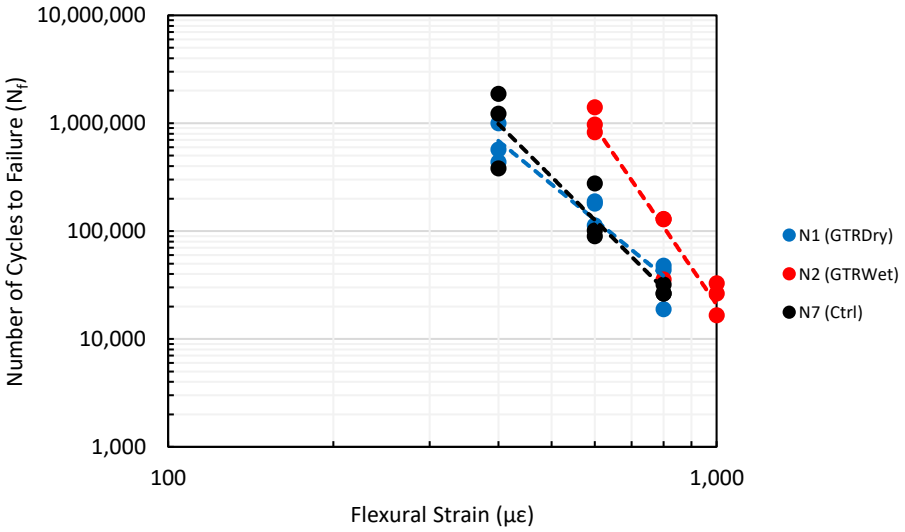

FIGURE 19 Fatigue life transfer functions (rubber-modified and control).

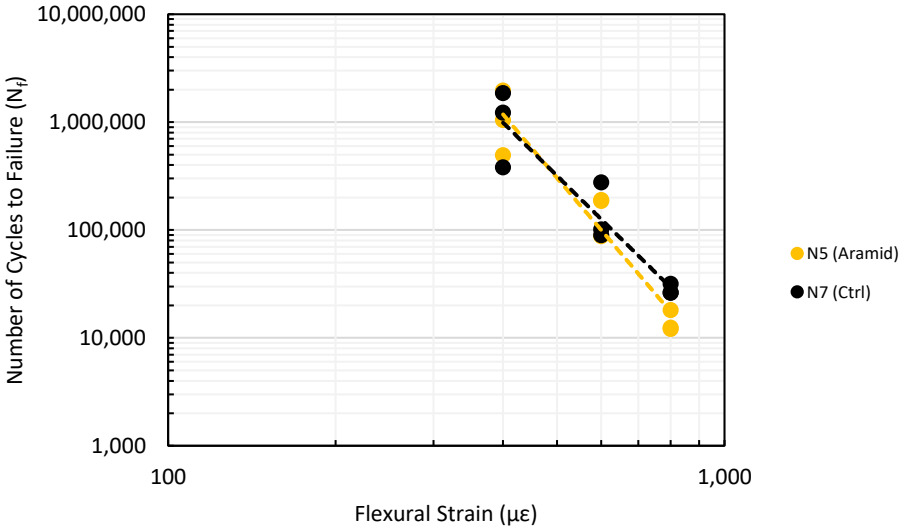

FIGURE 20 Fatigue life transfer functions (fiber-modified and control).

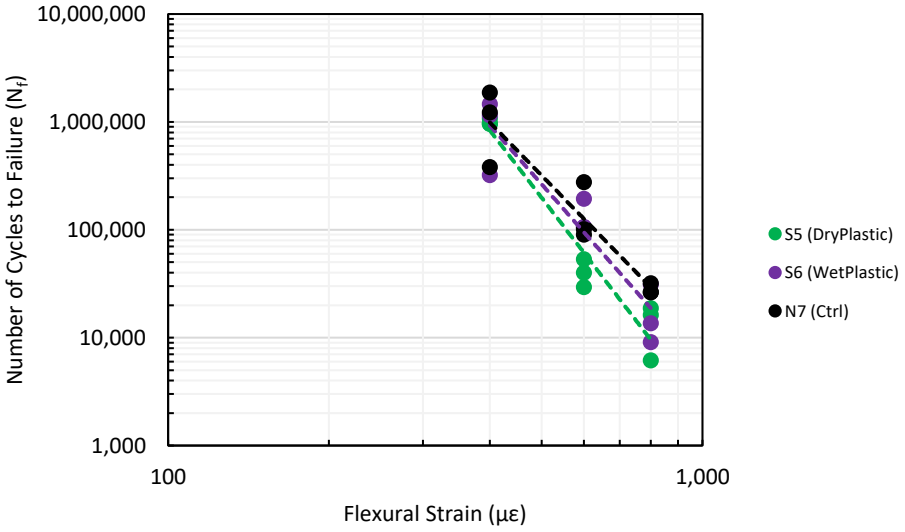

FIGURE 21 Fatigue life transfer functions (plastic-modified and control).

2.6.5 Laboratory Findings

As a path of Phase II of the AG Experiment, complex dynamic modulus (E*), direct tension cyclic fatigue, and bending beam fatigue tests were conducted to comprehensively characterize the performance of PMLC asphalt mixtures modified with additives. The findings presented in the previous four sections are summarized below.

- The control mixture had the highest average CT_{Index} at all aging conditions, followed by the wet process plastic mixture. The dry process plastic mixture had the lowest average CT_{Index} (Figure 10).
- All mixtures displayed adequate rutting resistance evaluated via the HWTT, HT-IDT, and IDEAL-RT (Figures 11, 12, and 13, respectively).

- Both rubber-modified mixtures had decreased E* values at low and intermediate temperatures relative to the control mixture (Figure 15). The wet process mixture displayed this behavior to a greater degree than the dry process mixture. The dry process plastic-modified mixture had significantly increased E* values relative to the control mixture, especially at intermediate and high temperatures (Figure 17). The E*of the other AG mixtures were significantly similar to the control mixture.

- The wet process rubber-modified mixture had the highest S_{app} parameter, indicating the highest laboratory fatigue resistance, followed by the dry process rubber-modified mixture (Figure 18). Conversely, the dry process plastic-modified mixture had the lowest S_{app} parameter, indicating the least amount of fatigue resistance.

- These findings align with beam fatigue test results, where the wet process rubber-modified mixture displayed significantly higher fatigue life relative to the other AG mixtures, while the dry process plastic-modified mixture displayed the lowest overall fatigue life (Figures 19 and 21).

- The dry process rubber-modified mixture had an increased S_{app} relative to the control mixture, but their fatigue life transfer functions were statistically similar. This indicates a slight disagreement between cyclic fatigue and beam fatigue test results.

- All other AG mixtures fell in between the wet process rubber-modified mixture and the dry process plastic-modified mixture in terms of their computed S_{app} parameters and fatigue life transfer functions, a finding that further confirms the agreement between the results of the direct tension cyclic fatigue test and the bending beam fatigue test (excluding the dry process rubber-modified mixture).

2.7 WESLEA and FlexPAVE™ Analysis

WESLEA for Windows 3.0 and FlexPAVE™ 1.1 were used to complete provisional structural coefficients for the six PMLC AG mixtures following the same methodology used in the Phase I analysis (Timm et al., 2022). Like Phase I, both simulation methods yielded similar provisional structural coefficients; therefore, only FlexPAVE™ results are shown for conciseness. Unlike the Phase I analysis, the granular base and subgrade moduli (E_{GB} and $E_{Subgrade}$) were based on the average backcalculated moduli (from FWD testing), rather than representative values based on historical moduli data.

Figure 22 presents provisional structural coefficients from the FlexPAVE™ percent damage simulation method. The rubber-modified mixtures were estimated to have the highest overall structural coefficients, and the wet plastic was predicted to have the lowest overall structural coefficient.

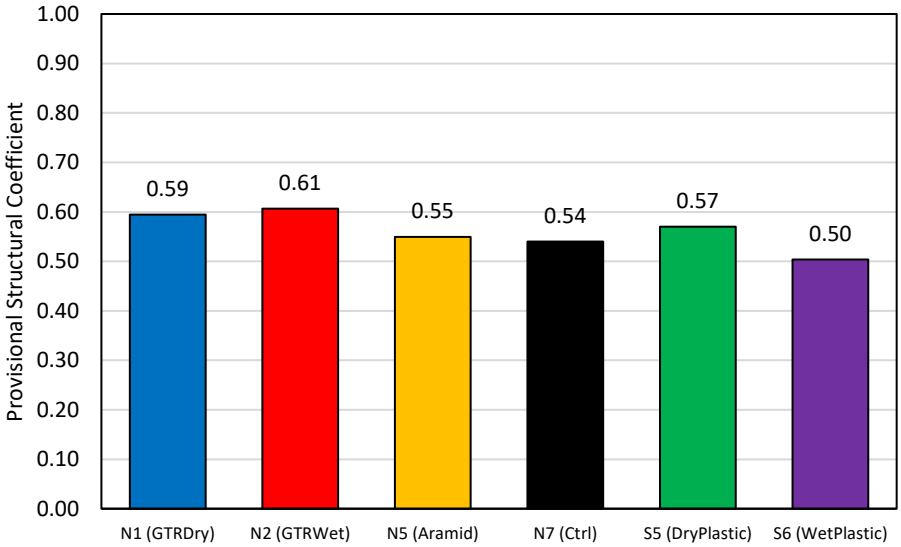

FIGURE 22 FlexPAVE™ provisional structural coefficients.

2.8 Phase II Mixture Production and Test Section Construction

Test sections were paved for each of the six AG mixtures in September 2021 at similar temperatures. The plant production temperature was approximately 330°F for all mixes. However, Sections N1, N2, and S6 experienced rain during paving days, which could impact construction quality and structural behavior of these test sections. Refer to Table 2 for a summary of each mix design and quality control testing results. All deviations were considered within acceptable tolerances of normal construction practices. Each test section was checked with a nuclear density gauge to determine if adequate compaction was achieved. Four random locations were tested at three offsets (inside, between, and outside wheelpath) with the nuclear density gauge set in backscatter mode. Three field cores were extracted from the end transition zone to calibrate the density gauge. The resulting average section compaction values are shown in Table 4. Density was not an issue, given that all values are greater than 92%. However, the N7 Control section had a considerably greater density than other test sections. The effect this may have on performance monitoring results, strain measurements, and backcalculated AC modulus is discussed in the following section.

TABLE 4 Phase II In-Place Density

Test Section	Average In-Place Density (% of G_{mm})
N1 (GTR Dry)	93.7%
N2 (GTR Wet)	94.1%

N5 (Aramid)	94.2%
N7 (Control)	95.9%
S5 (Dry Plastic)	93.5%
S6 (Wet Plastic)	93.9%

The sections were designed and constructed as 5.5-inch thick-lift pavements. Thick-lift paving was utilized for all sections to eliminate the possibility of slippage failure between lifts. This concept was crucial to the design, as the intended mode of failure for these sections was bottom-up fatigue cracking. Each mix was placed with conventional equipment used to construct past Test Track sections. Precision grinding was performed after paving to improve smoothness and IRI. Table 5 presents pre- and post-grind IRI data. It is evident that IRI for each section greatly improved with precision grinding.

TABLE 5 Phase II Pre- and Post-Grind IRI Data

Test Section	IRI (in/mile)	
	Pre-Grind	Post-Grind
N1 (GTR Dry)	175.96	72.96
N2 (GTR Wet)	179.72	82.83
N5 (Aramid)	214.42	155.80
N7 (Control)	238.18	125.00
S5 (Dry Plastic)	178.88	96.74
S6 (Wet Plastic)	152.03	79.61

As shown in Figure 23, the asphalt concrete (AC) lift thickness differed by various degrees from the design thickness (5.50 in), which was expected given the thick-lift paving method and inherent variability associated with different aspects of construction. To mitigate this variability, a normalization process was implemented to ensure a fair comparison of the sections and their measured strain responses. This normalization process is discussed in detail later in this chapter. Comprehensive information has also been published regarding as-built properties of the AG test sections (Foshee, 2022; Kmetz, 2023).

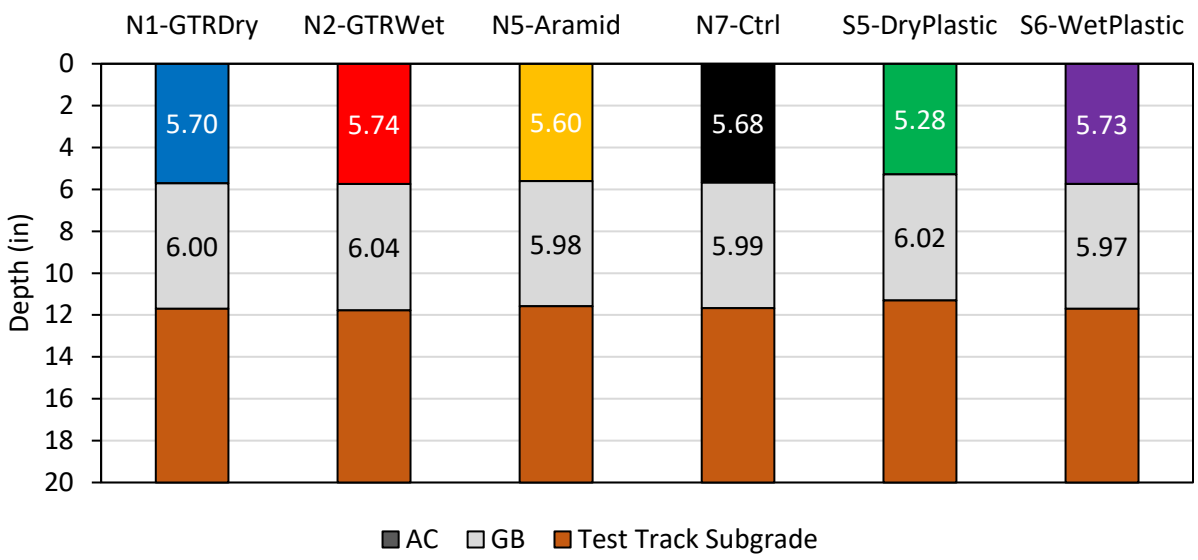

FIGURE 23 AG Experiment as-built cross sections.

2.9 Phase II Instrumentation

The test sections were instrumented with asphalt strain gauges (ASGs), earth pressure cells (EPCs), and thermocouple temperature probes to measure pavement response to traffic and the environment. ASGs measure the horizontal strain response of the pavement, EPCs measure vertical pressure the pavement experiences, and thermocouple probes capture the temperature gradient through the depth of the pavement. In each section, 12 ASGs were placed at the bottom of the AC layer, an EPC was placed at the top of the granular base (GB), and another EPC was placed at the top of the subgrade soil to measure structural response. A bundle of thermocouple temperature probes was also assembled to measure temperatures at the top, middle, and bottom of the AC layer and 3 inches into the GB layer. The instrumentation scheme and installation process were consistent with previous NCAT Test Track construction cycles and are documented in previous literature (Foshee, 2022 and Kmetz, 2023).

2.10 Phase II Test Section Performance Monitoring

Trafficking of the AG test sections began on November 10th, 2021, and concluded April 5th, 2024. Performance data were recorded weekly for each AG test section and included lane area and wheelpath cracking percentages, average rut depth, and ride quality (IRI). Falling weight deflectometer (FWD) testing was performed several times per month to monitor the in-situ moduli of the subgrade, subbase, and AC layers. The performance data collection procedures were consistent with previous research efforts at the NCAT Test Track and are documented in previous literature (Foshee, 2022 and Kmetz, 2023). Further trafficking of the AG sections will continue with the 2024 Test Track research cycle.

2.11 Phase II Test Track Performance Data

Performance data, including rut depth, cracking percentage, and ride quality, were recorded using a Pathway data collection van for each 200-ft AG section on the NCAT Test Track. FWD testing was performed inside, outside, and between wheelpaths at 4 random stations within each test section. The asphalt concrete (E_{AC}), granular base (E_{GB}), and subgrade ($E_{Subgrade}$) layer moduli were backcalculated from this testing. As previously detailed, the AG sections were also instrumented with ASGs, EPCs, and thermocouple temperature probes to measure and characterize structural response.

Figure 24 displays the ride quality, quantified by the International Roughness Index (IRI), versus trafficking level for the AG test sections through approximately 10 MESALs (million ESALs). The IRI magnitude between the test sections should not be compared since differences are due to thick-lift paving and surface grinding processes. Instead, any IRI changes concerning time or trafficking can be compared. No obvious changes in IRI were observed for any of the AG sections, indicating excellent ride quality performance thus far.

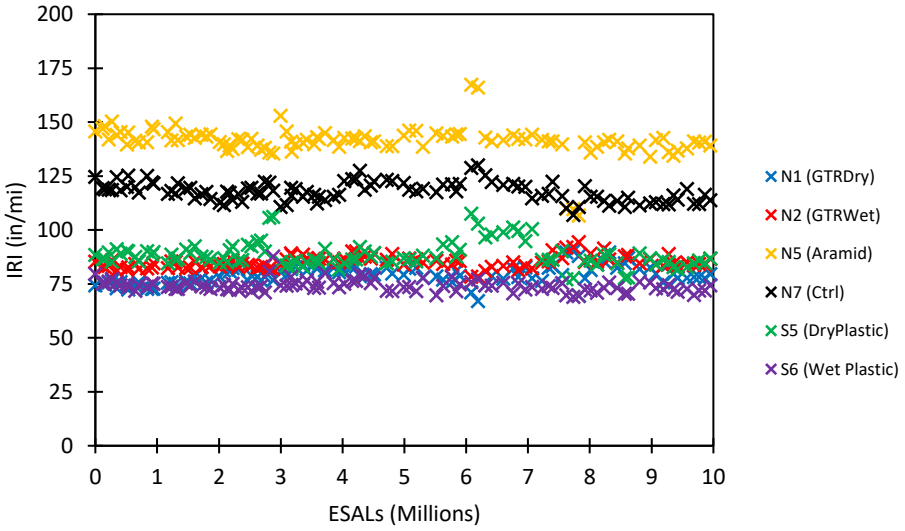

FIGURE 24 IRI vs. ESALs.

Figure 25 displays average rut depth versus trafficking level for the AG test sections through approximately 10 MESALs. As expected, average rutting depth in each AG section increased slightly as trafficking continued. Each test section displays a similar amount of rutting, but the levels are far below the failure threshold of 0.50 in. Using additive technologies did not negatively impact rutting performance of the mixtures.

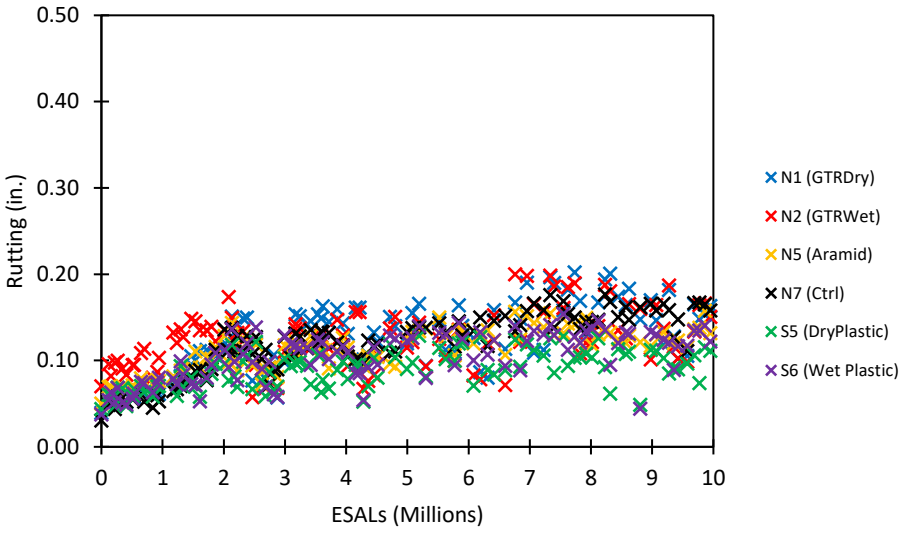

FIGURE 25 Average rut depth.

Figure 26 displays the percentage of cracking within the wheelpath area for each AG section versus time, with MESALs also plotted on the secondary y-axis. Only the cracking detected by the imaging van was plotted. Through April 2024 (approximately 10 MESALs), Sections N1 (GTR Dry), N2 (GTR Wet), and S5 (Dry Plastic) have displayed various levels of cracking. Cracking was manually observed in Section N1 (GTRDry) at approximately 2.51 million ESALs and was first detected by the Pathway van at 3.79 million ESALs. Section N1 (GTR Dry) has displayed the most severe level of cracking through April 2024 (relative to the other AG test sections), with approximately 27.3% of the wheelpath area cracked. Despite this, the section's ride quality has not suffered (Figure 24). Minor cracking was observed in Section N2 (GTR Wet) after 10 million ESALs, amounting to approximately 4.9% of the wheelpath area. Cracking was manually observed in Section S5 (Dry Plastic) at approximately 5.17 million ESALs and was first detected by the Pathway van at 5.98 million ESALs. Through 10 million ESALs, approximately 3.5% of the wheelpath area is cracked. Like Section N1 (GTR Dry), section's N2 (GTR Wet) and S5 (DryPlastic) haven't experienced an increase in IRI since cracking was first detected (Figure 24).

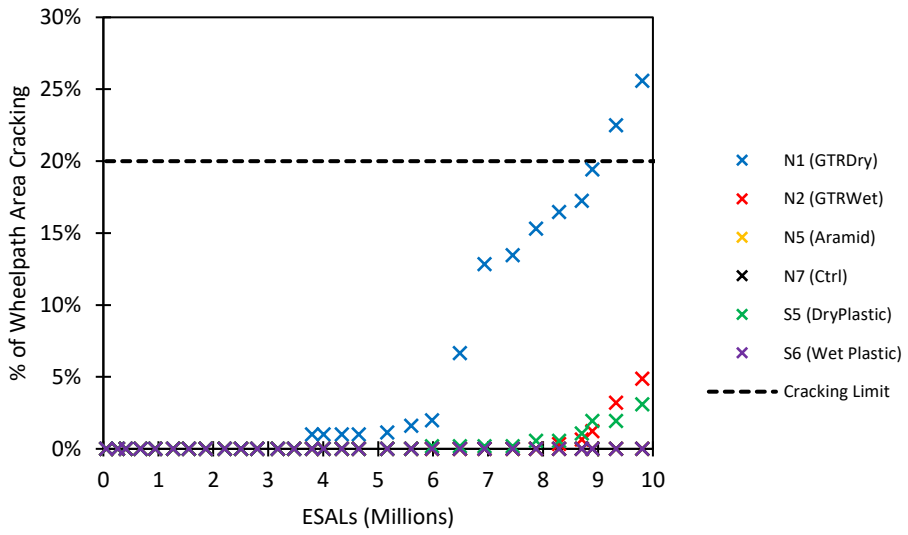

FIGURE 26 Percentage of wheelpath area cracking.

2.12 Phase II Test Track FWD Data

Figure 27 displays the average temperature-corrected, backcalculated AC layer moduli (E_{68}) for the rubber-modified, fiber-modified, and plastic-modified sections relative to the control. The backcalculated AC moduli were normalized to 68°F to observe changes in the AC moduli due to trafficking and independent of temperature effects (daily or seasonal variations). An ANOVA and post-hoc Tukey-Kramer Analysis was performed using an α of 0.05 to evaluate the average E_{68} for each test section. Further details regarding FWD backcalulation and moduli temperature correction have been published (Foshee, 2022 and Kmetz, 2023).

Through April 2024 (10 MESALs), N1 (GTR Dry) displayed an obvious decline in its backcalulated E_{68}, as shown by Figure 27. It is the only AG test section to display changes in E_{68} through the trafficking period thus far, due to the extensive cracking throughout the test section. Sections N2 (GTR Wet) and S5 (Dry Plastic) have relatively minor levels of cracking, and therefore the E_{68} of these sections have not displayed any observable declines.

The average E_{68} of the test sections are statistically different (Figure 28). Both N1 (GTR Dry) and N2 (GTR Wet) had a lower average E_{68} relative to N7 (Control), with N1 (GTR Dry) displaying the lowest among all sections. The average E_{68} of N5 (Aramid) was very similar, albeit slightly lower than that of N7 (Control). S5 (Dry Plastic) and S6 (Wet Plastic) had higher average E_{68} values compared to N7 (Ctrl), with S5 (Dry Plastic) displaying the highest values among all sections.

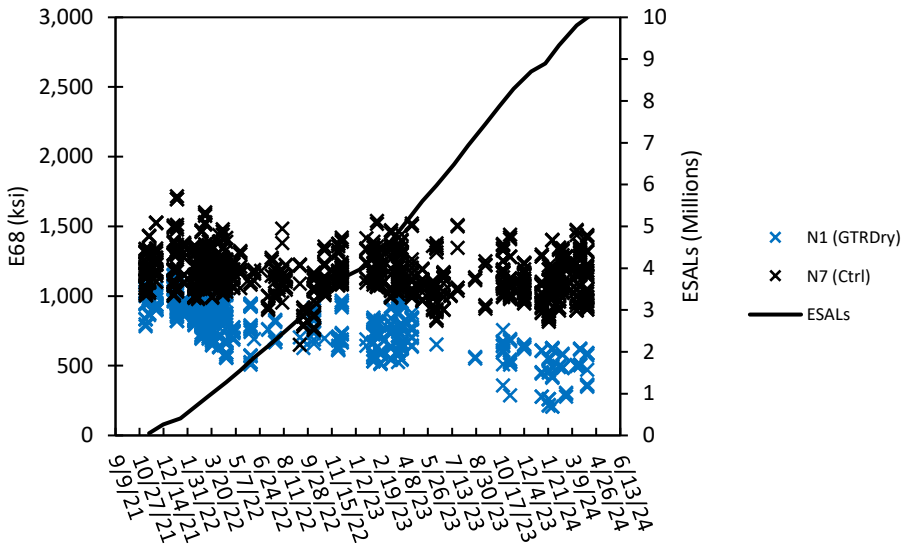

FIGURE 27 E_{68} (rubber-modified and control).

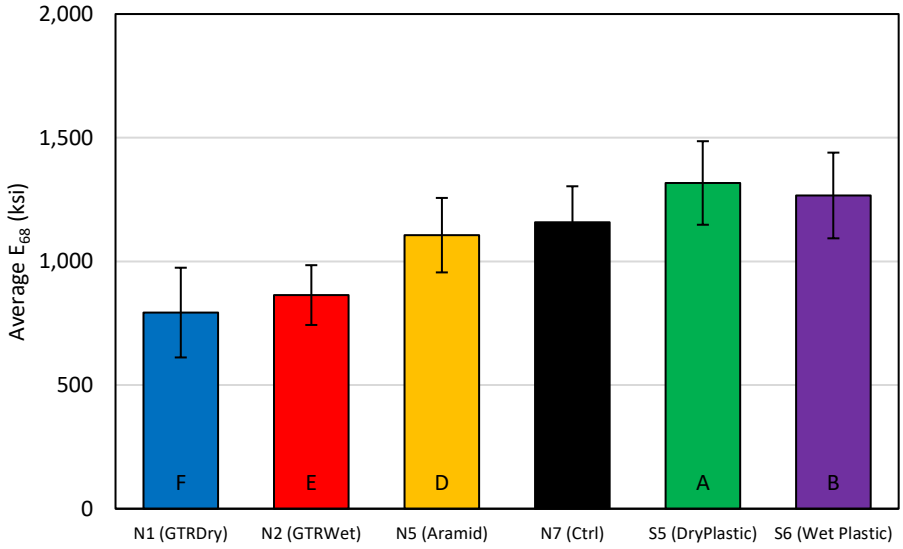

FIGURE 28 Average E_{68} of AG sections.

Figures 29 and 30 display the average backcalculated granular base (E_{GB}) and subgrade moduli ($E_{Subgrade}$), respectively. An ANOVA and Tukey-Kramer Analysis was performed using an α of 0.05 to evaluate the average E_{GB} and $E_{Subgrade}$ for each test section. Because neither moduli are prone to significant temperature effects, temperature correction was not necessary. Section N7 (Control) had significantly higher E_{GB} and $E_{Subgrade}$ relative to the other AG test sections. Conversely, N1 (GTRDry) was found to have the lowest E_{GB}, a factor that may have contributed to the cracking in this test section. Previous studies conducted at NCAT also found the $E_{Subgrade}$

of N7 (Control) to be higher than the other sections on the northern tangent of the Test Track, including N1 (GTR Dry), N2 (GTR Wet), and N5 (Aramid) (Taylor and Timm, 2009; Timm and Priest, 2006). It should also be noted that the NCAT Test Tack foundation layers are unconventional, with an $E_{Subgrade}$ greater than E_{GB}. Average ratios between E_{GB} and $E_{Subgrade}$ of 0.34 to 0.37 have been observed (Timm and Tutu, 2017).

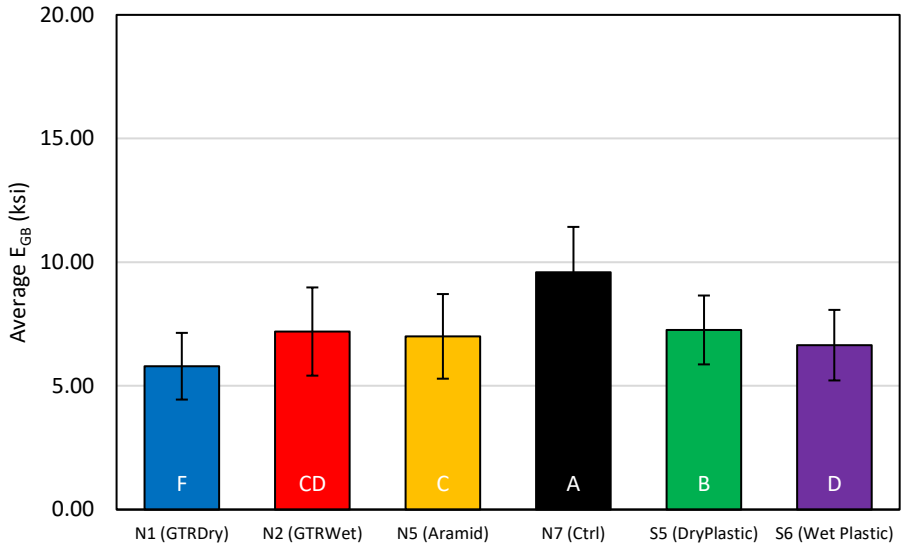

FIGURE 29 Average E_{GB} of AG sections.

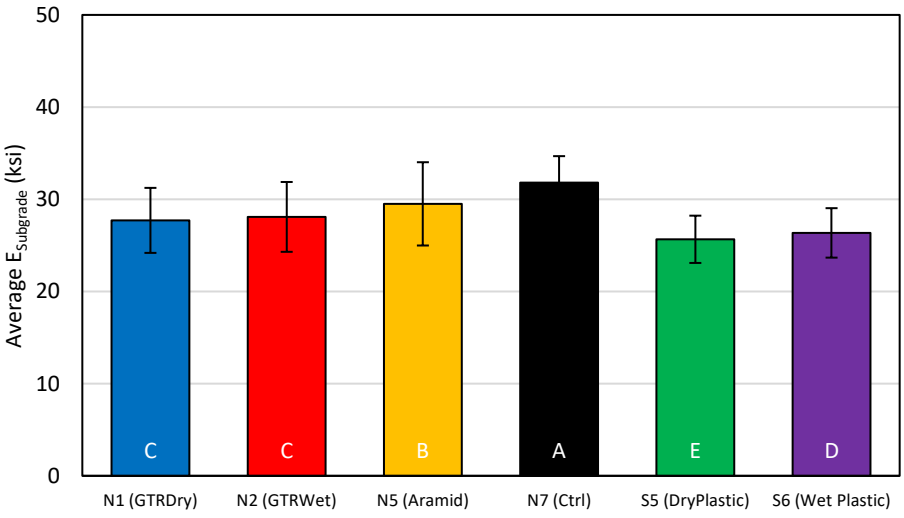

FIGURE 30 Average $E_{Subgrade}$ of AG sections.

2.13 Phase II Test Track Strain Data

Figure 31 displays the average thickness- and temperature-corrected field-measured strain response ($\mu\varepsilon_{cor}$) for each section. ANOVA and Tukey-Kramer analysis, using an α of 0.05, were performed to identify sections with statistically different or similar average $\mu\varepsilon_{cor}$ values. Further details regarding strain data collection, processing, and analysis have been published (Foshee, 2022; Kmetz, 2023).

The post-processed strain response data presented significant variation, particularly for N5 (Aramid). Regardless, sound observations were achieved. There were no obvious increases in $\mu\varepsilon_{cor}$ for any of the AG sections as of April 2024, despite the cracking measured in sections N1 (GTR Dry), N2 (GTR Wet), and S5 (Dry Plastic). However, this is likely because cracking in these sections has not developed within the ASG array area.

N1 (GTR Dry) had the highest strain response, followed by N2 (GTR Wet). N7 (Control) had the lowest at less than half of what was measured for N1 (GTR Dry). This increased strain level is likely what caused N1 (GTR Dry) to display cracking before any of the other AG test sections. The increased strain level could be due to various contributing factors, including reduced stiffness of the mixture relative to N7 (Ctrl), as displayed by its E* master curve (Figure 15) and its E_{68} (Figure 28).

N1 (GTRDry) had the lowest E_{GB} amongst all AG test sections as well as average flexural strain tolerance in the laboratory, as shown by its fatigue life transfer function (Figure 19). N2 (GTR Wet) also had high values of measured strain but displayed excellent flexural strain tolerance in lab testing (Figure 19). The strain tolerance of this asphalt mixture has likely mitigated fatigue cracking development, despite the high values of measured strain. S5 (Dry Plastic) had statistically similar average strain values to N5 (Aramid) and N7 (Control). The early cracking in S5 is likely due to its reduced strain tolerance, which was the lowest among all AG mixtures in lab testing (Figure 21).

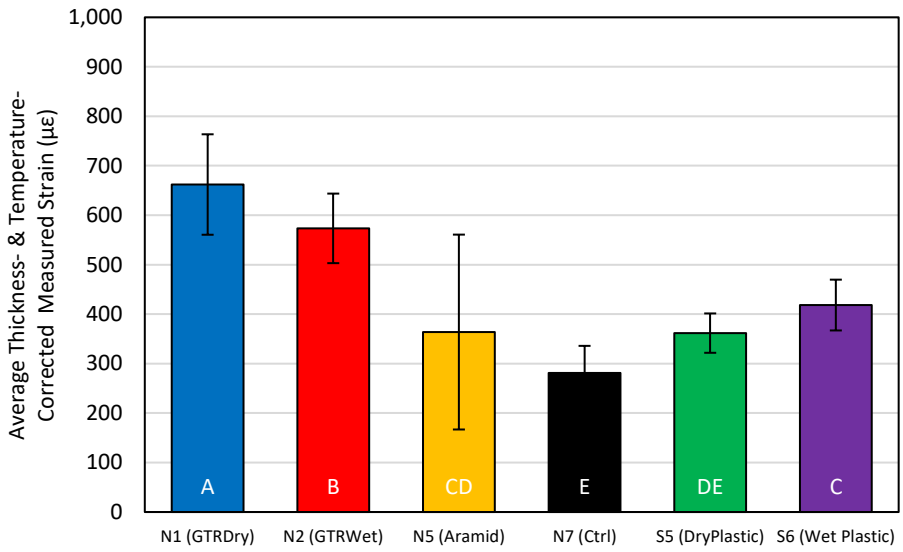

FIGURE 31 Average thickness- and temperature-corrected measured strain.

2.14 Summary of Phase II Findings

September 2021 through April 2024:

- None of the AG test sections displayed IRI increases (Figure 24). All sections show a similar increase in average rut depth, well below the 0.5" threshold (Figure 25).
- The dry process rubber mixture has the greatest amount of cracking, followed by the wet process rubber mixture, and then and the dry process plastic mixture (27.3%, 4.9%, and 3.5% of the wheelpath areas, respectively)(Figure 26).
- The dry process plastic mixture had the highest average backcalulated AC modulus (E_{68}), while the dry process rubber mixture had the lowest (Figure 27). The two plastic technologies had the highest average E_{68}, while the two rubber technologies had the lowest. The dry process aramid fiber technology and wet process SBS-modified control fell between the other mixtures in terms of average E_{68}.
- The dry process rubber mixture saw an obvious decline in average E_{68}, likely due to its high amount of measured cracking relative to the other sections (Figure 28). None of the other AG mixtures saw a decline in average E_{68}.
- The control mixture had the greatest average backcalculated granular base (E_{GB}) and subgrade moduli ($E_{Subgrade}$). This, along with its higher-than-average density, is likely why it had the lowest average measured strain response despite it not being the stiffest mixture (Figure 31).
- The dry process rubber mixture had the highest average strain response, followed by the wet process rubber. This, coupled with the dry process rubber mixture's average strain tolerance (Figure 19), led to the cracking observed in the test section. The wet process rubber mixture had excellent strain tolerance in the laboratory relative to the other AG mixtures, which likely helped it to resist cracking longer. Although it developed cracking, the dry process plastic mixture had the second lowest average strain response. The cracking is likely due to the mixture's reduced strain tolerance in relation to the other AG mixtures (Figure 21).

1.4.1: Development of Preliminary Framework for Additive Evaluation

One of the chief objectives of the Additive Group experiment is to develop a preliminary "framework" for the evaluation of new and existing additive technologies, utilizing the laboratory tests conducted in Phase I and II of the AG experiment, calibrated to the fatigue damage results/findings for the full-scale paved test sections. The intent of this framework is to provide state agencies with a method of predicting the in-field fatigue cracking performance of asphalt mixtures modified with additives, without the need for the construction of full-scale test sections; only requiring the battery of laboratory tests to be conducted. The development of the AG framework will continue as the AG test sections continue to receive accelerated traffic throughout the next (2024) Test Track research cycle and develop more severe fatigue cracking distresses.

2.15 References

Balanced Mix Design Resource Guide. National Asphalt Pavement Association (NAPA). https://www.asphaltpavement.org/expertise/engineering/resources/bmd-resource-guide. Accessed January 31, 2024.

Chen, C., A. Taylor, and N. Moore. *Validation of Rapid Rutting Test Procedures Using Plant Mixtures from the 2021 NCAT Test Track*. Asphalt Technology News, Vol. 35, No. 1, 2023, pp. 10-11.

Chen, C., F. Yin, A. Andriescu, R. Moraes, D. Mensching, N. Tran, A. Taylor, and R. West. Preliminary Validation of the Critical Aging Protocol for NCAT Top-down Cracking Experiment. *Journal of the Association of Asphalt Paving Technologists*, Vol. 89, 2020.

Foshee, M. M. *Early Characterization and Performance of Flexible Pavements Utilizing Asphalt Additives*. MS thesis. Auburn University, 2022.

Kmetz, M. H. *Laboratory and Field Characterization of Additive-Modified Asphalt Concrete Mixtures*. MS thesis. Auburn University, 2023.

Product Data Sheet: ACE XPTM. Surface Tech. https://surface-tech.com/wp-content/uploads/2023/07/ST-ACEXP-PDS.pdf. Accessed January 22, 2024

Taylor, A. J., and D. H. Timm. *Mechanistic Characterization of Resilient Moduli for Unbound Pavement Layer Materials*. NCAT Report 09-06, National Center for Asphalt Technology at Auburn University, 2009.

Timm, D. H., and A. L. Priest. *Material Properties of the 2003 NCAT Test Track Structural Study*. NCAT Report 06-01, National Center for Asphalt Technology at Auburn University, 2006.

Timm, D., F. Yin, N. Tran, M. Foshee, and C. Rodezno. Comparison of Relative Structural Characterization Methods for Additive-Modified Asphalt Materials, *Transportation Research Record 2676 (11)*, 676-688, 2022.

Tutu, K., and D. H. Timm. Determination of an Optimum Backcalculation Cross-Section for Unconventional Pavement Profiles. *Transportation Research Record: Journal of the Transportation Research Board, No. 2641*, Transportation Research Board of the National Academies, Washington, D.C., 2017, pp. 48–57.

Yin, F., C. Chen, R. Moraes, J. Sias, E. Dave, and F. Zhou. *Validation of Loose Mix Aging Procedures for Cracking Resistance Evaluation in Balanced Mix Design*. MnDOT Report NRRA202308, Minnesota Department of Transportation, 2023.

Zhou, F., R. Steger, and W. Mogawer. Development of a coherent framework for balanced mix design and production quality control and quality acceptance. *Construction and Building Materials*, Vol. 287, 2021.

3. ALABAMA DEPARTMENT OF TRANSPORTATION HIGH-PERFORMANCE OGFC MIXTURE DESIGN

Dr. Chen Chen

3.1 Background

Open-graded friction course (OGFC) asphalt mixtures are specially designed with gap-graded gradations and high air void contents typically ranging from 15% to 22%. OGFC surface layers are widely used by state highway agencies in the southeastern United States because of significant safety benefits, including reduced risk of hydroplaning, reduced splash and spray from vehicle tires, and improved visibility. The Alabama Department of Transportation (ALDOT) has used OGFC mixtures for many years. However, premature raveling in the OGFC layer is a recurrent issue, which is more prevalent when using certain aggregate types, particularly sandstone and slag.

Premature raveling is considered a material damage issue rather than a structural damage issue. It's typically caused by wear from the repeated shearing force between tire and pavement surface, moisture damage, or insufficient asphalt-aggregate bonding (West et al., 2021). A typical OGFC mixture in Alabama consists of a 12.5-mm nominal maximum aggregate size (NMAS), 0.3% cellulose fiber, and 6.0% PG 76-22 asphalt modified with styrene-butadiene-styrene (SBS).

In 2012, ALDOT sponsored three test sections (E9A, E9B, and E10) on the NCAT Test Track to evaluate three changes in mixture components to improve OGFC mixture durability in Alabama— using a finer gradation (i.e., 9.5 mm NMAS), a synthetic fiber, and ground tire rubber (GTR) modified binder. Laboratory and field performance results indicated these adjustments had the potential to improve the long-term performance of OGFC mixtures (Xie et al., 2019).

Another potential way to improve durability is to adjust ALDOT's design methodology to ensure adequate performance during the design phase. Currently, ALDOT uses an OGFC mix design methodology loosely based on the 1990 FHWA mixture design method, where the optimum binder content (OBC) is based on a surface constant determined using the oil absorption test (FHWA, 1990). However, the ALDOT method (ALDOT-259-97) differs from the FHWA method for gradation ranges, sample compaction method, and moisture susceptibility testing. Although ALDOT-259-97 is used to design all OGFC mixtures in Alabama, most mixtures have an OBC of 6.0% regardless of aggregate type, which is the minimum permissible binder content for OGFC mixtures per Section 420 of the ALDOT Specifications. Therefore, a more rigorous performance-based OGFC design methodology was used in this study to consider the mixture performance during the design phase, which is also called high-performance OGFC mixture design. This adjusted design method is based on NCHRP 01-55 and NCHRP 20-44/Task 18 studies (Watson et al., 2018; Tran et al., 2021), which uses the Superpave Gyratory Compactor (SGC) for laboratory

compaction and determines OBC based on mixture properties such as air voids, Cantabro loss, permeability, and moisture susceptibility.

3.2 Objective and Scope

The objective of this study was to validate the feasibility of the high-performance OGFC mixture design to improve durability through field performance evaluation. For this purpose, the adjusted design methodology was first used to design two OGFC mixtures with two local aggregate types. One mixture design was selected and placed on Section E9 of the NCAT Test Track, as shown in Figure 1. After construction, approximately 10 million equivalent single axle loads (ESALs) of traffic were applied using the Test Track's fleet of five heavily loaded trucks. Field performance was monitored throughout the traffic cycle from 2021 to 2024, which included rutting, cracking, texture, roughness, permeability, and friction.

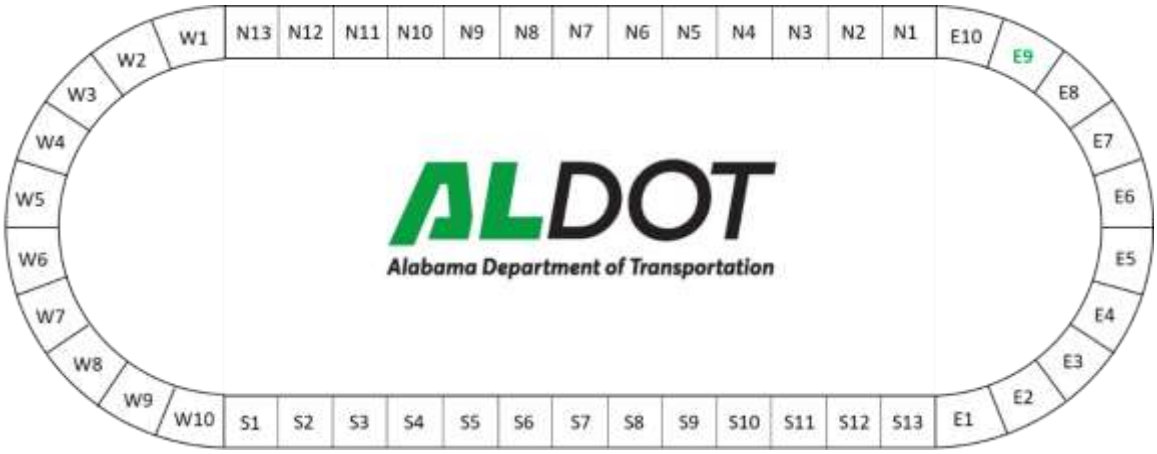

FIGURE 1 Location of ALDOT's Section E9 on the NCAT Test Track.

3.3 Laboratory Mixture Design and Performance Test Results

The high-performance OGFC mixture design procedure consists of three steps: 1) designing the aggregate blend to meet the gradation and voids in coarse aggregate (VCA) requirements; 2) determining OBC based on air voids (using the vacuum sealing method per AASHTO T331) and Cantabro loss results; and 3) verifying mixture draindown and moisture susceptibility at the OBC. All the mixture tests except for the draindown testing were performed on SGC specimens compacted with 50 gyrations. The loose mixtures were conditioned at 275°F for 4 hours prior to compaction. Compared to the 2-hour duration specified in AASHTO R30, a longer conditioning time of 4 hours prior to compaction is required to enhance binder absorption at the design stage. This adjustment consequently requires an augmentation in binder content, leading to improved durability. In addition, the draindown test was conducted on unconditioned loose mixtures at two temperatures (325°F and 350°F). Table 1 summarizes the mixture performance tests used in the high-performance OGFC mixture design along with associated performance properties, test parameters and criteria, and test standards.

TABLE 1 Laboratory Mixture Performance Testing Summary

Mixture Test	Performance Property	Test Parameters and Criteria	Test Standard
Cantabro	Raveling	Cantabro mass loss **(≤ 20%)**	AASHTO T401
Air voids (Vacuum Seal Method)	Permeability	Air voids **(15-20%)**	AASHTO T 209 and AASHTO T331
Tensile Strength Ratio (TSR)	Moisture susceptibility	TSR **(≥ 0.70)** and wet tensile strength **(≥ 50 psi)**	AASHTO T283
Draindown	Draindown	Draindown percentage **(≤ 0.3%)**	AASHTO T305

The adjusted design methodology was used to design OGFC mixtures with two types of aggregates, including one conventional granite aggregate (Nova Scotia granite) and one challenging aggregate (sandstone and slag). Table 2 presents a summary of both mixture designs including mixture components, blend gradation, volumetrics, and performance results. For each aggregate type, blend gradation was determined based on requirements specified in ALDOT-259-97. Both designs were ALDOT 12.5 mm OGFC. The sandstone and slag design consisted of 60% no. 78 sandstone, 20% no.8 sandstone, 5% 750 slag, and 15% 899 slag. The granite design included 24% no. 67 stone, 67% no. 7 stone, 6% screenings, and 1% baghouse fines. The asphalt binder was an SBS-modified PG 76-22 with 0.5% liquid anti-strip (LAS); 0.3% cellulose fibers by weight of total mix were also added to the mixtures. The SGC specimens for each aggregate type were prepared at multiple binder contents (BCs), and OBC was determined based on air voids and Cantabro results. VCA of the aggregate blend (VCA_{drc}) and mixtures (VCA_{mix}) at OBC were determined using the following equations. VCA_{drc} was required to be greater than VCA_{mix} to ensure the aggregate blend had adequate stone-on-stone contact.

$$VCA_{drc} = \left\langle \frac{([G_{ca} x\, \gamma_w] - \gamma_s)}{(G_{ca} x\, \gamma_w)} \right\rangle x\, 100$$

Equation 1

where

G_{ca} = bulk specific gravity of coarse aggregate,

γ_s = dry rodded unit weight of the coarse aggregate blend, and

γ_w = unit weight of water (62.3 lb/cf).

$$VCA_{mix} = 100 - \left(\frac{G_{mb}}{G_{ca}} x\, P_{ca}\right)$$

Equation 2

where

G_{mb} = bulk specific gravity of the compacted specimen,

G_{ca} = bulk specific gravity of coarse aggregate, and

P_{ca} = percent coarse aggregate stone.

TABLE 2 Summary of OGFC Mixture Designs with Two Aggregate Types

Property	OGFC Design #1	OGFC Design #2	Criteria
Mixture Component and Design Information			
Binder Type	PG 76-22 SBS	PG 76-22 SBS	N/A
Aggregate Type	Sandstone and Slag	Nova Scotia Granite	N/A
Blend Gsb	2.630	2.732	N/A
LAS Additive (%)	0.5	0.5	N/A
Cellulose Fiber (%)	0.3	0.3	N/A
N_{design}	50	50	50
Volumetric and Performance Results at OBC			
OBC (%)	7.0	7.0	≥ 6.0
VCA_{drc} (%)	39.8	42.1	$VCA_{drc} > VCA_{mix}$
VCA_{mix} (%)	39.5	42.0	
Vacuum Sealing Air Voids (%)	15.7	17.1	15-20%
TSR	0.78	0.91	≥ 0.70
Conditioned ITS (psi)	75.0	60.6	≥ 50
Draindown (%)	0.00	0.02	≤ 0.3
Blend Gradation			
Sieve (in.)	**Percent Passing (%)**		**Spec Limit**
25 mm (1”)	100	100	
19 mm (3/4”)	100	99	100
12.5 mm (1/2”)	87	93	85-100
9.5 mm (3/8”)	64	65	55-65
4.75 mm (#4)	18	17	10-25
2.36 mm (#8)	7	9	5-10
1.18 mm (#16)	6	6	
0.60 mm (#30)	5	5	
0.30 mm (#50)	5	3	
0.15 mm (#100)	4	3	
0.075 mm (#200)	3.7	2.7	2-4

Figure 2 illustrates the OBC determination for two OGFC designs with different aggregate types based on air voids (using the vacuum sealing method per AASHTO T331) and Cantabro loss results, and the specified criteria of both parameters were also shown in the figure. As expected, air voids and Cantabro loss results generally decreased with increasing binder contents for both designs. The sandstone and slag OGFC design met both criteria at binder contents of 6.5% and 7.0%, and the granite OGFC design met both criteria at binder content of 7.0%. In sum, an OBC of 7.0% was determined for both designs. Moisture susceptibility (TSR testing), draindown, and VCA results of two designs were further validated at the OBC of 7.0%, with all properties meeting the criteria, as shown in Table 2.

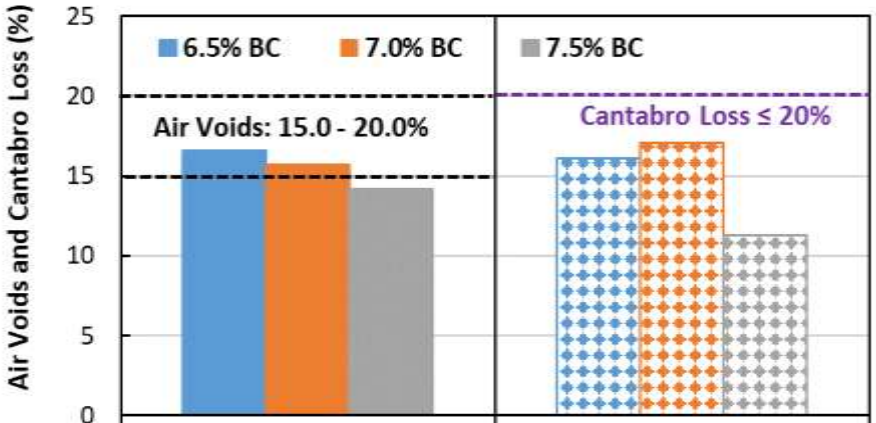

	Air Voids (%)	Cantabro Loss (%)
6.5% BC	16.6	16.1
7.0% BC	15.7	17.1
7.5% BC	14.2	11.3

OGFC mixture design with sandstone and slag.

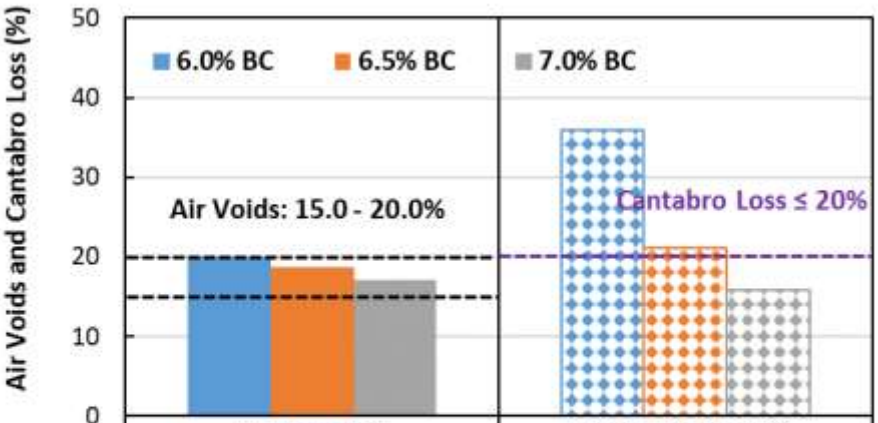

	Air Voids (%)	Cantabro Loss (%)
6.0% BC	20.0	35.9
6.5% BC	18.7	21.2
7.0% BC	17.1	15.8

OGFC mixture design with Nova Scotia granite.
FIGURE 2 OBC determination of two OGFC mixture designs.

3.4 Plant Mixture Production and Construction

To better determine the effectiveness of the modified design method, the OGFC mixture designed with sandstone and slag was produced and constructed on the 2021 NCAT Test Track. Table 3 shows the job mix formula (JMF) and quality control (QC) data including mixture component information, blend gradation, and volumetric results. The results of the QC testing of the plant-produced mixtures showed a slightly higher binder content and a finer blend gradation, especially in the finer fractions below #4 sieve, which resulted in significantly lower

air voids and voids in mineral aggregate (VMA) compared to the JMF data. Note that the resultant finer gradation during production was mainly caused by the high Los Angeles (LA) abrasion and segregation of the aggregate stockpiles, especially the sandstone stockpiles. The QC air voids of 12.5% fell significantly below the design threshold of 15.0% when tested with the vacuum sealing method. In addition, the difference of blend G_{sb} and G_{mm} between JMF and QC may also be caused by the changes in binder contents and blend gradation.

TABLE 3 JMF and QC Data of OGFC Mixture Designed with Sandstone and Slag

Property	JMF	QC
Total Binder Content (%)	7.0	7.2
Effective Binder Content (%)	5.7	5.9
Blend G_{sb}	2.630	2.669
G_{mb}	2.063	2.161
G_{mm}	2.447	2.471
Air Voids (%)	15.7	12.5
VMA	27	24.8
VFA	42	50
Dust Ratio	0.7	0.7
Sieve (in.)	**Percent Passing (%)**	
25 mm (1”)	100	100
19 mm (3/4”)	100	100
12.5 mm (1/2")	87	86
9.5 mm (3/8”)	64	66
4.75 mm (#4)	18	24
2.36 mm (#8)	7	13
1.18 mm (#16)	6	10
0.60 mm (#30)	5	9
0.30 mm (#50)	5	8
0.15 mm (#100)	4	6
0.075 mm (#200)	3.7	4.4

The OGFC mixture was produced and placed September 1, 2021. The temperature reached a high of 90°F and a low of 72°F, with a rainfall of 0.85 inches. Except for the changes made to the mix designs, this section was paved following common construction practices for OGFC mixtures in Alabama. The as-built lift thickness was 1.3 inches, which was greater than the planned thickness of 1.0 inch. Prior to construction, the original ALDOT OGFC section constructed in 2012 was milled and the tack coat was sprayed with a rate of 0.16 gal/sy. The existing underlying structure included 22.7 inches of HMA, 6 inches of graded aggregate base, and a stiff subgrade (approximately 30 ksi).

Plant-produced mixtures were also sampled during construction and characterized with Cantabro and TSR tests. Table 4 presents the air voids, Cantabro, and TSR test results of the laboratory and plant mixtures. As shown, the plant mixture yielded less air voids and Cantabro

loss and higher TSR and tensile strength compared to the lab mixture, which was attributed to the higher binder content and finer gradation of the plant mixture during production.

TABLE 4 Test Results of Plant-Produced OGFC Mixtures

Mix Type	Air Voids (%)	Cantabro Loss (%)	TSR	Conditioned ITS (psi)
Lab	15.7	17.1	0.78	75.0
Plant	12.5	14.8	0.89	149.5

3.5 Field Performance

This section presents the field performance of the ALDOT OGFC section throughout this research cycle with 10.0 million ESALs of trafficking (from 2021 to 2024).

3.5.1 Roughness

Pavement roughness represents irregularities in the pavement surface, which adversely affect vehicle ride quality. Roughness is typically affected by construction quality and pavement distress during service, such as potholes or shoving. Fewer changes and lower values in roughness indicate better durability and smoothness, respectively. In this study, roughness in the wheelpath was measured in accordance with AASHTO R 57 using an Automatic Road Analyzer (ARAN) Van, which was reported as Mean International Roughness Index (IRI) in inch/mile. Figure 3 shows roughness measurements as a function of traffic from 2021 to 2024. The OGFC section maintained a steady IRI around 80 inches/mile for the duration of this cycle, indicating excellent durability and smoothness.

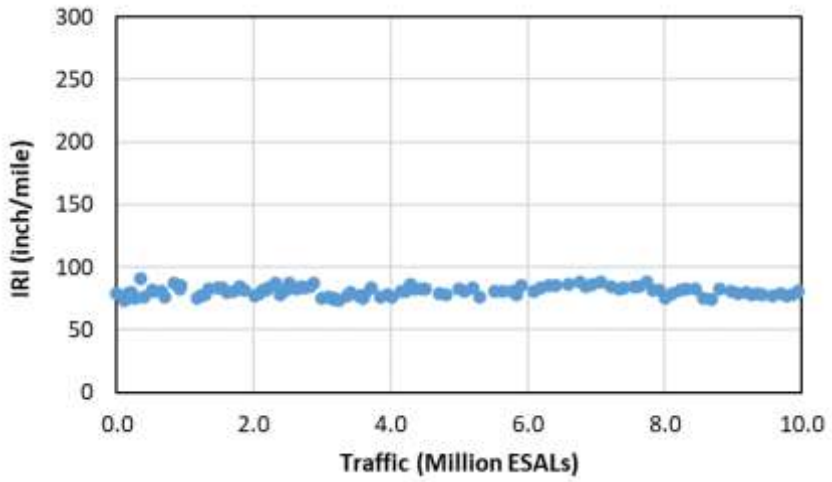

FIGURE 3 International roughness index results.

3.5.2 Macrotexture

Pavement macrotexture is defined as short wavelength (0.5 – 50 mm) irregularities on the pavement surface and is typically affected by aggregate gradation, void structure, and surface distress (i.e., raveling). Similar to roughness, fewer changes in macrotexture indicate better

durability. In this study, the macrotexture of the wheelpath is reported in mean profile depth (MPD), which typically increases when raveling occurs due to loss of aggregate. Figure 4 displays the MPD evolution with truck trafficking from 2021 to 2024. The macrotexture didn't change over 10.0 million ESALs, which was consistent with IRI results. The stability of the IRI and MPD results in this research cycle indicate good OGFC mixture durability without the occurrence of raveling.

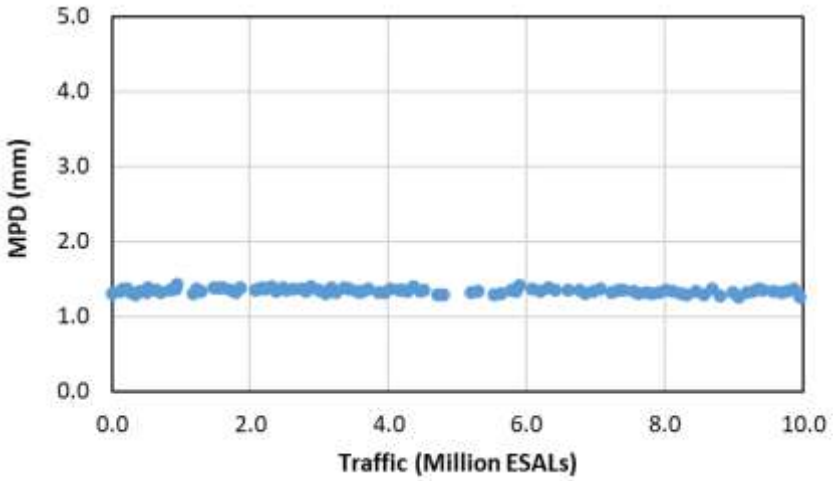

FIGURE 4 Mean profile depth results.

3.5.3 Rutting

Figure 5 shows the field rut depth of the OGFC section as a function of traffic. As presented, the rut depth slightly increased in the first two million ESALs and then remained constant at approximately 2.5 mm. Rut depth was significantly lower than the typical criterion of 12.5 mm, which indicated the mixture had excellent rutting resistance.

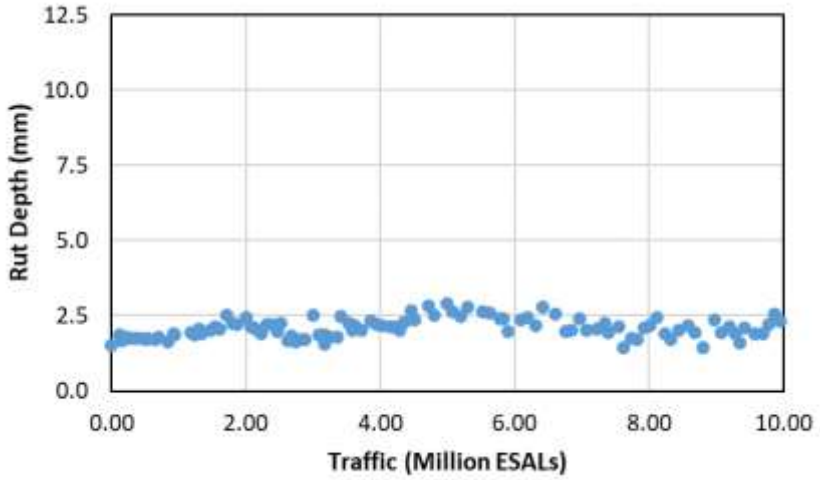

FIGURE 5 Field rut depth results.

3.5.4 Cracking

No cracking has been observed in the E9 section thus far, indicating this mixture has good cracking resistance.

3.5.5 Permeability

The permeability of OGFC plays an important role in the safety of pavements, which is also a primary reason for their use. In this study, the permeability of OGFC mixture was measured using the falling-head field permeameter on the section's wheelpath (Cooley, 1999). Figure 6 displays the field permeability results as a function of traffic. As presented, field permeability consistently reduced with traffic. This reduction in permeability over time is common in OGFC mixtures and may be attributed to the clogging of air voids with traffic loading. The OGFC section still has limited permeability (38 m/day) after 10 million ESALs of traffic, which was lower than the permeability criterion of 50 m/day recommended by NCHRP 01-55 project (Watson et al., 2018). The lower QC air voids for this mixture (12.5%) are the likely driver of the lower permeability levels in the field. However, this section showed permeability performance comparable to the other three ALDOT OGFC sections laid on the 2012 NCAT Test Track after 10 million ESALs (West et al., 2021).

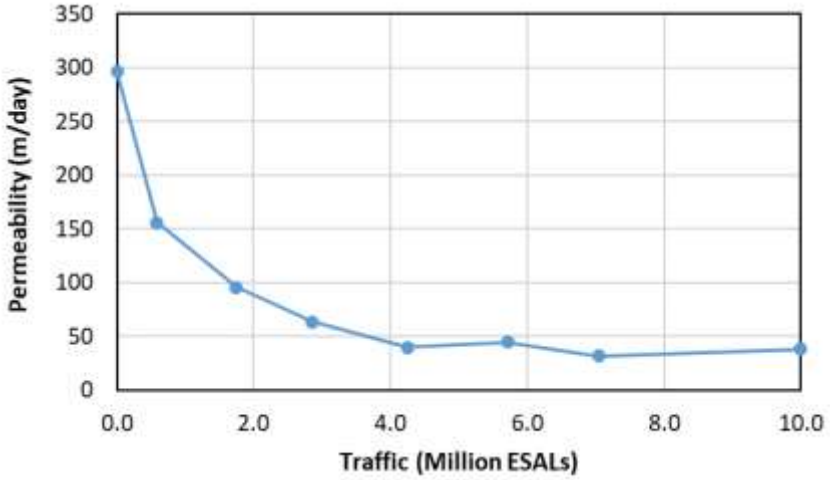

FIGURE 6 Field permeability results.

3.5.6 Friction

In this study, field friction performance was evaluated using a locked-wheel skid trailer (LWST) per AASHTO T 242, which was a trailer with a water supply and dispensing system, actuation brake control system, and one test wheel equipped with a specified ribbed test tire. The LWST was operated at a speed of 40 mph, and the water was sprayed ahead of the test tire while driving. The braking system was then activated to lock the test tire, and the resulting friction force between the tire and test surface was recorded by the system. The Friction number (FN) was calculated by dividing the friction force by the normal wheel load and multiplying it by 100.

Figure 7 shows the friction evolution of Section E9 as a function of trafficking. The FN increased after initial polishing, which was attributed to the removal of asphalt film. The FN then remained consistent over 10 million ESALs, which is higher than those of the three ALDOT OGFC sections prepared using granite aggregate.

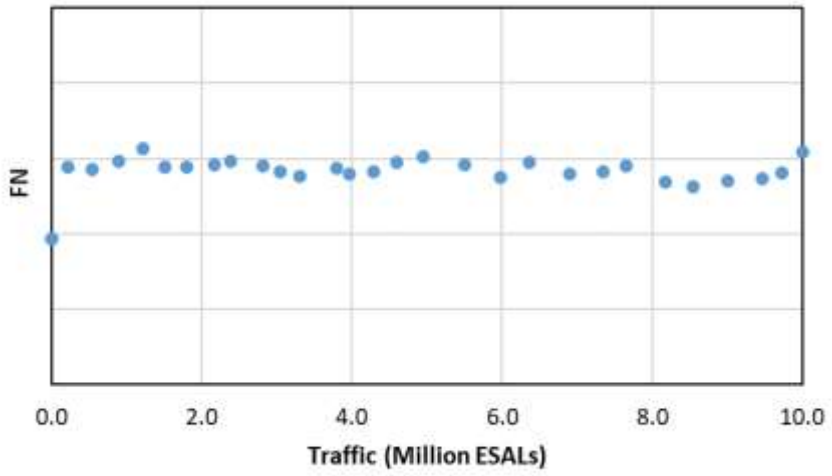

FIGURE 7 Field friction results.

3.6 Conclusions and Recommendations

Based on the laboratory test results and field performance evaluation at the Test Track from 2021 through 2024, the following conclusions and recommendations are made.

- The OBC determined using the high-performance OGFC design method was approximately 1.0% higher than the corresponding value based on the original ALDOT OGFC design method. In addition, no draindown was observed with the higher OBC due to the addition of stabilizing fiber.
- The QC air voids of 12.5% fell significantly below the design threshold of 15.0%, which may be caused by the higher binder content and finer blend gradation of the plant-produced mixture. The finer gradation during production was mainly caused by the high Los Angeles (LA) abrasion of and segregation of the aggregate stockpiles, especially the sandstone stockpiles.
- The OGFC section developed with the high-performance design method exhibited excellent smoothness, rutting resistance, and cracking resistance after 10 million ESALs. With the exception of permeability, field performance remained consistent for the duration of the research cycle, which indicated excellent durability without the occurrence of raveling.
- The field permeability of the section reduced with increasing trafficking. After 10 million ESALs of traffic, this OGFC section still has limited permeability (38 m/day), which is similar to the permeability of three 2012 ALDOT OGFC sections.

- The field friction performance improved after initial polishing due to the removal of asphalt film, and then it remained consistent over 10 million ESALs. This OGFC section constructed with sandstone and slag shows better friction performance than the three 2012 ALDOT OGFC sections using granite aggregate.
- Based on the preliminary results of this study, high-performance OGFC is recommended to replace the original ALDOT design method to improve the durability of OGFC mixtures in the field.

3.7 References

Cooley, L. A. *Permeability of Superpave mixtures: Evaluation of Field Permeameters*. NCAT Report No 99-01, National Center for Asphalt Technology at Auburn University, 1999.

Open-Graded Friction Courses FHWA Mix Design Method. Technical Advisory T 5040.31. Federal Highway Administration, U.S. Department of Transportation, Washington, D.C., 1990.

Tran, N., F. Gu, and D. Watson. *Validation of a Performance-Based Mix Design Method for Porous Friction Courses.* NCHRP Project 20-44, Task 18, 2021.

Watson, D., N. Tran, C. Rodezno, A. J. Taylor, and T. M. James Jr. *Performance-Based Mix Design of Porous Friction Courses*. NCHRP Project 01-55, 2018.

West, R., D. Timm, B. Powell, N. Tran, F. Yin, B. Bowers, C. Rodezno, F. Leiva, A. Vargas, F. Gu, R. Moraes, and M. Nakhaei. *Phase VII (2018-2021) NCAT Test Track Findings*. NCAT Report 21-03, National Center for Asphalt Technology at Auburn University, 2021.

Xie, X., N. Tran, D. Watson, and L. D. Blackburn. Five-Year Performance of Improved Open-Graded Friction Course on the NCAT Pavement Test Track. *Transportation Research Record: Journal of the Transportation Research Board*, Transportation Research Board of the National Academies, Washington, D.C., 2019.

4. ALABAMA DEPARTMENT OF TRANSPORTATION LONG-TERM PERFORMANCE EVALUATION OF HIGH-PERFORMANCE THINLAYS

Dr. Carolina Rodezno

4.1 Background

In the 2018 Test Track research cycle, the Alabama DOT (ALDOT) sponsored Sections N10 and N11 to evaluate two thinlay mixes. This experiment assessed the field performance of thinner overlays to provide ALDOT with alternatives suitable for pavement preservation on high-volume roads. At the end of the 2018 research cycle, both sections showed excellent performance with no cracking and minimal rutting. Trafficking was continued in the 2021 Test Track research cycle to assess long-term performance.

4.2 Objective and Scope

ALDOT continued sponsorship of Sections N10 and N11 to assess the long-term performance of two thinlay mixes for possible thinner overlay alternatives suitable for pavement preservation on high-volume roads. The thinlay mixes were: Section N10, a 4.75 mm NMAS stone matrix asphalt (SMA) mix, and Section N11, a 4.75 mm NMAS dense-graded Superpave mix.

4.3 Mix Design and Construction

Tables 1 and 2 summarize both mixtures' mix design and quality control data.

TABLE 1 ALDOT Thinlay Aggregate Fractions and Binder Content

Constitute Materials	N10 - SMA Thinlay	N11 - Superpave
Limestone	62%	58%
Granite	13%	
Fly ash	5%	
Fine fractionated RAP	20%	20%
Sand		22%
Cellulose Fibers	0.3%	
Binder grade/content	PG 76-22 SBS / 6.0%	PG 67-22 / 6.1%

ALDOT does not allow high percentages of carbonate aggregate in surface mixes due to pavement friction concerns. ALDOT Standard Specification Sections 423 and 424 limit the percentage of carbonate aggregate using the British Pendulum Tester (BPT) on aggregate source samples polished for 9 hours (BPN 9). According to the requirement set by ALDOT, a BPN of at least 35 is needed for a maximum allowable percentage of carbonate aggregate of 50. The limestone source used for N10 and N11 had a BPN 9 value of 26 at the time of construction. A waiver was granted by ALDOT to use higher percentages of limestone for this project than currently allowed due to a desire to use locally available materials.

TABLE 2 ALDOT Thinlay Mix Design and QA Data

Mix Design Parameters	N10		N11	
Design method	SMA		Superpave	
Compactive effort	50 blows		60 gyrations	
Binder grade	76-22 SBS		67-22	
Sieve, percent passing	Design	QC	Design	QC
$P_{3/8"}$	100	100	100	100
$P_{\#4}$	90	81	95	95
$P_{\#8}$	54	52	72	76
$P_{\#16}$	36	38	53	59
$P_{\#30}$	27	29	36	43
$P_{\#50}$	19	21	22	27
$P_{\#100}$	15	15	14	18
$P_{\#200}$	12.4	10.2	9.8	10.5
Total binder content (P_b), %	6.1	6.0	6.0	6.1
Eff. binder content (P_{be}), %	5.9	5.8	5.9	5.2
Dust/eff. binder ratio	2.1	1.8	1.6	2.0
RAP binder ratio	0.23	0.24	0.24	0.23
Rice sp. gravity (G_{mm})	2.509	2.495	2.513	2.492
Bulk sp. gravity (G_{mb})	2.421	2.465	2.429	2.412
VMA	17.8	15	17.5	15.4
VFA	80	82	81	79
Air voids, %	3.5	1.2	3.3	3.2
Compacted thickness (in)	0.75	0.80	N/A[1]	0.50
Mat density (% G_{mm})	94	93.8	94	91.5

[1]Target rate for this mix was 50 PSY.

To assess the performance of the thinlays without being impacted by the performance of the underlying layers, a structurally sound pavement was needed underneath. Therefore, a 7-inch asphalt base layer produced with a highly modified binder (HiMA) binder was placed and compacted in one lift beneath the thinlays.

Section N10 was constructed on August 29, 2018. The mix was produced at 340°F (163°C) with an average in-place density of 93.8%. The as-built lift thickness was 0.80 inches (19.1 mm). Figure 1 shows the mix placement and compaction of Section N10.

Section N11 was constructed on August 27, 2018. The N11 mix was produced at 325°F (171°C) with an average in-place density of 91.5%. The as-built lift thickness was 0.50 inches (12.7 mm). Figure 2 shows the mix placement and compaction activities on Section N11. The planned thickness/rate of both N10 and N11 were designated by ALDOT, highlighting that Section N10 was thicker for higher performance preservation and Section N11 was thinner for lower cost preservation.

FIGURE 1 N10 mix placement and compaction.

FIGURE 2 N11 mix placement and compaction.

4.4 Laboratory Testing

Plant-produced mix was obtained during construction to fabricate plant-produced lab-compacted (PMLC) samples for performance testing. No critical aging was performed before laboratory performance testing. Hamburg Wheel Tracking Tests (HWTT) were conducted to assess rutting resistance, and IDEAL-CT and I-FIT tests were conducted to evaluate mix cracking resistance using reheated (RH) PMLC samples. In addition, the Cantabro abrasion test was used to assess the mixture durability. The laboratory testing results are summarized in the Test Track Phase VII findings report and are reproduced here for convenience.

4.4.1 HWTT Results

Both mixes were assessed for rutting resistance using the HWTT, with testing conducted at 122°F (50°C). For each mix, two replicates were tested. The average rut depths at 10,000 passes and 20,000 passes for both mixtures are presented in Table 3. The results show slightly higher rut depths for N10 (SMA) than for N11 (Superpave). ALDOT specifies 10.0mm or less at 20,000 passes for SMA for ESAL Range E mixes with PG 76-22 binder and 10.0mm or less at 10,000 passes for ESAL Range E Superpave mixes with PG 67-22 binder. Both mixes have rut depths below the ALDOT specification criteria.

TABLE 3 Hamburg Wheel Tracking Test Results

Mix ID	Average Rut Depth (mm)	
	10,000 passes	20,000 passes
N10	3.5	5.0
N11	1.6	2.0

4.4.2 I-FIT and IDEAL-CT Test Results

The I-FIT and IDEAL-CT tests were used to assess intermediate-temperature cracking resistance using reheated (RH) PMLC samples. The I-FIT was performed according to AASHTO TP 124, while the IDEAL-CT was conducted per ASTM D8225-19. Table 4 shows the I-FIT and IDEAL-CT results for both mixes. The N10 mix exhibited higher FI than the N11 mix, but there was no statistical difference in the results. The Illinois DOT currently recommends a minimum FI criterion of 8 for asphalt surface mixes, and although state-specific FI criteria are likely needed to represent local climate conditions, the results for both mixes fell below the Illinois DOT requirement. IDEAL-CT results showed significantly higher CT_{Index} values for the N10 mix than the N11 mix, 50.4 and 12.7, respectively. ALDOT developed a special provision for Balanced Mix Design (BMD) in 2020 that requires an IDEAL-CT of 100 during production for ESAL range E mixes. Bot mixes failed this criterion. However, as presented in the next section, both sections performed well with minimal cracking.

TABLE 4 I-FIT and IDEAL-CT Test Results

Mix ID	I-FIT Results			IDEAL-CT		
	Average FI	Replicates	CV (%)	Average CT_{Index}	Replicates	CV (%)
N10	2.4	9	18.4	50.4	5	15.2
N11	1.6	7	20.5	12.7	6	11.0

4.4.3 Cantabro Test Results

Cantabro test results were used to assess the durability of the two mixes, conducted per AASHTO TP 108-14. Four samples of each mix were tested, and the results are presented in Table 5. The results show relatively low mass loss percentages for both mixes as an indication of adequate durability. In addition, the results were found to be statistically similar.

TABLE 5 Cantabro Abrasion Results

Mix ID	Average Cantabro Loss (%)	CV (%)
N10	5.8	4.9
N11	6.1	7.8

4.5 Field Performance

Sections N10 and N11 were subjected to an additional 10 million ESALs of heavy truck traffic in the eighth research cycle, applied over approximately two years. Trafficking started October 10, 2021. Surface cracking, rutting, and smoothness in terms of the international roughness index

(IRI) were monitored weekly. Surface friction was measured monthly using a locked-wheel friction test (LWFT) with a ribbed tire under wet conditions.

As indicated in Figure 3, rutting performance was excellent with less than 0.2 inches (5.1 mm) of rut depth for both sections. Although IRI numbers for both sections were high from the beginning of the cycle because of the uneven finish of the underlying thick base layers placed in one lift, roughness remained stable for the cycle's duration as presented in Figure 4. Very low severity cracking was first identified in both sections in February 2022. At the end of the cycle, both sections have less than 3% of the lane area cracked, as indicated in Figure 5. Figure 6 presents the LWFT results, where the friction numbers of both sections remained stable with a slight reduction over time, but still above the safety threshold of 30 that has been established at the NCAT Test Track. Both thinlays constructed with high percentages of limestone were able to maintain an acceptable friction performance after 20 million ESALs.

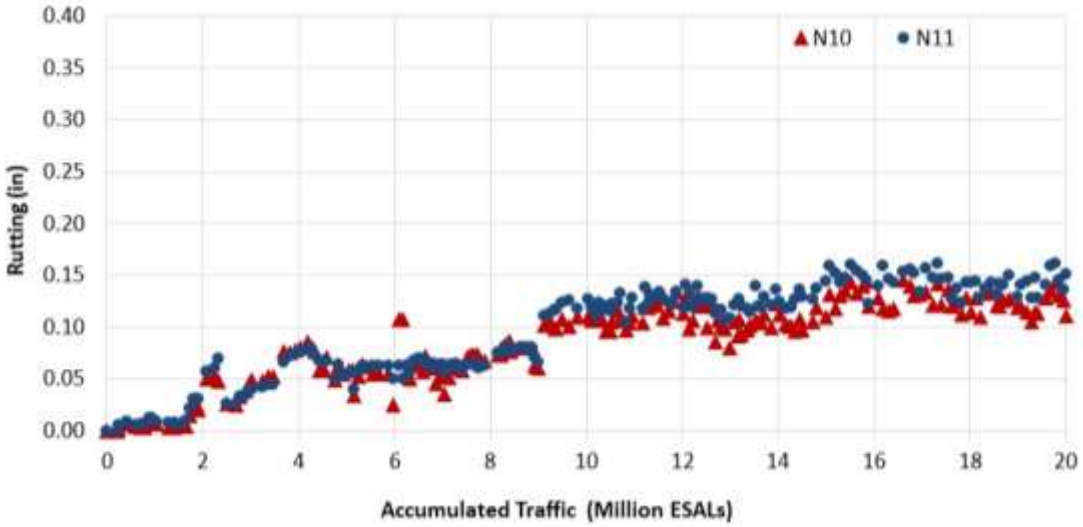

FIGURE 3 Field rutting data.

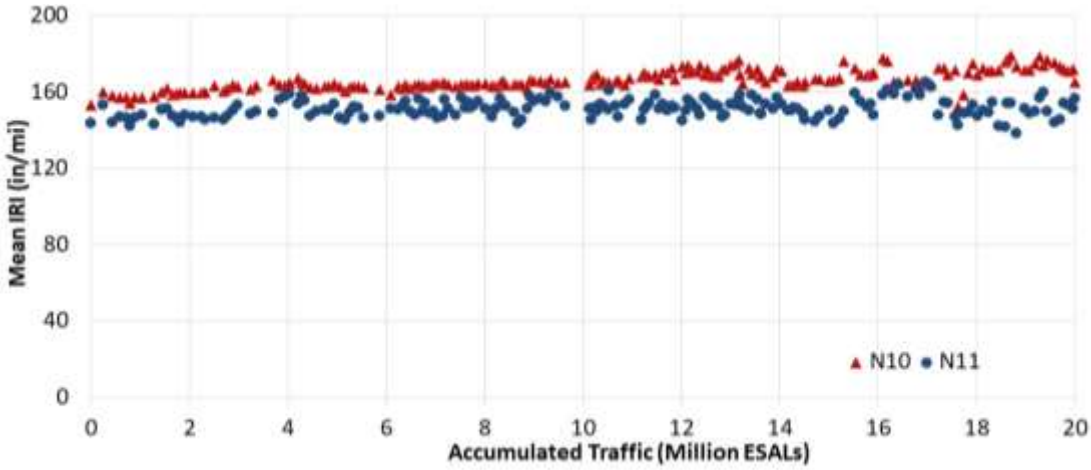

FIGURE 4 International roughness index data.

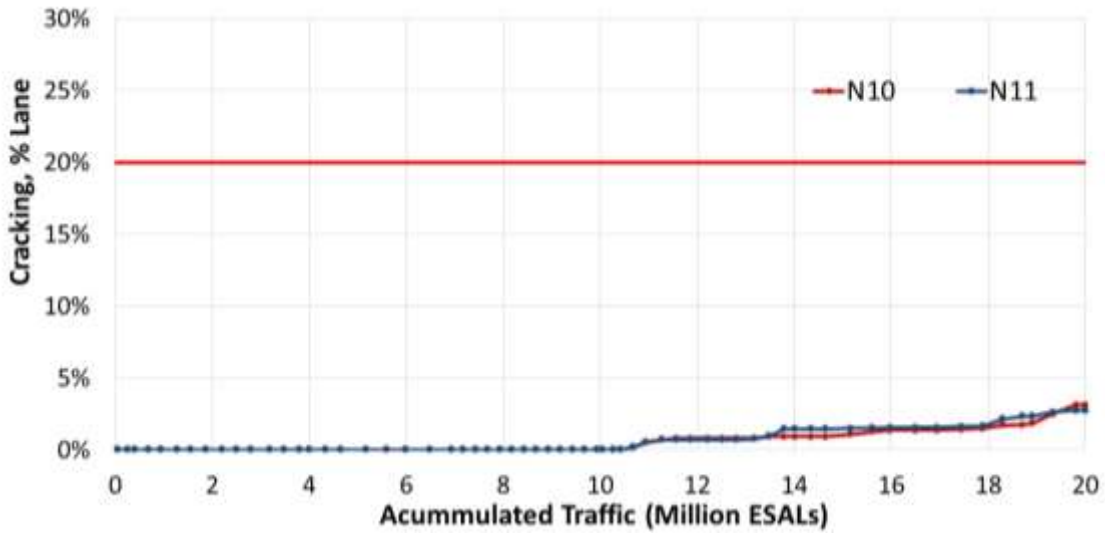

FIGURE 5 Cracking data.

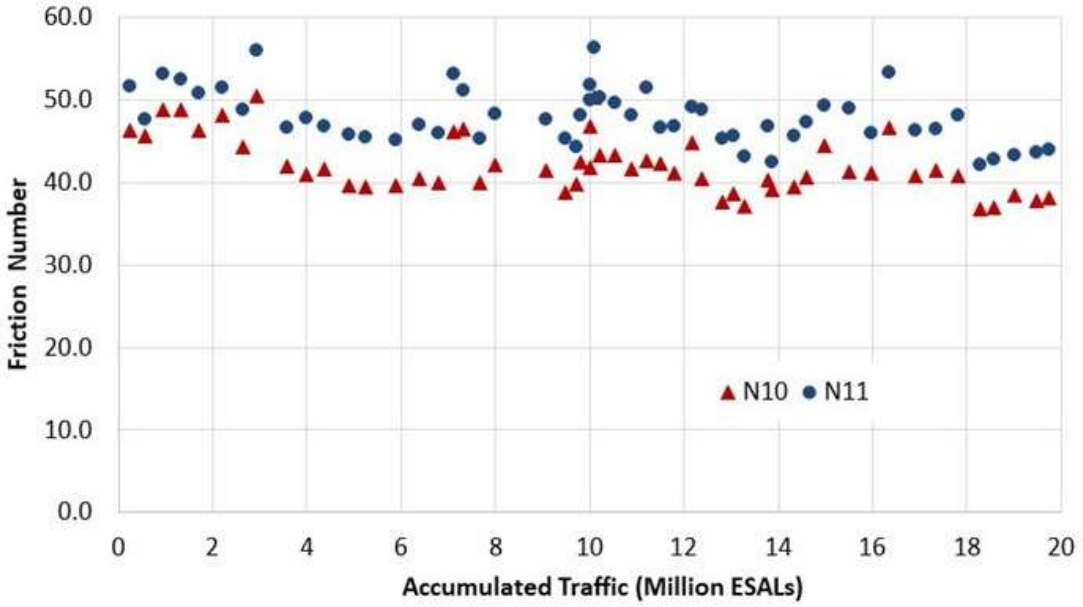

FIGURE 6 Locked-wheel friction tester data.

4.6 Summary and Conclusions

This experiment evaluated the long-term performance of two thinlay test sections, N10 and N11, each constructed with 4.75 mm NMAS mixes, one an SMA and the other a dense-graded Superpave mix. The findings of this study are summarized as follows—

- Both sections performed very well after 20 million ESALs with minimal rutting and cracking.
- Roughness in terms of IRI was high from the beginning of the 2018 test cycle but remained stable for both sections. The high initial numbers were attributed to the rough base layers placed in a single pass before placement of the surface layers.

- Friction number results showed slight reductions over time, but were above the general threshold from a safety perspective. This shows that despite the high percentage of limestone used for these mixes, the sections had adequate friction performance.
- The satisfactory performance of both test sections after 20 million ESALs of traffic provides ALDOT with two thinlay preservation options for high-traffic volume roads.

5. FLORIDA DEPARTMENT OF TRANSPORTATION IN-PLACE DENSITY STUDY

Dr. Randy West

5.1 Introduction

In 2018, the Florida DOT sponsored an experiment to evaluate the field performance of an asphalt pavement built with subsections intentionally constructed with a range of in-place densities. Although numerous research studies have explored the effects of relative density on pavement performance, most of those studies have been based on laboratory experiments (*1*). A commonly quoted axiom is that for a given mix design, a one percent decrease in the in-place density from the nominal 93% of theoretical maximum specific gravity (G_{mm}) will result in about a 10% reduction in a pavement's life (*2*). All state DOTs use in-place density as a pay item for asphalt pavement construction quality assurance (QA). This experiment is intended to provide further evidence to support the use of in-place density as a key measure of the quality of asphalt pavement construction.

This chapter provides a detailed update on the field performance of the test sections, summarizes the results of numerous laboratory tests on the mixtures compacted to the target densities of the test sections, and provides new information on the properties of the binders recovered from the test sections after five years of service. Chapter 7 of the previous NCAT Test Track report (*3*) provides a more complete literature review of the topic and thoroughly documents the construction of the test sections, the in-depth laboratory testing plan and corresponding results, and the field performance of the test sections through the first two years of trafficking. The test sections will remain in place through the next cycle, which will be completed in 2027.

5.2 Objective and Scope

The objectives of this experiment are to:

1) evaluate the effects of in-place relative density on pavement performance, and
2) characterize the mixture properties in the laboratory utilizing the same density levels achieved in the field.

To complete this research, a typical asphalt surface mix was placed and compacted in four 100-foot subsections of Sections E5 and E6 during the 2018 reconstruction of the NCAT Test Track. The surface layer was compacted to a nominal thickness of 1.5 inches to target densities ranging from 88% to 94% of G_{mm}. The underlying pavement is from the original construction of the NCAT Test Track and includes more than 20 inches of asphalt pavement.

5.3 Mix Design and Construction Data

The mix design for this experiment was performed by NCAT to meet the requirements of AASHTO M 323, using 100 gyrations. It is considered a typical surface mixture containing 20%

RAP and an SBS-modified binder, meeting the specifications for PG 76-22 with a continuous grade of 76.3 -27.3. The binder's delta Tc was -3.1, and its intermediate grade was 22.6°C. Table 1 shows a summary of the Job Mix Formula (JMF) and QA test results obtained during construction. Gradations, binder contents, and volumetric properties of the four subsections were generally consistent, except for higher $P_{\#200}$ content in subsections E5A and E5B.

TABLE 1 Mix Design and As-Produced Results for the Florida DOT Density Experiment

	JMF	E5A	E5B	E6A	E6B
$P_{3/4"}$, %	100	100	100	100	100
$P_{1/2"}$, %	98	99	99	98	98
$P_{3/8"}$, %	90	89	89	89	87
$P_{\#4}$, %	54	57	57	56	55
$P_{\#8}$, %	40	40	40	38	39
$P_{\#16}$, %	33	32	32	29	31
$P_{\#30}$, %	24	22	22	20	22
$P_{\#50}$, %	13	12	12	10	12
$P_{\#100}$, %	7	8	8	6	7
$P_{\#200}$, %	4.1	5.5	5.5	3.8	3.9
P_b, %	4.8	5.0	5.0	5.0	5.0
Air Voids, %	4.3	3.6	3.6	3.5	3.5
VMA, %	14.0	13.6	13.6	13.5	13.5
VFA, %	69	74	74	74	74
$P_{be}/P_{\#200}$	1.0	1.3	1.3	0.9	0.9

The in-place density of each subsection was determined by NCAT personnel from corrected nuclear measurements in the left wheel-path (LWP) and right wheel-path (RWP) at three random locations. The cores used for the nuclear gauge correction factors were obtained from the 25-foot transition area at the beginning of E5. Table 2 shows the results of the in-place density data for the four subsections. Through the remainder of this chapter, the sections are interchangeably referred to by their subsection number and the average initial in-place density of the subsections.

TABLE 2 In-Place Density Data (% of G_{mm}) for the Experimental Subsections

Location	Subsection			
	E5A	E5B	E6A	E6B
Random 1, LWP	93.2	90.7	88.5	88.9
Random 1, RWP	94.1	91.9	87.5	89.8
Random 2, LWP	93.3	91.9	88.8	90.1
Random 2, RWP	93.8	92.1	86.9	90.1
Random 3, LWP	93.2	93.3	87.8	89.8
Random 3, RWP	93.8	91.9	87.3	89.7
Average (%)	**93.6**	**92.0**	**87.8**	**89.7**
Std. Dev. (%)	0.37	0.84	0.73	0.43

5.4 Density Profiles

Approximately three years after the density experiment subsections were built and after they had accumulated 10 million ESALs of trafficking, additional testing was conducted using a density profiling system (DPS), shown in Figure 1. Using air-coupled ground penetrating radar technology, the DPS provides essentially continuous density data in the path that the device travels without the need for pavement coring (*4*).

FIGURE 1 DPS operated by Dr. Fabricio Leiva on the NCAT Test Track.

The DPS testing of E5 and E6 was conducted as part of Transportation Pooled Fund TPF-5(443) *Continuous Asphalt Mixture Compaction Assessment Using Density Profiling System (DPS)* (*5*). The objective of testing E5 and E6 was to evaluate the overall variability of DPS measurements. Ten DPS measurements (runs) were made along the same path between the wheelpaths of the test sections. Figures 2 and 3 show the DPS profiles of E5 and E6, respectively. At the time of testing, it can be seen from these two figures that the data from the ten DPS runs were very repeatable, but substantial variability existed in the between-wheelpath densities along some of the subsections. E5A is the first 100 feet and E5B is the second 200 feet of Figure 2. Similarly, E6A is the first 100 feet and E6B is the second 200 feet of Figure 3. Excluding the first 30 feet of the subsections yields the average and standard deviation for the subsections shown in Table 3. The point to be made from this data is that there is likely more spatial variability in the in-place densities of the subsections than expected from the six random locations summarized in Table 2. DPS data often have slightly higher standard deviations than a small set of cores or gauge readings because the DPS covers much more of the pavement area.

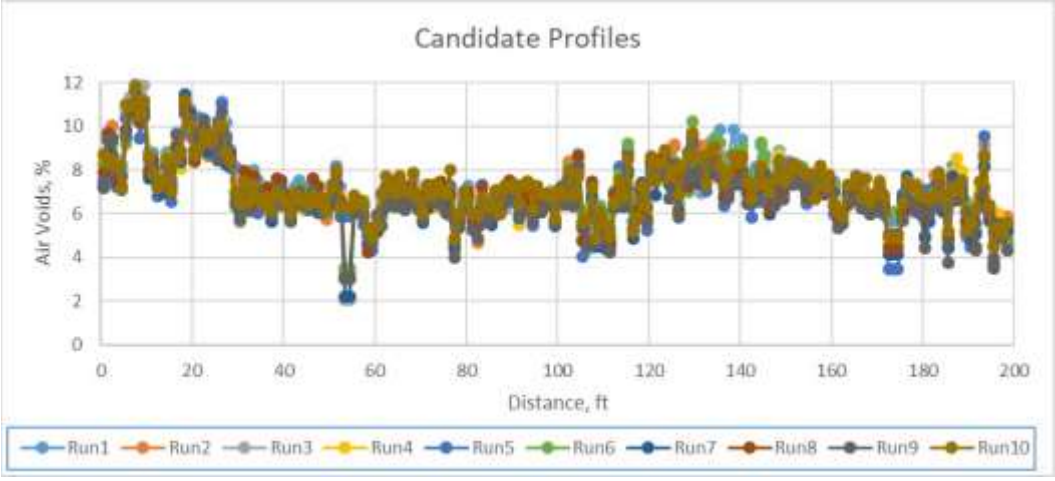

FIGURE 2 Plot of density profiles from between wheelpaths of Section E5.

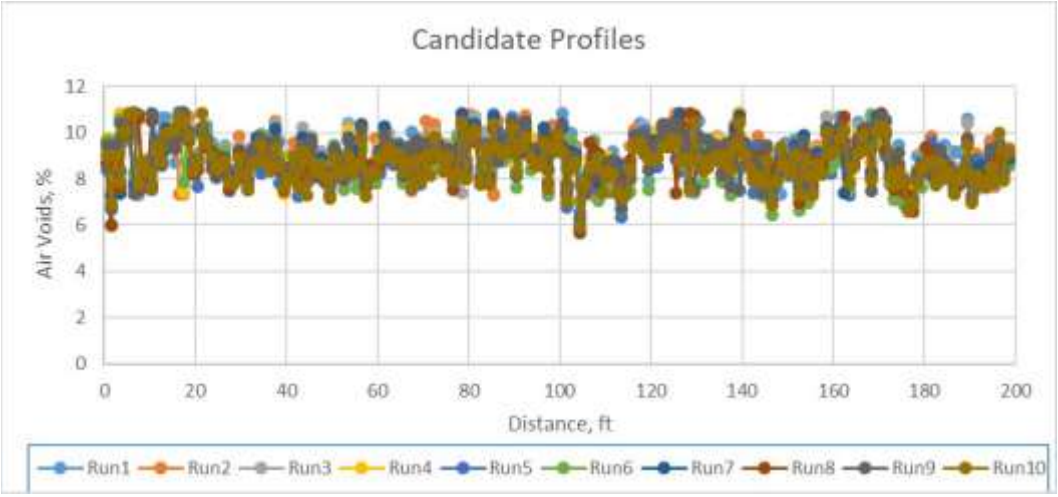

FIGURE 3 Plot of density profiles from between wheelpaths of Section E6.

TABLE 3 Average and Standard Deviations of the In-Place Air Voids Determined from DPS Testing after Three Years of Traffic

Location	Subsection			
	E5A	E5B	E6A	E6B
Average (%)	93.6	93.2	91.0	91.3
Std. Dev. (%)	0.82	1.16	0.76	0.86

5.5 Field Performance

The field performance of the subsections has been evaluated weekly for rutting, roughness (International Roughness Index, IRI), surface texture (mean profile depth), and cracking (expressed as a percentage of the lane and percentage of wheelpaths). Through nearly two cycles of heavy trafficking, the subsections are still performing very well, as summarized in Table 4. Rutting is very low in all subsections, and the IRI has changed very little. Interestingly, subsection E6A appears to have become slightly smoother after five years.

TABLE 4 Summary of Field Performance Data at 18.6 Million ESALs for the In-Place Density Experiment

Subsection (Avg. In-Place Density)	Rut Depth, mm	Change in IRI, in./mi.	Mean Profile Depth, mm	Cracking, % of Lane Area	Cracking, % of Wheelpaths
E5A (93.6% of G_{mm})	0.9	9.8	1.13	2.6	3.2
E5B (92.0% of G_{mm})	1.3	13.3	1.20	5.1	4.0
E6A (87.8% of G_{mm})	1.2	-0.7	1.40	6.8	7.2
E6B (89.7% of G_{mm})	1.2	14.0	1.31	5.6	7.2

Figures 4 and 5 show the progression of cracking for the subsections, expressed as a percentage of the wheelpaths and a percentage of lane area, respectively. For cracking data, one linear foot of cracking (any severity) is assumed to represent a one-square-foot area. When cracks become interconnected (i.e., alligator pattern), a virtual polygon is drawn around the cracked area, and the polygon area is used in the calculation of the percentage of the wheelpath or lane. The two cracking plots are similar except that E5B (92.0% of G_{mm}) is more closely grouped with E5A (93.6% of G_{mm}) for the plot of percentage of wheelpath cracking, but it is more closely grouped with E6A and E6B when considering the percentage of cracking by entire lane area. This difference is primarily due to more transverse cracks in E5B that are outside the wheelpaths.

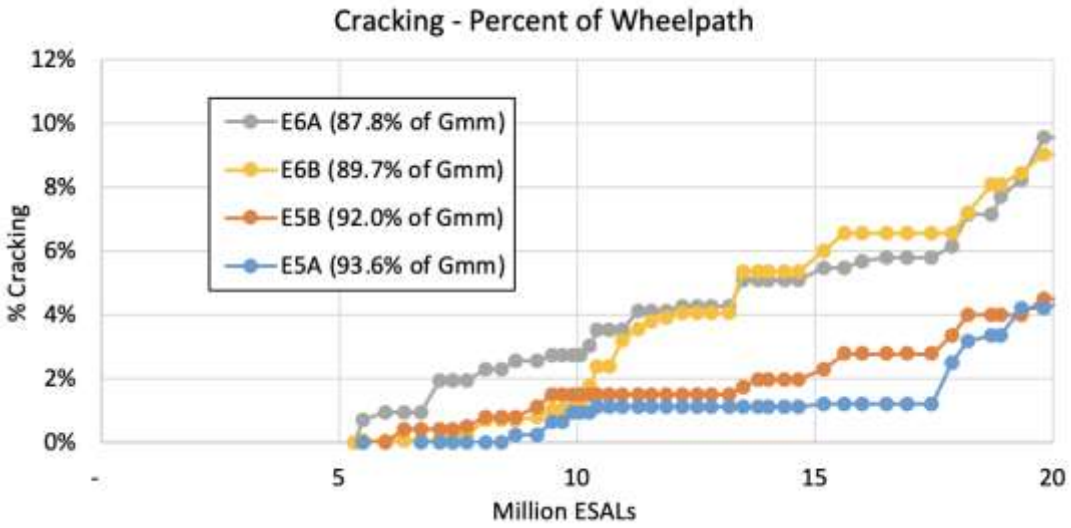

FIGURE 4 Cracking (percent of wheelpath) versus traffic.

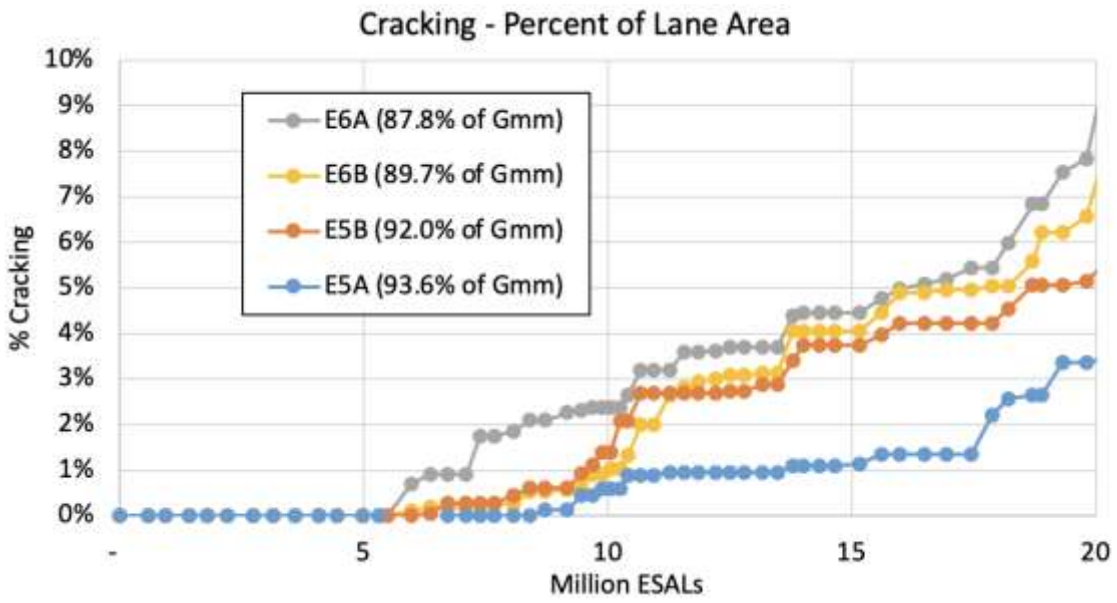

FIGURE 5 Cracking (percent of lane area) versus traffic.

Figures 6 and 7 provide representative photographs of the subsections. Overall, the subsections are performing well. Most cracks are categorized as minor severity (≤ 5 mm) and are barely discernable during the warmer months. Some cracks in E6A and E6B are more easily visible with some spalling beginning to occur.

E5A (93.6% of G_{mm}) overview

E5A (93.6% of G_{mm}) representative cracking

E5B (92.0% of G_{mm}) overview

E5B (92.0% of G_{mm}) representative cracking

FIGURE 6 Subsection overviews and representative cracking severity in April 2024.

E6A (87.8% of G_{mm}) overview

E6A (87.8% of G_{mm}) representative cracking

E6B (89.7% of G_{mm}) overview

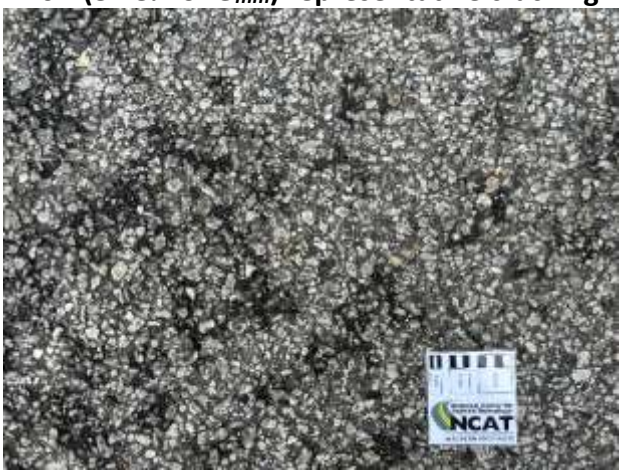

E6B (89.7% of G_{mm}) representative cracking

FIGURE 7 Subsection overviews and representative cracking severity in April 2024.

Crack maps of the four subsections are shown in Figure 8. As can be seen from these maps, the cracks in E5A (93.6% of G_{mm}) and E5B (92.0% of G_{mm}) are more dispersed throughout the section, whereas the cracking in E6A (87.0% of G_{mm}) and E6B (89.7% of G_{mm}) is more clustered. The reason for the clustering of cracks is unknown.

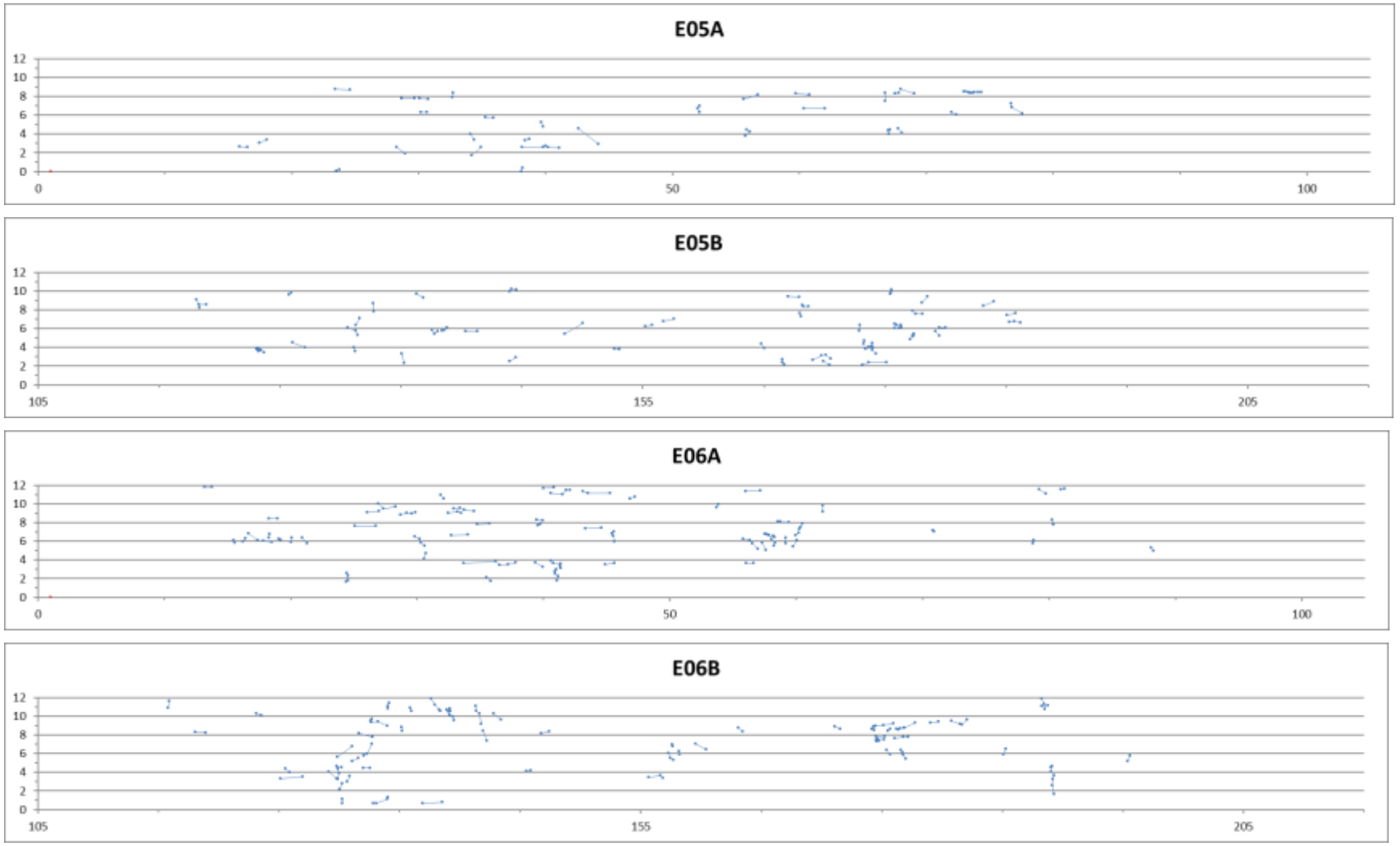

FIGURE 8 Crack maps for the Florida DOT in-place density subsections at 20 million ESALs.

Figure 9 shows the progression in surface texture for the subsections in the in-place density experiment. The shift in data at 10 million ESALs was due to a change in the inertial profiler used for pavement performance data collection at the beginning of the 2021 Cycle. In addition to the hardware change, the texture was reported natively in mean profile depth (MPD) for the 2021 data, whereas the previous profiler required a transfer function to convert mean texture depth (MTD) to MPD. This resulted in a noticeable but consistent increase in the reported surface texture results. In general, the ranking of MPD results for the density experiment subsections has stayed consistent over time with the lower density subsections having slightly higher MPD than the higher density subsections. In other words, subsections with higher in-place densities have less raveling.

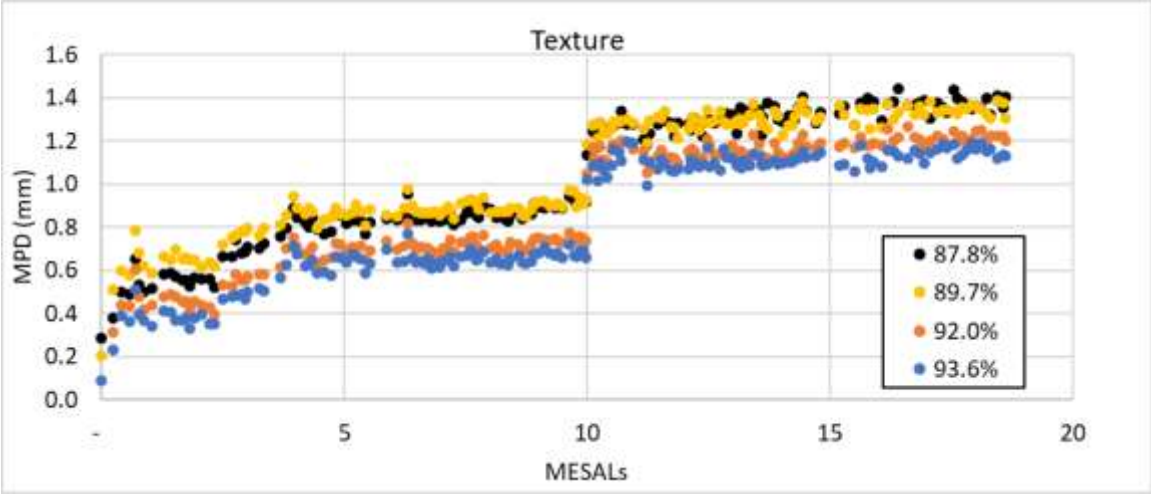

FIGURE 9 Progression of surface texture of the density subsections over two cycles.

5.6 Laboratory Testing of Plant-Produced Mixtures

Plant-produced loose mixtures sampled during construction were taken to the main NCAT laboratory for testing. Except where otherwise noted, the laboratory performance tests for this experiment were conducted on specimens made from re-heated, plant-produced mix. Test specimens were compacted to the following density targets: 6.5 ± 0.5% air voids for E5A, 8.0 ± 0.5% air voids for E5B, 12.0 ± 0.5% air voids for E6A, and 10.0 ± 0.5% air voids for E6B, corresponding to the target in-place air voids of the subsections. Table 5.5 lists the tests conducted on the sampled mixtures.

TABLE 5 Laboratory Tests Conducted on the Mixtures from the FDOT Density Study

Test Name	Test Method	Parameter	Reference(s)
IDEAL-CT	ASTM D8225	CT_{Index}	*6*
I-FIT	AASHTO T 393	Flexibility Index (FI)	*7, 8*
Cantabro	AASHTO TP 108	Mass loss, %	*11, 12*
Dynamic Modulus	AASHTO T 378	E*	*13*
Energy Ratio	no standard	ER	*14, 15*
Hamburg Wheel	AASHTO T 324	Rut Depth @ 20,000 passes	*16*
High-Temp. IDT	Draft ASTM method	IDT strength	*17-19*

5.6.1 Indirect Tensile Asphalt Cracking Test (IDEAL-CT)

The primary output of the IDEAL-CT is the parameter CT_{Index}. A higher CT_{Index} typically indicates an increased resistance to intermediate-temperature, load-related mixture cracking (*3*). However, one drawback of the IDEAL-CT has been the counterintuitive effect of specimen air voids on CT_{Index}. Previous studies have shown that for any given mixture, as specimen density is decreased (higher air voids) typically results in a higher CT_{Index}, which is the opposite of the expected behavior (*6*). That trend is clearly evident in Figure 10, which shows that the CT_{Index} increased as the average specimen air voids increased.

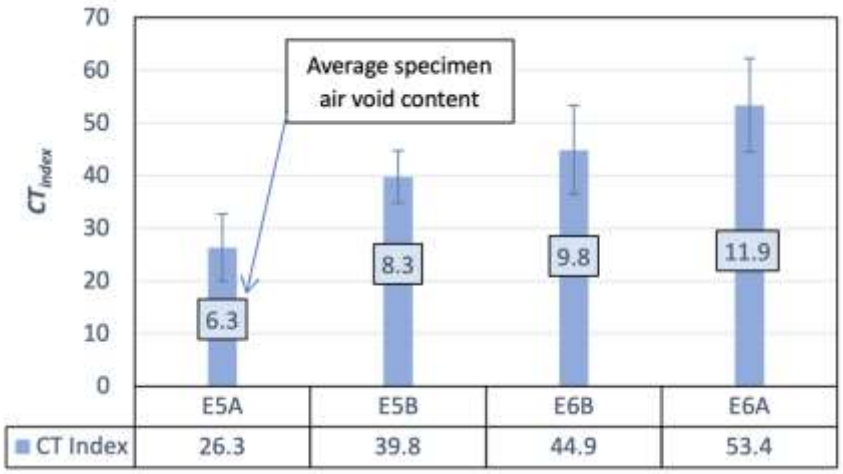

FIGURE 10 IDEAL cracking test results of subsections E5A, E5B, E6A, and E6B.

5.6.2 Illinois Flexibility Index Test (I-FIT)

Developed by the Illinois Center for Transportation at the University of Illinois, Urbana-Champaign, the Illinois Flexibility Index Test and its resulting index parameter, Flexibility Index (FI), has been shown to provide strong relationships with field performance in several studies (*7, 8*). The results of those studies led the Illinois DOT to set a minimum FI criterion of 8 for dense-graded asphalt mixtures.

The FI results from the four subsection mixtures are shown in Figure 11. The average FI results for each of the subsections are low compared to the Illinois DOT criterion but are higher than

many of the other research mixtures evaluated on the NCAT Test Track over the past few cycles. Like the CT_{Index}, FI has been shown to be counterintuitively affected by specimen air void contents. However, the expected trend of increasing FI with increasing specimen air void contents is inconsistent for these results. The higher FI results for E6B and E6A, compared to E5A and E5B, may be due to their lower $P_{\#200}$ contents, which were about 1.5% lower.

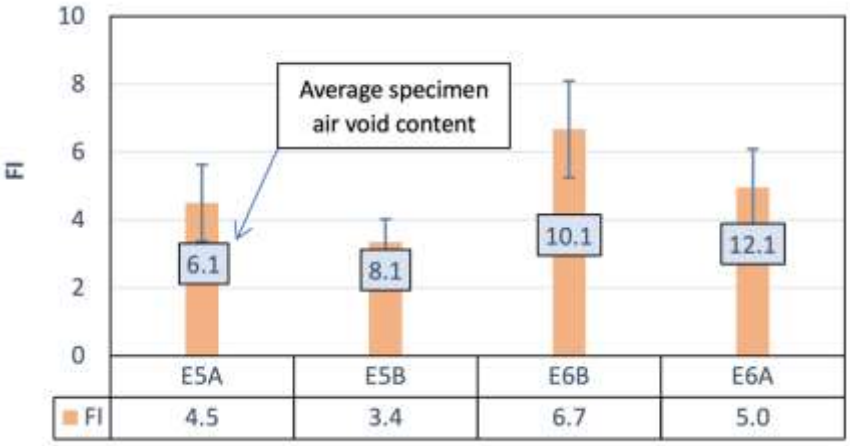

FIGURE 11 Flexibility Index test results of subsections E5A, E5B, E6A, and E6B.

5.6.3 Cantabro Test

The Cantabro abrasion test has primarily been used for the design of open-graded friction course (OGFC) mixtures as an indicator of durability and raveling potential (*9*). Doyle and Howard found that mass loss for dense-graded mixtures was typically less than 15% based on a limited data set and stated that the use of the Cantabro test for dense-graded mixtures was promising (*10, 11*). The Virginia DOT (VDOT) currently uses the Cantabro test, along with the IDEAL-CT and the Asphalt Pavement Analyzer (APA) as part of its BMD special provisions. The VDOT criterion is a maximum loss of 7.5 percent on N_{design} specimens (*12*).

Figure 12 shows the results of the Cantabro test conducted on the plant-produced mixture at the target field density levels and a sample compacted to N_{design}. No trend is observed for the effect of air void content on Cantabro results, perhaps except for E6A, which had a much higher mass loss for specimens with air voids at 12.0 ± 0.5%.

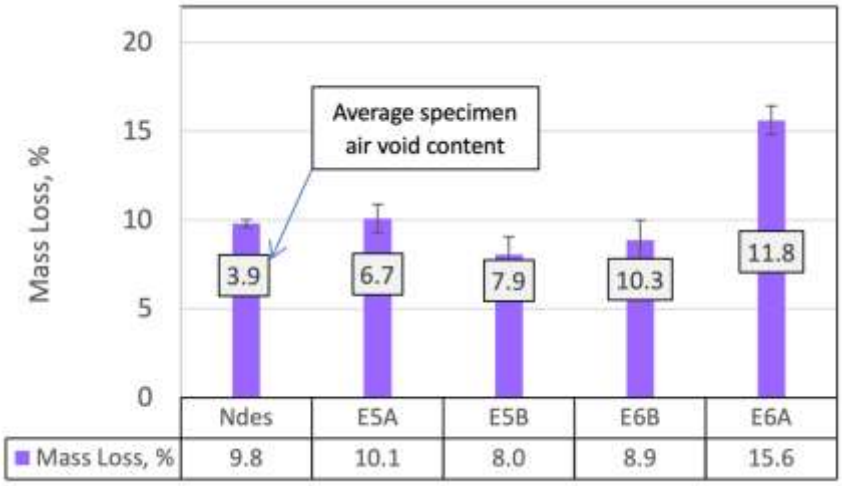

FIGURE 12 Cantabro test results of subsections E5A, E5B, E6A, and E6B.

5.6.4 Energy Ratio

The Energy Ratio (ER) test, developed at the University of Florida to assess an asphalt mixture's resistance to top-down cracking, is determined from a combination of three tests, each conducted at 50°F (10°C): resilient modulus, creep compliance, and indirect tensile strength. The ER testing procedures, analysis, and proposed criteria are reported elsewhere (*14, 15*). Researchers at the University of Florida reported that a higher ER provides better resistance to surface cracking (*14*). However, the recent Cracking Group experiment on the NCAT Test Track found ER to correlate poorly with top-down cracking of the test sections on the Test Track (*3*). Figure 13 shows the ER results for the mixture at the four density levels. There was no trend for the impact of air voids on ER results for this experiment.

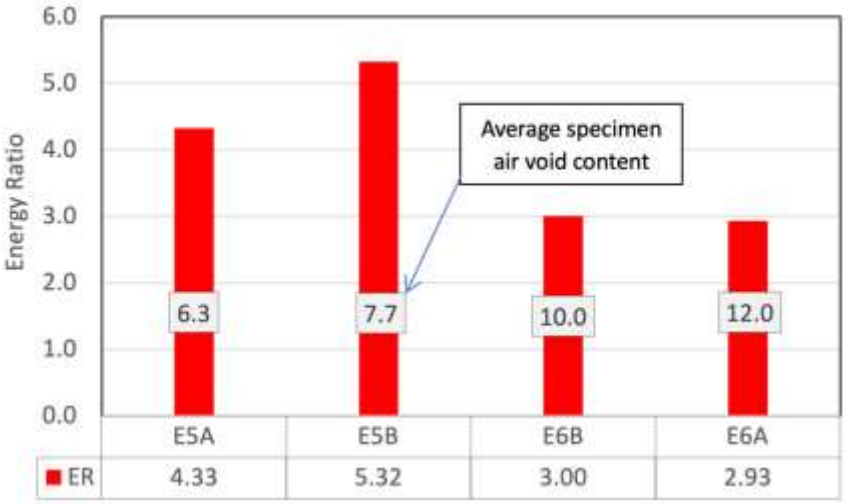

FIGURE 13 Energy ratio test results of subsections E5A, E5B, E6A, and E6B.

5.6.5 Dynamic Modulus (E)*

While dynamic modulus (E*) master curves have not been suggested as indicators of cracking resistance, they are used in most mechanistic pavement design methods and provide a measure of mixture stiffness over a range of loading frequencies and temperatures. As shown in Figure 14, the mixture with the lowest air void content (E5A) was the stiffest mixture at all temperatures and frequencies. On the other hand, specimens from Sections E6A and E6B had very similar master curves over the range of temperatures and frequencies.

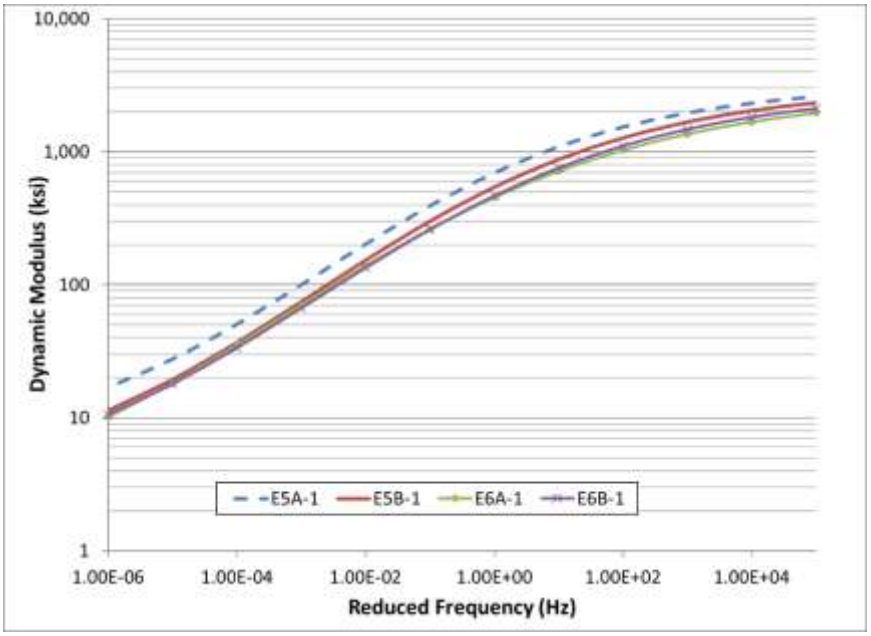

FIGURE 14 Master curves of subsections E5A, E5B, E6A, and E6B.

5.6.6 Hamburg Wheel Tracking Test (HWTT)

Figure 15 shows the HWTT rut depths after 20,000 passes. The mixtures did not have any signs of stripping. All four mixtures have good resistance to rutting, with all rut depths below 5 mm. These results are consistent with the observed field performance with regard to rutting. As expected, rut depths increased slightly as the specimen air void contents increased.

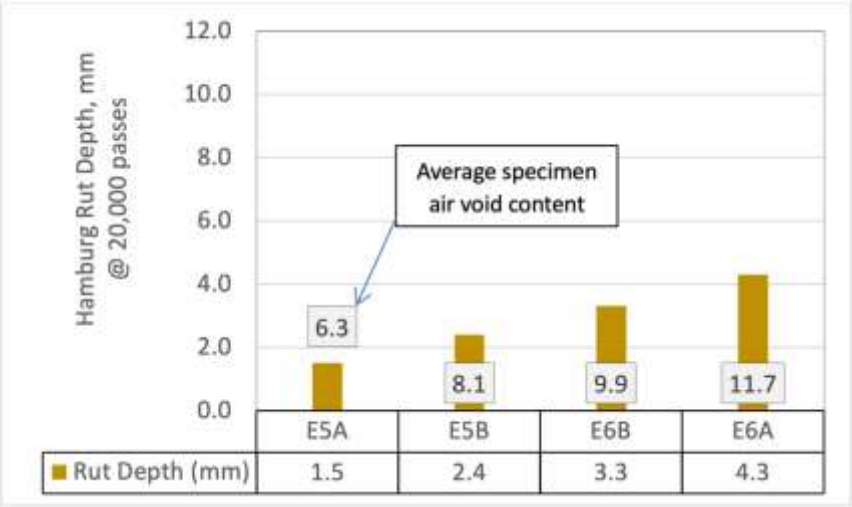

FIGURE 15 Hamburg test results of subsections E5A, E5B, E6A, and E6B.

5.6.7 High-Temperature Indirect Tensile (HT-IDT) Strength

Christensen et al. (*17*), reported that IDT strength at 20°C below the critical pavement temperature had a strong correlation with rutting measured at the FHWA pavement test facility. Those results led to preliminary guidelines for evaluating rut resistance based on IDT strengths. In 2007, Christensen and Bonaquist (*18*) revised the guidelines for HT-IDT strengths based on field-measured rut depths from test sections at NCAT, MnROAD, and WesTrack. Bennert et al. (*19*) have shown HT-IDT to be strongly correlated with rutting in the Asphalt Pavement Analyzer test and suggested the HT-IDT test as a surrogate for the APA for QA testing.

For this study, three replicate specimens were compacted in an SGC to 62 mm height at the as-constructed field densities for each subsection. Specimens were conditioned at 50°C ± 1°C (122°F ± 2°F) for two hours ± 10 minutes before testing, then tested within two minutes of removal from the chamber. Specimens were loaded monotonically at 50 mm/minute until the peak load was obtained. The indirect tensile strength (ITS) was then calculated from the peak load and specimen dimensions. Figure 16 shows the results of HT-IDT conducted for all four mixtures. The chart shows that high-temperature tensile strengths decreased with an increase in air void contents.

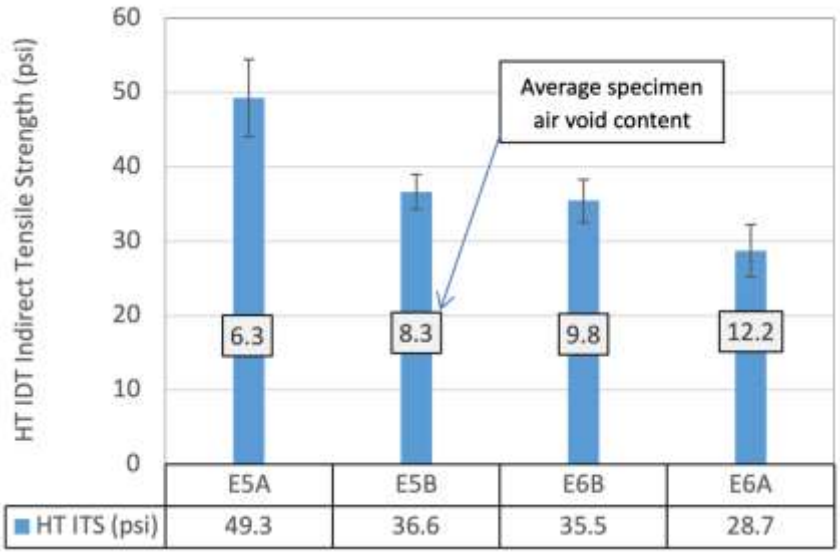

FIGURE 16 HT-IDT results of subsections E5A, E5B, E6A, and E6B.

5.7 Testing of Extracted Binders from Cores after Five Years

Cores from each subsection were obtained in December 2023 to evaluate the recovered binder property changes after five years of service. The cores were obtained from between the wheelpaths of the subsections. The 1.5-inch surface layers were separated, and air void contents were determined based on the original G_{mm} for each subsection. Then, the 1.5-inch cores were cut into an upper and lower portion (i.e., top and bottom), and the air void contents of each portion were also determined. Table 6 summarizes the average air void contents of the complete core (entire layer) and the upper (top) and lower (bottom) portions for each subsection.

TABLE 6 In-Place Air Void Contents of the Subsections Density Data (% G_{mm}) for the Experimental Subsections

Description	Subsection			
	E5A	E5B	E6B	E6A
Entire Layer	2.8%	3.7%	4.9%	7.5%
Top	2.7%	3.7%	4.8%	7.6%
Bottom	2.8%	4.1%	4.9%	8.2%
As-Constructed	6.4%	8.0%	10.7%	12.2%

These data show that the surface layers for each subsection have densified (air voids have decreased) significantly under traffic over the five years. The cores were taken in the center of the lane (between the wheel paths). It is evident this part of the pavement experienced wander of the trucks and trailers trafficked, which is a common occurrence in the curve sections. The subsections have densified between 3.6% and 5.8% of G_{mm}.

Asphalt binder from the top and bottom portions of the cores was extracted using ASTM D2172 *Standard Method for Quantitative Extraction of Asphalt Binder from Asphalt Mixture, Method*

A, with Trichloroethylene as the solvent. The asphalt binders were recovered from the solvent solution using ASTM D5404, *Standard Practice for Recovery of Asphalt Binder from Solution using a Rotary Evaporator*. The recovered asphalt binders were tested for high, intermediate, and low-temperature properties as described in AASHTO M320, *Standard Specification for Performance Graded (PG) Asphalt Binders*. In addition to the standard PG testing, the Dynamic Shear Rheometer (DSR) was used to measure sweeps of frequency (0.1 to 30 Hz) over a range of temperatures (-10 to 90°C) to allow for the creation of master curves of complex shear modulus (G*) vs frequency. Due to the age of the pavement from which the cores were taken, the asphalt binders from the tops and bottoms of the cores were tested in their as-recovered condition without further aging. Asphalt binder from a sample of production mix that had been stored at NCAT since construction was also extracted and recovered using the same procedures. The recovered asphalt binder from the construction mix was tested in its as-recovered condition as well. Table 7 summarizes the testing performed on the recovered asphalt binders.

TABLE 7 Laboratory Tests Conducted on the Recovered Binders from the FDOT Density Study

Test Name	Test Method	Parameter
Rotational Viscosity	AASHTO T 316	Viscosity @ 135°C, Pa-s
Dynamic Shear Rheometer, high temperature	AASHTO T 315	G*/sin(δ) = 2.20 kPa
Dynamic Shear Rheometer, intermediate temperature	AASHTO T 315	G*sin(δ) = 6,000 kPa
Bending Beam Rheometer	AASHTO T 313	Stiffness = 300 MPa, m-value = 0.300
Delta Tc (ΔTc)	n/a	ΔTc = T_{cont}, Stiffness – T_{cont}, *m*-value
Dynamic Shear Rheometer frequency sweep	n/a	G* @ 15°C, 0.005 rad/sec

It was expected that the recovered asphalt binders would show increased aging with decreasing in-place density, as higher air voids would allow more oxidative aging to occur within the thickness of the pavement. It was also expected that the recovered asphalt binders from the top portions of the subsections would exhibit increased aging when compared to the bottom portions, with in-place density affecting the magnitude of the difference.

Figure 17 shows the rotational viscosities of the recovered binders from the top and bottom of the four subsections and the recovered binder from the plant mix sample. While the viscosity values for the four subsections do not exactly follow the expected trend (subsection E6B has higher viscosity than subsection E6A, even though E6A has the lowest in-place density), the overall trend is as expected. The binders recovered from E6A (87.8% of G_{mm}) and E6B (89.3% of G_{mm}) had substantially higher viscosity values than the binders recovered from E5A (93.6% of G_{mm}) and E5B (92.0% of G_{mm}). This indicates that the binders in the subsections with lower in-place densities have aged more than the binders recovered from the subsections with higher in-place densities. The top portions of the E6A and E6B subsections have higher viscosities than their corresponding bottom portions, indicating that more aging occurs near the surface of the pavement. The binders recovered from the bottom portions of E6A and E6B have higher

viscosity values than the binders recovered from the bottom portions of E5A, E5B, and the production mix. This indicates increased aging throughout the thickness of those subsections, although the bottom portions are less aged than the top portions. For the higher-density subsections (E5A and E5B), there is less change in the viscosity of the top portions compared to the bottom portions. The viscosity values of the higher density subsections were closer to those of the production mix, indicating that overall these subsections aged less than the lower density subsections.

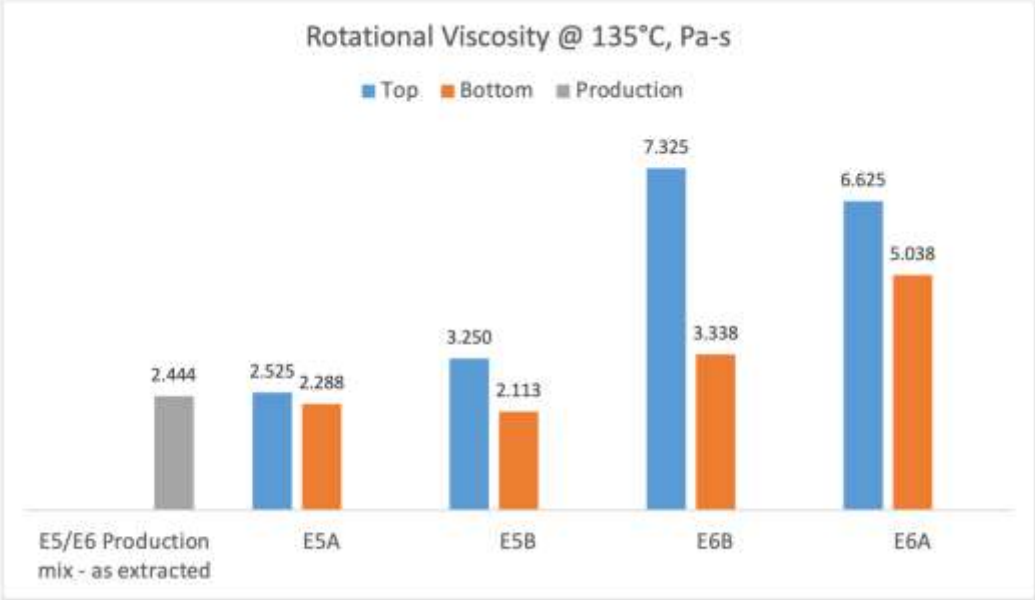

FIGURE 17 Viscosities of the recovered binders from the density experiment subsections.

Figure 18 provides comparisons of the high-temperature continuous grades (the temperature in °C where G*/sin(δ) = 2.20 kPa) of the recovered binders. High-temperature continuous grade is an indicator of high-temperature stiffness and is used to assess rutting potential in asphalt binders. Higher values of high-temperature continuous grade indicate increased rutting resistance. They can also indicate increased aging as the high-temperature continuous grade increases as the binder ages.

As with the rotational viscosity values, the high-temperature continuous grades shown in Figure 18 do not follow the exact expected trend of increased aging with decreased in-place density. The high-temperature continuous grades for subsection E6B are slightly higher than those of E6A. It is important to remember, however, that these results are based on field-aged binders that have been through the extraction and recovery procedure. Because of this, they have a large amount of inherent variability in their properties. Keeping this in mind, the high-temperature continuous grades for the subsections do meet the overall expected trend of increased high-temperature continuous grades for the lower in-place density subsections. The recovered binders from subsections E6A and E6B have high-temperature continuous grades for

both the top and bottom portions that are higher than those of subsections E5A and E5B. The high-temperature continuous grades for the tops and bottoms of subsections E6A and E6B are also higher than those of the production mix, indicating that the lower in-place densities led to increased aging throughout the thickness of these subsections. The high-temperature continuous grades for the tops of subsections E5A and E5B are much closer to those of the production binder, indicating less aging has occurred in the higher in-place density subsections. The bottom portions of these subsections actually have slightly lower values than the production mix. This was unexpected, but it is possible that the production mix experienced some aging during storage.

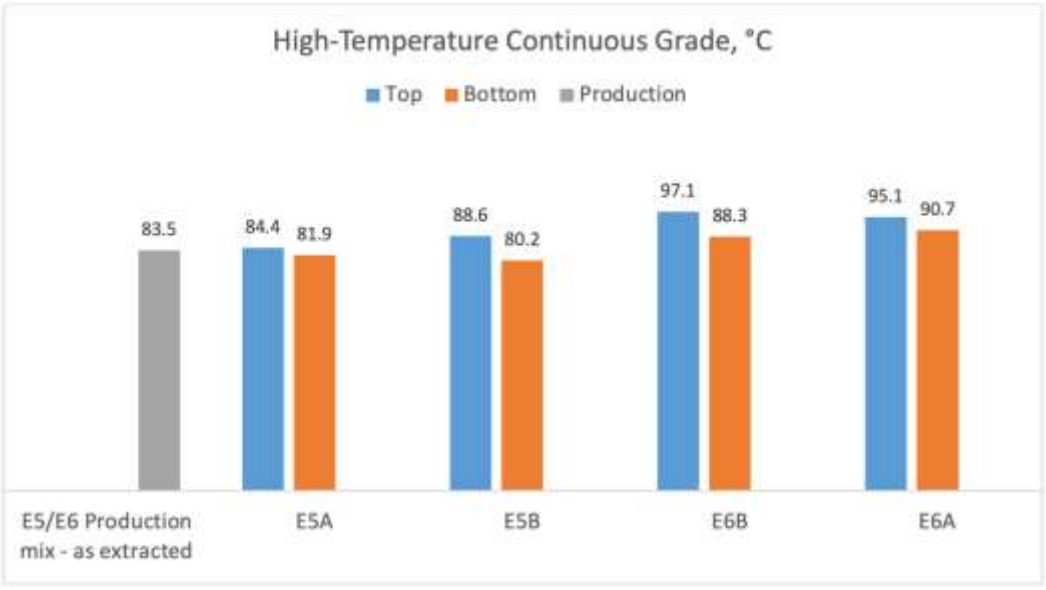

FIGURE 18 High-temperature continuous grade of the recovered binders from the density experiment subsections.

Figure 19 shows the intermediate-temperature continuous grades (the temperature in °C where G*sin(δ) = 6000 kPa) of the recovered binders. Intermediate-temperature continuous grade is an indicator of the recovered binder's ability to resist load-related fatigue cracking and is expected to increase as the binder ages. Warmer values of intermediate-temperature continuous grade indicate a loss in the binder's ability to resist fatigue cracking.

The results shown in Figure 19 match the trends shown in the previous two figures. The intermediate-temperature continuous grades of the recovered binders from the lower in-place density subsections are higher than those of the recovered binders from the higher in-place density subsections, indicating increased aging for those subsections. The recovered binders from the bottom portions of sections E6A and E6B have higher intermediate-temperature continuous grades than the recovered binders from the production mix and from the bottom portions of subsections E5A and E5B, indicating increased aging throughout the thickness of the

lower in-place density subsections. The recovered binders from subsections E5A and E5B have intermediate-temperature continuous grades closer to that of the production binder for both top and bottom portions indicating that they have aged less than subsections E6A and E6B. The recovered binder from the bottom portion of subsection E5B is significantly lower than that of the production binder. This could be due to the production binder aging during storage or could simply be an artifact of the inherent variability in both field cores and the extraction and recovery process.

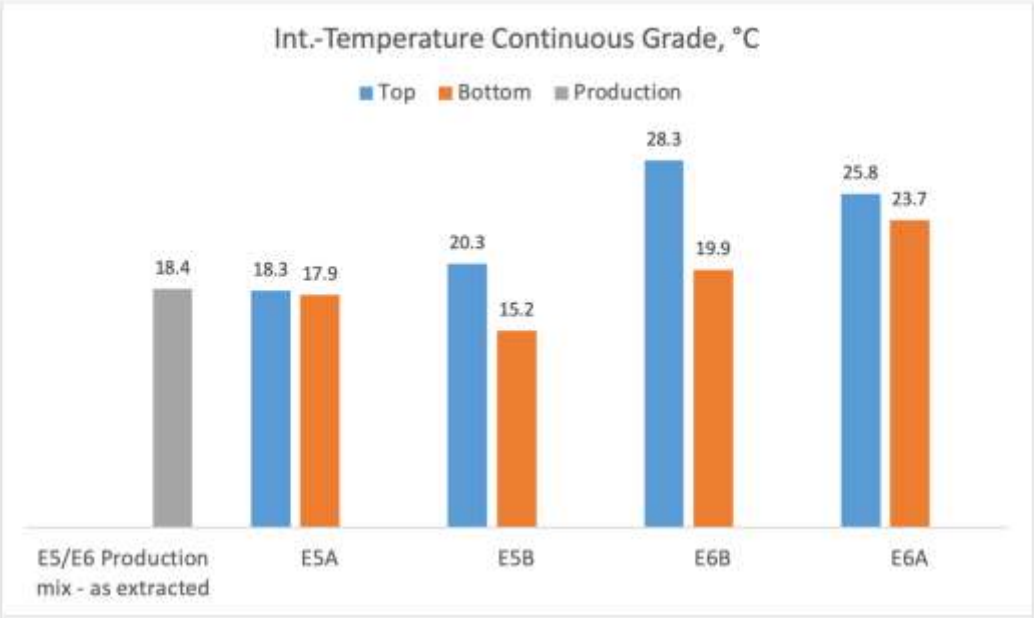

FIGURE 19 Intermediate-temperature continuous grade of the recovered binders.

Figure 20 shows the low-temperature continuous grades for the four subsections. The low-temperature continuous grade is defined as the warmest temperature, in °C, where either the BBR creep stiffness = 300 MPa or the *m*-value = 0.300. For these results, all of the low-temperature continuous grades were based on the m-value criteria as it was the warmer of the two values for all recovered binders. The low-temperature continuous grade is an indicator of the asphalt binder's ability to resist thermal cracking. As the binder ages, the low-temperature continuous grade is expected to increase (become warmer).

For the top portion of the cores, the recovered binders from the subsections all had low-temperature continuous grades warmer than the production mix low-temperature continuous grade. The recovered binders from the tops of subsections E6A and E6B had low-temperature continuous grades that were significantly warmer than that of the production mix, indicating increased aging. The recovered binders from the bottoms of subsections E6B and E6A also had low-temperature continuous grades that were significantly warmer than that of the production mix, indicating increased aging throughout the lower in-place density subsections. The

recovered binders from the bottoms of E5A and E5B had low-temperature continuous grades that were either comparable to or slightly colder than that of the production mix, indicating less aging.

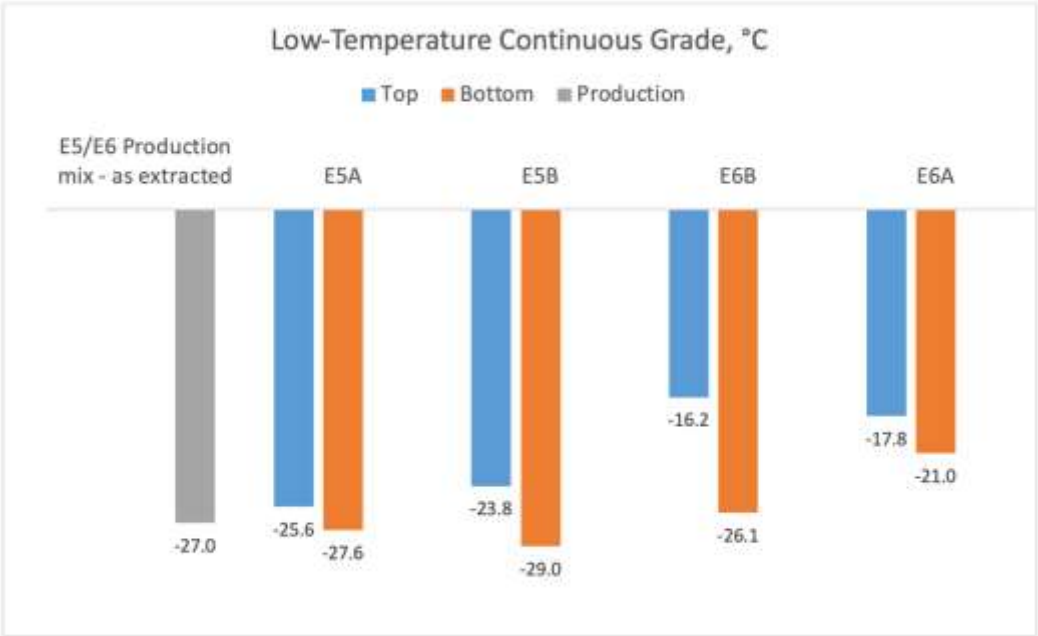

FIGURE 20 Low-temperature continuous grade of the recovered binders from the density experiment subsections.

Delta Tc is an indicator of the loss of relaxation properties of an asphalt binder that contributes to age-related embrittlement distresses of asphalt pavements. An asphalt binder with a lower (colder) Delta Tc is generally more susceptible to non-load-related (environmental) cracking (*20*). A Delta Tc value of -5°C has been proposed as the point where cracking can be expected. The Delta Tc parameter accounts for the loss in relaxation compared to stiffness as the numerical difference between the low-temperature continuous grade calculated using the Stiffness = 300 MPa criterion and the low-temperature continuous grade calculated using the m-value = 0.300 criterion. For example, a binder with a low-temperature continuous grade = -18.2°C based on stiffness, and a low-temperature continuous grade = -15.2°C based on m-value will have Delta Tc = -3.0°C.

Figure 21 shows the Delta Tc values for the binders recovered from the subsections of this experiment. Overall, the subsections with lower in-place densities had lower (worse) Delta Tc values for both the top and bottom portions compared to those of the higher in-place density subsections. The top portions of the higher in-place density subsections had Delta Tc values that were comparable to or slightly lower than those of the production mix, indicating aging in the top portions of those subsections. The bottoms of the higher in-place density subsections had higher (warmer) Delta Tc values than either the top portions of their corresponding

sections or those of the bottom portions of E6A and E6B. While the results shown in Figure 21 don't appear to follow the expected trends, they do match the field cracking data shown in section 5.5. The higher in-place density subsections all have Delta Tc values warmer than -5°C and experienced very little cracking. The lower in-place density subsections have Delta Tc values colder than -5°C for the top portions and while they also did not experience a large amount of cracking, the actual percentage of the lane width cracked was higher than that of the higher in-place density subsections. This indicates that the lower in-place density subsections have experienced higher aging than the higher in-place density subsections.

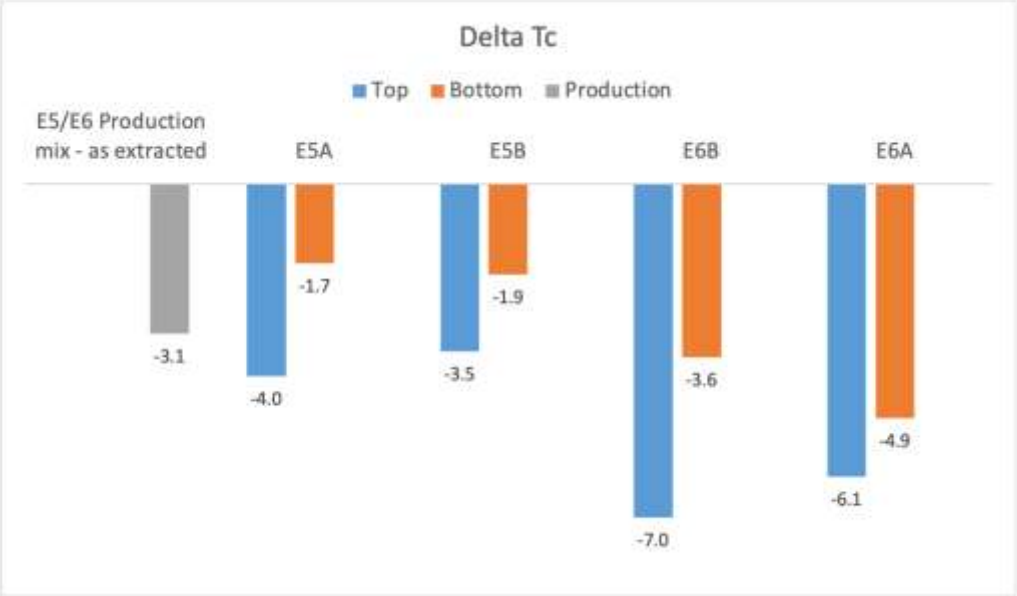

FIGURE 21 Delta Tc results for recovered binders from the density experiment subsections.

The Glover-Rowe parameter (GR) is another binder cracking parameter. The results of the DSR frequency sweeps over a range of temperature were shifted to fit the Christensen-Anderson model to create master-curves of complex shear modulus (G*) vs frequency at 15°C. The master curve results were used to obtain complex shear modulus (G*) and phase angle (δ) results for each binder and aging condition at 15°C and 0.005 rad/s. Master curves are necessary as these conditions cannot be measured directly using the DSR due to time constraints. The simplified version of Glover-Rowe shown in Equation 1 was used for the calculation:

$$GR = \frac{G^*(\cos\delta)^2}{\sin\delta}$$

Equation 1

Higher GR values indicate an increase in binder stiffness and a decreased resistance to cracking. A tentative maximum value of 180 kPa has been proposed for the GR parameter to identify crack initiation and 600 kPa for crack propagation (*20*).

Figure 22 shows the GR results for the recovered binders from the tops and bottoms of the subsections and the production mix. Once again, the results followed a similar trend to the criteria discussed previously. The recovered binders from the tops and bottoms of the lower in-place density subsections had significantly higher GR values than the recovered binders from the higher in-place density subsections and the production mix. This indicates increased aging throughout the thickness of these subsections. The recovered binders from the tops and bottoms of the higher in-place density subsections had GR values that were comparable to or slightly better than the production mix, indicating less aging for these subsections.

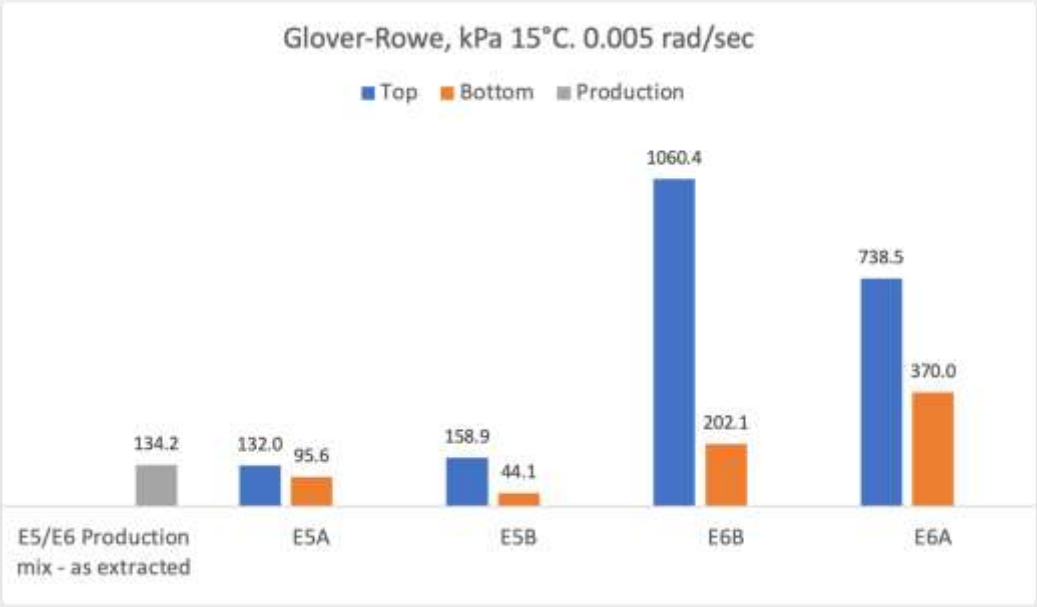

FIGURE 22 Glover-Rowe parameter of the recovered binders from the density experiment subsections.

5.8 Preliminary Findings

Based on the field performance and analysis of laboratory test results from the FDOT in-place density experiment through five years, the preliminary findings of this study are:

- Through five years of environmental exposure and 20 million ESALs of traffic, all of the in-place density experiment subsections are still performing very well. There are no practical differences in rutting among the subsections. There is a trend of increasing surface texture for sections having lower in-place densities, but the magnitudes of texture changes are not indicative of significant raveling. The test sections with lower as-constructed densities were the first to have visible cracks, and there is a trend of higher crack progression for those test sections, but the extent and severity of the cracking of all sections are still low at this time. Overall, the low-severity cracks are well dispersed throughout the subsections.

- Results of IDEAL-CT specimens compacted to represent the average as-constructed densities reveal that lower densities yield a higher CT_{Index}, which is the opposite of the expected behavior. This highlights the importance of using the standard specimen air void target of 7.0 ± 0.5% for the IDEAL-CT test. Otherwise, the results of the test may be confusing and not indicative of actual pavement performance.
- Other studies have shown that the results of the Illinois Flexibility Index Test (I-FIT) are also counterintuitively affected by specimen air void contents. The results of the I-FIT test in this experiment show that E6B (87.8% of G_{mm}) and E6A (89.7% of G_{mm}) have higher FI values compared to E5A (93.6% of G_{mm}) and E5B (92.0% of G_{mm}). It is recommended that I-FIT tests be conducted on specimens prepared with the standard air void target of 7.0 ± 0.5% to avoid the confusing effects of air voids on FI results.
- The results of Cantabro tests conducted on specimens at the target field density levels showed no general trend for the effect of air void content on Cantabro mass loss, except for E6A, which had a much higher mass loss for specimens with 12.0 ± 0.5% air void contents.
- The effect of specimen air void contents on Energy Ratio results was inconsistent among the subsections. Energy Ratio is not recommended as an indicator of top-down cracking.
- Hamburg Wheel Track results (rut depth at 20,000 passes) followed the expected trend of higher rut depths as average specimen rut depths increased. However, all four mixes performed well in the Hamburg and even the lower in-place density sections had rut depths well shy of established failure criteria.
- High-temperature indirect tensile strengths decreased as average specimen air void contents increased, as expected. The HT-IDT results were consistent with the HWTT results as indicators of rutting resistance.
- Cores were cut from the surface layers after approximately five years of service on the Test Track. Binders extracted from the cores were tested with many of the recommended rheological tests to assess the impact of in-place air voids on the aging of the binders.
    - Nearly all rheological properties generally followed the expected trend of significantly more stiffening and embrittlement of the binders for subsections having lower as-constructed in-place densities.
    - The binders recovered from the upper half of the cores were consistently stiffer and had a greater loss in relaxation properties compared to the binders recovered from the bottom half of the cores. These results confirm a significant aging gradient within a 1.5-inch surface layer, even for well-compacted asphalt pavement layers.

5.8 References

1. Tran, N., Turner, P., and Shambley, J. (2016). Enhanced Compaction to Improve Durability and Extend Pavement Service Life: A Literature Review, NCAT Report No. 16-02, National Center for Asphalt Technology at Auburn University, Auburn, AL.
2. Linden, R.N., Mahoney, J.P., and Jackson, N.C. (1989). "Effect of Compaction on Asphalt Concrete Performance." Transportation Research Record 1217, pp. 20–28, Transportation Research Board of the National Academies, Washington, D.C.
3. West, R., Timm, D., Powell, B., Tran, N., Yin, F., Bowers, B., Rodezno, C., Leiva, F., Vargas, A., Gu, F., Moraes, R., and Nakhaei, M. (2021) Phase VII (2018-2021) NCAT Test Track Findings, NCAT Report 21-03, National Center for Asphalt Technology at Auburn University, Auburn, AL.
4. Hoegh, K., Khazanovich, L., Dai, S., & Yu, T. (2015). Evaluating asphalt concrete air void variation via GPR antenna array data. *Case Studies in Nondestructive Testing and Evaluation*, 3, pp. 27-33.
5. Leiva, F., Brenes, A., Gatiganti, S., and Musselman J., (2022) DPS Publications, National Pooled Find TPF-5(443), Minnesota Department of Transportation, https://www.dot.state.mn.us/materials/dps/publications.html
6. Zhou, F., Im, S., Sun, L., & Scullion, T. (2017). Development of an IDEAL Cracking Test for Asphalt Mix Design and QC/QA. Journal of the Association of Asphalt Paving Technologists, pp. 549-577.
7. Al-Qadi, I., Ozer, H. Lambros, J., El Khatib, A., Singhvi, P., Khan, T., Rivera Pérez, J., and Doll, B. (2015). Testing Protocols to Ensure Performance of High Asphalt Binder Replacement Mixes using RAP and RAS. Illinois Center for Transportation Series No. 15-017, Illinois Center for Transportation, University of Illinois at Urbana-Champaign.
8. Al-Qadi, I.L., Lippert, D., Wu, S., Ozer, H., Renshaw, G., Said, M., Espinoza, F. (2017). Utilizing Lab Tests to Predict Asphalt Concrete Overlay Performance. FHWA-ICT-17-020, Urbana, IL, Illinois Center for Transportation, University of Illinois at Urbana-Champaign.
9. Watson, D. E., Cooley, L. A., Jr., Moore, K. A., and Williams, K., "Laboratory Performance Testing of Open-Graded Friction Course Mixtures," Transportation Research Record, Vol.1891, 2004, pp. 40–47.
10. Doyle, J. D. and Howard, I. L., (2011) Evaluation of the Cantabro Durability Test for Dense Graded Asphalt, Proceedings of Geo-Frontiers, Advances in Geotechnical Engineering Geotechnical Special Publication No. 211, ASCE, Reston, VA, 2011, pp. 4563–4572.
11. Doyle, J.D., and I.L. Howard (2016) Characterization of Dense-Graded Asphalt with the Cantabro Test, Journal of Testing and Evaluation, Vol. 44, No. 1, ASTM International, pp. 78-88.

12. Balanced Mix Design Resource Guide, Implementation Efforts, National Asphalt Pavement Association, Accessed March 11, 2024, https://www.asphaltpavement.org/expertise/engineering/resources/bmd-resource-guide/implementation-efforts
13. Bennert, T. A. (2009). Dynamic Modulus of Hot-Mix Asphalt, Report No. FHWA-NJ-2009-011. Center for Advanced Infrastructure & Transportation, Rutgers, The State University, Piscataway, NJ.
14. Roque, R., B. Birgisson, C. Drakos, and B. Dietrich (2004). Development and Field Evaluation of Energy-Based Criteria for Top-Down Cracking Performance of Hot Mix Asphalt. Journal of the Association of Asphalt Paving Technologists, Vol. 73, pp. 229-260.
15. Timm D. H., G. A. Sholar, J. Kim, and J. R. Willis, (2009). Forensic Investigation and Validation of Energy Ratio Concept. In Transportation Research Record: Journal of the Transportation Research Board, No. 2127, Transportation Research Board of the National Academies, Washington, D.C., pp. 43-51.
16. West, R., Timm, D., Willis, R., Powell, B., Tran, N., Sakhaeifar, M., Brown, R., Robbins, M., Vargas-Nordcbeck, A., Leiva Villacorta, F., Guo, X. and Nelson, J. (2012) Phase IV NCAT Pavement Test Track Findings. NCAT Report 12-10, National Center for Asphalt Technology at Auburn University, Auburn, AL.
17. Christensen, D. W., R. Bonaquist, D. A. Anderson, S. Gokhale, (2004). Indirect tension strength as a simple performance test, Transportation Research Circular, number E-C068, Washington D.C., pp. 44 – 57.
18. Christensen, D. W., and R. Bonaquist (2007). Using the Indirect Tension Test to Evaluate Rut Resistance in Developing Hot-Mix Asphalt Designs, Transportation Research Circular, number E-C124, Washington D.C., pp. 62 – 77.
19. Bennert T., Haas E., Wass E., Indirect Tensile Test (IDT) to Determine Asphalt Mixture Performance Indicators during Quality Control Testing in New Jersey. (2018). Transportation Research Record: Journal of the Transportation Research Board. https://doi.org/10.1177/0361198118793276
20. Anderson, R.M., King, G., Hanson, D., and Blankenship, P. (2011) Evaluation of the Relationship between Asphalt Binder Properties and Non-Load Related Cracking. Journal of the Association of Asphalt Paving Technologies: Volume 80, pp. 615-664).

6. GEORGIA DEPARTMENT OF TRANSPORTATION INTERLAYER STUDY FOR REFLECTIVE CRACK PREVENTION

Dr. Thomas Harman

6.1 Background

The Georgia Department of Transportation (GDOT) is dedicated to identifying cost-effective strategies to minimize reflective cracking. Their traditional approach involves applying a single layer of No. 7 stone as a surface treatment over an existing pavement before adding a leveling course topped with an asphalt overlay. This interlayer treatment's open texture creates a separation plane between the existing pavement and the asphalt overlay to absorb underlying cracks and prevent them from reflecting onto the surface. Unfortunately, the effectiveness of this method has not always met expectations.

In 2012, GDOT initiated two experimental sections (N12 and N13) at the NCAT Test Track to assess innovative techniques to reduce reflective cracking. These techniques were:

1) 0.70-inch double surface treatment complemented by a sand seal coat and
2) 1.10-inch open-graded interlayer (OGI).

Following exposure to twenty million equivalent single-axle loads (ESALs), the double surface treatment section exhibited reflective cracking in only 6% of the saw cuts. In contrast, the OGI section showed 50.5% of saw cuts reflecting through to the surface. The crack width in both sections was less than 0.24 inches (6 mm), which is considered low severity. Moreover, the OGI section demonstrated a lower final rut depth of 0.24 inches (6 mm), in contrast to 0.83 inches (21.0 mm) observed in the double surface treatment section.

In 2018, in a continued effort to explore effective methods for mitigating reflective cracking, GDOT extended support for these two sections into six potential solutions. Sections N12 and N13 were divided into three subsections: A, B, and C. The treatments included:

- N12-A, GlasGrid® CG100 interlayer by ADFORS Saint-Gobain,
- N12-B, PETROMAT® fabric interlayer,
- N12-C, chip seal using No. 7 stone,
- N13-A, chip seal with reclaimed asphalt pavement (RAP),
- N13-B, Arizona-style asphalt rubber gap-graded (ARGG) interlayer, and
- N13-C, open-graded Interlayer (OGI).

The Geosynthetic Materials Association randomly selected the two suppliers to have their products tested as part of the GDOT interlayer study (N12-A and N12-B). The 2018 testing cycle replicated the saw cut pattern and surface overlay mix used in the 2012 cycle, ensuring the selected treatment methods were the only variable influencing the performance against reflective cracking.

6.2 Section Preparation and Construction

In 2012, deep saw cuts 1/8 inches wide (3.2 mm) were executed across the full depth of the structural layer in the existing pavement to emulate cracking within the pavement structure. The existing pavement structure was part of the original Test Track perpetual deep foundation study (24 inches asphalt). In 2018, the sections were milled to maintain the finished surface profile, and the saw cuts were re-sanded.

As depicted in Figure 1, these cuts were longitudinally aligned at intervals of 3 feet (0.91 meters) across the lane width and 15 feet (4.57 meters) in the transverse direction. The area impacted by the saw cuts accounted for roughly one-third of the test section's total surface area, assuming an influence zone of 1 foot (0.30 meters) on each side of the crack. The cuts were subsequently filled with sand to prevent the cracks from resealing during construction and warm weather conditions. The saw-cut pattern for this cycle replicated that of the previous research cycle.

FIGURE 1 Deep saw cuts to simulate pavement cracks.

Section N12 was segmented into three subsections to evaluate different treatment methods: N12-A with GlasGrid®, N12-B with PETROMAT® fabric (Figure 2), and N12-C with a No. 7 stone, virgin chip seal (Figure 3, foreground). For subsections N12-A and N12-B, a PG 64-22 asphalt binder was applied as a tack coat at 0.30 and 0.27 gallons per square yard, respectively. Per the manufacturer, GlasGrid® CG100 can be installed on a milled surface or leveling course with a tack coat application ranging from 0.20 to 0.30, and PETROMAT® recommends a PG 70-XX

asphalt binder as the tack coat. A 9.5mm NMAS Superpave Type 2 mix served as the surface layer for all six sections. In N12-A and N12-B, the 9.5mm mix was placed at 2.82 and 2.76 inches, respectively.

FIGURE 2 Section N12-B geosynthetic PETROMAT® (foreground) and N12-A GlasGrid® (background) interlayers.

N12-C received a CRS-2h emulsion tack on the existing pavement with a residue application rate of 0.23 gallons per square yard. The 9.5mm mix was placed as a leveling course over all the remaining subsections at a thickness of approximately ¾ inch. The same 9.5mm NMAS was then placed as a surface layer. See Table 2 for as-constructed layer thicknesses.

FIGURE 3 Section N12-C chip seal with No. 7 stone (foreground) and N13-A chip seal with RAP (background).

Section N13 was divided into three subsections for various treatment methods: N13-A with an RAP chip seal RAP, (Figure 3), N13-B with an ARGG, and N13-C with an OGI. The existing pavement of N13-A received a CRS-2h emulsion tack with a residue application rate of 0.23 gallons per square yard. This is the same application rate as section N12-C. In hindsight, this rate should have been adjusted down to account for the precoated RAP aggregates. Blacklidge UltraFuse® trackless tack was employed for N13-B and N13-C subsections at 0.25 gallons per square yard.

The asphalt rubber gap-graded interlayer, shown in Figure 4a, featured a 1/2-inch (12.5 mm) NMAS gap-graded mix with granite aggregate and 7.4% ARB20 – asphalt rubber binder modified with 20% ground tire rubber (GTR). The OGI, depicted in Figure 4b, was a 1/2-inch NMAS porous friction course (PFC) with a PG 64-22 binder grade, designed according to GDOT special provision section 415, which targets an OBC between 4.50 to 5.25%. This mix omitted fiber stabilizer for cost considerations and utilized a reduced mix temperature of 250°F ± 20°F (121°C ± 11°C) to prevent drain-down. These mixes aimed to provide a discontinuity between the existing surface and overlay, thereby diminishing crack reflection.

a. ARGG interlayer **b. Open-graded interlayer**

FIGURE 4 Asphalt rubber gap-graded and open-graded asphalt interlayers.

Sections N12 and N13 used a 9.5 mm Type 2 surface mix with PG 64-22 compacted to 93.8% of maximum theoretical density. In Georgia, optimal asphalt content for Superpave mixes is determined based on 65 gyrations using a Superpave gyratory compactor. Notably, GDOT specifications distinguish between two 9.5 mm mixes: Type 1, with a finer gradation for leveling courses and thin overlays, and Type 2, typically employed as a surface course on busier roads. The mixture properties for the ARGG, OGI, and 9.5 mm Type 2 mixes are summarized in Table 1. Table 2 provides the as-constructed layer thickness of the six subsections.

TABLE 1 ARGG, OGI, and 9.5 mm Gradation and Mixture Properties

Sieve Size, inches (mm)	ARGG	OGI	9.5 mm
	Passing Percentage		
3/4 (19.0)	100	100	100
1/2 (12.5)	96	96	100
3/8 (9.5)	79	59	95
No. 4 (4.75)	40	14	64
No. 8 (2.36)	24	8	44
No. 200 (75µm)	3.4	2.0	5.9
Mixture Properties	**Percentage of Mixture**		
Asphalt Binder Content (P_b), %	7.4	4.5	5.6
Air Voids, %	6.0	22.2	4.1
Voids in Mineral Aggregate (VMA), %	19.9	30.8	15.4

TABLE 2 As-Constructed Layer Thickness (inches)

Section	N12-A	N12-B	N12-C	N13-A	N13-B	N13-C
Description	GlasGrid®	PETROMAT®	Chip-seal No. 7 stone	Chip-seal RAP	ARGG	12.5mm OGI
Total	2.82	2.76	2.64	2.65	2.92	3.04
9.5 mm Superpave	2.82	2.76	1.88	2.05	1.57	1.58
Interlayer	--	--	0.76	0.60	1.35	1.46

6.3 Field Performance

At the end of the loading cycle in April 2024, the evaluated sections have been subjected to over 20.08 million ESALs. Weekly field performance monitoring encompasses ride quality, rut depth, surface texture, and cracking assessments.

Figure 5 illustrates initial International Roughness Index (IRI) readings, highlighting that subsection N12-A started with a notably higher IRI than other subsections (200 in./mile). This discrepancy is attributed to interference from the adjacent Section N11, which boasts an IRI exceeding 150 inches per mile (93.2 inches/km), and the impact of the transverse joint. Across the board, none of the six subsections exhibited significant increases in IRI. Overall smoothness improved slightly for half of the subsections, as shown in Figure 6.

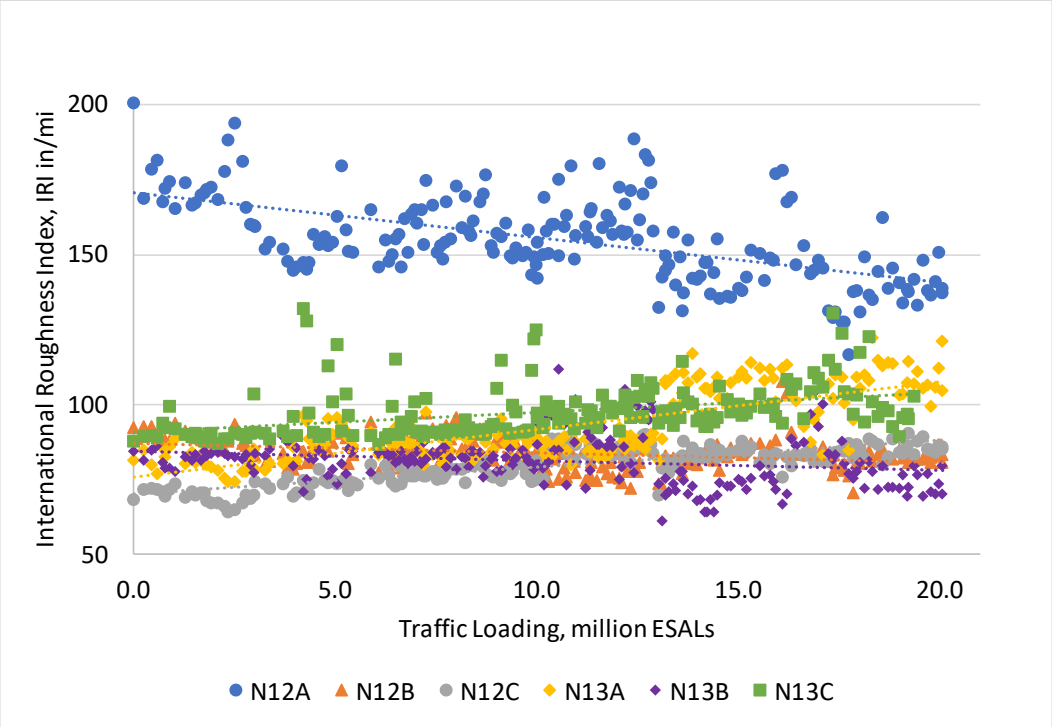

FIGURE 5 International Roughness Index measurements of N12 and N13.

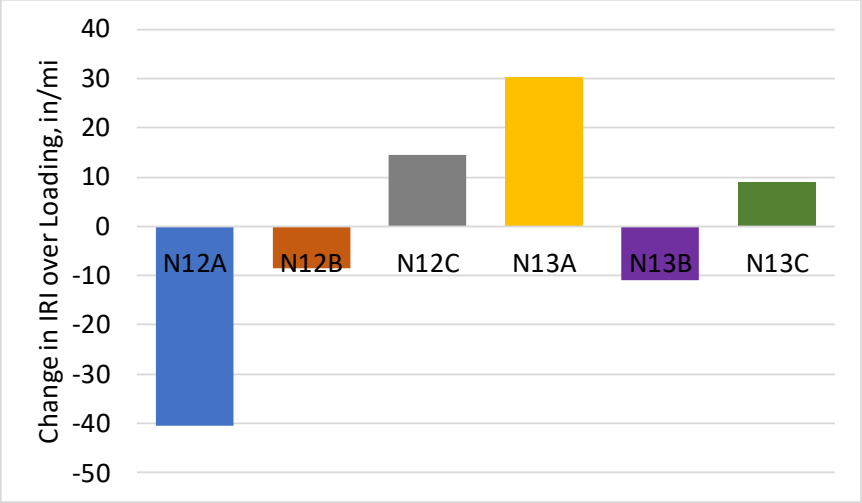

FIGURE 6 Change in IRI over trafficking for N12 and N13.

Figure 7 and Figure 8 capture variations in rut depth due to trafficking, with subsection N13-A (chip seal with RAP) displaying the most substantial change of 0.46 inches (11.7 mm).

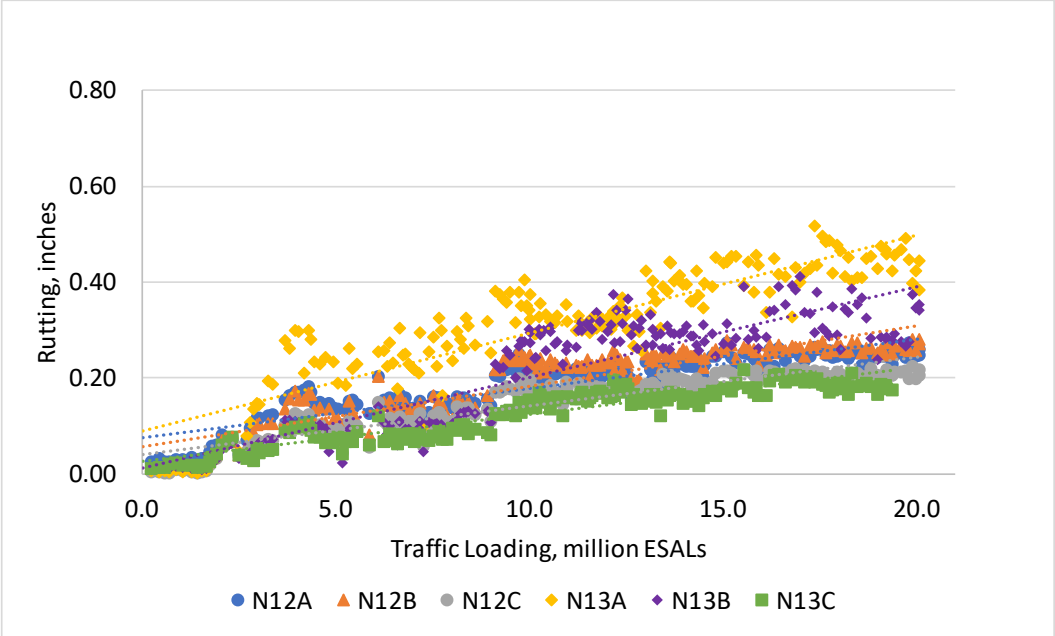

FIGURE 7 Rut depth comparison of N12 and N13.

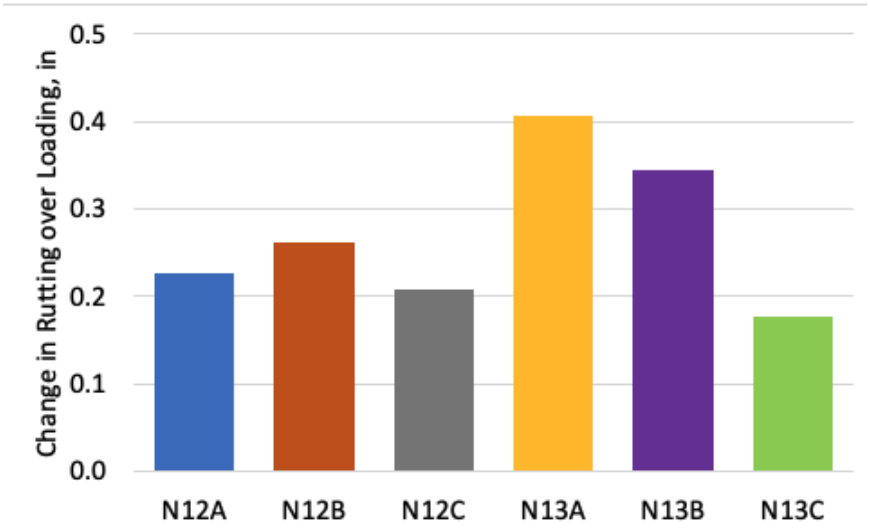

FIGURE 8 Change in rut depth over trafficking for N12 and N13.

Surface texture changes measured by mean profile depth (MPD) are presented in Figure 9. MPD is a key indicator of pavement macrotexture and is vital for assessing roadway safety and tire wear. Newly constructed asphalt pavements typically feature MPD values between 0.5 and 1.5 mm. All six subsections showcased similar MPD values, with a minor increase observed as trafficking progressed. Notably, there was no evidence of surface raveling.

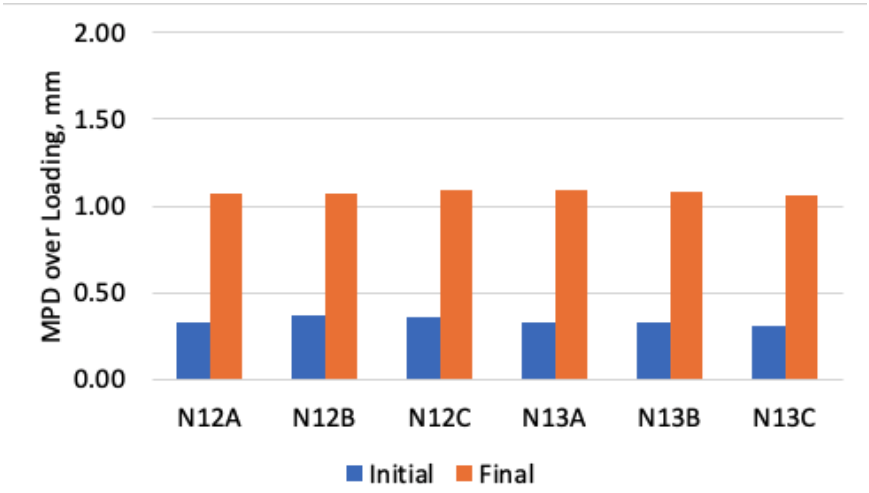

FIGURE 9 Mean texture depth comparison of N12 and N13.

Cracking performance data, depicted in Figure 10, indicates that no measurable cracking distress was observed in any subsection during the initial 15 million ESALs. In N13-B (ARGG), visible crack initiation was noted around 13.5 million ESALs, escalating to 1.3% of the lane area by approximately 15.6 million ESALs. By the end of the monitoring period, at 18.7 million ESALs, N13-C (OGI) exhibited 0.2% lane area cracking.

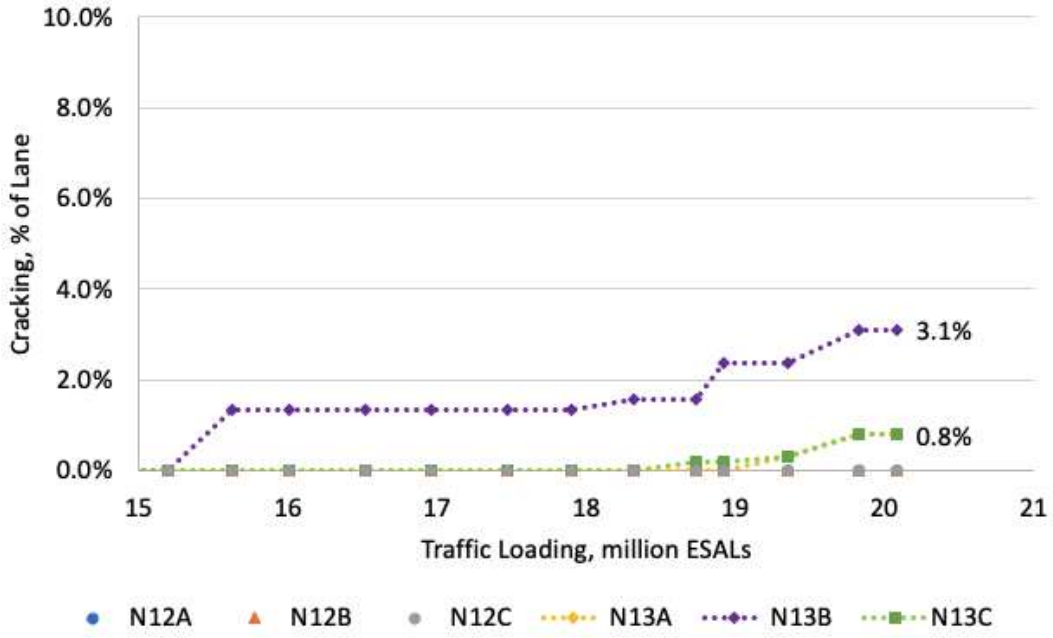

FIGURE 10 Change of cracking percentage of lane area over trafficking.

Figure 11 and Figure 12 view field performance from a balanced mix design perspective, where rutting and cracking are selected as key discriminators. In the 2012 construction cycle, N13 performed better in rutting resistance (OGI), and N12 performed better in reflective cracking (double sand-seal coat). In the 2018 construction cycle, N13-A had lower rutting resistance, and all mixtures performed well in reflective cracking resistance, with half having no reflective cracking (N12-A/B/C).

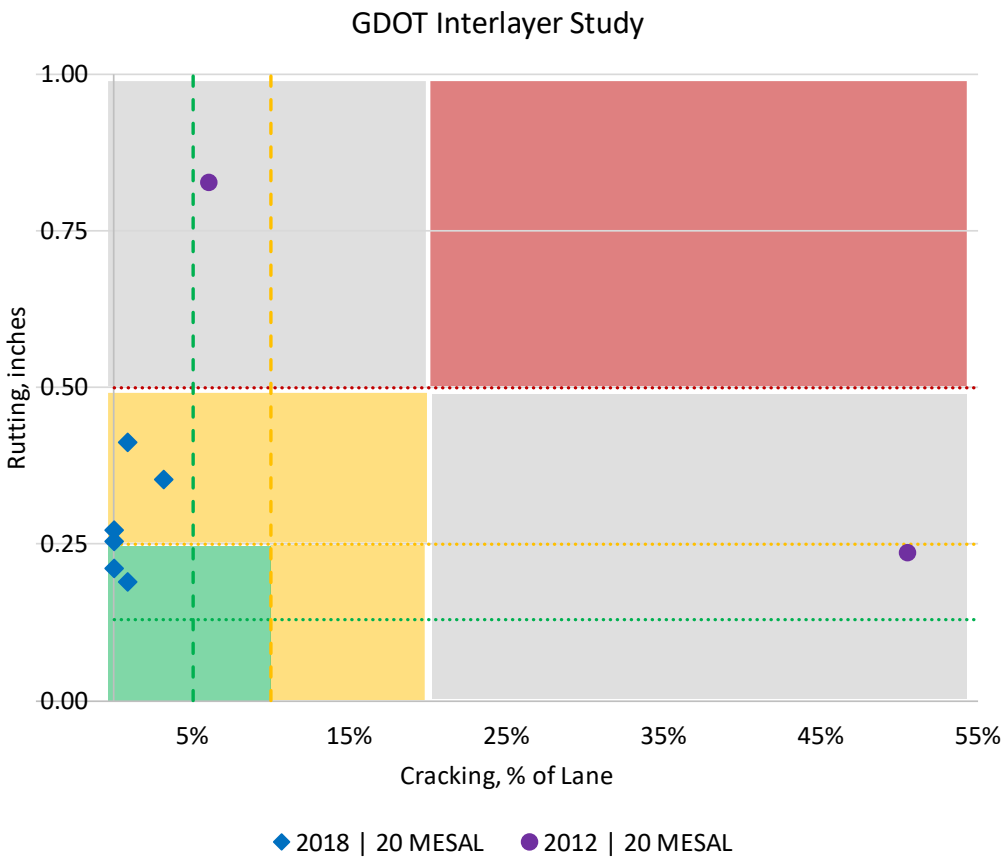

FIGURE 11 Rutting versus cracking field performance for 2012 and 2018 track construction.

The test sections that plot in the areas shaded in green, yellow, and red exhibited good, fair, and poor performance (rutting-cracking), respectively. Test sections that plot in the grey area exhibited poor performance for either rutting or cracking. These thresholds are for comparative purposes and do not directly relate to GDOT criteria.

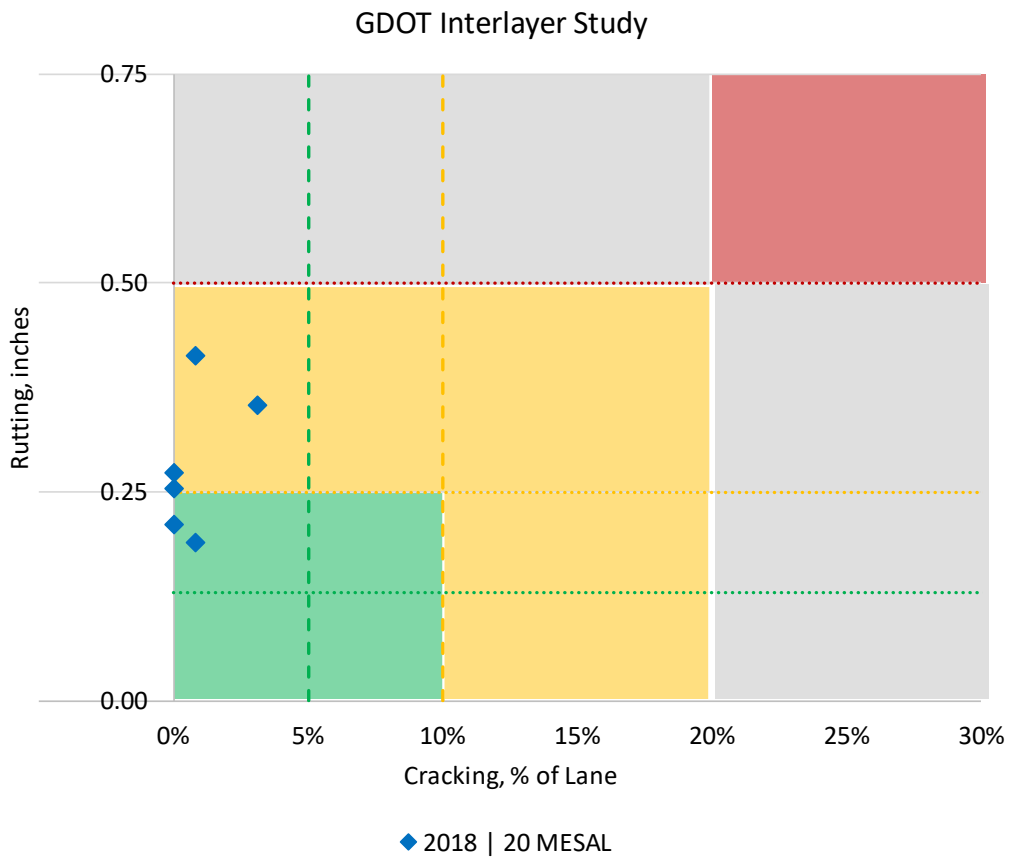

FIGURE 12 Rutting versus cracking field performance for 2018 track construction.

6.4 Pictorial View of Subsection at the End of the Research Cycle

The final surface after loading for each section is shown in Figures 13 through 18. The yellow superimposed line marks the start of each subsection.

FIGURE 13 Subsection N12-A GlasGrid®, 0.24-inch rutting, no cracking (April 2024).

FIGURE 14 Subsection N12-B PETROMAT®, 0.27-inch rutting, no cracking (April 2024).

FIGURE 15 Subsection N12-C virgin chip seal, 0.21-inch rutting, no cracking (April 2024).

FIGURE 16 Subsection N13-A RAP chip seal, 0.41-inch rutting, 0.8% cracking (April 2024).

FIGURE 17 Subsection N13-B ARGG, 0.35-inch rutting, 3.1% cracking (April 2024).

FIGURE 18 Subsection N13-B OGI, 0.19-inch rutting, 0.8% cracking (April 2024).

6.5 Summary of Observations

The six subsections were exposed to 20.08 million ESALs, allowing for a detailed analysis of each treatment method's effectiveness. Performance monitoring included weekly ride quality evaluations, rut depth, surface texture, and cracking. Key findings revealed some variations in the International Roughness Index (IRI), with minimal changes across subsections and

differences in rut depth changes and cracking patterns, indicating similar efficacy of treatment methods.

Key observations—

- A range of interlayer approaches can mitigate reflective cracking.
- An economic analysis should be conducted to evaluate similar approaches.
- This study highlights the importance of tailored treatment strategies to address reflective cracking, considering each pavement structure's specific conditions and demands.
- Consider a lower residual tack coat for a RAP chip seal compared to a Virgin chip seal.
- The ARGG used is likely too flexible for non-surface mix application.

GDOT's research provides valuable insights into the complexities of mitigating reflective cracking in asphalt pavements. By systematically evaluating a range of treatment methods, the study identifies promising solutions and underscores the necessity for ongoing innovation and testing in pavement maintenance and rehabilitation strategies.

7. KENTUCKY TRANSPORTATION CABINET BALANCED MIX DESIGN AND FRICTION EXPERIMENT

Nathan Moore

7.1 Background

In 2021, the Kentucky Transportation Cabinet (KYTC) began investigating implementing a Balanced Mix Design (BMD) specification using the Hamburg Wheel-Tracking Test (HWTT) as the rutting test and the Indirect Tensile Asphalt Cracking Test (IDEAL-CT) for the cracking test. They expected implementing BMD in Kentucky would increase the lifespan of their pavements. However, longer lifespans would lead to more traffic loading and the potential for extended polishing of exposed aggregates on the surface. This required a method for assessing the skid resistance of these pavements, as KYTC personnel were concerned if mixes produced under a BMD specification would have adequate friction at the end of their extended lifespans.

Previous NCAT Test Track research from 2015 to 2021 prompted KYTC to consider taking a closer look at an experiment focusing on friction. The KYTC-sponsored S7A and S7B test sections from the 2015 and 2018 research cycles were developed to study longitudinal joint performance and mix durability of finer mixes compared to coarse mixes. They opted to continue traffic on these sections in 2018 and quickly noticed that while longitudinal joints and mix durability were performing well, friction levels of the sections was much lower than expected (West, et al., 2021). Since the aggregates used to construct these mixes were considered skid-resistant in Kentucky, this outcome was surprising. Nonetheless, after 14 million equivalent single axle loads (ESALS), the monthly locked-wheel friction number (SN at 40 mph with a ribbed tire) dropped below 30 and continued to decline. Friction levels diminished to a point where a friction treatment was necessary to continue traffic. The sections were shot blast to restore friction and remained in place until the end of the cycle. However, this experience highlighted the need for a reliable method to identify mixes with poor potential skid resistance years after placement. Thus, KYTC opted to study the feasibility of designing asphalt mixes to achieve friction targets alongside BMD targets in the laboratory on the 2021 Test Track.

7.2 Objective and Scope

KYTC opted to place two half-sections on S7 (S7A and S7B) in 2021, as shown in Figure 1. The objective was to determine a method for predicting long-term skid resistance on asphalt pavements in the field using laboratory tests during mix design. This concept was referred to as “BMD + Friction” or simply “BMD+”. The idea was to use the BMD framework to design a mix to prevent rutting and cracking while improving skid resistance. Including friction within a BMD framework required proof that laboratory friction results accurately relate to field performance.

This objective required using the IDEAL-CT (ASTM D8225) and HWTT (AASHTO T324) tests for cracking and rutting, respectively, and the Three-Wheel Polishing Device (TWPD) and Dynamic Friction Test (DFT) (ASTM E1911) for accelerating polishing and friction measurement. Laboratory BMD testing was conducted after mixes were aged for 4 hours at 275°F (135°C) Both mixes were expected to pass KYTC volumetric specifications, preliminary IDEAL-CT and HWTT threshold values, and meet specific friction criteria. The S7A mix was intended to have "medium" friction, defined as achieving skid number results in the mid-30s at the end of its lifespan on the Test Track. The S7B mix was intended to have "high" friction, with skid number results in the mid-40s at the end of its cycle on the Test Track.

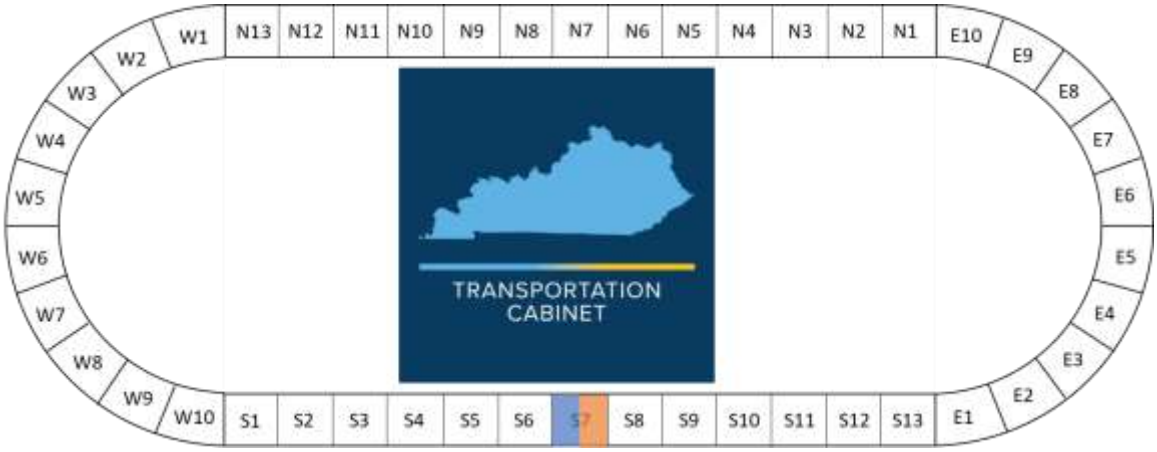

FIGURE 1 Test Track layout of KYTC Sections S7A and S7B.

7.3 Mix Design

Table 1 includes KYTC's initial proposed mix properties, volumetric criteria, and BMD threshold values for S7A and S7B. After some initial trials, it was clear there were too many criteria when combined with the friction targets and that some should be relaxed. The selection of aggregates available to achieve the higher friction target was extremely limited. Thus, air void requirements were expanded to a range between 2.5% and 4.0%. No VMA criterion was set for this work, as it was clear this would add another unnecessary limitation to the process. The only instructions regarding VMA for this work were to ensure that the VMA of the final designs was "reasonable."

TABLE 1 KYTC Criteria for Test Sections

Mix Parameter	Initial Proposed Criteria	Final Design Criteria
Mix NMAS	9.5 mm	9.5 mm
Binder Grade	PG 76-22	PG 76-22
RAP Content	≤ 15%	≤ 15%
Ndes	65	65
% Gmm at Ndes	96.5% (Va = 3.5%)	96.0 to 97.5 (Va between 2.5 – 4.0%)
IDEAL-CT	CT_{Index} ≥ 100	CT_{Index} ≥ 90
HWTT	Rut Depth @ 20K passes < 12.5 mm	Rut Depth @ 20K passes < 12.5 mm

Note: No VMA targets were applied.

Aggregate samples that could meet the necessary criteria, specifically the friction requirements, were sent from dozens of KYTC-approved sources for initial testing. KYTC personnel identified a handful of these sources with a high potential to achieve the necessary friction levels in asphalt mixes. These sources were tested by including them in various investigatory design blends and immediately proceeding with TWPD/DFT testing without regard to volumetric or BMD criteria. Since friction was the primary goal of this research, the aggregate sources were determined before multiple BMD and volumetric mix design trials were attempted. Figure 2 shows initial screening designs and the desired friction ranges to determine which aggregates would be used in the two blends. The aggregates were utilized in various combinations of low, high, and extremely high proportions of the coarse aggregate (retained on #4 sieve) in the total blends. Sandstone and granite were the only two aggregates that achieved the higher friction target. Of the remaining aggregates, the quartzite source was the only one that reached the medium friction target range. Sandstone and quartzite were also selected for further testing.

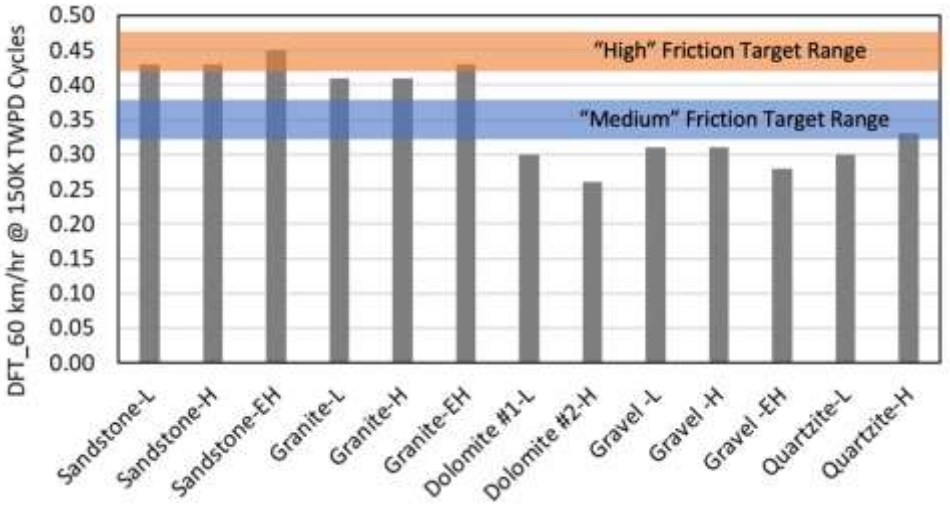

Note: L = low aggregate proportion in blend; H = high aggregate proportion in blend; EH = extremely high aggregate proportion in blend.

FIGURE 2 Initial aggregate blends to identify suitable friction aggregates.

KYTC requested two RAP sources from asphalt contractors in Kentucky, which were sent to NCAT for testing and inclusion in the mixes. Their friction properties were characterized by making lab-compacted slabs with 100% RAP and approximately 2.5% asphalt. The slabs were then polished in the TWPD and tested with the DFT at different intervals to determine their relative friction properties. Figure 3 shows the DFT results of two RAP sources with different friction levels.

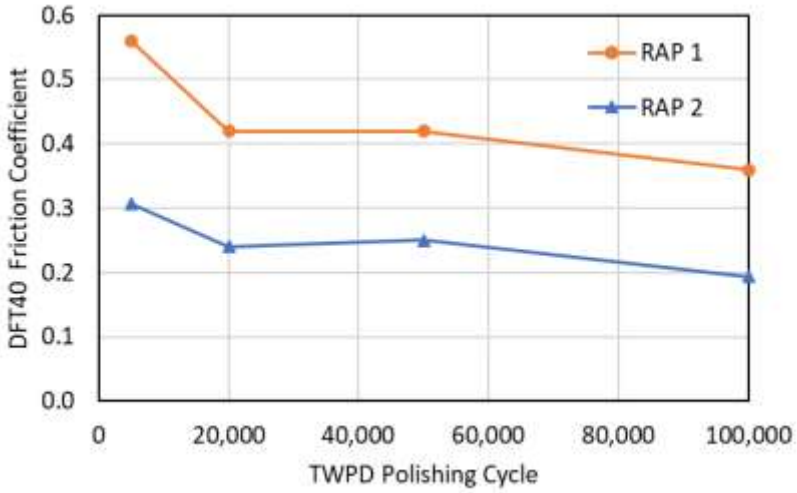

FIGURE 3 Characterization of RAP friction using the TWPD and DFT.

Once the RAP was characterized, aggregate blends were determined (including those shown in Figure 1). Due to multiple design criteria, the following mix design process was developed—

1. Evaluate RAP friction properties using the TWPD and DFT.
2. Establish initial aggregate blends for friction testing with the TWPD and DFT.
    - Estimate the optimum binder content.
    - If desired friction range is not achieved, change aggregate proportions or source.
3. Mix volumetric design specimens and evaluate volumetric results.
    - Use the estimated AC% from Step 2 and bracket by ± 0.5%.
    - Stop if air voids are too low.
    - Removing binder drastically decreases the probability of passing IDEAL-CT requirements.
4. Mix BMD specimens at maximum allowable AC% and check IDEAL-CT criteria.
    - If the design fails at the highest AC%, a blend change is needed.
5. Mix BMD specimens and check HWTT criteria.
    - If HWTT fails, retest CT_{Index} at a lower AC% and verify passing results before retesting HWTT. (This never occurred during the design process for these sections.)

In total, 26 unique design blends with six different coarse aggregate sources were tested for the two sections. This included 13 attempts with the sandstone aggregate to achieve a high friction mix and 5 blends with the quartzite aggregate for the medium friction mix. Unused trial blends failed for various reasons, such as failing DFT results, air voids out of the required range, or CT_{Index} below the minimum of 90. Leading up to construction, the best high friction mix design yielded a CT_{Index} of 91 with air voids of 2.8%. KYTC elected to relax the IDEAL-CT criterion from 100 to 90 and proceed with this mix. Table 2 shows a summary of the final JMFs for the two mixes.

TABLE 2 Mix Design Data of S7A (Medium Friction) and S7B (High Friction)

Sieve (in.)	Job Mix Design	
	S7A	S7B
25 mm (1”)	100	100
19 mm (3/4”)	100	100
12.5 mm (1/2")	100	100
9.5 mm (3/8”)	92	90
4.75 mm (#4)	51	54
2.36 mm (#8)	35	32
1.18 mm (#16)	24	24
0.60 mm (#30)	17	19
0.30 mm (#50)	12	16
0.15 mm (#100)	9	9
0.075 mm (#200)	6.4	6.0
Design Gyration (N_{design})	65	65
NMAS (mm)	9.5	9.5
Total Binder Content (%)	5.8	5.9
Virgin Binder Grade	PG 76-22	PG 76-22
RAP Binder Ratio (%)	17	10
Air Voids (%)	3.4	2.8
Blend G_{sb}	2.631	2.598
G_{mm}	2.465	2.404
G_{mb}	2.382	2.337
VMA (G_{sb}) (%)	14.7	15.2
V_{be}	11.3	12.4
VFA	77	83
Dust Proportion	1.3	1.1

The S7A and S7B mixes had asphalt contents of 5.8% and 5.9%, respectively. Both were coarse-graded mixes. The design air voids for S7A were 3.4% with a VMA of 14.7%. The design air voids and VMA for S7B were 2.8% and 15.2%, respectively. Both mixes had high VFAs due to the low air voids and high VMA. The dust proportion of S7A was 1.3, which was higher than the AASHTO M323 limit but within the KYTC limit of 0.6—1.4, while S7B had a dust proportion of 1.1. S7A

included 15% RAP (17% recycled binder replacement) and S7B contained 10% RAP (10% recycled binder replacement).

Figure 3 shows BMD results from both mix designs on a performance space diagram. The "sweet zone" represents the combination of test results that pass both BMD criteria. The original CT_{Index} target was relaxed from 100, as previously discussed. The CT_{Index} results for S7A and S7B were 110 and 91, respectively.

HWTT was conducted on Section S7A's final design (rut depths = 3.0 mm after 20K passes) but not S7B. The difficult and time-consuming process of designing the higher friction section continued until the day before paving, and the most promising blend had still not been tested with the HWTT. However, previous testing of a similar design resulted in rut depths of 5.9 mm after 20K passes. Therefore, it was assumed rutting would not be a concern since the aggregate structure was similar to the previous design and the binder grade was a PG 76-22. The rutting data representing S7B in Figure 4 are from the design similar to S7B, which already had HWTT results.

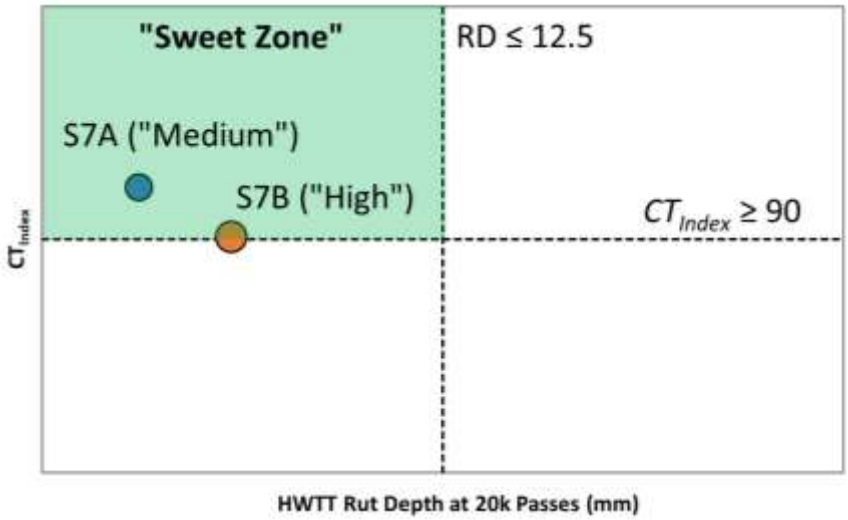

FIGURE 4 BMD performance diagram from S7A and S7B mix design testing.

7.4 Mix Production and Construction

The S7A "medium" friction mix was produced and placed August 19, 2021, with a high temperature of 92°F, a low temperature of 75°F, and no 24-hr rainfall. The mix had an average production temperature of 325°F and in-place density of 92.9%. Figure 5 shows laydown and compaction of Section S7A.

FIGURE 5 Construction of Section S7A.

The S7B “high” friction mix was also produced and placed August 19, 2021, with a high temperature of 92°F, a low temperature of 75°F, and no 24-hr rainfall. The mix had an average production temperature of 325°F and in-place density of 92.9%, which matched Section S7A. Figure 6 shows the laydown and compaction of S7B. Figure 7 shows the transition line between the two sections after six months of traffic, with S7A (with quartzite coarse aggregate) on the left and S7B (with sandstone coarse aggregate) on the right.

FIGURE 6 Construction of Section S7B.

FIGURE 7 Transition from S7A (left) to S7B (right).

Table 3 contains the QC data for S7A and S7B alongside the original JMF for comparison. The S7A mix ran slightly coarser than designed from the 3/8" (9.5 mm) sieve down to the #30 (0.60 mm) sieve, and S7B was significantly finer on the percent passing the #100 and #200 (0.15 mm and 0.075 mm) sieves. The dust in the S7B mix was 1.8% higher than the design, possibly due to the sandstone being a softer aggregate and breaking down in the plant during production. This pushed the dust proportion from 1.3 to 1.5, significantly outside of AASHTO M323 range and greater than KYTC's maximum allowable dust proportion of 1.4. The AC% measured during production dropped by 0.1% from design for S7A and 0.2% for S7B. The dust also influenced a drop in air voids to 2.1%. VMA dropped in both sections by approximately 1.0%

TABLE 3 Quality Control Data of S7A ("Medium" Friction) and S7B ("High") Mixes

Sieve (in.)	S7A		S7B	
	Design	QC	Design	QC
25 mm (1")	100	100	100	100
19 mm (3/4")	100	100	100	100
12.5 mm (1/2")	100	99	100	99
9.5 mm (3/8")	92	90	90	93
4.75 mm (#4)	51	47	54	55
2.36 mm (#8)	35	31	32	28
1.18 mm (#16)	24	22	24	24
0.60 mm (#30)	17	16	19	20
0.30 mm (#50)	12	12	16	16
0.15 mm (#100)	9	8	9	11
0.075 mm (#200)	6.4	6.2	6.0	7.8
Design Gyration (N_{design})	65	65	65	65
Total Binder Content (%)	5.8	5.7	5.9	5.7
Air Voids (%)	3.4	2.4	2.8	2.1
G_{sb}	2.631	2.620	2.598	2.604
G_{mm}	2.465	2.462	2.404	2.417
G_{mb}	2.382	2.402	2.337	2.367
VMA (G_{sb}) (%)	14.7	13.5	15.2	14.3
V_{be}	11.3	11.1	12.4	12.2
VFA	77	82	83	85
Dust Proportion	1.3	1.3	1.1	1.5

BMD tests were conducted on these mixes during production and results were returned within 4 or 5 hours of sampling. No additional conditioning or aging was performed on the mix samples. Thus, despite S7B having failing volumetrics in terms of dust proportion, this mix was quickly evaluated to determine if it decreased in cracking or rutting resistance. The IDEAL-CT and High Temperature Indirect Tensile Strength test (HT-IDT) were used for this process. Although not part of the original testing plan, the HT-IDT was used to test the rutting potential of every BMD mix produced on the 2021 Test Track. The results from samples taken during production are shown in Figure 8. Both mixes produced CT_{Index} values greater than 100. A summary of the results is provided in Table 4. BMD results from both sections were acceptable to the research team.

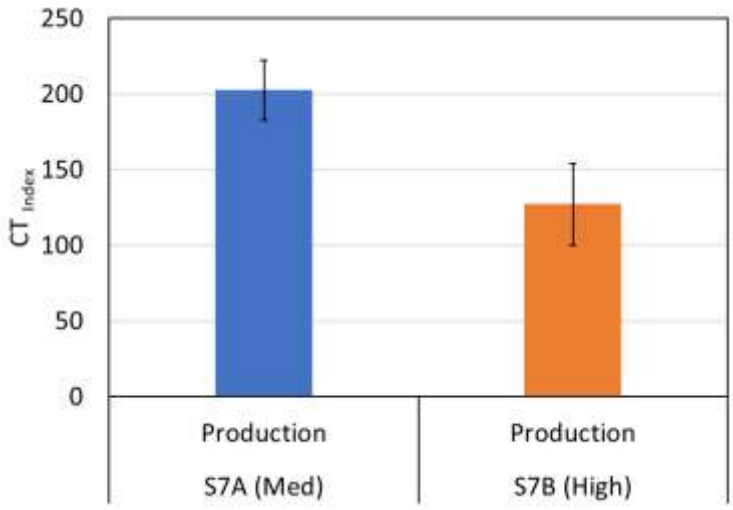

FIGURE 8 IDEAL-CT results from S7A and S7B BMD production testing.

TABLE 4 HT-IDT Results from S7A and S7B BMD Production Testing

Mix ID	N	ITS (psi)		
		Avg.	St. Dev.	CV (%)
S7A-Production	3	31.0	1.8	5.8
S7B-Production	3	35.0	0.3	1.0

7.5 Laboratory Testing and Data Analysis

A production sample was taken from each mix during construction and transported to the NCAT laboratory for future testing. The mix was later reheated in metal buckets to the compaction temperature to produce plant-mixed, lab-compacted (PMLC) performance testing results to compare to the lab-mixed, lab-compacted (LMLC) results from mix design. HWTT and IDEAL-CT were conducted to evaluate rutting and cracking resistance, respectively, of the mixes in Sections S7A and S7B. Figure 9 shows the results of these tests plotted in the same performance space diagram as in Figure 4. Arrows indicate the changes from design to reheated PMLC results. The reheated S7A PMLC mix remained in the "sweet zone," passing both HWTT and IDEAL-CT criteria. The S7B reheated PMLC mix dipped below the CT_{Index} threshold to 74 but remained well below the HWTT threshold. Field evaluation was necessary to determine the quality of the S7B mix and the validity of the IDEAL-CT threshold of 90 as a performance threshold for the KYTC mixes.

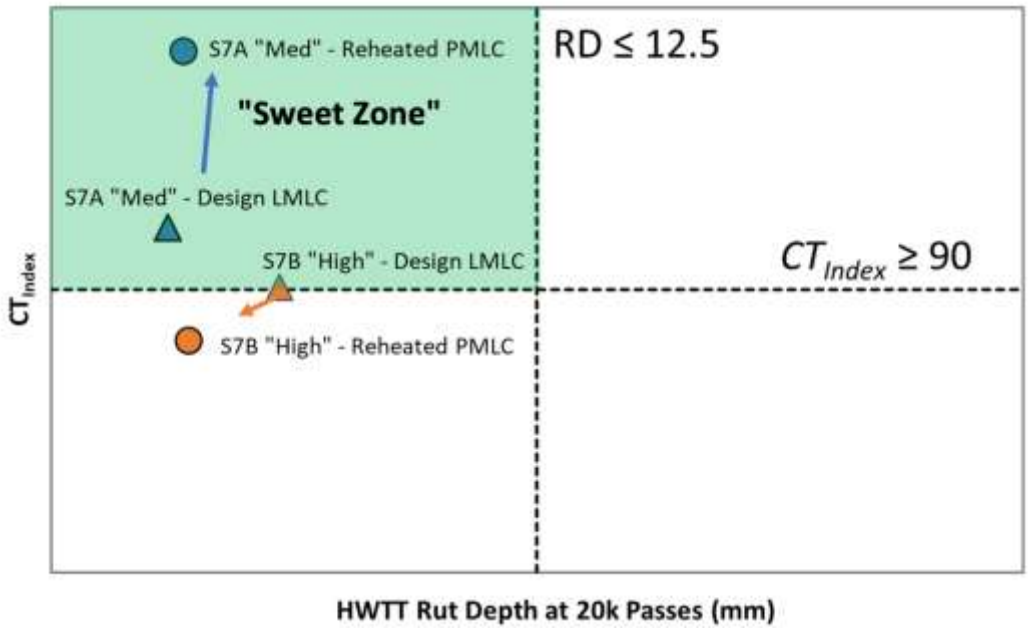

FIGURE 9 BMD performance diagram from S7A and S7B reheated mix testing.

Figure 10 displays a comparison of LMLC and PMLC DFT results on slabs compacted from loose mix. Both demonstrated slight declines in the DFT results from the mix design to production. However, the drop was minor. In general, this indicates the DFT may not be sensitive to minor mixture changes. This behavior was also noticed during the mix design process. Asphalt mixture friction is more sensitive to aggregate properties and major gradation changes, which affect texture, rather than volumetric changes (AASHTO, 2022).

Section S7A produced DFT results at 40 km/hr of 0.34 compared to 0.37 from design. Showing a smaller magnitude decline, the S7B mix produced DFT results of 0.42 compared to 0.43 from design. Both mixes remained in the expected ranges of mid-30s for S7A and mid-40s for S7B based on DFT and TWPD testing. Ultimately, friction testing in the field would verify or refute these findings.

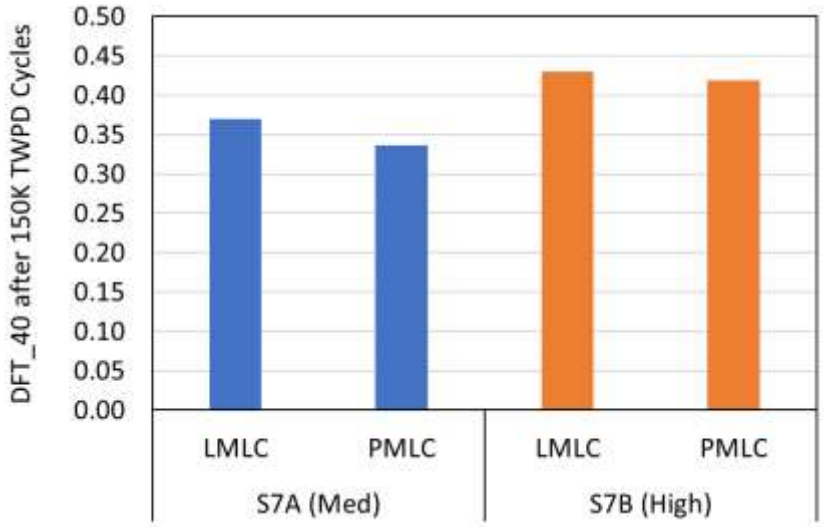

FIGURE 10 Comparison of S7A and S7B LMLC and PMLC DFT results.

7.6 Field Performance

Truck traffic on the 2021 NCAT Test Track began in November 2021. Throughout trafficking, surface cracking, rutting, smoothness, and surface texture were monitored weekly using an automated pavement condition survey vehicle. Friction was measured monthly using a locked-wheel friction trailer with a ribbed tire at 40 mph (SN40R). Figure 11 displays the skid performance of the two KYTC-sponsored sections. The orange and blue shaded regions indicate the expected range of final skid resistance performance for each section at the end of 10 million ESALs based on the mix design DFT results (i.e. the shaded ranges represent the DFT results from design x 100 ± ≈ 3 SN units). Until 8.2 million ESALs, with only a few exceptions, the sections had friction performance that almost perfectly matched expectations. In November 2023, the friction performance of both sections dipped below their expected performance ranges after 8.5 million ESALs but recovered to near or above the midpoint of the expected ranges at 10 million ESALs. It is expected that lack of precipitation was responsible for the temporary friction decline near the end of the research cycle. Based on historical skid testing on the NCAT Test Track, it is expected that both of these mixes will not polish much further and the friction levels will remain near their current SN values for the duration of their experimental usage on the track.

Regardless, the average difference between the sections was 5.1 skid units. This is the same difference found in the DFT results from the LMLC slabs of the two mixes (0.05 DFT units x 100). Only once in 26 tests did the skid resistance of the medium friction mix (S7A) surpass the high friction mix (S7B), and at that point (6.9 million ESALs) they were only 0.4 SN units different. Therefore, the DFT demonstrated the ability to identify mixes with superior friction performance in the laboratory mix design process.

FIGURE 11 SN40R performance of S7A and S7B.

Figure 12 shows the Mean Profile Depth (MPD) of the sections. Section S7A was 8% coarser on the #4 sieve compared to Section S7B, as previously shown in Table 3. The coarser gradation of S7A compared to S7B is likely the reason for the increased macrotexture. The texture of both sections slightly decreased over time, likely due to densification of the surface mixes and lack of raveling due to sufficient asphalt contents. The texture of both sections is as expected when compared to previous Test Track sections with similar gradations (Moore, 2023).

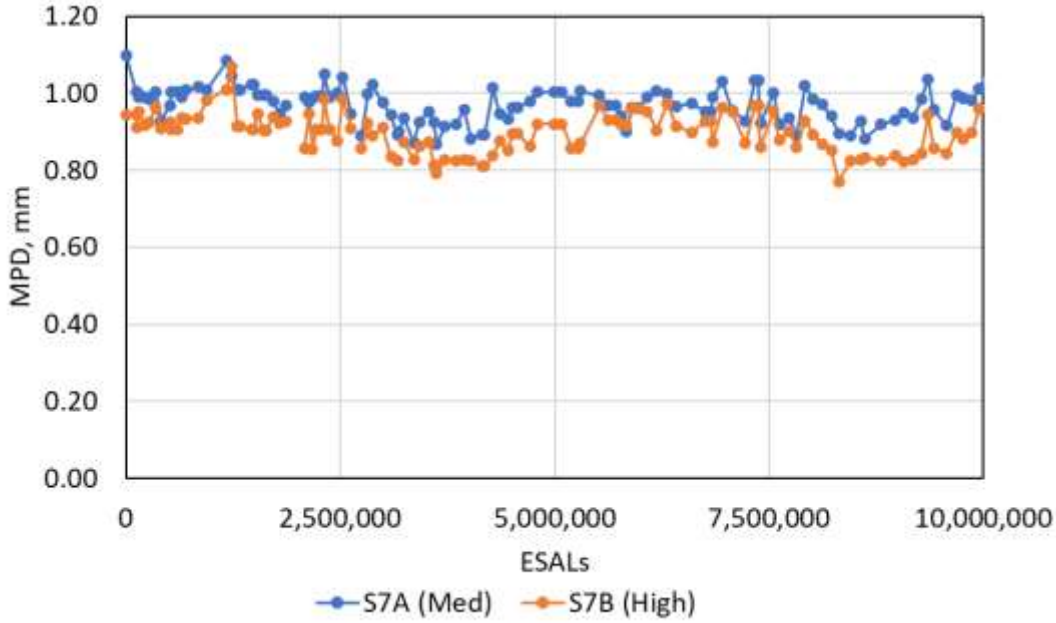

FIGURE 12 MPD performance of S7A and S7B.

Figures 13-15 show the cracking, rutting, and rideability of the two sections. Figure 13 highlights the lack of cracking in either section after 10 million ESALs. Figure 14 shows the rutting performance of Sections S7A and S7B. At 10 million ESALs, neither section had rut depths more than 0.2 inches, well below the failure threshold of 0.5 inches used at the track. Therefore, the BMD tests accurately identified both mixes as resistant to cracking and rutting up to 10 million ESALs on the NCAT Test Track.

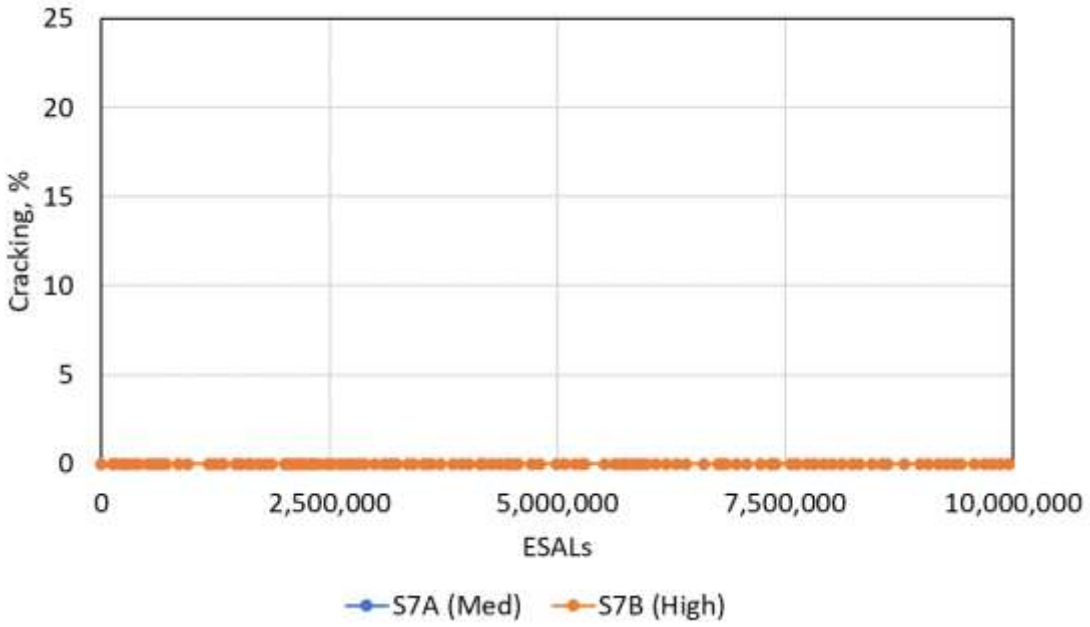

FIGURE 13 Cracking performance for Sections S7A and S7B.

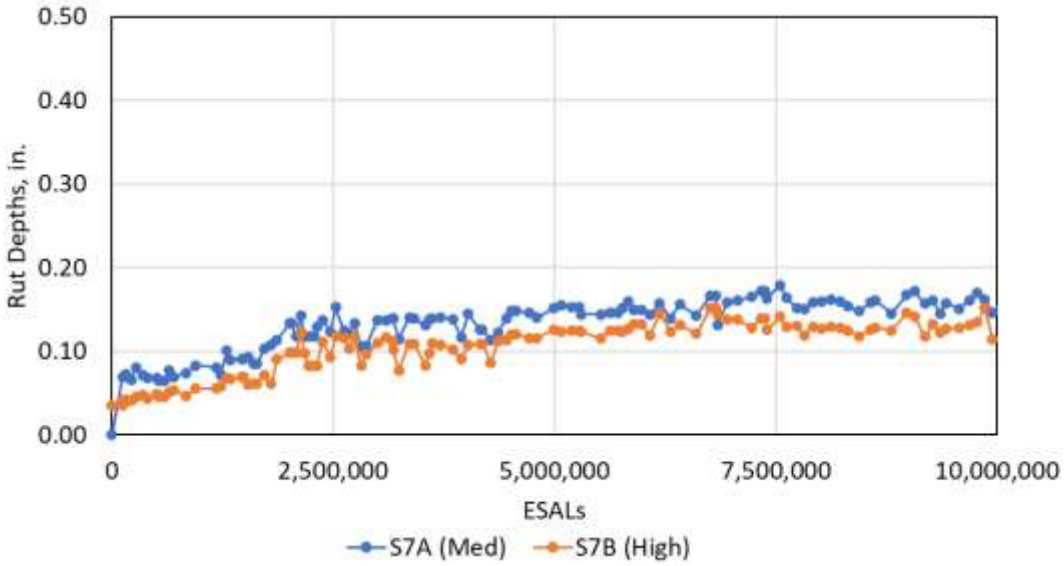

FIGURE 14 Rutting performance of Sections S7A and S7B.

Figure 15 displays rideability, expressed as IRI as in/mile. In both cases, ride performance was good. S7A had relatively consistent ride quality, except for the noise in the data from approximately 6 to 7 million ESALS. An adjacent section was repaved during this time which caused the temporary bump in the overall IRI measurements due to the short section length. Discounting this event, the ride in Section S7 remained between 70 and 80 in/mile until the end of the experiment. The ride in S7B was even smoother, hovering consistently between 55 and 65 in/mile.

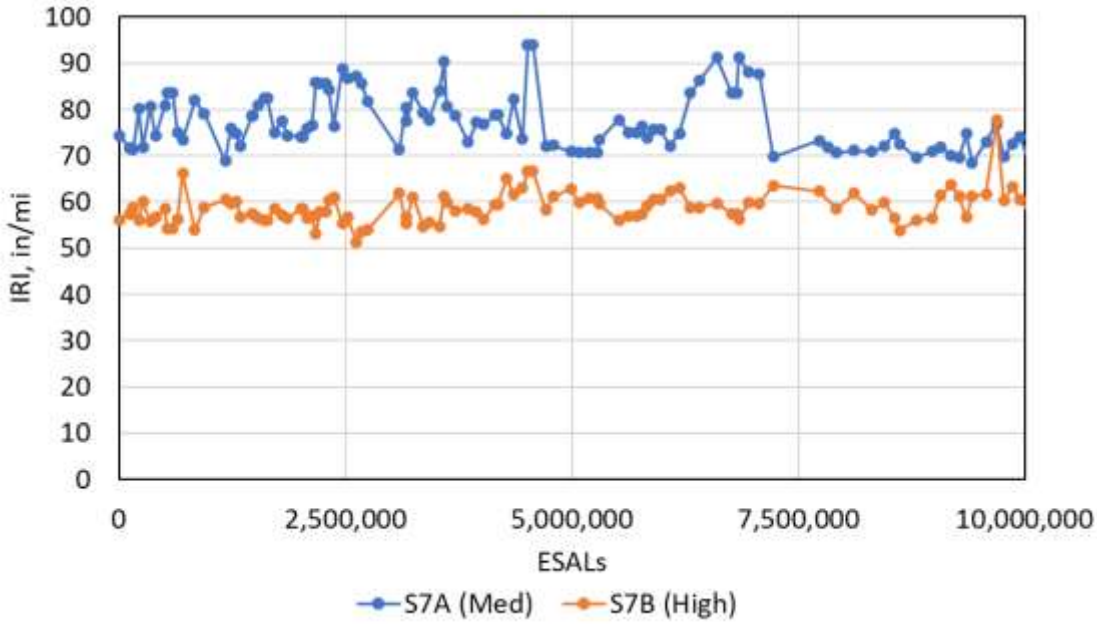

FIGURE 15 IRI performance of Sections S7A and S7B.

7.7 Conclusions and Recommendations

Based on the laboratory and field performance results after 10 million ESALs, the following conclusions and recommendations are made.

- The S7A and S7B BMD results accurately relate to field performance in terms of little to no rutting or cracking for either section.
- S7B demonstrated suitable field performance despite the volumetric properties of the plant-produced mix being considered failures by KYTC.
- DFT results from laboratory-produced asphalt slabs can relate to field performance of the same mix and discriminate between mixes with varying friction characteristics.
- The TWPD/DFT system can be used in a mix design framework similar to BMD to eliminate mixes with poor friction properties and create mixes that will meet minimum friction levels in the field.

- Blanket aggregate classifications should be replaced with DFT criteria on asphalt mixes to avoid incorrect predictions of pavement performance based on unreliable aggregate tests.
- If friction is added to a mix design specification, volumetric requirements must be relaxed. Friction is primarily affected by aggregate type and gradation, and locking in an aggregate type or gradation to meet friction requirements will limit mix design options. Strict volumetric requirements will further restrict mix design options and prevent mixes with a potential for acceptable performance from being produced.
- Sections S7A and S7B are recommended for traffic continuation in the next research cycle to further monitor their performance and the validity of the BMD thresholds used in this experiment.
- KYTC should consider shot blasting these sections to add data to their previous sections that required shot blasting due to low friction. Shot blasting these sections would provide KYTC with estimations of expected long-term frictional life extension benefits of shot blasting of sections with varying friction levels (low, medium, and high). Shot blasting is not expected to affect the cracking or rutting potential of the sections.

7.8 References

Guide for Pavement Friction, 2nd Edition. American Association of State Highway and Transportation Officials. Washington, D.C., 2022.

Moore, N. *Friction: Dynamics of Macro-Texture related to Friction*. Asphalt Technology News, 35(2). National Center for Asphalt Technology at Auburn University, 2023.

West, R., D. Timm, B. Powell, N. Tran, F. Yin, B. Bowers, C. Rodezno, F. Leiva, A. Vargas, F. Gu, R. Moraes, and M. Nakhaei. *NCAT Report 21-03: Phase VII (2018-2021) NCAT Test Track Findings*. National Center for Asphalt Technology at Auburn University, 2021.

8. MISSISSIPPI DEPARTMENT OF TRANSPORTATION STABILIZED FOUNDATION PAVEMENT

Dr. David Timm

8.1 Introduction

As documented in the Phase VII Test Track report (West et al., 2021), challenging soil conditions are sometimes mitigated by stabilizing with cementitious material to improve the load carrying capacity of flexible pavements. The Mississippi DOT (MDOT) routinely uses this strategy by cement- or lime-stabilization of soils and other granular materials. Though often used by MDOT and other state agencies, there is little data available to support mechanistic-empirical (M-E) analysis and design of these stabilized foundation pavements.

To expand the knowledge base of stabilized foundation pavements, MDOT sponsored a section (S2) for the 2018 NCAT Test Track research cycle, which continued into the 2021 research cycle due to good performance. As previously documented (West et al., 2021), this section features subgrade and base materials local to Mississippi that were hauled to and placed at the Test Track. These materials were stabilized in place with lime (subgrade) and cement (base) over which asphalt concrete (AC) layers were constructed. The materials are representative of those often stabilized in Mississippi due to their relatively low quality for road building. Pavement response sensors were embedded during construction to enable direct mechanistic response measurement under live truck traffic and falling weight deflectometer (FWD) loading.

The short-term goal of the section was to fundamentally characterize the structural characteristics of the stabilized foundation pavement, measure its response to environmental changes, and track surface performance. The experiment's long-term goal is to gather the necessary M-E properties to perform transfer function calibration in order to provide more accurate distress predictions for this pavement type. As will be covered in this chapter, the pavement has not yet experienced any significant distress or performance deterioration, other than some very minor between wheelpath cracking, during the first two test cycles (approximately 20 million equivalent single axle loads (ESALs)), so additional trafficking is recommended for the next test cycle.

8.2 Construction and Instrumentation

As the construction and instrumentation of the section were extensively documented in the 2018 Test Track report, this section will only provide a brief overview. Interested readers can refer to the earlier report (West et al., 2021) for more detail.

The cross-section of Section S2 is shown in Figure 1, where the thicknesses are based on average as-built surveyed depths from 12 locations across the section. The pavement section includes four AC layers over a cement treated base (CTB), over lime treated soil (LTS), on top of a Mississippi subgrade (MS Subgrade). Asphalt strain gauges (ASGs) were installed to measure flexural strains at the bottom of the AC in the direction of travel, while the earth pressure cells

(EPCs) were placed to measure vertical compressive stresses at critical depths (AC/CTB interface, CTB/LTS interface, and LTS/MS subgrade interface). Temperature probes were installed vertically to measure temperatures at the top, middle, and bottom of the AC and 3 inches into the cement treated layer.

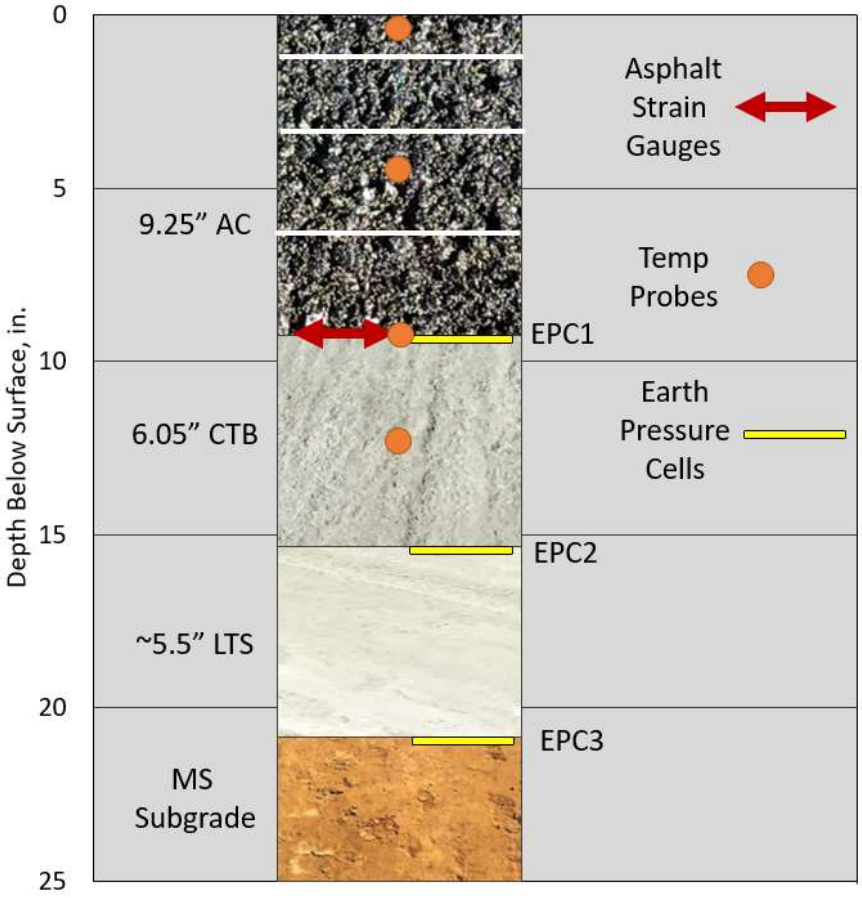

FIGURE 1. Section S2 cross-section (West et al., 2021).

8.3 Trafficking and Field Performance

Trafficking of the first test cycle began on November 26, 2018 and concluded on February 27, 2021, after applying 10,023,907 ESALs. The section was then left in place with no trafficking, while other sections were subjected to forensic investigation and reconstruction in preparation for the 2021 research cycle. Trafficking of that cycle began November 10, 2021 and concluded April 5, 2024, after applying an additional 10,052,142 ESALs, for a total of 20.1 million ESALs over both test cycles.

As with all other Test Track sections, Section S2 was measured frequently for rutting and roughness during the two research cycles and was inspected for cracking on a regular basis. Figure 2 shows the section on February 8, 2021, near the end of the first two-year trafficking cycle. Figure 3 shows the section after trafficking was completed in April, 2024. The following

sections document the field performance both in terms of time and traffic application (expressed as ESALs).

FIGURE 2. Test Section S2 near the end of first trafficking cycle.

FIGURE 3. Test Section S2 after completion of second trafficking cycle.

8.3.1 Rutting

Rutting progression is presented in Figure 4, where rut depths are shown on the left vertical axis and cumulative ESALs are on the right vertical axis. The x-axis spans both test cycles. Note that the flattened part of the ESAL series represents the break in traffic between test cycles.

Rutting increased primarily during the first spring and summer (April 2019 through September 2019) up to about 0.10 inches. At that point, it leveled off. The section did not experience increased rutting through the second summer, maintaining rut depths around 0.10 inches. The increase at the very end of the first test cycle from 0.10" to 0.15" is likely related to a change in data acquisition software rather than a true increase in rutting, as this jump was not evident in manual rut depth measurement. In either case, rutting did not exceed 0.20" after the application of 10 million ESALs and most likely leveled off at 0.10" after primary rutting occurred during the first summer. When ESAL applications resumed in 2021, there was no significant increase in rutting over time. This is likely due to primary consolidation of the mix having already been achieved during the first test cycle and some aging of the materials limiting the amount of additional AC rutting. Since the Test Track defines rutting failure at 0.5", and MDOT would not address rutting until it exceeded 0.2" on interstate sections and 0.25" on non-interstate sections, the rutting performance of the section through 20 million ESALs is considered excellent. This is not unexpected, since rutting is not a primary concern for stabilized foundation pavement.

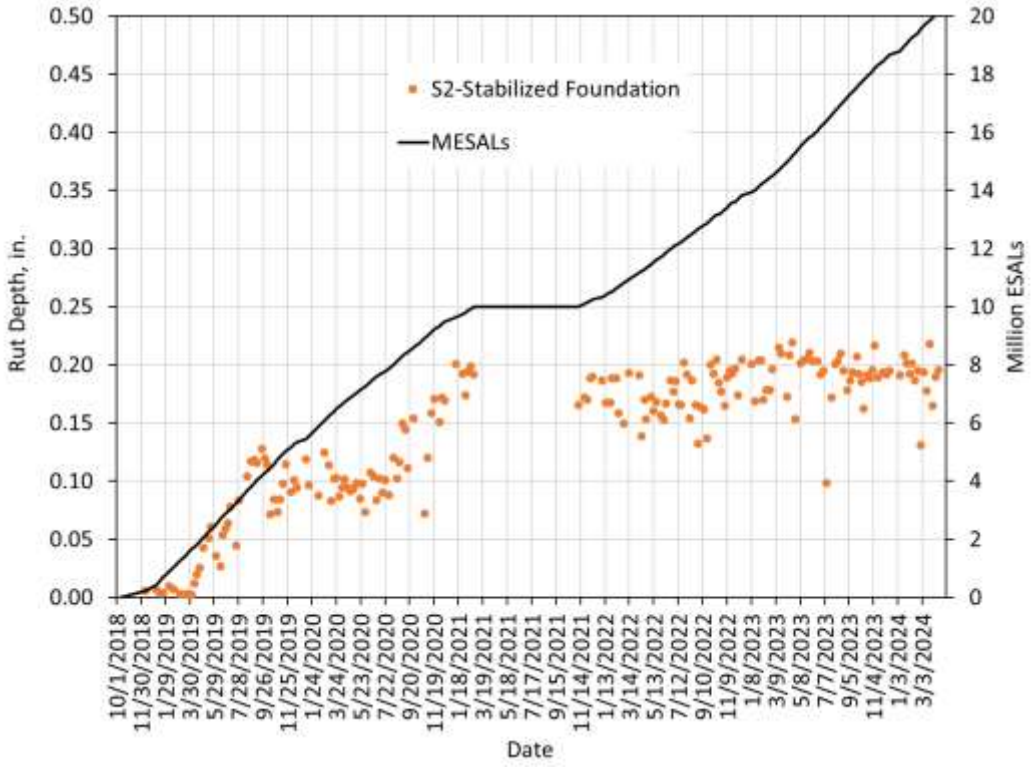

FIGURE 4. Section S2 rutting performance.

8.3.2 Cracking

No cracking was observed in the section after the first 2 years and 10 million ESALs. There were, however, a few randomly located pop-outs. Figure 5 shows one of the largest pop-outs. The time this pop-out occurred is unknown, and it was not deemed detrimental to the section's structural integrity.

FIGURE 5 Pop-out in Section S2.

Minor longitudinal between-wheelpath cracking developed during the second test cycle. The cracking was first observed April 24, 2023 at 15.3 million ESALs. Figure 5 shows one of the larger cracks. In subsequent months, the cracking would literally disappear depending on the time of year. This was especially evident during warmer months, and it was assumed the asphalt was able to flow back together, or self heal, at elevated temperatures. This also supported the notion that the cracking was top-down, though no forensics were performed on the cracks. At the conclusion of the test cycle, this cracking represented 1% of the lane area and was not considered detrimental to the section's structural integrity.

FIGURE 5 Minor between-wheelpath longitudinal cracking in S2.

8.3.3 Ride Quality

Ride quality was nearly constant over traffic application. As shown in Figure 6, IRI is plotted on the left vertical axis, and cumulative ESALs are on the right vertical axis. The IRI varied between 60 and 70 in/mile with no significant increase over time. Overall, the section exhibited excellent ride quality through 20 million ESALs.

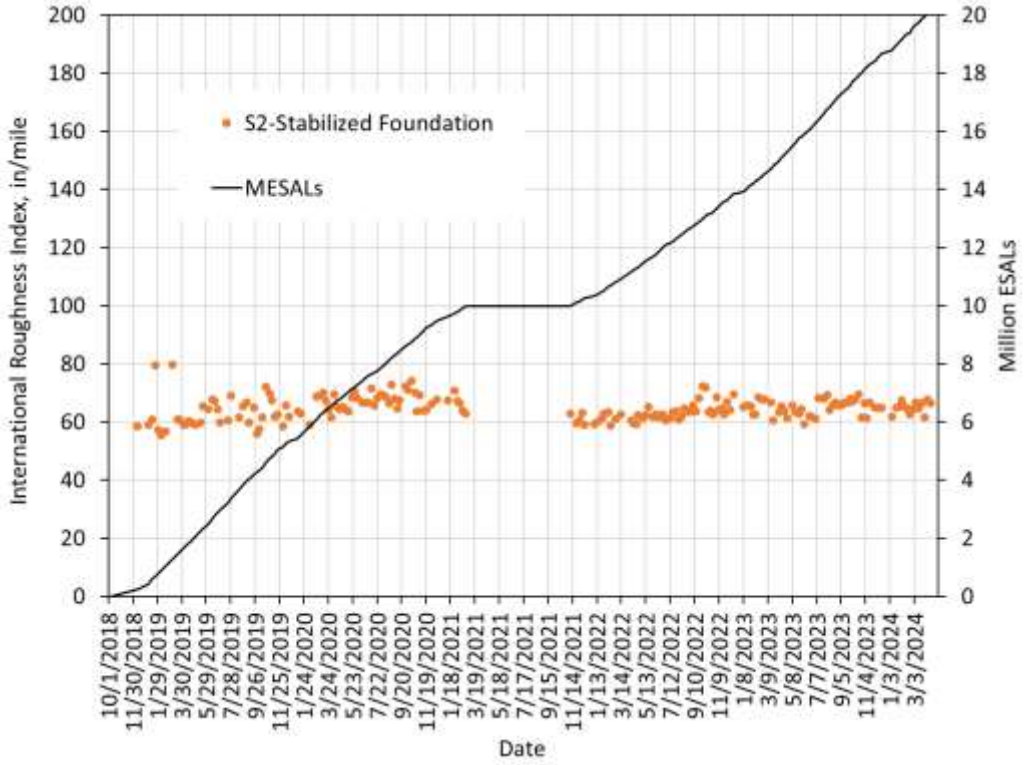

FIGURE 6 Section S2 smoothness data.

8.4 Structural Response Characterization

The performance data indicated excellent performance through 20 million ESALs despite minor longitudinal between-wheelpath cracking. The next portion of this investigation was to characterize the structural response through direct measurement under truck loading and FWD testing.

During the experiment, structural response was measured on a weekly basis using the asphalt strain gauges (ASGs) and earth pressure cells (EPCs) embedded during construction. Response measurements consisted of at least 15 truck passes from which the 95th percentile measurement was used to represent the “best hit” on that collection day. Truck speed was approximately 45 mph during each measurement. Though all axles were measured, only single axle strain responses are presented herein for brevity. Despite some variation, each axle typically weighed approximately 20,000 lbs with dual tires. The data presented below

represents measurements normalized to a reference temperature of 68°F. This process has been previously documented (McCarty, 2019).

8.4.1 Pressure Measurements

As detailed in Figure 1, three earth pressure cells were installed to measure the vertical pressure at the top of the cement treated base (CTB), at the top of the lime treated soil (LTS), and at the top of the Mississippi subgrade (Subgrade), respectively. Figure 7 shows the temperature-normalized pressure measurements from both test cycles versus the measurement date, following the process described by McCarty (2019). The gap in the middle of each data set represents the break between test cycles.

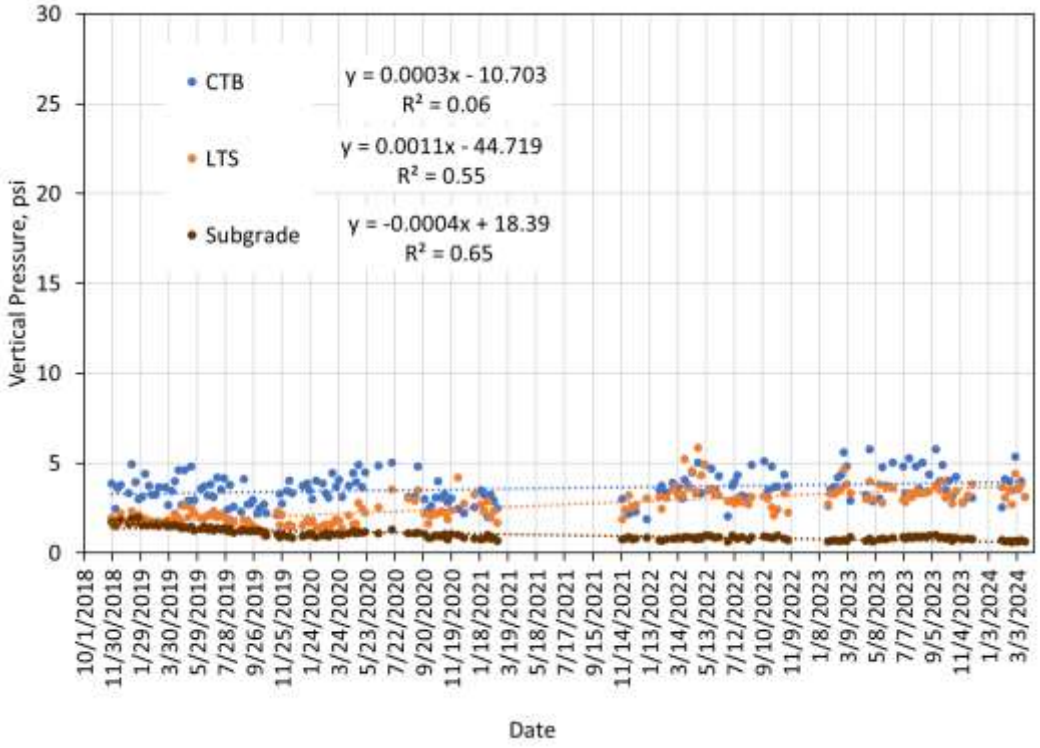

FIGURE 7 Vertical pressure in Section S2 at 68°F versus date.

While all the pressures are low (i.e., < 5 psi), the data in Figure 7 clearly show the vertical stress gradient versus depth. The average pressure on top of the CTB is about 3.6 psi, the average pressure on top of the LTS is about 2.6 psi, and the average pressure on top of the subgrade is only about 1.0 psi. In each case, the slope of the trendline on the data is relatively flat, meaning not much change in pressure measurements over time, which indicates a structurally healthy test section. If cracking were present, the pressures would increase due to loss of structural integrity.

8.4.2 Strain Measurements

As well documented in the 2018 Test Track report (West et al., 2021), maximum tensile strain levels in Section S2 tended to decrease with increasing temperature. Extensive earlier analysis and simulation work demonstrated this behavior was a function of the stabilized base providing excessive restraint to the bending of the AC layer. This caused a predominantly compressive mode at elevated temperatures when the AC modulus was less than the stabilized base modulus. That analysis is not repeated here, but the behavior was also observed during the 2021 research cycle.

Figure 8 shows the maximum tensile strain versus mid-depth AC temperature for both test cycles, where there is a clear downward trend with increasing mid-depth temperature. Strain levels are relatively low, ranging between 20 to 100 me. Tensile strains in this range are unlikely to initiate cracking at the bottom of the AC, since a well-accepted modern endurance limit for AC to prevent cracking is 100 me (Newcomb, et al., 2020).

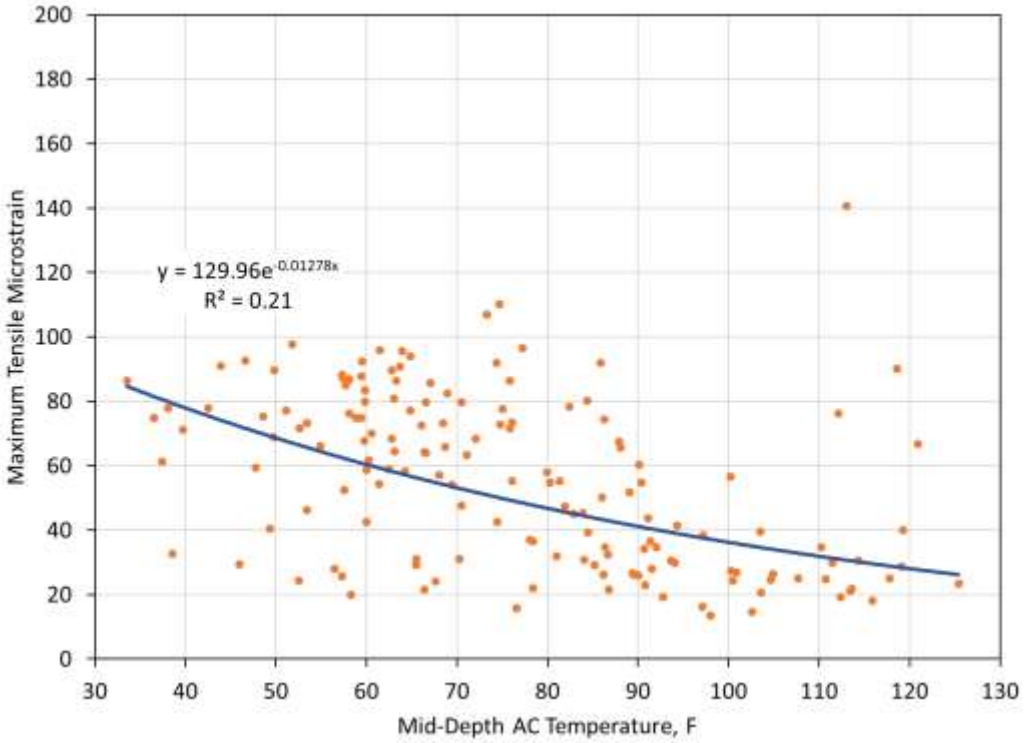

FIGURE 8 Section S2 maximum tensile strain versus mid-depth AC temperature.

Following established procedures from the Test Track (West et al., 2021), and as was done with the above pressure data, maximum tensile strain levels from Figure 8 were normalized to a reference temperature of 68°F and plotted versus the measurement date in Figure 9. Though there appears to be a downward shift in the data, the fitted trendline shows, on average, less

than a 10 microstrain decrease since the start of the experiment. This will be monitored into the next test cycle, but to date, these strain levels indicate a structurally healthy test section.

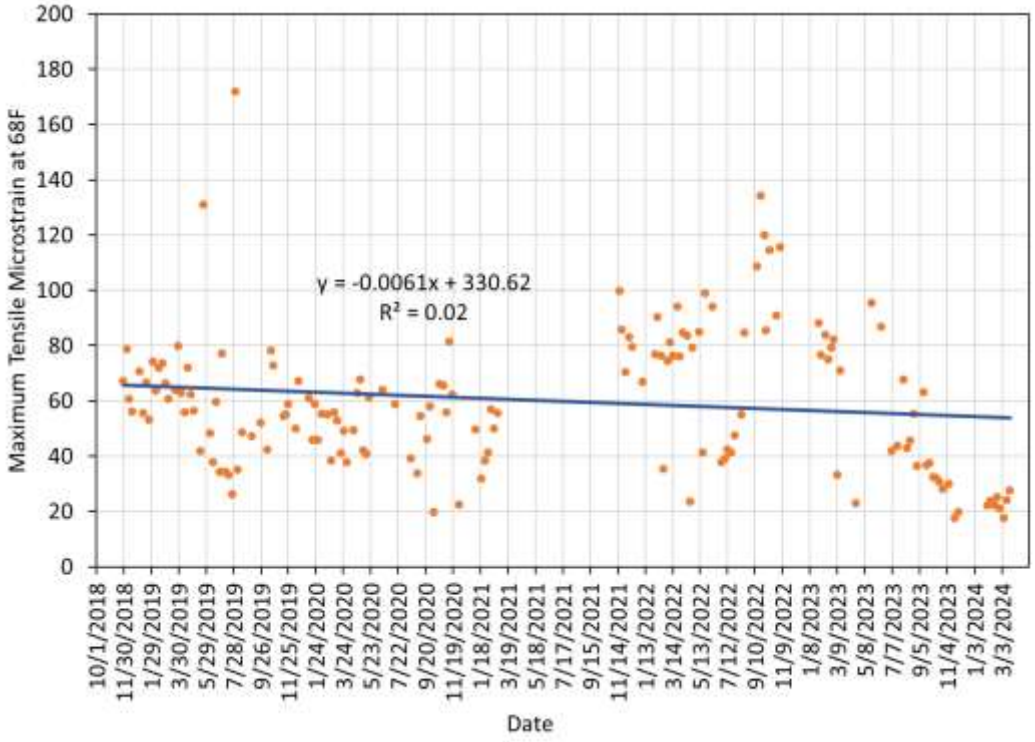

FIGURE 9 Section S2 maximum tensile strain at 68°F versus date.

8.4.3 Falling Weight Deflectometer Testing and Backcalculation

Through both test cycles, FWD testing was conducted multiple times per month with a Dynatest 8000. This FWD has nine sensors with a standard spacing of 0, 8, 12, 18, 24, 36, 48, 60, and 72 inches from the load center. Testing was conducted at four longitudinal stations in the section with three lateral offsets (inside wheelpath, outside wheelpath, and between wheelpath) at each station. The four stations represented each of three 50 ft subsections and the middle of the gauge array, respectively. Stations 1, 2, and 3 represent the subsections, and Station 4 was in the gauge array. Stations 1, 2, and 3 were originally determined by random number generation in the 50 ft subsections at the time of construction but then held fixed during trafficking. Each FWD test consisted of two seating drops followed by three replicate drops at various load levels. Only data from the 9,000 lb load level are discussed in this chapter.

An extensive investigation was conducted by Nakhaei (2021) to evaluate the effectiveness of using EVERCALC 5.0 to backcalculate layer properties for Section S2. The study determined conventional backcalculation techniques would not apply to a flexible pavement with a stabilized foundation. Therefore, an in-house customized program (MASTIC) was developed to backcalculate layer properties in both test cycles. Further details may be found in Nakhaei

(2021) and West et al. (2021). Only the backcalculated layer properties are presented below for brevity.

Figure 10 shows the backcalculated AC moduli through both test cycles, with the gap in the middle of the data resulting from the break between test cycles. The seasonal cycling is clearly evident, approaching 200 ksi in the warmest summer months and 3,000 ksi in the coldest months. The modulus values look nearly identical between cycles, indicating no change in structural health over time. This supports the hypothesis that the observed cracking is top-down and did not impact the structural integrity of the section.

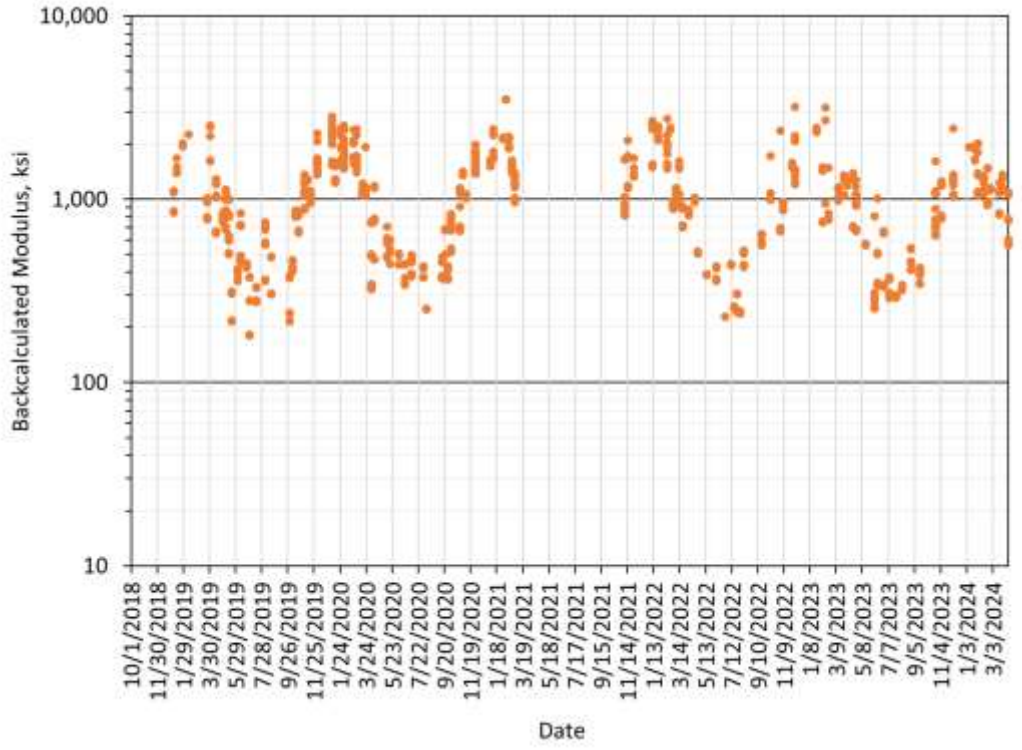

FIGURE 10 Backcalculated AC modulus versus time in Section S2.

The backcalculated moduli for the cement treated base (CTB), the lime treated soil (LTS), and the Mississippi subgrade (Subgrade) are shown in Figure 11 over the two test cycles. As expected, there is no apparent seasonal cycling since these layers do not contain materials with temperature dependent behavior. The significant variation is attributed to the in-place stabilization that occurred within the LTS and CTB layers. Also, since the values are relatively constant over both test cycles, there is no indication of subsurface pavement damage.

For future pavement modeling purposes, it is instructive to compute averages and standard deviations of each layers' modulus values. These are shown in Figure 12 through the whisker box plot, where the bars are the average values and the whiskers represent plus/minus one standard deviation. The backcalculated modulus for the CTB is approximately 1,400 ksi, the LTS

is approximately 450 ksi, and the subgrade soil is approximately 31 ksi. The modulus values for CTB and LTS are reasonable for these material types and were previously shown to be comparable to laboratory-measured values (West et al., 2021). The subgrade, however, appears excessively high for this material type. As was previously theorized (West et al., 2021), the high modulus is believed to be a function of the stress-sensitive nature of the soil subjected to such low stress levels (i.e., ~1 psi as shown in Figure 7) that it yields a relatively high modulus in this pavement cross section. In fact, this is the reason for building stabilized layers above this soil, as they limit the stresses reaching the soil to extract better performance out of an otherwise weak material.

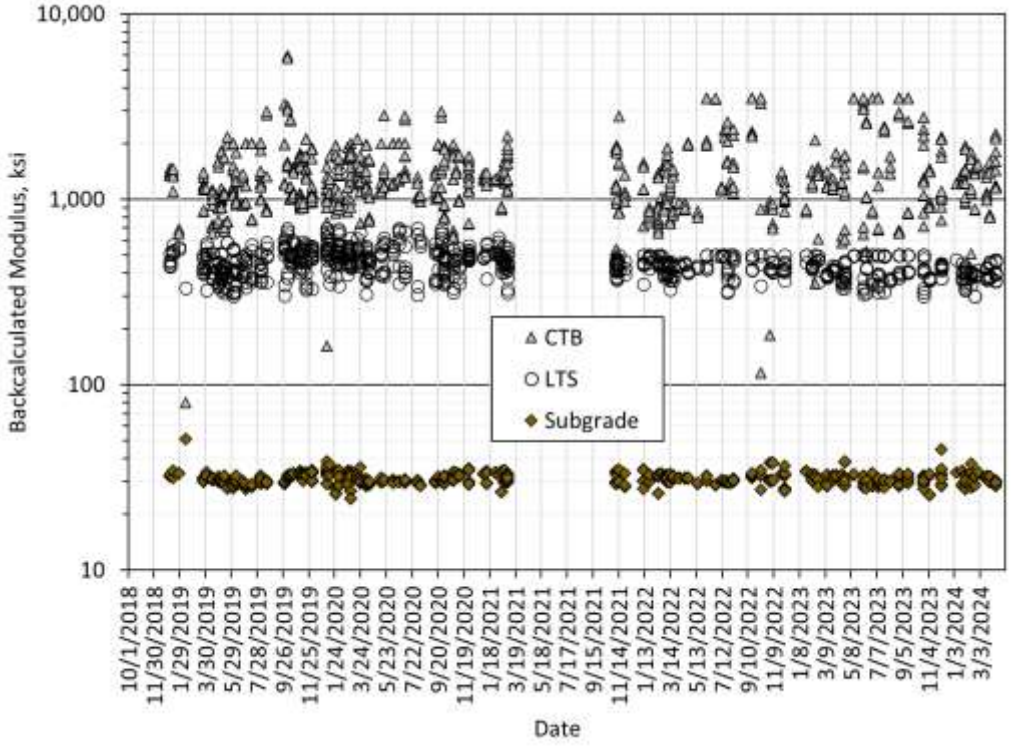

FIGURE 11 Backcalculated foundation layer moduli versus time in Section S2.

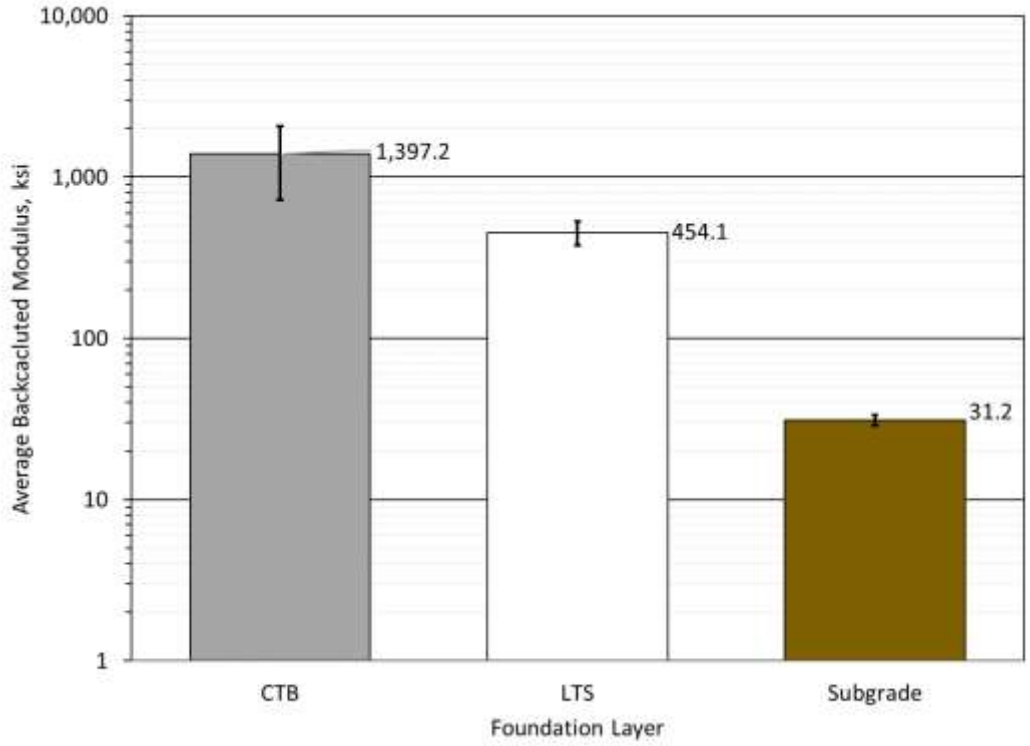

FIGURE 12 Average foundation backcalculated layer moduli in Section S2.

A final examination of the backcalculated AC moduli centered on normalizing the AC modulus values from Figure 10 to a reference temperature of 68°F and plotting against date. The data were first plotted against their corresponding mid-depth AC temperatures at the time of testing (Figure 13) to generate an exponential trendline that could normalize the data to 68°F. This process has been previously documented by McCarty (2019). The normalized data were then plotted in Figure 14 to look for any time-related trends indicating pavement damage. Since the trend is relatively flat, there is no sign of pavement damage, which again supports the previous hypothesis that the limited longitudinal cracking did not adversely affect the structural health of the pavement section after the completion of two test cycles.

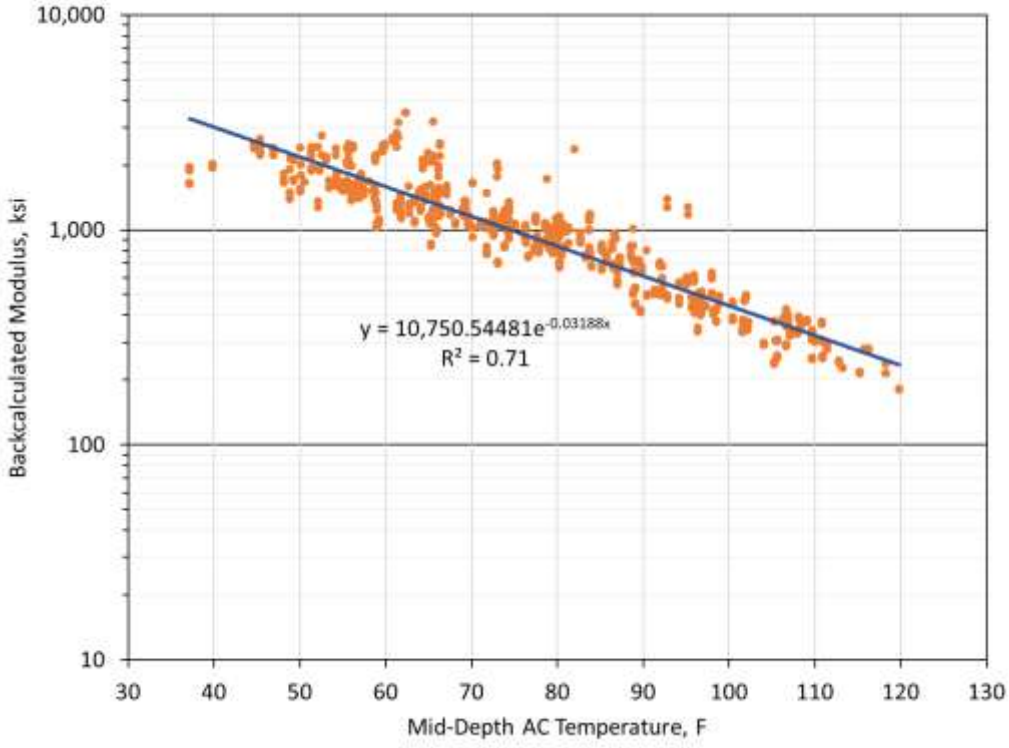

FIGURE 13 Backcalculated AC modulus versus temperature in Section S2.

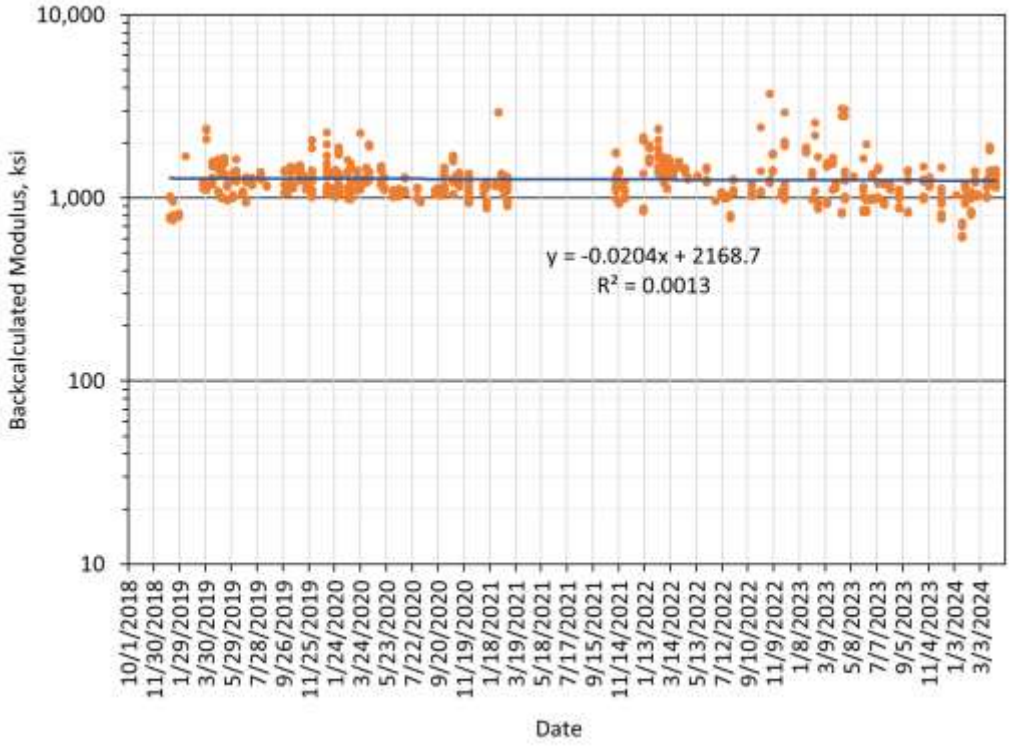

FIGURE 14 Backcalculated AC modulus at 68°F versus time in Section S2.

8.5 Summary, Conclusions, and Recommendations

Section S2 was constructed for the Mississippi DOT to evaluate the fundamental behavior and performance of a flexible pavement with a stabilized foundation. Based on the results presented in this chapter, the following conclusions and recommendations are made:

- The stabilized foundation section exhibited excellent performance over the full 20 million ESALs. Rutting was less than 0.20", only minor between wheelpath cracking was observed, and smoothness did not change appreciably over time.
- It is difficult to determine the exact nature of the between wheelpath cracking at this time. Future forensic investigation will help determine the origin and mechanism of cracking.
- Measured vertical stresses were as expected: stresses decreased with depth and were exponentially influenced by temperature. Stresses in the deeper pavement layers (LTS and subgrade) were less affected by AC temperature.
- Tensile strain levels measured at the bottom of the AC were very low (less than 100 microstrains), which was expected from relatively thick AC over a stabilized foundation. Bottom-up cracking is not expected to occur.
- Given the section's excellent performance, it is recommended to leave it in place for another 10 million ESALs during the 2024 research cycle. Continued surface performance monitoring (i.e., rutting, cracking and ride quality) and subsurface characterization (i.e., stress, strain measurement and FWD testing) will continue. Linkages between the performance measurements and structural characterization will provide needed data sets for M-E analysis and design of stabilized foundation sections.

8.6 References

McCarty, C. *Early Characterization and Performance of a Flexible Thick Lift Pavement*. M.S. Thesis, Auburn University, 2019.

Nakhaei, M. *Full-Scale Mechanistic and Performance Investigation of a Flexible Pavement with a Stabilized Foundation*, Doctoral Dissertation, Auburn University, 2021.

Newcomb, D., D. Timm, and J. Willis. *Perpetual Pavements: A Manual of Practice*. Quality Improvement Publication 130, National Asphalt Pavement Association, 2020.

West, R., D. Timm, B. Powell, N. Tran, F. Yin, B. Bowers, C. Rodezno, F. Leiva, A. Vargas, F. Gu, R. Moraes, and M. Nakhaei. *Phase VII (2018-2021) NCAT Test Track Findings*. NCAT Report 21-03, National Center for Asphalt Technology at Auburn University, 2021.

9. MISSISSIPPI DEPARTMENT OF TRANSPORTATION SPRAY-ON REJUVENATOR EXPERIMENT

Dr. Raquel Moraes

9.1 Background

Asphalt binder near the pavement surface becomes stiff and brittle over time due to age hardening from oxidation. This leads to surface deterioration, including non-load-associated distresses and top-down fatigue cracking. Rejuvenating seals, commonly referred to as spray-on rejuvenators, offer a solution by preserving the functional and structural integrity of existing asphalt pavements and reducing subsequent deterioration. Rejuvenators can also be combined with emulsified water-based or asphalt-based emulsions and/or other materials, such as polymers, to seal low-severity surface cracks and inhibit raveling. These treatments are formulated to address the stiffening and brittleness of the asphalt binder in the upper 9 mm (3/8 inch) of the surface layer. They can renew the hardened and oxidized asphalt binder by penetrating the asphalt material near the surface.

Spray-on rejuvenators are cost-effective pavement preservation treatments when applied to asphalt pavement surfaces that are still in good condition. These treatments are not recommended for pavements with low surface permeability, poor surface texture, large cracks, rutting, shoving, or other structural deficiencies (*1*). They can typically be applied every three to four years to prolong pavement life (*1, 2*). These treatments should be applied using well-calibrated distributors to spread the material as evenly as possible to achieve optimum coverage and penetrate surface cracks. The application rate depends on surface texture, level of oxidative aging, degree of cracking, and the specific product used. Spray-on rejuvenators are recommended for non-trafficked surfaces, such as shoulders, gores, or dikes, or trafficked surfaces when there is adequate surface texture, such as aged and raveled hot mix surfaces, chip-sealed surfaces, and open-graded asphalt surfaces (*1*).

It's crucial to consider that spray-on rejuvenators will immediately decrease pavement friction and skid resistance. The curing time of a spray-on rejuvenator product and its effect on friction is influenced by the application rate, the existing pavement surface condition, and weather conditions during application. Therefore, traffic control and temporarily reduced speed limits after application are often necessary for the safety of motorists and to protect the integrity of the rejuvenation treatment applied to the pavement.

9.2 Research Objective

As part of NCAT's 2018 Test Track research cycle, the Mississippi Department of Transportation sponsored a spray-on rejuvenator experiment in Section S3. The study's objective was to evaluate the field performance of two spray-on rejuvenator products commercially available in the United States, including their short- and long-term effectiveness in renewing asphalt surfaces and their effects on surface friction after application. The study was recommended for traffic continuation in the 2021-2024 research cycle for further monitoring and evaluating the applied products' long-term performance. The rejuvenating capability of each product was assessed based on rheological parameters and surface friction measurements obtained before and after application of the spray-on rejuvenator products.

9.3 Research Methodology

9.3.1 Materials

Two spray-on rejuvenator products were applied over the surface of Section S3, a 1.5" mill/inlay asphalt pavement section constructed in 2012, after the section experienced around 20 million equivalent single axle loads (ESALs) of traffic without presenting rutting or cracking distresses (Figure 1). The hot mix asphalt (HMA) of Section S3 was a dense-graded mix with sand and gravel containing 25% reclaimed asphalt pavement (RAP) and an asphalt content of 6.8%. The asphalt binder used in the design was a neat binder with a performance grade (PG) 67-22.

FIGURE 1 S3-A and S3-B application of spray-on rejuvenators.

The spray-on rejuvenator products utilized in this study were ReGenX® and Delta Mist™, listed in this report as S3-A and S3-B, respectively. The application rate, water dilution rate, and residual application rate of the products were determined following manufacturer recommendations, and this information is described in Table 1.

TABLE 1 Section S3 Spray-on Rejuvenator Products and Application Parameters

ReGenX® (S3-A)	Composition	Bio-Based
	Manufacturer Description	An age-regenerating surface treatment sprayed onto existing asphalt pavements using conventional distributor trucks or other common applicator systems. It penetrates the pavement, healing the aged and oxidized asphalt. Routine treatment every 4-5 years greatly extends the life of pavements. Does not require re-stripping. (*3*)
	Application Date	October 31st, 2018
	Application Rate	0.07 gal/yd^2
	Residual	20% (originally 60%)
	Dilution Rate	2:1
	Residual Application Rate	0.014 gal/yd^2
	Composition	Plant-Based

Delta Mist™ (S3-B)	Manufacturer Description	An emulsified version of Delta S® recycling agent that penetrates the surface and softens the asphalt binder to improve cohesion while retarding crack propagation. (*4*)
	Application Date	November 16th, 2018
	Application Rate	0.10 gal/yd^2
	Residual	20%
	Dilution Rate	Undiluted
	Residual Application Rate	0.020 gal/yd^2

The layout considering the untreated (control) and treated areas of Section S3 is depicted in Figure 2. Field cores were obtained from the beginning or end of each subsection for the laboratory rheological evaluation of asphalt binders extracted and recovered from the treated sections.

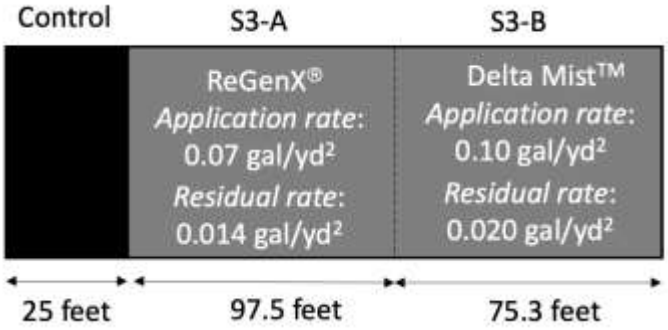

FIGURE 2 Test Track layout of Section S3.

Figure 3 shows the pavement surfaces of Section S3, including control, 1 month post-application, and 24 months post-application of the spray-on rejuvenator products. For section S3-A, the cores were collected from the diamond ground portion of the section that existed before the application of spray-on products for this study.

FIGURE 3 Section S3 pavement surfaces 1 month and 24 months after treatment application.

9.3.2 Experimental Plan

A schematic of the testing matrix utilized in this study for the untreated (control) and treated sections is shown in Figures 4 and 5, respectively. A modified version of the Federal Aviation Administration's (FAA) P-632 (Bituminous Pavement Rejuvenation) specification (*5*), the

procedure widely used to recognize the performance of spray-on rejuvenators, was used in this experiment. The modification includes the addition of the following rheological tests: Superpave Performance Grade (PG), Delta Tc (ΔT_c), Multiple Stress Creep Recovery (MSCR), and Frequency Sweep. The P-632 specification evaluates the rejuvenation capability of spray-on products by rheological parameters [e.g., complex modulus (|G*|), complex viscosity (η*), and phase angle (δ) at 60°C, 10 rad/s] of binders extracted and recovered from the upper 3/8-inch (9 mm) of treated pavement surfaces 30-45 days after product application. The parameters are determined using the Dynamic Shear Rheometer (DSR). Pavement friction characteristics tested 24 and 96 hours after the application of spray-on rejuvenator products and tested at no less than 180 days or greater than 360 days after the application are also included in the FAA P-632 specification.

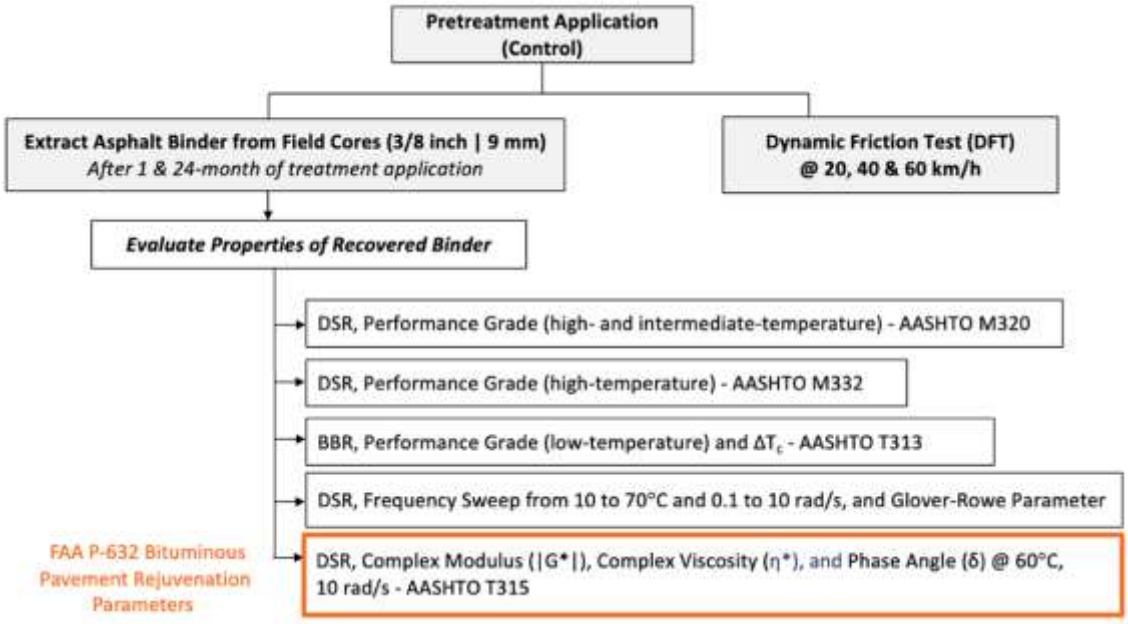

FIGURE 4 Testing matrix performed on untreated (control) section.

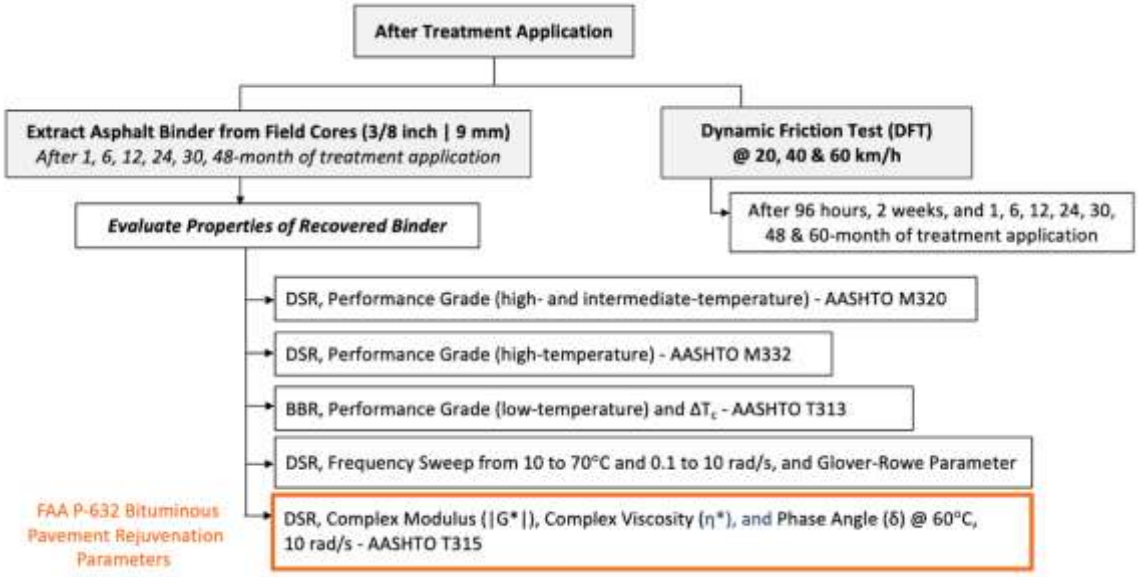

FIGURE 5 Testing matrix performed on treated sections.

For a spray-on rejuvenator to be classified as effective per the FAA P-632 specification, the extracted binder from samples of the upper 3/8-inch (9 mm) of the surface of a treated pavement must exhibit changes as listed in Table 2, when compared to the values from untreated (control) samples from the same pavement in the same timeframe.

TABLE 2. FAA P-632 Requirements

Property of Recovered Binder	Test Method	Age of Asphalt Pavement	
		≤ Three years	> Three years
Absolute Viscosity at 60°C, (P)	ASTM D 2171	≥ 25% Decrease	≥ 40% Decrease
|G*| at 60°C (kPa)	AASHTO T315		
η* at 60°C (Pa.s)			
δ at 60°C (°)		Report	

Note: Changes are based on the values of the control (untreated) asphalt binder.

9.3.3 Asphalt Binder Extraction and Recovery

The asphalt binders were extracted per ASTM D 2172 (method A) using trichloroethylene and recovered per ASTM D 5404 from upper 3/8-inch (9 mm) samples from field cores. For each treated pavement section, the asphalt binders were extracted and recovered from field cores at several time intervals after application of the spray-on rejuvenator products (i.e., 1 month, 6 months, 12 months, 18 months, 24 months, 30 months, and 48 months). Due to the short length of the control sections (Figure 3), the asphalt binders were extracted and recovered from field cores 1 and 24 months after the application of the spray-on rejuvenator products on the treated sections.

9.4 Laboratory Evaluation of Binders

9.4.1 Superpave PG and ΔT_c Parameter

Performance grades of the extracted binders were determined following AASHTO M320 (T315). The ΔT_c was determined based on Bending Beam Rheometer (BBR) results. ΔT_c is the numerical difference between the low continuous grade temperatures determined from the BBR stiffness criterion of 300 MPa and the m-value criterion of 0.3 (*6*). The ΔT_c parameter is used to assess the loss of stress relaxation properties of asphalt binders. Generally, a more positive (or less negative) ΔT_c value is desired for asphalt binders with better ductility and block cracking resistance. However, the applicability of ΔT_c to severely aged and polymer-modified asphalt (PMA) binders has been questioned and warrants further investigation (*7, 8*). PG and ΔT_c results for the extracted binders without additional aging are summarized in Table 3, with Figure 6 highlighting the comparisons of untreated (control) versus treated sections.

TABLE 3 PG and ΔT_c Results for Extracted Binders

Section	Field Aging Interval	T_{cont}, High (°C)	T_{cont}, Intermediate (°C)	T_{cont}, Low S (°C)	T_{cont}, Low m-value (°C)	ΔT_c (°C)	PG HT (°C)	PG LT (°C)
S3 Control	1 month after treatment	103.9	39.3	-19.4	-4.0	-15.4	100	-4
	24 months after treatment	104.4	41.4	-17.9	-2.9	-15.0	100	2
S3-A	1-month	94.1	34.0	-19.8	-11.6	-8.2	94	-10
	6-month	97.8	35.5	-17.5	-9.8	-7.7	94	-4
	12-month	100.5	35.8	-18.9	-6.4	-12.5	100	-4
	24-month	101.9	38.0	-18.7	-7.0	-11.7	100	-4
	30-month	109.3	42.0	-20.8	-4.0	-16.8	106	-4
	48-month	110.5	41.7	-15.7	-2.8	-12.9	106	2
S3-B	1-month	97.8	33.3	-18.9	-9.2	-9.7	94	-4
	6-month	101.6	37.0	-12.4	-6.6	-5.8	100	-4
	12-month	102.9	39.4	-16.8	-5.9	-10.9	100	-4
	24-month	101.4	38.0	-19.1	-5.0	-14.1	100	-4
	30-month	103.9	39.6	-17.0	-2.9	-14.1	100	2
	48-month	107.2	41.7	-16.6	-5.4	-11.2	106	-4

Compared to the control data obtained 24 months after treatments were applied, a decrease in the continuous true grade (pass/fail temperature) of the extracted binders present in the surface of the section was observed at high, intermediate, and low temperatures. This indicates an overall softening of the binder on the surface of the treated sections. This decrease was observed up to the 24-month field aging interval for the S3-A treatment. For the S3-B treatment, a decrease in the continuous true grade (pass/fail temperature) was observed up to a 30-month field aging interval at high and intermediate temperatures, while at low-temperature, T_{cont} S (stiffness) was slightly higher and T_{cont} m-value was equal to the control.

When comparing both treatments after a 48-month field aging interval, the S3-B treatment resulted in lower continuous true grade at high and low temperatures. At intermediate temperature, both treatments presented equal continuous true grade.

Regarding the effects of the treatments on the durability of the extracted binders, applying the treatments effectively improved cracking resistance of the binder at the pavement surface, as indicated by less negative ΔT_c values, even after a 48-month field aging interval. For S3-A and S3-B, the highest improvement in ΔT_c was observed at the 6-month field aging interval.

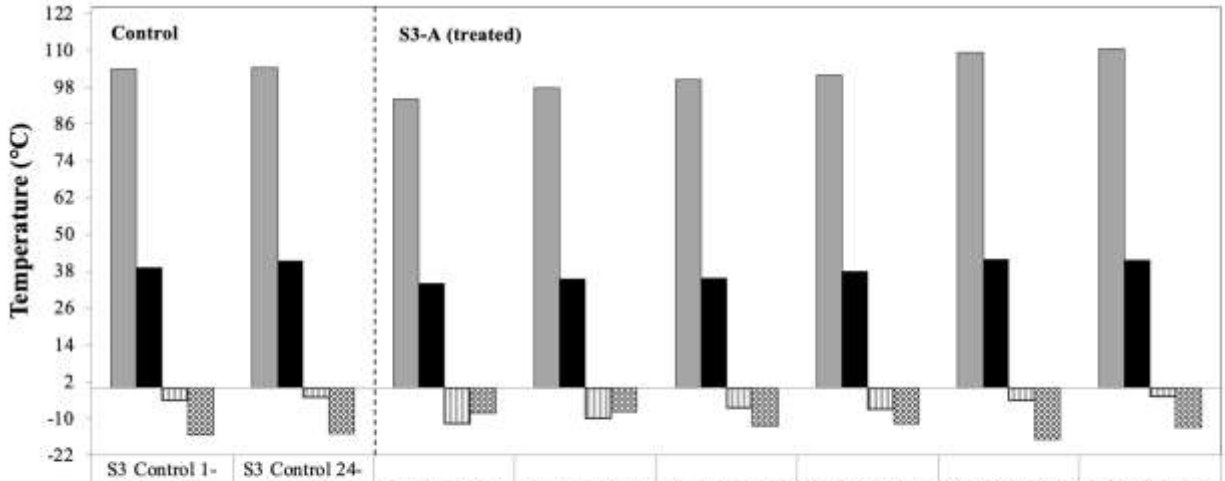

	S3 Control 1-month after treatment	S3 Control 24-month after treatment	S3-A 1-month	S3-A 6-month	S3-A 12-month	S3-A 24-month	S3-A 30-month	S3-A 48-month
PGH	103.9	104.4	94.1	97.8	100.5	101.9	109.3	110.5
PGI	39.3	41.4	34.0	35.5	35.8	38.0	42.0	41.7
PGL	-4.0	-2.9	-11.6	-9.8	-6.4	-7.0	-4.0	-2.8
ΔTc	-15.4	-15.0	-8.2	-7.7	-12.5	-11.7	-16.8	-12.9

(a) S3 control vs. S3-A

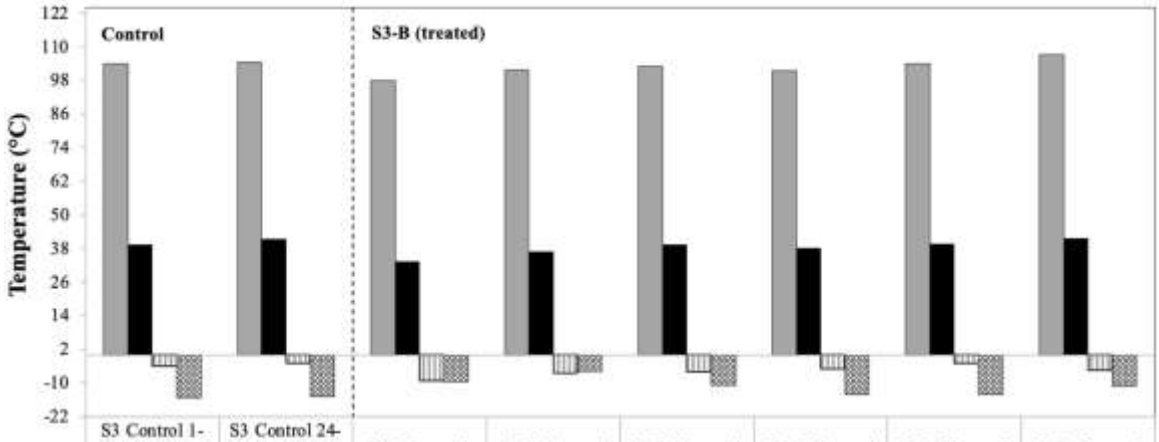

	S3 Control 1-month after treatment	S3 Control 24-month after treatment	S3-B 1-month	S3-B 6-month	S3-B 12-month	S3-B 24-month	S3-B 30-month	S3-B 48-month
PGH	103.9	104.4	97.8	101.6	102.9	101.4	103.9	107.2
PGI	39.3	41.4	33.3	37.0	39.4	38.0	39.6	41.7
PGL	-4.0	-2.9	-9.2	-6.6	-5.9	-5.0	-2.9	-5.4
ΔTc	-15.4	-15.0	-9.7	-5.8	-10.9	-14.1	-14.1	-11.2

(b) S3 control vs. S3-B

FIGURE 6 PG and ΔT_c results.

9.4.2 Multiple Stress Creep and Recovery (MSCR) Test

The MSCR test per AASHTO M332 (T350) evaluated the elastic response and rutting resistance of the extracted binders. The test was conducted on the extracted binders at 64°C. The test applied 20 loading cycles at a low-stress level of 0.1 kPa and 10 cycles at a high-stress level of 3.2 kPa. Each loading cycle consisted of 1 second of creep and 9 seconds of recovery. For data analysis, strain responses were used to calculate percent recovery ($\%R_{3.2}$) and non-recoverable creep compliance (J_{nr}) using Equations 1 and 2, respectively. A higher $\%R_{3.2}$ value indicates better binder elasticity and a lower J_{nr} value indicates better rutting resistance. MSCR results are provided in TABLE 4, Figure 7, and Figure 8.

$$\%R = \frac{\varepsilon_r}{\varepsilon_r + \varepsilon_{nr}} * 100\% \qquad \text{Equation 1}$$

Where

ε_r = recoverable strain, and

ε_{nr} = non-recoverable strain.

$$J_{nr} = \frac{\varepsilon_{nr}}{\sigma} \qquad \text{Equation 2}$$

Where

σ = creep stress.

TABLE 4 MSCR Results for Extracted Binders

Section	Field Aging Interval	Testing Temperature	J_{nr} @ 3.2kPa (1/kPa)	%R @ 3.2kPa (%)	Traffic Rating
S3 Control	1 month after treatment	64°C	0.004	69.9	E
	24 months after treatment		0.006	68.5	
S3-A	1-month		0.030	50.9	
	6-month		0.021	60.1	
	12-month		0.010	65.8	
	24-month		0.009	66.4	
	30-month		0.002	77.1	
	48-month		0.003	75.6	
S3-B	1-month		0.019	57.7	
	6-month		0.012	64.2	
	12-month		0.007	66.0	
	24-month		0.009	66.3	

	30-month		0.006	67.9	
	48-month		0.004	71.0	

*E = extreme traffic loading (>30 million ESALs and <20 km/h).

Compared to the control data obtained 24 months after treatment application, Figure 7 indicates that the spray-on rejuvenator products seemed to increase the overall magnitude of $J_{nr3.2}$, which indicates an overall softening of the binder on the surface of the treated sections. This increase in $J_{nr3.2}$ was observed up to the 24-month field aging interval for treatments S3-A and S3-B. All the extracted binders had almost negligible $J_{nr3.2}$ values and traffic rating "E" (E = extreme traffic loading). Thus, no rutting distress was observed, corresponding with PGH and field results.

Up to the 12-month field aging interval, $J_{nr3.2}$ values for the S3-A product were higher than the S3-B product, capturing the higher softening effect of the S3-A treatment. At the 24-month field aging interval, both treatments resulted in an equal $J_{nr3.2}$ value. As field aging progressed, a change occurred, and the binder treated with product S3-B presented slightly higher $J_{nr3.2}$ values than the S3-A up to 48 months after treatment application. The same trend was observed when considering the PGH data presented in Section 1.4.1. However, the observed differences may not be significant due to the very low $J_{nr3.2}$ values below 0.1 kPa^{-1}.

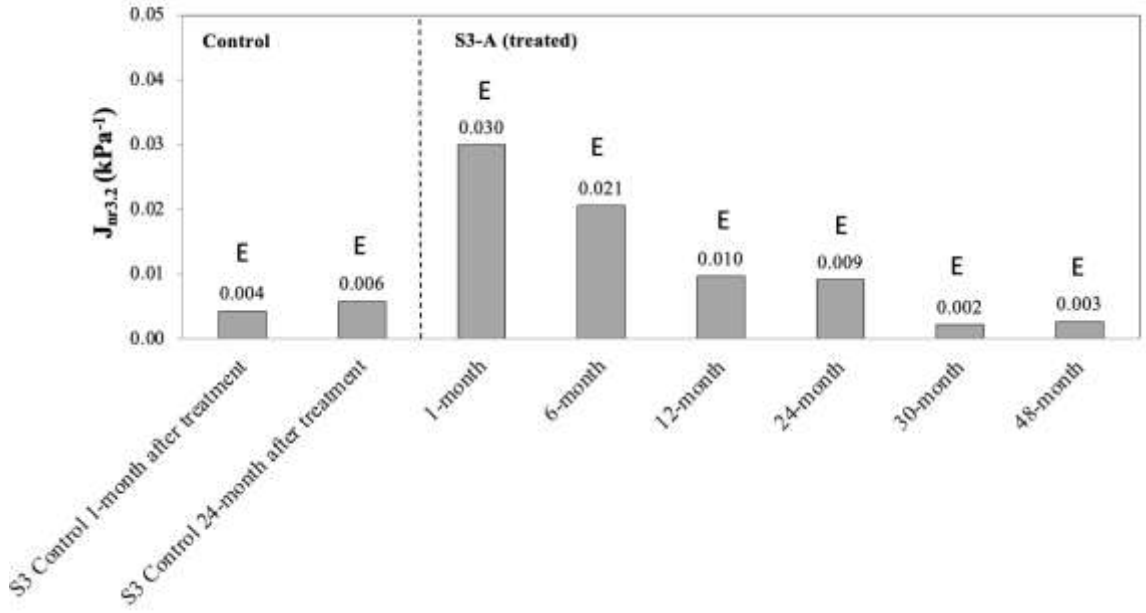

(a) S3 control vs. S3-A

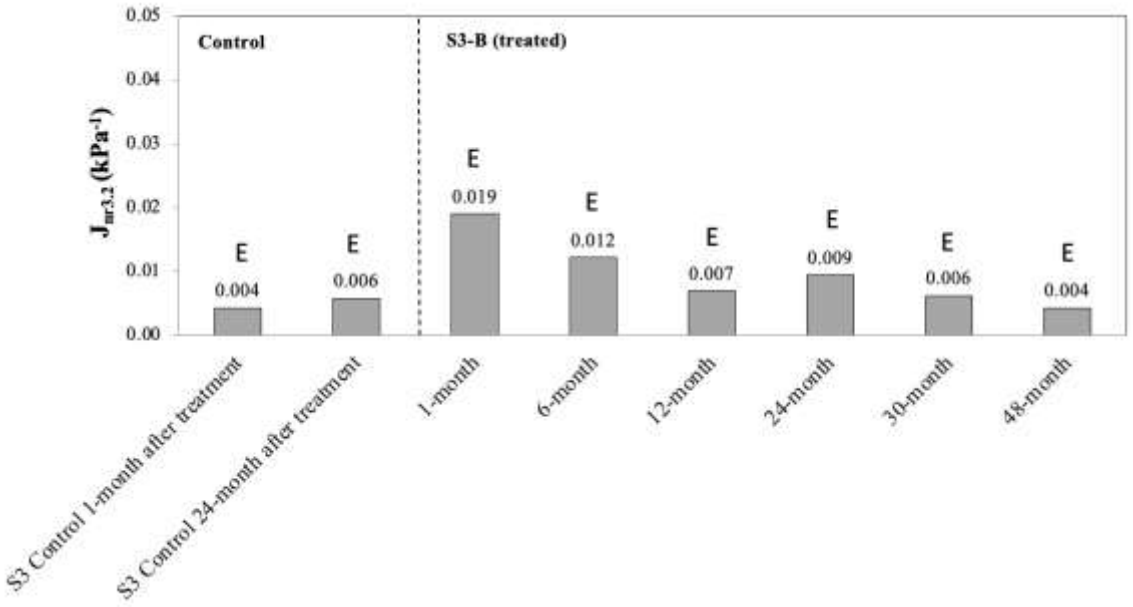

(b) S3 control vs. S3-B

FIGURE 7 MSCR $J_{nr3.2}$ Results. E = extreme traffic loading (>30 million ESALs and <20 km/h).

Figure 8 indicates that a decrease in $\%R_{3.2}$ values was observed 1 month after application of the spray-on products, followed by a slight increase as field aging progressed up to 48 months after product application. The $\%R_{3.2}$ values of the extracted binders (control and treated) should be interpreted cautiously since they are influenced by the low $J_{nr3.2}$ values, which are also influenced by the selected testing temperature of 64°C per the Alabama climate. Researchers have reported that the behavior of the MSCR $\%R_{3.2}$ parameter is highly influenced by the creep compliance $J_{nr3.2}$ of binders, regardless of the presence and content of polymer (*10, 11*). As $J_{nr3.2}$ decreases, an increase in $\%R_{3.2}$ is often observed.

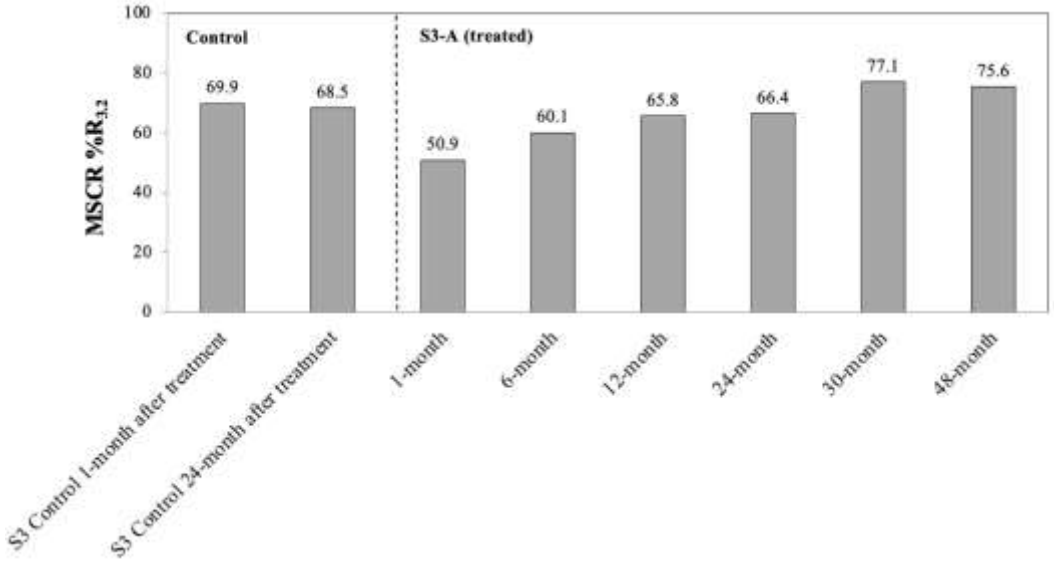

(a) S3 control vs. S3-A

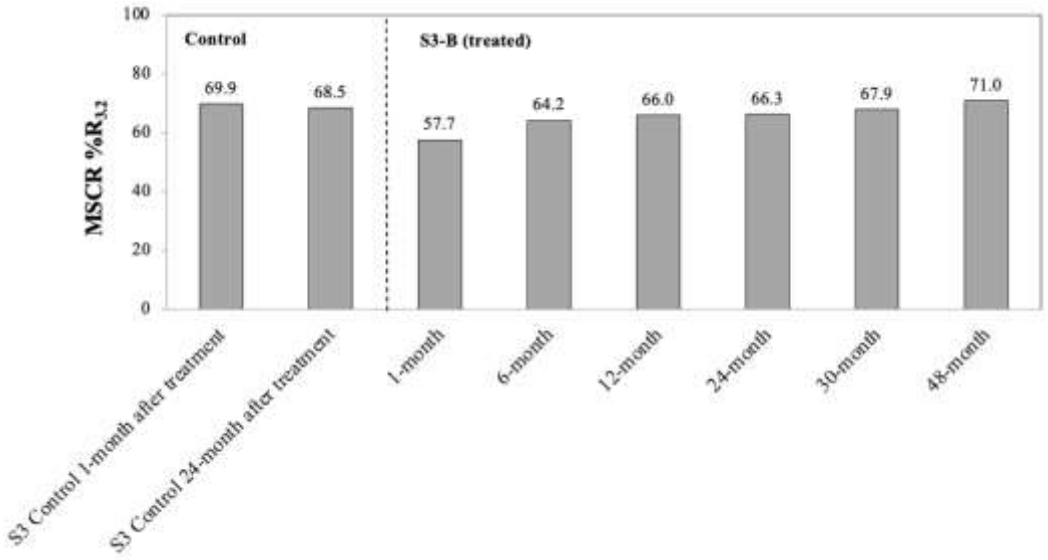

(b) S3 control vs. S3-B

FIGURE 8 MSCR $\%R_{3.2}$ results.

9.4.3 FAA P-632 Parameters |G|, η*, and δ at 60°C and 10 rad/s*

The complex shear modulus (|G*|), complex viscosity (η*), and phase angle (δ) of the extracted binders were determined before and after the application of the spray-on rejuvenator products. The DSR parallel plate geometry at 60°C and a frequency of 10 rad/s was used, representing higher temperatures and the shearing action corresponding to a traffic speed of about 55 mph (90 km/h). As indicated in Figure 9(a), the S3 control binder showed a stiffness increase of 30.1% (from 367.7 to 478.5 kPa) during the 24-month field aging interval. Applying the spray-on rejuvenator products S3-A and S3-B decreased the binder stiffness of the S3 control. As the field aging interval increased (from 1 month to 48 months of field aging), the stiffness of the treated sections also increased. However, after a 30-month field aging interval, the treated sections still showed complex modulus values smaller than the S3 control before treatment application (i.e., 367.7 kPa). Product S3-A showed a decrease in |G*| of 6.9%, while product S3-B showed a decrease of 14.6%. When comparing both treatments after a 48-month field aging interval, the S3-B product resulted in a binder with much lower stiffness (427.0 kPa) than the S3-A product (743.2 kPa). The same trend was observed when considering the complex viscosity (η*) (Figure 10). When considering the P-632 requirement (Table 2) of a decrease in |G*| ≥ 40% 30-45 days after product application, only product S3-A passed with a

decrease of 64.1% in |G*|. For the same time interval, product S3-B presented an increase of 12.1% in |G*|.

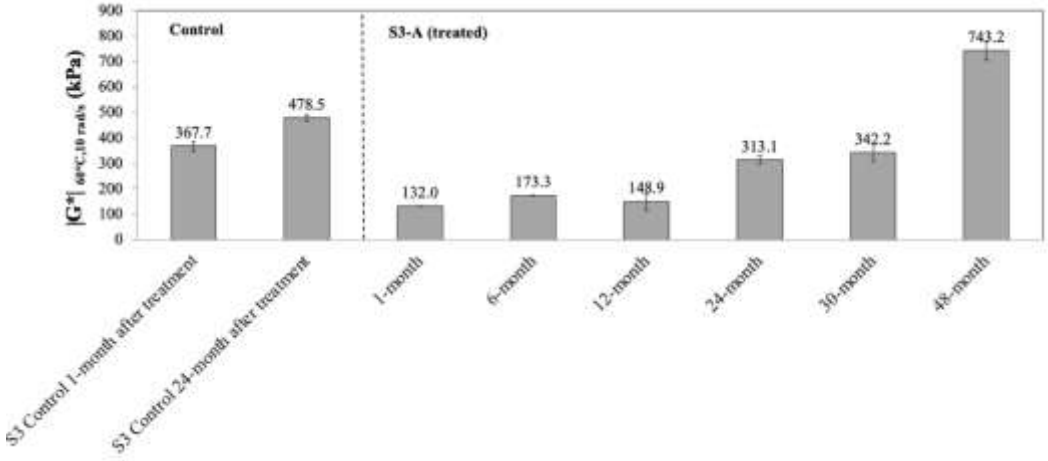

(a) S3 control vs. S3-A

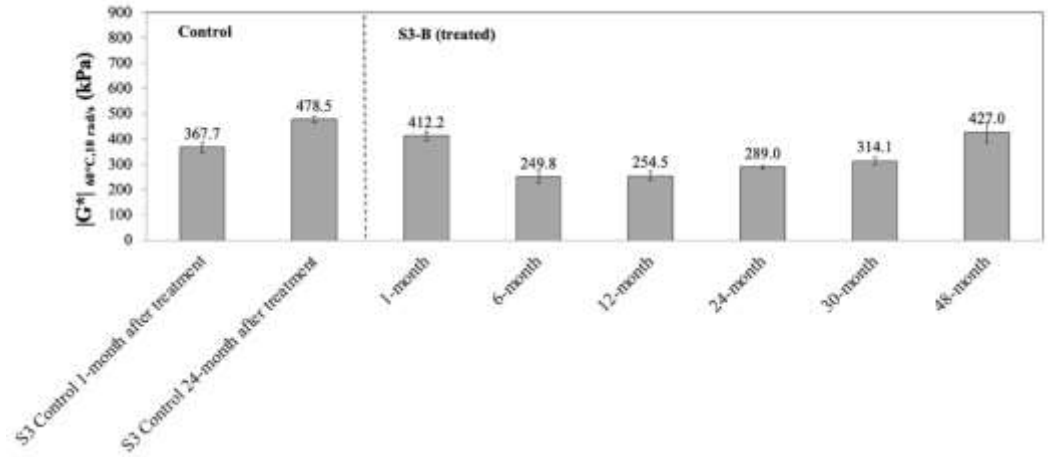

(b) S3 control vs. S3-B

FIGURE 9 Effect of field aging on |G*| at 60°C and 10 rad/s.

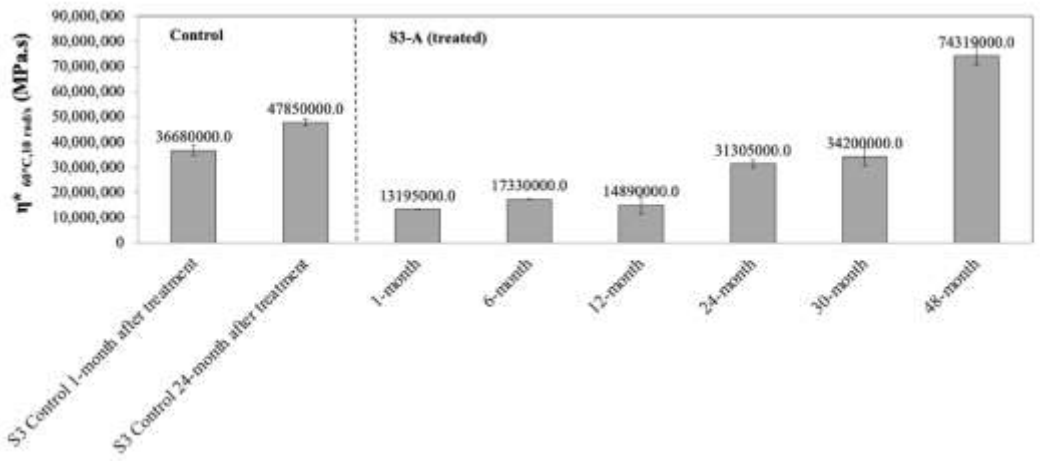

(a) S3 control vs. S3-A

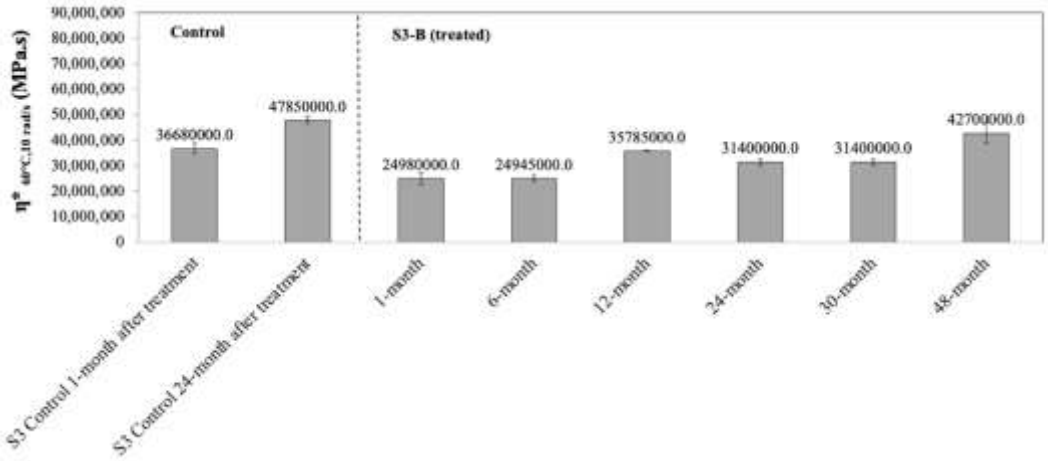

(b) S3 control vs. S3-B

FIGURE 10 Effect of field aging on η* at 60°C and 10 rad/s.

This NCAT field study has shown that the restoration capacity of a spray-on rejuvenating treatment increases rapidly after application due to the decrease in asphalt binder stiffness. However, it then begins to slowly decrease with oxidative aging due to the embrittlement of the binder. Therefore, the 30-45 days aging time proposed in the FAA P-632 procedure, described in Section 1.3.2 of this report, can be misleading in assessing a spray-on rejuvenator product's long-term effectiveness.

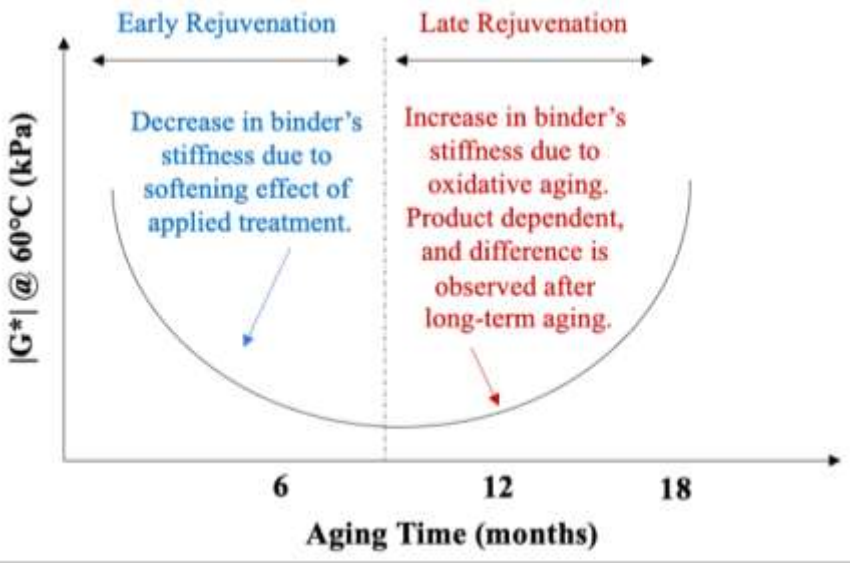

FIGURE 11 Hypothesized behavior of spray-on rejuvenator products.

Figure 12 indicates that product S3-A was more effective than product S3-B in decreasing binder stiffness (|G*|) for up to 12 months of field aging. As field aging progressed to 24 months, a change occurred, and the binder treated with product S3-B presented lower |G*| values for up to 48 months after treatment application.

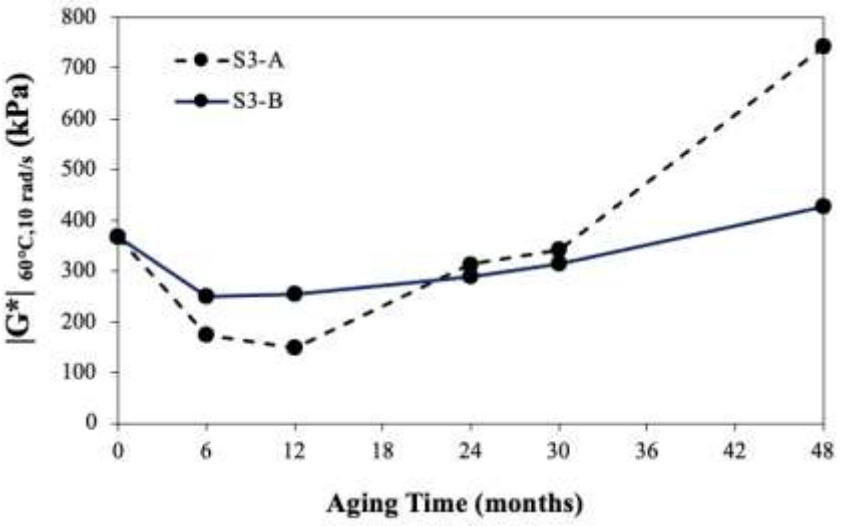

FIGURE 12 Effect of field aging on |G*| at 60°C and 10 rad/s for Section S3 after treatment with products S3-A and S3-B.

With aging, for a given temperature, the phase angle (δ) decreases as the asphalt binder stiffens. As indicated in Figure 13, this behavior was observed for the control and treated binders as the field aging interval increased. When the spray-on rejuvenator products were applied to the surface of Section S3, lowering the stiffness of the control binder, an increase in δ was observed at a given temperature (i.e., 60°C). Compared to the control data obtained 24 months after treatment application, the increase in δ was observed up to a 24-month field

aging interval for the S3-A product and up to 30 months after application for the S3-B product. When comparing both treatments after a 48-month field aging interval, the S3-B product resulted in a slightly higher δ than S3-A. All the extracted and recovered binders presented a phase angle greater than 42° (AASHTO M320), possibly indicating they would have the viscous behavior required at intermediate temperature to limit cracking. For the S3-B treatment, the effect on phase angle was apparent after a 6-month field aging interval, with the value obtained after 1-month being like the control binder considering test variability.

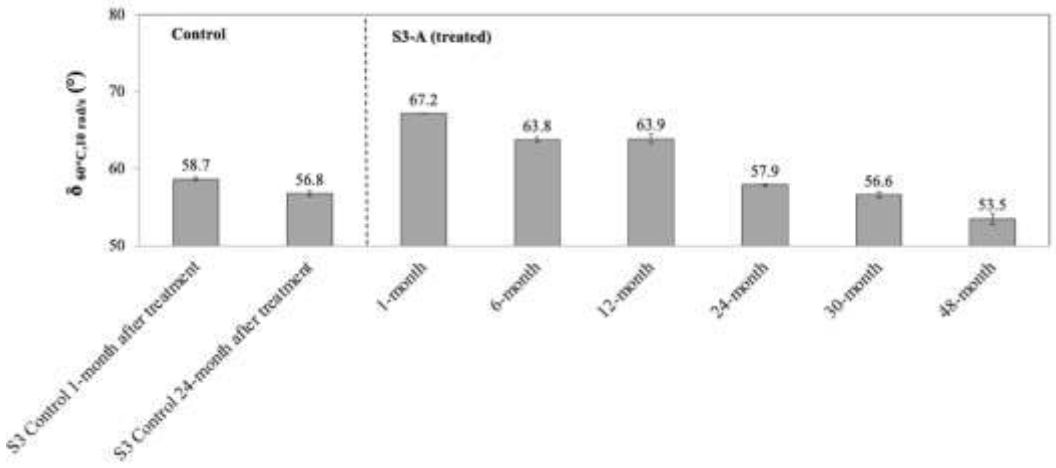

(a) S3 control vs. S3-A

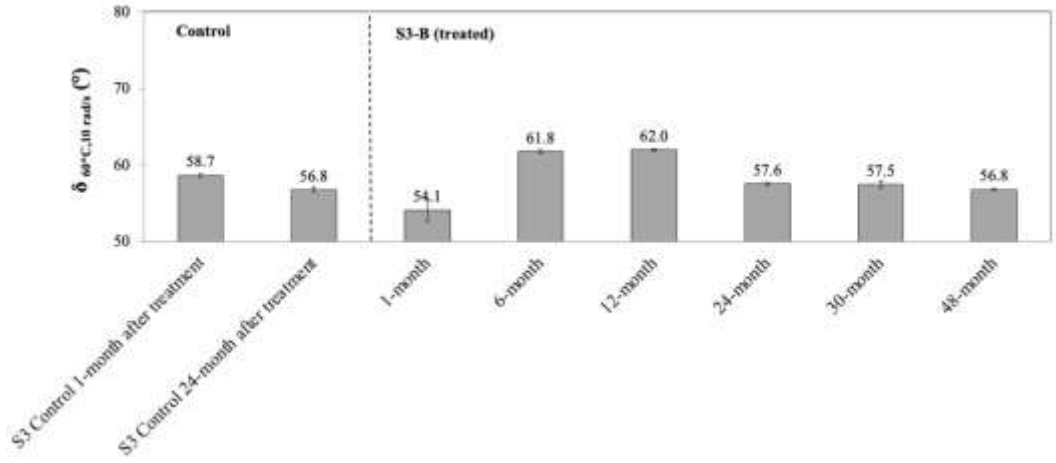

(b) S3 control vs. S3-B

FIGURE 13 Effect of field aging on δ at 60°C and 10 rad/s.

9.4.4 Glover-Rowe (G-R) Parameter

The *G-R* parameter evaluated the extracted binders' ductility and block cracking potential. To determine the *G-R* parameter, a DSR frequency sweep test was conducted at multiple test temperatures (i.e., 10, 20, 30, 40, 50, 60, and 70°C) over an angular frequency range of 0.1 to 10 rad/s. During the test, the peak-to-peak strain of the binder sample was controlled at 1% to ensure its behavior remained in the linear viscoelastic range. For data analysis, RHEA software

was used to construct a limited DSR master curve by fitting the G*| and phase angle (δ) data to the discrete relaxation and retardation spectra (*9*). Then, the binder |G*| and δ at 15°C and 0.005 rad/s were determined, from which the *G-R* parameter was calculated using Equation 3. Generally, a high *G-R* parameter indicates low ductility and high block cracking susceptibility.

$$G - R\ Parameter = \frac{|G^*|\cos(\delta)^2}{\sin(\delta)} \qquad \text{Equation 3}$$

Where

|G*| = binder shear complex modulus at 15°C (59°F) and 0.005 rad/s, and

δ = binder phase angle at 15°C and 0.005 rad/s.

Table 5 presents the |G*|, δ, and *G-R* Parameter Results at 15°C and 0.005 rad/s of the extracted binders.

TABLE 5 |G*|, δ, and *G-R* Parameter Results at 15°C and 0.005 rad/s

Sample	Field Aging Interval	15°C, 0.005 rad/s (unaged)		
		|G*| (kPa)	δ (°)	G-R (kPa)
S3 Control	1-month	5577.0	42.8	4410.8
	24-month	5704.0	42.0	4700.7
S3-A	1-month	1368.0	52.8	626.0
	6-month	1802.0	50.9	924.9
	12-month	1516.0	47.8	923.0
	24-month	3852.0	44.5	2795.9
	30-month	4328.0	39.7	4016.7
	48-month	4903.0	41.5	4148.3
S3-B	1-month	2059.0	46.6	1341.7
	6-month	2488.0	48.2	1483.5
	12-month	1733.0	47.0	1100.2
	24-month	3228.0	43.7	2439.1
	30-month	4065.0	43.1	3167.1
	48-month	4020.0	44.0	2994.1

Figure 14 presents the *G-R* parameter results on a Black Space diagram, with the binder |G*| at 15°C and 0.005 rad/s plotted on the y-axis *versus* δ at the same condition on the x-axis. As aging increased for each binder, the |G*| and δ data migrated from the lower right corner to the upper left corner of the Black Space diagram. The dashed and bold curves represent the two preliminary *G-R* parameter criteria of 180 kPa and 600 kPa, respectively, for the onset of block cracking and visible surface cracking. It should be noted that these criteria were developed

based on a limited number of unmodified binders and a PG 58-28 climate in Pennsylvania; thus, their broad applicability remains unknown and needs further investigation.

It is encouraging that the S3-A and S3-B treatments significantly decreased the stiffness of the control binder, even after a 48-month field aging interval. The treated binders exceeded the criterion for visible surface cracking regardless of the field aging interval. However, it should be noted that Section S3 was an eight-year-old pavement (containing 25% RAP) when the treatments were applied, considering that surface treatments are most effective if applied early before the asphalt binder properties age to critical cracking conditions. Furthermore, results are subject to the assumption that a Black Space diagram is valid for comparing all binders, with the *G-R* parameter damage zone limits in Figure 14 defined only for unmodified binders used in a PG 58-28 climate. When comparing both products, the binder treated with the S3-A product exhibited the highest relative change in Black Space (i.e., its aging pathways were longer), indicating greater aging susceptibility than the S3-B product.

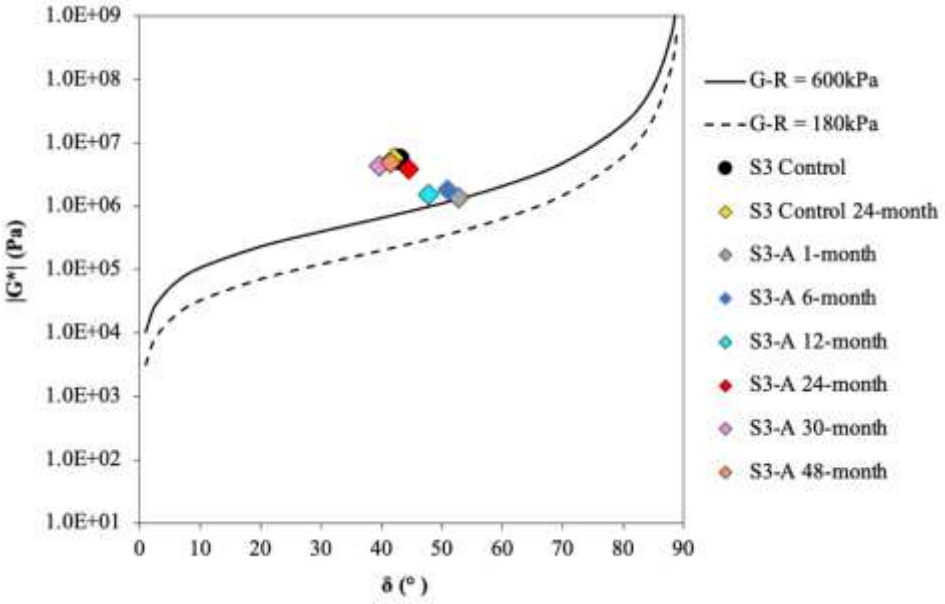

(a) S3 control vs. S3-A

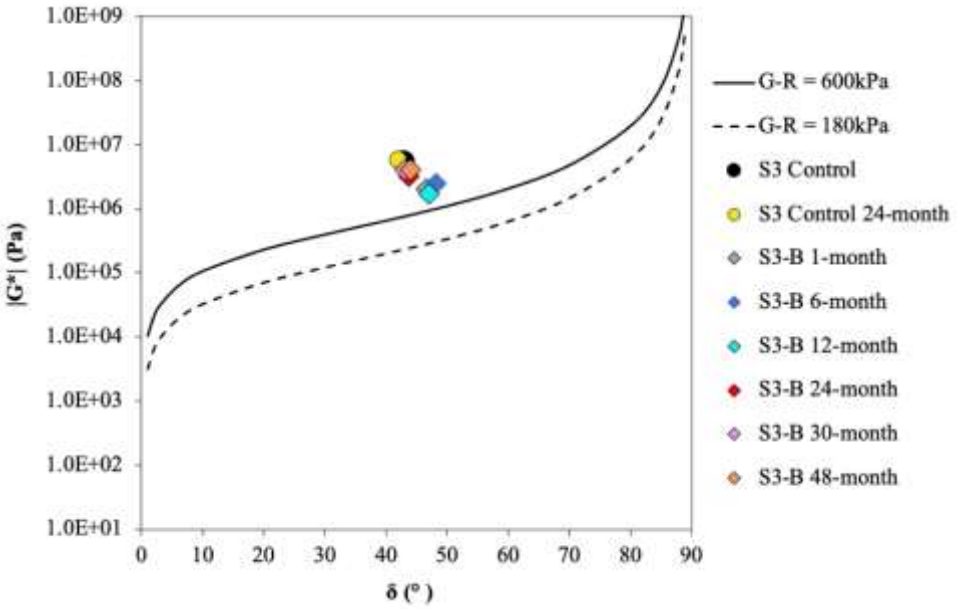

(b) S3 control vs. S3-B

FIGURE 14 |*G| and δ Results at 15°C and 0.005 rad/s on a Black Space Diagram.**

Up to the 12-month field aging interval, the *G-R* parameter values for the S3-A product were lower than the S3-B product values, capturing the higher softening effect of the S3-A treatment (Figure 15). As field aging progressed, a change occurred, and the binder treated with product S3-B presented lower *G-R* parameter values than the S3-A up to 48 months after treatment application. The same trend was observed when considering the previously presented PGH, $J_{nr3.2}$, and $|G^*|_{60°C,\ 10\ rad/s}$ data.

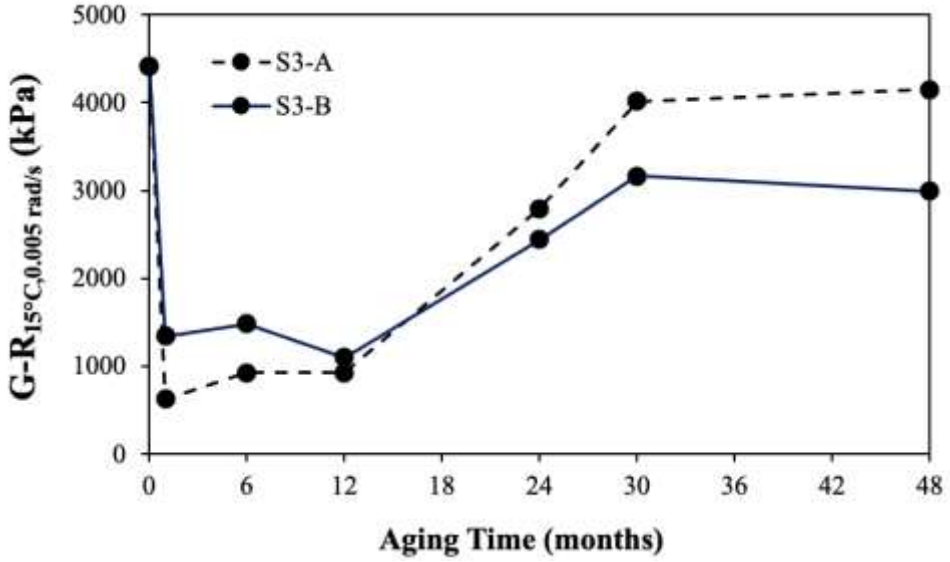

FIGURE 15 Effect of field aging on *G-R* parameter at 15°C and 0.005 rad/s for Section S3 after treatment with products S3-A and S3-B.

To further investigate the effect of additives on the stiffness and embrittlement of the control binder, a *G-R* effectiveness index was calculated per Equation 4, where a lower index value is desired for treatments that are more effective in restoring the *G-R* parameter of the control binder after extended aging.

$$\boldsymbol{G-R_{Effectiveness\ Index}} = \frac{\boldsymbol{G-R_{Treated}}}{\boldsymbol{G-R_{Control}}} \qquad \text{Equation 4}$$

Figure 16 presents the *G-R* effectiveness index for the extracted binders after several field aging intervals. Perhaps the most valuable observation is that the control binder, presenting very poor relaxation properties (ΔT_c = -15.4°C), experienced a significant net reduction (improvement) in the *G-R* effectiveness index with the two applied treatments. S3-A and S3-B presented *G-R* effectiveness indices below 1.0 after a 48-month field aging interval, indicating the stiffness and embrittlement of the treated binders were considerably better than the control binder after extended aging. Product S3-A had the lowest (best) *G-R* effectiveness index up to the 12-month field aging interval among the two applied treatments. As field aging progressed, product S3-B presented lower *G-R* effectiveness index values than S3-A up to 48 months after treatment application.

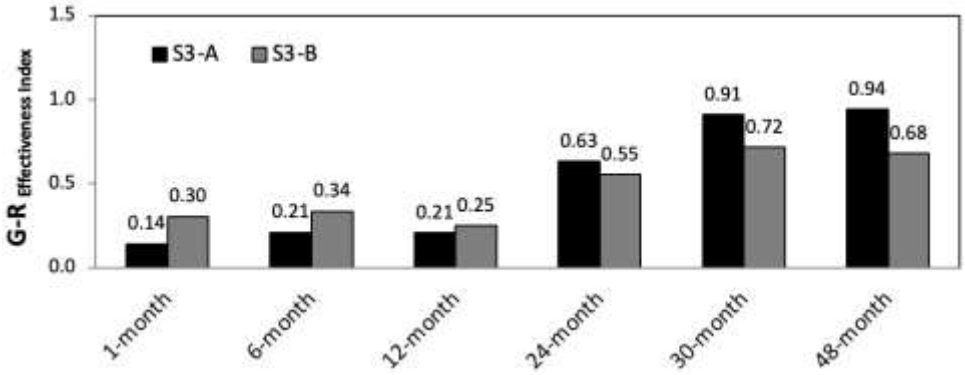

FIGURE 16 *G-R* effectiveness index of binders after field aging.

9.4.5 Friction Results

Pavement surface frictional properties of Section S3 as a function of speed were measured using the Dynamic Friction Tester (DFT). The DFT consists of a horizontal spinning disk fixed with three spring-loaded rubber sliders that contact the pavement surface (Figure 17). A water spray system is used to simulate wet conditions. When the disk is lowered onto the test surface, the DFT measures the torque generated by the sliders' resistive force to calculate the friction coefficient of the asphalt pavement surface. Velocity is also measured to indicate the relationship between the coefficient of friction and speed. Each DFT test includes three replicate measurements as described in ASTM E 1911. This study selected speeds of 20, 40, and 60 km/h for measuring friction properties of the pavement surface of Sections S3-A and S3-B. Heitzman and Moore indicated that 40 km/h DFT speed produces the most repeatable measure (*12*). Therefore, this speed was used for detailed analysis.

FIGURE 17 Dynamic friction tester.

Figure 18 shows the average friction number (F_n) at 40 km/h before and at several intervals after applying the two spray-on rejuvenator products. The initial time interval of 96 hours and 72 hours for collecting the friction values for Sections S3-A and S3-B differed due to weather conditions. For the two evaluated products, pavement surface friction decreased initially after treatment application but improved with time. When comparing the products and the first obtained friction value after treatment application, product S3-A showed the highest decrease in friction (29.6%), while product S3-B showed the least decrease in friction (3.7%). Two weeks after treatment application, products S3-A and S3-B showed friction values equal to (0.27) and higher (0.30) than the S3 control section, respectively. The long-term test results indicate the applied products did not show adverse effects on pavement friction compared with the friction of the control section.

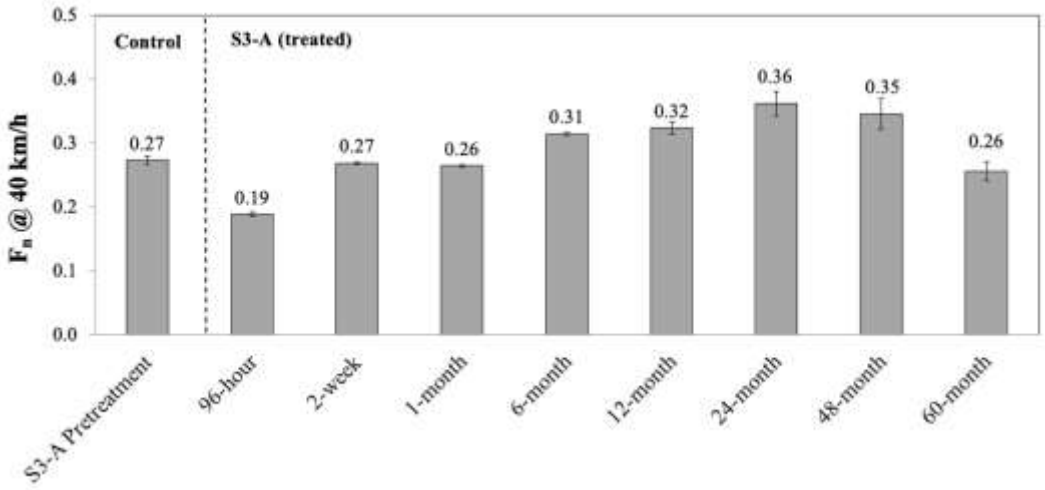

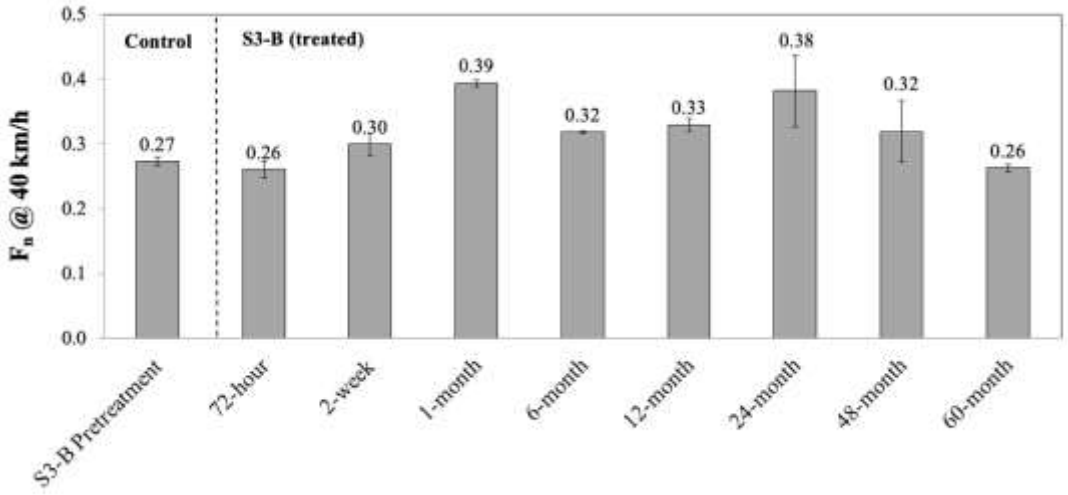

FIGURE 18 Average F_n at 40 km/h at several time intervals.

9.5 Field Performance Evaluation

Subsections S3-A and S3-B were trafficked by approximately 20 million ESALs of heavy truck traffic after applying the spray-on treatments. Truck traffic occurred Monday evenings through Saturday mornings from 2018 to 2024. Surface condition surveys were conducted weekly on Mondays to collect rutting, cracking, ride quality, and surface texture data.

Due to the length restriction of the S3 control section (Figure 2), it was not possible to evaluate its field performance. As indicated previously (Section 1.3.1), the S3-A and S3-B spray-on rejuvenator products were applied after Section S3 was subjected to 20 million ESALs of truck traffic since construction without presenting rutting and cracking distresses.

9.5.1 Rutting

Rutting in the wheel path was evaluated using the Pathway PathRunner inertial profiler and the ALDOT beam procedure (ALDOT T392). This method utilizes a four-foot beam with a dial gauge to measure rut depths along predetermined locations in the wheel path of each test section with accuracy within ± 2.5 mm.

Figure 19 compares rut depth versus traffic ESALs for S3-A and S3-B. S3-A rut depth was slightly higher than S3-B (5.3 and 3.8 mm, respectively). However, all rut depths are below the typical maximum field rut depth threshold of 12.5 mm.

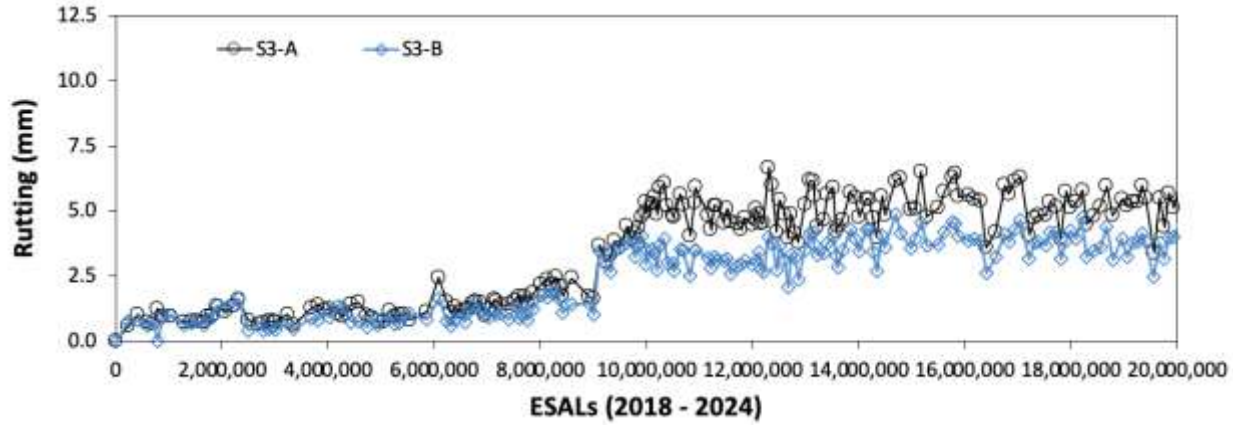

FIGURE 19 Field rut depth measurements.

9.5.2 Surface Cracking

The procedure for gathering surface cracking data commenced by visually examining each test section. Subsequently, the identified surface cracks were systematically mapped and quantified. The size of the cracked area was assessed by measuring the length of the cracks within the test section. This data was then employed to calculate the percentage of lane area impacted by surface cracking (Figure 20).

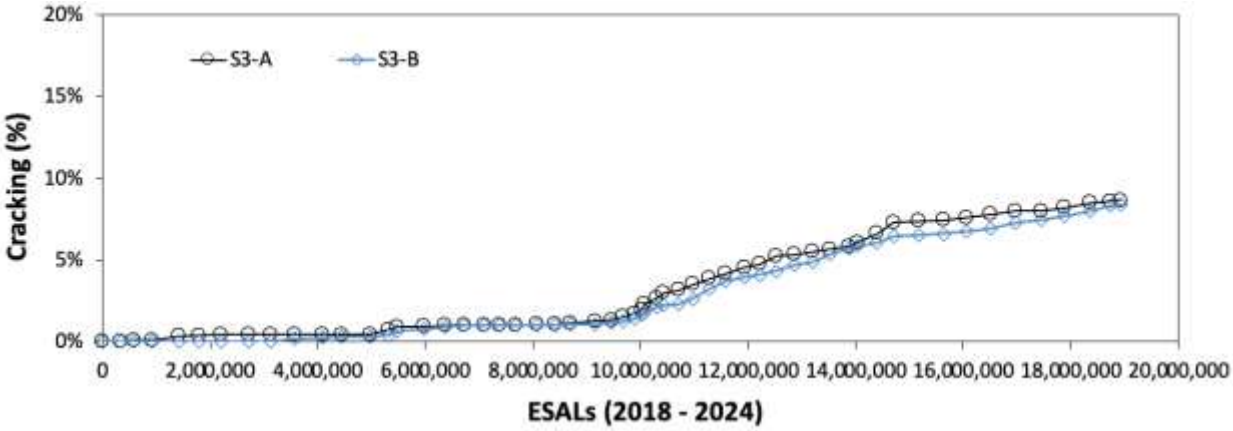

FIGURE 20 Field cracking measurements.

For Section S3 treated with product S3-A, the first cracks started after around 584,084 ESALs and approximately 2 months after treatment application, with 0.1% of lane area cracked. For Section S3 treated with product S3-B, the first cracks started after around 3,581,376 ESALs and approximately 9 months after treatment application, with 0.2% of lane area cracked. Approximately 65 months after treatment application and 20 million ESALs of truck traffic, the two treated sections remain below the maximum lane area cracked limit of 20%. The section treated with product S3-A presented 8.5% of lane area cracked, while the section treated with product S3-B presented 8.2%. The type of cracking observed was classified as block cracking.

Table 6 summarizes the ΔT_c and *G-R* binder cracking parameters and the cracking field performance for the two treated sections. After a 1-month field aging interval, the treated

sections presented ΔT_c values below the minimum threshold of -5°C (*6*), but no cracking was observed in the field. As field aging progressed, the ΔT_c values became more negative, and cracking was observed in the treated sections. Regarding the *G-R* parameter threshold for visible surface cracking, S3-A at 1 month post-treatment and S3-B at 1 and 6 months after treatment application presented *G-R* values above the threshold 600 kPa, and no cracking was observed in the field. As aging progressed up to the 48-month field aging interval, *G-R* values increased above the threshold for visible surface cracking (i.e., 600 kPa), and cracking was observed in the field.

TABLE 6 ΔT_c and $G\text{-}R_{15°C,\ 0.005\ rad/s}$ Binder Cracking Parameters, Field Cracking Performance and ESALs.

Sample	Field Aging Interval	ΔT_c (°C)	G-R (kPa)	Cracking (%)	ESALs 2018 – 2024
S3-A	1-month	-8.2	626.0	0.0	329,764
	6-month	-7.7	924.9	0.4	2,196,281
	12-month	-12.5	923.0	0.4	4,971,971
	24-month	-11.7	2795.9	1.3	9,156,176
	30-month	-16.8	4016.7	2.7	10,301,014
	48-month	-12.9	4148.3	7.6	16,066,569
S3-B	1-month	-9.7	1341.7	0.0	329,764
	6-month	-5.8	1483.5	0.0	2,196,281
	12-month	-10.9	1100.2	0.3	4,971,971
	24-month	-14.1	2439.1	1.1	9,156,176
	30-month	-14.1	3167.1	2.1	10,301,014
	48-month	-11.2	2994.1	6.8	16,066,569

9.5.3 Ride Quality

Ride quality (pavement roughness) was assessed through international roughness index (IRI) measured by the Pathway PathRunner inertial profiler. Figure 21 shows ride quality data expressed as IRI. IRI values were 99.3 in/mile for S3-A and 82.8 in/mile for S3-B. A fleet accident in subsection S3-A resulted in the need for a wrecker to remove a damaged trailer set. During the removal process, one of the trailers overturned, impacting Section S3-A. Therefore, the slightly higher IRI measured for S3-A is likely due to the higher lane area cracks obtained from the accident. Note that cracking originating from this accident is not included in the field cracking results presented in Figure 20.

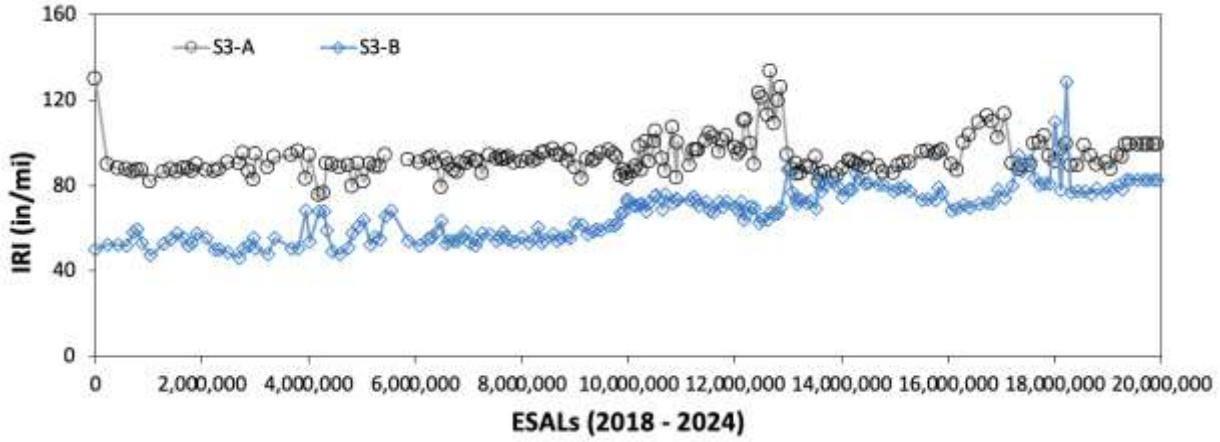

FIGURE 21 Ride quality (IRI) measurements.

9.5.4 Surface Macrotexture

During the seventh research cycle (2018-2021), the surface texture of each subsection was assessed through mean texture depth (MTD) and measured using the Dynatest inertial profiler. For the eighth research cycle (2021-2024), the surface texture of each subsection was assessed through mean profile depth (MPD) and measured using the Pathway PathRunner inertial profiler. This resulted in increased mean depth measurements. Figure 22 compares MTD and MPD measurements for the S3 subsections. At the end of trafficking for the eighth research cycle, MPD results were almost identical for the two subsections: 1.24 mm for S3-A and 1.26 mm for S3-B.

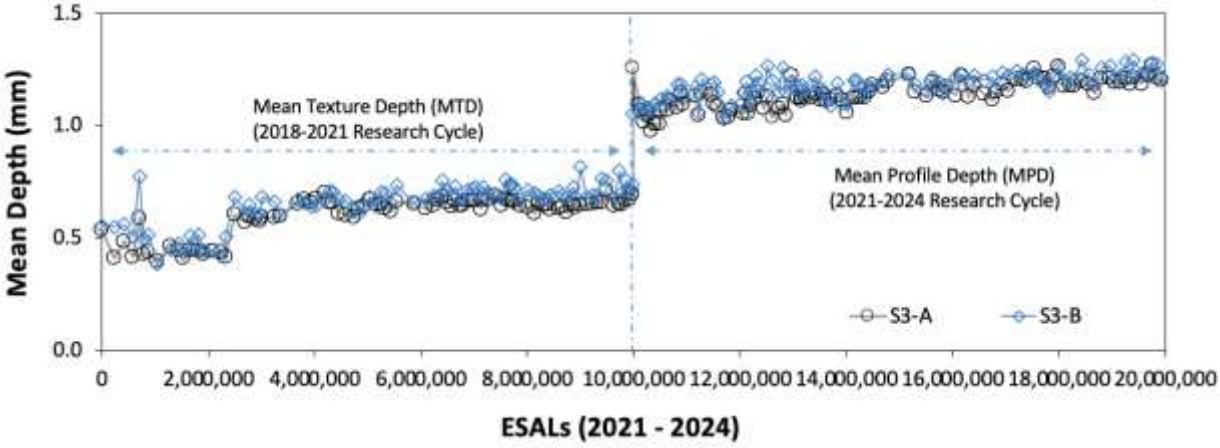

FIGURE 22 Surface macrotexture measurements.

9.6 Conclusions and Recommendations

This research evaluated the short- and long-term field performance of two spray-on rejuvenator products. Extending the evaluation over a longer period enabled a more thorough assessment of each product, as it was found that a longer aging time was necessary to distinguish their effectiveness in decreasing stiffness and improving the relaxation properties of the asphalt binder. Key findings from the research include the following—

- After a 48-month field aging interval, treatment S3-B resulted in lower continuous true grade at high and low temperatures compared to S3-A, with equal grades at intermediate temperature.
- Both spray-on rejuvenator products increased $J_{nr3.2}$ up to the 24-month field aging interval. However, the control and treated binders had almost negligible $J_{nr3.2}$ values and traffic rating "E" (E = extreme traffic loading).
- After a 30-month field aging interval, the treated sections presented $|G^*|_{60°C,\ 10\ rad/s}$ values smaller than the S3 control before treatment application. Product S3-A showed a decrease in |G*| of 6.9%, while product S3-B showed a decrease of 14.5%. When comparing both treatments after a 48-month field aging interval, the S3-B product resulted in a binder with much lower stiffness (427.0 kPa) than the S3-A product (743.2 kPa). The same trend was observed for complex viscosity (η*).
- *G-R* parameter values for the S3-A product were lower than values for the S3-B product, capturing the higher softening effect of the S3-A treatment. As field aging progressed, a change occurred, and the binder treated with product S3-B presented lower *G-R* parameter values than S3-A, up to 48 months after treatment application. The same trend was observed for PGH, $J_{nr3.2}$, and $|G^*|_{60°C,\ 10\ rad/s}$ data.
- When comparing the products and the first obtained friction value after treatment application, product S3-A showed the highest decrease in friction (29.6%), while product S3-B showed the smallest decrease in friction (3.7%).
- Two weeks after treatment application, products S3-A and S3-B showed friction values equal to (0.27) and higher (0.30) than the S3 control section, respectively. Between 6 and 60 months after treatment application, S3-A and S3-B presented similar friction values, regardless of field aging interval.
- Rut depths were similar for Sections S3-A and S3-B (5.3 and 3.8 mm, respectively) and below the typical maximum field rut depth threshold of 12.5 mm.
- Approximately 65 months after treatment application and 20 million ESALs of truck traffic, the two treated sections remained below the maximum lane area cracked limit of 20%. The section treated with product S3-A presented 8.5% of lane area cracked, while the section treated with product S3-B presented 8.2%. The type of cracking observed was classified as block cracking.
- IRI values were 99.3 and 82.8 in/mile for S3-A and S3-B, respectively.
- At the end of truck trafficking for the eighth research cycle, MPD results were almost identical for the two subsections: 1.24 mm for S3-A and 1.26 mm for S3-B.

Key takeaways from the research include the following—

- A decrease in the continuous true grade (i.e., pass/fail temperature) of the extracted binders present on the surface of the section was observed at high, intermediate, and low temperatures, indicating binder softening on treated sections.

- Treatments improved cracking resistance, evidenced by less negative ΔT_c values, even after a 48-month field aging interval, with maximum improvement between 6 and 12 months.

This NCAT field study has shown that the restoration capacity of a spray-on rejuvenating treatment increases rapidly after application due to the decrease in asphalt binder stiffness but then begins to slowly decrease with oxidative aging due to the embrittlement of the binder. Therefore, the 30-45 days aging time proposed in the FAA P-632 procedure, described in Section 1.3.2 of this report, can be misleading in assessing a spray-on rejuvenator product's long-term effectiveness.

In summary, the spray-on rejuvenator products assessed in this study are a good option for preventing or slowing surface deterioration of pavements. They are convenient to use since they don't require specialized equipment and can effectively restore the surface condition of existing pavements.

9.7 References

1. Hanson, D., G. King, M. Buncher, J. Duval, P. Blankenship, and M. Anderson. *Techniques for Prevention and Remediation of Non-Load Related Distresses on HMA Airport Pavements (Phase I)*. Airfield Asphalt Pavement Technology Program, 2009.
2. Estakhri, C., and H. Agarwal. *Effectiveness of Fog Seals and Rejuvenators for Bituminous Pavement Surfaces*. Research Report 1156-1F, Research Study 2-18-87-1156, Texas State Department of Highways and Public Transportation, 1991.
3. Blacklidge. ReGenX®Performance Surface ReGeneration. https://blacklidge.com/products/regenx/
4. Collaborative Aggregates, LLC. About Delta Mist. https://collaborativeaggregates.com/deltamist/
5. Federal Aviation Administration (FAA). Guidelines and Procedures for Maintenance of Airport Pavements. Advisory Circular AC 150/5370-10H, 2018.
6. Anderson, M., G. N. King, D. I. Hanson, and P. B. Blankenship. Evaluation of the Relationship between Asphalt Binder Properties and Non-Load Related Cracking. *Journal of the Association of Asphalt Paving Technologists*, Vol. 80, 2011, pp. 615-664.
7. Kluttz, R. Q. Prepared Discussion on Relationships Between Mixture Fatigue Performance and Asphalt Binder Properties. *Journal of the Association of Asphalt Paving Technologists*, Vol. 88, 2019.
8. Elwardany, M., J. P, Planche, and G. King. Universal and Practical Approach to Evaluate Asphalt Binder Resistance to Thermally Induced Surface Damage. *Construction and Building Materials*, Vol. 255, 2020.
9. Baumgaertel, M., and H. H. Winter. Determination of Discrete Relaxation and Retardation Time Spectra from Dynamic Mechanical Data. *Rheologica Acta*, Vol. 28(6), 1989, pp. 511-519.
10. Rodezno, C., R. Moraes, M. Fortunatus, and F. Yin. Recycled Asphalt Binder Study (No. 0092-19-04), Final Report. Wisconsin Dept. of Transportation. 2021

11. Bahia, H., D. Swiertz, and A. Kilger. *Modified Binder (PG+) Specifications and Quality Control Criteria (No. 0092-14-20) TPF-5(302)*. Extension Final Report, Wisconsin Dept. of Transportation, 2018.
12. Heitzman, M., and J. Moore. *Evaluation of Laboratory Friction Performance of Aggregates for High Friction Surface Treatments*. NCAT Report 17-01, National Center for Asphalt Technology at Auburn University, 2017.

10. NORTH CAROLINA DEPARTMENT OF TRANSPORTATION EFFECTS OF TACK COAT TYPE AND RATE ON INTERFACE SHEAR BOND STRENGTH

Dr. Raquel Moraes

10.1 Background

The long-term performance of asphalt pavements is fundamentally related to the bond developed between pavement layers. Asphalt pavements are designed to behave as a bonded single flexible layer under loading. However, asphalt pavements typically consist of multiple layers, and the bond strength of the interface between these layers is critical to ensuring that the pavement will act as a monolithic structure and not experience distress. When pavement layers are not properly bonded, the layers exhibit independence, resulting in an alteration to the stress distribution profile. Therefore, tack coats play a critical role in the overall performance of asphalt pavements. Distresses related to poor bonding typically occur as delamination, which can lead to slippage cracking and fatigue cracking (*1*).

(a)

(b)

FIGURE 2 (a) Delamination and (b) slippage cracking (*2*).

Pavement surfaces with different physical conditions (e.g., new, old, or milled) require different tack coat application rates to achieve a proper interface bond. Furthermore, the appropriate application rate also varies by tack coat material type. Excessive tack coat is detrimental since it can act as a lubricant, creating a slippage plane between the pavement layers (*3*). Additionally, excessive material can be drawn into an overlay, negatively affecting mixture properties and

creating the potential for bleeding in thin overlays. On the other hand, failure to use or insufficient tack coat can also cause pavement slippage and debonding (*4*). Therefore, it's crucial to accurately design the amount of tack coat to produce the optimum outcome.

10.2 Research Objective

As part of the 2021-2024 Test Track research cycle at the National Center for Asphalt Technology (NCAT), the North Carolina Department of Transportation (NCDOT) sponsored a tack coat experiment in Section W4 (the 4th section in the west curve) (Figure 2). The study aimed to assess 1) the effect of tack coat type and rate on initial and long-term interface shear bond strength under the influence of aging and traffic loading, and 2) whether NCDOT's mixture specifications are sufficient to ensure the stability of high recycled content mixes under realistic, high shear stress conditions.

FIGURE 2 Section W4 for the 2021-2024 research cycle.

10.3 Research Methodology

10.3.1 Materials

Two tack coat products, a PG 67-22 binder and CRS-1h (a cationic rapid-set emulsion with a relatively low asphalt emulsion viscosity made with hard base asphalt), were applied over the surface of Section W4, a 1.5" milled asphalt pavement section (Figure 3). Section W4 was constructed in 2018 and experienced around 10 million ESALs of traffic without presenting rutting and cracking distresses before milling in 2021.

FIGURE 3 Tack coat application after milling in Section W4.

Section W4 was divided into three subsections for this study, W4-A, W4-B, and W4-C. The layout with corresponding tack coat products is depicted in Figure 4. PG 67-22 tack was applied at 0.06 gal/yd^2 (0.060 gal/yd^2 residual rate) for the first 100 feet (Section W4-A), CRS-1h was applied at 0.06 gal/yd^2 (0.036 gal/yd^2 residual rate) for the next 50 feet (Section W4-B), and at 0.10 gal/yd^2 (0.060 gal/yd^2 residual rate) for the final 50 feet (Section W4-C). These application rates were calculated to allow application (Section W4-B) and residual (Section W4-C) rates equal to the PG 67-22 tack rate in Section W4-A. The tack coat application rate is the total amount of liquid asphalt sprayed by the distributor, while the tack coat residual rate is the amount of asphalt binder remaining after the water has evaporated from the emulsion (*5*). The residual asphalt binder is the amount that effectively provides the bond between two pavement layers (*6*).

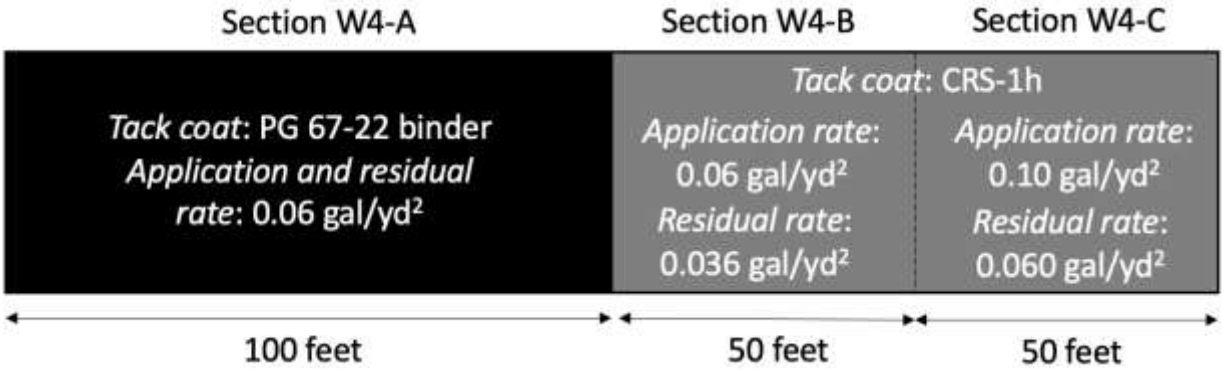

FIGURE 4 Test track Section W4 layout.

10.3.2 Asphalt Mixture

Table 1 presents the job mix formula (JMF) of the W4 mixture (used as a surface mix after the tack coat was applied) provided by the Barnhill Contracting Company in North Carolina. The W4 mix was an NCDOT RS9.5C mix with a 9.5 mm nominal maximum aggregate size (NMAS). The mix used a PG 58-28 neat binder, a blend of granite and sand, 25% RAP, and 4% RAS by weight

of the mix. The mix had an optimum binder content (OBC) of 6.2%, design air voids of 4.0%, and voids in the mineral aggregate (VMA) of 17.8% at 65 gyrations. The resultant RAP and RAS binder replacement of the mix were 19.4% and 12.9%, respectively. The mix was designed using the Volumetric Design with Asphalt Pavement Analyzer (APA) rut performance verification.

TABLE 1. Mix Design and Quality Control (QC) Data of W4 Mixture

Compactive effort (N_{des})	65 gyrations	
Binder PG	58-28	
Sieve (in.)	**Job Mix Design**	**Quality Control**
25 mm (1”)	100	100
19 mm (3/4”)	100	100
12.5 mm (1/2")	100	99
9.5 mm (3/8”)	97	97
4.75 mm (#4)	79	78
2.36 mm (#8)	65	64
1.18 mm (#16)	55	53
0.60 mm (#30)	41	45
0.30 mm (#50)	25	23
0.15 mm (#100)	13	13
0.075 mm (#200)	7.8	9.5
Binder content (P_b)	6.2	6.0
Effective binder content (P_{be})	6.1	6.0
RAP binder replacement (%)	19	20
RAS binder replacement (%)	13	13
Total binder replacement (%)	32	33
G_{mm}	2.437	2.432
G_{mb}	2.342	2.387
Air voids (%)	3.9	1.9
Aggregate gravity (G_{sb})	2.674	2.660
VMA (%)	17.8	15.7
VFA (%)	78	88
Dust proportion	1.3	1.6

10.3.3 Experimental Plan

This study was divided into four tasks, including (1) rheological evaluation of the tack coat products (Figure 5), (2) interface bond shear strength evaluation of field cores (Figure 6), (3) pavement friction evaluation, and (4) field performance evaluation.

In Task 1, the tack coat products were subjected to rheological evaluation using the Dynamic Shear Rheometer (DSR) and Bending Beam Rheometer (BBR), including Superpave Performance Grade (PG), Delta T_c (ΔT_c), and Multiple Stress Creep Recovery (MSCR) tests. In Task 2, the ALDOT-430 test was used to evaluate the effect of tack coat type and rate on initial and long-term shear bond strength between pavement under the influence of aging and traffic loading. In Task 3, friction properties of Sections W4-A, W4-B, and W4-C were monitored using the Dynamic Friction Tester (DFT). Task 4 focused on field performance evaluation on the NCAT Test Track.

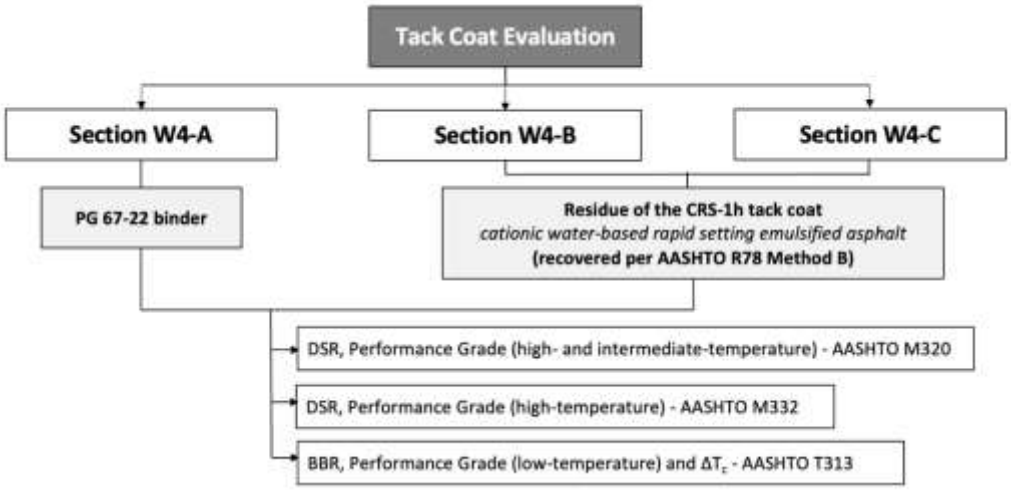

FIGURE 5 Binder testing matrix.

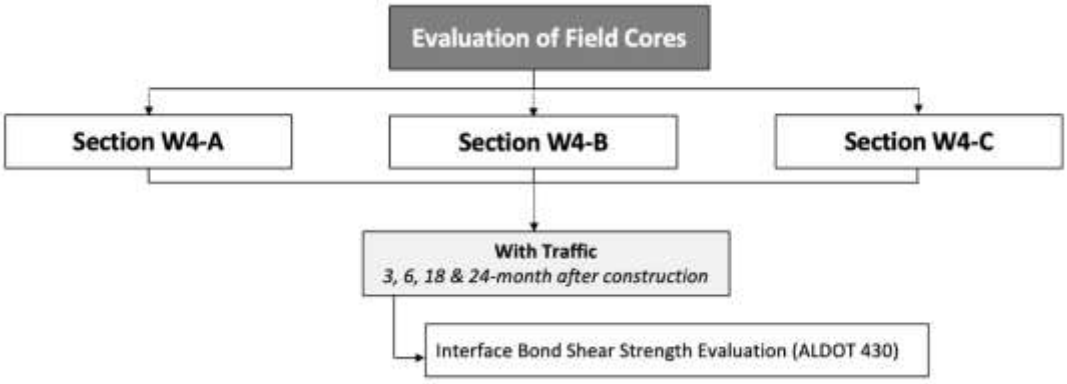

FIGURE 6 Evaluation of interface bond shear strength of field cores.

10.4 Laboratory Evaluation of Binders

10.4.1 Superpave PG and ΔT_c Parameter

Performance grades of the PG 67-22 binder and the residue of the CRS-1h emulsion were determined following AASHTO M320 (T315). For the CRS-1h tack coat, the binder was recovered per AASHTO R78 Method B. Samples were aged following standard Superpave procedures, including RTFO per AASHTO T240 and 20 hours in the pressure aging vessel (PAV) at 100°C per AASHTO R28.

The ΔT_c was determined based on the BBR results. ΔT_c is the numerical difference between the low continuous grade temperatures determined from the BBR stiffness criterion of 300 MPa and the m-value criterion of 0.3 (*7*). The ΔT_c parameter has recently been used to assess the loss of stress relaxation properties of asphalt binders. Generally, a more positive (or less negative) ΔT_c value is desired for asphalt binders with better ductility and block cracking resistance. PG and ΔT_c results for the binders are summarized in Table 2.

TABLE 2 PG and ΔT_c Results for Binders

Tack coat type	T_{cont} high (°C)	T_{cont} intermediate (°C)	T_{cont} low S (°C)	T_{cont} low m-value (°C)	ΔT_c (°C)	PG
PG 67-22 binder	68.4	23.9	-25.6	-24.6	-1.0	64-22
CRS-1h residue	66.7	15.6	-31.0	-40.0	9.0	64-28

The following observations can be drawn based on the binder test results—

- Based on the continuous true grade (i.e., pass/fail temperature), PG 67-22 binder has higher stiffness compared to CRS-1h residue at high, intermediate, and low temperatures (including both S-based and m-value).
- Since a more negative ΔT_c value suggests higher susceptibility to non-load-related cracking, PG 67-22 binder is more susceptible than the CRS-1h residue.

10.4.2 Multiple Stress Creep and Recovery (MSCR) Test

The MSCR test per AASHTO M332 (T350) evaluated elastic response and rutting resistance of the binders. The test was conducted on binders at 64°C after RTFO aging. The test applied 20 loading cycles at a low-stress level of 0.1 kPa and 10 cycles at a high-stress level of 3.2 kPa. Each loading cycle consisted of 1 second of creep and 9 seconds of recovery. For data analysis, strain responses were used to calculate percent recovery ($\%R_{3.2}$) and non-recoverable creep compliance (J_{nr}) using Equations 1 and 2, respectively. A higher $\%R_{3.2}$ value indicates better binder elasticity, and a lower J_{nr} value indicates better rutting resistance.

$$\%R = \frac{\varepsilon_r}{\varepsilon_r + \varepsilon_{nr}} * 100\% \qquad \text{Equation 1}$$

Where, ε_r = recoverable strain; and ε_{nr} = non-recoverable strain.

$$J_{nr} = \frac{\varepsilon_{nr}}{\sigma} \qquad \text{Equation 2}$$

Where, σ = creep stress.

Table 3 presents the MSCR results of the binders. The PG 67-22 binder had a notably lower $J_{nr,3.2}$ value than the CRS-1h residue, indicating a stiffer binder and better rutting resistance (as observed with the Superpave PG results). Nevertheless, both binders presented an "S" (standard traffic loading) MSCR traffic rating. The CRS-1h residue had a lower $\%R_{3.2}$ value than the PG 67-22 binder, since the $\%R_{3.2}$ parameter was highly influenced by the lower creep compliance $J_{nr,3.2}$ of the PG 67-22 binder.

TABLE 3 MSCR Results for Binders

Tack coat type	MSCR $J_{nr,3.2}$ (1/kPa)	MSCR $\%R_{3.2}$ (%)	Traffic rating
PG 67-22 binder	2.51 (S)	0.89	S
CRS-1h residue	3.27 (S)	0.34	S

* S = standard traffic loading (<10 million ESALs and >70 km/h)

10.5 Interface Bond Shear Strength Evaluation

The ALDOT 430 procedure was used in this study to evaluate the effects of tack coat type and rate on initial and long-term shear bond strength under the influence of aging and traffic loading. This test is performed on six-inch (150-mm) diameter field cores. Specimens are preconditioned at 77°F (25°C) for at least 2 hours before positioning within the bond strength device, ensuring vertical alignment with traffic direction and precise centering of the marked layer interface between the edge of the shearing frame and the edge of the reaction frame (Figure 7). The shearing frame can move while the reaction frame is immobile. The assembly is then incorporated into the Marshall Stability testing apparatus, placing the loading head on the top of the bonded interface. By employing a vertical shear load in a controlled displacement mode (2 inches/minute), the Marshall Stability test determines peak shear loading and corresponding displacement of the interface. Interface bond strength is calculated by dividing the maximal shear load (lb.) by the specimen's cross-sectional area (in^2). Adequate test validation requires a minimum of three specimens per testing protocol.

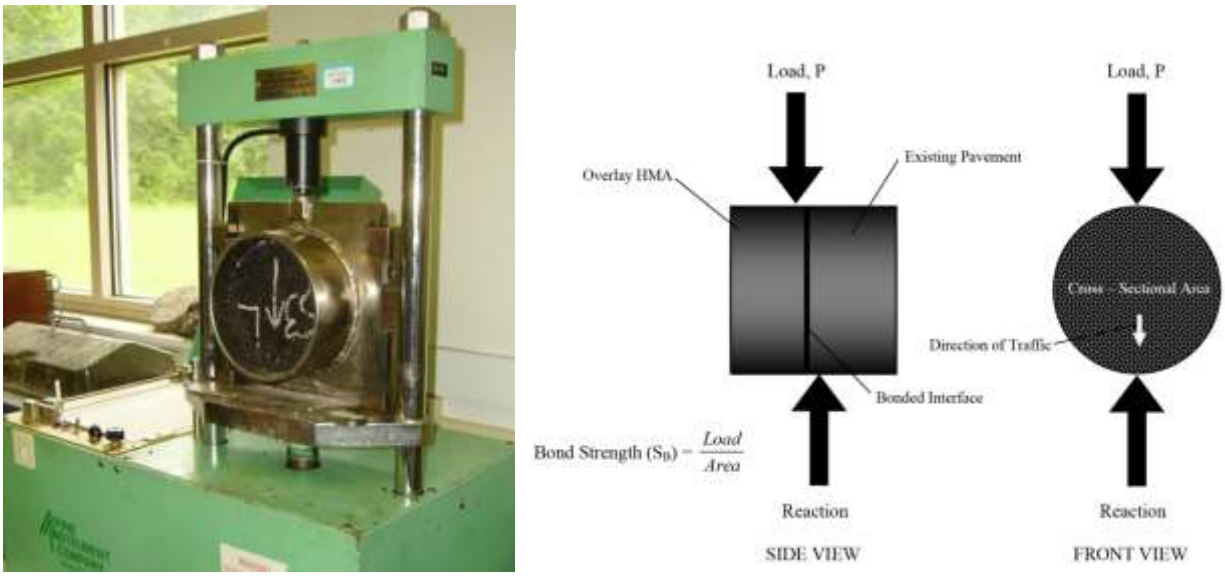

FIGURE 7 ALDOT 430 Bond Strength Testing Apparatus.

The average interface bond strength for the field cores obtained from Sections W4-A, W4-B, and W4-C are shown in Figure 8. Field cores were extracted from the wheel paths of each subsection at different field aging intervals (i.e., 3, 6, 18, and 24 months after construction) after truck trafficking was initiated. The following observations related to tack coat type and rate can be drawn based on the interface bond strength results—

- Section W4-B (CRS-1h applied at 0.06 gal/yd^2 with 0.036 gal/yd^2 residual rate) presented the highest bond strength value regardless of the field aging interval.
- Sections W4-A (PG 67-22) and W4-B (CRS-1h) used a 0.06 gal/yd^2 tack coat application rate but had different residual rates (W4-A, 0.060 gal/yd^2 residual rate; W4-B, 0.036 gal/yd^2 residual rate). The increase in bond strength between 3 and 24 months after construction was slightly higher for W4-A (38.4%) than for W4-B (35.9%).

- Section W4-C (CRS-1h applied at 0.10 gal/yd^2 with 0.060 gal/yd^2 residual rate) showed the highest increase (i.e., 40.2%) in bond strength between 3 and 24 months after construction.

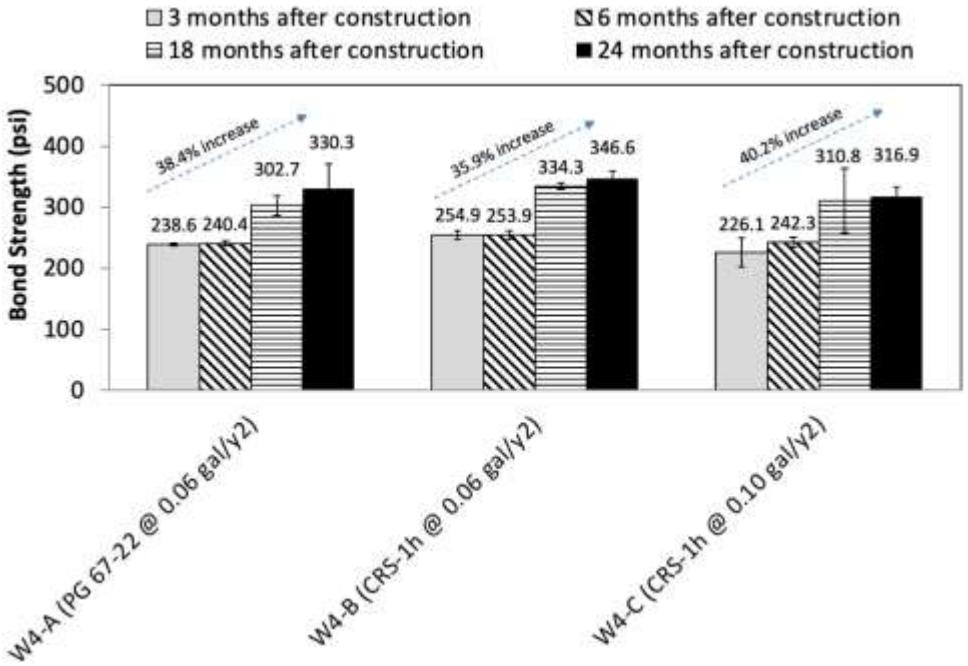

FIGURE 8 W4 interface bond strength after different field aging intervals.

10.6 Friction Evaluation

Pavement surface frictional properties of Section W4 as a function of speed were measured using the DFT after 3 and 18 months of construction (Figure 9). The DFT consists of a horizontal spinning disk fixed with three spring-loaded rubber sliders that contact the pavement surface. A water spray system is used to simulate wet conditions. When the disk is lowered onto the test surface, the DFT measures the torque generated by the sliders' resistive force to calculate the friction coefficient of the asphalt pavement surface. Velocity is also measured to indicate the relationship between the coefficient of friction and speed. Each DFT test includes three replicate measurements as described in ASTM E 1911. This study selected speeds of 20, 40, and 60 km/h for measuring friction properties of the pavement surface of Sections W4-A, W4-B, and W4-C. Heitzman and Moore indicated that 40 km/h DFT speed produces the most repeatable measure (*8*). Therefore, this speed was used for detailed analysis.

FIGURE 9 Dynamic friction tester (DFT).

Figure 10 shows the average friction number (F_n) at 40 km/h 3 and 18 months after construction of Section W4. Subsections W4-A, W4-B, and W4-C presented similar friction values regardless of the field aging interval. As expected, friction values decreased over time due to applied traffic.

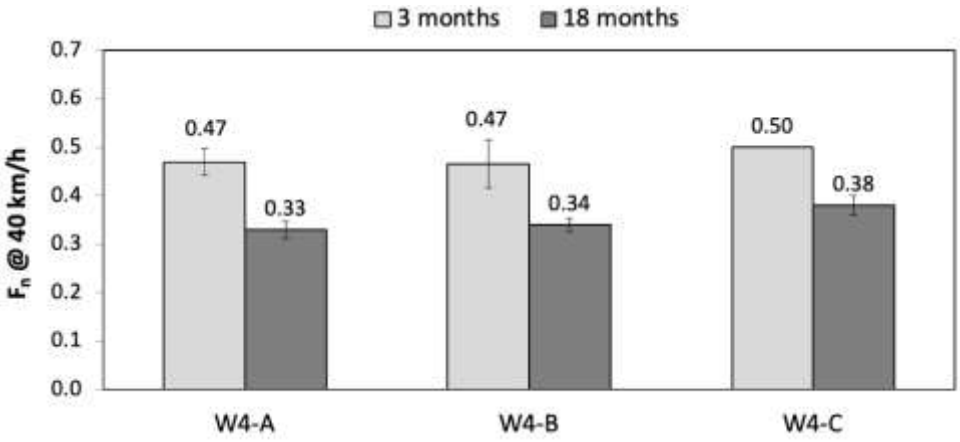

FIGURE 10 Average F_n at 40 km/h after different field aging intervals.

10.7 Field Performance Evaluation

As part of the eighth research cycle, subsections W4-A, W4-B, and W4-C were trafficked starting November 9, 2021, and approximately 10 million ESALs were applied by the end of fleet operations on April 03, 2024. Truck traffic occurred Monday evenings through Saturday mornings. Surface condition surveys were conducted weekly on Mondays to collect rutting, cracking, ride quality, and surface texture data.

10.7.1 Rutting

Rutting in the wheel path was evaluated using the Pathway PathRunner inertial profiler and the ALDOT beam procedure (ALDOT T392). This method utilizes a four-foot beam with a dial gauge to measure rut depths along predetermined locations in the wheel path of each test section with accuracy within ± 2.5 mm.

Figure 11 compares rut depth versus traffic ESALs for W4-A, W4B, and W4-C. Rut depths were similar for Sections W4-B and W4-C (1.4 and 1.8 mm, respectively) and slightly lower for Section W4-A (0.5 mm). However, all rut depths are below the typical maximum field rut depth threshold of 12.5 mm.

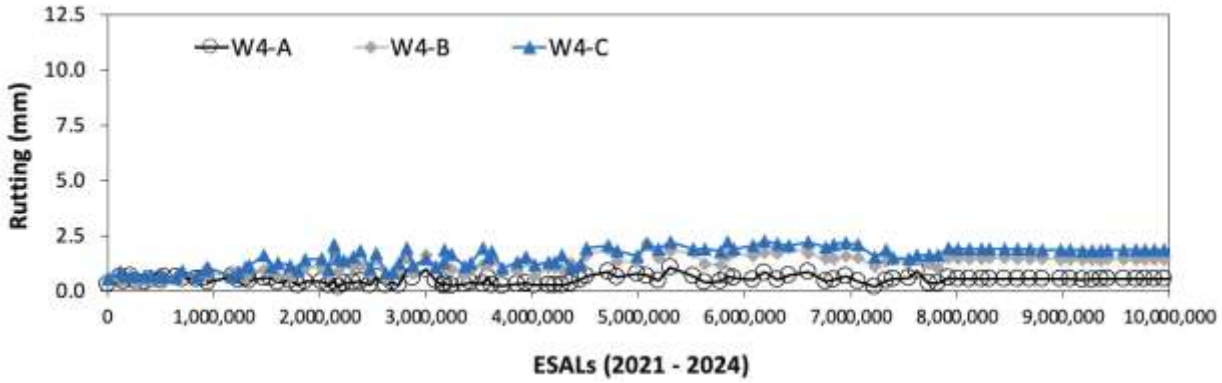

FIGURE 11 Field rut depth measurements.

10.7.2 Surface Cracking

The procedure for gathering surface cracking data commenced by visually examining each test section. Subsequently, the identified surface cracks were systematically mapped and quantified. The size of the cracked area was assessed by measuring the length of the cracks within the test section. This data was then employed to calculate the percentage of lane area impacted by surface cracking. After approximately 10 million ESALs were applied by the end of fleet operations in 2024, no cracking was observed in subsections W4-A, W4-B, and W4-C (Figure 12).

FIGURE 12 Panoramic view of Section W4.

10.7.3 Ride Quality

Ride quality (pavement roughness) was assessed through international roughness index (IRI) measured by the Pathway PathRunner inertial profiler. FIGURE shows ride quality data expressed as IRI. The extraction of field cores from the wheel paths of each subsection (for interface bond strength evaluation) affected the overall smoothness of Section W4. Overall IRI values were 140.8, 103.7, and 129.1 in/mile for W4-A, W4-B, and W4-C, respectively.

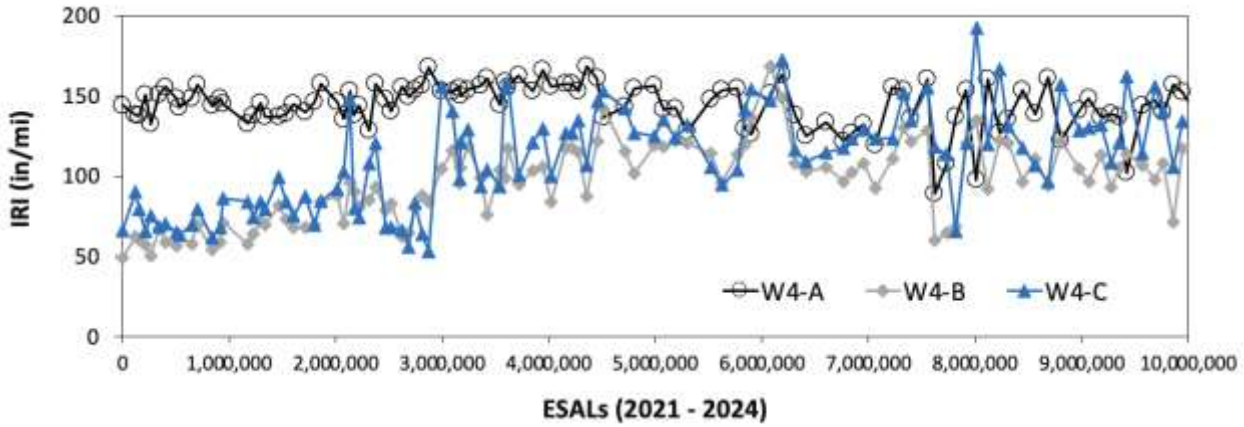

FIGURE 13 Ride quality (IRI) measurements.

10.7.4 Surface Macrotexture

The surface texture of each subsection was assessed through mean profile depth (MPD) and measured using the Pathway PathRunner inertial profiler. Figure 14 compares MPD measurements for the W4 subsections. A minor increase in macrotexture can be seen due to removing asphalt film on the pavement surface at the onset of truck trafficking. At the end of trafficking for the eighth research cycle, MPD results were almost identical for the three subsections: 0.97 mm for W4-A, 0.94 mm for W4-B, and 0.91 mm for W4-C.

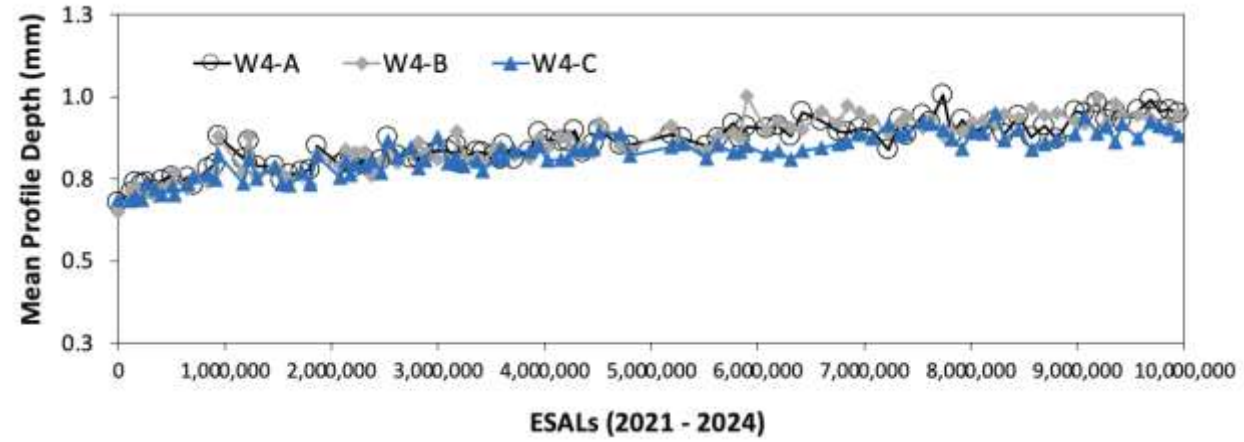

FIGURE 14 Surface macrotexture (MTD) measurements.

10.8 Conclusions and Recommendations

This experiment evaluated 1) initial and long-term effects of tack coat type and rate on interface shear bond strength under the influence of aging and traffic loading, and 2) whether NCDOT's mixture specifications can ensure the stability of high recycled content mixes under realistic, high shear stress conditions. The experiment compared interface bond shear strength and field performance of sections with varied tack coat types and application rates under the same pavement structure, traffic, and climatic conditions.

Section W4, a 1.5” milled asphalt pavement section, was divided into three subsections (W4-A, W4-B, and W4-C). A PG 67-22 binder was applied at 0.06 gal/yd^2 (0.060 gal/yd^2 residual rate) for the first 100 feet (Section W4-A), then CRS-1h was applied at 0.06 gal/yd^2 (0.036 gal/yd^2 residual rate) for the next 50 feet (Section W4-B) and at 0.10 gal/yd^2 (0.060 gal/yd^2 residual rate) for the final 50 feet (Section W4-C). The mix was a PG 58-28 neat binder, a blend of granite and sand, 25% RAP, and 4% RAS. The subsections were trafficked for 10 million ESALs from November 9, 2021, through April 3, 2024. Their field performance, including rutting, cracking, ride quality, and surface macrotexture, was monitored weekly. Based on laboratory test results and field performance of Sections W4-A, W4-B, and W4-C, the following conclusions can be drawn—

- Section W4-B (CRS-1h applied at 0.06 gal/yd^2 with 0.036 gal/yd^2 residual rate) presented the highest interface shear bond strength value, regardless of field aging interval.
- Section W4-A (PG 67-22) and Section W4-B (CRS-1h) used a 0.06 gal/yd^2 tack coat application rate with different residual rates (W4-A, 0.060 gal/yd^2 residual rate; W4-B, 0.036 gal/yd^2 residual rate). Throughout 3 to 24 months post-construction, Section W4-A recorded a slightly higher bond strength increase of 38.4% compared to W4-B's increase of 35.9%.
- Section W4-C (CRS-1h applied at 0.10 gal/yd^2 with 0.060 gal/yd^2 residual rate) showed the highest increase (40.2%) in bond strength between 3 and 24 months after construction.
- The three subsections W4-A, W4-B, and W4-C presented similar friction values, regardless of field aging interval.
- Rut depths were similar for Sections W4-B and W4-C (1.4 and 1.8 mm, respectively) and slightly lower for Section W4-A (0.5 mm). All rut depths are below the typical maximum field rut depth threshold of 12.5 mm.
- None of the subsections cracked during the eighth research cycle, where approximately 10 million ESALs were applied by the end of fleet operations in 2024.
- The extraction of field cores from the wheel paths of each subsection for interface bond strength evaluation affected the overall smoothness of Section W4. IRI values were 140.8, 103.7, and 129.1 in/mile for W4-A, W4-B, and W4-C, respectively.
- At the end of truck trafficking for the eighth research cycle, MPD results were almost identical for the three subsections: 0.97 mm for W4-A, 0.94 mm for W4-B, and 0.91 mm for W4-C.

In summary, tack coat type and rate can influence interface shear bond strength over time. The experiment also highlights the capability of NCDOT’s mixture specifications to produce stable high recycled content mixes under realistic, high-shear stress conditions. W4-A, W4-B, and W4-C showed good field performance after 10 million ESALs. The study supports maintaining these subsections for traffic continuation, allowing for a thorough field cracking, rutting, texture, and friction performance evaluation.

10.9 References

13. Willis, J., and D. Timm. Forensic Investigation of a Rich-Bottom Pavement, NCAT Report 06-04, National Center for Asphalt Technology at Auburn University, 2006.
14. Florida Department of Transportation. *Pavement Conditions*. https://www.fdot.gov/programmanagement/implemented/urlinspecs/pavement.shtm
15. Flexible Pavements of Ohio. *Proper Tack Coat Application*. Technical Bulletin, Columbus, OH, May 2001.
16. Texas Department of Transportation. Proper Use of Tack Coat. Technical Advisory 2001-1, Construction and Bridge Divisions, Austin, TX, June 2001.
17. California Department of Transportation. *Tack Coat Guidelines*. Division of Construction, State of California, April 2009.
18. Mohammad, L. N., M. A. Elseifi, A. Bae, N. Patel, , J. Button, and J. A. Scherocman. NCHRP Report 712: Optimization of Tack Coat for HMA Placement. National Cooperative Highway Research Program, Washington, D.C., 2012.
19. Anderson, M., G. N. King, D. I. Hanson, and P. B. Blankenship. Evaluation of the Relationship between Asphalt Binder Properties and Non-Load Related Cracking. *Journal of the Association of Asphalt Paving Technologists*, Vol. 80, pp. 615-664, 2011.
20. Heitzman, M., and J. Moore. Evaluation of Laboratory Friction Performance of Aggregates for High Friction Surface Treatments. NCAT Report 17-01, National Center for Asphalt Technology at Auburn University, 2017.

11. OKLAHOMA DEPARTMENT OF TRANSPORTATION BALANCED MIX DESIGN EXPERIMENT

11.1 Background

The Oklahoma Department of Transportation (ODOT) started implementing balanced mix design (BMD) in 2017. The first draft of ODOT's provisional BMD specification required using the Hamburg Wheel Tracking Test (HWTT) (AASHTO T 324) and the Illinois Flexibility Index Test (I-FIT) (AASHTO T 393) to evaluate rutting and cracking resistance, respectively. Based on the findings of several research studies, ODOT replaced the I-FIT with the Indirect Tensile Asphalt Cracking Test (IDEAL-CT) (ASTM D8225) as its BMD cracking test in 2019. Those studies found that both tests could discriminate asphalt mixes with different cracking resistance (Al-Qadi et al., 2015; Zhou et al., 2017), but the IDEAL-CT is simpler and faster and, thus, more suitable for quality control (QC) and acceptance testing during production.

ODOT's current provisional BMD specification uses the *Volumetric Design with Performance Optimization* approach per AASHTO PP 105 to design asphalt mixtures that meet their performance requirements but not necessarily Superpave volumetric requirements. The design air voids content is relaxed to 3.0 to 4.0% at a design gyration (N_{design}) of 50 for mixtures containing a PG 64-xx, 65 for PG 70-xx, and 80 for PG 76-xx binder. The minimum voids in mineral aggregate (VMA) criteria vary from 12.5% to 16.5% as a function of nominal maximum aggregate size (NMAS). The HWTT criteria are based on the number of passes to reach 12.5 mm rut depth at 50°C, where a minimum of 10,000 passes is required for mixtures containing a PG 64-xx, 15,000 for PG 70-xx, and 20,000 passes for PG 76-xx binder. The IDEAL-CT criteria include a minimum cracking tolerance index (CT_{Index}) of 100 for surface mixes and 60 for non-surface mixes, regardless of virgin binder grade. Both the HWTT and IDEAL-CT are conducted on specimens short-term aged for 4 hours at 135°C per the previous AASHTO R 30. Production acceptance is purely based on volumetric properties without performance test requirements.

11.2 Scope and Objectives

As shown in Figure 1, ODOT sponsored three BMD sections on the NCAT Test Track: S1 in the 2018 research cycle and N8 and N9 in the 2021 cycle. S1 was a 5.0-inch mill-and-inlay section using a BMD surface mix with 12% reclaimed asphalt pavement (RAP). N8 was a 5.5-inch mill-and-inlay section using a BMD surface mix with 30% RAP and a bio-based recycling agent (RA). N9 was built as a 1.5-inch mill-and-inlay section designed as a BMD mix with 12% recycled tire rubber (RTR) added dry during production, and the underlying structure was a perpetual pavement where a small amount of top-down cracking remained after milling. This cracking was also present during reconstruction for the 2018 cycle.

The overall objective of these three sections was to support ODOT in implementing mixture performance testing and criteria for BMD while exploring the responsible use of RAP and RTR. For Section N9, an additional objective was to assess the performance of the rubber-modified mix and its potential to prevent reflection cracking from the underlying layer. The recurrence of reflective cracking with the new rubber-modified BMD is compared to the previous cycle conventional BMD mix to quantify the impact of the rubber additive.

FIGURE 1 ODOT's BMD sections (S1, N8, and N9) on the NCAT Test Track.

11.3 Section S1– BMD with Low RAP

11.3.1 Mix Design

Table 1 presents the job mix formula (JMF) and quality control (QC) data of the surface and base mixes. Note that the JMF data was provided by an asphalt contractor in Oklahoma, while the QC data was collected at NCAT during Test Track construction. The surface mix was an ODOT S4 mix with 12.5 mm NMAS. It used a PG 70-28 SBS modified binder, a blend of granite, chat, and sand, as well as 12% RAP. The base mix was an ODOT S3 mix with 19 mm NMAS. It used a PG 64-28 SBS modified binder, a blend of granite and sand, and 30% RAP. To mitigate the stiffening impact of high RAP, a tall-oil-based RA was added at 3.1% dosage by weight of virgin binder. Both the surface and base mixes were designed using the *Performance Modified Volumetric Design* approach as described in AASHTO PP 105. Figure 2 presents the contractor's HWTT and I-FIT results of the surface and base mixes on a performance diagram, where the dashed lines represent ODOT's BMD criteria in 2018. Both mixes fell within the "sweet zone" of the performance diagram with expected balanced rutting and cracking performance.

TABLE 1 Mix Design and QC Data of S1 Surface and Base Mixes

Sieve (in.)	Job Mix Design		Quality Control	
	S1 Surface	S1 Base	S1 Surface	S1 Base
25 mm (1”)	100	100	100	100
19 mm (3/4”)	100	98	100	99
12.5 mm (1/2")	94	89	94	89
9.5 mm (3/8”)	88	83	90	84
4.75 mm (#4)	63	62	68	63
2.36 mm (#8)	37	42	41	42
1.18 mm (#16)	24	28	28	28
0.60 mm (#30)	17	19	20	19
0.30 mm (#50)	10	12	13	12
0.15 mm (#100)	5	7	7	7
0.075 mm (#200)	4.5	5.7	5.4	5.2
Design Gyration	65	65	65	65
NMAS (mm)	12.5	19	12.5	19
OBC (%)	5.8	5.2	5.5	5.1
Virgin Binder	70-28 SBS	64-28 SBS	70-28 SBS	64-28 SBS
RAP Binder Ratio (%)	11	30	11	31
RA Dosage (% weight of virgin binder)	-	3.1	-	3.1
Air Voids (%)	3.4	3.4	2.3	2.7
Blend G_{sb}	2.619	2.610	2.632	2.614
G_{mm}	2.410	2.450	2.432	2.459
G_{mb}	2.329	2.367	2.377	2.392
VMA (%)	16.2	14.0	14.7	13.1
V_{be} (%)	12.8	10.6	12.4	10.4
VFA (%)	79	76	85	79
Dust Proportion	0.8	1.3	1.0	1.2

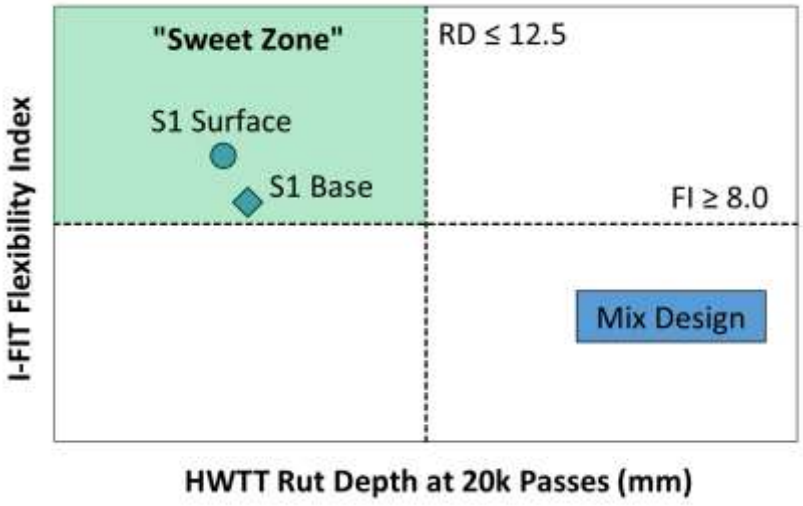

FIGURE 2 HWTT versus I-FIT performance diagram of S1 surface and base mixes from mix design testing (RD = rut depth; FI = flexibility index).

11.3.2 Mix Production and Construction

Section S1 was built as a 5.0-inch mill-and-inlay, consisting of a 2-inch surface mix over a 3-inch base mix. The section was built over an existing perpetual pavement with 24 inches of asphalt mixes from previous Test Track research cycles. Both the surface and base mixes were produced with virgin binders at the same performance grade but from different sources than those used in mix design. The base mix was produced and placed on September 20, 2018, and the surface mix was produced and placed the next day. Climate conditions were ideal for paving with a 24-hour high temperature of 92°F, a low temperature of 73°F, and no rainfall.

As shown in Table 1, QC testing of the base mix indicated a slight reduction in the total binder content from 5.2% in mix design to 5.1% at production, but there were no significant changes in the combined aggregate gradation. Although the mix had a reduction in air voids from 3.4% in mix design to 2.7% at production and a reduction in VMA from 14.0% to 13.1%, these differences were within ODOT's production tolerance. The base mix was produced at approximately 305°F and had an in-place density averaging 94.6%. Figure 3 shows the laydown and compaction of the base mix.

FIGURE 3 Laydown and compaction of S1 base mix.

QC testing of the surface mix showed a reduction in total binder content from 5.8% in mix design to 5.5% at production but no significant changes in combined aggregate gradation. The mix had a notable reduction in air voids from 3.4% in mix design to 2.3% at production and a reduction in VMA from 16.2% to 14.7%, but these changes were within ODOT's production tolerance. The surface mix was produced at approximately 325°F and had an in-place density averaging 96.1%. Figure 4 shows the laydown and compaction of the surface mix.

FIGURE 4 Laydown and compaction of S1 surface mix.

11.3.3 Laboratory Testing and Data Analysis

During construction, plant mixes were sampled at the Test Track and transported to the NCAT lab, where they were reheated for BMD performance testing with the HWTT and I-FIT. In addition, the IDEAL-CT test was conducted to explore its feasibility as a potential surrogate test for the I-FIT. To consider the effect of asphalt aging on mixture durability and cracking resistance, the I-FIT and IDEAL-CT were conducted on both reheated and critically aged specimens. The critical aging (CA) protocol was loose mix aging for 8 hours at 135°C to simulate a critical field aging condition of 70,000 cumulative degree days, where top-down cracking starts to develop after 4 to 5 years of in-service in Alabama (Chen et al., 2018; Chen et al., 2020).

Figure 5 presents the performance diagram of the reheated specimens, where the I-FIT results are plotted on the y-axis against the HWTT results on the x-axis (using rut depth at 20,000 passes). Mix design results provided by the contractor are also presented for comparison purposes (note that no mix design verification was conducted at NCAT due to schedule challenges). For both mixes, the reheated specimens from production had similar HWTT but significantly reduced I-FIT results compared to the mix design specimens. The reheated specimens failed ODOT's previous I-FIT criterion and, thus, fell outside the "sweet zone" of the performance diagram, as shown in Figure 5. The difference in the HWTT and I-FIT results from mix design versus production could be due to several factors, including a change in virgin binder source, changes in the mix associated with plant production, and between-lab variability associated with sample preparation and testing. Further discussions of these factors can be found in Chapter 13 of the previous NCAT Test Track findings report (West et al., 2021).

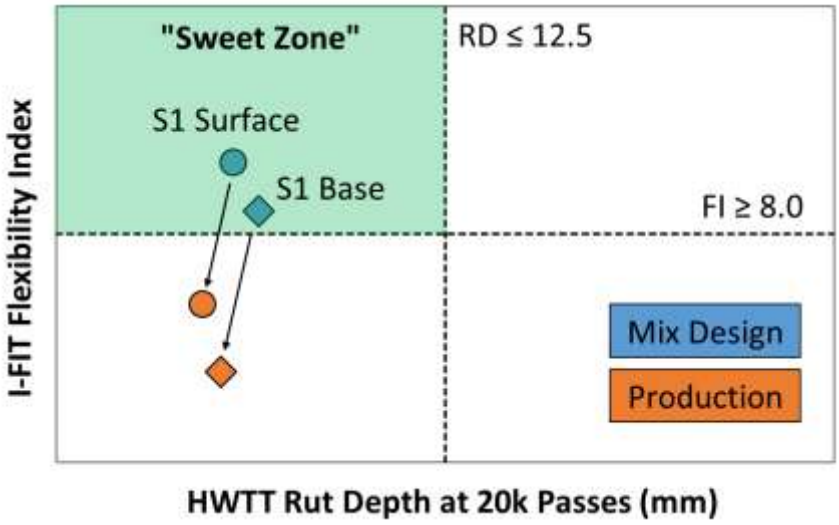

FIGURE 5 HWTT-versus-I-FIT performance diagram of S1 surface and base mixes from mix design versus production testing.

Figures 6 and 7 present the I-FIT and IDEAL-CT results, respectively, of reheated and critically aged specimens from production. For both mixes, the critically aged specimens showed reduced cracking resistance compared to the reheated specimens, as indicated by reduced *FI* and CT_{Index} results. The reheated specimens did not meet ODOT's current IDEAL-CT criteria for mix design (i.e., minimum CT_{Index} of 100 for surface mixes and 60 for non-surface mixes).

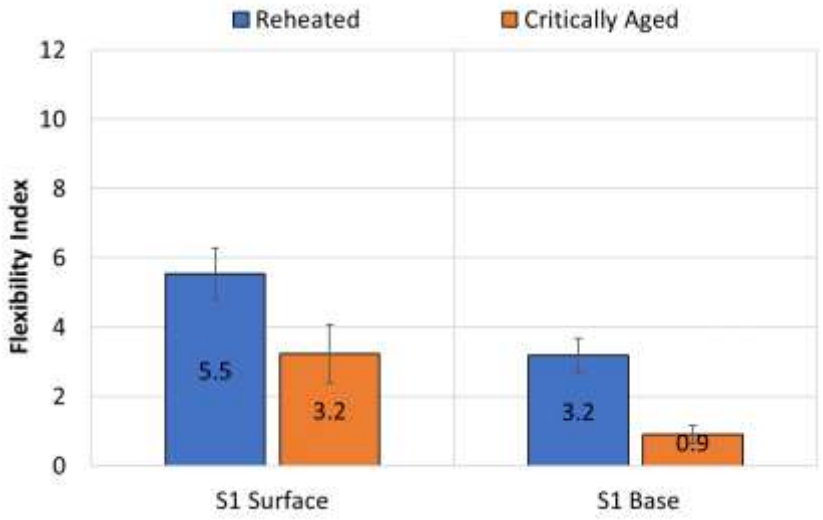

FIGURE 6 I-FIT results of reheated versus critically aged specimens for S1 surface and base mixes.

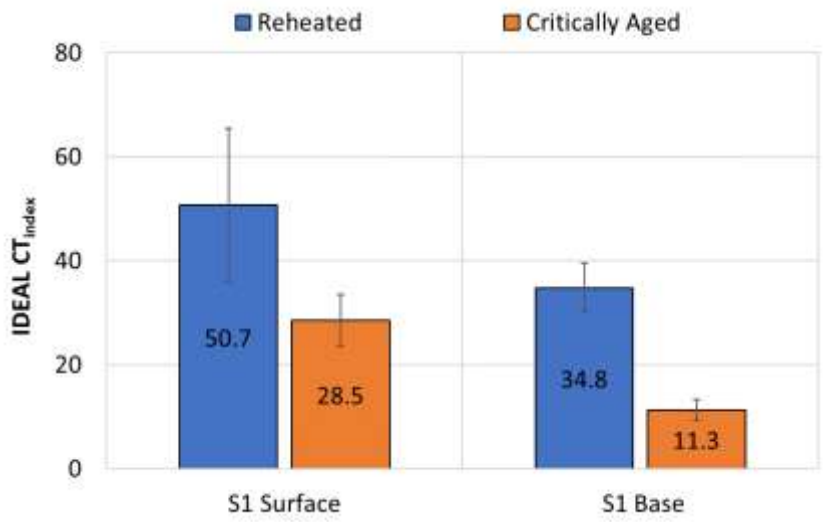

FIGURE 7 IDEAL-CT results of reheated versus critically aged specimens for S1 surface and base mixes.

11.3.4 Field Performance

Section S1 started trafficking on October 10, 2018. As of April 12, 2024, approximately 20 million ESALs were applied. Surface cracking, rutting, and smoothness data were monitored on a weekly basis using an automated pavement condition survey vehicle. Overall, Section S1 performed extremely well with no surface cracking, less than 0.3 inches of rutting, and a steady international roughness index (IRI), as shown in Figures 8 and 9.

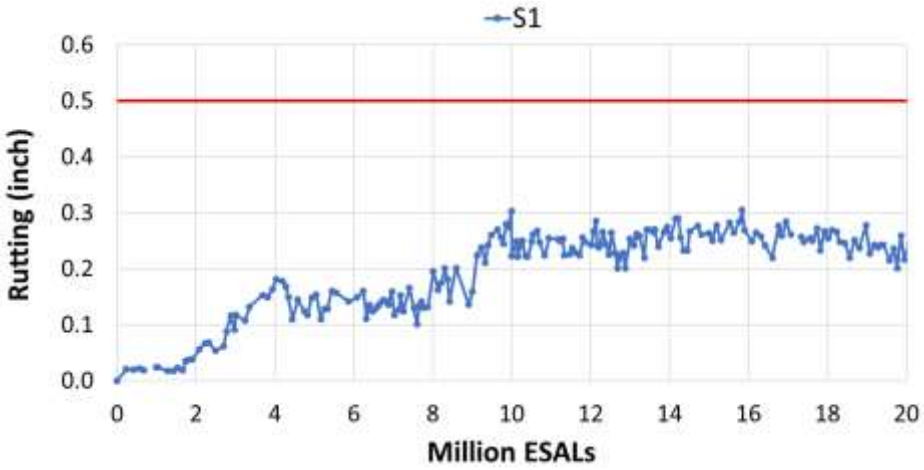

FIGURE 8 Field rutting data of Section S1.

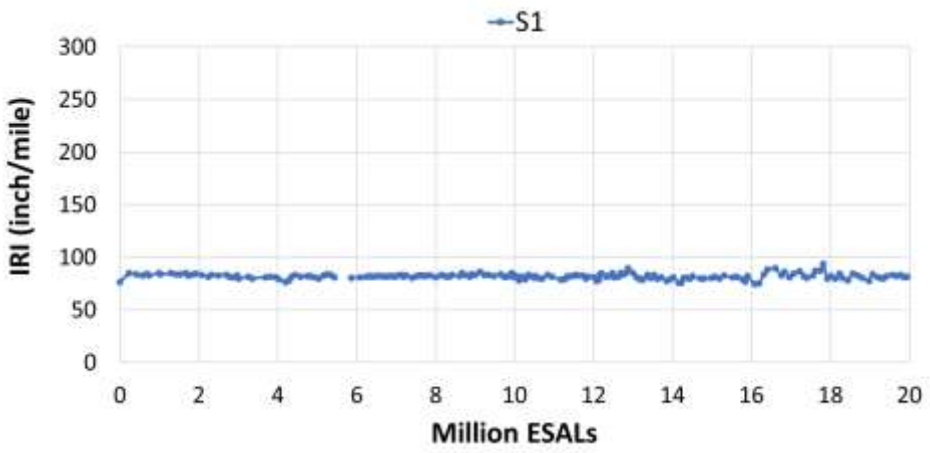

FIGURE 9 Field smoothness data of Section S1.

11.3.5 Findings and Conclusions

For both the surface and base mixes, the production mix had similar rutting resistance but significantly reduced cracking resistance compared to the mix design. The production mix passed the HWTT criterion but failed ODOT's previous I-FIT and current IDEAL-CT criteria, which indicated the mixes had good rutting resistance but could be susceptible to cracking. Nevertheless, the section performed well with minimal rutting and no surface cracking after 20 million ESALs. The discrepancy between the I-FIT/IDEAL-CT results and field cracking performance suggests that ODOT's BMD cracking criteria may be over-conservative for asphalt pavements with a robust underlying condition.

11.4 Section N8– BMD with High RAP and Recycling Agent

11.4.1 Mix Design

Table 2 presents the JMF and QC data of the surface and base mixes used in Section N8. The surface mix was an ODOT S4 mix with 12.5 mm NMAS, which was designed at NCAT using the same aggregate stockpiles (a blend of granite, chat, and sand) as the surface mix of Section S1 from the 2018 research cycle, except for an increased RAP content from 12% to 30% and a bio-based RA added at 3.0% by weight of virgin binder. The base mix used the same mix design as Section S1 from the 2018 research cycle, which was an ODOT S3 mix with 19 mm NMAS. It used a PG 64-28 SBS modified binder, a blend of granite and sand, 30% RAP, and a tall-oil-based RA at 3.1% by weight of virgin binder.

TABLE 2 Mix Design and QC Data of N8 Surface and Base Mixes

Sieve (in.)	Job Mix Design		Quality Control	
	N8 Surface	N8 Base	N8 Surface	N8 Base
25 mm (1”)	100	100	100	100
19 mm (3/4”)	100	98	100	99
12.5 mm (1/2")	92	89	94	88
9.5 mm (3/8”)	84	83	86	79
4.75 mm (#4)	63	62	62	59
2.36 mm (#8)	44	42	42	39
1.18 mm (#16)	29	28	28	26
0.60 mm (#30)	20	19	20	18
0.30 mm (#50)	13	12	13	13
0.15 mm (#100)	7	7	8	10
0.075 mm (#200)	5.2	5.7	6.5	8.5
Design Gyration	65	65	65	65
NMAS (mm)	12.5	19	12.5	19
OBC (%)	5.8	5.2	5.7	4.9
Virgin Binder	70-28 SBS	64-28 SBS	70-28 SBS	64-28 SBS
RAP Binder Ratio (%)	30	30	34	40
RA Dosage (% weight of virgin binder)	3.0	3.1	3.0	3.1
Air Voids (%)	3.3	3.4	0.8	2.8
Blend G_{sb}	2.619	2.610	2.629	2.667
G_{mm}	2.429	2.450	2.442	2.490
G_{mb}	2.349	2.367	2.422	2.419
VMA (%)	15.5	14.0	13.1	13.7
V_{be} (%)	12.2	10.6	12.3	10.9
VFA (%)	80	76	94	79
Dust Proportion	1.0	1.3	1.3	1.8

11.4.2 Mix Production and Construction

Section N8 was built as a 5.5-inch mill-and-inlay, consisting of a 2.3-inch surface mix over a 3.2-inch base mix. The section was built over an existing pavement from the 2015 Cracking Group experiment, which included 6.5 inches of asphalt mixes and 6 inches of aggregate base over the Test Track subgrade. The base mix was produced and placed on September 7, 2021, and the surface mix was produced and placed two days later. Climate conditions were ideal for paving, with temperatures ranging from 70°F to 90°F and less than 0.2 inches of rainfall.

As shown in Table 2, the surface mix had 1.3% more dust and 0.1% less asphalt binder at production compared to the JMF. The higher dust content of the production mix was a primary factor causing an approximately 2.5% reduction in air voids and VMA. Nevertheless, the V_{be} only changed by 0.1% from design to production. The surface mix was produced at 335°F and had an in-place density averaging 96.1%. The base mix had 2.8% more dust and 0.3% less asphalt binder at production compared to the mix design. Air voids and VMA reduced by 0.6% and 1.1%, respectively, which caused a 0.5% decrease in the V_{be}. The base mix was produced at 305°F and had an in-place density averaging 93.4%.

11.4.3 Laboratory Testing and Data Analysis

During construction, the surface mix was sampled at the Test Track and transported to the NCAT lab. Part of the mix was immediately compacted without reheating to make hot-compacted specimens, while the rest was stored in 5-gallon buckets and compacted later as reheated specimens. Both the hot-compacted and reheated specimens were tested with the IDEAL-CT and HWTT for BMD performance evaluation. The IDEAL-CT was also conducted on specimens that were critically aged for an additional 8 hours at 135°C after reheating to evaluate the long-term cracking resistance of the mix.

Figure 10 presents the performance diagram of the hot-compacted and reheated specimens, where the IDEAL-CT results are plotted on the y-axis against the HWTT results on the x-axis (using the rut depth at 15,000 passes). The two horizontal dashed lines represent ODOT's IDEAL-CT criteria from 2020 and 2023. As shown, the mix passed ODOT's IDEAL-CT and HWTT criteria and, thus, was located inside the "sweet zone" of the performance diagram with balanced rutting and cracking resistance.

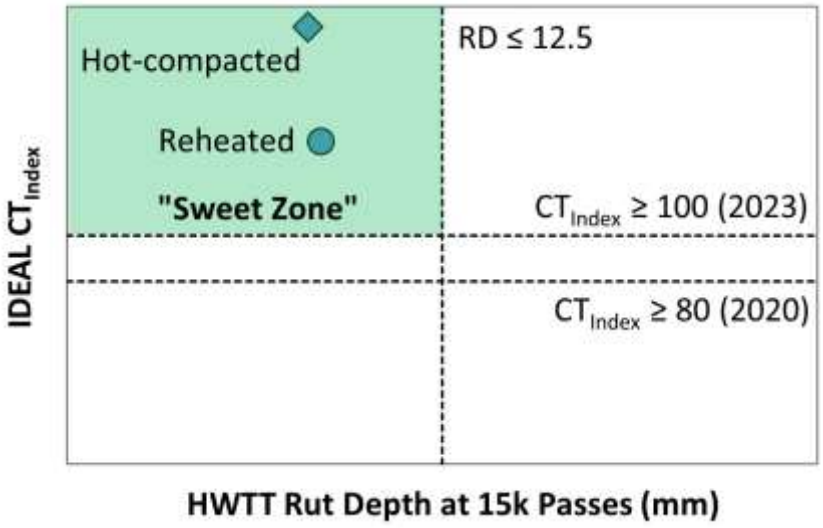

FIGURE 10 HWTT-versus-IDEAL-CT performance diagram of N8 surface mix.

Figure 11 presents the IDEAL-CT results of the hot-compacted, reheated, and critically aged specimens. The hot-compacted specimens had the highest average CT_{Index}, followed by the reheated specimens and the critically aged specimens, respectively, which indicated mix reheating and critical aging both had a detrimental impact on the cracking resistance of the mix due to oxidation and stiffening of the asphalt binder. The CT_{Index} decreased from 140.9 to 42.6 after critical aging, which was a reduction of approximately 70%. This reduction was more pronounced than the range reported by Vivanco et al. (2022), which may be attributed to the increased aging susceptibility of the mix due to the use of RA (Yin et al., 2019).

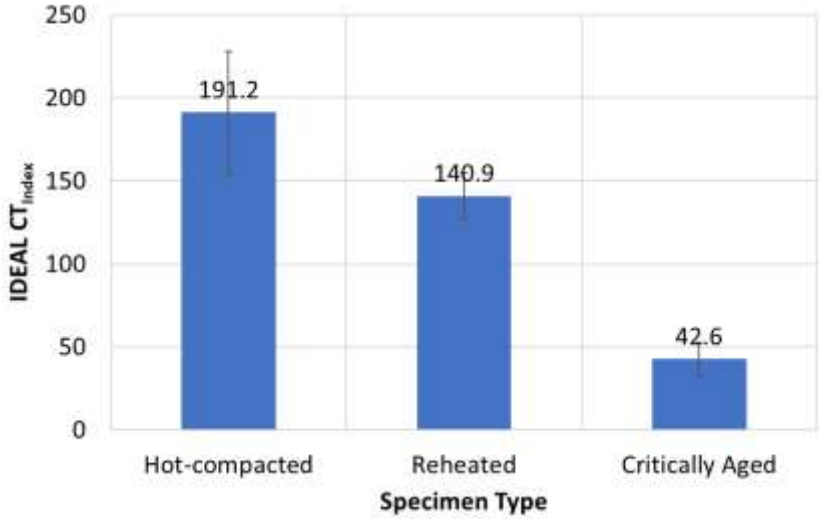

FIGURE 11 IDEAL-CT results of N8 surface mix.

11.4.4 Field Performance

Section N8 began trafficking on November 9, 2021. As of April 12, 2024, approximately 10 million ESALs were applied. Surface cracking, rutting, smoothness, and surface texture were monitored on a weekly basis using an automated pavement condition survey vehicle. Section N8 performed extremely well with no cracking, less than 0.2 inches of rutting, and steady international roughness index (IRI) and mean profile depth (MPD) after 10 million ESALs, as shown in Figures 12 through 14.

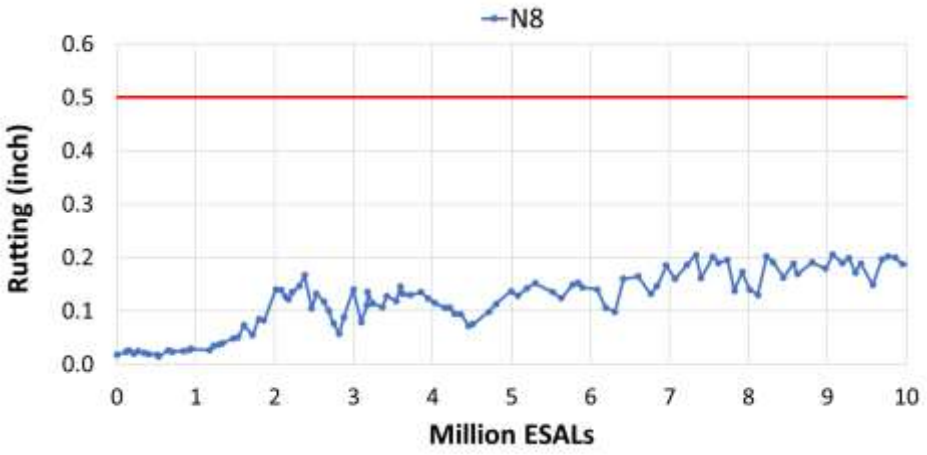

FIGURE 12 Field rutting data of Section N8.

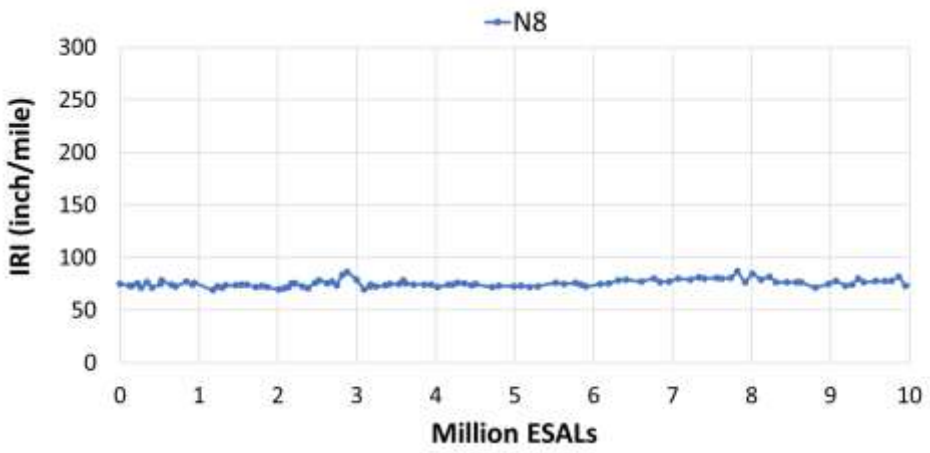

FIGURE 13 Field smoothness data of Section N8.

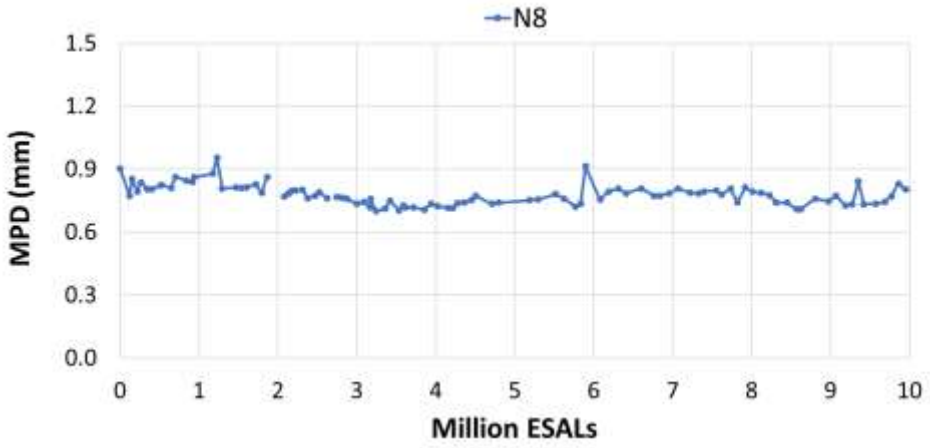

FIGURE 14 Field surface texture data of Section N8.

11.4.5 Findings and Conclusions

Although having significantly lower air voids and VMA on the production sample than ODOT's specification requirements, the surface mix with 30% RAP and a bio-based RA showed balanced rutting and cracking resistance in the BMD performance tests. This highlights the need to relax volumetric requirements for asphalt mixtures designed with BMD (especially those containing high RAP contents), provided they meet performance test requirements. Reheating and critical aging were detrimental to the cracking resistance of the mix, as indicated by a reduction in CT_{Index}. The section performed well with minimal rutting and no surface cracking after 10 million ESALs, which agrees with the performance test results compared to ODOT's BMD criteria.

11.5 Section N9– BMD with Dry RTR

11.5.1 Existing Pavement Condition

The existing pavement of Section N9 was constructed in 2006 as a perpetual pavement with 14 inches of asphalt mix over 9.6 inches of aggregate base and a soft subgrade that was

representative of the soil in Oklahoma. The pavement had excellent field performance through three research cycles from 2006 to 2015. No cracks developed after trafficking of 20 million ESALs, but top-down cracking along the left wheel path began to show in 2012 during the third research cycle.

In the 2015 research cycle, Section N9 was reconstructed as an open-graded friction course (OGFC) for ODOT to evaluate the friction performance of OGFC mixes using locally available aggregates. For the 2018 cycle, the top 1.5 inches of the OGFC and underlying mixes were milled, and a 1.5-inch surface layer using PG 70-28 SBS binder was placed to support ODOT's BMD implementation efforts. At the end of the 2018 research cycle in 2021, the section had only 3.3% of the lane area cracked, with the first cracking observed along the left path in January 2020. This cracking was expected because of existing cracking in the underlying layer. In July 2021, the top 1.5 inches of asphalt mix were milled in preparation for the 2021 research cycle.

11.5.2 Mix Design

The N9 (2021) surface mix was designed to replicate the N9 (2018) surface mix using a similar aggregate structure and stockpile while replacing the PG 76-28 SBS binder with a PG 58-28 plus 12% RTR. Table 3 presents a comparison of Section N9's JMF and QC data for the 2021 and 2018 cycles. As shown, the gradations of the two mixes were very similar with some variation due to stockpile gradation changes over time.

The RTR supplier recommended conditioning laboratory-prepared mixtures at 325°F for 4 hours to "activate" the rubber and achieve the required compaction level. However, conditioning the mix at a higher temperature than the standard short-term oven aging temperature reduced the cracking resistance of the mix, resulting in low IDEAL-CT CT_{Index} results. Therefore, the short-term aging procedure was modified to achieve compaction without sacrificing cracking performance. The modified procedure consisted of 30-minute conditioning aging at 325°F, followed by 3.5 hours of aging at 275°F. Upon completion of short-term aging, the mixture was brought back to a range between 315-325°F for compaction.

TABLE 3 Mix Design and QC Data of N9 Surface Mixes for the 2018 and 2021 TT Cycle

Sieve (in.)	Job Mix Design		Quality Control	
	N9 (2018)	N9 (2021)	N9 (2018)	N9(2021)
19 mm (3/4”)	100	100	100	100
12.5 mm (1/2")	100	100	100	99
9.5 mm (3/8”)	97	97	97	94
4.75 mm (#4)	77	73	76	73
2.36 mm (#8)	50	48	48	46
1.18 mm (#16)	34	33	33	30
0.60 mm (#30)	25	24	26	21
0.30 mm (#50)	18	16	18	14
0.15 mm (#100)	10	9	9	8
0.075 mm (#200)	6.5	5.5	6.0	5.4
Design Gyration	80	80	80	80
NMAS (mm)	9.5	9.5	9.5	9.5
OBC (%)	5.6	5.8	5.6	5.7
Virgin Binder	76-28 SBS	58-28	76-28 SBS	58-28
RAP Binder Ratio (%)	14	15	15	15
Air Voids (%)	4.0	3.3	2.1	2.5
Blend G_{sb}	2.642	2.646	2.663	2.665
G_{mm}	2.462	2.430	2.478	2.450
G_{mb}	2.364	2.350	2.427	2.388
VMA (%)	15.5	16.4	14.0	15.5
P_{be} (%)	4.9	5.7	5.0	5.6
VFA (%)	74	80	85	84
Dust Proportion	1.3	1.0	1.2	1.0

Two mix trials were developed to finalize the design of the 2021 N9 surface mix, and the mixture component and mixture performance of each are summarized in Table 4. The first trial with 5.8% OBC yielded a CT_{Index} of 84.3 and 12,900 passes to 12.5 mm rut depth, which met the preliminary cracking criterion but failed the rutting criterion due to early stripping. Based on the observation of the N9 mix in the 2018 research cycle, this was attributed to the susceptibility of the aggregate blend to stripping. To address this issue, the second trial incorporating 0.5% liquid anti-strip (LAS) agent was further evaluated with HWTT and IDEAL-CT. As shown in Table 4, the passes to 12.5 mm rut depth were greater than the minimum criterion of 15,000 passes for PG 70-xx, but CT_{Index} failed the preliminary criterion of 80.

TABLE 4 Trial Mix Design Results for N9 Surface Mix

Design ID	OBC (%)	LAS (%)	CT_{Index}	Passes to 12.5mm Rut Depth	Stripping Inflection Point
Design Trial #1	5.8	0	84.3	12,900	5,600
Design Trial #2	5.8	0.5	65	15,600	10,167

Since the N9 mix with this aggregate didn’t experience stripping failure in the field during the 2018 research cycle and considering the special modifications to the aging procedure when incorporating dry rubber, ODOT decided to move forward with this design at an optimum AC content of 5.8% AC and incorporated an antistrip agent.

Issues with specimen expansion were encountered when working with the mix modified with dry rubber additive. Specimen expansion is typical for mixes incorporating certain rubber or plastic additives, where the gyratory specimens expand above the target height after immediately extruding them from the mold, as illustrated in Figure 15. To mitigate this issue, specimens must cool under a fan in the gyratory molds while the specimen is still under pressure from the gyratory ram for at least 15 to 30 minutes after compaction. States that use rubber mixtures regularly recommend similar protocols to account for specimen expansion (Caltrans, 2023).

FIGURE 15 Typical expansion with RTR specimens.

11.5.3 Mix Production and Construction

Section N9 was built as a 1.5-inch mill-and-inlay on a 14-inch asphalt pavement. The mix was produced and placed on September 10, 2021, with a 24-hour high temperature of 85°F, a low temperature of 64°F, and no rainfall over 24 hours. As shown in Table 3, quality control testing of the production mix closely matched JMF gradation, while the asphalt content was 0.1% lower than the target. Other volumetric requirements, such as VMA, were very close to the target. However, the production mix had 2.5% air voids while the JMF results indicated 3.3% air voids. The mix had an average production temperature of approximately 335°F and in-place density of 95.7%. Figure 16 shows the mix laydown and compaction for Section N9.

FIGURE 16 Laydown and compaction of N9 surface mix.

11.5.4 Laboratory Testing and Data Analysis

During construction, the N9 mix was sampled and then transported to the NCAT lab. Part of the mix was compacted without reheating to make hot-compacted specimens, while the rest was stored in 5-gallon buckets and compacted later to fabricate reheated specimens. Both the hot-compacted and reheated specimens were tested with the IDEAL-CT and HWTT for BMD performance evaluation. The IDEAL-CT was conducted on specimens critically aged for an additional 8 hours at 275°F after reheating to evaluate the cracking resistance of the mix after aging.

Figure 17 shows the IDEAL-CT results of the hot-compacted, reheated, and critically aged specimens. The reheated specimens had the highest average CT_{Index}, followed by the hot-compacted specimens and then the critically aged specimens. The hot-compacted and reheated results exceeded CT_{Index} results obtained during the design phase and met the preliminary ODOT IDEAL-CT criterion of 80. Although the hot compacted specimens were expected to yield higher CT_{Index} results than the reheated specimens, cooling in the gyratory molds (to prevent specimen expansion) caused the hot-compacted specimens to remain in the oven for an excessive length of time while waiting for compaction. Hence, these specimens were oven-aged significantly longer than a typical hot-compacted specimen, which likely reduced their cracking resistance relative to the re-heated specimens.

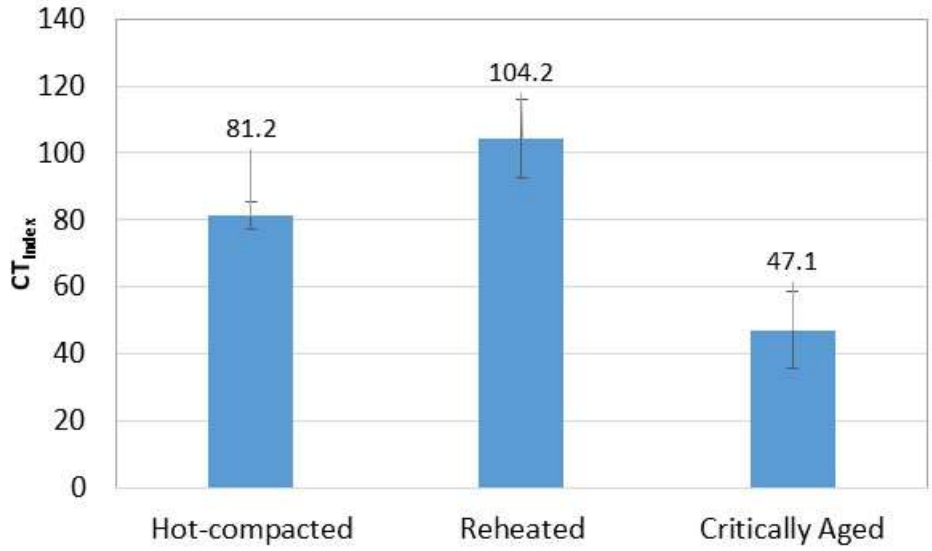

FIGURE 17 IDEAL-CT results of N9 surface mix.

As shown in Figure 18, HWTT results of hot-compacted specimens improved the number of passes from 15,600 obtained during the design phase to 17,400 to reach a 12.5 mm rut depth. However, the reheated specimens dropped to 6,700 passes to 12.5 mm rut depth, with a stripping inflection point (SIP) of 5,000 passes, indicating the mix was highly susceptible to stripping. Similar results regarding stripping potential were reported for the 2018 N9 mixture with the same aggregate type. Despite the discrepancies in production mix results, no signs of moisture damage or significant rutting are evident in the field.

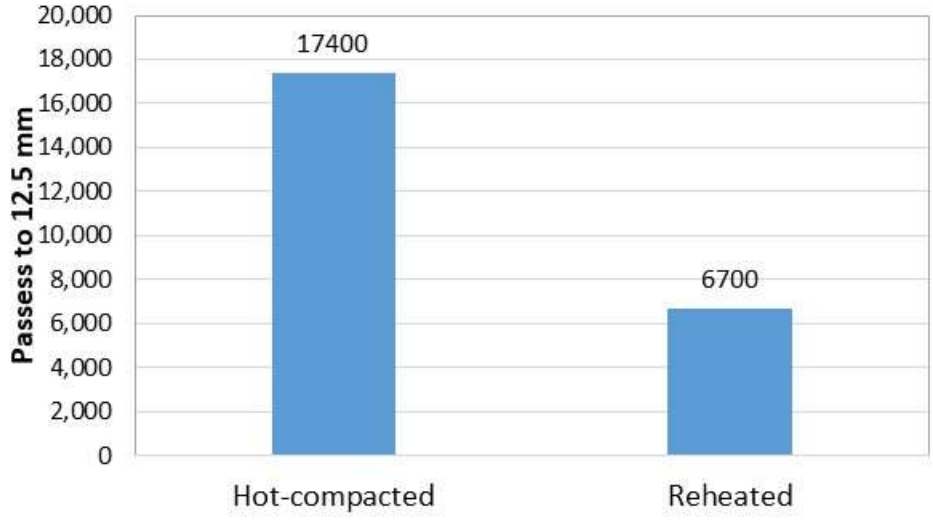

FIGURE 18 HWTT results of N9 surface mix.

11.5.5 Field Performance

Trafficking of N9 started on November 9, 2021. As of April 12, 2024, approximately 20 million ESALs were applied. Surface cracking, rutting, and smoothness were monitored every week using an automated pavement condition survey vehicle. Figures 19, 20, and 21 show the overall rutting, smoothness in terms of IRI, and cracking performance of Section N9 compared to the previous research cycle.

As presented in Figure 19, rutting of the 2021 N9 section was higher than the 2018 N9 section at approximately 0.17 in, but this number is still significantly lower than the 0.5-in threshold. IRI was almost identical at approximately 60 in/mile (Figure 20). The bump in IRI numbers at around 2 million ESALs was due to issues regarding the transition from Section N8 into N9. Repairs conducted in October 2022 lowered these numbers. The first crack in Section N9 (2021) was detected on November 14, 2023. At the end of the research cycle, cracking measured 0.2%. When compared to the N9 (2018) section, the first crack appeared after approximately 5.5 million ESALs, and 3.3% cracking was shown at the end of the research cycle. These results indicate that the 2021 N9 mix exceeded the cracking performance of the 2018 N9 mix, as shown in Figure 21.

FIGURE 19 Field rutting data of Section N9 (2018 and 2021 test cycles).

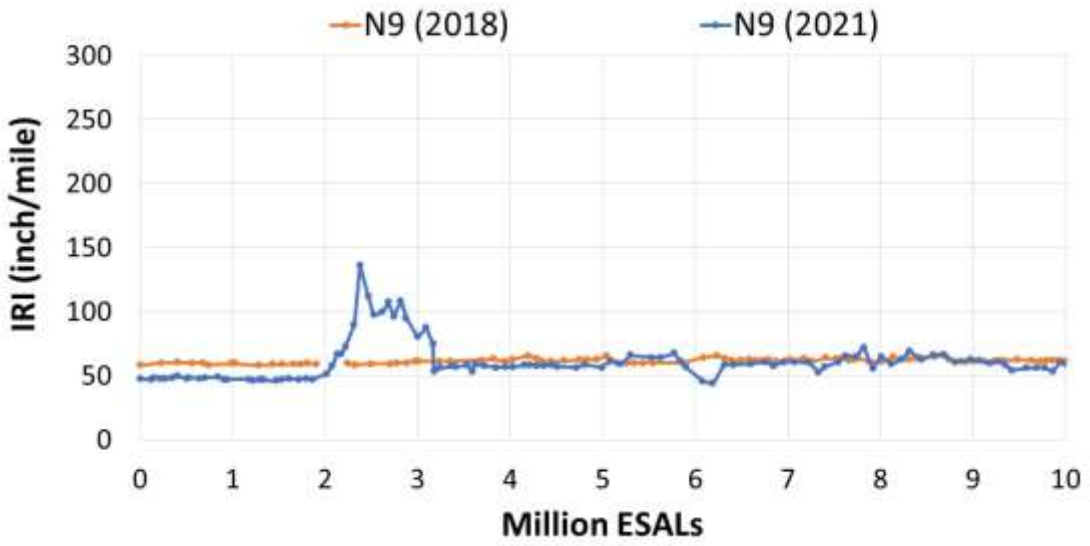

FIGURE 20 Field smoothness data of Section N9 (2018 and 2021 test cycles).

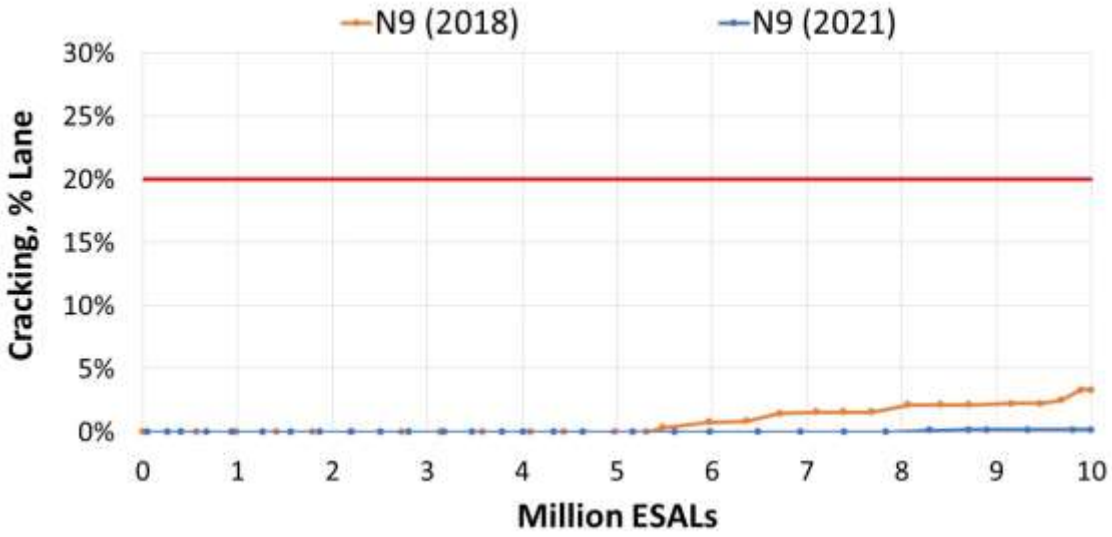

FIGURE 21 Cracking data of Section N9 (2018 and 2021 test cycles).

11.5.6 Findings and Conclusions

Although the N9 (2021) mix design incorporating RTR didn't meet the preliminary BMD ODOT thresholds, the mixture should have satisfactory performance based on its field performance and considering the modifications required in laboratory conditioning to activate the RTR and achieve specimen compaction. This is an important consideration if ODOT decides to allow the use of RTR in asphalt mixtures.

For the N9 surface mix, the production mix (hot-compacted and reheated specimens) showed improved cracking resistance compared to the mix design. However, the results are mixed for rutting resistance when comparing the production mix (reheated specimens) and the mix design results, which suggests the mixture was susceptible to rutting and moisture damage.

Similar results were reported for the 2018 N9 mixture regarding moisture susceptibility potential and were partially attributed to changes in the mix associated with plant production.

Despite the difference in BMD results between the production mix and the design mix, the section performed well with minimal rutting, excellent smoothness, and only 0.2% cracking. Field performance results showed that the 2021 N9 mix outperformed the N9 mix from the previous cycle, demonstrating the dry rubber additive delayed the appearance of reflective cracking.

References

Al-Qadi, I.L., H. Ozer, J. Lambros, A. El Khatib, P. Singhvi, T. Khan, J. Rivera-Perez, and B. Doll. *Testing Protocols to Ensure Performance of High Asphalt Binder Replacement Mixes Using RAP and RAS*. Illinois Center for Transportation/Illinois Department of Transportation, 2015.

Chen, C., F. Yin, A. Andriescu, R. Moraes, D. Mensching, N. Tran, A. Taylor, and R. West. Preliminary Validation of the Critical Aging Protocol for NCAT Top-down Cracking Experiment. *Journal of the Association of Asphalt Paving Technologists*, Vol. 89, 2020.

Chen, C., F. Yin, P. Turner, R. C. West, and N. Tran. Selecting a Laboratory Loose Mix Aging Protocol for the NCAT Top-Down Cracking Experiment. *Transportation Research Record: Journal of the Transportation Research Board*, No. 2672, Transportation Research Board of the National Academies, Washington, D.C., 2018, pp.359-371.

Standard Specifications 2023 Edition. California Department of Transportation (CALTRANS), 2023. https://dot.ca.gov/-/media/dot-media/programs/design/documents/2023_stdspecs-a11y.pdf

Vivanco Sala, D., N. Tran, F. Yin, and B. F. Bowers. Evaluating Impact of Corrected Optimum Asphalt Content and Benchmarking Cracking Resistance of Georgia Mixtures for Balanced Mix Design Implementation. *Transportation Research Record: Journal of the Transportation Research Board*, No. 2676(5), 2022, pp. 13-29.

West, R., D. Timm, B. Powell, N. Tran, F. Yin, B. Bowers, C. Rodezno, F. Leiva, A. Vargas, F. Gu, and R. Moraes. Phase VII (2018-2021) NCAT Test Track Findings. NCAT Report 21-03, National Center for Asphalt Technology at Auburn University, 2021.

Yin, F., F. Kaseer, E. Arámbula-Mercado, and A. Epps Martin. Characterising the Long-Term Rejuvenating Effectiveness of Recycling Agents on Asphalt Blends and Mixtures with High RAP and RAS Contents. *Road Materials and Pavement Design*, 18(sup4), 2017, pp. 273-292.

Zhou, F., S. Im, L. Sun, and T. Scullion. Development of an IDEAL Cracking Test for Asphalt Mix Design and QC/QA. *Road Materials and Pavement Design*, 18(sup4), 2017, pp. 405-427.

12. SOUTH CAROLINA DEPARTMENT OF TRANSPORTATION FULL-DEPTH RAPID REBUILD

Dr. David Timm

12.1 Introduction

As discussed in the Phase VII Test Track report (West et al., 2021), the asphalt concrete (AC) layer of flexible pavement is typically comprised of multiple lifts paved in succession and bonded together with tack. This method optimizes pavement structure and increases economy by using various AC mix designs, binder grades, and lift thicknesses. However, this approach has some disadvantages. First, construction time can prove problematic when placing multiple lifts, and potential drop-offs between lanes can create operational hazards. Additionally, slippage failures can occur, even when tack is applied. More rapid construction methods using single, thick-lift construction are needed to mitigate these issues.

The South Carolina DOT (SCDOT) has been investigating using thick-lift construction in high-traffic areas where relatively short lane closures can help maintain higher levels of service to the public. Successful projects in South Carolina using up to 5 inches in a single lift have been completed where a pavement section is milled and inlaid with new material in a relatively short time (i.e., overnight). There is a desire to mill and inlay to even greater depths in a single lift. However, questions regarding in-place density, rutting, cracking performance, and as-built smoothness necessitate accelerated pavement testing before attempting on high-volume roadways in South Carolina. To that end, SCDOT sponsored a section in the 2018 Test Track research cycle that was paved 8 inches thick in one pass. Section S9, the so-called “thick-lift” section, was built to answer the following questions:

1. Could thick-lift AC be adequately compacted?
2. How long after paving will an 8-inch lift take to reach a temperature where it can be subjected to traffic?
3. Could a thick-lift pavement achieve sufficient smoothness during construction?
4. Will a thick-lift pavement perform well under heavy trafficking? If sufficient compaction was not achieved, rutting and premature cracking could occur.
5. Will a thick-lift pavement behave like a conventional multi-lift pavement in terms of pavement response (i.e., stress, strain, deflection) under loading?

To answer these questions, the thick-lift section was designed and built in the summer of 2018 under the guidance and direction of SCDOT. The Phase VII report thoroughly addressed the first three questions with the following main findings (West et al., 2021):

1. The construction of a single 8-inch lift is viable. Care should be taken regarding the cooling time needed to open to traffic, but this can be somewhat controlled by coordinating the time of year and time of day for paving. In practice, SCDOT found nighttime placement in cold weather months is optimal, while paving in weather above 70^{o}F creates longer cooling times and subpar smoothness (Selkinghaus, 2021).

2. Achieving density with an 8.05-inch lift was a non-issue. Density exceeding 95% of the theoretical maximum specific gravity, as measured with cores, was accomplished with standard rollers and roller patterns; no specialized processes or equipment were needed.
3. As-built smoothness can be an issue with thick-lift paving and certainly was with this section. The problem was rectified somewhat with diamond grinding. If paving crews were given more opportunities to pave thick lifts, as-built smoothness could be greatly improved. In practice, SCDOT has found that having an additional lane for material transfer vehicles, trucks, and rollers can help minimize dips in the longitudinal pavement profile (Selkinghaus, 2021).

Questions 4 and 5, listed above, were addressed over the first 10 million equivalent single axle loads (ESALs) in the Phase VII report but will be evaluated more extensively as part of this report since the section was left in place to receive another 10 million ESALs in its second test cycle.

12.2 Construction and Instrumentation of the Thick-Lift Section

Previous publications extensively documented the construction and instrumentation of the thick-lift section (S9); therefore, only a brief overview is provided in this report (McCarty, 2019; West et al., 2021). Figure 1 shows the pavement cross-section where the thicknesses represent a section-wide average measured at 12 different locations. The granular base of crushed granite is commonly used in other sections at the Test Track. The subgrade is native to the Test Track and classifies as an A-4 (0) soil. The AC was classified as an SCDOT “Type B Intermediate Special,” which is used for rehabilitation repairs, interstates, and high-volume primary routes. The thick-lift mix was a dense graded 12.5 mm NMAS mix with a PG 64-22 binder and 25% RAP. The target mix design air voids are usually around 2.5 to 3.0% for these thick-lift mixes to make them easier to compact in the field (Selkinghaus, 2021); this mix was designed for 2.5% air voids with 75 design gyrations. The resulting asphalt content was 5.75%, of which 4.37% was new binder and 1.38% came from the RAP. The AC layer was placed in a single 8” lift on top of the existing granular base.

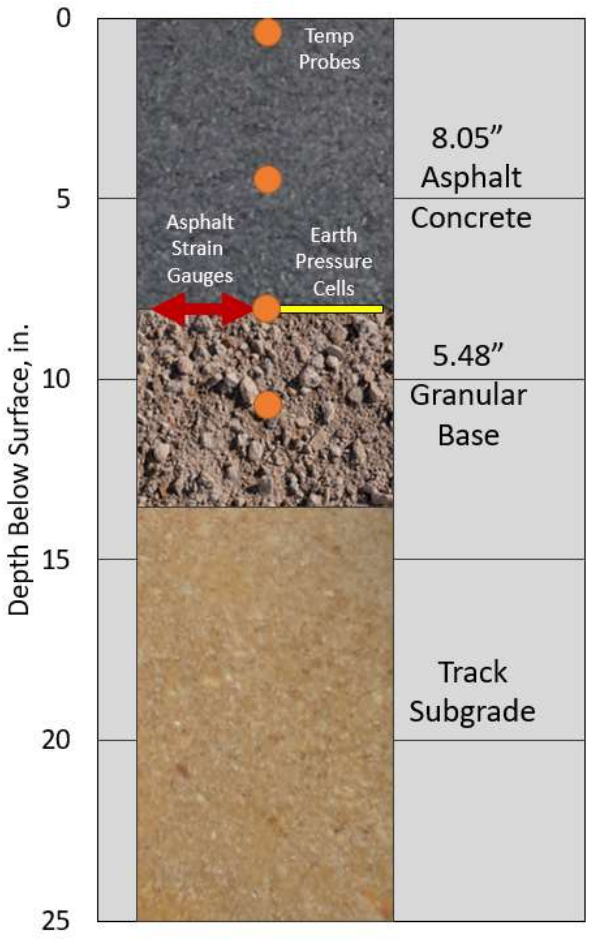

FIGURE 1 Thick-lift cross section (S9).

12.3 Field Performance

Trafficking of the first test cycle began November 26, 2018 and concluded February 27, 2021 after applying 10,023,907 ESALs. The section was then left in place with no trafficking while other sections were subjected to forensic investigation and reconstruction in preparation for the 2021 research cycle. Trafficking of that cycle began November 10, 2021 and concluded April 5, 2024, after applying an additional 10,052,142 ESALs, for a total of 20.1 million ESALs over the two test cycles.

As with all Test Track sections, the thick-lift section was measured frequently for rutting and roughness and inspected for cracking during each cycle. The following sections document the field performance in terms of both time and traffic application, expressed as equivalent single axle loads. Though ESALs are a convenient expression of traffic, they were applied by five triple-trailer trucks traveling at 45 mph with steer axles weighing approximately 11 kips, drive tandem axles weighing approximately 40 kips, and 5 trailing single axles weighing approximately 20.5 kips. These axle weights and groups resulted in a truck factor of approximately 10 ESALs/truck.

12.3.1 Rutting

Rutting progression for the thick-lift section is presented in Figure 2, where rut depths are plotted on the left y-axis and total ESALs are plotted on the right y-axis. Rutting increased primarily during the first spring and summer (April 2019 through September 2019) up to about 0.15 inches. At that point, it leveled and did not increase through the second summer, maintaining rut depths around 0.15 inches. The increase at the very end of the first test cycle from 0.15" to 0.25" is believed to be related to a change in the data acquisition software rather than a true increase in rutting, as this jump was not evident in manual methods of rut depth measurement. In either case, rutting did not exceed approximately 0.25" after the application of the first 10 million ESALs and most likely leveled off at 0.15" after primary rutting occurred during the first summer. When trafficking resumed in the second test cycle, rutting did not increase appreciably through the next 5 million ESALs, which included the first summer of the second cycle. Some additional rutting (~0.05 inches) accumulated during the the second cycle and the section ended at 0.3 inches of rutting after 20 million ESALs, which was well below the failure threshold of 0.5 inches. This critical finding indicates that despite concerns about the potential for excessive rutting with thick-lift paving, it did not occur.

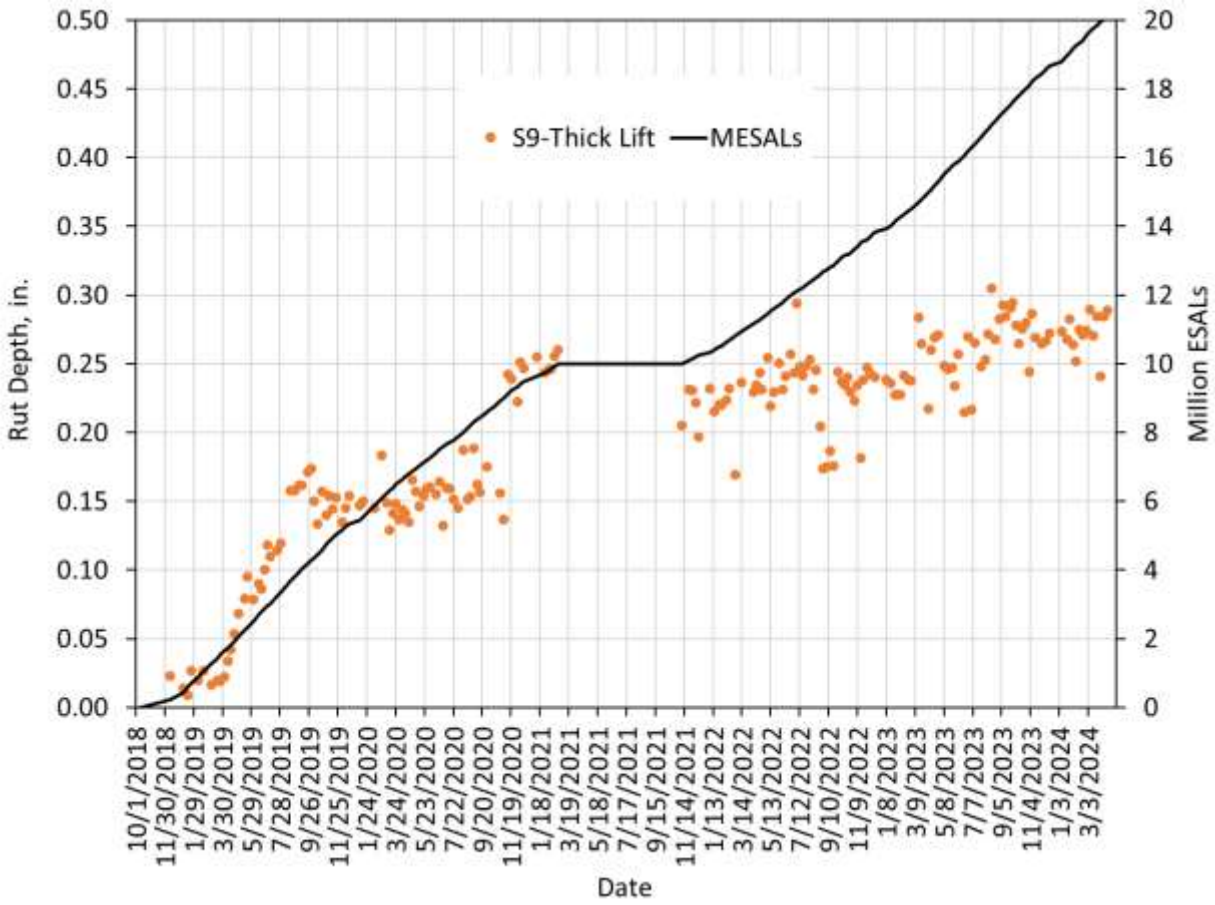

FIGURE 2 Section S9 thick lift rutting performance.

12.3.2 Cracking

A small amount of cracking was first observed in mid-December 2020 after approximately 9.4 million ESAL applications. The hairline cracks were aligned in the direction of travel and were at the edges of the wheelpath. At the end of the first cycle, the cracking represented a total of 0.7% of the lane area or 1.1% of the wheelpath area. At that time, one crack was located at the edge of the outside wheelpath near the gauge array, while another was further along the section at the edge of the outside wheelpath. Figures 3 and 4 show the two cracks lightly highlighted for easier identification. Traffic moves from bottom to top in each photo.

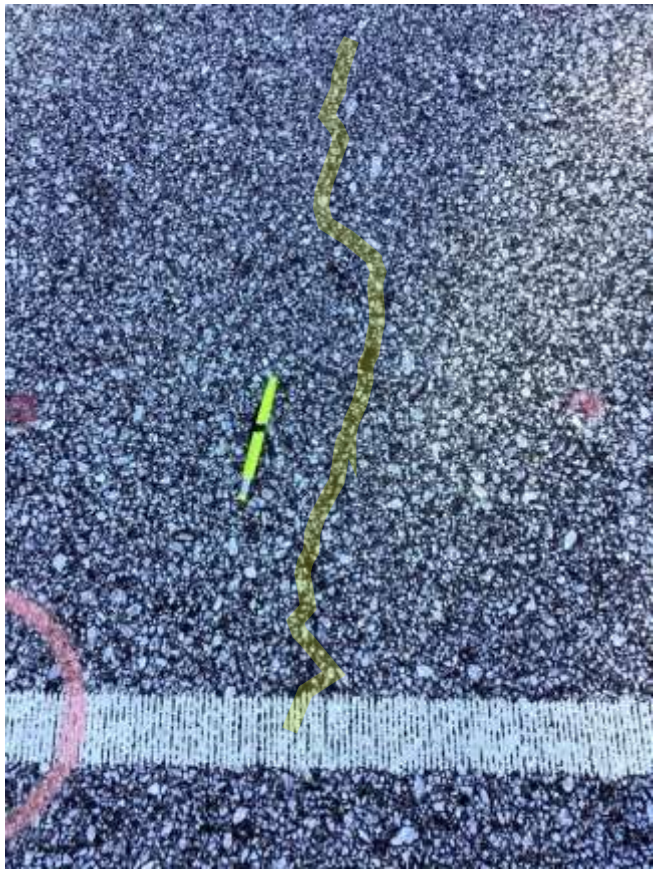

FIGURE 3 Longitudinal crack at edge of outside wheelpath in S9 at end of first test cycle.

FIGURE 4 Longitudinal crack at edge of inside wheelpath in S9 at end of first test cycle.

As shown in Figure 5, the area of cracking increased to 10% of lane area and 15% of wheelpath area after 20 million ESALs in the next test cycle without an observable increase in severity. Figure 6 shows cracking severity at the end of the second test cycle. Despite the increase in cracking extent, as will be shown below, there was not a measurable change in the structural capacity as quantified by strain measurements and backcalculated asphalt concrete modulus.

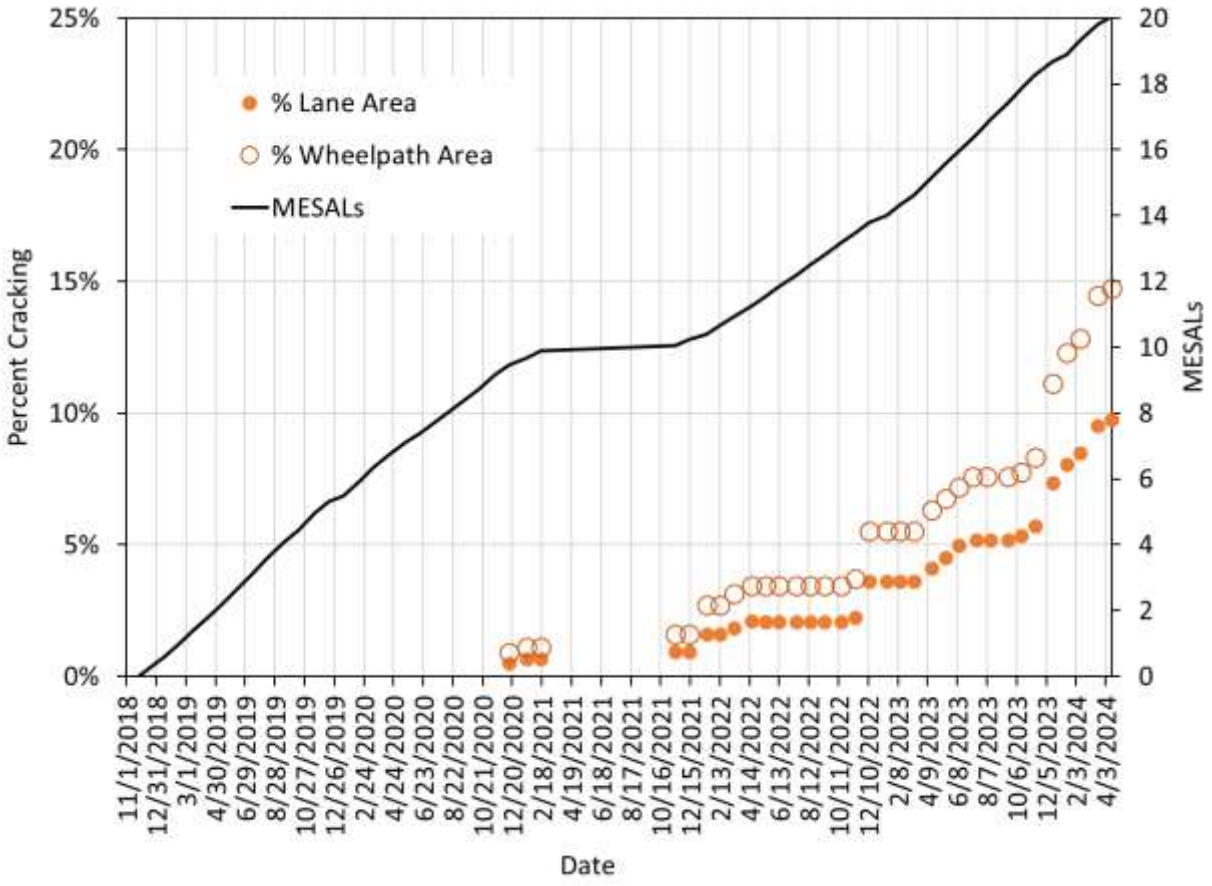

FIGURE 5 Section S9 thick lift cracking versus time.

FIGURE 6 Longitudinal crack at edge of inside wheelpath in S9 at end of second test cycle (with and without highlighting).

Given its magnitude, amount, and orientation, the cracking appears to be top-down. As will be presented in the structural characterization section, the stress, strain, and backcalculated modulus data support this assertion. Destructive forensic coring and/or trenching will be conducted to check this hypothesis after the next test cycle is completed in 2027.

12.3.3 Ride Quality

Though initial roughness was higher than optimal as a result of the thick build, ride quality in this section improved with ESAL applications. The trendline in Figure 7 shows IRI decreased by nearly an average of 15 inches/mile since the start of trafficking in 2018. The traffic had a

smoothing effect on an initially relatively rough pavement; this phenomenon is also sometimes seen in smoothness data of asphalt overlaid rubblized pavements.

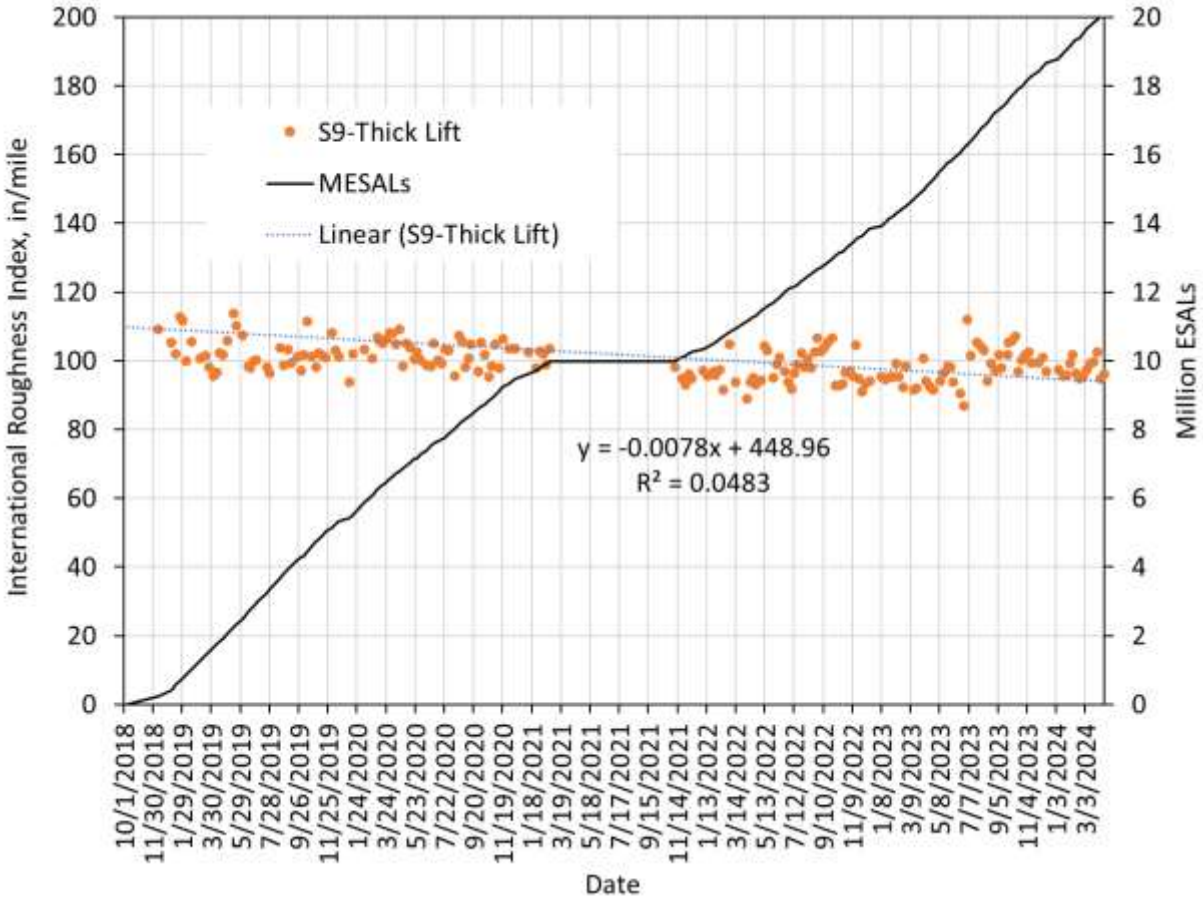

FIGURE 7 Section S9 thick-lift ride quality data.

12.4 Structural Response Characterization

The construction and performance data indicated that an 8-inch thick-lift section could be built successfully and, despite minor top-down cracking, exhibit excellent performance through 20 million ESALs. The next portion of this investigation was to characterize the structural response through direct measurement under truck loading and falling weight deflectometer testing.

12.4.1 Structural Responses Measured with Embedded Instrumentation

Structural response measurements were made weekly during the two test cycles using asphalt strain gauges (ASGs) and earth pressure cells (EPCs) embedded during construction, shown schematically in Figure 8. Response measurements consisted of at least 15 truck passes, from which the 95th percentile highest measurement was used to represent the “best hit” on that collection day. Trucks were traveling at approximately 45 mph during each measurement, and though all axles were measured, only single-axle responses are presented herein for brevity.

There was some variation among all the single axles, but they typically weighed approximately 20,000 lb with dual tires.

The measured tensile strain response versus time is plotted in Figure 8, which clearly shows seasonal effects on the section response. Peak tensile strain levels are achieved in the warmer summer months, while lower strains are seen during cooler times of the year. The short-term cycling in the data stems from collecting data alternating between the mornings and afternoons on a week-to-week basis. Figure 8 resembles other multi-lift sections measured in this fashion at the Test Track in previous cycles.

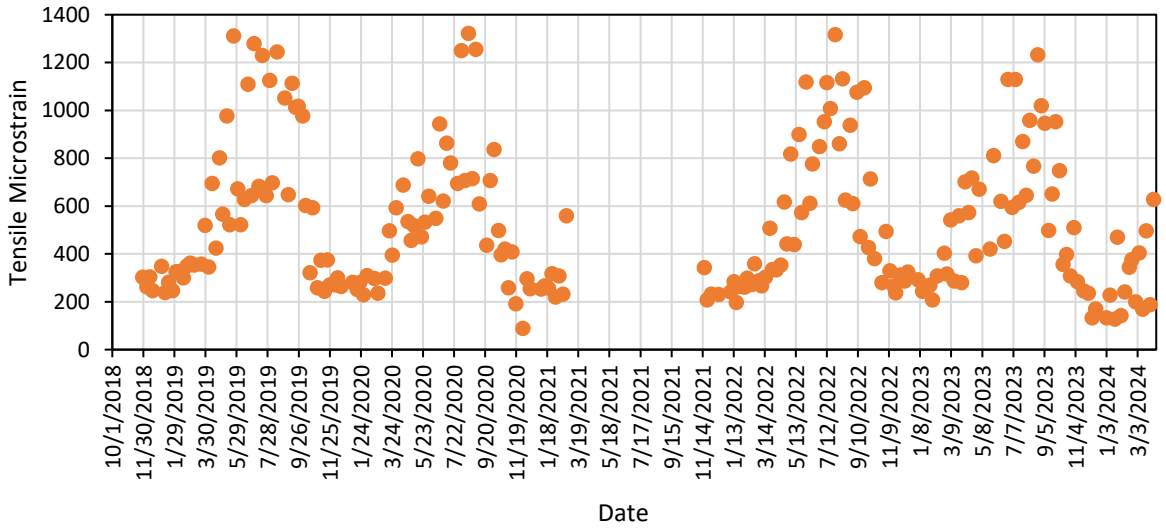

FIGURE 8 Section S9 thick-lift tensile strain versus time.

The strain readings from Figure 8 were plotted against the mid-depth temperature at the time of measurement, as depicted in Figure 9. The strong influence of temperature seen in Figure 8 is quantified in Figure 9 with the exponential trendline fitted to the data. The relatively high R^2 (exceeding 0.93) means the variation in measured strain response is primarily caused by temperature changes with some scatter potentially due to wheel wander and other random variations.

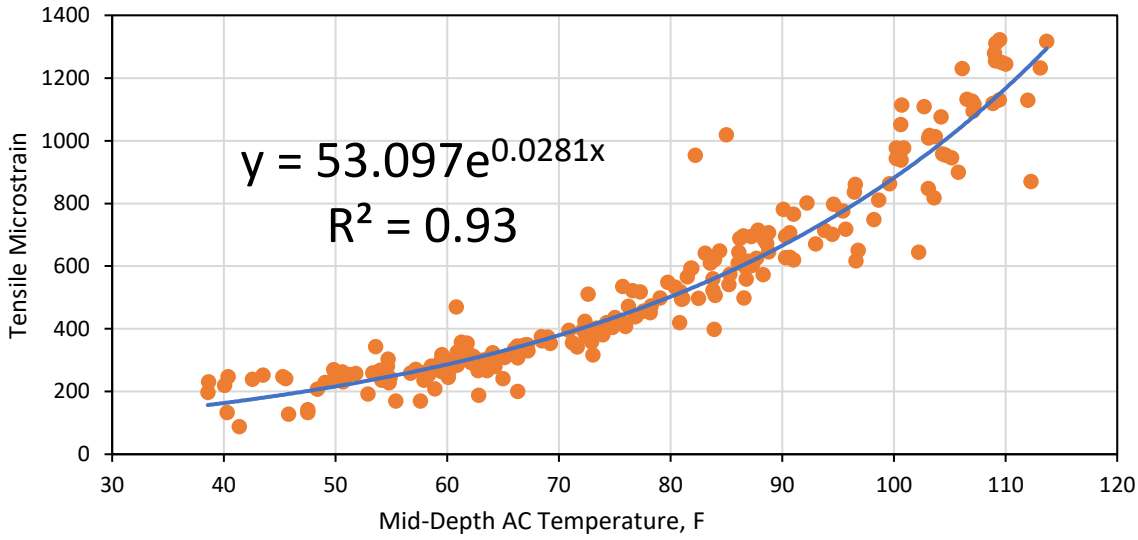

FIGURE 9 Section S9 thick-lift tensile strain versus temperature.

The regression equation from Figure 9 was used to normalize the strain data to a reference temperature following well-established Test Track procedures as documented by McCarty (2019). The normalized tensile strain at 68°F is plotted versus time in Figure 10. The relative stability of the measurements and slight decrease shown by the trendline indicates good structural health. Had the cracking been more severe, or bottom-up, strain levels would have increased over time rather than remaining stable or slightly decreasing.

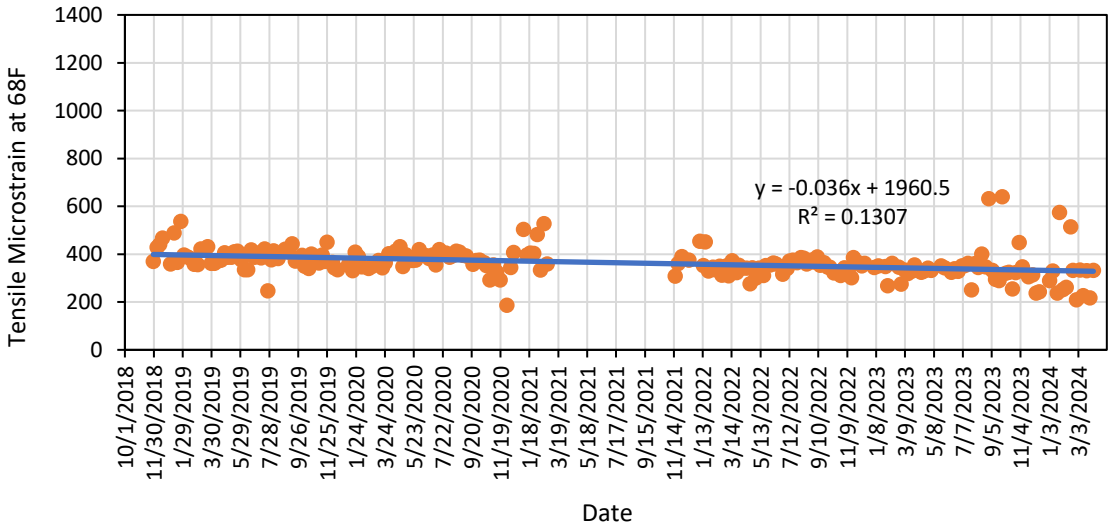

FIGURE 10 Section S9 thick-lift tensile strain at 68°F versus date.

Figures 11, 12, and 13 were created using the base pressure measurements. The data closely mimics the strain data regarding the importance of pavement temperature on the measured response (Figure 11). The exponential function fitted to the data (Figure 12) again quantifies the

strong influence of temperature, and the pressures normalized to 68°F (Figure 13) show steady and slightly declining pressure over time. Like the strain data, these measurements indicate good structural health and are consistent with measurements in other multi-lift sections at the Test Track.

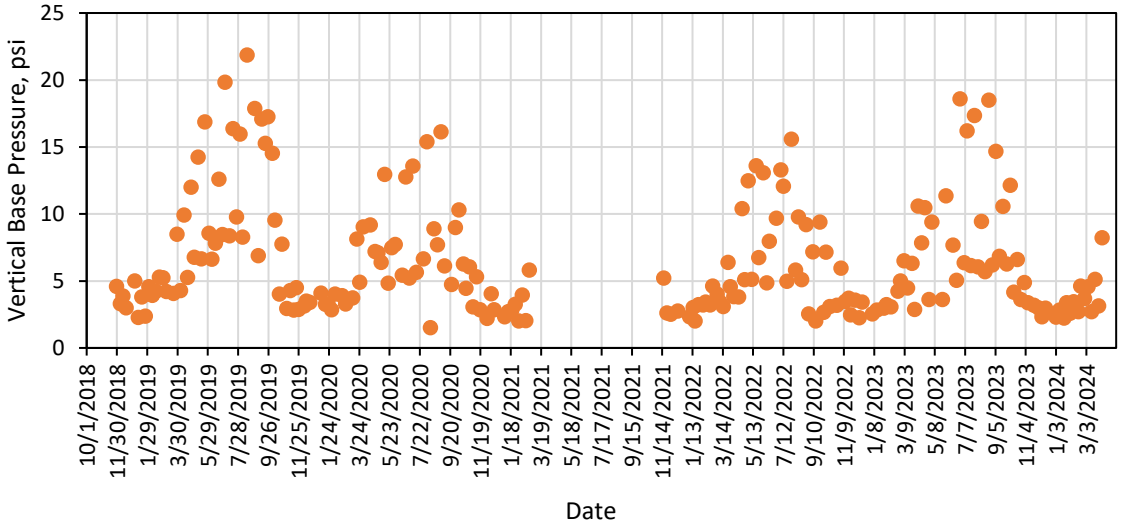

FIGURE 11 Section S9 thick-lift compressive stress versus time.

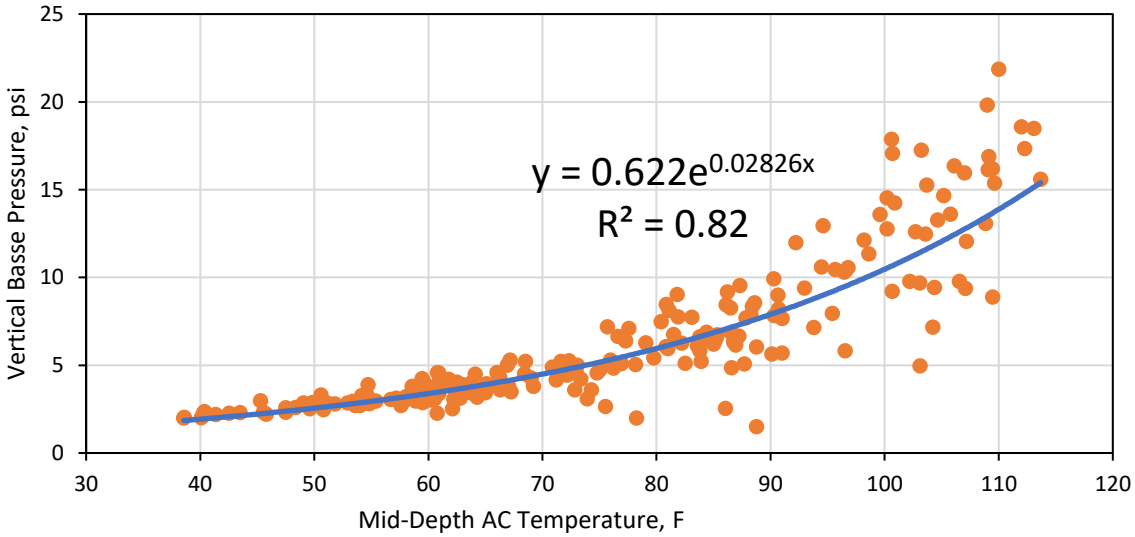

FIGURE 12 Section S9 thick-lift compressive stress versus temperature.

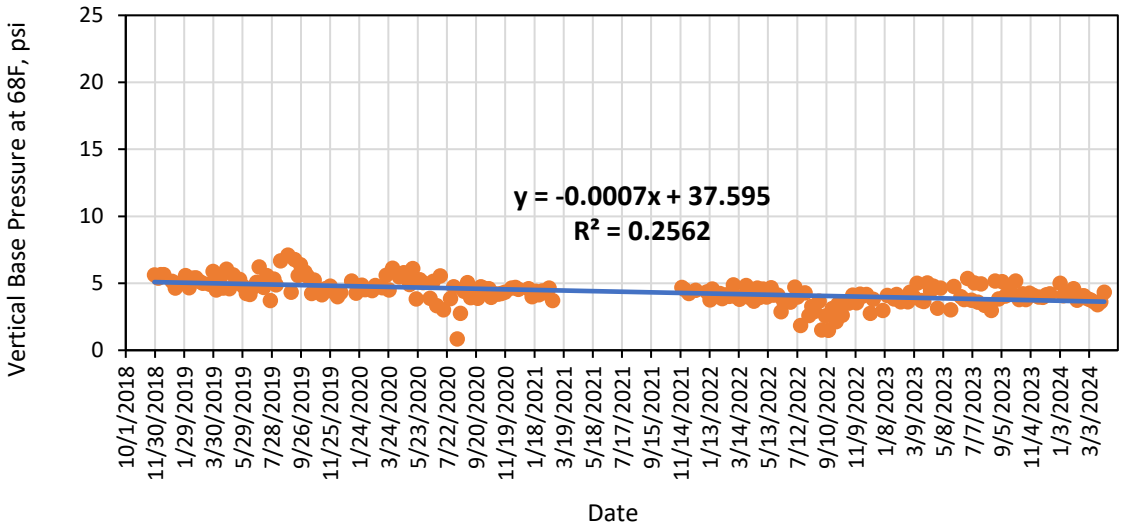

Figure 13 Section S9 thick-lift compressive stress at 68°F versus date.

12.4.2 Falling Weight Deflectometer (FWD) Testing and Backcalculation

FWD testing was conducted several times per month during each two-year trafficking cycle using a Dynatest 8000 FWD with nine sensors using standard spacing at 0, 8, 12, 18, 24, 36, 48, 60, and 72 inches from the load center. Testing was conducted at four random locations in the section with three lateral offsets at each location (inside wheelpath, outside wheelpath, and between wheelpaths). Each FWD test consisted of two seating drops followed by three replicate drops at 6,000, 9,000, and 12,000 lb, respectively. The data presented below pertains only to the 9,000 lb loading, as this is the AASHTO 1993 Design Guide standard load level for overlay design and most closely replicates single-axle loading of the track's trucks.

Backcalculation of the deflection basins was conducted using EVERCALC 5.0, with the cross-section depicted in Figure 14. A previous study found that combining the aggregate base layer with 16 inches of the Test Track subgrade resulted in more accurate backcalculation results and was used for this study (Tutu and Timm, 2017). Note that Figure 14 shows the average as-built thicknesses, but the surveyed depths from each of the 12 FWD test locations were used on a location-by-location basis for backcalculation. Only AC modulus values resulting in less than 3% root mean square error between measured and predicted deflection basins are presented.

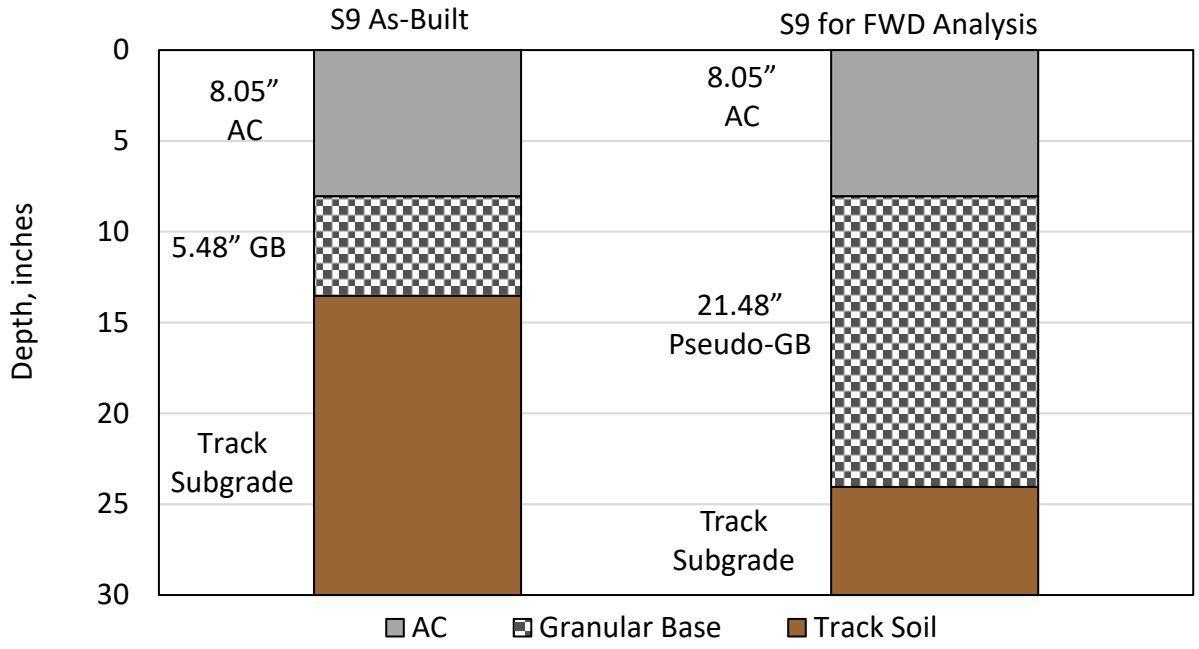

FIGURE 14 Section S9 thick-lift as-built and backcalculation cross-sections (West et al., 2021).

Figure 15 plots the backcalculated AC moduli versus test date where the seasonal effects are readily apparent, much like the measured strain and stress responses presented above. This is similar to observations of other multi-lift sections at the Test Track. The AC modulus changes by approximately an order of magnitude from summer to winter. This profound influence of temperature on the modulus is the reason why the other measured responses are also significantly affected. The vertical spread of the data on any given date represents the spatial variability across the section (random locations and offset wheelpath).

When backcalculated AC moduli were plotted against the corresponding measured mid-depth temperature (Figure 16), the influence of temperature was very strong ($R^2 > 0.88$) and followed an exponential trendline, much like the strain and pressure data. Following the same temperature normalization process used with the strain and pressure data, the AC modulus corrected to 68°F were plotted against time in Figure 17. The data's remarkable stability over time indicates a structurally healthy section. Modulus would decrease if AC cracking was becoming an issue.

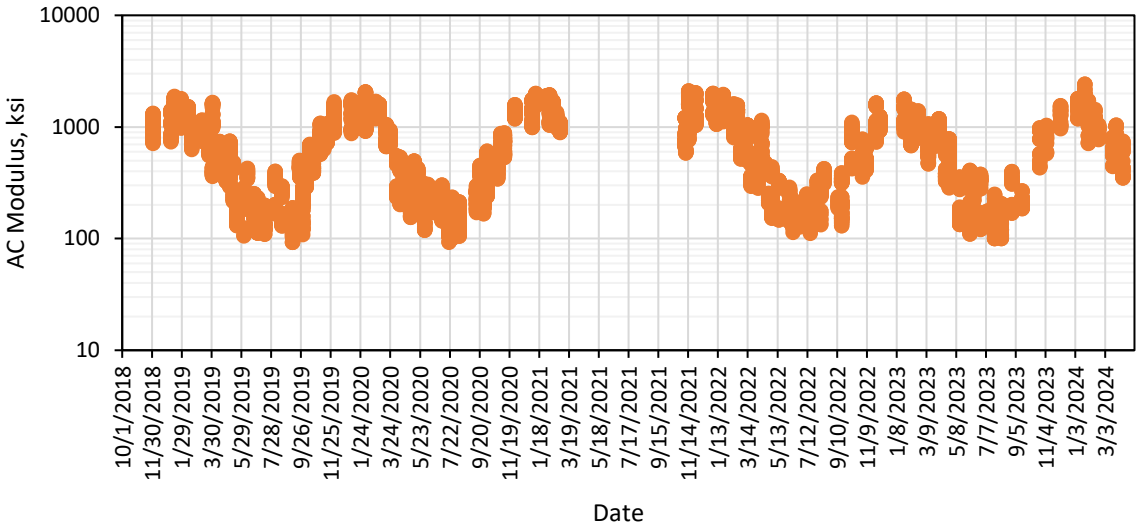

FIGURE 15 Section S9 thick-lift backcalculated AC modulus versus date.

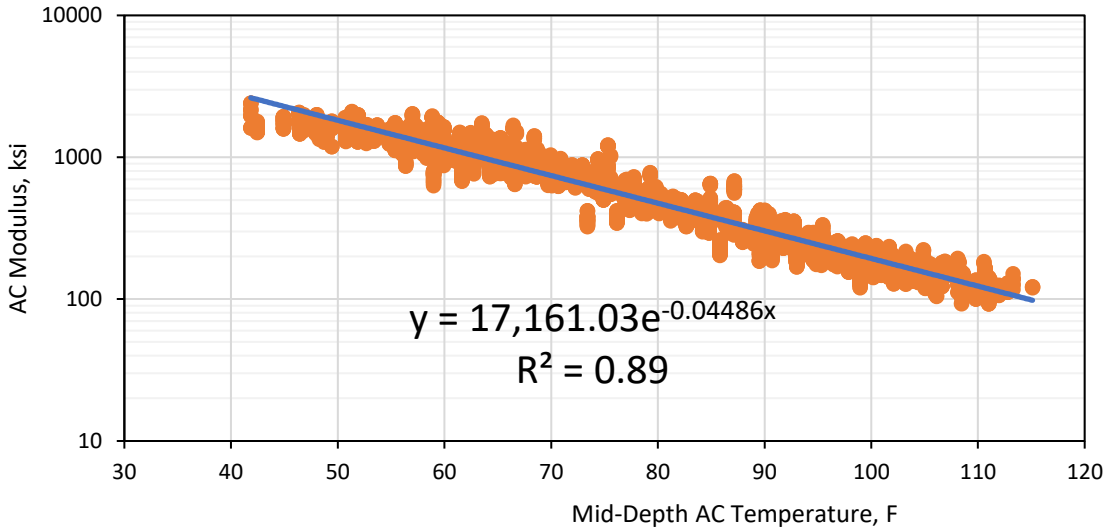

FIGURE 16 Section S9 thick-lift backcalculated AC modulus versus temperature.

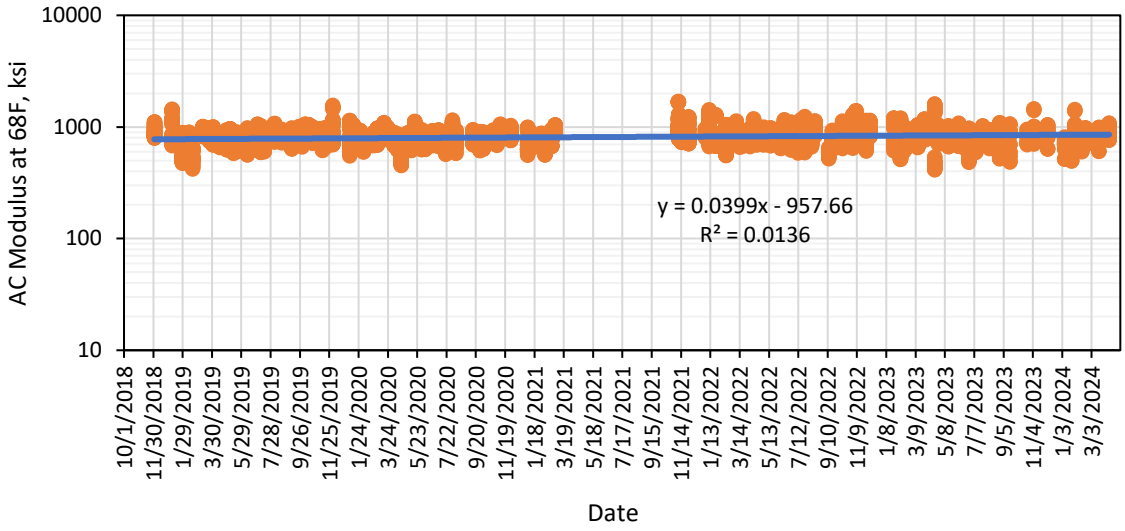

FIGURE 17 Section S9 thick-lift backcalculated AC modulus versus date at 68°F.

12.5 Summary, Conclusions, and Recommendations

Section S9 was constructed for the SCDOT as a single thick-lift pavement to evaluate the constructability, performance, and structural characteristics of this rapid reconstruction technique. Based on the results presented in this chapter, the following conclusions and recommendations are made:

1. The thick-lift section exhibited excellent performance over the 20 million ESAL applications. Rutting was less than 0.30”, some top-down cracking developed, and smoothness got better over time. Premature or excessive rutting, which was a potential liability for this construction technique, was not evident and should not be a problem provided that adequate compaction is achieved during construction.
2. The thick-lift section behaved similarly to other conventional multi-lift sections concerning measured mechanistic response and backcalculation of deflection basins. As expected, the influence of temperature was evident in measured pavement responses and backcalculated AC moduli. The temperature-corrected data were remarkably consistent over time, indicating good structural health despite the cracking observed in the section.
3. It is recommended to leave this section in place for another 10 million ESALs during the 2024 research cycle to observe the progression of cracking and determine if it begins to compromise the structural health of the section.

12.6 References

McCarty, C. *Early Characterization and Performance of a Flexible Thick Lift Pavement*. M.S. Thesis, Auburn University, 2019.

Selkinghaus, C. *Personal Communication*. South Carolina Department of Transportation, May 14, 2021.

West, R., D. Timm, B. Powell, N. Tran, F. Yin, B. Bowers, C. Rodezno, F. Leiva, A. Vargas, F. Gu, R. Moraes, and M. Nakhaei. *Phase VII (2018-2021) NCAT Test Track Findings*. NCAT Report 21-03, National Center for Asphalt Technology at Auburn University, 2021.

Tutu, K., and D. H. Timm. Determination of an Optimum Backcalculation Cross-Section for Unconventional Pavement Profiles. *Transportation Research Record: Journal of the Transportation Research Board, No. 2641*, Transportation Research Board of the National Academies, Washington, D.C., 2017, pp. 48–57.

13. TENNESSEE DEPARTMENT OF TRANSPORTATION BALANCED MIX DESIGN USING A GYRATORY COMPACTOR WITH MARSHALL COMPACTOR COMPARISON

Dr. Benjamin F. Bowers, Tiana Y. Lynn Wright

13.1 Background

The Tennessee Department of Transportation, like many agencies, is interested in using Balanced Mix Design (BMD) of asphalt mixtures to enhance their pavement performance. TDOT conducted a benchmarking study (Lynn and McDonald 2023) and selected two tests for mix acceptance on high-volume roads: the indirect tension asphalt cracking test (IDEAL-CT) for cracking and the Hamburg Wheel Tracking Test (HWTT) for rutting. To meet the proposed/tentative BMD specification, a CT_{Index} minimum of 100 is required on Superpave gyratory compacted (SGC) specimens along with a maximum HWTT rut of 12.5 mm after 20,000 passes.

Beyond an interest in investigating how use of the proposed BMD thresholds perform under heavy traffic, there is an interest in whether or not specimens made using a 4-inch Marshall hammer can be used to produce IDEAL-CT specimens. TDOT uses 75 blow Marshall Mix Design for the design of asphalt mixtures. If TDOT is to fully implement BMD, bypassing the use of a SGC is ideal since most contractors do not currently have an SGC in their lab. There has been little to no work investigating the use of a 4-inch Marshall specimen for IDEAL CT, though mathematically it is plausible. The equation to calculate a CT_{Index} is as follows:

$$CT_{Index} = \frac{t}{62} \times \frac{l_{75}}{D} \times \frac{G_f}{|m_{75}|} \times 10^6$$

Where t = thickness, l_{75} = the displacement at 75% of the peak load, D = the diameter of the specimen, G_f = the failure energy, and m_{75} = the load at 75% of the peak load. By including the thickness and the diameter of the specimen, there is a theoretical correction for a specimen with a size other than the standard 150 mm diameter x 62.0 +/- 1.0 mm height SGC specimen. The standard Marshall specimen is a 4-inch (101.6 mm) diameter by 63.5 +/- 1.27 mm height specimen.

13.2 Mix Designs

TDOT provided an accepted mix design from a contractor that achieved a CT_{Index} of 165, significantly higher than the required CT_{Index} of 100. Materials from this mix design were shipped to NCAT where the design was adjusted to move the CT_{Index} closer to 100. The mixture was a ½ inch dense-graded hot mix asphalt with a PG 70-22 binder and 28% RAP by aggregate weight (27% RAP binder replacement). The mixture was adjusted by the following steps: (1) adding RAP to the maximum amount allowable by TDOT in base and binder mixtures of 35% which is beyond the current allowable in surface mixtures of 20%, both when fractionated RAP is used, (2) reducing the total binder content to the minimum allowable of 5.7%, (3) reducing

any antistrip additives to the minimum allowable amount given that may affect performance beyond antistripping benefits, and (4) reducing the total binder content below that of the TDOT minimum *or* adjusting the gradation. All mix design iterations were compacted using a Marshall hammer with 75 blows per side. The IDEAL-CT test was conducted on SGC specimens each step of the way and the final materials combination was tested on the HWTT to ensure that the rutting criteria was still met.

Figure 1 provides the CT_{Index} results after the mix adjustment process. In the figure, the use of "R" indicates the RAP content, and the following percentage indicates the binder content (e.g., 35R 6.1% = 35% RAP at a 6.1% binder content). The final mix design gradation and volumetrics are provided in Figure 2 and Table 1. The final NCAT adjusted mix design resulted in a CT_{Index} of 110 by increasing the RAP content to 35% by weight of aggregate (also 35% by RAP binder contribution), reducing the total binder content to TDOT's minimum of 5.7%, and reducing the liquid antistripping agent content to the minimum allowable. This mixture also met the HWTT requirements. The gradation of the final NCAT adjusted mix design was close to that of the original TDOT mix design (TDOT JMF). The differences between the NCAT 28% RAP and TDOT JMF are attributed to material variability. The Voids in the Mineral Aggregate (VMA) and Voids Total in the Mix (VTM) are lower for the NCAT adjusted mix design compared to the TDOT JMF. It should be noted that TDOT uses G_{se} in the calculation of VMA. The mixture was further adjusted by lowering the total binder content to 5.6%, which is 0.1% lower than TDOT's minimum, but this resulted in a CT_{Index} lower than 100.

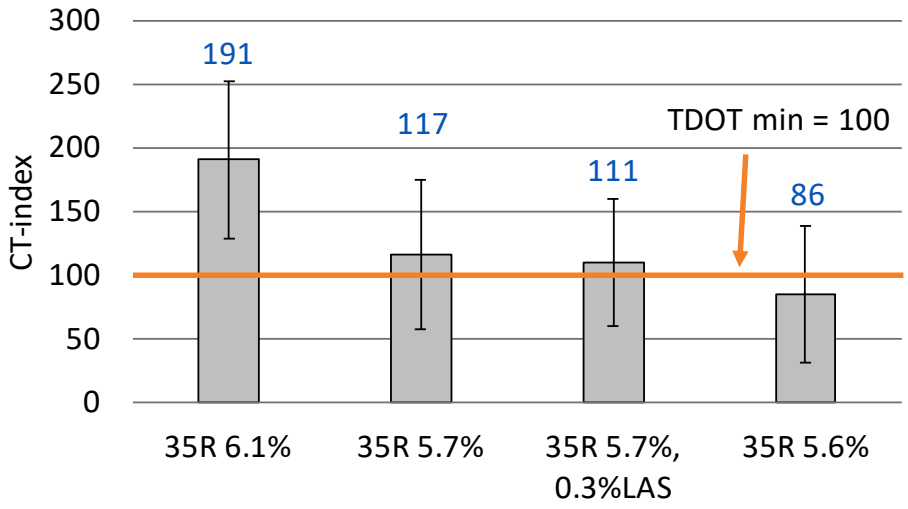

FIGURE 1 Results of BMD testing for adjusted mixtures; 35R 5.7%, 0.3% LAS is the selected design.

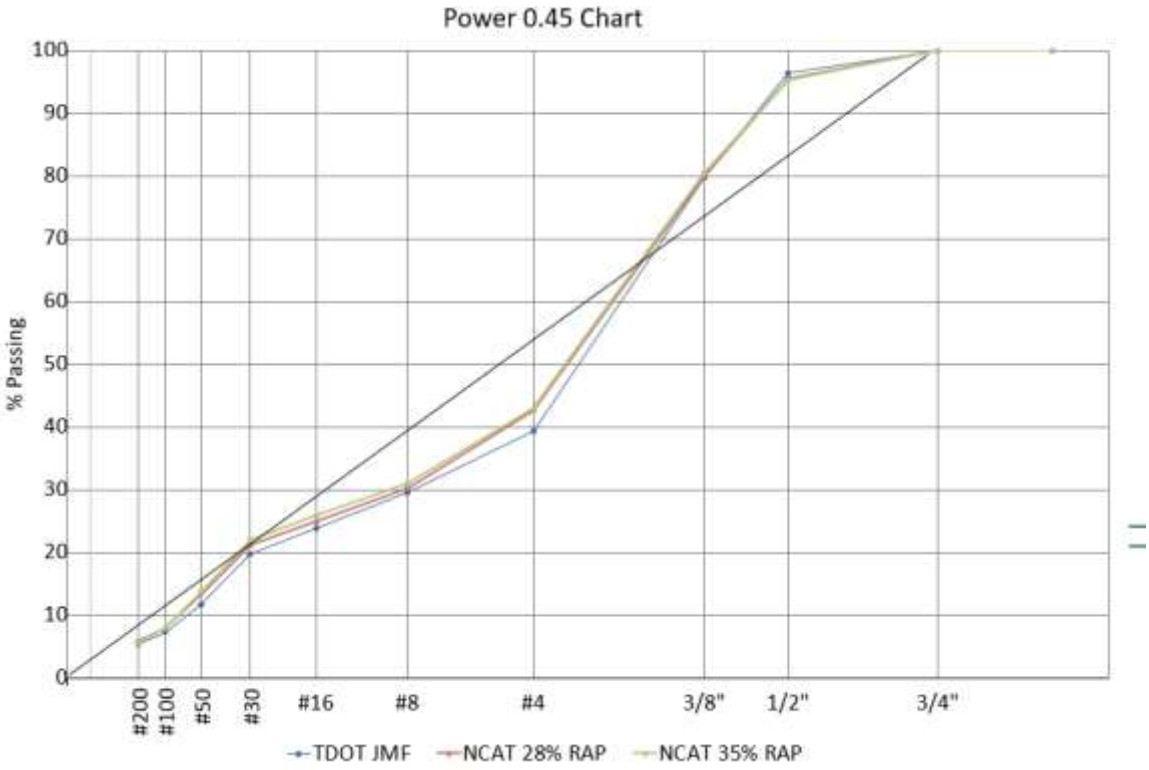

FIGURE 2 Results of BMD testing for adjusted mixtures.

TABLE 1 Volumetric Results for Marshall Compacted Specimens Meeting Original TDOT JMF And Adjusted NCAT JMF

Volumetric Data at 75 Blows Per Side		
	TDOT JMF	**NCAT JMF**
Gmm	2.415	2.422
Avg. Gmb	2.321	2.344
Avg. Height (mm)	-	63.06
Total Asphalt Content (%)	6.1	5.7
Avg. VTM (%)	3.9	3.2
Gse	2.646	2.637
VMA (%)	17.6	16.2
VFA (%)	78.0	80.2
Dust to Asphalt Ratio	0.880	0.996
CT_{Index}	~165	110
Hamburg (mm)	~6.00	5.05

13.3 Test Section and QC Results

Test section S4 was selected to investigate the TDOT BMD thresholds. TDOT elected to do a mill and overlay of 1.5 inches, with the existing asphalt in section S4 left in place. This final section had a 1.6-inch BMD dense graded overlay, approximately 22.4 inches of existing hot mix asphalt (HMA), and 6 inches of aggregate base over subgrade. The mix design used was the NCAT adjusted mix design, NCAT JMF, with 35% RAP, 5.7% total binder, and 0.3% liquid antistrip (LAS). Figure 3 provides a visual cross section for section S4.

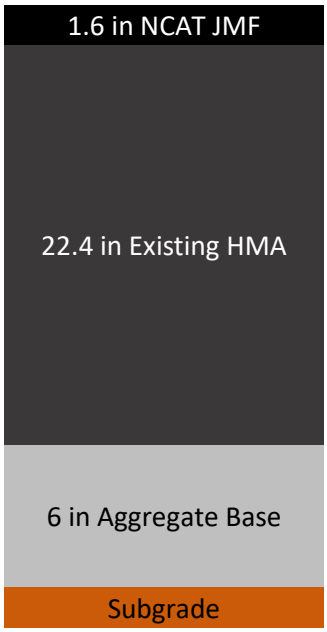

FIGURE 3 TDOT Test Section S4.

The quality control data is provided in Table 2. Interestingly, the average CT_{Index} dropped to 85.1 on the SGC, below the minimum threshold of 100. The production mixture did have 0.1% less binder than the target (5.6% instead of 5.7%), though that is well within production tolerance. However, it is well established that adding or removing asphalt binder from a mixture will impact the CT_{Index} result. Further, the mix had 1.4% more material passing the #200 sieve, which can also contribute to a stiffening of the binder mastic. The mixture passed the HWTT at 3.7 mm after 20,000 passes.

Table 2. Target and Quality Control Data from Section S4 Construction

Sieve Size	Target	Quality Control
25 mm (1")	100	100
19 mm (3/4")	100	100
12.5 mm (1/2")	95	98
9.5 mm (3/8")	80	87
4.75 mm (#4)	43	47
2.36 mm (#8)	31	31
1.18 mm (#16)	26	24
0.60 mm (#30)	22	20
0.30 mm (#50)	14	14
0.15 mm (#100)	8	9
0.075 mm (#200)	5.7	7.1
Mix Properties / Volumetrics	**Target**	**Quality Control**
Binder Content (Pb), %	5.7	5.6
Rice Gravity (Gmm)	2.422	2.428
Bulk Gravity (Gmb)	2.344	2.353
Air Voids (Va), %	3.2	3.1
Voids in the Mineral Aggregate, %	16.2	15.8
Voids Filled with Asphalt, %	80	81

13.4 Performance Data

It was important to evaluate two elements of the TDOT specification. First, is a CT_{Index} of 100 and a HWTT maximum of 12.5 mm after 20,000 passes sufficient to prevent rutting and cracking on high traffic roadways in Tennessee? Secondly, is it possible to use a Marshall compacted specimen to test the CT_{Index} of a mixture?

After 10 million ESALs the test section exhibited no cracking. The rutting had increased slightly from an average of 1.8 mm over the first 1 million ESALs to 3.2 mm over the most recent 1 million ESALs. The average IRI throughout the life of the pavement is 88.7 in/mile with a minimum of 76.4 in/mile and a maximum of 102.1 in/mile. The IRI in the last 1 million ESALs was 88.0 in/mile. Thus, the performance of the pavement to date indicates that the selected BMD criteria do result in a pavement that will perform under these conditions with this structure. The rutting and IRI results are provided in Figures 4 and 5.

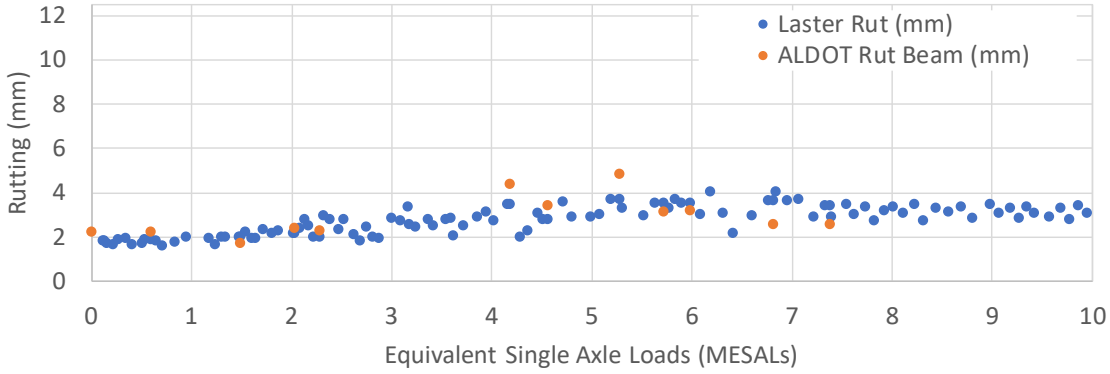

FIGURE 4 Rutting results.

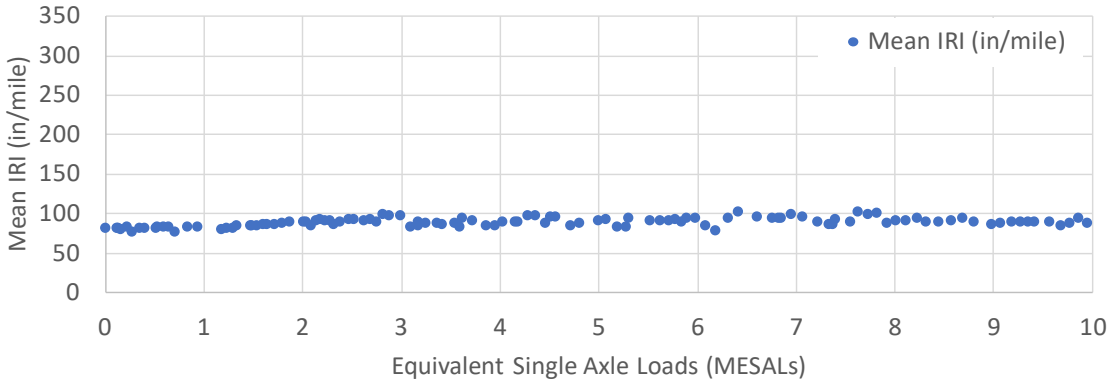

FIGURE 5 IRI results.

During mix design *and* production, CT_{Index} specimens were created using both the 6-inch diameter SGC and 4-inch diameter Marshall hammer. The 6-inch SGC specimens were then tested using a hydraulic load frame and the 4-inch Marshall specimens were tested on a screw-

type load frame in accordance with ASTM D8225-19 and the CT_{Index} was calculated. It should be noted that the hydraulic load frame did not have enough travel to test the smaller specimens. A minimum of five replicates were used for each of the tests. Figure 6 provides the results of testing. It is notable that the Marshall specimen produced a lower CT_{Index} than its paired SGC specimen in both the design and production phase. As noted earlier, the lower production values for both tests were likely due to construction variability. This is not surprising when considering the work of Wright et al. (2024) which showed that slight changes in binder content and gradation within production tolerances can yield results below the design BMD thresholds. However, with the data provided it is hard to conclude anything other than that the Marshall specimen and the SGC specimen do *not* yield the same result. Understanding why this is the case will require additional testing of mixes to understand the cause(s) of the difference as well as whether there is a reasonable offset that can be applied to normalize the specimens. It should also be noted that meeting the target air void criteria within a tolerance of ± 0.5 percent is vital to achieving repeatable and meaningful CT_{Index} results. This was found to be more challenging to achieve in the laboratory with the Marshall than with the SGC. With the SGC, the height of the final specimen is fixed to a target when the SGC is set to height control mode (62 mm). With the Marshall hammer, Marshall samples have an allowable variance in final height at a given number of blows (63.5 mm ± 2.5 mm) – which can lead to additional variance in air voids. Hence it is vital to not only control the mass of mix going into the mold but the height of the final specimen as well to get Marshall specimens that meet the air void requirement for IDEAL-CT testing.

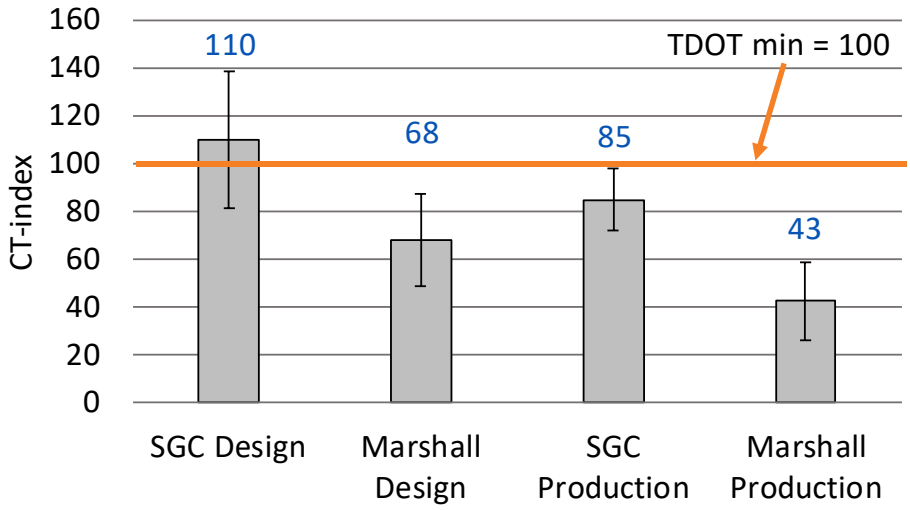

FIGURE 6 Comparison of design and production IDEAL-CT specimens.

13.5 Summary, Conclusions, and Recommendations

An approved TDOT contractor's HMA mix design was modified to lower its CT_{Index} value to move closer to the TDOT BMD threshold of 100 while not compromising its ability to pass the HWTT.

This mixture was then placed on the NCAT Test Track in an effort to investigate whether the TDOT BMD thresholds for high traffic were sufficient to withstand 10 million ESALs of heavy truck traffic. Further, considering TDOT is a Marshall mix design state, the use of a 4-inch Marshall specimen for the IDEAL-CT test was investigated. The following conclusions were drawn from this study:

- The TDOT BMD mix design thresholds (CT_{Index} > 100 and HWTT < 12.5 mm after 20,000 cycles) yielded acceptable results on the NCAT Test Track after 10 million ESALs.
- CT_{Index} results collected during production (CT_{Index} = 85) were lower than the design (CT_{Index} = 110) and threshold (CT_{Index} = 100). This is not surprising considering the work of Wright et al. (2024) which showed currently accepted production mixture variability can result in test values outside BMD thresholds.
- For this mixture, use of a 4-inch Marshall specimen for IDEAL-CT testing does not provide the same result as the standard 6-inch SGC specimen. Marshall compaction results were lower than the companion 6-inch SGC specimens.

It is recommended that TDOT continue to confidently investigate using their current BMD criteria of CT_{Index} > 100 and HWTT < 12.5 mm after 20,000 cycles as it showed promise on the NCAT Test Track after 8.6 million ESALs. It is recommended that more mixtures are tested using the 150 mm SGC versus a 4-inch Marshall specimen for IDEAL-CT testing. This will help establish whether or not there is a relationship between specimen sizes and compaction type that will enable the use of 4-inch Marshall specimens in BMD.

13.6 References

1. Lynn, T.A. and M.P. McDonald. Development of a Balanced Mix Design Procedure for Tennessee Mixtures. Tennessee Department of Transportation Final Report RES2019-05, Nashville, TN, 2023.
2. Wright, T.Y.L., B. Bowers, S. Diefenderfer, I. Evaluation of the Influence of Production Tolerance Limits on Virginia Balanced Mixtures. *Transportation Research Record: Journal of the Transportation Research Board*, DOI: 10.1177/03611981231222248, 2024.

14. TEXAS DEPARTMENT OF TRANSPORTATION BALANCED MIX DESIGN EXPERIMENT

Dr. Fan Yin, Nathan Moore

14.1 Background

The Texas Department of Transportation (TxDOT) has a long history of using mixture performance tests for asphalt mix design and is a leading agency in implementing balanced mix design (BMD). In 2018, TxDOT developed a special provision for BMD that requires the Hamburg Wheel-Tracking Test (HWTT) (Tex-242-F) for evaluating rutting and moisture resistance and uses the Overlay Test (OT) (Tex-248-F) for evaluating cracking resistance. The HWTT temperature is 50°C, and the criterion is based on the number of passes to 12.5mm rut depth. A minimum threshold of 10,000 passes for mixtures using a PG 64-xx (or lower) binder, 15,000 passes for a PG 70-xx binder, and 20,000 passes for a PG 76-xx (or higher) binder is required.

TxDOT previously used Cycles to Failure (N_f) as their OT cracking parameter, which is defined as the number of cycles corresponding to a 93% reduction of the initial peak load. Although this parameter was effective in discriminating asphalt mixtures with different cracking potential, it had high variability with an average reported coefficient of variation between 30 and 50% (West et al., 2018).

TxDOT adopted two new OT parameters to address this limitation, Critical Fracture Energy (CFE) and Crack Progression Rate (CPR), based on a research study conducted by the University of Texas at El Paso (UTEP) (Garcia et al., 2017). CFE is defined as the energy required to initiate a crack on the bottom of the specimen at the first loading cycle, which characterizes the fracture properties of the specimen during the crack initiation phase. CPR is defined as the reduction in load required to propagate cracking under cyclic loading conditions, which characterizes the flexibility and fatigue properties of the specimen during the crack propagation phase. TxDOT's current OT test criteria for surface mixtures include a minimum CFE threshold of 1.0 lb.-in./in.^{2} and a maximum CPR threshold of 0.45. In addition to the HWTT and OT requirements, TxDOT's most recent BMD special specification also includes requirements for the Delta T_c (ΔT_c) parameter of asphalt binder (greater than or equal to -6.0°C after 20 hours of PAV aging), maximum allowable reclaimed asphalt pavement (RAP) and recycled asphalt shingles (RAS) contents, and recycled binder ratios for surface mixtures.

14.2 Objective and Scope

TxDOT sponsored Sections S10 and S11 in the 2018 research cycle to compare the field performance of asphalt mixtures designed using a BMD approach versus the traditional volumetric approach, as shown in Figure 1. Section S10 was constructed with a BMD mix, while Section S11 used a volumetric mix. Both sections were built as 2.5-inch mill-and-inlays on top of a 4.5-inch existing asphalt pavement. TxDOT sought to answer two questions from this experiment: Will the BMD mix have a potential rutting issue? Are the current OT test criteria sufficient, or do they need to change to ensure satisfactory cracking performance?

In the 2021 research cycle, TxDOT added Section N6 to further investigate the BMD specification limit for the OT CPR of 0.45. This third mix was designed as close as possible to the 0.45 CPR limit using the same virgin materials from the previous two mixes. The test section was constructed with a pavement structure similar to S10 and S11.

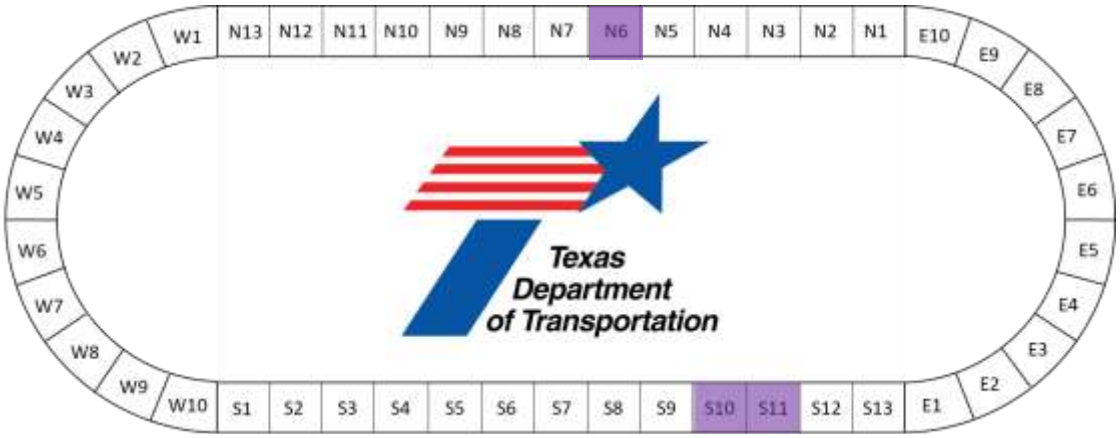

FIGURE 1. Layout of TxDOT Sections S10, S11, and N6 on the NCAT Test Track.

14.3 Existing Pavement Conditions

Sections S10 and S11 were constructed in 2009 as part of the first Group Experiment at the NCAT Test Track. Their existing pavements had 7 inches of asphalt mix over 6 inches of graded aggregate base and a stiff subgrade (approximately 30 ksi). Both sections had approximately 15 to 20% of the lane area cracked after 14 million equivalent single axle loads (ESALs) of trafficking through April 2014. At that point, they were converted to the Pavement Preservation Experiment. Section S10 was divided into two sub-sections and treated with scrub cape and scrub seal, respectively. Section S11 was also divided into two sub-sections, with one treated with chip seal and the other remaining untreated as a control section. In May 2018, the top 2.5 inches of both sections were milled for the preparation of the 2018 research cycle. Figure 2 shows the fatigue cracking in the underlying pavement after milling. These two sections allow TxDOT to determine if a BMD mix would still outperform a volumetric mix in terms of cracking resistance with a challenging underlying pavement condition.

FIGURE 2. Fatigue cracking in underlying pavement of Sections 10 and S11 after milling.

The existing pavement of Section N6 was also originally built in 2009. In 2014, after 17.5 million ESALs, half of the section was treated with micro surfacing, and the other half was left untreated. The untreated section was milled and inlaid with a new asphalt mix in May 2020 due to severe rutting. Therefore, it is assumed the underlying surface in N6 did not have the same cracking severity after milling as the surfaces in S10 and S11. In 2021, 2.5 inches were milled from the entire surface of Section N6, and a new mix design was placed for TxDOT to further validate their BMD cracking test criteria.

14.4 Mix Design

Table 1 presents the job mix formula (JMF) and quality control (QC) data for S10 BMD, N6 BMD, and S11 volumetric mixes. The S10 and S11 mixes, placed in 2018, were designed by UTEP by adjusting a TxDOT-approved 12.5 mm SP-C surface mix design. They used the same component materials, including a PG 70-22 styrene butadiene styrene (SBS) modified binder from the same binder supplier, fractionated RAP, and a blend of granite and dolomitic limestone. The S10 BMD mix had a RAP content of 18.1%, which is higher than that of the S11 volumetric mix (i.e., 16.0%). Despite this difference, the two mixes had the same RAP binder replacement ratio of 20%. The N6 BMD mix was designed with the same virgin materials as S10 and S11 but in different proportions. The gradation was between the other two mixes, as shown in Table 1.

All three mixes were designed with 4.0% air voids at 50 design gyrations. The S11 volumetric mix had an optimum binder content (OBC) of 4.7% and 15% voids in mineral aggregate (VMA) (calculated using aggregate G_{se} per TxDOT specifications). The S10 BMD mix was designed with a slightly coarser gradation, a higher OBC of 5.5%, and a higher VMA (G_{se}) of 16.6%, which was expected to provide improved mixture durability and cracking resistance. The N6 mix had an OBC of 5.3% and 16.4% VMA, which was expected to have lab and field performance between that of S10 and S11.

TABLE 1. Mix Design and QC Data of S10 BMD, S11 Volumetric, and N6 BMD Mixes

Sieve (in.)	Job Mix Design			Quality Control		
	S10	S11	N6	S10	S11	N6
25 mm (1”)	100	100	100	100	100	100
19 mm (3/4”)	100	100	100	100	100	100
12.5 mm (1/2”)	93	92	94	93	95	94
9.5 mm (3/8”)	82	81	81	78	82	86
4.75 mm (#4)	52	53	52	46	55	53
2.36 mm (#8)	30	34	33	27	37	32
1.18 mm (#16)	21	24	23	19	25	21
0.60 mm (#30)	16	17	16	14	17	15
0.30 mm (#50)	11	12	12	11	12	11
0.15 mm (#100)	7	7	8	8	8	7
0.075 mm (#200)	4.9	4.8	5.0	5.2	5.7	5.2
Design Gyration (N_{design})	50	50	50	50	50	50
NMAS (mm)	12.5	12.5	12.5	12.5	12.5	12.5
Total Binder Content (%)	5.5	4.7	5.3	5.3	4.4	5.2
Virgin Binder Grade	PG 70-22 (SBS)	PG 70-22 (SBS)	PG 70-22 (SBS)	PG 70-22 (SBS)	PG 70-22 (SBS)	PG 70-22 (SBS)
RAP Binder Ratio (%)	20	20	19	19	20	19
Air Voids (%)	4.0	4.0	4.0	2.4	3.6	3.9
Blend G_{se}	2.668	2.656	2.684	2.660	2.651	2.715
G_{mm}	2.450	2.470	2.493	2.451	2.475	2.503
G_{mb}	2.353	2.370	2.394	2.393	2.387	2.407
VMA (G_{se}) (%)	16.6	15.0	16.4	14.8	14.0	16.0
V_{be} [calculated with VMA (G_{se}), %]	12.6	11.0	12.4	12.4	10.4	12.1
VFA [calculated with VMA (G_{se}), %]	76	73	76	84	74	76
Dust Proportion	0.9	1.0	0.9	1.0	1.3	1.0
Extracted Binder Grade	-	-	-	PG 82-16	PG 82-16	-

The S10 BMD and N6 BMD mixes were designed with the *Volumetric Design with Performance Verification* approach (Approach A), as described in AASHTO PP 105-20. Using this approach, OBC was first determined based on the Superpave volumetric analysis and was then verified with the HWTT and OT to ensure compliance with rutting and cracking test requirements. Figure 3 presents the performance diagram from mix design testing with the HWTT total rut depth at 15,000 passes plotted on the x-axis versus the OT CPR results on the y-axis. The two dashed lines represent TxDOT’s performance test criteria. As shown, the S10 BMD and N6 BMD mixes fell within the “sweet zone” of the performance diagram (by passing both the HWTT and OT criteria) with the expectation of having balanced rutting and cracking resistance. On the other hand, the S11 volumetric mix passed the HWTT requirement but failed the OT CPR requirement and was located outside the “sweet zone” of the performance diagram. Note that the N6 mix was deliberately designed to have cracking resistance between that of the S11 volumetric mix and the S10 BMD mix, per TxDOT’s request.

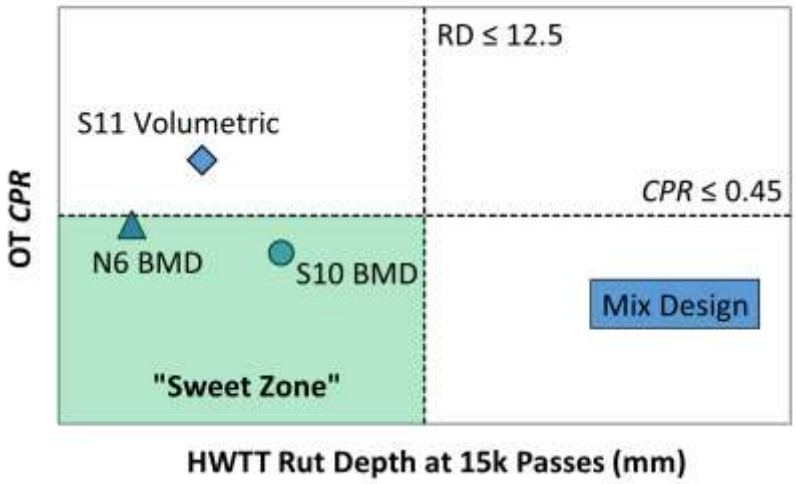

FIGURE 3. Performance diagram from mix design testing.

14.5 Mix Production and Construction

The BMD mix for Section S10 was produced and placed on September 18, 2018, with a high temperature of 91°F, a low of 73°F, and no rainfall. As shown in Table 1, QC testing of the plant mix showed a reduction in the total binder content from 5.5% in mix design to 5.3% at production, as well as moderate changes in the 3/8", #4, and #8 fractions. The production mix had 2.4% lab-molded air voids and 14.8% VMA (G_{se}) at 50 gyrations (N_{design}), and 4.0% lab-molded air voids and 16.2% VMA (G_{se}) at a reduced N_{design} of 35 gyrations. The production mix met TxDOT's special specification for *Superpave Mixtures – Balanced Mix Design*, except that the percent passing on the #8 sieve size was 1% lower than the allowed master gradation limits. The extracted binder of the plant mix was graded at PG 82-16. The mix was produced at approximately 305°F and had an in-place density averaging 95.9%. Figure 4 shows the laydown and compaction of the BMD mix for Section S10.

FIGURE 4. Constructing Section S10 with a BMD mix.

The S11 volumetric mix was produced and placed on September 17, 2018, with a high temperature of 93°F, a low temperature of 72°F, and no rainfall. As shown in Table 1, QC testing showed a reduction of asphalt content from 4.7% in mix design to 4.4% at production and slight

changes in the 1/2", 3/8”, #16, and minus #200 fractions. The plant mix had 3.6% lab-molded air voids and 14.0% VMA (G_{se}) at 50 gyrations (N_{design}), which met TxDOT’s specification for Item 341, *Dense-Graded Hot-Mix Asphalt*. The extracted binder of the plant mix was graded at PG 82-16, which was the same as that of the S10 BMD mix. The S11 mix was produced at approximately 300°F and had an in-place density averaging 95.4%. Figure 5 shows the laydown and compaction of the volumetric mix for Section S11.

FIGURE 5. Constructing Section S11 with a volumetric mix.

The BMD mix in Section N6 was produced and placed on September 13, 2021, with a high temperature of 89°F, a low of 67°F, and no rainfall within the previous 24 hours. As shown in Table 1, there were no major differences between the JMF and the QC results. The asphalt content was deliberately targeted to run slightly lower than the JMF to slightly push the OT CPR result from 0.43 closer to the 0.45 threshold. This resulted in an asphalt content of 0.1% less than the JMF at QC testing. The gradation was essentially the same for the QC sample compared to the JMF, except the percent passing the 3/8” sieve was 5% finer. The volumetrics from QC testing were also similar to the JMF, within typical production tolerances. The mix was produced at approximately 320°F and had an in-place density averaging 93.3%. Figure 6 shows the laydown and compaction of the BMD mix for Section N6.

FIGURE 6. Constructing Section N6 with a BMD mix.

14.6 Laboratory Testing and Data Analysis

During test section construction, the plant mix was sampled from the Test Track and transported back to the NCAT laboratory, where it was reheated to fabricate plant-mixed, lab-compacted (PMLC) specimens for performance testing. HWTT and OT were conducted to evaluate the rutting and cracking resistance, respectively, of the three plant-produced mixes and determine their compliance with TxDOT's performance test criteria. In addition, the Indirect Tensile Asphalt Rutting Test (IDEAL-RT per ASTM D 8360-22) and Indirect Tensile Asphalt Cracking Test (IDEAL-CT per ASTM D8225-19) were performed to explore their feasibility as surrogate tests to HWTT and OT, respectively, for BMD production testing. OT and IDEAL-CT tests were conducted on both reheated and critically aged PMLC specimens to consider the effect of asphalt aging on mixture cracking resistance. The critical aging (CA) protocol used was loose mix aging for 8 hours at 135°C, which is expected to simulate a critical field aging condition of 70,000 cumulative degree days where top-down cracking starts to develop after four to five years in service in Alabama (Chen et al., 2018; Chen et al., 2020).

Figure 7 presents the HWTT and OT results of the re-heated PMLC specimens on a performance diagram. The S10 BMD mix fell within the "sweet zone" of the performance diagram, while the S11 volumetric mix fell outside the "sweet zone." As expected, the N6 mix was close to TxDOT's CPR threshold, with an average of 0.46. The OT and HWTT results for the three mixes fell in line as expected during the design process. Specifically, the S10 BMD mix was the most cracking resistant, followed by the N6 BMD mix, which was right at the OT design criterion. The S11 volumetric mix fell outside the "sweet zone" with inadequate cracking resistance. All three mixes had passing HWTT results. The S10 BMD mix met both TxDOT's HWTT and OT criteria and was expected to have balanced rutting and cracking resistance. The S11 mix failed to meet TxDOT's OT criteria and was expected to have reduced cracking resistance compared to the S10 and N6 mixes. Despite the production sample being 0.01 outside of the "sweet zone," the N6 mix was still expected to have superior cracking resistance compared to S11 and inferior performance compared to S10. However, field evaluation was necessary to quantify the pavement life-extension benefits associated with BMD optimization for Sections N6 and S10.

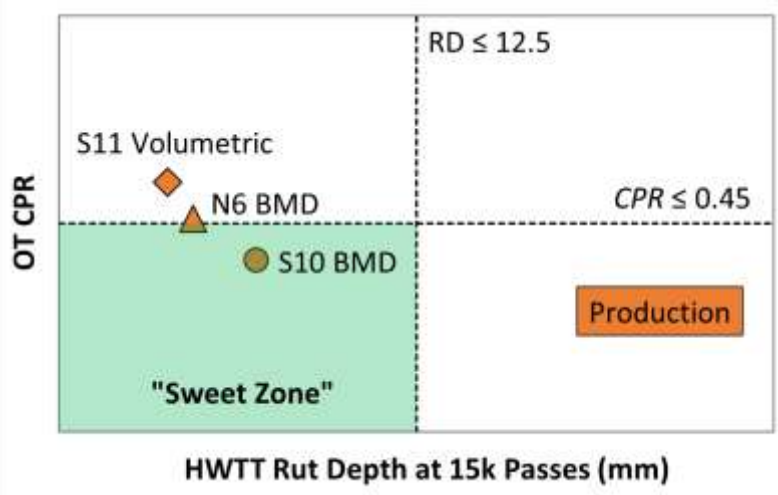

FIGURE 7. Performance diagram from production testing using reheated PMLC specimens.

Figure 8 presents the OT results of the short-term aged LMLC, reheated PMLC, and critically aged PMLC specimens for S10 BMD, S11 volumetric, and N6 BMD mixes. Note that the LMLC specimens for S10 and S11 were tested at UTEP, while the reheated and critically aged PMLC specimens were tested at NCAT. NCAT conducted all testing for N6. The reheated PMLC results were similar to the short-term aged LMLC results for all three mixes, indicating the mixes did not change much from design to construction. The CA protocol of loose mix aging for 8 hours at 135°C yielded a significant increase in the CPR results, which indicated reduced cracking resistance, possibly due to increased mix embrittlement and reduced relaxation properties. The S10 BMD production mix was expected to have the best cracking resistance due to its lowest CPR results among the three mixes at both aging conditions. The N6 mix had lower CPR results than the S11 mix at the reheated condition, but similar results at the critically aged condition. This result indicated the long-term cracking performance of the two mixes could be similar.

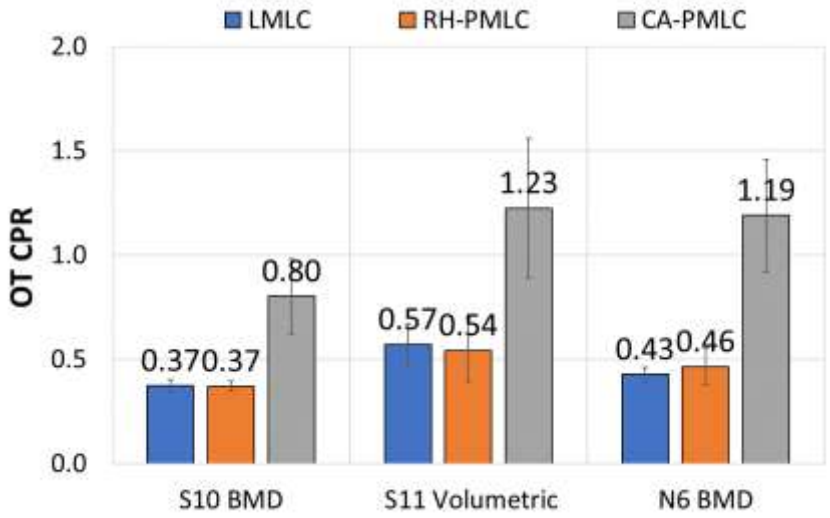

FIGURE 8. OT CPR results of short-term aged LMLC, reheated PMLC, and critically aged PMLC specimens.

Figure 9 presents the IDEAL-CT results of reheated and critically aged PMLC specimens. At both aging conditions, the S10 BMD mix showed significantly higher CT_{Index} results compared to the N6 and S11 mixes, indicating better cracking resistance. These results agree with the OT results in Figure 8 and highlight the potential of using IDEAL-CT as a surrogate test to OT for BMD production testing.

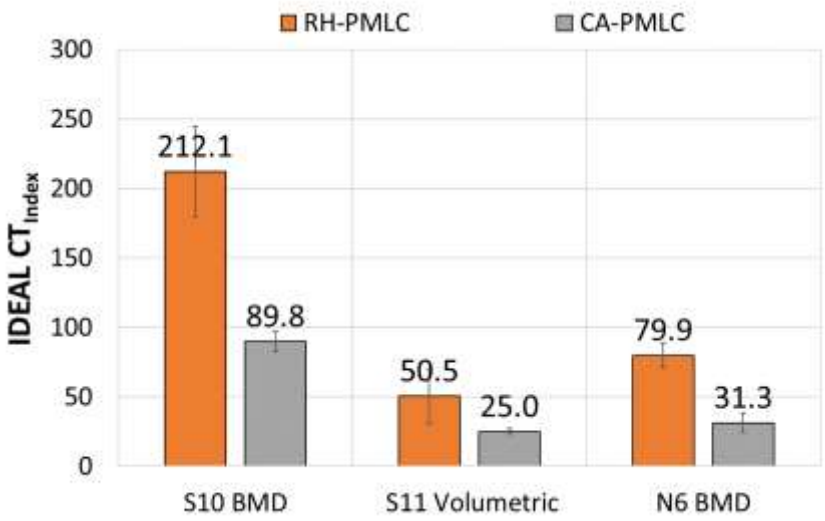

FIGURE 9. IDEAL CT_{Index} results of reheated and critically aged PMLC specimens.

Figure 10 presents the IDEAL-RT results of reheated PMLC specimens. As shown, the S10 mix had a lower RT_{Index} and thus, was expected to have reduced rutting resistance relative to the S11 volumetric mix. The RT_{Index} of the N6 BMD mix was slightly less than the midpoint between the S10 and S11 mixes. These results agree with the HWTT rut depth results in Figure 7 and highlight the potential of using the IDEAL-RT test as a surrogate to HWTT for BMD production testing. However, the correlation between these tests cannot be determined due to limited data availability in the study.

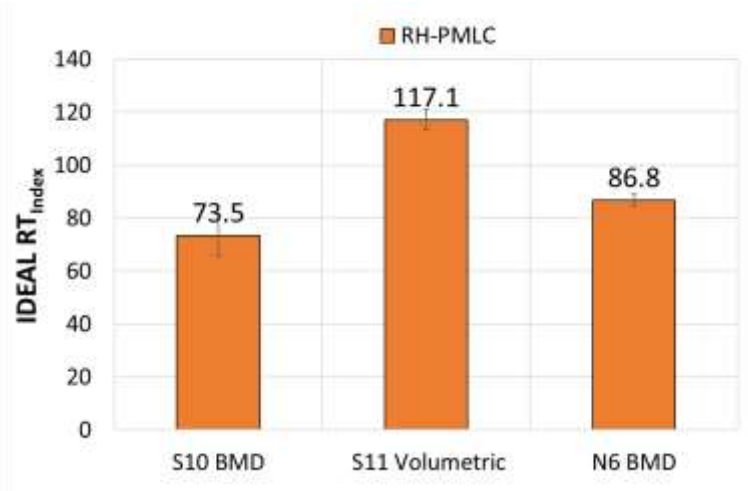

FIGURE 10. IDEAL RT_{Index} results of reheated PMLC specimens.

14.7 Field Performance

Trafficking of S10 and S11 started in October 2018, and trafficking of N6 started in November 2021. This three-year offset requires plotting field performance on an x-axis indicating traffic (in million ESALs) instead of time. Section S11 failed due to cracking and was milled in June 2023 after approximately 15.8 million ESALs of traffic. Throughout trafficking of the test sections,

surface cracking, rutting, smoothness, and surface texture were monitored on a weekly basis using an automated pavement condition survey vehicle. Additionally, surface friction was measured each month using a locked-wheel friction trailer.

Figure 11 presents the field rutting data. Section S10 had approximately 0.3 inches of rutting after 20 million ESALs, while Section S11 had approximately 0.2 inches of rutting before it was milled at around 15.8 million ESALs. Section N6 had approximately 0.2 inches of rutting after 10 million ESALs. For Sections S10 and S11, most rutting occurred in the summer of 2019 and then leveled off. Section N6 experienced upticks in rutting during the summers of 2022 and 2023, but the rut depth after 10 million ESALs was significantly lower than the 0.5-inch threshold. Although Section S10 rutted slightly more than Section S11, it was far from exceeding the maximum rutting threshold of 0.5 inches. Overall, the field rutting data in Figure 11 agrees with the HWTT and IDEAL-RT results, which indicates reduced but adequate rutting resistance of the two BMD mixes (S10 and N6) compared to the S11 volumetric mix.

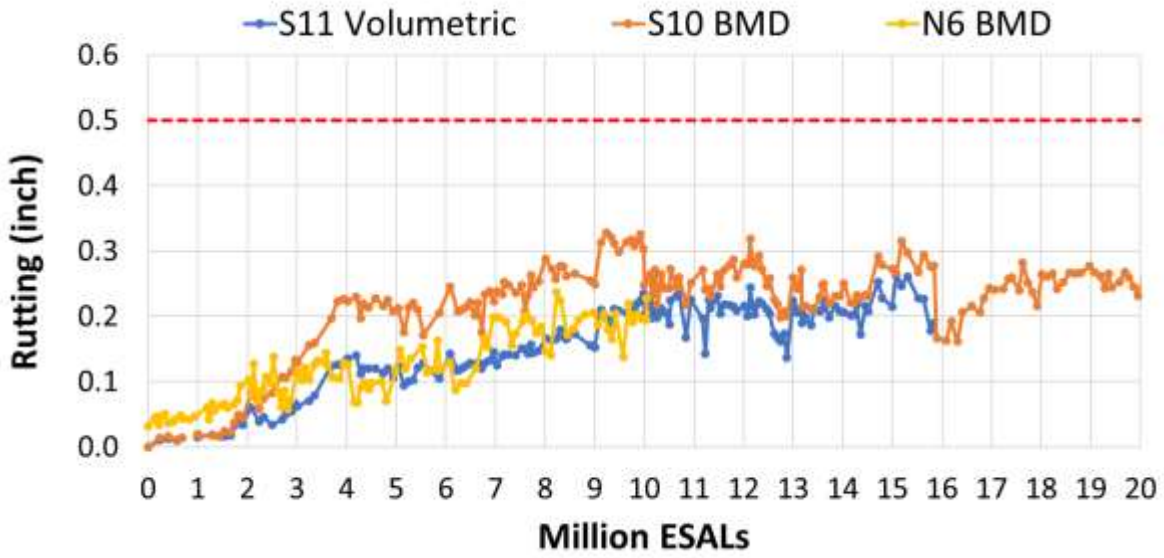

FIGURE 11. Field rutting data.

Figure 12 presents the surface cracking data, where cracking is expressed as a percentage of the lane area cracked. As observed, Section S10 exhibited excellent cracking performance with approximately 11.0% of cracked lane area after 20 million ESALs, while Section S11 reached over 20% of cracked lane area at around 14.5 million ESALs. The cracking in Section S11 progressed to approximately 25.7% before it was milled at around 15.8 million ESALs. The field cracking data agreed with the laboratory OT and IDEAL-CT results, which indicated that the S10 BMD mix had better cracking resistance than the S11 volumetric mix. Forensic analysis of Section S11 by coring the cracked areas showed that cracking was caused by the reflection of previously existing cracking in the underlying layer. The field cracking data of Section S10 versus S11 also highlights the benefit of BMD in extending the lifespan of asphalt overlays despite having a challenging underlying pavement condition, which can provide significant cost savings and environmental benefits from the life-cycle cost analysis and life-cycle assessment perspectives, respectively. After 10 million ESALs, no cracking had occurred in Section N6.

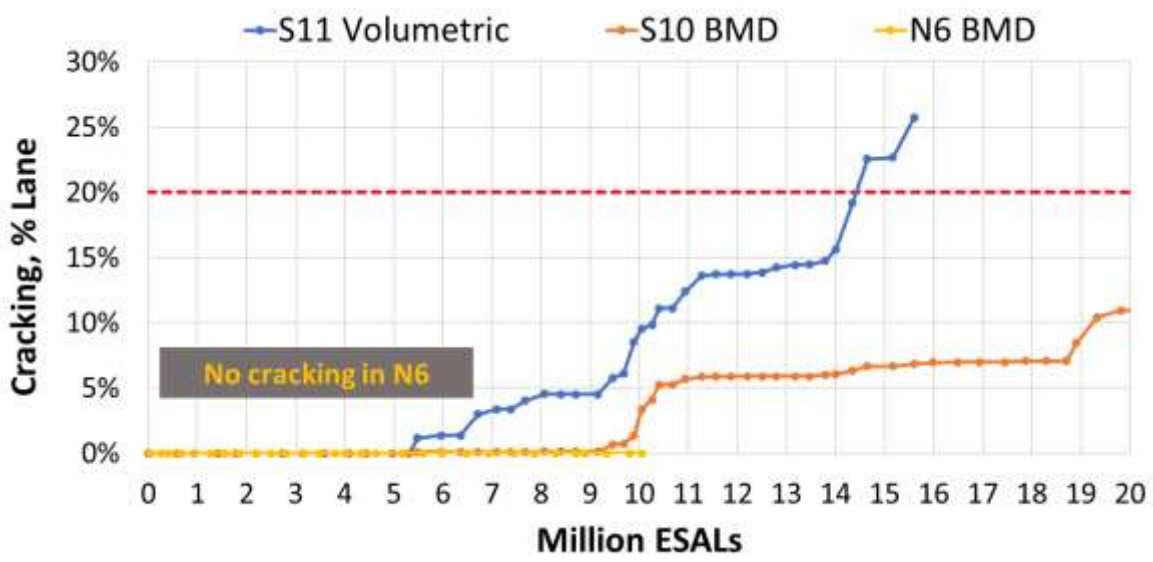

FIGURE 12. Field cracking data.

Figures 13 through 15 present the international roughness index (IRI), mean texture depth (MTD), mean profile depth (MPD), and skid number (tested with ribbed tire) results. As shown in Figure 13, Sections S10 and S11 did not experience significant changes in IRI through the first 6.0 million ESALs. At that time, maintenance patches were applied in the transition areas of the test sections, which caused a steep increase in IRI. After that, the IRI of Section S11 gradually increased over time, while Section S10 fluctuated around 150 to 200 inches per mile up to approximately 16.0 million ESALs. Section N6 showed a steady IRI of around 70 inches per mile throughout 10 million ESALs.

Texture data from the 2018 research cycle was reported in MTD. At the beginning of the 2021 Track cycle, texture results were reported in MPD instead. Therefore, texture data for S10 and S11 was recorded in MTD for the first 10 million ESALs, while all the other texture data was in MPD. Nonetheless, the three sections have similar MPD results, albeit at different time intervals. Section S10 had a higher initial MTD than Section S11, likely due to coarser aggregate gradation. Nevertheless, the two sections had similar MTD results until Section S11 was milled at approximately 15.8 million ESALs, as shown in Figure 14.

The skid number, measured at 40 mph with a ribbed tire, declined in the first year of trafficking from greater than 45 after construction to approximately 30 after 5 million ESALs for all three sections, as shown in Figure 15. After approximately 5 million ESALs, a running average of the skid numbers remained around 30 for the remainder of traffic and often dipped below 30. Despite marginally meeting the Test Track's skid number threshold of 25, Sections S10, S11, and N6 consistently showed the lowest friction numbers on the Test Track during the two research cycles.

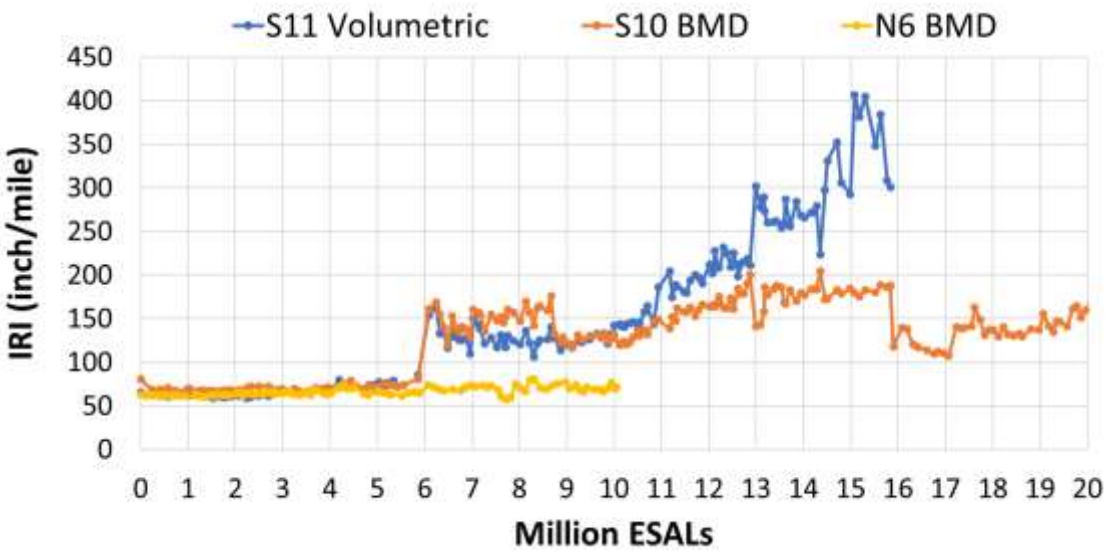

FIGURE 13. Field smoothness data.

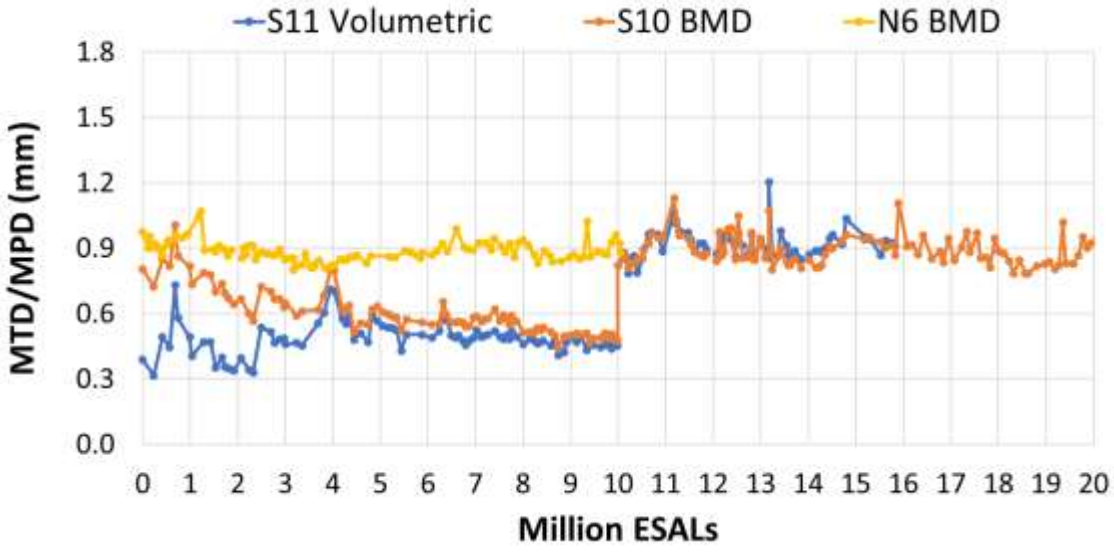

FIGURE 14. Field texture data.

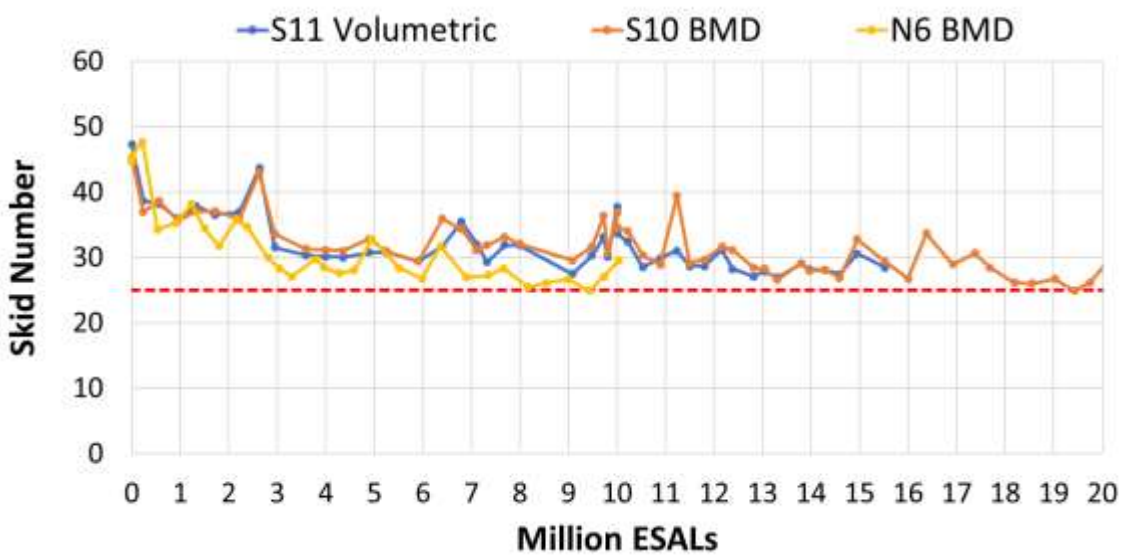

FIGURE 15. Field friction data.

14.8 Conclusions and Recommendations

Based on the laboratory test results and field performance data, the following conclusions and recommendations are made.

- The S11, N6, and S10 mixes were designed with varying degrees of gradation coarseness, with S10 being the coarsest, S11 the least coarse, and N6 between S10 and S11. Because of the gradation differences, S10 had the highest asphalt content and VMA, followed by N6 and S11, respectively.
- OT and HWTT testing of all three mixes produced the expected results, with higher asphalt content resulting in better cracking resistance and lower rutting resistance. All three mixes passed HWTT requirements, but only N6 and S10 passed the OT cracking requirement during design. The IDEAL-CT and IDEAL-RT results from plant-produced mixes agreed with OT and HWTT results in terms of ranking the mixes.
- All sections performed well after 10 million ESALs. Section S10 had more rutting but less cracking than Section S11, while Section N6 had rutting performance between that of S10 and S11. Overall, the field performance data agreed with the laboratory test results. Section S11 exceeded the 20% lane cracked threshold at 14.5 million ESALs and was subsequently removed from the experiment. Section S10 had 11.0% of the lane cracked after 20 million ESALs, while Section N6 did not exhibit any cracking after 10 million ESALs. The cracking performance difference between Sections S10 and S11 highlights the life extension benefits of BMD over the volumetric mix design, despite having a challenging underlying pavement condition.
- Possibly because of the coarser gradation, Section S10 had higher MTD than Section S11 after construction, but the difference significantly reduced over time. All three sections had similar MPD beginning in 2021.

- All three sections showed similar friction characteristics and were consistently some of the lowest skid resistance sections at the Test Track for the 2018 and 2021 research cycles.
- Sections N6 and S10 are recommended for traffic continuation in the next research cycle to further monitor and evaluate their long-term performance on the Test Track. This performance data will be highly valuable for TxDOT to quantify the benefits of implementing BMD in extending the service life of asphalt pavements in Texas.
- Due to the low skid resistance of Sections N6 and S10, it is recommended that TxDOT consider a friction treatment in the 2024 research cycle. A potential candidate that would have a negligible effect on the overall purpose of the BMD experiment is shot blasting. If the skid resistance of the sections declines further, a treatment must be applied for safety purposes.

References

Chen, C., F. Yin, A. Andriescu, R. Moraes, D. Mensching, N. Tran, A. Taylor, and R. West. Preliminary Validation of the Critical Aging Protocol for NCAT Top-down Cracking Experiment. *Journal of the Association of Asphalt Paving Technologists*, Vol. 89, 2020.

Chen, C., F. Yin, P. Turner, R. C. West, and N. Tran. Selecting a Laboratory Loose Mix Aging Protocol for the NCAT Top-Down Cracking Experiment. *Transportation Research Record: Journal of the Transportation Research Board,* No. 2672, Vol. 28, 2018, pp. 359-371.

Garcia, V. M., A. Miramontes, J. Garibay, I. Abdallah, G. Carrasco, R. Lee, and S. Nazarian. Alternative Methodology for Assessing Cracking Resistance of Hot Mix Asphalt Mixtures with Overlay Tester. *Road Materials and Pavement Design*, Vol. 18(sup4), 2017, pp. 388-404.

West, R., C. Rodezno, F. Leiva, and F. Yin. *Development of a Framework for Balanced Mix Design*. Project NCHRP 20-07/Task 406 Final Report, 2018.

Yin, F., A. Taylor, and N. Tran. *NCAT Report 20-02: Performance Testing for Quality Control and Acceptance of Balanced Mix Design*. National Center for Asphalt Technology at Auburn University, 2020.

15. VIRGINIA DEPARTMENT OF TRANSPORTATION LONG-TERM PERFORMANCE OF CCPR SECTION N4

Dr. David Timm, Dr. Benjamin Bowers

15.1 Introduction

An experiment to determine the viability of using cold central plant recycled (CCPR) asphalt mix as a base layer in a flexible pavement began in 2012 at the direction of the Virginia Department of Transportation (VDOT). The original experiment featured three test sections at the Test Track and complimented a study that began in 2011 on I-81 in Virginia featuring a range of recycling techniques (West et al., 2021). The three test sections used reclaimed asphalt pavement (RAP) obtained from the I-81 project. The purpose of the experiment at the Test Track was to characterize the field performance and quantify the structural characteristics under accelerated trafficking.

The sections exceeded their performance expectations during the first test cycle (2012 to 2014), totaling 10 million equivalent single axle load (ESAL) applications. The sections were left in place for another test cycle (2015 to 2017), again performing well to a total of 20 million ESALs. At that point, VDOT elected to continue trafficking into a third cycle (2018 to 2021) on the two sections at structural extremes (i.e., thickest and thinnest overall cross sections) while taking the third section out of service. After the third test cycle, 30 million ESALs were applied to these two test sections, and VDOT elected to remove the thickest section and continue trafficking the thinnest overall cross-section to 40 million ESALs. This chapter documents the long-term performance and structural responses of the section. For additional investigations of the VDOT CCPR Test Track sections, interested readers may refer to earlier publications by Timm et al. (2015), Diefenderfer et al. (2016), Timm et al. (2021), and West et al. (2021).

15.2 Test Section N4

Figure 1 shows Section N4, featuring CCPR as a base layer between the dense-graded Superpave mix and the granular base layer. The section was built on the native Test Track subgrade, which is classified as an AASHTO A-4 soil, over which a crushed granite base of 6 inches was placed. Details regarding the base and subgrade materials were documented in a prior report (Taylor and Timm, 2009).

The CCPR layer was comprised of 100% RAP material hauled from the I-81 project in Virginia. It was mixed with 2% foamed PG 67-22 binder and 1% Type II hydraulic cement by weight of the dry RAP mixture. The Superpave dense-graded asphalt concrete (AC) layer on top of the CCPR was a 19 mm nominal maximum aggregate size (NMAS) mixture with 30% RAP and a PG 67-22 binder. The binder content was 4.6%, and in-place air voids were 7.4%. The stone mix asphalt (SMA) surface AC layer was a 12.5 mm NMAS with 12.5% RAP and a PG 76-22 binder. The binder content was 6.0%, and the in-place air voids were 4.7%.

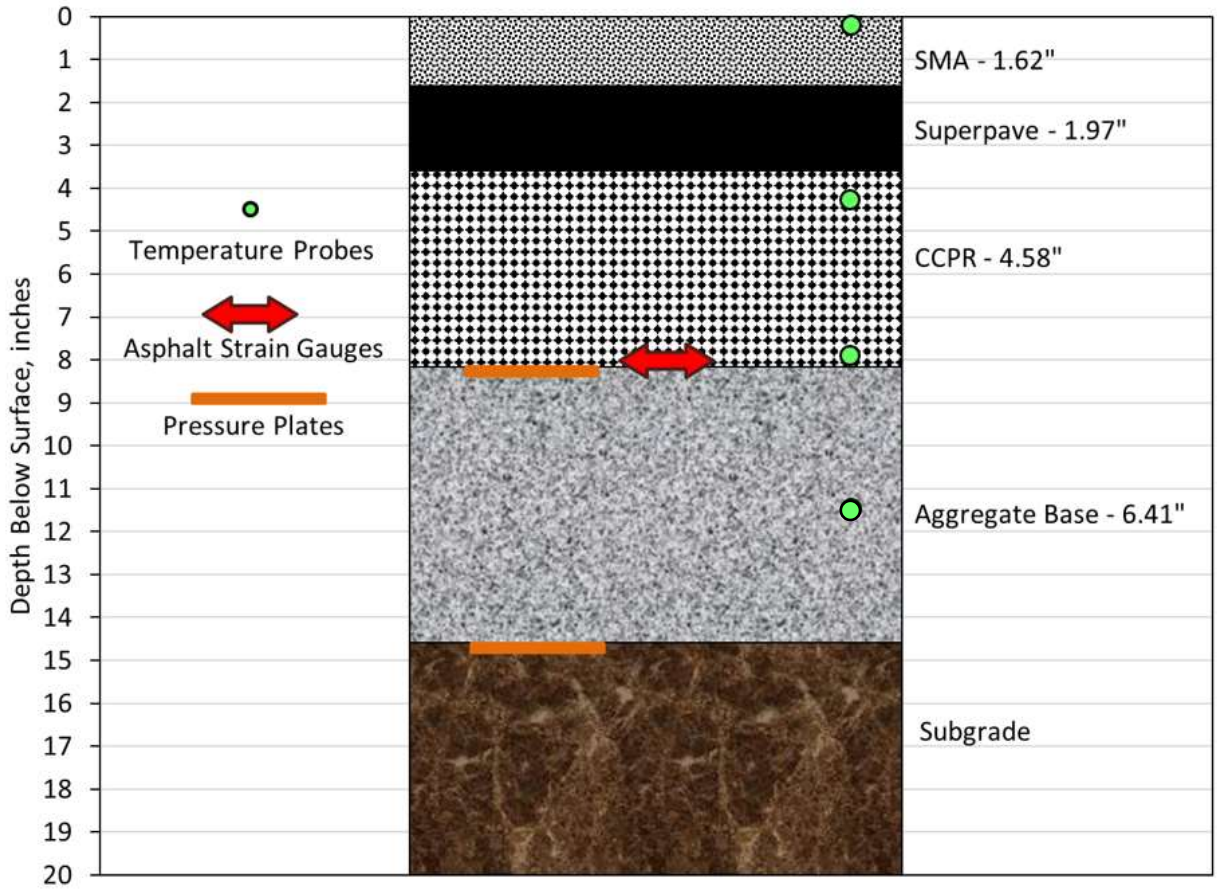

FIGURE 1 CCPR average as-built thickness and depth of instrumentation in N4.

15.3 Performance

The CCPR sections were built in the summer of 2012, with trafficking beginning October 23, 2012. Section N4 was subjected to four full cycles of trafficking amounting to approximately 40 million ESALs During each cycle, the section was monitored on a weekly basis for cracking, rutting, and ride quality, as described below.

15.3.1 Cracking

The section was inspected weekly for cracking during each research cycle. No cracks were observed during the first two test cycles (20 million ESALs). However, minor cracking was observed near the end of the third test cycle on January 25, 2021, after the application of 29.6 million ESALs. Cracking was confined to the outside wheelpath, was primarily transverse to the direction of travel (though there were some interconnecting longitudinal cracks) and was spread evenly along the length of the section. The cracks were relatively tight, and there was no evidence of pumping or fines at the surface. Figure 2 shows some of the cracks highlighted to provide better visualization. The pavement surface was wet during this visual inspection.

FIGURE 2 Sample cracking in N4 on 1/25/2021 (29.6 million ESALs).

Subsequent inspections on later dates revealed much less cracking, which did not appear to progress or worsen during the last 400,000 ESAL applications of the third test cycle. As of February 15, 2021 (29.9 million ESALs), 0.5% of the lane area and 0.1% of the wheelpath area cracked, as determined from inspection of high-resolution crack mapping images. Both values were considered quite low and did not indicate a pavement experiencing cracking failure. The lane area had more reported cracking than the wheelpath, which indicates more cracking outside the wheelpaths than within. This may be indicative of top-down cracking rather than bottom-up. The forensic investigation presented later in this chapter reveals the nature of the cracking, but after the third test cycle, VDOT elected to keep the section in place for another 10 million ESALs during the 2021 research cycle. During this time, lane area cracking grew to 3.4% and wheelpath cracking increased to 2.8%. Cracking severity also increased, particularly in the inside wheelpath. For example, Figure 3 shows clear wheelpath fatigue cracking with dust at the surface, that could be indicative of fines pumping from below, or aggregates grinding against each other under traffic, at approximately 39.1 million ESALs on January 22, 2024. This will be fully investigated in future forensic investigation of the section.

FIGURE 3 Wheelpath fatigue cracking in N4 on 1/22/2024 (39.1 million ESALs).

15.3.2 Rutting

Figure 4 contains all the rutting data gathered over the four test cycles for Section N4. Rutting reached approximately 0.25 inches in the first test cycle and remained largely stable through the next two test cycles to 20 million ESALs and 30 million ESALs, respectively. At the end of the third test cycle, there was a change in the data acquisition software that led to seemingly higher rut depths but was not supported by physical wireline measurements made on the track. Therefore, the circled data in Figure 4 can be considered offset from the previous data due to software rather than an actual increase in rutting. Interestingly, the fourth test cycle, from 30 to 40 million ESALs, saw a steady increase in rutting from approximately 0.3 inches to 0.4 inches. This increase may be partly due to loss of base support, as the section began experiencing more severe cracking and fines pumping from below. The forensic investigation will fully investigate this in the future. The section ended its life at a total average rut depth of 0.4 inches.

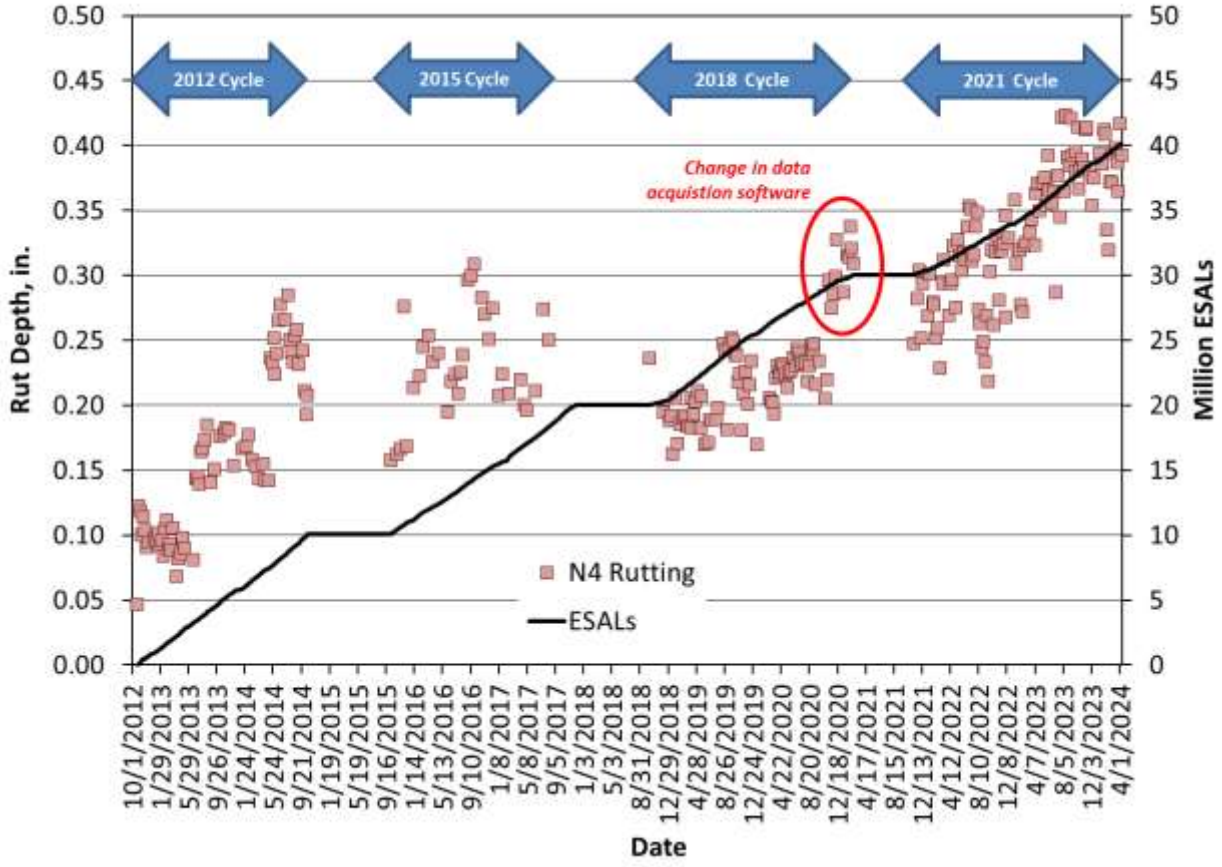

FIGURE 4 N4 rutting performance.

15.3.3 Ride Quality

Figure 5 contains ride quality data for Section N4 over the four test cycles, expressed as the International Roughness Index (IRI). The section had relatively steady IRI for the first three cycles through 30 million ESALs. However, with increasing extent and severity of cracking, and increasing rutting during the fourth test cycle, IRI climbed from approximately 80 inches/mile to nearly 140 inches/mile.

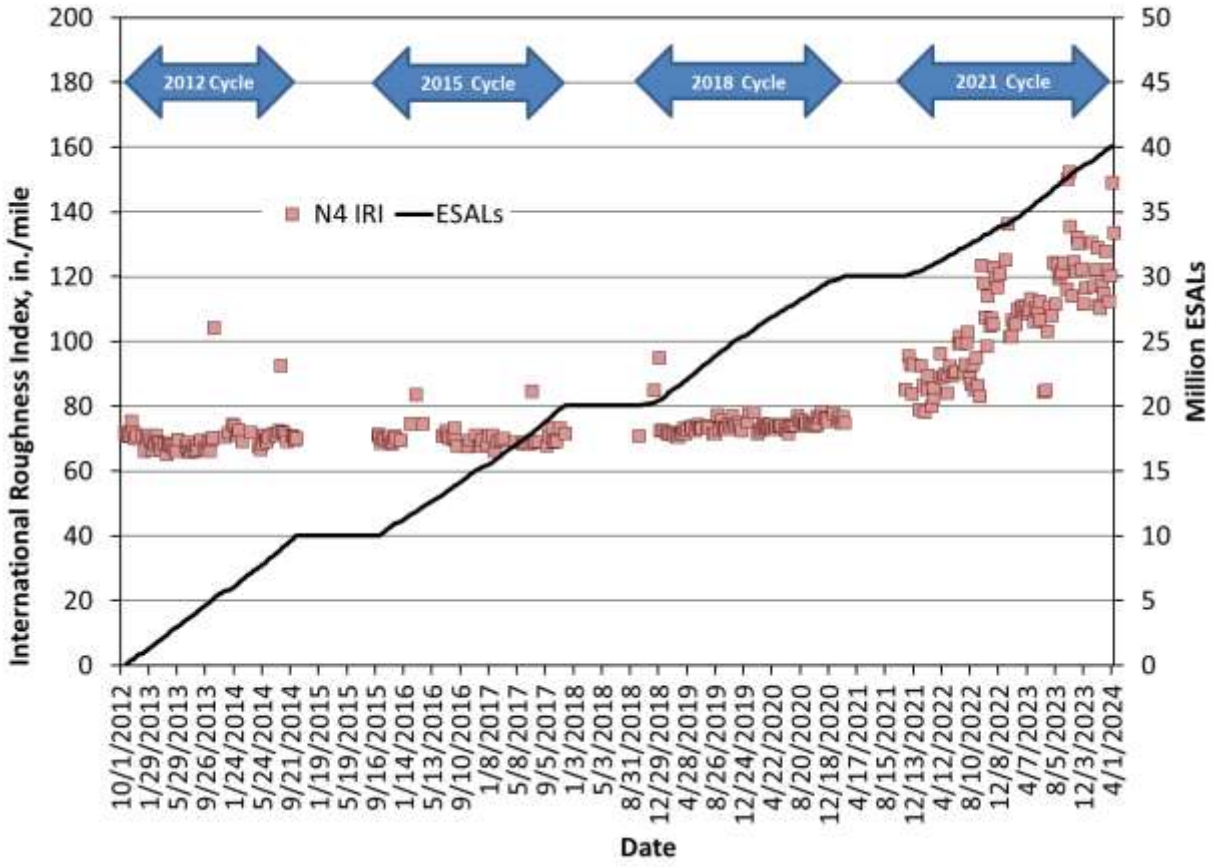

FIGURE 5 N4 ride quality.

15.4 Structural Characterization

Section N4 was instrumented with strain gauges and earth pressure cells to measure in situ pavement responses under truck loading. As shown in Figure 1, the strain gauges were positioned to measure horizontal tensile strain at the bottom of the CCPR layer, and the pressure cells were placed at the CCPR/aggregate base and aggregate base/subgrade interfaces, respectively. Additionally, the section was subjected to frequent falling weight deflectometer (FWD) testing and backcalculation, which is discussed below.

15.4.1 Measured Strain Responses

Figure 6 shows the measured tensile strain response versus time over the four test cycles. Note that the strain gauges stopped working in July of 2022, so no further data were available, and it is difficult to discern whether the cracking that developed over the fourth test cycle corresponded with increasing strain levels in the section since they were not measured. To help answer this question, the data in Figure 6 were plotted against mid-depth AC/CCPR temperature in Figure 7 and organized according to the test cycle. The limited data from the 2021 cycle does not show an apparent increase in strain through July 2022, but the severity of

cracking did not increase significantly until after this date. Also, the gauges are not located in the area with the worst cracking in the section. Only one working gauge was operational in the 2021 cycle, which could have biased the data into a lower range.

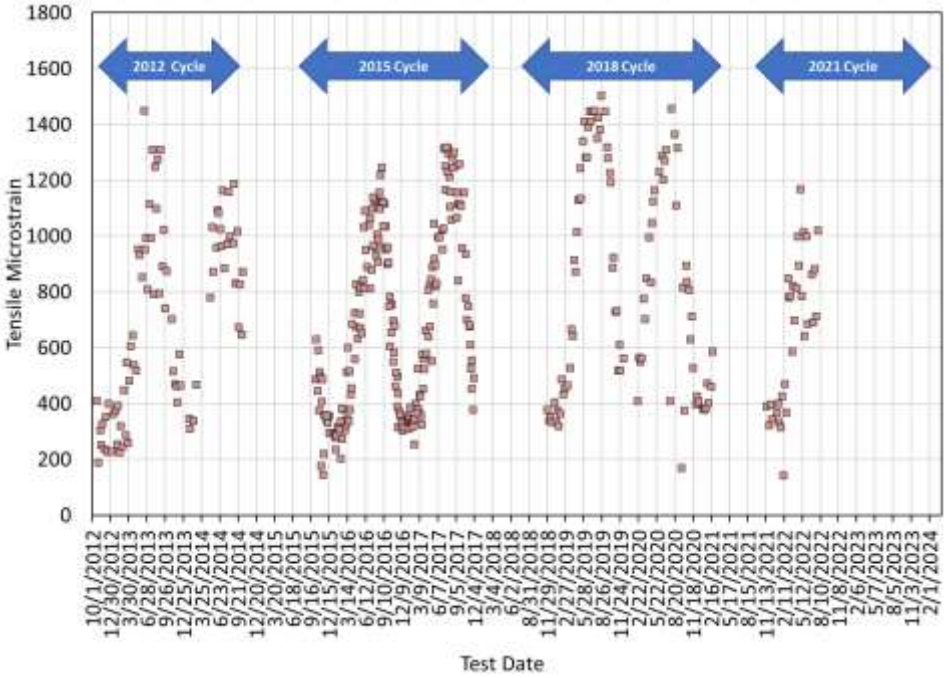

FIGURE 6 Measured strain responses in N4.

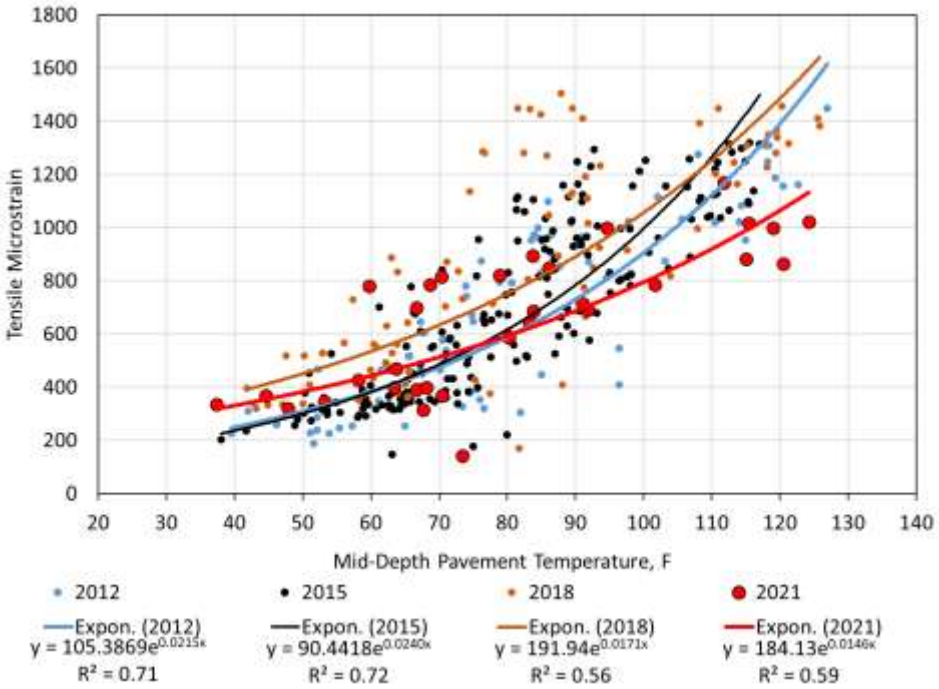

FIGURE 7 Measured strain responses in N4 versus temperature.

The vertical pressures measured at the CCPR/aggregate base interface are plotted in Figure 8. Unlike the strain data, there is a clear increasing trend in vertical pressure over time. Due to this increase, the lowest pressures measured in the fourth test cycle are as high as the highest pressures measured in the first test cycle. This behavior is attributed to increasing levels of distress in the section; both rutting and cracking would increase the pressure reaching the base layer.

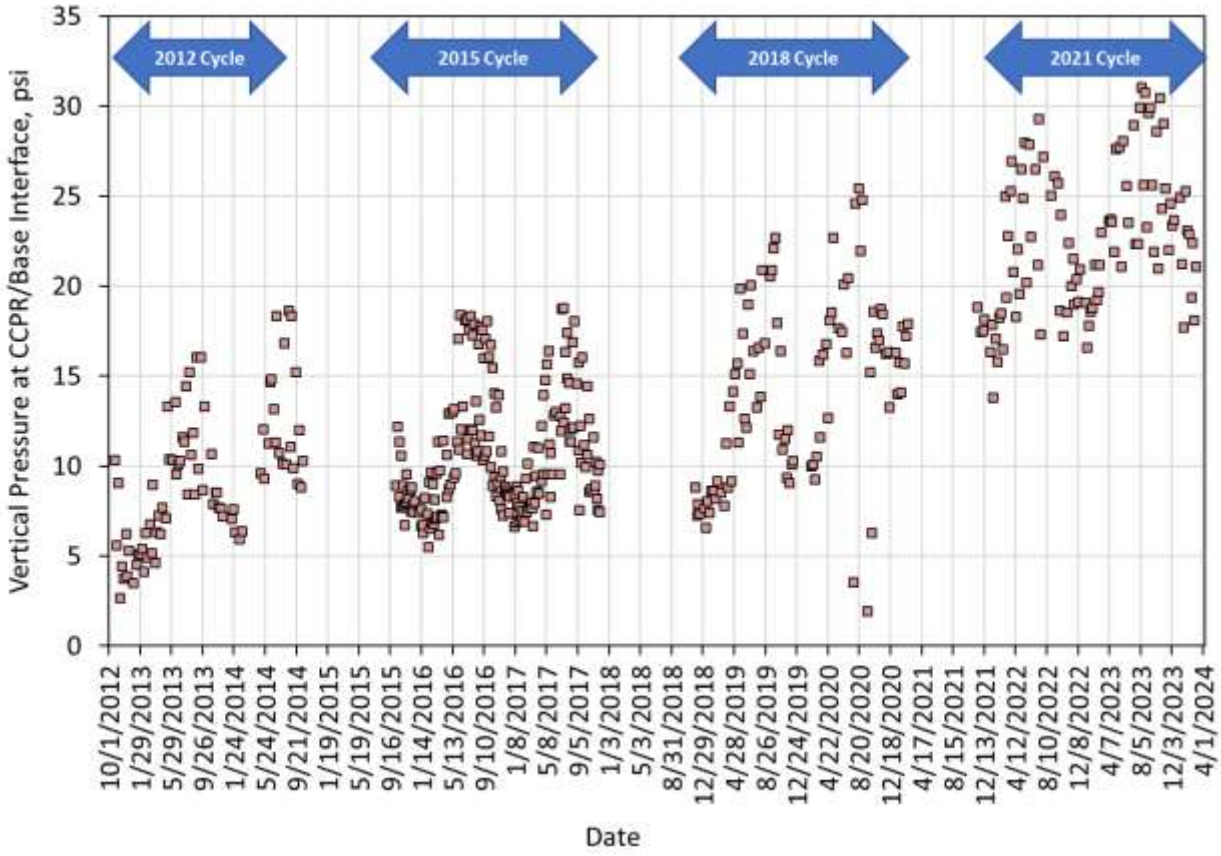

FIGURE 8 Measured vertical pressure in N4 versus date.

To further analyze the increase in pressure versus the test cycle, the data in Figure 8 were plotted against their corresponding mid-depth AC/CCPR temperatures and organized by test cycle. The first two test cycles are nearly identical, and there wasn't any appreciable distress during those cycles. The third cycle is slightly higher but had much more scatter, making it more difficult to discern. However, as noted above, the fourth cycle showed a clear increase in pressure despite the relatively higher degree of scatter compared to the first two cycles. Again, this is attributed to accumulating pavement damage in the fourth test cycle.

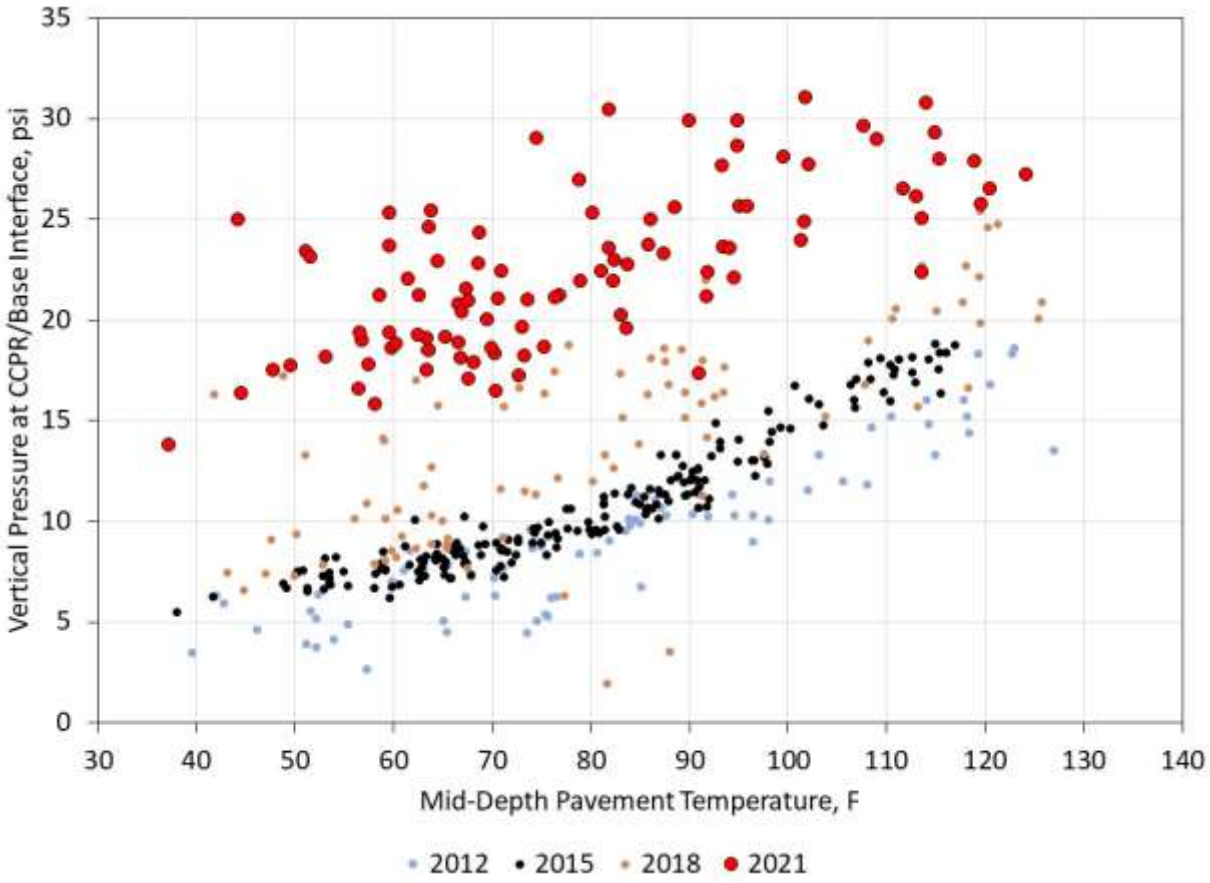

FIGURE 9 Measured vertical pressure in N4 versus temperature.

15.4.2 FWD Testing and Backcalculated AC Moduli

Falling weight deflectometer (FWD) testing was frequently conducted with a Dynatest 8000 FWD using a nine-sensor arrangement followed by multi-layer backcalculation to determine layer properties. Testing was conducted at multiple longitudinal stations in each section representing 50-foot subsections and in the middle of the instrumentation array. At each station, locations within the wheelpaths and between the wheelpaths were both tested. Though FWD testing was performed at multiple loading levels, only data pertaining to the 9,000 lb loading is included in this analysis. Mid-depth temperatures using embedded temperature probes were recorded at the time of testing. Backcalculation of the layer moduli was accomplished with EVERCALC 5.0, and a root mean square error (RMSE) limited to less than 3% was used to ensure reliable results. For this analysis, AC and CCPR were combined into one layer (i.e., layer 1). This decision was based on laboratory |E*| testing where a master curve was successfully developed for CCPR materials, indicating it behaves more like an asphalt concrete material than an aggregate base (Diefenderfer and Link, 2014; Timm et al., 2025). The aggregate base and subgrade layers were layers 2 and 3 in the backcalculation process.

Figure 10 shows the backcalculated AC/CCPR modulus over time during the four test cycles. The seasonal temperature effects are seen within each test cycle, and the first two cycles yielded very similar results in terms of the range of modulus values. The third test cycle, during which damage appeared near the very end, produced slightly lower modulus values. The fourth test cycle, where the extent and severity of cracking and rutting increased, showed a marked decrease in modulus.

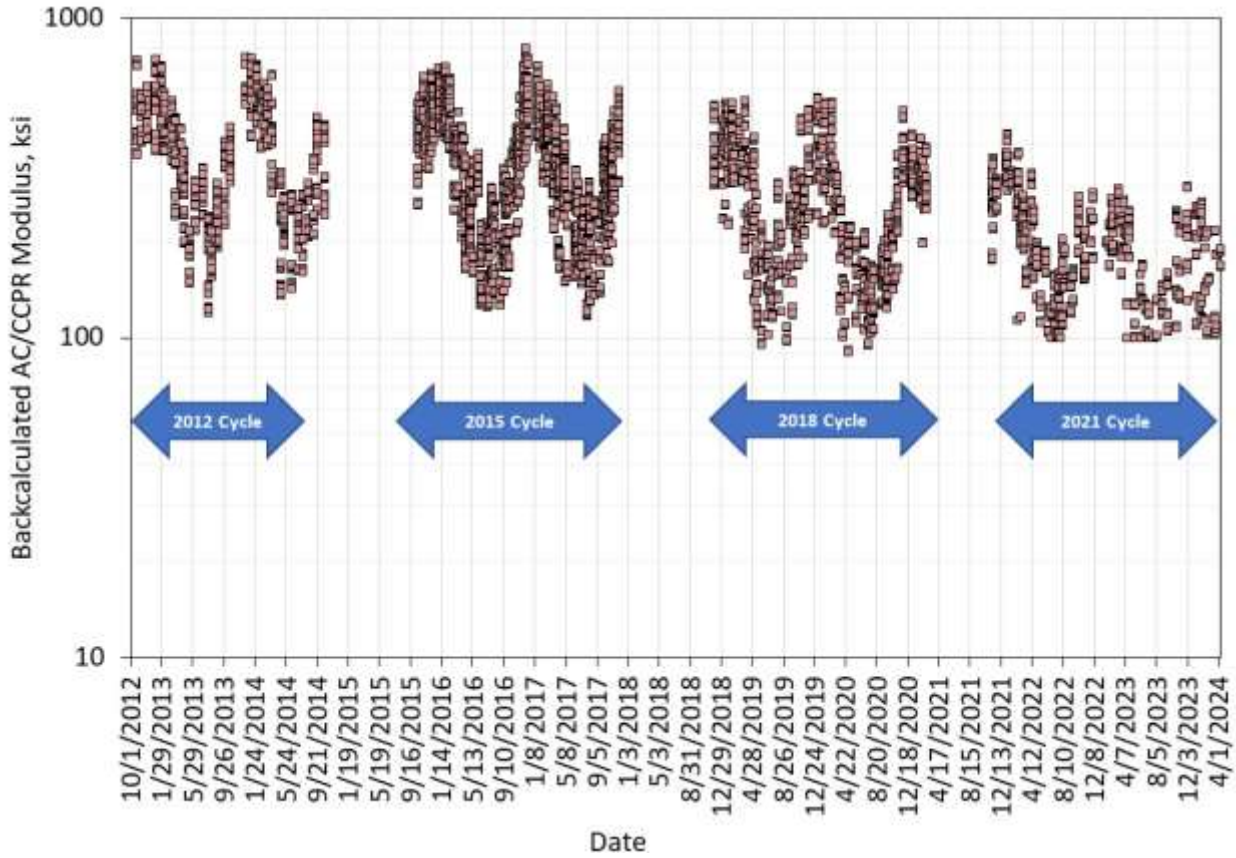

FIGURE 10 Backcalculated AC/CCPR modulus versus time in N4.

To see the effects of time and temperature, the data in Figure 10 were plotted in Figure 11 against their corresponding pavement mid-depth temperature measured at the time of FWD testing and grouped based on the test cycle. The data and trendlines in Figure 10 for the first two cycles show very similar behavior between test cycles. In the third cycle (2018), modulus decreases by about 33% across the temperature spectrum compared to the first two, and there is approximately another 27% decrease between the 2018 and 2021 test cycles. This totals a 50% decrease in modulus in the last test cycle compared to the first two cycles. The pavement clearly experienced structural pavement damage measurable by the FWD in the last two test cycles.

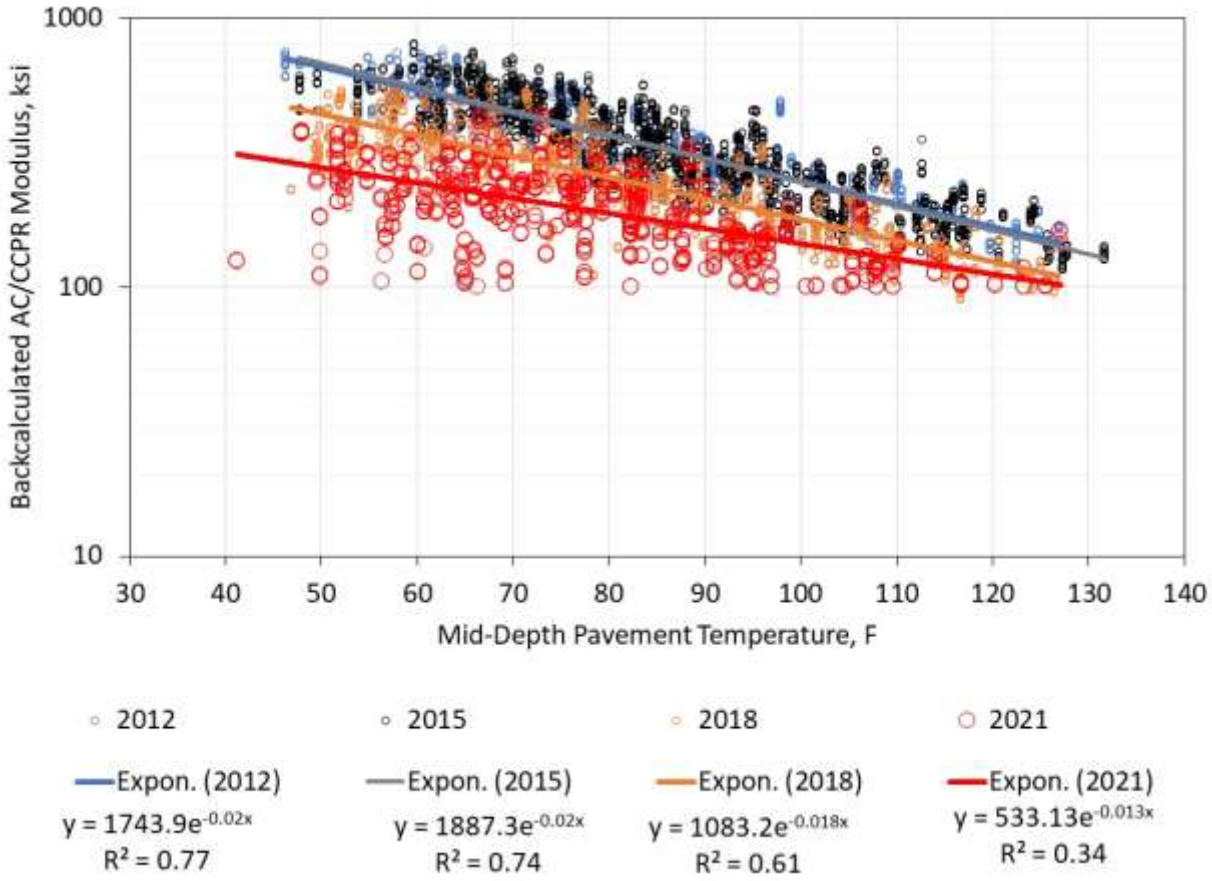

FIGURE 11 Backcalculated AC/CCPR modulus versus mid-depth AC/CCPR temperature.

An exponential trendline, with the same form shown at the bottom of Figure 11, was fit to the entire data set to capture the overall effect of temperature on backcalculated AC/CCPR modulus over the four test cycles. As shown in Figure 12, the data have considerable scatter since the series includes all four test cycles, in addition to spatial variability, but the trendline equation was used to normalize the data to a reference temperature of 68°F, following previously established procedures (Diefenderfer et al., 2016), which are then plotted versus time in Figure 13.

Figure 13 supports the above assertions that the first two test cycles did not result in any structural pavement damage. A decline in AC/CCPR modulus began in the third cycle, followed by the current test cycle, which had a significant reduction in modulus tied to the increasing extent and severity of cracking.

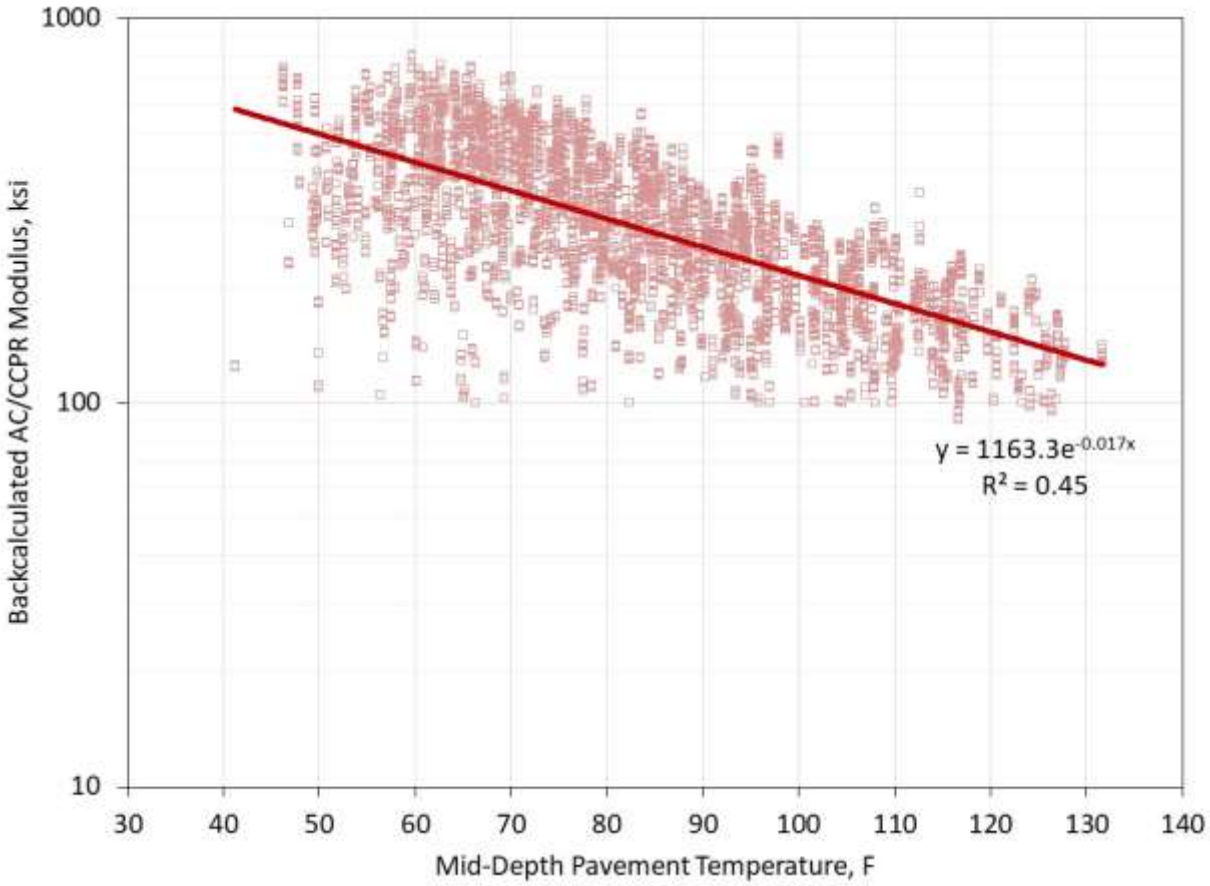

FIGURE 12 Backcalculated AC/CCPR modulus versus mid-depth AC/CCPR temperature – all cycles grouped.

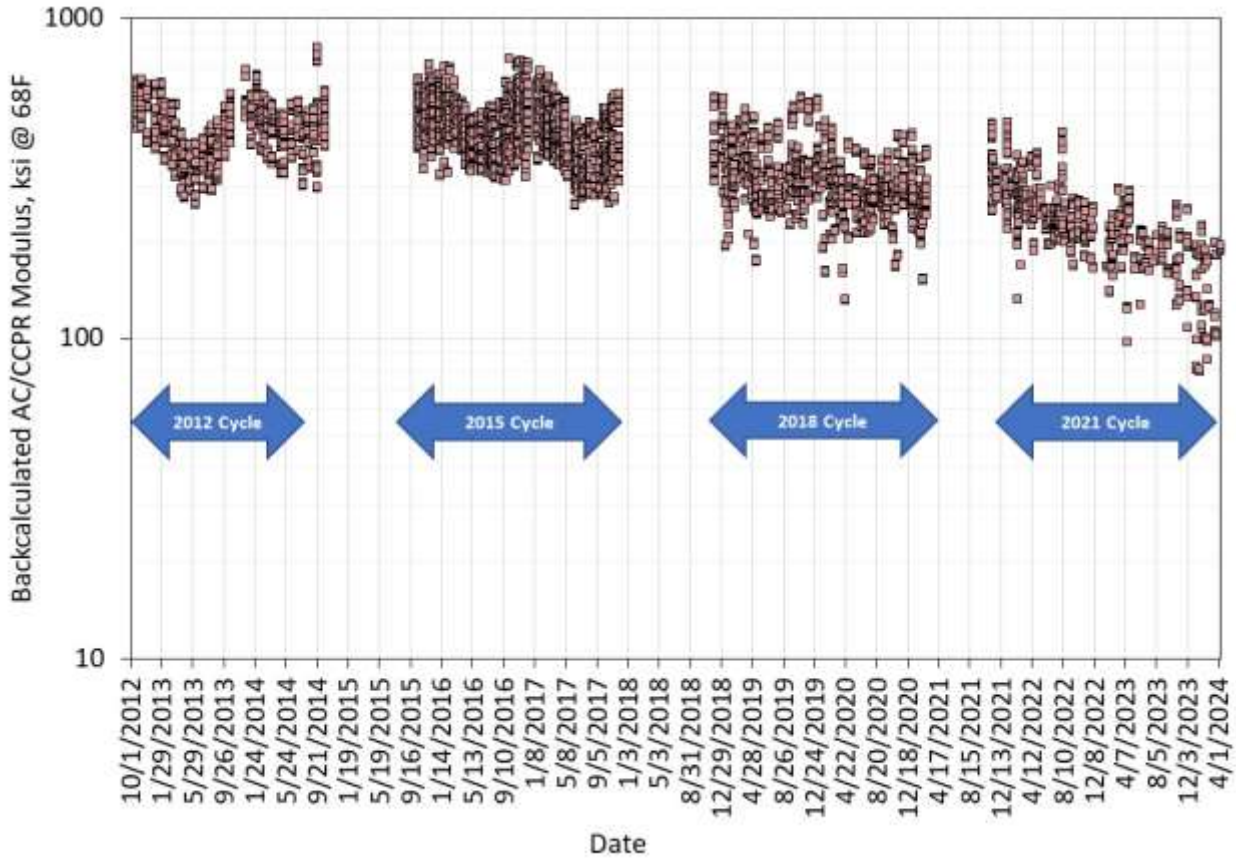

FIGURE 13 Backcalculated AC/CCPR modulus versus date normalized to 68°F.

15.5 Summary, Conclusions, and Recommendations

This investigation focused on the thinnest remaining CCPR section from a group of three sections originally built in 2012 for VDOT. Based on the data presented in this chapter, the following conclusions and recommendations are made.

The section far surpassed its expected performance with excellent rutting, IRI, and virtually no cracking through the first 30 million ESALs. All three performance measures showed degradation during the final 10 million ESALs, but this should not detract from the overwhelmingly positive performance history. In fact, the primary reason for leaving the section in place for the final 10 million ESALs was to gain a better understanding of how a CCPR pavement would deteriorate.

The strain sensors were not working for much of the 2021 test cycle. Although it is difficult to draw any definite conclusions, the section experienced significant strain levels (e.g., exceeding 1,000 με in the summer) throughout the four test cycles, which contributed to the eventual fatigue cracking in the section.

The vertical pressure data indicated a significant increase during the third and fourth test cycles. This was especially noticeable during the fourth cycle, where the measured pressures were approximately double that of the first cycle. This was attributed to structural pavement damage.

The backcalculated AC/CCPR moduli, much like the pressure data, showed clear signs of pavement damage during the third and fourth test cycles. When normalized for temperature to 68^{o}F, the AC/CCPR moduli decreased by about 50% from the first test cycle to the last.

15.6 References

Diefenderfer, B. K., M. A. Diaz-Sanchez, D. H. Timm, and B. F. Bowers. *Structural Study of Cold Central Plant Recycling Sections at the National Center for Asphalt Technology (NCAT) Test Track.* Final Report VTRC 17-R9, Virginia Transportation Research Council, 2016.

Diefenderfer, B. K. and S. D. Link. Temperature and Confinement Effects on the Stiffness of a Cold Central-Plant Recycled Mixture. *Proceedings of the 12th International Society for Asphalt Pavements Conference*, Raleigh, NC, 2014.

Taylor, A. J., and D. H. Timm. *Mechanistic Characterization of Resilient Moduli for Unbound Pavement Layer Materials*. NCAT Report No. 09-06. National Center for Asphalt Technology at Auburn University, 2009.

Timm, D. H., B. K. Diefenderfer, B. F. Bowers and G. Flintsch. Utilization of Cold Central Plant Recycled Asphalt in Long-Life Flexible Pavements. *Transportation Research Record, Journal of the Transportation Research Board*, Vol. 2675, Issue 11, 2021.

Timm, D. H., M. Diaz-Sanchez, and B. Diefenderfer. Field Performance and Structural Characterization of Full-Scale CCPR Pavements. Presented at 94th Annual Meeting of the Transportation Research Board, Washington, D.C., 2015.

West, R., D. Timm, B. Powell, N. Tran, F. Yin, B. Bowers, C. Rodezno, F. Leiva, A. Vargas, F. Gu, R. Moraes, and M. Nakhaei. *Phase VII (2018-2021) NCAT Test Track Findings*. NCAT Report 21-03, National Center for Asphalt Technology at Auburn University, 2021.

16. VIRGINIA DEPARTMENT OF TRANSPORTATION THIN OVERLAY ON RE-RECYCLED COLD CENTRAL PLANT RECYCLED ASPHALT MIXTURES

Dr. Benjamin Bowers, Dr. David Timm

16.1 Background

Beginning in 2012, the Virginia Department of Transportation (VDOT) began investigating the use of Cold Central Plant Recycled (CCPR) asphalt mixtures as a base layer in a flexible pavement cross section under heavy traffic conditions. Two of the three sections constructed in 2012 with a CCPR base layer at the Test Track performed well for three test cycles totaling 30 million equivalent single axle load (ESAL) applications (one was taken out of service at the end of two track cycles), and VDOT decided to investigate whether CCPR could be re-recycled into another CCPR layer (West et al., 2021). As the CCPR process continues to grow as a maintenance and rehabilitation technique for existing asphalt pavements, and as a way to construct new pavements or lanes using existing RAP stockpiles, the ability to re-recycle the pavement with existing CCPR material should be considered. The term re-recycling is used here to describe the process where an existing recycled pavement is recycled again into a new layer. This concept is particularly important when considering the use of CCPR as a method to reduce carbon emissions and potential applications beyond the primary networks and into the secondary network where RAP tends to be scarcer. Further, considering the success of Section N4 (see Chapter 16) over the last three track cycles, VDOT also decided to investigate how surface layer thicknesses over CCPR can potentially be reduced to increase potential applications across their network while maintaining performance (West et al., 2021).

16.2 Test Sections

To investigate the re-recyclability of CCPR along with the reduction in overlay thickness, a track section named S12-2021 was constructed using 6 inches of aggregate base beneath 5 inches of re-recycled CCPR and a two-inch SMA overlay (Figure 1). This track section complements Section N4 from the 2012 test track cycle, hereafter referred to as N4-2012, with four inches of AC, the top two being SMA, on top of 5 inches of CCPR on top of the aggregate base and subgrade (Figure 1). The CCPR used for re-recycling Section S12-2021 was from the original Section S12, constructed during the 2012 test track cycle, hereafter referred to as S12-2012. The CCPR layer from Section S12-2012 had the same RAP source, mix design, and placement time as the CCPR layer of Section N4-2012. The expectation was that N4-2012 would have to be reconstructed during the 8th track cycle and the track section would be rebuilt as is with exception of re-recycling the in-place CCPR (henceforth named N4-Future). This would allow for comparison of original recycling vs re-recycling (N4-2012 vs N4-Future) as well as thin overlay vs thicker overlay (S12-2021 vs N4-Future). An array of asphalt strain gauges were placed on top of the aggregate base, beneath the CCPR layer to study the performance of the pavement during trucking operations.

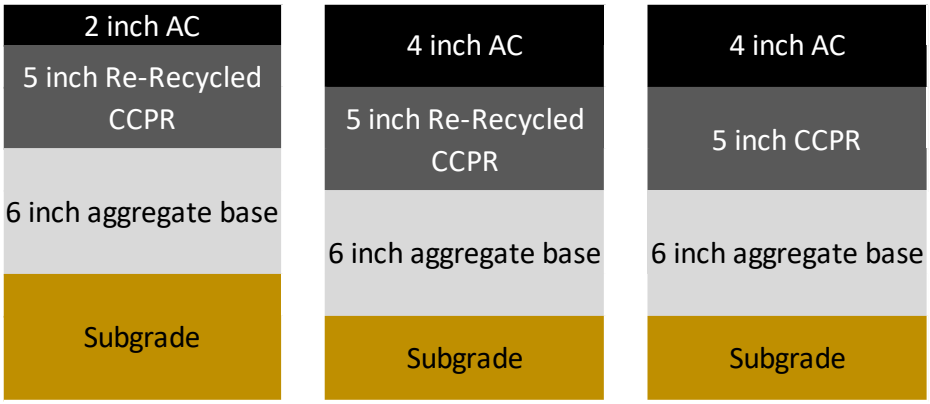

FIGURE 1 Cross section of S12 and the proposed N4 if reconstruction was required.

In order to perform the mix design for the re-recycled CCPR layer, the existing asphalt layers from Section S12-2012 was milled so that the milling unit barely touched the top of the CCPR layer. Next, the CCPR layer was milled, and the reclaimed CCPR material was stockpiled. The reclaimed CCPR material was sampled from the stockpile for mix design. Figure 2 shows the milling process, and Figure 3 shows the reclaimed CCPR millings (stockpiled). The existing stabilized layer from Section S12-2012 beneath the CCPR was removed and replaced with the typical test track subgrade and six inches of aggregate base material to closely match the condition and thickness of the unbound layers of Section N4-2012.

FIGURE 2 SMA and dense graded asphalt layer milling (left) and CCPR layer milling (right).

FIGURE 3 Stockpiled reclaimed CCPR millings.

A black rock gradation (an aggregate gradation with the asphalt coating still present) was performed on the reclaimed CCPR millings, and a mix design using foamed asphalt as the recycling agent in accordance with AASHTO MP 38 and AASHTO PP 94 was performed. An ignition gradation (an aggregate gradation after the asphalt coating has been removed by the ignition oven process) was also performed to compare with the original S12-2012 gradation, which did not have a black rock gradation performed. The gradation of the reclaimed CCPR millings (post ignition) was finer than that of the original RAP (post ignition) used in the original S12-2012 mix design, as shown in Figure 4. Interestingly, the mix design for the re-recycled CCPR yielded the same recycling agent content and active filler content as the original 2012 CCPR mix design (S12-2012). However, the average dry strength and wet strength were both reduced compared to the Section S12-2012. The re-recycled mix design information, including the quality control results from the field, is provided in Table 1.

It should be noted that the re-recycled CCPR hereafter will be referred to as "2nd Generation re-recycled CCPR" due to a 3rd re-recycling effort that will be discussed later in this chapter. The 2nd generation re-recycled CCPR mix was produced using a Wirtgen KMA 240i located on the NCAT Test Track property. The mix was immediately hauled to the test Section and placed using a conventional paver, then compacted using a compaction train consisting of 3 rollers capable of applying each of the following: a vibratory steel drum, oscillatory, static steel drum, and rubber tire rollers. The vibratory roller and oscillatory roller were both capable of rolling in static mode. The average wet density achieved in the field for the 2nd generation re-recycled CCPR layer was 132.4 pcf.

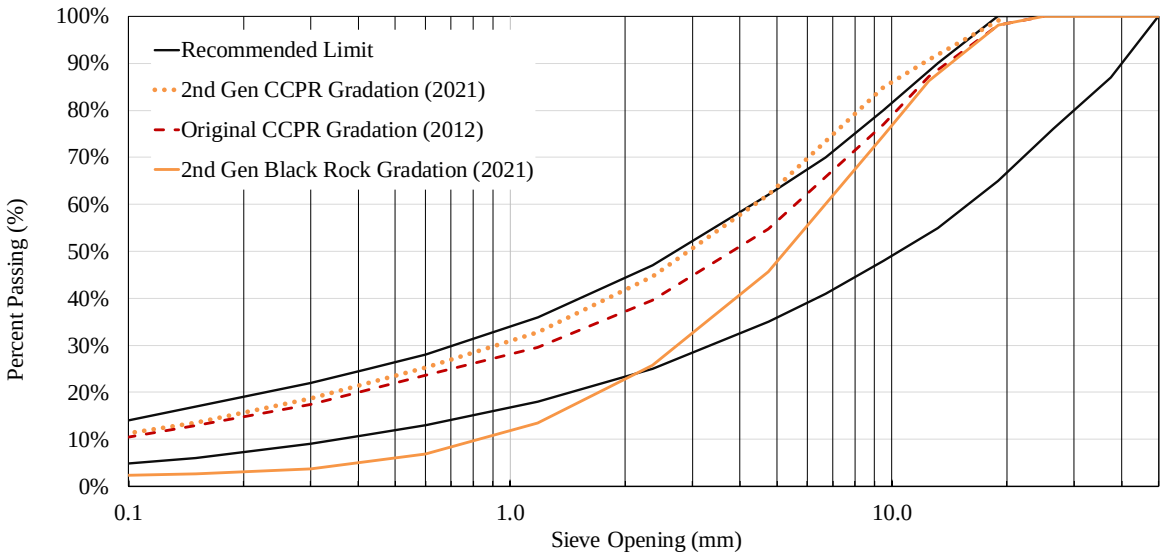

FIGURE 4 Black-rock gradation of re-recycled CCPR versus the original (2012) CCPR.

TABLE 1 Mix Design Comparison Between the S12-2012 Mix Design, the 2nd Generation Re-Recycled CCPR mix design, and the 2nd Generation Re-Recycled CCPR QC Data

Material / Test	S12-2012 Design	2nd Gen Re-Recycled CCPR Design	2nd Gen Re-Recycled CCPR QC
Recycling agent (foam), %	2.0	2.0	2.3 (Furnace)
Active filler content (cement), %	1.0	1.0	1.0
Optimum moisture content, %	-	6.8	6.9
Average dry strength (min 45 psi)	83	65	55
Average wet strength (min 35 psi)	63	55	35
Tensile Strength Ratio, %	76	85	63
Dry Density (lab), pcf	-	126.4	127.6

The two-inch thick SMA surface mix placed over the 2nd generation re-recycled CCPR layer was designed by a VDOT contractor. The mix was produced at the East Alabama Paving (EAP) plant in Opelika, AL, using raw materials that were shipped from Virginia. The binder grade used in the SMA was a PG 76-22. The SMA design was similar to that used for Section N4-2012 and Section S12-2012. The mix design information and quality control data of the plant produced mixture are provided in Table 2.

TABLE 2 Mix Design and QC Data for the SMA Layer

Sieve Size	Target	Quality Control
25 mm (1")	100	100
19 mm (3/4")	100	100
12.5 mm (1/2")	85	88
9.5 mm (3/8")	65	69
4.75 mm (#4)	26	27
2.36 mm (#8)	20	19
1.18 mm (#16)	18	17
0.60 mm (#30)	17	15
0.30 mm (#50)	16	14
0.15 mm (#100)	13	12
0.075 mm (#200)	10	8.6
Mix Properties / Volumetrics	**Target**	**Quality Control**
Binder Content (Pb), %	6.3	6.4
Eff. Binder Content (Pb), %	6.2	6.3
Dust to Effective Binder Ratio, %	1.6	1.4
Rice Gravity (Gmm)	2.639	2.631
Bulk Gravity (Gmb)	2.560	2.575
Air Voids (Va), %	3.0	2.2
Aggregate Gravity (Gsb)	2.942	2.937
Voids in the Mineral Aggregate (VMA), %	18.5	17.9
Voids Filled with Asphalt (VFA), %	84	88
Avg. Mat Compaction, % of Gmm	-	97.9

Note: Blackrock RAP gradation was performed and is presented in this table.

16.3 2nd Generation Re-recycled CCPR Performance

Trafficking of Section S12-2021 commenced in November of 2021. By February 2022, with approximately 0.8 million ESALs, it was noticed that cracking had begun to form in the wheelpaths throughout the Section (0.2% cracking in the wheelpath). The section was promptly cored in multiple locations, and no full-depth cores could be retrieved intact. It appeared that the CCPR layer had not completely cured. By the end of April 2022, with approximately 1.3 million ESALs, significant cracking had occurred – 14.1% in the wheelpaths as shown in Figure 5 - and began to bridge across the centerline. Rutting was also prevalent in this period with an average rut depth of 0.24 inches at approximately 1.3 million ESALs (Figure 6). Performance data of the 2nd generation re-recycled CCPR Section in terms of cracking, rutting, IRI, measured strain data, and backcalculated layer moduli are provided in Section 15.5.

FIGURE 5 Cracking in Section S12 at approximately 1.3 million ESALs (April 2022).

FIGURE 6 Rutting in Section S12 (April 2022).

It had rained the day before the 2nd generation re-recycled CCPR mix was placed, and the aggregate base had become very wet. The research team worked to ensure that the aggregate base was dry and could support the placement of the CCPR layer, which, in fact, appeared to be sufficient according to tests such as the dynamic cone penetrometer test. However, the vibratory roller is believed to have potentially pulled water up into the CCPR mixture when compacting, causing a reduction in curing. The asphalt overlay was placed the next day, which may have further exacerbated the pulling of moisture into the CCPR layer from the aggregate base layer while compacting and would have prevented further curing by sealing the surface.

Maintenance or rehabilitation was deemed required due to the level of cracking and rutting that had occurred. It has been hypothesized that the 2nd generation re-recycled CCPR mix did not cure prior to traffic loading, and the lack of stiffness beneath the SMA overlay caused the rutting and fatigue to occur. This was further confirmed when the surface was saw cut and removed to collect CCPR materials for mix design of a 3rd generation re-recycled CCPR. By the time the surface was removed, the CCPR layer appeared to have cured (Figure 7).

FIGURE 7 Material collection for mix design of 3rd generation re-recycled CCPR.

16.4 Design and Construction of 3rd Generation Re-Recycled CCPR

The 2nd generation re-recycled CCPR materials were collected by sampling from the saw cut portions and crushed using a jaw crusher to perform the 3rd generation re-recycled CCPR mix design. A black rock gradation was performed on the milled 2nd generation re-recycled CCPR. Interestingly, the 2nd generation re-recycled CCPR millings were further coarsened, as shown in Figure 8. This may be caused by the bonds made by the cement and/or foamed asphalt binder, causing the mixture to stick together, or a construction related cause, such as the speed of the milling machine and/or the drum.

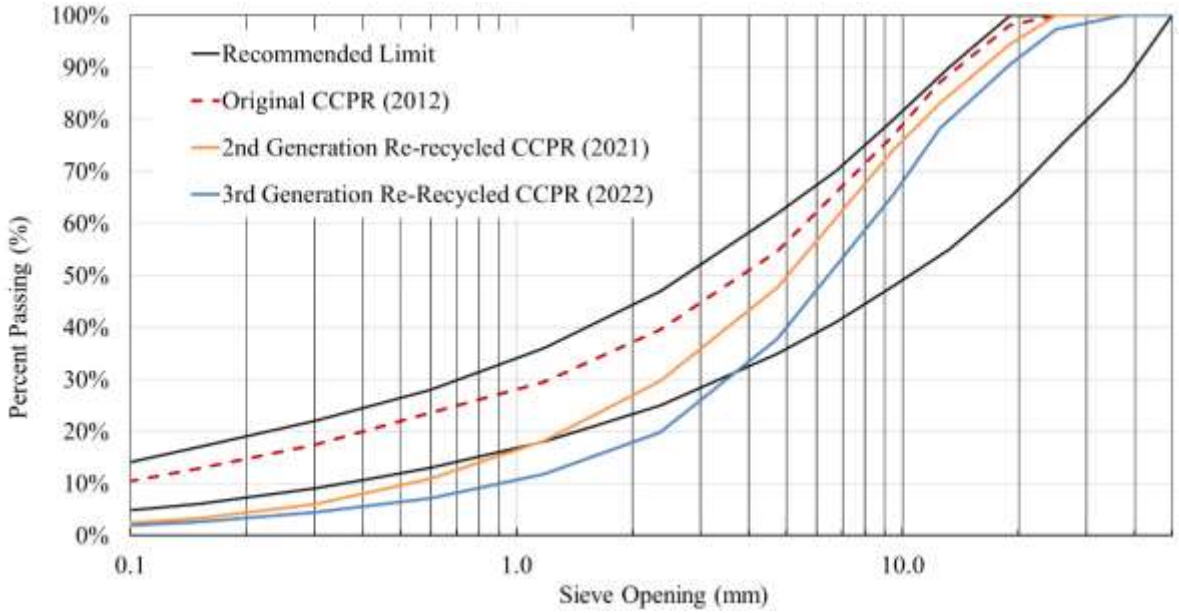

FIGURE 7 Black rock gradation of milled CCPR material comparing the original CCPR (S12-2012) to the 2nd generation re-recycled CCPR (S12-2021).

The mix design was performed using the same methodology described earlier in this chapter. The final mix design yielded a recycling agent content of 2.1% (foamed PG 67-22), a lower maximum dry density, and lower average dry strength and wet strength values compared to the 2nd generation re-recycled CCPR. It is hypothesized that the lower strength values were a byproduct of having additional asphalt cement in the mix (original RAP, S12-2012, and S12-2021). The mix design results are presented in Table 3.

TABLE 3 Mix Design Results For 2nd Generation and 3rd Generation Re-Recycled CCPR

Material / Test	2nd Generation Re-Recycled CCPR	3rd Generation Re-Recycled CCPR
Recycling agent (foam), %	2.0	2.1
Active filler content (cement), %	1.0	1.0
Optimum moisture content, %	6.8	6.8
Maximum Dry Density, pcf	133.4	128.0
Average dry strength (min 45 psi), psi	65	53
Average wet strength (min 31.5 psi), psi	55	34
Tensile Strength Ratio, %	85	64

The 3rd generation re-recycled CCPR mixture was then placed and compacted. The SMA layer was then replaced using a Virginia mixture. The mix design is provided in Table 4. The final layer thicknesses were 1.7 inches for the SMA surface and 4.6 inches for the 3rd generation recycled CCPR.

TABLE 4 Mix Design and QC Data for the SMA Layer

Sieve Size	Target	Quality Control
25 mm (1")	100	100
19 mm (3/4")	100	100
12.5 mm (1/2")	85	90
9.5 mm (3/8")	65	69
4.75 mm (#4)	26	23
2.36 mm (#8)	20	15
1.18 mm (#16)	18	13
0.60 mm (#30)	17	12
0.30 mm (#50)	16	11
0.15 mm (#100)	13	9
0.075 mm (#200)	10	7.1
Mix Properties / Volumetrics	**Target**	**Quality Control**
Binder Content (Pb), %	6.3	6.2
Eff. Binder Content (Pb), %	6.2	6.2
Dust to Effective Binder Ratio, %	1.6	1.2
Rice Gravity (Gmm)	2.639	2.638
Bulk Gravity (Gmb)	2.560	2.443
Air Voids (Va), %	3.0	7.4
Aggregate Gravity (Gsb)	2.942	2.936
Voids in the Mineral Aggregate (VMA), %	18.5	22.0
Voids Filled with Asphalt (VFA), %	84	66
Avg. Mat Compaction, % of Gmm	-	94.5

16.5 2nd Generation and 3rd Generation Re-Recycled CCPR Performance Data

Just prior to reconstruction, the cracking in the 2nd generation re-recycled CCPR reached nearly 10% by lane area at 3.2 illion ESALs, as shown in Figure 8. Since the construction of the 3rd generation re-recycled CCPR, no detectable cracking has occurred in the SMA surface through approximately 5.5 million ESALs. Figure 9 shows that rutting of the 2nd generation re-recycled CCPR reached 12.3 mm at 3.2 million ESALs. The 3rd generation re-recycled CCPR currently has around 7 mm of rutting and appears stable at approximately 5.5 million ESALs. The mean IRI for

the 2nd generation re-recycled CCPR climbed to over 200 in/mile prior to construction of the 3rd generation re-recycled CCPR. The 3rd generation re-recycled CCPR is relatively stable, around 140 in/mile, which is where it has been since the reconstruction, as shown in Figure 10.

The rutting and IRI values are believed to be caused by the SMA mix rutting. As can be seen in the QC data, the SMA layer is low in fines compared to the target and also has high air voids. This could have contributed to instability in the SMA, leading to the SMA mix rutting. The research team took cores in the transition zone at the end of the Section and found that the CCPR layer was intact, but the SMA layer appeared to be extremely malleable, as shown in Figure 11.

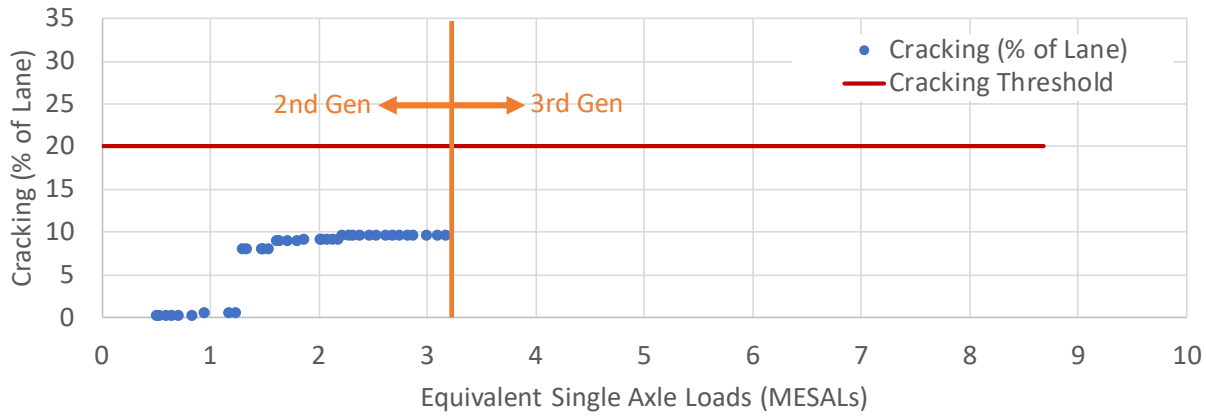

FIGURE 8 Percent cracking in the lane.

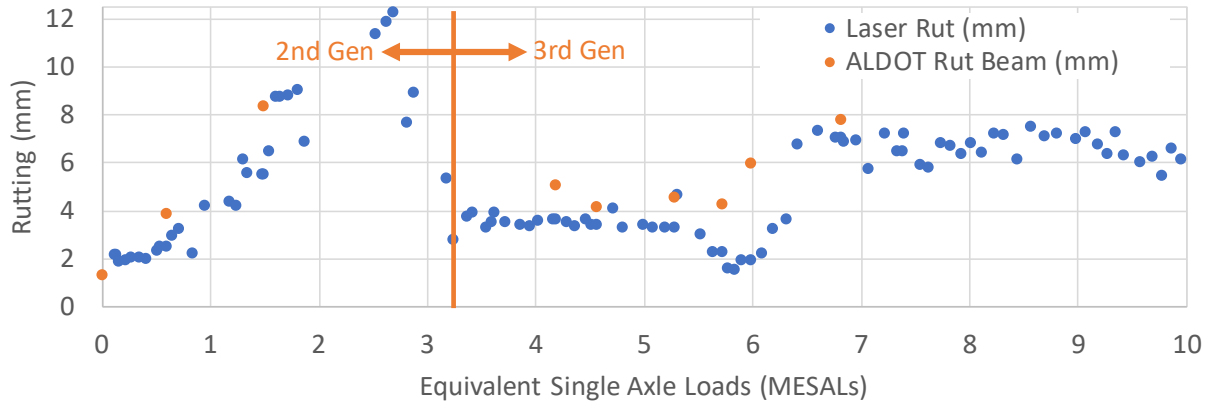

FIGURE 9 Average section rutting.

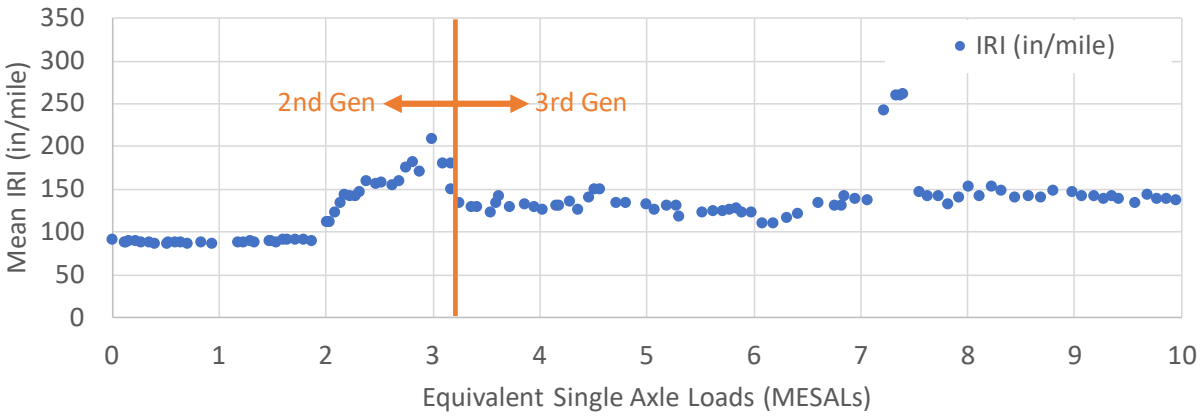

FIGURE 10 Mean international roughness index (IRI).

FIGURE 11 A core sample of the SMA layer in the transition zone at the end of the Section.

The tensile strain versus temperature is shown in Figures 12 and 13. The increase in strain as the temperature increases exhibits the viscoelastic nature of asphalt materials. Further, there is an obvious increase in tensile strain between the re-recycled CCPR (S12-2021) and the original CCPR (N4-2012). This is attributed to the thinner overlay (two inches), which is half the thickness of Section N4-2012 (four inches). The difference in the 2nd and 3rd generation re-

recycled CCPR is also noticeable, with the 3rd generation CCPR exhibiting a linear trend that is parallel to Section N4 with the four-inch overlay. The 2nd generation re-recycled CCPR had a steeper linear trend, which may be a function of the premature cracking that occurred in the Section. The strong correlation between tensile strain and temperature for the 3rd generation re-recycled CCPR, shown in Figure 13, suggests that the readings are not being affected by unobservable cracking in the CCPR layer.

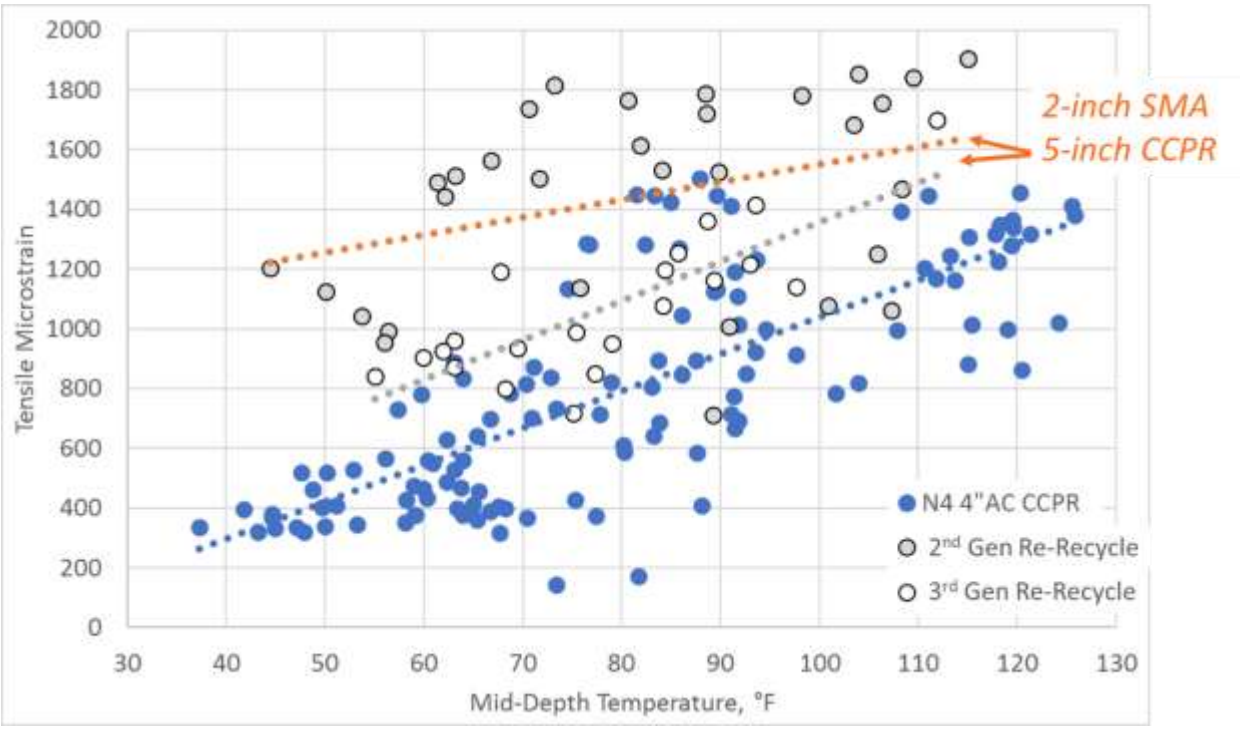

FIGURE 12 Tensile strain vs. temperature.

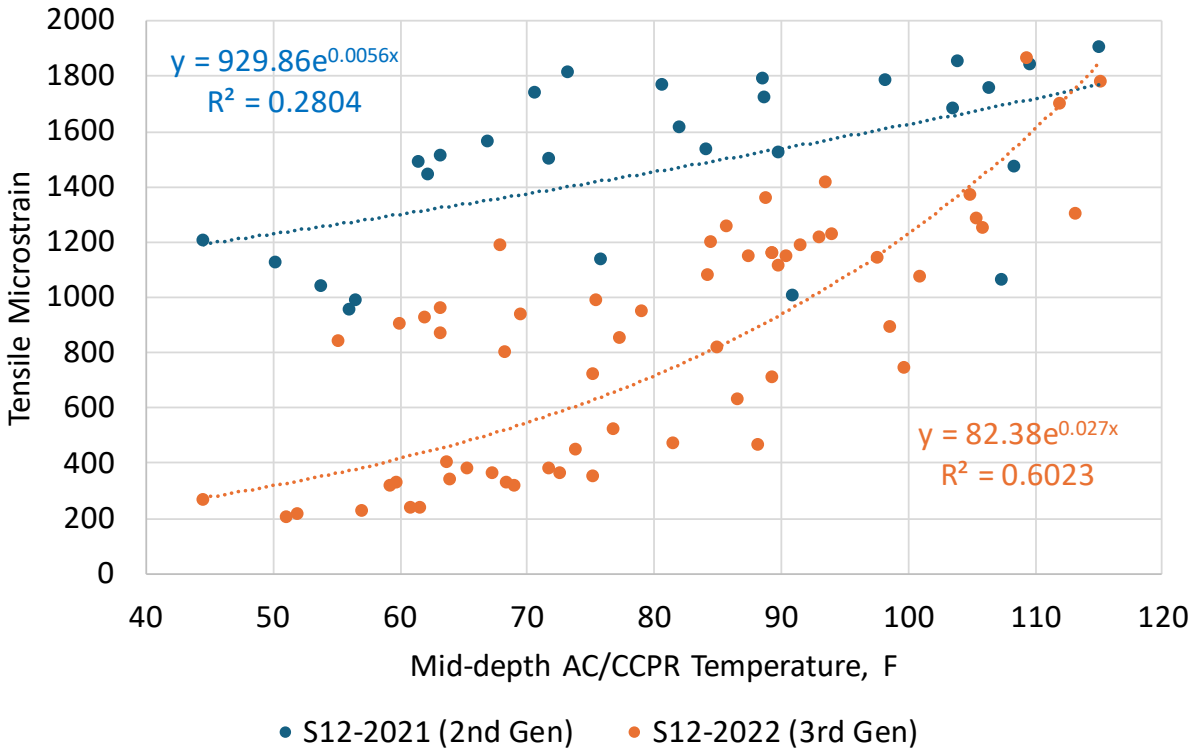

FIGURE 13 Mid-depth AC/CCPR temperature versus tensile microstrain for the 2nd and 3rd generation re-recycled CCPR.

Falling weight deflectometer (FWD) testing was conducted on multiple weeks of every month during the trafficking of the section. The layer moduli of Section S12-2021 were backcalculated assuming three layers, where the SMA and CCPR layers were modeled as one layer, and the aggregate base and subgrade were modeled as two different layers using the EVERCALC backcalculation tool. A maximum root mean square error (RMSE) of 3% was used for the backcalculation. The majority of the deflection data used for backcalculation yielded high RMSE values of over 3%. This caused much of the data to be removed, leaving only 12% of the 1527 samples. The backcalculated AC/CCPR moduli values corrected to 68°F of Section S12-2021 (2nd Gen) and S12-2022 (3rd Gen) over time are presented in Figure 14. The backcalculated AC/CCPR moduli data for S12-2021 (2nd Gen) has a range of 113 to 273 ksi with an average of 200 ksi, while S12-2022 (3rd Gen) has a range of 94 to 384 ksi and an average of 254 ksi.

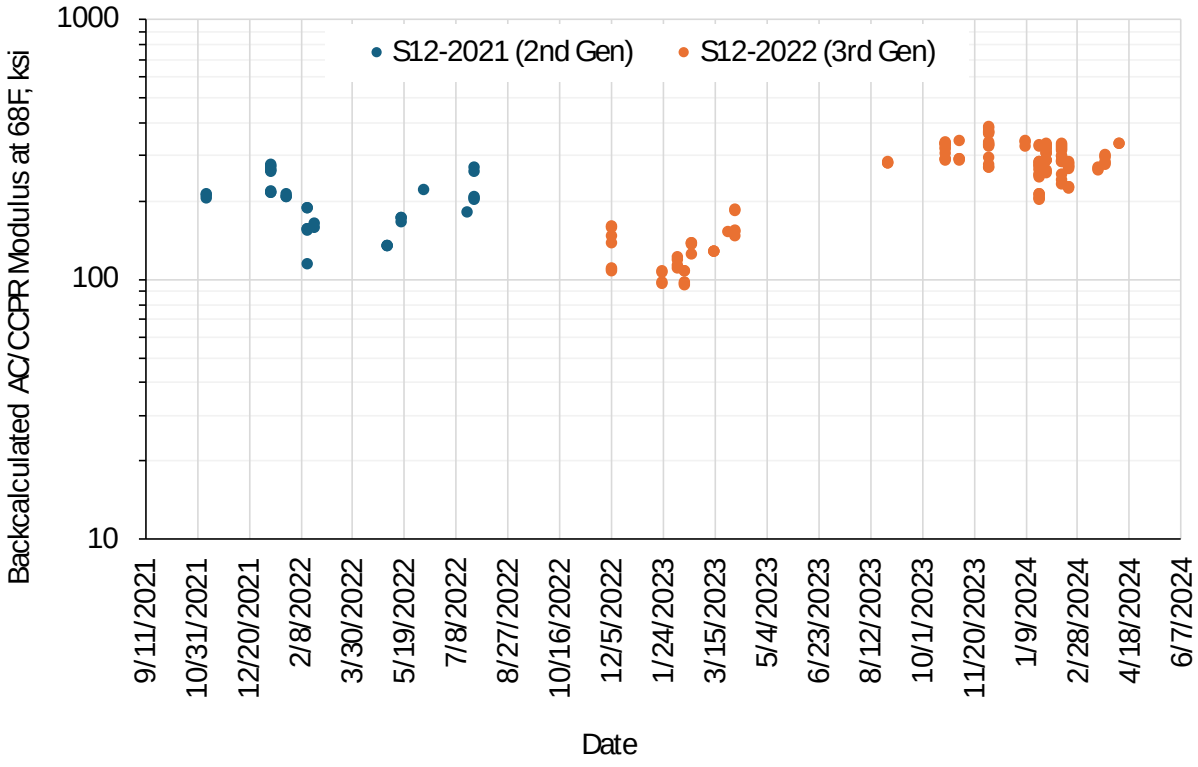

FIGURE 14 Backcalculated AC/CCPR modulus at 68F over time.

16.6 Summary, Conclusions, and Recommendations

Section S12-2021 was constructed to investigate two areas of interest to VDOT: (1) The performance of re-recycled CCPR and (2) whether a two-inch SMA overlay will provide sufficient structure to withstand traffic. The following conclusions have been drawn from this study:

- It is possible to re-recycle CCPR and achieve good early performance.
- The use of a two-inch SMA surface yields good early performance.
- The re-recycled CCPR mixtures exhibited a lower indirect tensile strength than their predecessors, which may be due to the presence of additional asphalt binder from past recycling efforts.
- Inadequate curing, due to the presence of additional water beyond that of the optimum moisture content of the mixture, should be considered during construction.

It is recommended that studies are continued to investigate the re-recyclability of CCPR, including the impact of adding fines to the mixture in an effort to increase the dry and wet strengths.

16.7 References

West, R., D. Timm, B. Powell, N. Tran, F. Yin, B. Bowers, C. Rodezno, F. Leiva, A. Vargas, F. Gu, R. Moraes, M. Nakhaei. *Phase VII (2018-2021) NCAT Test Track Findings*. NCAT Report 21-03, National Center for Asphalt Technology, Auburn University, 2021.

17. DENSE GRADED ASPHALT THINLAY ON CCPR AND REJUVENATED CCPR

Dr. Benjamin F. Bowers, Elizabeth Turochy, Dr. R. Buzz Powell

17.1 Background

Cold recycled (CR) pavements can provide a sustainable option for roadway rehabilitation, reconstruction, and construction. The CR process comprises of mixing Reclaimed Asphalt Pavement (RAP) millings from either a stockpile or directly from an existing roadway with a recycling agent (foamed or emulsified asphalt binder), which then forms a new pavement base layer once compacted. By using nearly 100% RAP material, cold recycling reduces the need for virgin materials and thus the material cost. Emissions produced during pavement production are also reduced by using fewer hauling trucks to transport materials and mixing them at ambient temperatures, which is critical considering national interest in environmental reporting through Environmental Product Declarations (EPD) for infrastructure products. Cold Central Plant Recycling (CCPR) is a subset of CR, where the millings and additives are all mixed in a centrally located plant and then distributed into dump trucks and placed with a typical asphalt paver.

With growing interest in asphalt rejuvenating agents in hot mix asphalt (HMA) to increase RAP contents, there has subsequently been interest in how these rejuvenating agents might benefit CR mixtures. While research on typical CR pavements containing foamed asphalt binder or emulsion and their behavior is prevalent, little work has been published on the performance of CR pavements containing rejuvenators. Of the limited work, Bowers et al. (2019) found that a rejuvenated CCPR mixture produced dynamic modulus (stiffness) values between that of hot mix asphalt and conventional cold recycled mixtures (Bowers 2019). Sections incorporating CCPR layers have been placed at the National Center for Asphalt Technology (NCAT) Test Track; however, none include a rejuvenator. With this in mind, CCPR mixture designs with and without rejuvenators were developed to be placed on the NCAT Test Track off-ramp to explore the impact of rejuvenators on the design, construction, and field performance of cold recycled pavement mixtures.

17.2 Test Sections

To evaluate the effect of rejuvenators on the design, construction, and field performance of CCPR, an HMA base (control) as well as five different CCPR mixture designs were developed to be placed in sections on the NCAT Test Track off-ramp (section ID denoted in parenthesis): HMA control (R5), foamed asphalt with active filler (cement) (R6), engineered emulsion (R7), emulsified bio-based rejuvenator (R8), CR rejuvenator (R9), and anionic emulsion with a bio-based rejuvenator (R10). Each experimental mixture was placed as a 4-inch-thick layer above 6 inches of aggregate base, then surfaced with a 1-inch-thick asphalt concrete (AC) Thinlay, as shown in Figure 1.

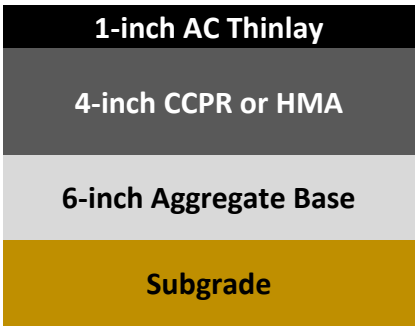

FIGURE 1 Standard cross section of off-ramp section.

A single RAP source from Georgia was selected for the five CCPR mix designs. The foamed asphalt with active filler, anionic emulsion with bio-based rejuvenator, and CR rejuvenator mixture designs were developed at the NCAT Laboratory, and the engineered emulsion and emulsified bio-based rejuvenator mixture designs were developed by their respective manufacturers. AASHTO PP 94 (Standard Specification for Determination of Optimum Asphalt Content of Cold Recycled Mixture with Foamed Asphalt) or AASHTO PP 86 (Standard Practice for Emulsified Asphalt Content of Cold Recycled Mixture Designs) were followed during the mixture design process, dependent on the mixture. Prior to the mixture design phase, black rock gradation (an aggregate gradation with the asphalt coating still present) and a washed gradation were performed on the RAP, along with the proctor density test (AASHTO T180, Method D), to determine the optimum moisture content. The rejuvenator contents were selected based upon manufacturers recommendations. The dry and conditioned strengths of each mixture design were determined via either Indirect Tensile Strength (ITS) testing (foam) or Marshall Stability (MS) testing (emulsion and rejuvenated mixtures), and moisture susceptibility was evaluated by tensile strength ratio (TSR) or Marshall Stability ratio (MSR). The final mixture designs were selected based on the ability of the mixture to meet the required minimum strengths and TSR or MSR while also achieving the most economically viable design (i.e., the least amount of recycling and/or rejuvenating agent needed to meet these requirements). All final material dosages and mixture properties are shown in Table 1.

TABLE 1 Mixture Designs and Strengths

Material / Test	Foamed Asphalt + Active Filler	Anionic Emulsion + Bio-Based Rejuvenator	CR Rejuvenator	Engineered Emulsion	Emulsified Bio-Based Rejuvenator
Foamed Asphalt or Emulsion Content (%)	2.00	3.50	-	3.0	*
Cement Content (%)	1.00	-	-	-	-
Rejuvenator Content (% by weight of RAP binder)	-	7.00	0.90	-	*
Added Water (%)	2.00	2.00	0.00	0.00	*
RAP Moisture Content (%)	3.87	4.37	4.88	5.63	5.07
Produced Mixture Moisture Content (%)	6.00	6.42	4.98	6.71	7.85
Average Dry Strength (min either 45 psi or 1250 lb)	49.9 psi	1349.4 lb	1159.1 lb	3366.2 lb	45.8 psi*
Average Conditioned Strength	41.2 psi	1163.8 lb	1350.6 lb	3181.6 lb	-
TSR or MSR	0.83	0.86	1.17	0.95	*
Dry Density (lab), pcf	124.25	130.94	133.56	130.7	123.46*

*Information related to the mixture design process was not provided by the manufacturer. The dry strength and density values provided were determined via lab-mixed, lab-compacted specimens post-construction.

The CCPR mixtures were produced on the NCAT Test Track property using one of two portable plants. The foamed asphalt and engineered emulsion mixtures were produced in a Wirtgen KMA 240i (Figure 2), and the anionic emulsion with bio-based rejuvenator, CR rejuvenator, and emulsified bio-based rejuvenator mixtures were produced in a Pugmill Systems Portable Pugmill (Figure 3). The production equipment selection was made by the research sponsors. Once produced, the mixtures were then immediately loaded into a dump truck, hauled to the off-ramp, and placed using a conventional paver, then compacted using a series of vibratory steel drum, oscillatory, static steel drum, and rubber tire rollers. All rollers were provided by Hamm and were models HD 140i, HP 180i, and HD 90i PH (oscillatory).

FIGURE 2 Wirtgen KMA 240i.

FIGURE 3 Pugmill Systems portable pugmill.

Wet densities were determined for each section using a nuclear density gauge, with the results shown in Table 2. Due to construction scheduling, the five CCPR sections were placed on different days. However, all sections were allowed a minimum of two days to cure prior to being surfaced with a 1-inch thick, 4.75 mm nominal maximum aggregate size thinlay of HMA in a single, continuous pass.

TABLE 2 Field Wet Density by Section

Mixture	Field Wet Density (pcf)	% Density
Foamed Asphalt with Active Filler	127.7	97.0
Anionic Emulsion with Bio-Based Rejuvenator	135.1	97.0
CR Rejuvenator	132.5	94.9
Engineered Emulsion	131.7	94.4
Emulsified Bio-Based Rejuvenator	132.6	lab density unk.

The HMA control section (not pictured) was placed first. The CCPR sections were then placed in the following order: foamed asphalt with active filler (Figure 4a), engineered emulsion (Figure 4b), CR rejuvenator (Figure 4c), emulsified bio-based rejuvenator (Figure 4d), and emulsified bio-based rejuvenator (Figure 4e). The photos in Figure 4 were taken at various points during the compaction process for each section. During production, it was noted that the emulsified bio-based rejuvenator mixture contained a low amount of recycling agent. Due to the limited amount of recycling/rejuvenating agent available, it was decided to apply the remaining recycling/rejuvenating agent to the surface of the mixture, like what is often done in practice with this product. This was performed on approximately half of the section, while the remaining portion was left at the lower recycling/rejuvenating agent content. Finally, the HMA thinlay was placed (Figure 4f).

FIGURE 4 Paved CCPR Sections on off-ramp; (a) foamed asphalt with active filler, (b) engineered emulsion, (c) CR rejuvenator, (d) emulsified bio-based rejuvenator; (e) emulsified bio-based rejuvenator, and (f) HMA thinlay overlay.

All CCPR sections were compacted until refusal for density immediately after paving, apart from the anionic emulsion with bio-based rejuvenator mixture. During initial field compaction, the emulsion was seen flushing out of the surface. It is believed that this is due to the elevated RAP moisture content (from recent rainfall) combined with the additional water in an anionic emulsion ultimately increased the total fluid content beyond the optimum. All rollers were immediately removed from the mat, and the section was allowed to dry for a few hours and then compacted with no issues.

17.3 Off-Ramp Field Performance

Surface performance data, including ride quality and rutting data, was collected using the NCAT Pathways automated distress van on a weekly basis for the off-ramp sections. Figure 5 shows

the cracking in each of the sections after just beyond 180,000 ESALs. All sections, except for the CR rejuvenator and Anionic Emulsion with Bio-Based Rejuvenator sections, have no detectable cracking, and even those with cracking are well below the cracking threshold of 20 percent of the total lane. The mean International Roughness Index (IRI) expressed in inches/mile is shown in Figure 6. Apart from the CR rejuvenator and Anionic Emulsion with Bio-Based Rejuvenator sections, all sections are performing around or below an IRI of 100 with little to no change since trafficking began. The rutting in mm for each section is shown in Figure 7. Rut depths of less than 4 mm were reported for all sections, again except for the CR rejuvenator section and anionic emulsion with bio-based rejuvenator sections. The increase in IRI and rutting began to accelerate around 21,000 equivalent standard axle load (ESAL) applications for the Anionic Emulsion with Bio-Based Rejuvenator section. It is hypothesized that the increased IRI and rut depth for the anionic emulsion with bio-based rejuvenator section could be a result of the elevated moisture contents at the time of placement, as mentioned previously, combined with a slower cure process due to the anionic emulsion. This would cause a lack of stability in the base beneath the thinlay, which would lead to both rutting and IRI issues, as well as cracking, which appeared around 46,000 ESALs. The increase in rutting for the CR rejuvenator began around the same time as the anionic emulsion with bio-based rejuvenator, but it was not as intense. The IRI did not start to increase until approximately 37,000 ESALs. While curing may have also been an issue for this section, the rejuvenator did not include any emulsion or other recycling agent which would add additional water to the mixture. This section has stabilized and maintained an average rut depth of 7.2 mm since approximately 54,000 ESALs.

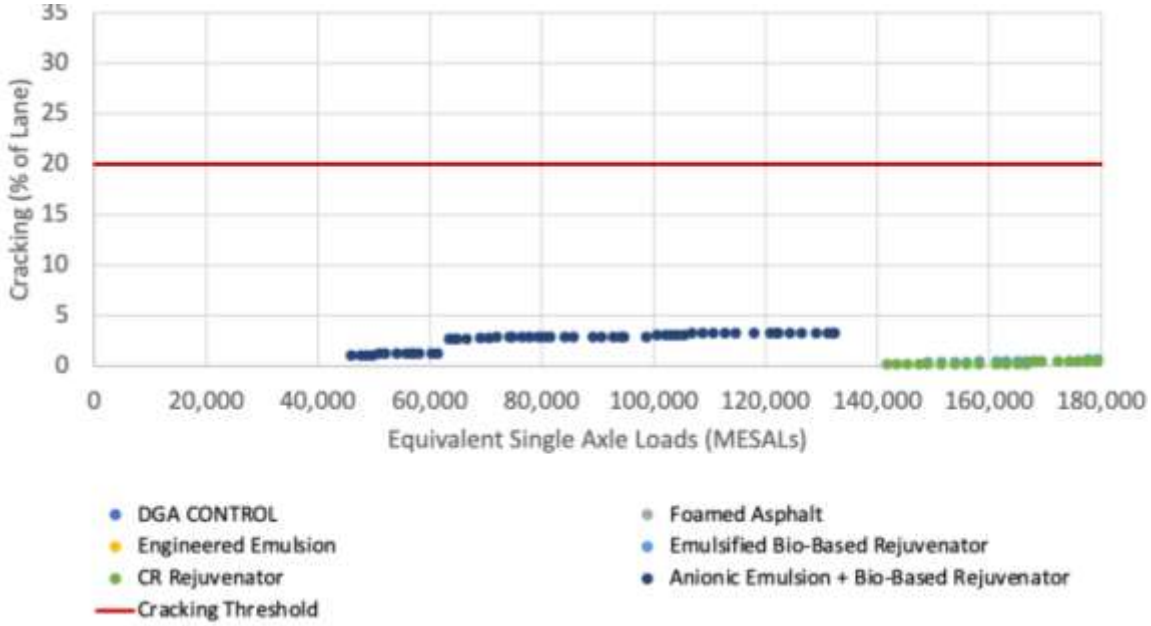

FIGURE 5 Cracking by percentage of the lane area. If no points are shown for a section in the legend, that indicates no cracking has occurred.

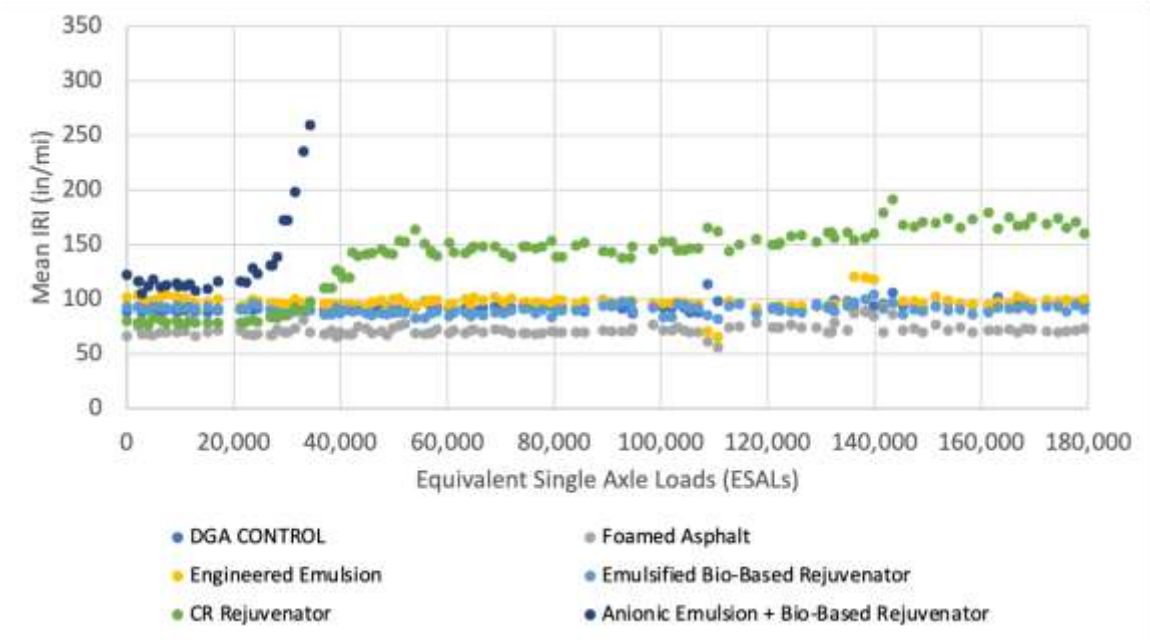

FIGURE 6 Mean IRI.

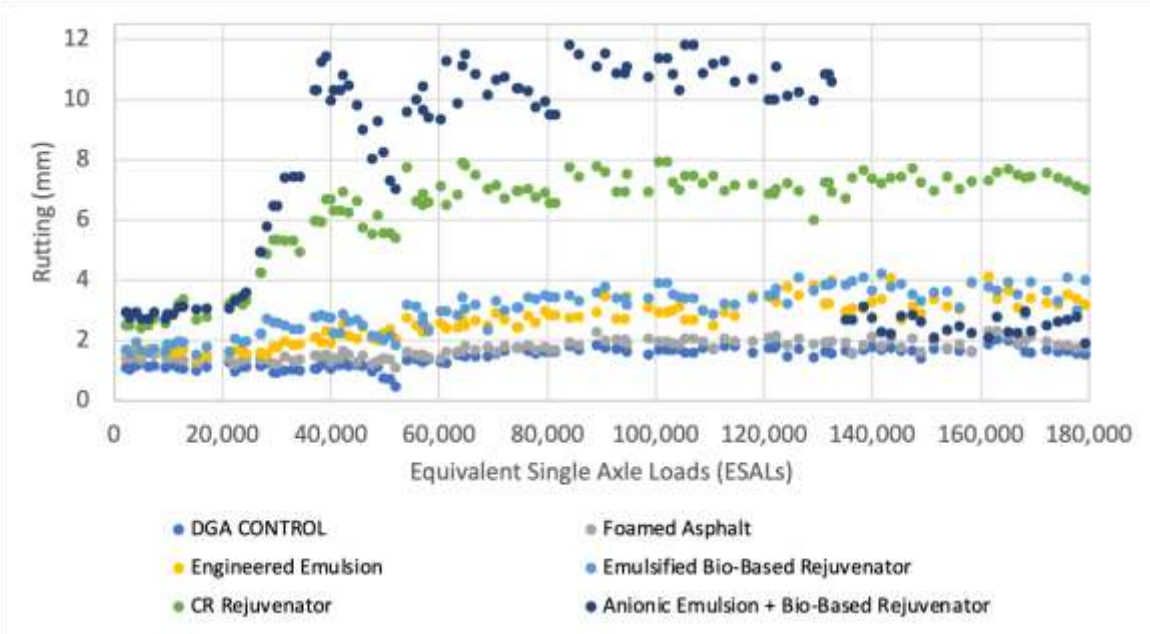

FIGURE 7 Off-Ramp rutting by section.

17.4 Summary, Conclusions, and Recommendations

The off-ramp study was conducted to investigate the impact of rejuvenators on the design, construction, and field performance of CCPR mixtures. Based on the data collected, the following findings, conclusions, and recommendations were identified:

- The plant production and construction of the rejuvenated CCPR mixtures was like a typical CCPR mixture.

- Some, but not all, rejuvenated CCPR mixtures can perform at least equivalent to typical CCPR mixture and DGA mixture with a thin overlay.
- The IRI and rutting increased for both the anionic emulsion with bio-based rejuvenator section as well as the CR rejuvenator section. This is believed to be a byproduct of insufficient curing and/or high moisture levels in the mixture during compaction.

It is recommended that further field research be conducted on rejuvenated CR mixtures, along with laboratory performance testing, to compare with field performance data. More information about the mix design process can be found in Turochy and Bowers (2024).

17.5 Funding and Support

The authors appreciate the funding and support from Blackledge Emulsions, Ingevity, Pavement Restorations, Inc., and Soylei Innovations.

17.6 References

Bowers, B.F., Diefenderfer, B.K., Wollenhaupt, G., Stanton, B., and Boz, I. (2019) Laboratory Properties of a Rejuvenated Cold Recycled Mixture Produced in a Conventional Asphalt Plant. *ASCE TD&I Conference Proceedings*, 2019.

Turochy, E. and Bowers, B.F. (2024). Design, Placement, Laboratory and Field Evaluation of Rejuvenated Cold Recycling Asphalt Mixtures. *Transportation Research Record: Journal of the Transportation Research Board.* In press.

18. CARGILL EVALUATION OF BMD MIXTURE WITH HIGH RAP AND ANOVA ASPHALT REJUVENATOR IN COMPARISON TO LOWER RAP MIX WITH WARM MIX/COMPACTION AID ADDITIVE

Dr. Nam Tran

18.1 Introduction

Approximately 100 million tons of asphalt materials are removed annually from roads (*1*). These materials can be reused as reclaimed asphalt pavement (RAP) in new asphalt mixtures, which reduces material costs, conserves natural resources, and saves landfill space. Despite the potential for increased RAP content, the national average RAP content in new asphalt mixtures has remained around 22% (*2*), as state departments of transportation (DOTs) are hesitant to permit higher levels due to concerns about performance and increased maintenance costs. However, strategies have been developed to improve the durability of these mixtures, such as using recycling agents and the balanced mix design (BMD).

For this experiment, a high RAP (45%) surface mixture was designed using Cargill's Anova™ 1815 asphalt recycling agent at 3% by weight of the total binder following a BMD approach. This mixture was placed in 2018 on the NCAT Test Track for field evaluation as part of the seventh research cycle (2018 through 2021). The Anova asphalt recycling agent was used to restore the performance properties of the RAP binder, which helped mitigate the impact of high RAP content on the long-term performance of the asphalt mixture. This mixture was compared to a lower RAP (30%) surface mixture, which contained the Anova™ 1501 additive (adhesion promotor/warm mix/compaction aid) at 0.5% by weight of the total binder. Both mixtures were built on the same pavement structure and tested under the same traffic and climatic conditions.

Before paving on the Test Track, the two mixtures were tested according to the Virginia Department of Transportation's (VDOT) BMD provisional specification released in 2018. This specification includes three laboratory tests: the Asphalt Pavement Analyzer (APA), the Indirect Tensile Asphalt Cracking Test (IDEAL-CT), and the Cantabro abrasion test. These tests evaluate the susceptibility of asphalt mixture to rutting, cracking, and raveling, respectively.

During Test Track construction, three plant-produced mixtures were tested using several performance tests in the laboratory, and the data were analyzed to assist the field evaluation at the Test Track.

- The first asphalt mixture, which had 30% RAP with a PG 64-22 binder and contained a standard amount of the Anova adhesion promotor/compaction aid (CA) additive, was placed in the surface layer of Section N3A (referred to as the 30% RAP+CA mixture).
- The second asphalt mixture had 45% RAP with a PG 64-22 binder and Anova asphalt recycling agent (RA) and was paved in the surface layer of Section N3B (referred to as the 45% RAP+RA mixture). Sections N3A and N3B are each 100 feet long.

- The 45% RAP mixture was also produced without the Anova recycling agent for laboratory testing only (referred to as the 45% RAP mixture) and was not placed on the Test Track.

Truck trafficking for the seventh research cycle started on November 26, 2018, and approximately 10 million equivalent single axle loads (ESALs) were applied by the end of fleet operations on February 28, 2021. The two test sections, N3A (30% RAP+CA) and N3B (45% RAP+RA), showed comparably good field performance after 10 million ESALs. They were kept in place for traffic continuation in the eighth research cycle (2021 through 2024) for a thorough evaluation of long-term field performance.

This chapter summarizes the experimental plan, mix design process, laboratory evaluation of the three plant-produced asphalt mixtures, and field performance of the two test sections in the two research cycles from 2018 through 2024.

18.2 Research Methodology

18.2.1 Experimental Plan

This study was divided into four tasks, as illustrated in Figure 1, including (1) mix design, (2) mix production and placement, (3) laboratory performance testing, and (4) field performance evaluation. In Task 1, mix designs were conducted to meet the volumetric criteria. Adjustments were then made to optimum binder contents and recycling agent dosage to meet performance thresholds required by VDOT's 2018 provisional BMD specification. Table 1 provides a detailed summary of the VDOT provisional BMD specification.

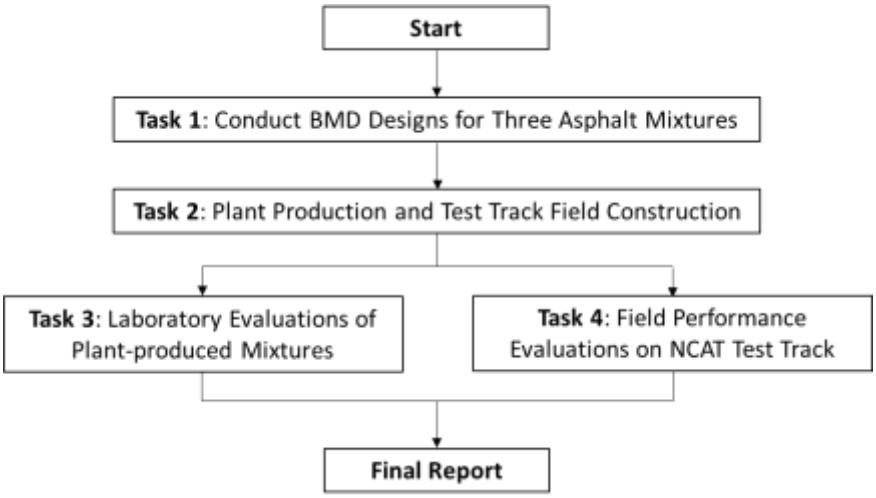

FIGURE 1 Experimental plan.

TABLE 1 Performance Testing Requirements in VDOT's BMD Provisional Specification

Test	Procedure	Specimens	Criteria
Asphalt Pavement Analyzer (APA) rutting	Testing is conducted to 8,000 cycles at 64°C with a wheel load of 120 lb and a rubber hose pressure of 120 psi.	Two replicates of two pills (150 mm in diameter by 75 ± 2 mm high) are prepared to achieve target air voids of 7 ± 0.5%. Note: Lab-produced loose mix is short-term aged for 2 hours at the design compaction temperature.	Rutting depth ≤ 8.0mm
Cantabro Abrasion Test	Testing is conducted to 300 rotations at a speed of 30-33 rotations per minute.	Three replicates (150 mm in diameter by 115 ± 5 mm high) are compacted to N_{design}. Specimen air voids are reported. Note: Lab-produced loose mix is short-term aged for four hours at 135°C prior to compacting.	Mass loss ≤ 7.5%
Indirect Tension Asphalt Cracking Test (IDEAL-CT)	Testing is conducted after specimens are conditioned at 25 ± 1°C for 2 ± 0.5 hours. After a contact load of 0.1 ± 0.02 kN is applied, loading is applied using load-line displacement control at 50 mm/minute.	Three replicates (150 mm in diameter by 62 ± 2 mm high) are compacted to 7 ± 0.5% air voids. Note: Lab-produced loose mix is short-term aged for 4 hours at 135°C prior to compacting.	CT_{index} ≥ 70

18.2.2 Materials

Both the 30% RAP+CA and 45% RAP+RA mix designs shared a nominal maximum aggregate size (NMAS) of 9.5 mm but differed in RAP content. The aggregates utilized in this study, including two trap rock aggregate stockpiles (#8 and #10) and one source of RAP, were the same as those in the VDOT-approved volumetric mix design. To simulate potential aggregate breakdown during plant production, 1% baghouse fine passing #200 material from the #10 aggregate was included in the final design gradations. Chemung Contracting in Virginia provided the aggregates and RAP.

The virgin asphalt binder used in this study was a PG 64–22, the same performance grade used in the approved volumetric mix design. The asphalt binder was provided by the asphalt supplier, Ergon Asphalt and Emulsions, who supplied all the binders for the 2018 Test Track.

Another difference between the two mix designs, aside from RAP content, was the use of chemical additives. The 45% RAP+RA mix design contained Anova 1815 recycling agent, a chemically modified vegetable oil-based recycling agent. This additive was designed to chemically balance and reactivate aged asphalt binder, thereby allowing more recycled materials (RAP and RAS) to be used in asphalt mixtures. In the laboratory, Anova 1815 was added directly to the asphalt binder, followed by low shear blending for 3 to 5 minutes to achieve homogeneity. For the Test Track construction, the recycling agent was injected in-line at the asphalt plant, but it can also be blended with asphalt binder at the terminal for field production (*4*). The optimum dosage selected for this study was 3.0% of the total weight of the asphalt binder. The 45% RAP mixture was also produced without the recycling agent for laboratory testing only and was not placed on the Test Track.

The 30% RAP+CA mix had no recycling agent but contained the Anova 1501 additive. The additive was designed to improve workability, facilitate compaction at lower temperatures, and enhance asphalt mixture resistance to moisture damage. The selected dosage rate for this additive is 0.5% by the total weight of the asphalt binder (*5*).

18.3 Volumetric and BMD Mix Designs

For this study, two mix designs were required—one for the 30% RAP+CA mix containing 30% RAP with a PG 64-22 binder and Anova 1501 additive, and another for the 45% RAP+RA mixture consisting of 45% RAP with the same PG 64-22 binder and Anova 1815 recycling agent. The 45% RAP mix design was also used to produce another mixture without the recycling agent for laboratory testing only. The sponsor-recommended dosages of the warm-mix additive and recycling agent were pre-blended with the base binder during the mix design.

Chemung Contracting in Virginia provided a VDOT-approved volumetric mix design (N_{des} = 50). To ensure it met all VDOT volumetric requirements, the 30% RAP+CA mix design with 30% RAP was verified first. Then, the aggregate gradation of this mixture was adjusted to create a design gradation for the 45% RAP+RA mixture with 45% RAP. The volumetric optimum binder content of the 45% RAP+RA mixture was selected to meet all the VDOT volumetric requirements. The volumetric properties of the two mix designs are provided in Table 2.

TABLE 2 Volumetric Mix Designs for N3A (30% RAP+CA) and N3B (45% RAP+RA) Mixtures

Design method:	Volumetric mix design		
Compactive effort (N_{des}):	50 gyrations		
Binder PG:	64-22		
Mix properties	**30% RAP+CA**	**45% RAP+RA & 45% RAP**	**Criteria**
% Total AC (P_b):	5.2	5.2	
Rice gravity (G_{mm}):	2.729	2.717	
Bulk gravity (G_{mb}):	2.620	2.608	
Design air voids (V_a):	4.0	4.0	4.0
VMA*:	16.3	16.7	Min. 16.0
VFA:	76	77.3	70 - 85
Dust-to-eff. binder ratio:	1.1	1.2	0.7 - 1.3
Eff. binder content (P_{be}):	4.89	4.96	
Abs. binder content (P_{ba}):	0.31	0.31	
% AC contribution from RAP:	1.33	2.20	
% Virgin binder:	3.86	3.04	
% RAP binder replacement:	26	42	
Agg. bulk gravity (G_{sb}):	2.973	2.963	
Agg. effective gravity (G_{se}):	3.000	2.989	
Agg. absorption (A_{bs}):	0.88	0.96	

*VMA was calculated based on G_{se} instead of G_{sb}

The performance tests required in the VDOT provisional BMD specification were conducted for these mixtures after the volumetric mix design. These tests included APA for rutting, Cantabro

for raveling, and IDEAL-CT for cracking. The thresholds for accepting a BMD mix design based on the results of these tests are summarized in Table 1.

In the first round of BMD testing, the volumetric mix designs for both mixtures met the APA rutting and Cantabro abrasion test criteria but not the IDEAL-CT cracking threshold, as shown in Figure 2. The VDOT provisional BMD specification permits adjustments to the volumetric properties of a BMD mix design beyond the VDOT volumetric limits. Therefore, the binder and recycling agent contents could be adjusted to meet the IDEAL-CT cracking threshold without altering design gradations. For the 30% RAP+CA mixture, binder content was increased, while for the 45% RAP+RA mixture, both the binder and recycling agent contents were adjusted. The final BMD mix designs for the 30% RAP+CA and 45% RAP+RA mixtures, as shown in Figure 2 and Table 3, met VDOT's BMD performance test requirements shown in Table 1.

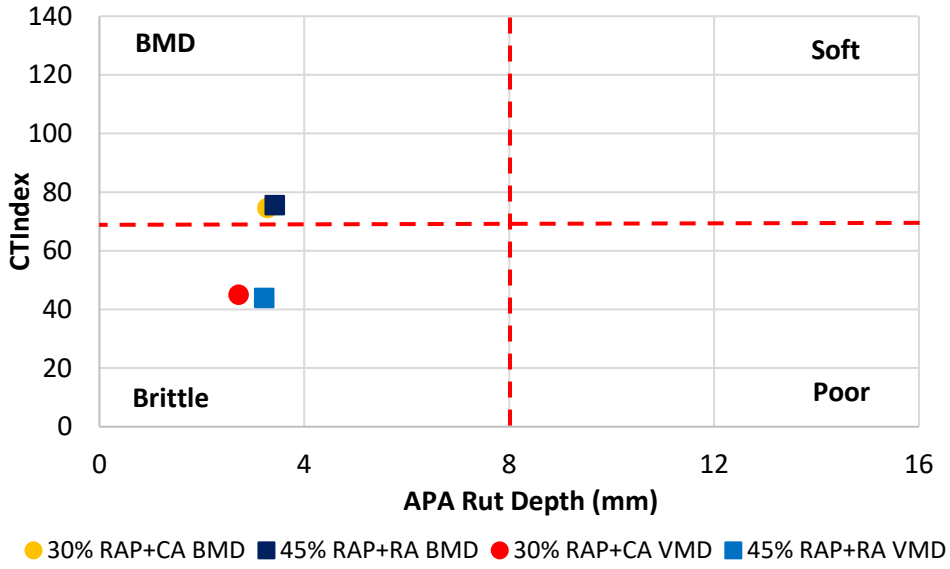

FIGURE 2 Volumetric mix design (VMD) vs. balanced mix design (BMD).

18.4 Plant Production and Paving at the Test Track

Based on the BMD mix designs, the two mixtures were produced and placed on the Test Track on September 6, 2018. The 30% RAP+CA mixture was produced with the Anova 1501 warm-mix additive (in-line blended), and the mix temperature was approximately 310°F when it left the plant. After the 30% RAP+CA mix was produced, the in-line pump was switched to the Anova 1815 recycling agent to produce the 45% RAP+RA mixture, and the temperature of this mixture was approximately 315°F when it left the plant. In addition, a third mixture was also produced based on the same 45% RAP+RA BMD mix design without either additive for laboratory testing only.

The 30% RAP+CA mixture was placed in Section N3A (100 feet long). The paver was then hot-stopped to clean out the mix from the hopper. The 45% RAP + RA mixture was then placed in Section N3B (100 feet long), as shown in Figure 3.

The temperature measured behind the paver for the 30% RAP+CA mixture was 290°F, and in-place density was 96.2% of G_{mm} of the as-produced mix. Due to an incident that delayed paving, the temperature measured behind the paver for the 45% RAP+RA mixture was lower at 279°F. However, since the recycling agent was also designed for use as a warm-mix additive, the 45% RAP+RA mixture still compacted well with a 96.8% in-place density. Table 3 summarizes the design and construction data for the two test sections.

FIGURE 3 Paving Sections N3A (30% RAP+CA) and N3B (45% RAP+RA).

TABLE 3 BMD Design and Construction Data for Sections N3A and N3B

Design method:	BMD		24 Hour High Temp. (F):	87
Compactive effort (N_{des}):	50 gyrations		24 Hour Low Temp. (F):	74
Binder PG:	64-22		24 Hour Rainfall (in):	0
Paving	**N3A (30% RAP+CA)**		**N3B (45% RAP+RA)**	
As-built sublot lift thickness(in):	1.5		1.5	
Approx. underlying AC (in):	9.5		9.5	
Tack coat:	NTSS-1HM		NTSS-1HM	
Undiluted target tack rate (gal/sy):	0.1		0.1	
Approx. avg. temp. at plant (F):	310		315	
Avg. mat compaction (%G_{mm}):	96.2		96.8	
Sieve Size	**Design**	**QC**	**Design**	**QC**
25mm (1"):	100	100	100	100
19mm (3/4"):	100	100	100	100
12.5mm (1/2"):	100	100	100	100
9.5mm (3/8"):	97	95	97	96
4.75mm (#4):	61	56	61	56
2.36mm (#8):	38	36	38	38
1.18mm (#16):	27	26	28	27
0.6mm (#30):	20	18	21	20
0.3mm (#50):	14	11	15	13
0.15mm (#100):	9	7	10	9
0.075mm (#200):	5.5	4.9	6.3	6.1
Mix Properties				
Binder content (P_b):	5.5	6.0	5.8	6.0
Eff. binder content (P_{be}):	5.2	5.7	5.5	5.7
Dust-to-eff. binder ratio:	1.1	0.9	1.1	1.1
RAP binder replacement (%):	24	25	38	38
RAS binder replacement (%):	0	0	0	0
Total binder replacement (%):	24	25	38	38
Rice gravity (G_{mm}):	2.715	2.679	2.691	2.664
Bulk gravity (G_{mb}):	2.636	2.608	2.628	2.624
Air Voids (V_a):	2.9	2.7	2.3	1.5
Aggregate gravity (G_{sb}):	2.973	2.966	2.963	2.949
VMA:	16.2	17.3	16.5	16.3
VFA:	82	85	86	91

18.5 Laboratory Evaluation of Plant-Produced Mixtures and Binders

To assist the field evaluation, all three plant mixtures were sampled during production for laboratory evaluation. The plant-produced mixtures were used to prepare plant-mixed, lab-compacted (PMLC) specimens for performance testing in the NCAT laboratory. Table 4 includes the laboratory tests conducted to evaluate the following mixture performance properties:

- Cracking and fracture: IDEAL-CT, Overlay Test (OT), Illinois Flexibility Index Test (I-FIT), Disc-Shaped Compact Tension (DCT) Test.
- Rutting: APA and Hamburg Wheel Tracking Test (HWTT).
- Durability/raveling: Cantabro Abrasion Test.
- Moisture susceptibility: Tensile Strength Ratio (TSR).

To compact test specimens, the loose mix was reheated and split to sample size. Depending on the loose mix aging condition planned in Table 4 for each performance test, test specimens were compacted after the split samples were either reheated to the compaction temperature or were compacted after the loose mix samples were critically aged for 8 hours at 135°C after reheating.

TABLE 4 Laboratory Evaluation Plan

Test	N3A (30% RAP+CA)		N3B (45% RAP+RA)		45% RAP	
	Reheated	Aged[2]	Reheated	Aged	Reheated	Aged
Mixture Tests (by NCAT)						
Virginia Specification						
IDEAL-CT (VDOT)	x	x	x	x	x	x
APA (VDOT)	x		x			
Cantabro	x		x		x	
Other Specifications						
OT (NJDOT B-10)	x	x	x	x	x	x
I-FIT (AASHTO TP124)	x	x	x	x	x	x
DCT (ASTM D7313)	x	x	x	x	x	x
TSR (AASHTO T283)	x		x			
HWTT (AASHTO T324)	x		x			
Binder Tests (by Cargill)						
Extract/recovery/PG[1]	x	x	x	x	x	x

[1]Includes RAP and base asphalt binder sampled during construction; [2]Plant mix was reheated and critically aged for 8 hours at 135°C prior to compaction (*6*); [3]These mixtures were tested at 400 microstrains only; [4]These mixtures were tested at both 400 and 600 microstrains.

During production, the PG 64-22 binder used to produce the asphalt mixtures was sampled to verify its performance grade (PG). In addition, asphalt binders were extracted and recovered from the three plant-produced mixtures for testing. Extraction of the asphalt binder was performed per ASTM D2172 (centrifuge method) and was recovered following the ASTM D1856 procedure. The recovered asphalt binder was subjected to several levels of aging before testing, as summarized in Table 5. The recovered asphalt binder was graded per ASTM D7643 as well as guidelines in the NCHRP 452 report (*7*). All the extracted binder testing was conducted at the Cargill laboratory.

TABLE 5 Aging Procedures

Aging Level	Description
HTPG: As extracted LTPG: As extracted + RTFO	Standard aging method, calibrated to correspond to standard M320 grades.
HTPG: As extracted + RTFO + 40-hr PAV LTPG: As extracted + RTFO + 40-hr PAV	Additional PAV testing, reflecting an extended (2 x PAV) aging of asphalt binder.

*HTPG: high temperature performance grade; LTPG: low temperature performance grade; RTFO: rolling thin film oven; PAV: pressurized aging vessel (conducted at 100°C).

18.5.1 Extracted Asphalt Binder Test Results

Table 6 provides a summary of extracted binder test results for the three plant-produced mixtures tested in the Cargill laboratory, including (1) 30% RAP+CA mixture with 30% RAP and a warm mix additive placed in Section N3A, (2) 45% RAP+RA mixture with 45% RAP and recycling agent placed in Section N3B, and (3) 45% RAP mix without recycling agent produced for laboratory testing only.

Asphalt binders were extracted and recovered from the three plant-produced mixtures after they were reheated and reduced to sample size. They were then aged at two aging levels before testing. The first aging level is the same as the standard aging procedure for extracted binders described in AASHTO M320. The second aging level was an extended binder aging protocol in which the extracted asphalt binder was subjected to twice the standard PAV aging time of 20 hours (2 x PAV aging). As shown in Table 6, the continuous high-temperature performance grade (HTPG) was determined based on the extracted binder and the RTFO+2PAV aged binder. The continuous low-temperature performance grade (LTPG) was determined based on the RTFO-aged and RTFO+2PAV-aged binders. Based on the Bending Beam Rheometer (BBR) results, S-BBR is the temperature where stiffness, *S*, equals 300 MPa, while m-BBR is the temperature where *m-value* equals 0.300. ΔT_c is the difference between the S-BBR and m-BBR. The following observations can be drawn based on the binder test results:

- The 45% RAP binder appeared to be the stiffest, followed by the 30% RAP+CA binder and then the 45% RAP+RA binder based on the HTPG and S-BBR.
- Based on the m-BBR results, the 45% RAP+RA binder was the most flexible. The 45% RAP binder appeared more flexible than the 30% RAP+CA binder for the first aging level, which was not expected, but they were similar for the extended aging level.
- Since a lower (more negative) ΔT_c value suggests higher susceptibility to non-load-related cracking, the 30% RAP+CA binder would be the most susceptible, which was also not expected. The 45% RAP binder was more cracking susceptible than the 45% RAP+RA binder for the first aging level, but they were similar for the extended aging level.

In summary, based on the test results of the extracted binders, the 45% RAP+RA binder showed improved long-term cracking resistance without an adverse effect on its rutting resistance compared to the other two binders. In addition, the 30% RAP+CA and 45% RAP binders would have similar rutting and long-term cracking performance, which was unexpected.

TABLE 6 Test Results for Asphalt Binders Extracted from Plant-Produced Mixtures

Binder Aging Level	Mix ID	HTPG (°C)	S-BBR (°C)	m-BBR (°C)	ΔTc (°C)	PG
HTPG: As extracted LTPG: As extracted + RTFO	30% RAP+CA	76.7	-23.8	-14.6	-9.2	76 – 10
	45% RAP+RA	75.9	-24.0	-22.0	-2.0	70 – 22
	45% RAP	78.8	-21.5	-18.6	-2.9	76 – 16
HTPG: As extracted + RTFO + 2PAV LTPG: As extracted + RTFO + 2PAV	30% RAP+CA	91.2	-20.7	-12.8	-7.9	88 – 10
	45% RAP+RA	90.5	-22.8	-17.0	-5.9	88 – 16
	45% RAP	94.3	-18.6	-12.9	-5.7	94 – 10

18.5.2 Lab Performance Test Results for Plant-Produced Mixtures

Tensile Strength Ratio (TSR) Test Results. The moisture susceptibility of the three mixtures was evaluated per AASHTO T283 on test specimens compacted using reheated plant mix samples. The results are presented in Figure 4. All mixtures met the minimum TSR of 0.80 required for moisture resistance, with the 30% RAP+CA mix having the highest TSR.

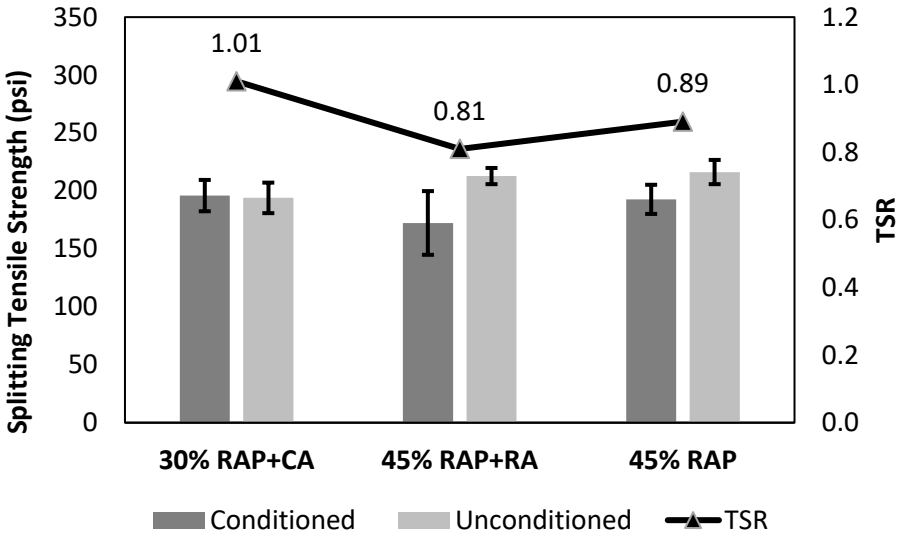

FIGURE 4 TSR Test results for reheated plant mixtures.

Asphalt Pavement Analyzer (APA) Test Results. The rutting resistance of the plant mixtures was evaluated using both the APA and HWTT. Testing was only conducted for the reheated 30% RAP+CA mixture (30% RAP+CA) and the 45% RAP+RA mixture with the recycling agent (45% RAP+RA). The rutting resistance of the 45% RAP mixture without the recycling agent was expected to be similar to or better than the 45% RAP+RA mixture due to its similar mixture composition and absence of a recycling agent. The APA results are summarized in Table 7. Rut depth was measured using both manual and automatic methods. Numerically, the 45% RAP+RA mixture recorded a higher rut depth in both methods of measurement. The Coefficient of Variation (COV) was higher for the 45% RAP+RA mixture in both manual and automated average rut depth measurements. The p-values of the one-way ANOVA statistical test ($\alpha = 0.05$)

suggested no significant difference between average rut depths of the 30% RAP+CA and 45% RAP+RA mixes for both methods of rut depth measurement. Both mixtures exhibited excellent rutting resistance, with rut depths averaging well below the maximum APA criterion of 8.0 mm at a test temperature of 64°C.

TABLE 7 APA Rutting Test Results for Reheated Plant Mixtures

Parameter	Mix Identifier	Average	COV	P-Value
Manual rut depth (mm)	30% RAP+CA	2.97	0.22	0.267
	45% RAP+RA	3.44	0.69	
Automated rut depth (mm)	30% RAP+CA	2.97	0.23	0.382
	45% RAP+RA	3.37	0.84	

Hamburg Wheel Tracking Test (HWTT) Results. Table 8 summarizes the HWTT results for evaluating the rutting resistance of reheated 30% RAP+CA and 45% RAP+RA mixtures. The average HWTT rut depths were almost the same for the two mixtures after 10,000 and 20,000 passes at 50°C, and no stripping inflection points (SIP) were observed. Based on the p-values of a one-way ANOVA ($\alpha = 0.05$) test, there was no statistical difference between the average HWTT rut depths of the reheated 30% RAP+CA and 45% RAP+RA mixtures at either 10,000 or 20,000 passes. The HWTT rutting results appeared to agree with the APA rutting results, suggesting both mixtures had good rutting resistance.

TABLE 8 HWTT Rutting Results for Reheated Plant Mixtures

Parameter	Mix Identifier	Average	COV	P-Value
10,000 passes	30% RAP+CA	2.51	0.07	0.760
	45% RAP+RA	2.55	0.02	
20,000 passes	30% RAP+CA	3.15	0.11	0.875
	45% RAP+RA	3.10	0.03	

Illinois Flexibility Index Test (I-FIT) Results. Figure 5 compares the FI results of the three plant-produced mixtures under two aging conditions. These results were determined after an outlier analysis was conducted on the replicate FI results at a 5% significance level as specified in ASTM E178. Numerically, the reheated 45% RAP+RA mixture recorded the highest average FI, suggesting the 45% RAP+RA mixture had better cracking resistance than the others.

A one-way ANOVA ($\alpha = 0.05$) statistical test was conducted, and the resulting p-value (0.007) suggested significant differences among the average FI values of the three mixtures. However, the p-value did not specifically indicate where the significant differences occurred. For this reason, the Tukey-Kramer test was conducted, with grouping results shown in Figure 5. For mixtures sharing the same letter, their average flexibility indexes were not statistically different. The Tukey-Kramer statistical groupings of the reheated FI results suggest significant differences between the average FI of the 45% RAP+RA and 45% RAP mixes (i.e., with and without recycling agent), as they did not share the same letter. However, the reheated 30%

RAP+CA mixture shares a letter with both the reheated 45% RAP+RA and 45% RAP+RA mixtures. The higher cracking resistance observed in the reheated 45% RAP+RA mixture compared to the 45% RAP mixture was attributed to the effect of the recycling agent.

Figure 5 also shows the I-FIT results of the critically aged 30% RAP+CA, 45% RAP+RA, and 45% RAP mixtures. The average FI values of all three mixtures were below 0.5. While the FI results were statistically different, they were considered not practically different in this case. In summary, in the reheated condition, the 45% RAP+RA mixture showed higher FI results than the other mixtures. However, the three mixtures aged quickly during the critical aging process, resulting in all average FI values below 0.5, which could lead to a concern about the long-term cracking resistance of these mixtures.

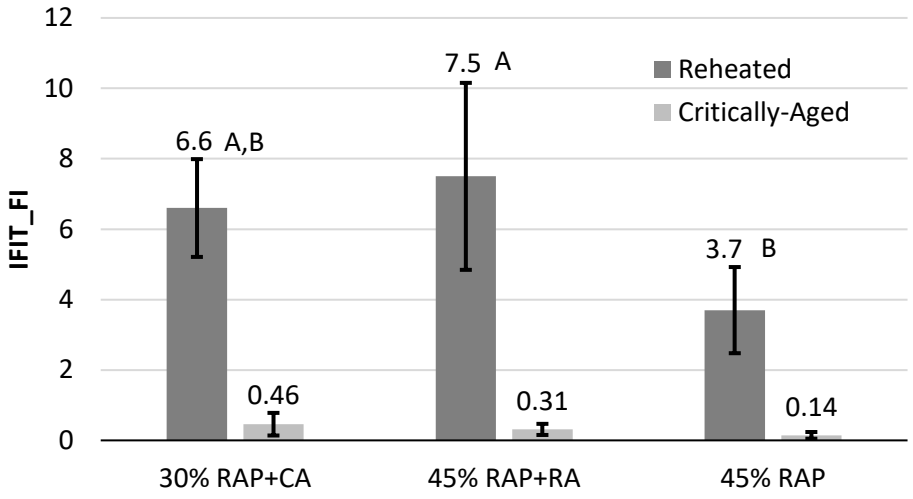

FIGURE 5 Comparison of reheated and critically aged I-FIT results.

Overlay Test (OT) Results. The Overlay Test was conducted per NJDOT B-10, where the number of cycles to failure (N_f) is reported as an index that represents the resistance of an asphalt mixture to reflective cracking. The higher the N_f, the better its resistance. Results for the plant-produced mixtures are summarized in Figure 6 after an outlier test (ASTM E178) was conducted. The reheated 45% RAP+RA mixture showed higher resistance to reflective cracking than the other mixtures. Also, the difference in the N_f of the three reheated mixtures was statistically significant at a 5% significance level (i.e., $\alpha = 0.05$). Tukey-Kramer statistical groupings showed this significant difference was due to the N_f of the reheated 45% RAP mixture. The OT results of the critically aged mixtures are also shown in Figure 6. Like the critically aged I-FIT results, the N_f of the three plant-produced mixtures dropped significantly after critical aging and were not statistically significant at a 5% significance level. In summary, the reheated 45% RAP+RA mixture showed higher resistance to cracking than the other two

reheated mixtures. The three mixtures aged significantly during critical aging, leading to similar critically aged cycles to failure.

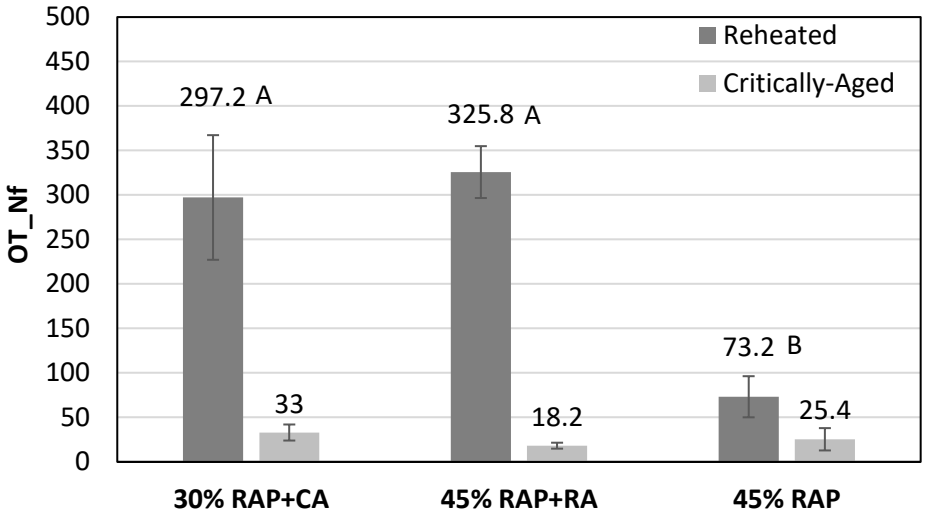

FIGURE 6 Comparison of reheated and critically aged OT results.

Disc-Shaped Compact Tension (DCT) Test Results. The DCT test was conducted at 12°C to evaluate the resistance of the three plant-produced mixtures to low-temperature cracking. The fracture energy (FE) results determined from DCT testing the reheated mixtures are shown in Figure 7 after performing an outlier analysis (ASTM E178). The reheated 45% RAP+RA mixture had the highest average FE, followed by the reheated 30% RAP+CA mixture and the reheated 45% RAP mixture. However, the difference was not statistically significant based on a one-way ANOVA statistical test at a 5% significance level. DCT results of the critically aged mixtures are also presented in Figure 7. The difference among the average FE of the critically aged mixtures was not statistically significant, though they were very close to being statistically significant based on a one-way ANOVA at a 5% significance level. While critical aging did not appear to significantly affect the DCT results of the 30% RAP+CA and 45% RAP (without recycling agent), the effect was significant for the 45% RAP+RA.

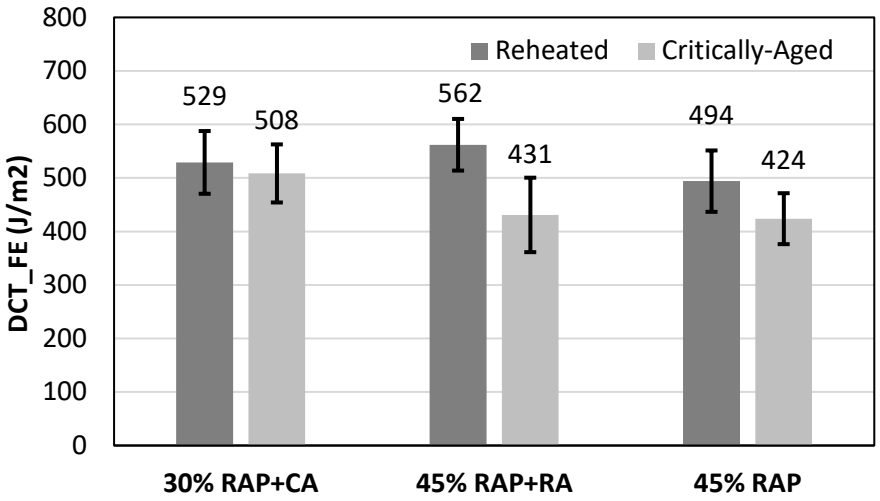

FIGURE 7 Comparison of reheated and critically aged DCT test results.

Indirect Tension Asphalt Cracking Test (IDEAL-CT) Results. The cracking resistance of the reheated mixtures was also evaluated based on CT_{Index} determined by the IDEAL-CT, as shown in Figure 8. The CT_{Index} results differed from the other cracking test results, with the reheated 30% RAP+CA mixture having the highest average CT_{Index}, followed by the reheated 45% RAP+RA mixture and the reheated 45% RAP mixture. The VDOT provisional BMD specification requires a minimum CT_{Index} threshold of 70, which only the reheated 30% RAP+CA mixture met.

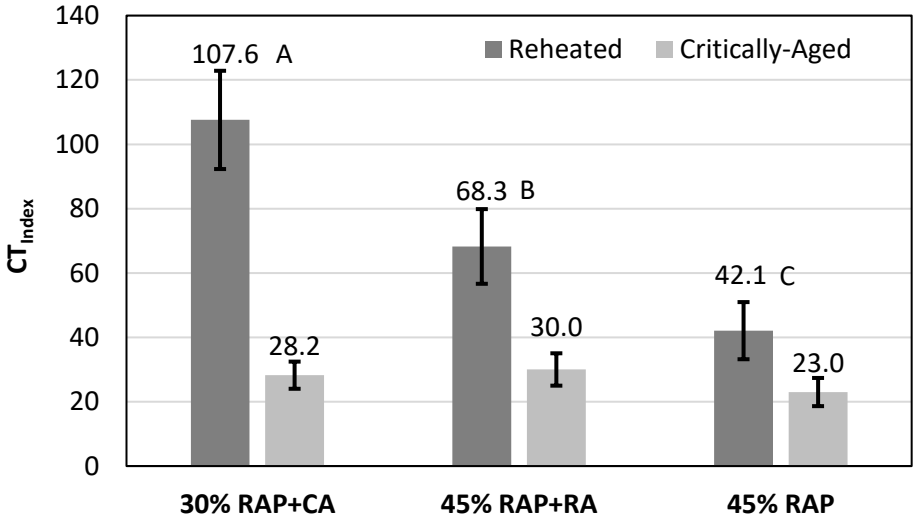

FIGURE 8 Comparison of reheated and critically aged IDEAL-CT results.

The p-value of a one-way ANOVA suggested a statistical difference in CT_{Index} values for the three reheated mixtures, and Tukey-Kramer statistical groupings showed significant differences among CT_{Index} values for the three reheated plant mixtures. A one-way ANOVA was conducted

for the three critically aged mixtures, suggesting their CT_{Index} values were statistically different at a 5% significance level (p-value = 0.035). The Tukey-Kramer statistical groupings showed the statistical difference only existed between the average CT_{Index} of the critically aged 45% RAP+RA and 45% RAP. In summary, while CT_{Index} values for the reheated plant mixtures were significantly different, they became closer to each other for the critically aged mixtures.

Cantabro Abrasion Test Results. The Cantabro abrasion test was conducted on the reheated plant mixtures compacted to N_{des}, and the results are illustrated in Figure 9. All three mixtures showed average mass losses higher than the maximum Cantabro mass loss threshold of 7.5% required in the VDOT provisional BMD specification. However, the reheated 45% RAP+RA mixture recorded statistically lower mass loss, with the other two mixtures having statistically the same mass loss values at a 5% significance level.

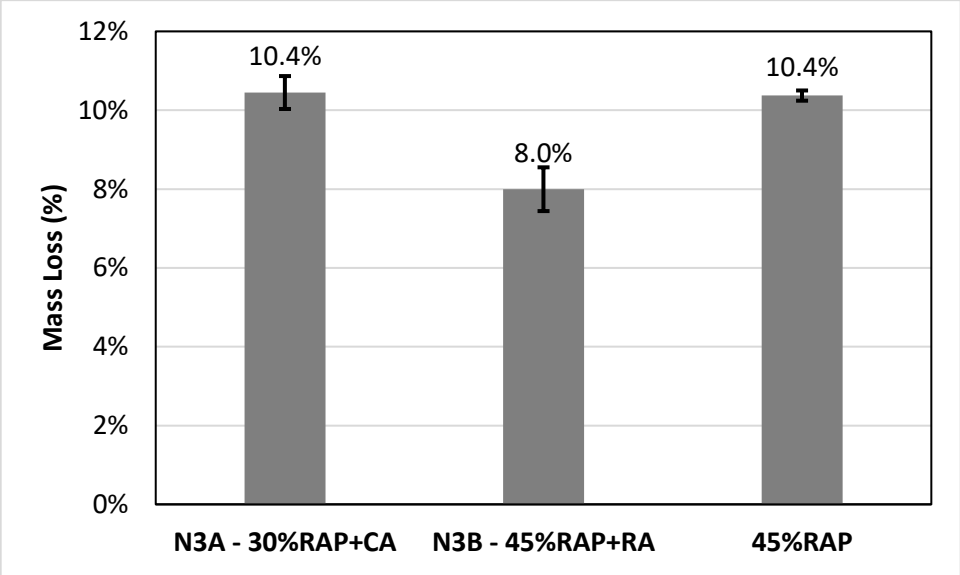

FIGURE 9 Cantabro abrasion test results for reheated plant mixtures.

18.6 Field Performance Evaluation

As part of the seventh research cycle, the 30% RAP+CA and 45% RAP+RA asphalt mixtures were trafficked starting November 26, 2018, and 10 million ESALs were applied by the end of fleet operations on February 28, 2021. Truck traffic was then halted for most of 2021 for the reconstruction of the eighth research cycle. It restarted on November 9, 2021, for the eighth research cycle, and approximately 10 million ESALs were applied to these test sections by the end of fleet operations on April 12, 2024.

Truck traffic operated on the Test Track from a Monday evening shift through a Saturday morning shift. Surface condition surveys were conducted every Monday to collect rutting, surface cracking, ride quality, and surface texture data. The ride quality of each pavement surface was measured based on the international roughness index (IRI). Surface texture was

measured based on mean texture depth (MTD) in the seventh research cycle and based on mean profile depth (MPD) in the eighth research cycle using the Pathway PathRunner inertial profiler. Rutting in the wheel paths of each test section was measured using the Pathway PathRunner inertial profiler and the ALDOT beam procedure, as per the ALDOT T-392 standard specification. This method uses a four-foot beam with a dial gauge to measure rut depths along the wheel path at predetermined locations in each test section of the Test Track. The accuracy of the rut depths obtained using the ALDOT beam method is estimated to be ± 2.5 mm.

Surface cracking data were obtained by an initial visual inspection of the test section, and observed surface cracks were then mapped and measured. The area of the cracked section was determined by conducting a linear measurement of cracks within each test section, which was then used to calculate the percent lane area of surface cracking.

18.6.1 Rutting

The rutting data collected for both research cycles for Sections N3A and N3B are compared in Figure 10. Rut depths were almost identical and below 5.0 mm for both sections in the first 10 million ESALs. While field rut depth for Section N3A remained unchanged, rut depth for Section N3B increased slightly by about 2.5 mm for the second 10 million ESALs. However, this is still below the typical maximum field rut depth threshold of 12.5 mm.

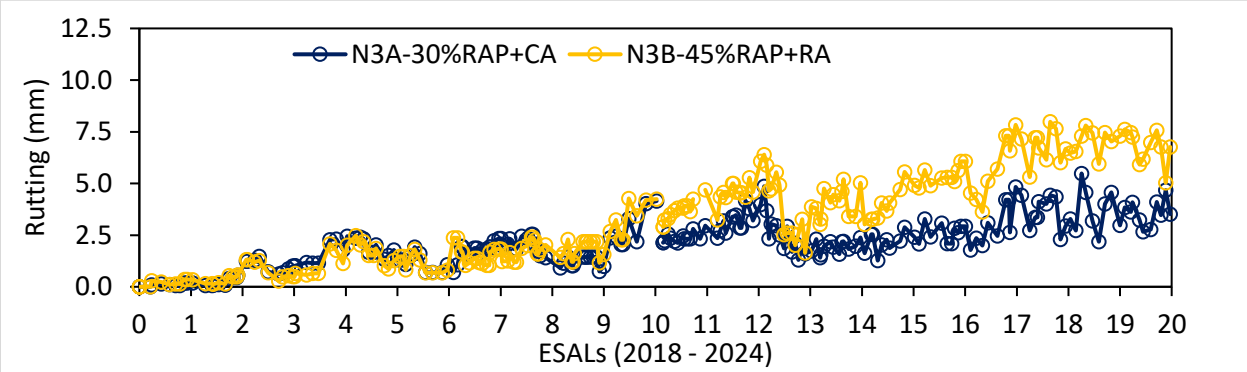

FIGURE 10 Field rut depth measurements.

The field rutting performance appeared to agree with the APA and HWTT results for the reheated plant mixtures summarized in Table 9. Their APA and HWTT results were below the VDOT maximum APA rut depth threshold of 8.0 mm and the commonly used maximum HWTT rut depth criterion of 12.5 mm, suggesting satisfactory rutting performance in the field.

TABLE 9 Summary of APA and HWTT Results for Reheated Plant Mixtures

Mix ID	APA Rut Depth (mm)		HWTT Rut Depth (mm)	
	Manual	Automated	10,000 passes	20,000 passes
30% RAP+CA	2.97	2.97	2.51	3.15
45% RAP+RA	3.44	3.37	2.55	3.10

*Average results of each measurement sharing the same letter are not statistically different.

18.6.2 Surface Cracking

Some signs of near-surface cracking initiation were observed in both sections in the last week of truck trafficking for the first 10 million ESALs in February 2021. They continued to grow slowly in the eighth research cycle (i.e., 10 to 20 million ESALs), reaching 2.5% of the lane area for Section N3A and 1.3% of the lane area for Section N3B, as shown in Figure 11. The amount of cracking shown in both sections is far below the 20% limit set for the Test Track.

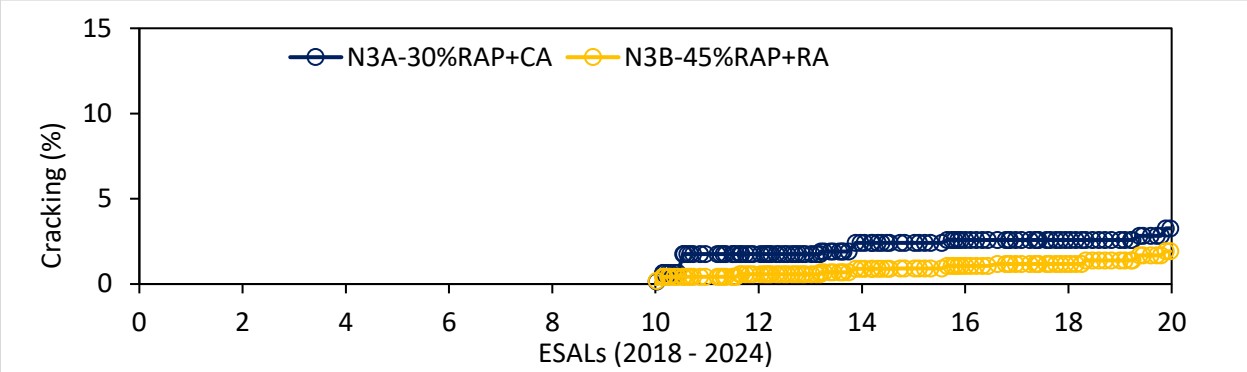

FIGURE 11 Field surface cracking measurements.

Table 10 summarizes the cracking test results for the plant mixtures under two aging conditions. The laboratory cracking test results indicate the two mixtures have similar cracking resistance, except for the IDEAL-CT test results for the reheated plant mixtures. These lab results align with the field cracking performance observed thus far.

TABLE 10 Summary of Cracking Test Results for Plant Mixtures

Mix ID	IFIT_FI		OT_N_f		IDEAL_CT_{Index}	
	Reheated	Critically Aged	Reheated	Critically Aged	Reheated	Critically Aged
30% RAP+CA	6.6	0.46	297	33	108	28
45% RAP+RA	7.5	0.31	325	18	68	30
Statistically significant?	No	No	No	No	Yes	No

*Average results of each measurement sharing the same letter are not statistically different.

18.6.3 Ride Quality

Figure 12 shows the ride quality data for Sections N3A and N3B, expressed as IRI. The rough transition at the beginning of Section N3A affected its overall smoothness in the seventh research cycle (i.e., the first 10 million ESALs). However, after the transition was repaired, the ride quality of both sections remained good throughout the eighth research cycle (i.e., up to 20 million ESALs).

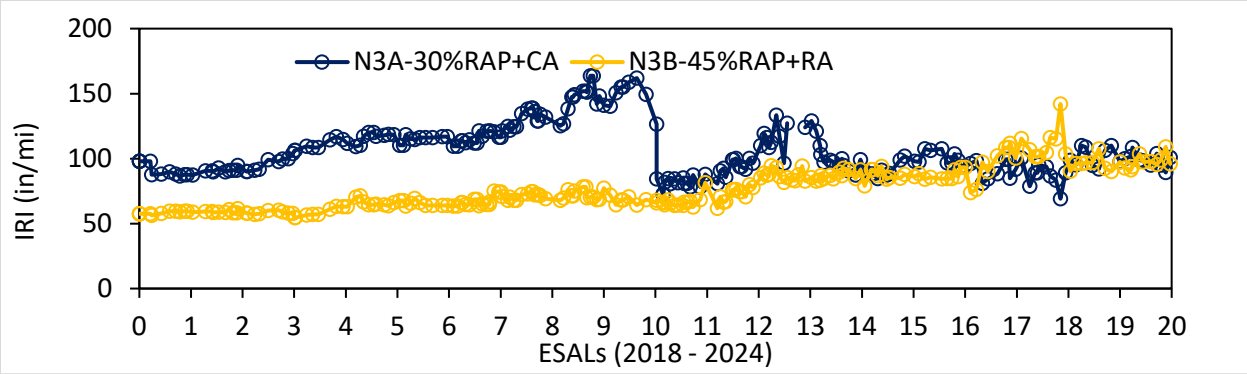

FIGURE 12 Ride quality (IRI) measurements.

18.6.4 Surface Macrotexture

Figure 13 compares mean texture depth (MTD) measurements in the first 10 million ESALs and mean profile depth (MPD) measurements from 10 to 20 million ESALs for Sections N3A and N3B. The results were almost identical for the two test sections. Macrotexture measurements increased due to the removal of asphalt film on the pavement surface at the onset of truck trafficking and stayed almost the same throughout the seventh research cycle. The increase in MPD from the seventh to the eighth research cycle at around 10 million ESALs was due to a new survey van and the change from MTD to MPD.

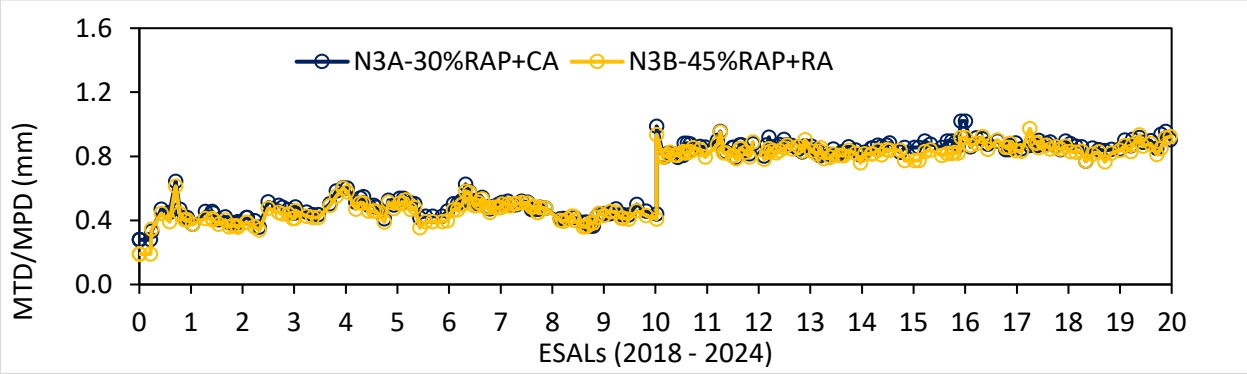

FIGURE 13 Surface macrotexture measurements (MTD in 2018-2021 and MPD in 2021-2024).

While the Cantabro mass loss results, as summarized in Table 11, were above the VDOT maximum mass loss requirement of 7.5%, there was no sign of raveling observed in the two test sections after 20 million ESALs.

TABLE 11 Summary of Cantabro Mass Loss Results for Reheated Plant Mixtures

Mix ID	Cantabro Mass Loss (%)
30% RAP+CA	10.5 (B)
45% RAP+RA	8.0 (A)
Statistically significant?	Yes

*Average results with different letters are statistically different.

18.7 Summary and Conclusions

This experiment was conducted to evaluate the effectiveness of Anova asphalt recycling agent in balancing the cracking and rutting performance of high RAP mixtures within the BMD framework. The experiment was conducted by comparing the field performance of two surface mixtures (30% RAP+CA and 45% RAP+RA) under the same pavement structure, traffic, and climatic conditions. A third mixture with 45% RAP was produced for laboratory testing only.

Section N3A was milled and inlaid with a 30% RAP+CA mixture produced with 30% RAP and a PG 64-22 binder with Anova 1501 Adhesion promoter/warm mix/compaction Aid additive, and Section N3B was milled and inlaid with a 45% RAP+RA mixture produced with 45% RAP, a PG 64-22 binder, and Anova 1815 recycling agent. Both sections were trafficked for 10 million ESALs from November 26, 2018, through February 28, 2021, in the seventh research cycle, and another 10 million ESALs from November 9, 2021, through April 28, 2024, in the eighth research cycle. Their field performance, including rutting, cracking, ride quality, and surface macrotexture, was monitored weekly.

Both mixtures were designed based on the VDOT 2018 provisional BMD specification, in which they were designed and tested to evaluate their resistance to rutting, cracking, and raveling using the APA, IDEAL-CT, and Cantabro tests, respectively. The two mixtures were then produced and sampled during construction for laboratory testing. A 45% RAP mixture was also produced without a recycling agent for laboratory testing only (without paving on the Test Track). The three mixtures were evaluated using a battery of laboratory performance tests to support the field evaluation experiment.

Based on the field performance of Sections N3A and N3B and laboratory test results for the BMD mix designs and the three plant-produced mixtures, the following conclusions can be drawn.

- The BMD approach using the APA, IDEAL-CT, and Cantabro abrasion tests is effective in improving mix resistance to cracking and raveling without causing a detrimental effect on rutting resistance. Both the 30% RAP+CA and 45% RAP+RA mixtures were designed to meet the VDOT provisional BMD specification with similar APA and IDEAL-CT results in their balanced mix designs.
- Both the BMD mixtures were produced, placed, and compacted to achieve good in-place density (i.e., 96.2% of G_{mm} for Section N3A and 96.8% of G_{mm} for Section N3B) on the NCAT Test Track.
- Both sections showed good and almost identical field rutting performance in the seventh research cycle (10 million ESALs), which also agreed with the APA and HWTT results for the reheated plant-produced mixtures sampled during construction. While rutting in Section N3A stayed almost the same in the eighth research cycle (i.e., from 10 to 20 million ESALs), rutting in Section N3B increased slightly by about 2.5 mm, reaching

about 7.5 mm. However, this is still below the typical maximum field rut depth of 12.5 mm.

- Neither section cracked until the end of the seventh research cycle. Cracks continued to grow slowly in the eighth research cycle (i.e., 10 to 20 million ESALs), reaching 2.5% of the lane area for Section N3A and 1.3% of the lane area for Section N3B. Laboratory cracking test results suggested a significant decrease in I-FIT, OT, and IDEAL-CT test results after critical aging, which is representative of approximately five years of field aging at the Test Track. Thus, it is important to continue monitoring the future cracking performance of these test sections.
- The transition area of Section N3A was very rough due to an unrelated issue, which affected the ride quality measurement for Section N3A. After it was repaired, both sections showed good ride quality and almost identical, consistent surface macrotexture measurements throughout the eighth research cycle.
- The effect of the recycling agent on cracking test results was more profound on reheated plant-produced mixtures and less on critically aged plant mixtures when comparing the 45% RAP+RA mixture to the 45% RAP mixture without the recycling agent.

In summary, Anova asphalt recycling agent was used to improve the cracking resistance of a high RAP mixture within the BMD framework without affecting the mixture's resistance to rutting when compared to a lower RAP BMD mix containing an adhesion promoter/warm mix/compaction aid additive. Sections N3A and N3B showed good field performance after 20 MESALs without any significant distress and will be kept in place for traffic continuation in the next research cycle to allow for a thorough field cracking and rutting performance evaluation.

18.8 References

1. Boomquist, D., G. Diamond, M. Oden, B. Ruth, and M. Tia. *Engineering and Environmental Aspects of Recycled Materials for Highway Construction*. Report No. FHWA-RD-088, FHWA, Washington, D.C., 1993.
2. NAPA. *Asphalt Pavement Industry Survey on Recycled Materials and Warm-Mix Asphalt Usage: 2021*. National Asphalt Pavement Association, Greenbelt, MD, 2022.
3. Cargill. ANOVA® 1815 Rejuvenator Product Data. Cargill, Incorporated, 2020. https://www.cargill.com/doc/1432177154791/anova-rejuvenator-1815-pds.pdf
4. Cargill. ANOVA® 1501 Warm Mix Additive: Production, Testing and Compaction Details. Cargill, Incorporated, 2020. https://www.dot.ny.gov/divisions/engineering/technical-services/technical-services-repository/details/anova_1501.pdf
5. Chen, C., F. Yin, P. Turner, R. C. West, and N. Tran. Selecting a Laboratory Loose Mix Aging Protocol for the NCAT Top-Down Cracking Experiment. *Transportation Research*

Record, *2672*(28), Transportation Research Board of the National Academies, Washington, D.C., 2018, pp. 359-371.

6. McDaniel, R., and M. Anderson. *NCHRP Report 452: Recommended Use of Reclaimed Asphalt Pavement in the Superpave Mix Design Method: Technician's Manual*. Transportation Research Board, National Research Council, Washington, D.C., 2001.

19. SOYLEI BIOPOLYMER-MODIFIED ASPHALT MIXTURE

Dr. Nam Tran

19.1 Introduction

The demand for longer-lasting asphalt pavements with improved performance has increased the need for modified asphalt binders. These modified binders can meet Superpave performance grade (PG) requirements for high traffic or challenging environmental conditions that unmodified binders cannot achieve (*1*). Various materials, such as polymers and oils, have been utilized as modifiers and additives to enhance the properties of asphalt binders (*2, 3, 4, 5*).

Asphalt polymers have traditionally been derived from petroleum-based sources. However, recent advancements have led to bio-based polymers. Iowa State University has developed a bio-based polymer through controlled radical polymerization of acrylated epoxidized high-oleic soybean oil using epoxidized benzyl soyate as the solvent. This innovative biopolymer, which includes epoxidized benzyl soyate (EBS), can enhance asphalt binder resistance to oxidative aging, as the epoxide rings within EBS react to form crosslinks, effectively blocking nucleophilic sites where asphalt oxidation occurs.

Preliminary laboratory tests have shown that a biopolymer with EBS can restore the performance properties of deteriorated asphalt binders and maintain their characteristics even after prolonged aging. However, a full-scale accelerated field experiment is required to validate the promising laboratory results and support the adoption of this biopolymer product by state highway agencies.

19.2 Research Objective and Scope

The objective of this study was to evaluate the impact of the new biopolymer on asphalt binder, plant-produced mixture, and field performance of the mixture on the NCAT Test Track. The modified biopolymer asphalt binder was blended at an asphalt terminal and then transported to the East Alabama Paving (EAP) facility in Opelika, Alabama. The biopolymer-modified asphalt mixture was produced at the EAP asphalt plant and paved in the surface layer of Section W10 at the NCAT Test Track.

The performance of the biopolymer-modified binder and mixture was compared to a conventional styrene-butadiene-styrene (SBS) polymer binder and its corresponding mixture, which was placed in Section E5A. During construction, samples of the asphalt binder and loose mix were collected for lab testing to support the field performance assessment.

The two test sections, W10 and E5A, were constructed in 2018 and evaluated under the same heavy truck traffic loading conditions during the seventh research cycle at the NCAT Test Track. The truck trafficking for the seventh research cycle commenced on November 26, 2018, and by the end of operations on February 28, 2021, around 10 million equivalent single axle loads (ESALs) were applied to these test sections. Both sections demonstrated similar field

performance after 10 million ESALs. They were kept in place for traffic continuation in the eighth research cycle from 2021 to 2024 to allow for an in-depth evaluation of their field performance. This chapter provides a detailed summary of the experimental plan, the lab evaluation of asphalt binders and mixtures placed in Sections W10 and E5A, and their field performance during the two research cycles from 2018 through 2024.

19.3 Experimental Plan

This study was divided into four main tasks, illustrated in Figure 1: (1) mix design, (2) mix production and paving, (3) laboratory performance testing, and (4) field performance evaluation.

FIGURE 1 Experimental plan.

The pavement structures of Sections W10 and E5A were originally built for the first research cycle in 2000. They were designed with sufficient thickness to ensure no structural damage would occur during testing. Surface distresses, including rutting and surface (or near surface) cracking, have only been observed in the original pavement sections at the NCAT Test Track. In 2018, the surface layers of these sections were milled and replaced with new mixtures for this field performance evaluation.

19.4 Mix Design

The new surface mixtures paved in Sections W10 and E5A were produced based on the same mix design except for the virgin asphalt binders. The surface mixture for Section W10 was produced using a binder modified with EBS biopolymer, while the control surface mixture in Section E5A was produced with a binder modified with SBS polymer. These binders were modified from two base binders by different suppliers, which may affect the field performance of the mixtures.

The aggregate gradation used in the mix design was a 12.5 mm nominal maximum aggregate size (NMAS) blend of 20% processed reclaimed asphalt pavement (RAP) with a binder content of 5.5%, granite 78s, granite 89s, and local sand, with size ranges defined in AASHTO M43. Table 1 shows the properties of the aggregates used in the mix design, and Table 2 summarizes the volumetric mix design parameters.

TABLE 1 Aggregate Properties

Property	RAP	GRN 78s	GRN 89s	Sand
Cold feed percentage (%)	20	38	24	18
Bulk specific gravity (G_{sb})	2.624	2.627	2.570	2.716
Apparent specific gravity (G_{sa})	2.678	2.682	2.650	2.745
Absorption (%)	0.8	0.8	1.2	0.4

TABLE 2 Summary of Mix Design Volumetric Parameters

Property	Value
Design Air Voids (VTM), %	4.0
Total Combined Binder (Pb), %wt	5.3
Effective Binder (P_{be}), %	4.9
Dust Proportion (DP)	1.0
Maximum Specific Gravity (G_{mm})	2.466
Voids in Mineral Aggregate (VMA), %	15.3
Voids Filled with Asphalt (VFA), %	73.7

19.5 Mixture Production and Paving

The control surface mixture for Section E5A was produced and placed on August 29, 2018, based on the volumetric mix design. The control mixture was made using an SBS-modified asphalt binder PG 76-22. On November 16, 2018, the experimental mixture was produced and paved based on the same mix design, except a biopolymer-modified binder PG 70-16 was used. In both mixtures, a liquid antistrip agent was used at a dosage of 0.5% by weight of the total binder. The target lift thickness for both mixtures was 1.5 inches, and the target mix temperature was 320°F. In-place density was comparable for both sections, with 93.2% of G_{mm} of the as-produced mix for Section E5A and 93.3% of G_{mm} for Section W10. Figure 2 shows the two test sections after construction. Table 3 summarizes the design and construction data for both test sections.

FIGURE 2 Paving of Sections E5A and W10.

TABLE 3 Design and Construction Data for Control and Experimental Sections

Design/Paving	**E5A - Control Mix**		**W10 - Experimental Mix**	
Design Method:	VMD		VMD	
Compactive Effort (N_{des}):	100 gyrations		100 gyrations	
Binder PG:	76-22 SBS		70-16 Biopolymer	
24 Hour High Temp. (F):	89		60	
24 Hour Low Temp. (F):	70		32	
24 Hour Rainfall (in):	1.08		0.00	
As-Built Sublot Lift Thickness(in):	1.5		1.8	
Approx. Underlying AC (in):	22.5		22.5	
Type of Tack Coat Utilized:	NTSS-1HM		PG67-22	
Undiluted Target Tack Rate (gal/sy):	0.1		0.06	
Approx. Avg. Temp. at Plant (F):	320		340	
Avg. Mat Compaction (%Gmm):	93.2		93.3	
Sieve Size/Mix Property	**Design**	**QC**	**Design**	**QC**
25mm (1"):	100	100	100	100
19mm (3/4"):	100	100	100	100
12.5mm (1/2"):	98	99	98	98
9.5mm (3/8"):	90	89	90	88
4.75mm (#4):	54	57	54	56
2.36mm (#8):	40	40	40	38
1.18mm (#16):	33	32	33	31
0.6mm (#30):	24	22	24	22
0.3mm (#50):	13	12	13	11
0.15mm (#100):	7	8	7	7
0.075mm (#200):	4.1	5.5	4.1	3.7
Binder Content (Pb):	4.8	5.0	4.8	4.9
Eff. Binder Content (Pbe):	4.2	4.3	4.2	4.3
Dust-to-Eff. Binder Ratio:	1.0	1.3	1.0	0.9
RAP Binder Replacement (%):	20	22	20	22
RAS Binder Replacement (%):	0	0	0	0
Total Binder Replacement (%):	20	22	20	22
Rice Gravity (Gmm):	2.491	2.472	2.491	2.477
Bulk Gravity (Gmb):	2.384	2.384	2.384	2.373
Air Voids (Va):	4.3	3.6	4.3	4.2
Aggregate Gravity (Gsb):	2.637	2.622	2.637	2.625
VMA:	14.0	13.6	14.0	14.0
VFA:	69	74	69	70

19.6 Laboratory Evaluation

Testing plans for evaluating the asphalt binders and mixtures are shown in Figure 3. During construction, representative samples of the virgin binders and plant-produced asphalt mixtures were collected. The representative binder samples were taken from the tankers upon delivery, while the representative loose mix samples were obtained by diverting mix from the conveyor of the material transfer machine going into the paver onto a flatbed truck. The flatbed then transported the mix to the Test Track laboratory, where the mixes were shoveled into five-gallon buckets and labeled. A total of 16 buckets of each mixture were sampled for this study.

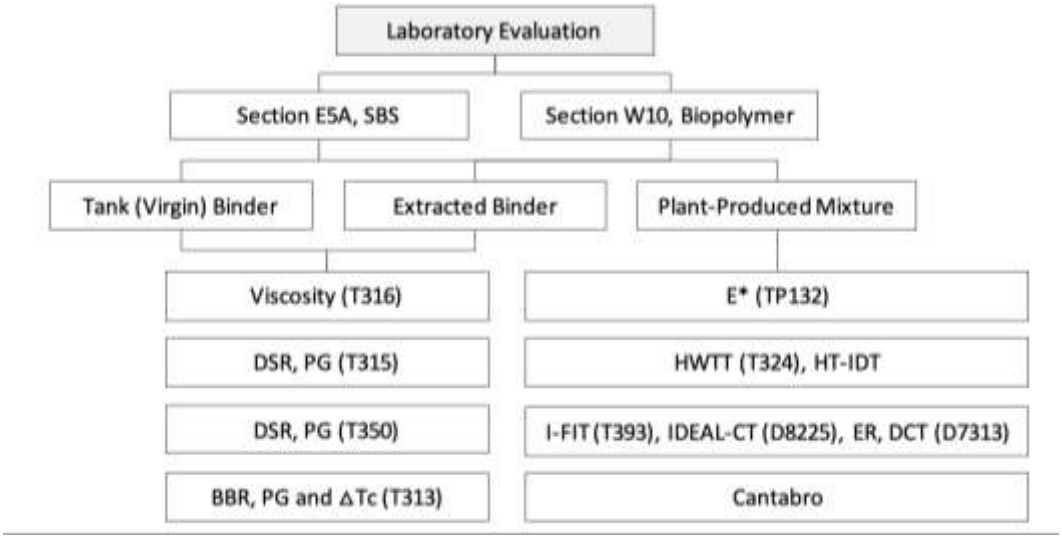

FIGURE 3 Testing plan performed for asphalt binder evaluation.

As part of the laboratory binder evaluation, the virgin binders were assessed. Asphalt binders were extracted from the plant-produced mixtures following ASTM D2172 (method A) using trichloroethylene and then recovered per ASTM D5404. The rheological evaluation of the recovered binders was conducted for both test sections to compare with the virgin binders sampled during production.

For the laboratory mixture evaluation, the plant-produced mixture was reheated to 150°C (compaction temperature) for two hours and then reduced to the testing size using the quartering method described in AASHTO R47. The theoretical maximum specific gravity (G_{mm}) test was performed on both mixtures according to AASHTO T209, and the results were 2.478 and 2.491 for the E5A and W10 mixes, respectively. AASHTO T166 was followed to obtain the bulk specific gravity of the mixes. For mixture performance testing, the specimens were targeted to have 7.0% air voids after cutting or coring based on the in-place densities achieved in the two test sections. A description of each test method and its results follows.

19.6.1 Asphalt Binder Evaluation

Rotational Viscosity. Viscosity refers to a fluid's resistance to flow and is used to determine the handling properties of asphalt binders. The rotational viscosity test was conducted in compliance with AASHTO T316 at 135ºC. Figure 4 displays the rotational viscosity values of the asphalt binders used in Sections E5A (control, modified with SBS) and W10 (modified with EBS biopolymer). As anticipated, using RAP increased asphalt binder viscosity (results of the binders extracted and recovered from plant-produced mixtures), especially for the biopolymer-modified binder. All tested binders, with or without the addition of aged RAP binder, showed viscosity values below the Superpave Brookfield rotational viscosity limit for asphalt binders at 135ºC, which is 3 Pa.s.

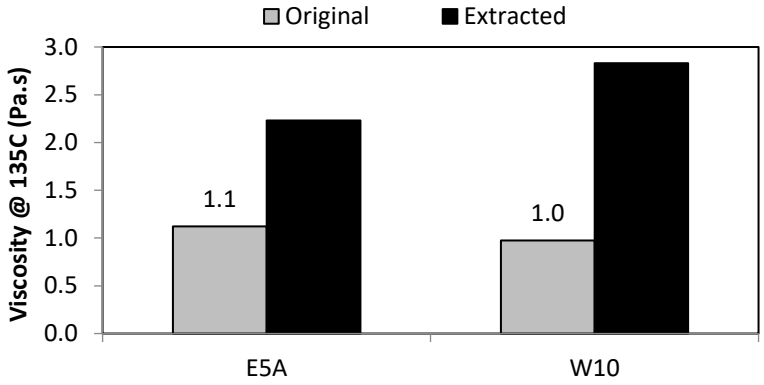

FIGURE 4 Rotational Viscosity at 135ºC.

Performance Grading (PG) and ΔTc. Table 4 shows the critical high, intermediate, and low temperatures and the ΔT_c (S-critical temperature – m-critical temperature) of the asphalt binders utilized in Sections E5A and W10. The results were obtained by conducting the following tests:

- The Dynamic Shear Rheometer (DSR) per AASTHO T315 was used to characterize the viscous and elastic behavior of unaged, rolling thin film oven (RTFO) aged and pressure aging vessel (PAV) aged binders.
- The Bending Beam Rheometer (BBR) per AASHTO T313 was used to measure the rheological characteristics of PAV-aged binders at low temperatures.

As shown in Table 4, the extracted asphalt binders from the two plant-produced mixtures had higher high-temperature continuous grades than the virgin asphalt binders. The addition of RAP binder had a slightly higher effect on the properties of the W10 binder, resulting in a slightly larger increase in the high-temperature continuous grade before and after RTFO aging. For the intermediate-temperature grade, the W10 virgin binder exhibited a higher continuous grade than the E5A virgin binder. For the low-temperature grade, the W10 virgin binder showed a higher continuous than the E5A virgin binder regarding both stiffness and m-value.

Initial BBR stiffness and m-value results showed the E5A virgin and extracted binders had better low-temperature cracking resistance than the W10 binders. Both the E5A virgin binder and W10 virgin binder showed acceptable ΔTc. After adding RAP, the stress relaxation of binders changed significantly, lowering ΔTc (i.e., it becomes more negative). The W10 extracted binder showed lesser cracking susceptibility (ΔTc = -6.6) than the E5A extracted binder (ΔTc = -7.3). Before and after mixture production, all binders were found to be "m-controlled" (i.e., failure potentially controlled by inadequate stress relaxation).

TABLE 4 ΔTc, High, Intermediate and Low Pass/Fail Binder Temperature

Sample	T_{cont} High unaged (°C)	T_{cont} High RTFO (°C)	T_{cont} Low S (°C)	T_{cont} Low m-value (°C)	ΔT_c
E5A Virgin	76.3	77.2	-27.3	-24.7	-2.6
E5A Extracted	89.7	88.4	-26.6	-19.2	-7.3
W10 Virgin	73.6	75.7	-24.6	-21.6	-3.0
W10 Extracted	92.0	89.1	-22.6	-16.0	-6.6

Table 5 presents the final PG of the asphalt binders before and after production of the mixtures containing RAP. Typically, asphalt binders with a broader PG range (i.e., useful temperature interval - UTI) are thought to provide better pavement performance under a given traffic and environmental condition. The addition of RAP increased the stiffness of the total binder in both asphalt mixtures. An increase in true PG was observed for both E5A and W10 binders with the low PG of the extracted E5A binder changing from -22°C to -16°C. However, there was no difference in UTI for the extracted asphalt binders from the two mixtures.

TABLE 5 PG and Useful Temperature Interval of Binders

Sample	PG High Temp. (°C)	PG Low Temp. (°C)	UTI (°C) (PG High Temp. - PG Low Temp.)
E5A Virgin	76	-22	98
E5A Extracted	88	-16	104
W10 Virgin	70	-16	86
W10 Extracted	88	-16	104

Multiple-Stress Creep-Recovery (MSCR) Test. The test was conducted at 64°C in accordance with AASHTO T350 to measure the non-recoverable creep compliance (J_{nr}) and percent recovery (%R) of RTFO-aged binders. The MSCR results are presented in Table 6 and indicate the E5A virgin binder has lower non-recoverable creep compliance (J_{nr}) than the W10 virgin binder. The MSCR grading was PG 64E-22 (Extremely Heavy) for the E5A virgin binder as compared to PG 64V-16 (Very Heavy) for the W10 virgin binder.

TABLE 6 MSCR High-Temperature PG Classification of Asphalt Binders at 64°C

Sample	J_{nr} @ 3.2, kPa^{-1}	% diff J_{nr}	%R @ 3.2, kPa^{-1}	High Temp. PG (°C)
E5A Original	0.33	33.4	59.9	64E
E5A Extracted	0.09	5.7	58.7	64E
W10 Original	0.65	33.4	29.5	64V
W10 Extracted	0.09	16.6	59.9	64E

Figure 5 shows the E5A virgin binder has a higher percent recovery rate (59.9%) compared to the W10 virgin binder (29.5%), suggesting the E5A binder is more resistant to permanent deformation. All binders passed the J_{nr} percent-difference parameter, indicating no negative effect on stress susceptibility.

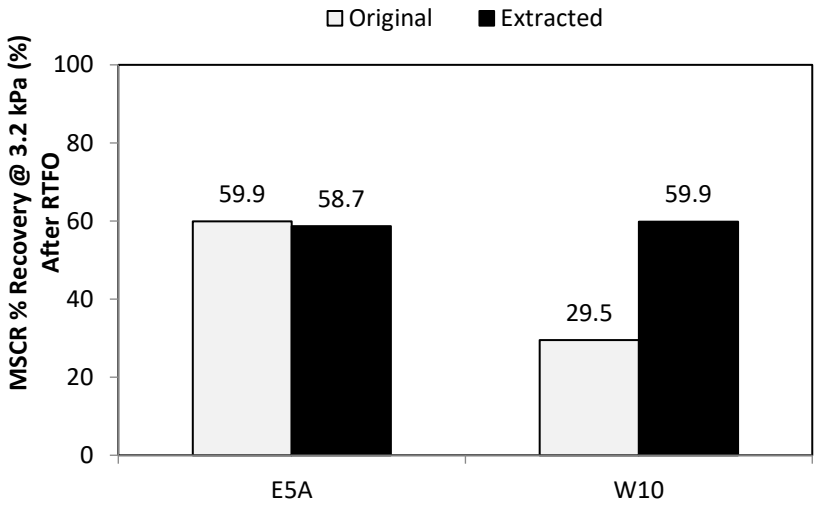

FIGURE 5 MSCR percentage recovery at 64°C.

Figure 6 indicates that the addition of oxidized RAP binder resulted in a reduction of J_{nr} for the extracted binders. Therefore, the improvement in the %Recovery parameter for the W10 extracted binder can be attributed to the aged binder coming from the RAP. Evaluation of the binder properties after exposure in the field will allow a better understanding of the influence of the biopolymer on the overall performance of the asphalt binder.

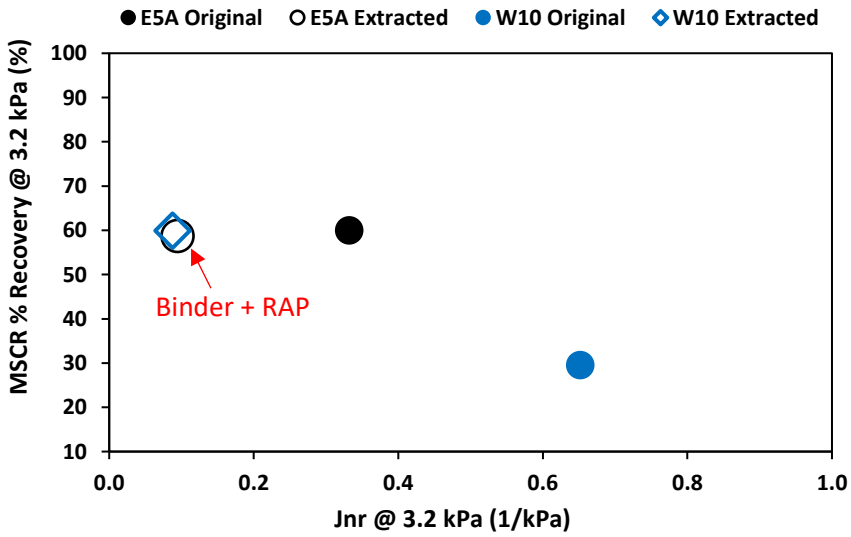

FIGURE 6 MSCR percentage recovery versus J_{nr} at 3.2 kPa and 64°C.

19.6.2 Asphalt Mixture Evaluation

Dynamic Modulus (E*). The testing process was carried out for each asphalt mixture based on AASHTO TP 132 guidelines using an Asphalt Mixture Performance Tester (AMPT). Three asphalt specimens that met target air voids were tested for each mixture. These specimens were 38 mm in diameter and 110 mm tall. The tests were conducted at three different temperatures (4, 20, and 40°C) and three loading frequencies (10, 1, and 0.1 Hz) for each temperature. Specimens were also tested at 0.01 Hz at the 40°C test temperature. The collected data was used to develop the E* master curve for each mixture. This allowed the relative stiffness of the two mixtures to be analyzed across a broad range of temperatures and loading rates.

Figure 7 shows the E* master curves for the E5A (control) and W10 mixtures. The results indicate both mixtures had similar stiffness at higher loading rates and lower temperatures (as seen on the right-hand side of the curve). However, the mixture with the biopolymer binder was stiffer than the SBS-modified control mixture throughout the rest of the curve, with higher temperatures and slower loading rates (as shown on the left-hand side of the curve).

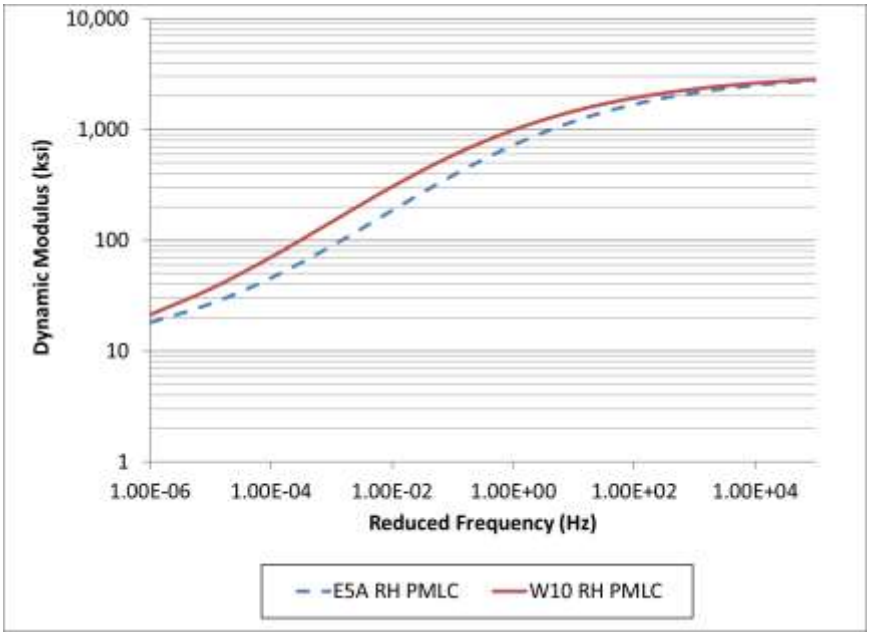

FIGURE 7 Dynamic modulus master curves.

Hamburg Wheel Tracking Test (HWTT). The test was performed per AASHTO T324 on asphalt specimens submerged in 50°C water to evaluate their rutting resistance and moisture susceptibility. The results of the HWTT for the E5A control and W10 mixtures are provided in Table 7. Both mixes showed rut depths of less than 2 mm after 10,000 and 20,000 passes, significantly less than the common threshold criteria of 12.5 mm at 20,000 passes. Neither mixture exhibited any signs of stripping in the Hamburg test.

TABLE 7 Summary of Hamburg Wheel Tracking Results

Mix	Rut Depth at 10,000 passes (mm)	Rut Depth at 20,000 passes (mm)	Rut Depth of 12.5 mm (# passes)	Stripping Inflection Point (# passes)
E5A	1.28	1.51	>20,000	>20,000
W10	1.48	1.68	>20,000	>20,000

Illinois Flexibility Index Test (I-FIT). The test was conducted per AASHTO T393 at 25°C to assess mixture resistance to intermediate temperature cracking. The results obtained from I-FIT are presented in Figure 8. The E5A control mix demonstrated an average flexibility index (FI) of 4.5, while the W10 biopolymer mixture showed an FI of 2.0. A two-sample t-test was conducted at a 5% significance level, which showed the E5A control mix had a statistically higher FI score than the W10 biopolymer mix (p-value = 4.9e-5 < α), suggesting that based on the I-FIT test, the SBS-control mix is more resistant to cracking than the W10 EBS-modified mix.

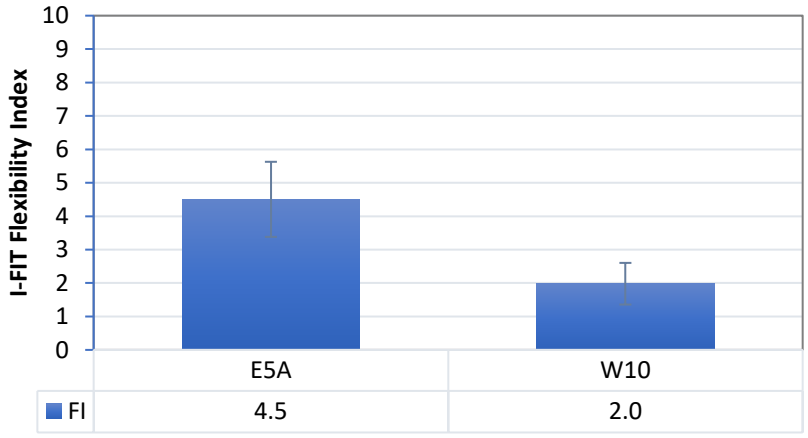

FIGURE 8 I-FIT flexibility index results.

Energy Ratio (ER). An Energy Ratio evaluation was conducted to assess asphalt mixture resistance to top-down cracking by performing three indirect tension (IDT) tests on the same mixture specimens. Testing was carried out on IDT specimens trimmed to a thickness of 50 mm and equipped with horizontal and vertical strain gauges. The three tests were resilient modulus (ASTM D7369), creep compliance (AASHTO T322), and indirect tensile strength (ASTM D6931). The Energy Ratio is the ratio of the dissipated creep strain energy threshold of the mixture (DCSEHMA) and the minimum dissipated creep strain energy required to resist top-down cracking (*7*). The dissipated creep strain energy is required beyond the elastic region to initiate cracking. The higher the Energy Ratio, the more resistant the mixture should be to top-down cracking.

Table 8 shows the results of the Energy Ratio analysis. At the test temperature of 10°C, both mixtures showed similar properties in the three component tests (resilient modulus, creep compliance, and fracture energy). This resulted in both mixes having a similar Energy Ratio, with the control having an Energy Ratio of 4.3 and the W10 mix having an Energy Ratio of 4.8.

TABLE 8 Energy Ratio Results

Mix	Resilient Modulus (GPa)	Creep Compliance Rate	IDT Fracture Energy (kJ/m^3)	$DCSE_{HMA}$ (kJ/m^3)	Energy Ratio
E5A	13.14	3.586 E-06	3.2	2.97	4.3
W10	12.96	3.290 E-06	3.6	3.27	4.8

Indirect Tensile Asphalt Cracking Test (IDEAL-CT). The test was conducted according to ASTM D8225 at 25°C to evaluate mixture resistance to intermediate temperature cracking. The CT_{Index} values for the two mixtures were determined using IDEAL-CT test data, as shown in Figure 9. The W10 mix had an average CT_{Index} of 17.2 with a standard deviation of 4.3, while the E5A mixture had an average CT_{Index} of 26.3 with a standard deviation of 6.4. To determine the statistical significance difference of the means assuming equal variances, a two-sample t-test was conducted at a 95% confidence interval. The t-test showed the W10 biopolymer mixture had a statistically lower CT_{Index} than the E5A control mix (p-value = 0.024 < α = 0.05), suggesting the biopolymer mixture would be less resistant to cracking in comparison to the SBS-control mixture, based on the IDEAL-CT test results.

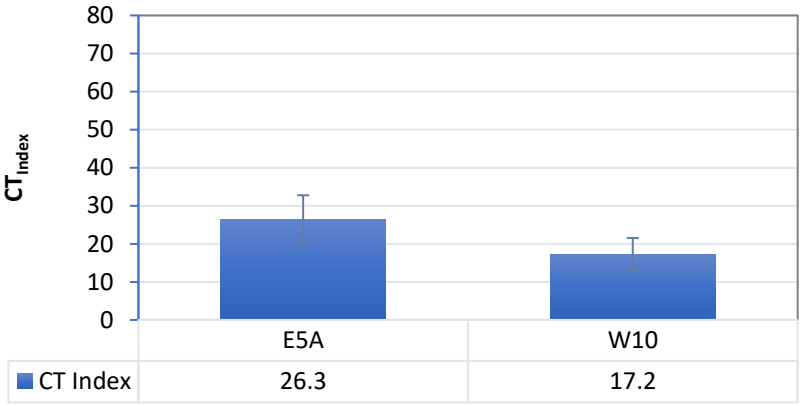

FIGURE 9 IDEAL-CT results.

High Temperature Indirect Tensile Test (HT-IDT). The HT-IDT test was performed similarly to the IDEAL-CT test, except the temperature was set at 50.2°C. This test was conducted to determine the rutting resistance of the asphalt mixes. Higher IDT strength at high temperatures generally indicates better relative rutting resistance. As shown in Figure 10, the average IDT strength of the W10 biopolymer mix was 69.5 psi, while that of the E5A control mix was 49.3 psi. The biopolymer sample had a standard deviation of 14.2 psi, while the control had a deviation of 5.2 psi. The results of a two-sample t-test showed the IDT strength of the biopolymer-modified mixture was statistically higher than that of the SBS-control mix (p-value = 0.036 < α = 0.05). Therefore, the biopolymer asphalt mixture was found to be more resistant to rutting than the control mix in the HT-IDT test.

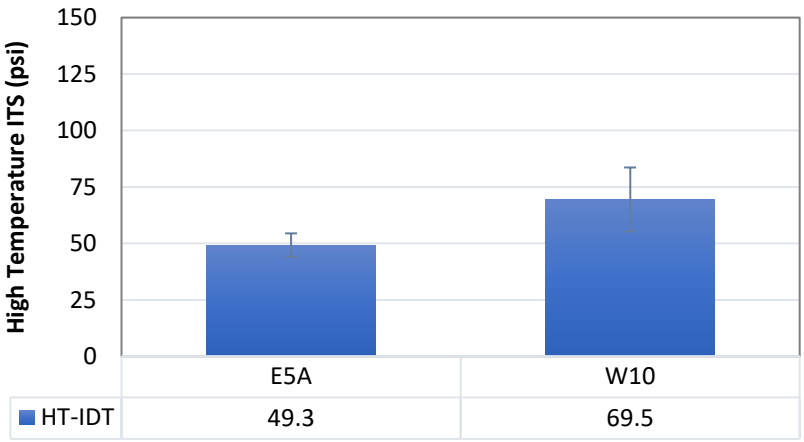

FIGURE 10 High-temperature indirect tensile test results.

Cantabro Percentage Loss. The Cantabro test evaluates the raveling potential of asphalt mixtures according to AASHTO TP108. VDOT specifies a maximum Cantabro Mass Loss of 7.5% for specimens compacted to N_{design} for BMD surface mixes (*8*). A summary of the Cantabro mass loss and air voids of the specimens compacted to N_{design} is presented in Figure 11. The W10 mixture, which contains the biopolymer-modified binder, showed a 12% mass loss and an average air void content of 4.8%. The E5A control mixture had a mass loss of 9.8% and an average air void content of 3.9%. A two-sample t-test indicated a significantly higher mass loss for the W10 mix than the control mix at N_{design} (p-value = 0.02 < α = 0.05). Moreover, the W10 mix also had statistically higher air voids than the control mix at N_{design} (p-value = 0.003 < α = 0.05).

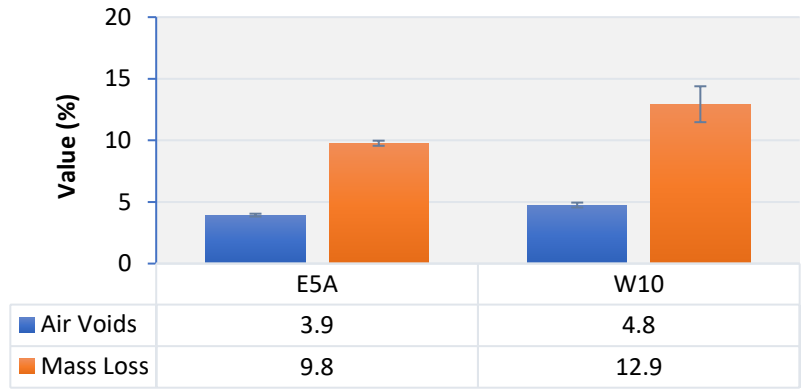

FIGURE 11 Cantabro mass loss of specimens compacted to N_{design}.

Figure 12 shows Cantabro loss conducted at the same target air void content of 6.5±0.5%. The biopolymer mixture had an 11.3% mass loss, while the SBS mixture had a 10.1% mass loss. A two-sample t-test of the mass loss values showed no significant difference in average mass loss between the control and W10 mixtures (p-value = 0.072 > α = 0.05). This indicates air voids in the specimen can significantly affect Cantabro loss results.

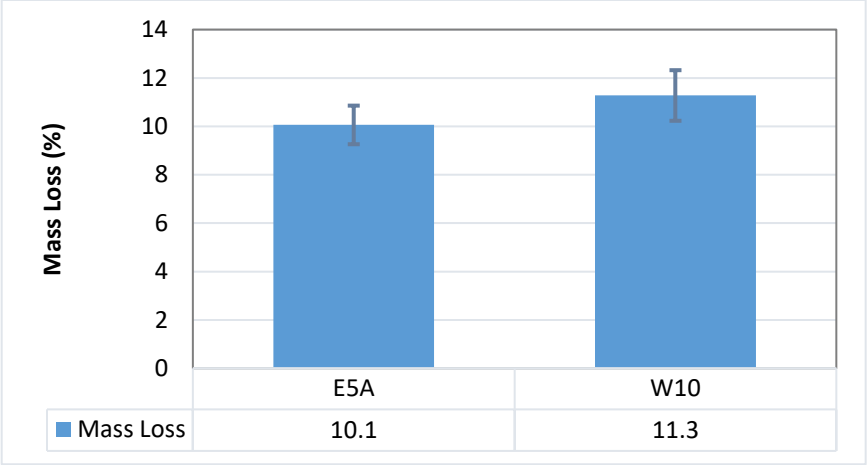

FIGURE 12 Cantabro mass loss of specimens compacted to 6.5 +/- 0.5 percent air voids.

Disk Shaped Compact Tension (DCT) Test. The two mixtures were also evaluated for their resistance to low-temperature cracking using the DCT test, following ASTM D7313, at a test temperature of -12°C. Figure 13 shows the DCT fracture energy (FE) (J/m^2) of the mixtures tested. The E5A mixture had an average FE of 604.5 J/m^2 with a standard deviation of 56.8 J/m^2 (CV of 9.4%), whereas the W10 mix had an average FE of 510.3 J/m^2 with a standard deviation of 81.7 J/m^2 (CV of 16.0%). A statistical analysis of the DCT FE results showed the E5A mix had statistically higher fracture energy than the W10 mixture (p-value = 0.043 < α = 0.05), suggesting the biopolymer mixture would be less resistant to low-temperature cracking than the SBS mixture. However, both mixtures can provide satisfactory performance for moderate traffic levels (10 to 30 million ESALs) based on the minimum fracture energy threshold of 460 J/m^2 proposed in a previous study (*9*).

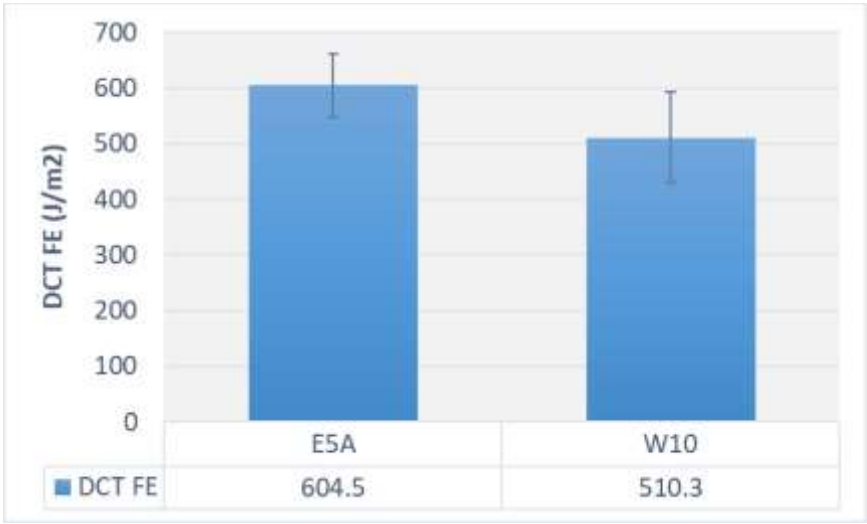

FIGURE 13 DCT fracture energy results.

19.7 Field Performance

Section E5A (control, SBS modified) and W10 (modified with EBS biopolymer) were evaluated for rutting, cracking, roughness, and macrotexture at the NCAT Test Track for 20 million ESALs, as shown in Figure 14.

Figure 14a compares the rut depth measurements for the control E5A and biopolymer W10 sections. The average rut depth of the biopolymer section was around 4.5 mm after 10 million ESALs in 2021, with the average rut depth of the control section around 2.0 mm. These values stayed almost the same after another 10 million ESALs were applied in the eighth research recycle from 2021 through 2024. Both mixtures have shown good rutting resistance, and their values are smaller than the maximum rut depth limit of 12.5 mm.

Figure 14b compares cracking measurements for the two test sections. The first crack was observed in Section E5A on November 20, 2020. At the end of the seventh research cycle on February 28, 2021, low-severity cracking measured in Section E5A was 0.4% of the lane area, while no cracking was observed in Section W10. The first crack was observed in Section W10 in the eighth research cycle on February 16, 2022. At the end of the eighth research cycle, low-severity cracking was observed in both sections, with 2.7% of the lane area in Section E5A and 3.4% of the lane area in Section W10.

For each section, pavement roughness was quantified using the International Roughness Index (IRI). Roughness increases are commonly associated with pavement distress. As shown in Figure 14c, the change in roughness over time for the E5A control and W10 sections was similar. Despite slight fluctuations in pavement smoothness, the overall IRI of Section W10 was 120 in/mile and 105 in/mile for Section E5A.

The final field performance assessment was surface macrotexture based on mean profile depth (MTD), as shown in Figure 14d. The change in surface macrotexture over time for the two test sections was almost identical. The increase in MPD from the seventh to the eighth research cycle (i.e., around 10 million ESALs) was due to the use of a new survey van.

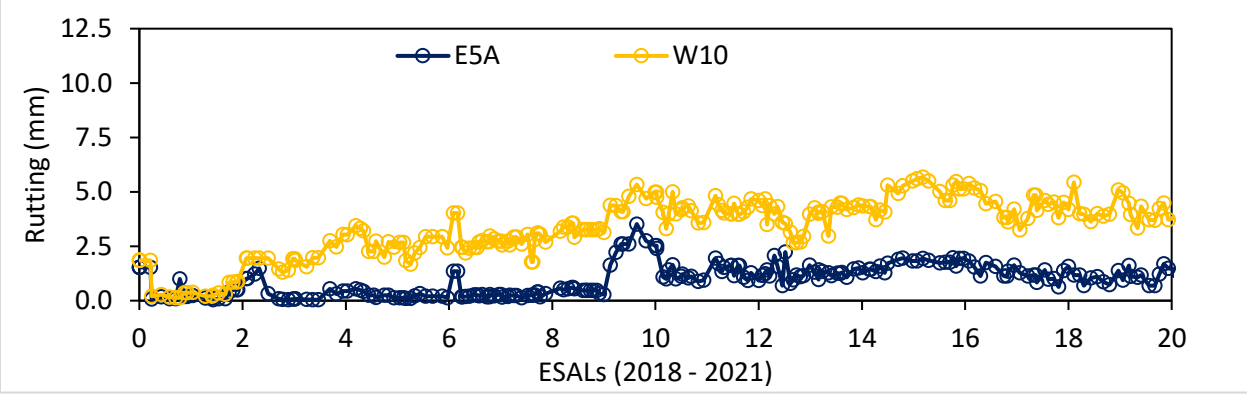

a. Rutting

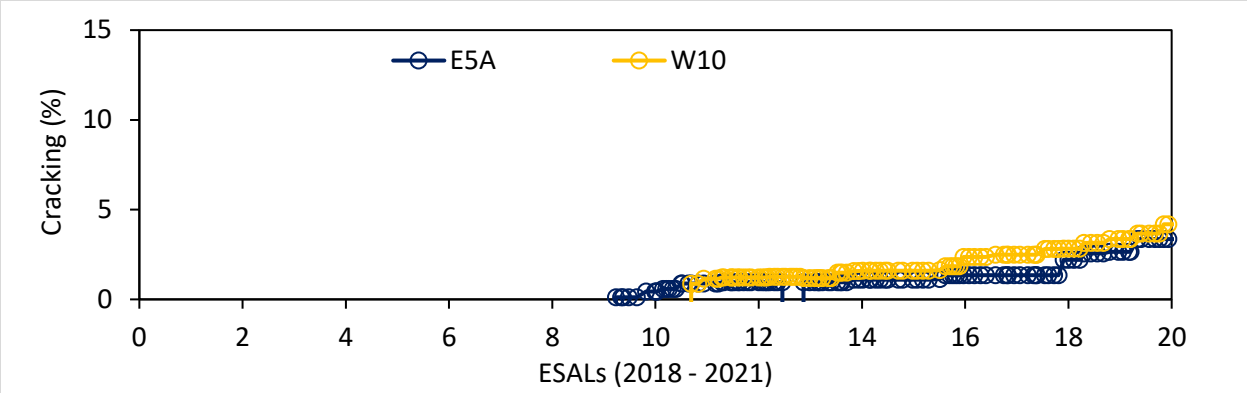

b. Cracking

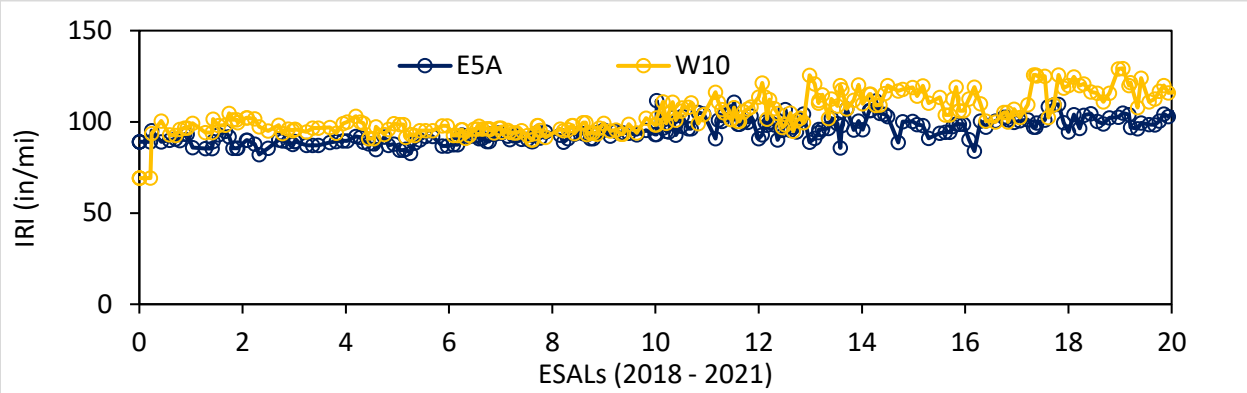

c. IRI

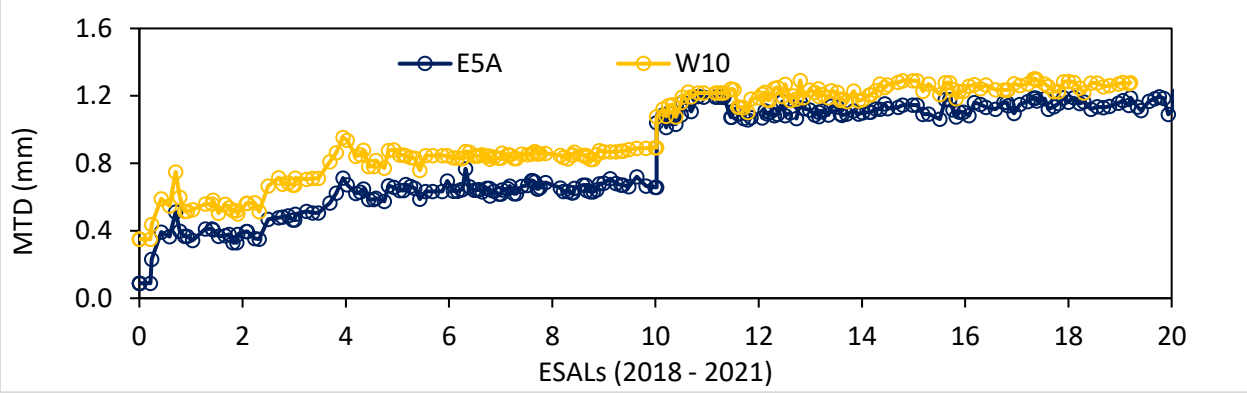

d. MPD

Figure 14 Field performance of Sections E5A and W10.

19.8 Summary and Conclusions

The surface layer of Section W10 was milled and inlaid with a new asphalt mixture with an EBS biopolymer binder in 2018. This section was compared to a control section (E5A) in the seventh and eighth research cycles (2018 through 2024). The surface layer of E5A was also paved with an asphalt mixture based on the same mix design, but it was produced using an SBS-modified PG 76-22 binder. The test sections were monitored weekly for rutting, cracking, smoothness,

and macrotexture under truck traffic. In addition, asphalt binders and plant mixtures were sampled during construction for a comprehensive laboratory evaluation to support the field evaluation. This chapter summarizes the results of the laboratory study along with field performance data collected in the two research cycles from 2018 through 2024.

The following observations were made regarding laboratory binder characterization—

- The biopolymer-modified binder (W10) had lower high-temperature stiffness than the SBS-modified binder (E5A). Higher stiffness at high temperatures may indicate increased rutting resistance.
- The high-temperature grade of the biopolymer-modified binder in Section W10 was more affected by the incorporation of the RAP binder compared to the SBS-modified binder in Section E5A. As a result, the asphalt binder from the W10 plant-produced mixture was stiffer than the binder from the E5A mixture.
- At intermediate temperatures, the stiffness of the biopolymer-modified binder (W10) was higher than the SBS-modified binder (E5A). The addition of RAP binder further increased the binder's intermediate-temperature stiffness for both mixtures. Like high-temperature stiffness, the asphalt binder from the biopolymer-modified plant mix had a higher increase in stiffness at intermediate temperatures.
- At low temperatures, both original binders showed similar negative values of ΔT_c (i.e., -2.6^{o}C for E5A and -3.0^{o}C for W10) and were found to be m-controlled. However, after the addition of RAP binder (extracted from plant-produced mixes), ΔT_c values for E5A and W10 significantly decreased to -7.3^{o}C and -6.6^{o}C, respectively.

The following observations were made based on mixture performance testing of the re-heated plant-produced mixtures—

- Based on the results of the Dynamic Modulus (E*) test, the biopolymer-modified mixture was generally stiffer than the control SBS mixture across most of the tested temperatures and frequencies. This finding is consistent with other laboratory rutting test results.
- Both mixtures performed well in the Hamburg test, showing rutting less than 2 mm without any signs of stripping. The W10 mixture exhibited higher IDT strength than the control at a temperature of 50.2°C. However, neither mixture was expected to show significant rutting on the NCAT Test Track.
- Both the I-FIT and IDEAL-CT cracking tests were performed at 25°C to compare the cracking resistance of the control mix (E5A) and the W10 mixture. The results indicated the control mix would have better cracking resistance than the W10 mixture. However, the Energy Ratio test conducted at 10°C showed the cracking resistance of both mixtures was comparable. Furthermore, the DCT test, conducted at a low temperature

of -12°C, showed the control mix (E5A) may have better low-temperature cracking resistance than the W10 mixture.

- According to the Cantabro test results, the W10 mix demonstrated less durability than the control mix at N_{design}. However, the W10 mix had a higher air void content at N_{design}, which could have contributed to its higher mass loss. When compacted to the same target air void content, there was no significant difference in Cantabro mass loss values of the two mixtures.

After 20 million ESALs of trafficking, both test sections have shown similar field performance. Both sections exhibited good rutting with final rut depths below 5.0 mm. At the end of the eighth research cycle, low-severity cracking was observed in both sections, with 2.7% of the lane area in Section E5A and 3.4% of the lane area in Section W10.

These sections will be kept in place for a new experiment in the ninth research cycle. The section will be divided into two sub-sections: one will be treated with a spray-on rejuvenator, and the other will be used as the control. The experiment will allow for an evaluation of the spray-on rejuvenator while continuing to evaluate the long-term performance of the biopolymer-modified asphalt binder against the conventional SBS-modified asphalt section.

19.9 References

1. Bahia, H. U., D. I. Hanson, M. Zeng, H. Zhai, M. A. Khatri, and R. M. Anderson. *NCHRP Report 459: Characterization of Modified Asphalt Binders in Superpave Mix Design.* TRB, National Research Council, Washington, D.C., 2001.
2. Li, Y., R. Moraes, E. Lyngdal, and H. U. Bahia. Effect of Polymers and Oils Modification on the Aging Susceptibility of Asphalt Binders. *Transportation Research Record: Journal of the Transportation Research Board*, No. 2574, Vol. 1, Transportation Research Board of the National Academies, Washington, D.C., 2016, pp. 28-37.
3. Moraes, R., and H. U. Bahia. Effect of Mineral Fillers on the Oxidative Aging of Asphalt Binders: A Laboratory Study Using Mastics. *Transportation Research Record: Journal of the Transportation Research Board*, No. 2506, Transportation Research Board of the National Academies, Washington, D.C., 2015, pp. 19-31.
4. Golalipour, A. *Investigation of the Effect of Oil Modification on Critical Characteristics of Asphalt Binders.* University of Wisconsin–Madison, 2013.
5. Ruan, Y., R. R. Davison, and C. J. Glover. Oxidation and Viscosity Hardening of Polymer-Modified Asphalts. *Energy and Fuels,* Vol. 17, 2003, pp. 991-998.
6. Bonaquist, R. *NCHRP Report 673: A Manual for Design of Hot Mix Asphalt with Commentary.* NCHRP, Washington, D.C., 2011.
7. Roque, R., B. Birgisson, C. Drakos, and B. Dietrich. Development and Field Evaluation of Energy-Based Criteria for Top-Down Cracking Performance of Hot Mix Asphalt (with discussion). *Journal of the Association of Asphalt Paving Technologists*, Vol. 73, 2004.

8. Diefenderfer, S. D., Boz, I., & Habbouche, J. (2023). *Balanced Mix Design for Surface Mixtures: 2021 and 2022 Plant Mix Schedule Pilots* (No. FHWA/VTRC 23-R19). Virginia Transportation Research Council (VTRC).
9. Dave, E. V., Oshone, M., Schokker, A., & Bennett, C. E. Disc shaped compact tension (DCT) specifications development for asphalt pavement, 2019.

20. EVALUATION OF MIXTURE PERFORMANCE AND STRUCTURAL CAPACITY OF PAVEMENTS USING US POLYCO BINDER FORMULATION

20.1 Introduction

In 2021, US Polyco sponsored a full-scale test section at the NCAT test track featuring a new binder formulation referred to as Sigmabond HP comprised of styrene-butadiene-styrene (SBS) polymer and Sigmabond Tire Rubber (TR). Mixtures produced with this binder formulation are expected to have an improved cracking and rutting performance compared to mixtures with polymer-modified binders containing 3% SBS, which is commonly specified by state agencies for mixtures subjected to high traffic volumes.

20.2 Objective and Scope

The objective of the research was to design, produce, and pave an asphalt mixture with US Polyco-modified binder Sigmabond HP on Section S8 of the NCAT Test Track and to compare its performance with that of a control mix with a conventional SBS-modified binder asphalt mixture. The control mix with a PG 76-22 SBS binder was built on Section N7 as part of the Additive Group Study. The design for both sections included a 5.5-inch asphalt layer over a 6-inch aggregate base on top of the existing Test Track subgrade. With this design, bottom-up fatigue cracking was anticipated as the failure mode.

20.3 Overall Experimental Plan

The experimental plan for this study was divided into two phases. Phase I consisted of a laboratory characterization using a dense-graded asphalt mix. The mixture was designed using a Sigmabond HP-modified binder and an SBS-modified binder following a balanced mix design (BMD) approach to evaluate their rutting and cracking resistance. In addition, the mixtures were characterized to conduct theoretical structural pavement analysis to predict pavement performance at the NCAT Test Track. Phase II included the construction and instrumentation of two full-scale test sections, as well as structural and performance evaluation, which comprised applying accelerated traffic, monitoring, and evaluating the performance of the test sections for the duration of the test track cycle. The field performance, in terms of rutting, cracking, and smoothness, was monitored weekly. In addition, laboratory testing was conducted on the production mix sampled during the construction of these test sections to support the field experiment. The next sections summarized the details of the work conducted on each phase and their corresponding outcome.

20.4 Phase I Experimental Plan

Figure 3 presents the experimental plan of the Phase I study. A 12.5 mm nominal maximum aggregate size (NMAS) dense-graded mix design with 20% reclaimed asphalt pavements (RAP) was used for both experimental mixes. Phase I utilized a Balanced Mix Design and advanced mixture characterization for structural analysis to predict and compare the pavement performance of the control and US Polyco test sections. The mixtures were compared in terms of the optimized BMD results using the Hamburg Wheel Tracking Test (HWTT) and IDEAL-CT, and theoretical structural pavement analysis in terms of fatigue performance using dynamic modulus

(E*) and cyclic fatigue as inputs for WESLEA and FlexPave™ programs to predict equivalent pavement fatigue cracking performance and provisional asphalt layer structural coefficients.

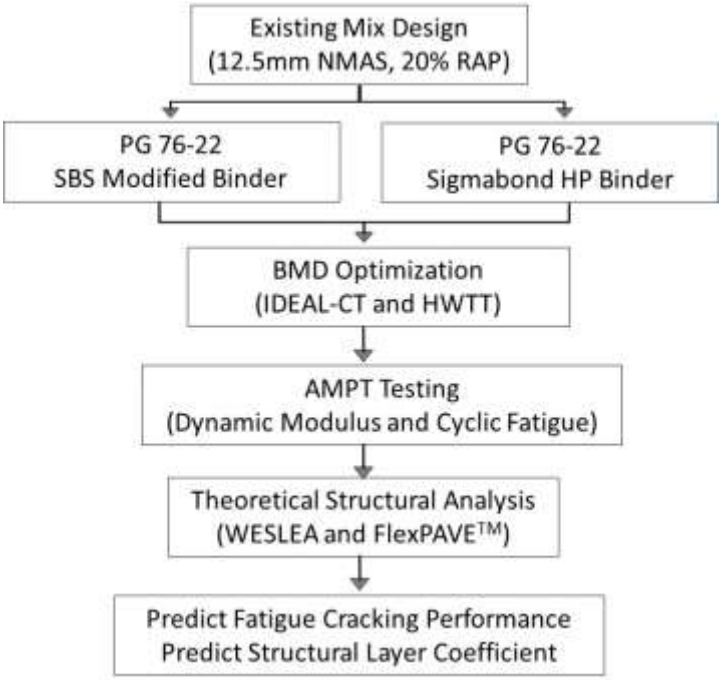

Figure 3. Experimental Plan of Phase I Study

Materials and Mix Design

Table 2 summarizes the binder performance grade results of the PG 76-22 SBS modified binder and the US Polyco Sigmabond HP binder. The Sigmabond HP binder was graded as PG 76-22 with a true grade of PG 77.9-28.9 with an improved Delta T_c (less negative) compared to the PG 76-22 SBS binder.

Table 2. Performance Grade Results

Binder ID	PG 76-22 SBS Modified	Sigmabond HP
Viscosity@135°C (PaS)	1.45	3.88
Original High-temp. Grade	78.1	86.9
RTFO High-temp. Grade	78.9	77.9
Intermediate-temp. Grade	23.9	17.5
Low-temp. Grade (stiffness)	-25.5	-30.6
Low-temp. Grade (m-value)	-23.4	-28.9
PAV Delta T_c	-2.1	-1.6

True Grade	78.1-23.4	77.9-28.9
PG Grade	76-22	76-22

The base asphalt mix design used in the experiment was a 60-gyrations 12.5mm nominal maximum aggregate size (NMAS) dense-graded mix that contained a blend of granite and manufactured sand, 20% reclaimed asphalt pavement (RAP), and 1% baghouse fines. The gradation and aggregate percentages are presented in Table 3. The RAP had a binder content of 5.7% and the extracted RAP binder had a high-temperature PG of 100.9°C. The control mix and Sigmabond HP mix used the same base mix design, varying only the binder utilized.

Table 3. Gradation of the Base Mix Design

Sieve	% Passing
3/4"	100
1/2"	98
3/8"	89
#4	55
#8	41
#16	33
#30	22
#50	12
#100	7
#200	4.5
Aggregate Percentages	
Aggregate type	% of total aggregate
Granite 78's	26
Granite 89's	25
Manufactured sand	28
RAP	20
Baghouse fines	1

20.4.1 BMD Testing

The control mix and Sigmabond HP mix were was optimized to meet the BMD criteria based on IDEAL-CT and HWTT testing. For IDEAL-CT, a cracking tolerance index (CT_{Index}) of 50 was selected for good cracking resistance based on research conducted at the NCAT Test Track *(West et al., 2021).* The IDEAL-CT was conducted by ASTM D8225-19. For HWTT, a maximum rut depth of 12.5 mm at 20,000 passes was set as the criterion for rutting resistance. HWTT was conducted following the AASHTO T 324 standard method at a temperature of 50°C. IDEAL-CT and HWTT samples were tested after short-term oven-aged (STOA) conditioning by AASHTO R 30 consisting of loose mix samples for four hours at 135°C before compaction.

The mix optimization consisted of conducting IDEAL-CT at multiple asphalt contents and selecting the optimum binder content (OBC) that would meet the CT_{Index} criterion. The mixtures were then tested with HWTT at the OBC to ensure adequate rutting resistance, as indicated by their rut depth at 20,000 passes.

20.4.2 AMPT Testing for Structural Evaluation

E* testing was performed following AASHTO TP132-19 using an Asphalt Mixture Performance Tester (AMPT) equipment to characterize the stiffness of the asphalt mixtures. Tests were conducted on STOA mixtures. Specimens were prepared per AASHTO PP99-19 specification. Three replicates for every asphalt mixture that met the air void criteria (7.0 ± 0.5%) were used for testing. Specimens were tested at three temperatures (4, 20, and 35 °C) and three loading frequencies (10, 1, and 0.1 Hz) at each testing temperature. The data collected was used to construct the| E*| master curves for the asphalt mixtures using the time-temperature superposition principle per AASHTO R84-17 at the 20°C reference temperature by using the generalized sigmoidal function as shown in Equation 1.

$$\log|E^*| = \delta + \frac{\alpha}{1 + e^{\beta+\gamma\log(\omega)}} \qquad \text{Equation 1}$$

Where,
E* = dynamic modulus;
α, β, δ, and γ = fitting parameters; and
ω = reduced frequency.

Cyclic Fatigue test was also conducted to evaluate the fatigue damage resistance of the asphalt mixtures using specimens prepared in the same manner as for the E* test discussed above. The Cyclic Fatigue test was conducted following AASHTO TP 133-19. In this evaluation, the test temperature was selected at 21°C based on the climate high-temperature grade requirement of the mix design. The test was conducted with a constant frequency of 10 Hz. The test generates a plot of both specimen modulus and phase angle versus the number of cycles applied, where the phase angle increases until it peaks and then drops off. The fatigue data were analyzed using FlexPAVE™ to determine the damage characteristic curve represented by the relationship between the pseudo-stiffness (C) and the material integrity indicator (S). E* and cyclic fatigue test results were used as inputs to FlexPAVE™ to model the fatigue performance of the pavement structure. Finally, the apparent damage capacity index, S_{app} was calculated using cyclic fatigue test results. This parameter accounts for the effects of the material's toughness and modulus on its resistance to fatigue and is a measure of the amount of fatigue damage a mix can endure under loading (*Castorena et al., 2021*). This index is calculated using Equation 2.

$$S_{app} = 1000^{\frac{\alpha}{2}-1} \frac{a_T^{\frac{1}{\alpha+1}\left(\frac{D^R}{C_{11}}\right)^{\frac{1}{C_{12}}}}}{|E^*|^{\alpha/4}} \qquad \text{Equation 2}$$

Where,

S_{app}=Apparent damage capacity index;
a_T = time-temperature shift factor at a given temperature from E* master curve.
D^R= average reduction in pseudo-stiffness per cycle

20.4.3 WESLEA and FlexPAVE Analysis

Two structural analyses were conducted in this study to determine provisional structural coefficients to assess the structural capacity of the mixtures. The first used layered elastic analysis in WESLEA for Windows (Version 3.0) to determine tensile strain levels at the bottom of the asphalt layer in the cross-section under evaluation. The moduli (E) of these unbound materials were based on representative values obtained through back-calculation of falling weight deflectometer data from previous research cycles at the Test Track (*Taylor and Timm, 2009*). The Poisson ratios were assumed based on typical values for these material types. The moduli of the asphalt layers were based on the E* testing at 20°C and 10Hz. The sections were modeled as 5 inches of AC over 6 inches of granular base to simulate their planned as-built cross-sections at the Test Track. The simulated loadings were based on the single axles of the Test Track vehicles, which weigh approximately 20,000 lb or 5,000 lb per tire with an inflation pressure of approximately 100 psi. After the maximum tensile strain at the bottom of the asphalt layer was computed with WESLEA, the transfer functions generated from AMPT cyclic fatigue testing were used to estimate the number of cycles to bottom-up fatigue cracking (N) for each section.

Following the fatigue life predictions based on a 5.0-in asphalt pavement, additional WESLEA simulations were conducted to determine the thickness required of the US Polyco section to yield approximately the same number of cycles to failure as the control section. These simulations maintain the same material properties of the different layers but vary the asphalt layer thickness of the section. The resulting thicknesses were used to estimate the corresponding structural coefficients for use in the AASHTO 1993 Design Guide of Pavement Structures. This computation assumed a structural coefficient for the asphalt mix in the PG 76-22 control section of 0.54, corresponding to the value currently used for this material by the Alabama Department of Transportation. This value is multiplied by the asphalt layer thickness to obtain a structural number (SN) of 2.7 for the asphalt layer. Since the US Polyco section was designed as structurally equivalent (i.e., SN = 2.7) but with different thicknesses, structural coefficients were determined by dividing 2.7 by the corresponding estimated thicknesses from the WESLEA simulations using Equation 3:

$$a_{1e} = \frac{D_c}{D_e} a_{1c} \qquad \text{Equation 3}$$

Where,

a_{1e} = asphalt structural layer coefficient for the experimental mix.
a_{1c} = asphalt structural layer coefficient for PG 76-22 control mix = 0.54.
D_c = asphalt layer thickness of PG 76-22 control pavement section = 5 inches.

D_e = equivalent layer thickness of additive-modified experimental pavement section.

The second structural analysis was conducted using the FlexPAVE™ program. FlexPAVE™ uses viscoelastic continuum damage theory to account for the effects of loading rate and temperature on the asphalt pavement response and distress mechanisms. The program utilizes three-dimensional finite element analysis with moving loads to compute the mechanical response under various traffic loads. The program relies on the Enhanced Integrated Climatic Model (EICM) to provide representative climatic conditions for pavement response calculations and performance predictions.

The structural analysis with FlexPAVE focused on fatigue cracking assessment because it was the expected distress anticipated for these sections. The inputs used for the FlexPAVE™ analysis were selected to simulate the traffic, climate, and subgrade conditions of the NCAT Test Track and the anticipated pavement structure. The cross sections were identical to the ones used in the WESLEA analysis. A pavement design life of 2 years was utilized (based on the trafficking duration at the NCAT test Track). Design speeds of 45 mph and daily ESAL counts of 13,699 (with no traffic growth) were chosen to estimate the Test Track conditions.

The predicted percentage damage (% damage) at the end of pavement design life was used as the primary analysis parameter to compare the predicted fatigue performance. To obtain the equivalent layer thicknesses and provisional structural coefficients of the US Polyco and control section, iterative FlexPAVE™ simulations were conducted with varying asphalt layer thicknesses. The iteration process was repeated until an equivalent pavement section with approximately equal predicted percent damage in FlexPAVE™ as the pavement section with 5.0 inches of asphalt layer using the PG 76-22 control mix was found. The corresponding asphalt layer thickness of the equivalent pavement section was defined as the equivalent layer thickness. The provisional structural coefficient was then calculated using Equation 3.

20.5 Phase 1 Test Data Analysis and Test Results

20.5.1 BMD Performance Testing

Table 4 summarizes the CT_{Index} results for the Sigmabond HP modified mix compared to the PG 76-22 SBS modified mix at three different binder contents used in the BMD optimization. Based on these results, the OBC of the Sigmabond HP mix was selected as 5.6%, which was the same as the PG 76-22 control mix. Although the performance of the Sigmabond HP mix in terms of CT_{Index} is significantly higher than the control mix at this binder content, it was decided to keep the binder content the same to facilitate the performance comparison of the mixes. Table 5 presents the HWTT results of the two mixes at the OBC of 5.6%. After 20,000 passes, the mixes had a similar rut depth, with only a 0.3 mm difference.

Table 4. Summary of IDEAL-CT CT_{Index} Results

Mix ID	AC%	No. of Samples	CT_{Index}		
			Avg.	St. Dev.	CV%
PG 76-22 SBS Modified	5.1	5	41.6	7.2	17.3
	5.4	4	47.8	6.8	14.2

	5.6	5	54.1	6.2	11.4
	6.0	5	112.3	17.3	15.4
Sigmabond HP	5.1	6	43.0	6.6	15.3
	5.6	6	89.6	20.8	23.3
	6.0	6	136.8	20.7	15.1

Table 5. Summary of HWTT Results

Mix ID	Rut Depth at 20k passes (mm)	Stripping Inflection Point
PG 76-22 SBS Modified	2.5	>20,000
Sigmabond HP	2.2	>20,000

20.5.2 AMPT Results

Table 7 summarizes the average E* results of the PG 76-22 SBS modified, and the Sigmabond HP modified mixtures. As can be seen, the control mix has relatively higher E* values than the Sigmabond HP mix, particularly at the intermediate temperature of 20°C. The difference in E* results tend to decrease at high-temperature low frequency (i.e. 40°C, 0.1Hz).

Table 6. Summary of Average E* Results of the Control and US Polyco Mixtures

Temperature (°C)	Frequency (Hz)	Average E* (ksi)	
		PG 76-22 SBS Modified Mix	US Polyco Sigmabond HP
4	10	1882	1723
4	1	1455	1291
4	0.1	1047	901
20	10	948	760
20	1	575	435
20	0.1	306	227
40	10	238	195
40	1	100	86
40	0.1	45	42

The representative S_{app} results from the Cyclic Fatigue test yielded values of 50.4 and 21.7 for the Sigmabond HP and control mix, respectively. Since a higher Sapp is desired for better fatigue damage resistance, the results suggested that the Sigmabond HP mix had the potential to improve the fatigue damage resistance of the control mix significantly.

20.5.3 Structural Analysis Results

The results of the WESLEA analysis are presented in Figure 4 and Table 7. Figure 4 shows the tensile strain levels at the bottom of the asphalt layers, and the corresponding cyclic fatigue transfer functions and predicted cycles to failure are shown above each section. Table 7 summarizes the predicted asphalt thicknesses to equivalent fatigue lives. These thicknesses translate into a structural coefficient of 0.75 for the US Polyco-modified mixture. As indicated, the predicted performance of the experimental section with respect to the control mixture significantly improved with a percent change in the structural coefficient of approximately 39%.

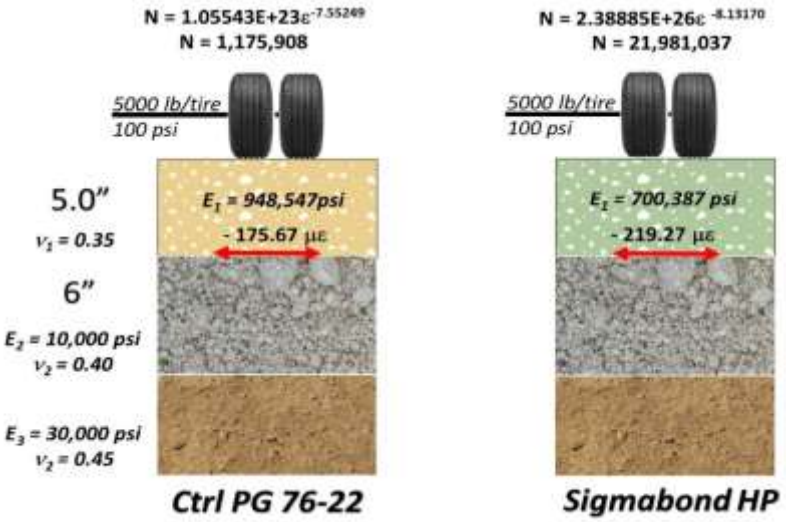

Figure 4. WESLEA Strain and Fatigue Life Predictions at 5 inches Asphalt

Table 7. Summary of WESLEA Analysis Results

Parameter	Control Mix	Sigmabond HP
Equivalent AC Thickness (in)	5.0	3.6
Layer Coefficient	0.54 (assumed)	0.75

The results of the FlexPAVE™ analysis are presented in Table 8. The results compared the predicted % damage evolution for the two mixtures, the equivalent asphalt thicknesses for equivalent lives, and the corresponding layer coefficients. Similar to the results obtained with the WESLEA analysis, the experimental mixtures showed a significant improvement in the predicted fatigue damage, which translated into a reduced equivalent thickness and an increase of 36% in its structural coefficient with respect to the control section.

Table 8. FlexPAVE™ Analysis Results

Parameter	Control Mix	US Polyco Mix
% Damage	30.8	23.4
Equivalent AC (in)	5.0	4.0
Layer Coefficient	0.54 (assumed)	0.68

20.6 Phase 2 Experimental Plan

Phase 2 of this research study included constructing, trafficking, and monitoring its field performance. In addition, the plant mix was sampled to conduct BMD testing to characterize the performance of the field mix.

20.6.1 Construction and Mix Design

Section S8 was constructed on September 28, 2021, while the control section in N7 was constructed on September 3, 2021. In constructing the sections, thick-lift paving was employed to prevent slippage failure between lifts. The target thickness was 5.5-inch. Table 9 provides a summary of the mix design of the US Polyco section and the control section and the results from quality control testing of the mixtures. Although the quality control indicators in this table are comparable for the control and US Polyco sections, it is important to point out that the control section had greater density than the US Polyco section with values of 95.9% and 93.5%, respectively. In addition, the control section was built 0.4 in thicker.

Figure 5 shows mix placement and compaction activities in Section S8. Mixes were placed with no issues reported.

Table 9. Mix Design Information

Mix Design Parameters	S8		N7	
Binder Grade	Sigmabond HP		PG 76-22	
Sieve	Design	QC	Design	QC
19 mm (3/4")	100	100	100	100
12.5 mm (1/2")	98	98	98	97
9.5 mm (3/8")	89	86	89	84
4.75 mm (#4)	55	54	55	54
2.36 mm (#8)	41	40	41	41
1.18 mm (#16)	33	32	33	32
0.60 mm (#30)	22	21	22	20
0.30 mm (#50)	12	12	12	10
0.15 mm (#100)	7	8	7	6
0.075 mm (#200)	4.5	4.7	4.5	4
Total Binder Content (P_b), %	5.6	5.5	5.6	5.7
Eff. Binder Content (P_{be}), %	5.0	4.9	5	5
Dust/Binder Ratio	0.9	1.0	0.9	0.8
RAP Binder Ratio	21	20	21	20
Rice Sp. Gravity (G_{mm})	2.453	2.472	2.453	2.455
Bulk Sp. Gravity (G_{mb})	2.344	2.388	2.344	2.369
Air Voids, %	4.4	3.4	4.4	3.5
VMA	15.8	14.7	15.8	15.1
VFA	72	77	72	77
Mat Density (% G_{mm})	NA	93.5	NA	95.9

As built- thickness (in)	NA	5.3	NA	5.7

Figure 5. S8 Mix Placement and Compaction

20.6.2 Phase II BMD Results

Phase II BMD evaluation was conducted on plant-mixed lab-compacted (PMLC) specimens. The IDEAL-CT test was conducted in accordance with ASTM D8225-19 at 25°C at three aging conditions: production PMLC, re-heated (RH) PMLC, and critically aged (CA) PMLC. The production specimens were compacted during mix production with no reheating, the re-heated (RH) PMLC specimens were prepared by re-heating loose mix that was sampled during production, finally, the critically aged (CA) specimens were compacted from loose mix aged for 8 hours at 135°C to simulate approximately 5 years of field aging at the NCAT Test Track *(Chen et al., 2020*). In general, the average CT_{Index} for the production specimens was greater than that for the re-heated samples while the average CT_{Index} for the re-heated specimens was greater than that of the critically aged specimens. The control mixture had a greater average CT_{Index} value at different aging conditions relative to the US Polyco mix.

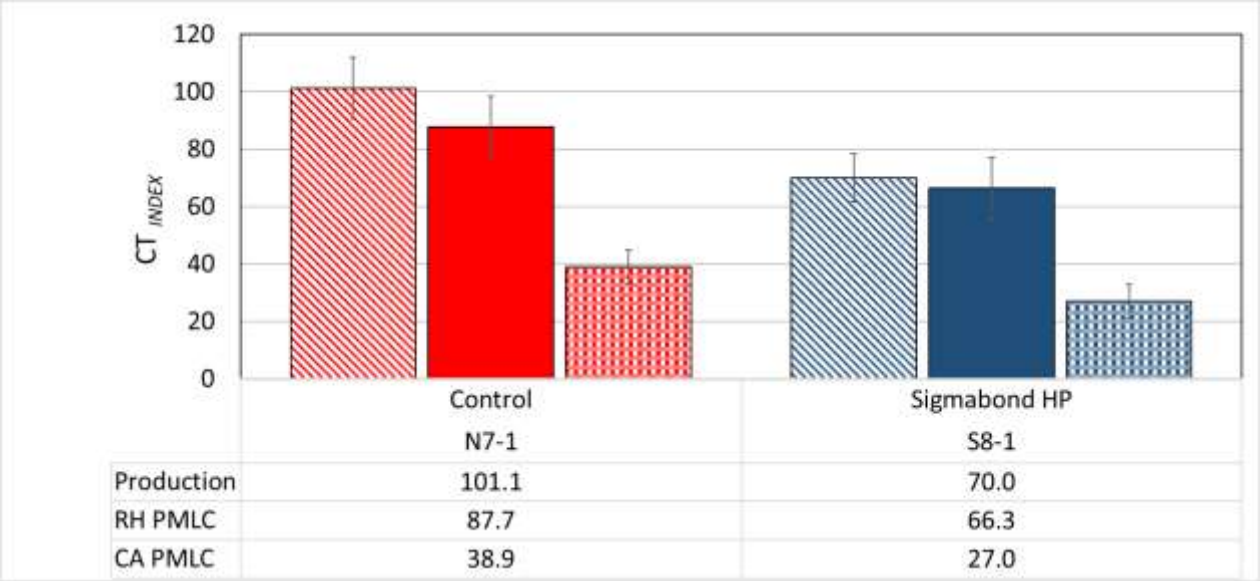

Figure 6. IDEAL-CT Result for Plant-Produced Mix at Different Aging Conditions

Rutting was characterized by HWTT conducted per AASHTO T 324-22, the tests were conducted on PMLC and RH PMLC specimens compacted to 7.0 ± 0.5% air voids. The HWTT was conducted on four specimens per mix (two-wheel tracks with 2 specimens per track). All rutting tests were conducted on specimens conditioned in water at 50°C. The HWTT results are shown in Figure 7. No stripping was observed in the HWTT for both mixes, and all the final test rut depths after 20,000 passes were very low.

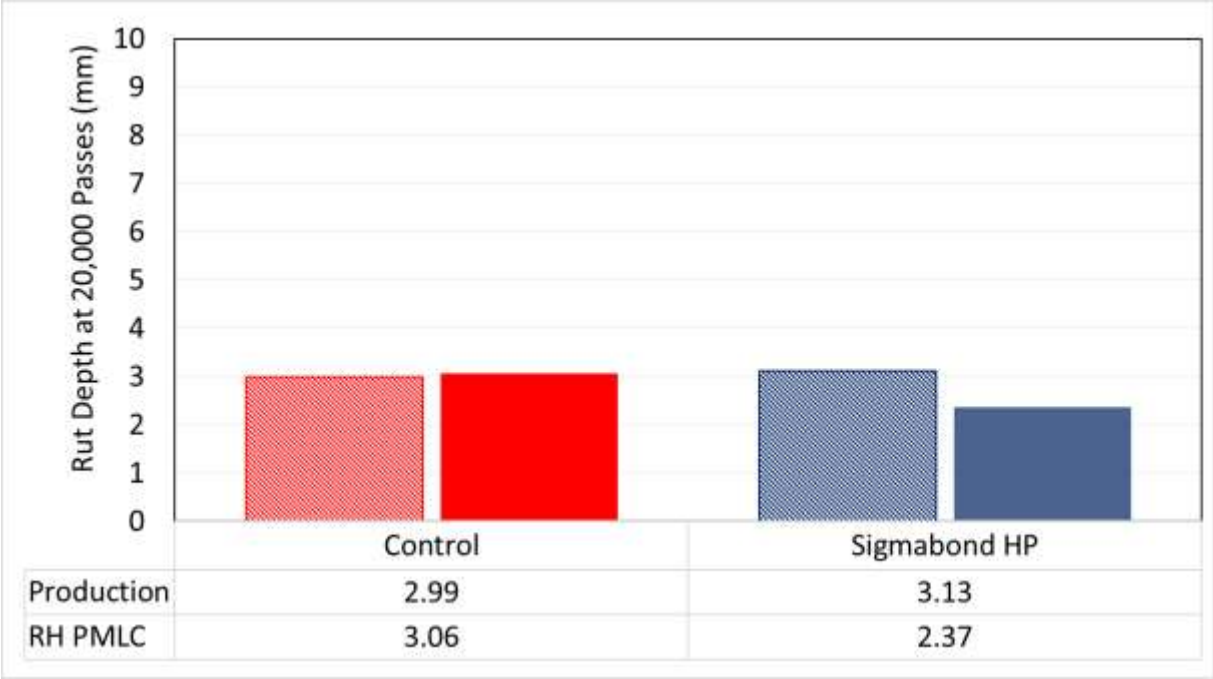

Figure 7. HWTT Result for Plant-Produced Mix at Different Aging Conditions

20.6.3 Phase II Test Track Field Performance

Traffic began on November 10, 2021, for the 2021 research cycle. Once accelerated trafficking began on the experimental sections, surface performance data collection started. Cracking, rutting, and roughness field performance measurements were taken to monitor the sections' performance over time and due to the accelerated traffic. After 1 million ESALs of trafficking (March 2022), isolated cracking was observed in the test section at approximately 35 feet into the section. Cracking continued to progress but was limited to the same area. Figure 8 illustrated the progression of the cracking at approximately 1.2 million ESALs of trafficking.

Figure 8. Cracking in Section S8 at approximately 1.2 million ESALs (April 2022).

A forensic investigation was conducted to investigate the early cracking in the section on June 6, 2022. Cores were extracted in the distressed and non-distressed areas, as presented in Figure 12. As shown in Figure 13 cores from the distressed area indicated cracking initiated at the bottom of the asphalt layer (bottom-up cracking). Limited cores extracted in non-distressed areas showed no signs of cracking.

Figure 9. Cores Extracted in Section S8 in Distress Area (June 2022).

Figure 10. Closeup of Cores Extracted in Section S8 in Distress Area

Binder was extracted from cores from the distressed area for further rheological testing. Table 10 shows the binder results of the original Sigmabond HP binder evaluated in Phase I, as well as the results of the binder extracted from cores. As indicated, the extracted binder was significantly stiffer, with a more negative Delta Tc value than the original binder. In addition to binder rheological testing, US Polyco requested an external laboratory to conduct Fourier Transform Infrared Spectroscopy (FTIR) testing to determine the polymer content of the extracted binder. It was reported that the extracted binder had less than half the intended polymer level

formulated (1.25%). It is important to point out that the US Polyco-modified binder was transported from Texas in a heated tanker, and during production, the binder was directly run off the tanker. It is possible that the first binder offloaded from the trailer (the first portion of the test section paved and area of distress) was around the heating tube and heat damaged, causing binder degradation.

Table 10. Performance Grades of Original Sigmabond HP Binder and Binder Extracted from Cores from Distressed Area

Binder ID	Sigmabond HP	Sigmabond HP Extracted from Cores
Viscosity@135°C (PaS)	3.88	-
Original High-temp. Grade	86.9	-
RTFO High-temp. Grade	77.9	89.1
Intermediate-temp. Grade	17.5	23.1
Low-temp. Grade (stiffness)	-30.6	-28.1
Low-temp. Grade (m-value)	-28.9	-24.4
PAV Delta T_c	-1.6	-3.7
True Grade	77.9-28.9	89.1-24.4
PG Grade	76-28	88-22

The decision was made by US Polyco to partially rebuild the test section's first 70 feet and leave the remaining section in place. Partial reconstruction of the test section took place on October 19, 2022 (Figure 13). For performance monitoring, the first portion of the section (rebuilt) is referred to as section S8A, and the remaining section is S8B.

Figure 11. Partial Reconstruction of Section S8 (October 2022)

20.7 Field Performance

Trafficking of the sections at the track started on November 10, 2021 while trafficking on section S8A started on October 20, 2022, after reconstruction activities took place. At the end of the research cycle, 10 million ESALs were applied to section S8B, and 6.9 million ESALs were applied to section S8A. As indicated in Figure 11, rutting performance for S8A and S8B was comparable to that of the control section, with less than 0.25 rut depth for both sections. IRI results for section S8B were comparable to the control section as indicated in Figure 13. However, IRI results for section S8A were high due to a rough transition from previous section S7. IRI results improved in section S8A after approximately 4 million ESALs of trafficking had been applied as a result of maintenance activities on the transition portion of the section. Similar to the control section, S8A and S8B showed no sign of cracking.

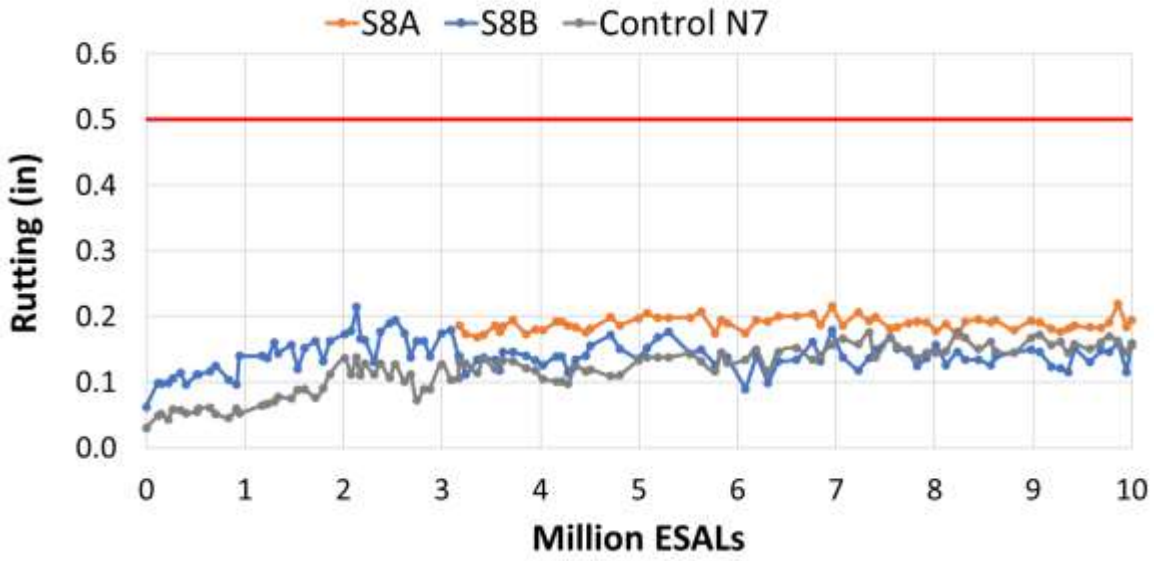

Figure 12. Field Rutting Data-US Polyco Sections on S8A and S8B

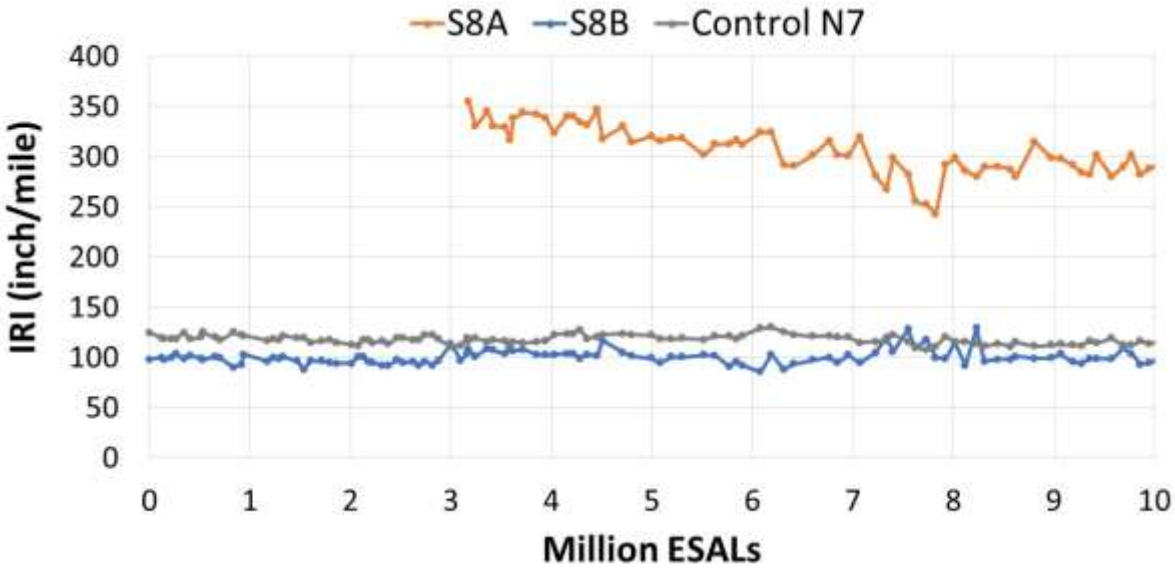

Figure 13. Field Smoothness Data-US Polyco Sections on S8A and S8B

20.8 Findings and Conclusions

This report evaluates US Polyco Sigmabond HP-modified asphalt mixtures compared to conventional SBS-modified mixtures. The study encompassed laboratory testing and full-scale field experiments to assess the performance of these mixtures in terms of fatigue resistance, rutting resistance, and overall structural capacity. The study was conducted in two phases: a laboratory experiment in Phase I and a field performance evaluation at the NCAT Test Track in Phase II. Key findings are summarized as follows:

- The BMD evaluation conducted in Phase I showed that the US Polyco mix significantly exceeded the IDEAL-CT CT_{Index} of the control SBS-modified mix and had comparable rutting performance in the HWTT.
- The structural analyses conducted with WESLEA and FlexPave™ using dynamic modulus and cyclic fatigue test results showed improved structural capacity of the US Polyco mix compared to the control mix.
- As constructed results showed, the US Polyco mix had comparable quality control data as the control mix regarding gradation and AC content, but the control section had a higher in-place density and was built 0.4in thicker.
- Performance test results conducted on plant-mixes showed that the US Polyco mix had lower IDEAL-CT CT_{Index} than the control and had comparable rutting performance in HWTT.
- The US Polyco experimental section experienced isolated cracking at approximately 35 feet into the section, which was attributed to lower than intended polymer content (degradation), possibly as a result of the tanker binder around the tube being heat damaged. Partial reconstruction of approximately 75 feet (section S8A) of the US Polyco section occurred in October 2022.
- At the end of the cycle, after 10 million ESALs, sections S8A and S8B have comparable performance as the control mix with no cracking and comparable rutting. The excellent field performance supported the decision to leave approximately 2/3 of the original section in place for the remaining research cycle.

References

Castorena, C., S. Underwood, Y. R. Kim, K. Lee, N. Tran, and A. Taylor. Ruggedness and Interlaboratory Studies for Asphalt Mixture Performance Tester (AMPT) Cyclic Fatigue Test: Phase I Report. Report No. FHWA-HRT-21-057. May 2021.

Chen, C., Yin, F., Andriescu, A., Moraes, R., Mensching, D., Tran, N., Taylor, A., and West, R. (2020). Preliminary Validation of the Critical Aging Procedure for NCAT top-down cracking experiment. Journal of the Association of Asphalt Paving Technologists, 89, 323-362.

Taylor, A.J. and D.H. Timm. Mechanistic Characterization of Resilient Moduli for Unbound Pavement Layer Materials. Report No. 09-06, National Center for Asphalt Technology, Auburn University, 2009.

West, R., Timm, D., Powell, B., Tran, N., Yin, F., Bowers, B., Rodezno, C., Leiva, F., Vargas, A., Gu, F. and Moraes, R., 2021. Phase VII (2018-2021) NCAT test track findings. NCAT Report, pp.21-03.

21. BASF Evaluation of Hybrid B2Last® Modified Asphalt Pavement

Dr. Nam Tran, Matthew Kmetz, Dr. David Timm

21.1 Background

The long-term durability of asphalt mixtures is essential for extending the life of roadways, thereby contributing to transportation efficiency and safety. Various methods have been explored to enhance the long-term performance of asphalt mixtures, with additives and modifiers showing promising results. Currently, styrene-butadiene-styrene (SBS) is the most used asphalt modifier. As a non-reactive polymer, SBS does not chemically react with asphalt binder. Instead, it forms a polymer network, providing specific performance improvements. While SBS is widely used, it has limitations, especially at higher dosages, including potential polymer separation affecting modified asphalt binder's storage stability and increased viscosity during asphalt processing and application (Becker et al. 2001).

Unlike the SBS polymer, the reactive isocyanate-based modifier chemically reacts with asphalt binder components. When blended with asphalt binder, the highly reactive isocyanate groups (-NCO) of the modifier chemically react with the hydroxyl groups containing active hydrogen atoms (-OH) present in the most polar fractions (i.e., asphaltenes and resins) of asphalt binder to form a polymer (Carrera et al. 2010). This chemical reaction helps overcome the issues of increased viscosity and phase separation encountered with conventional modified asphalt binders, potentially allowing a higher modifier dosage. Moreover, reactive isocyanate-modified asphalt binders show improved adhesive bonds at the asphalt-aggregate interface, potentially reducing moisture susceptibility. The reactive isocyanate-based modifier, known as B2Last® by BASF, can be used by itself or with other modifiers and additives to modify asphalt binders to meet the highest performance grades currently specified by state departments of transportation (DOTs).

Given the limited number of pavements utilizing a reactive isocyanate-based modifier, a study was initiated to construct a test section with a B2Last®-modified mixture on the exit ramp at the NCAT Test Track in 2020 (Tran et al. 2024). The project aimed to demonstrate the constructability of an asphalt mixture modified with the B2Last® modifier in the field and compare its performance with that of a control SBS-modified mixture. The project involved milling an approximately 2-inch thick surface layer of two 100-foot sections with similar foundation support on the exit ramp. One section was resurfaced with a B2Last®-modified mixture and the other with a conventional SBS-modified mix. The two sections were subjected to the truck traffic getting off the Test Track, which was approximately 6,000 equivalent single axle loads (ESALs) per month. In addition, a laboratory testing program was also conducted to test the binders and field cores to assist the field performance monitoring program. The mixtures have shown no significant difference in laboratory performance test results. In addition, after being trafficked for over 160,000 ESALs since May 27, 2020, the two pavement sections have performed well with no cracking, very low rutting (less than 2 mm), no change in roughness after field cores were extracted for laboratory testing, and almost identical macrotexture.

After the successful 2020 experiment on the exit ramp at the NCAT Test Track, a full-scale structural pavement experiment was scheduled for the 2021 NCAT Test Track research cycle. In this experiment, the B2Last® modifier was formulated with a conventional SBS to create a highly modified asphalt binder.

21.2 Objective and Scope

The objective of the full-scale structural experiment on the NCAT Test Track was to determine (a) the contribution of a hybrid B2Last®+SBS modified asphalt mixture to the overall structural capacity to mitigate bottom-up fatigue cracking and structural rutting in the unbound layers and (b) the resistance of the hybrid B2Last®+SBS modified surface asphalt mixture to rutting and top-down cracking under heavy truck traffic.

One structural experiment section was built with the hybrid B2Last®+SBS modified asphalt mixture for field performance evaluation in the 2021 Test Track research cycle. The hybrid B2Last®+SBS pavement section was compared with the control section of the Additive Group (AG) experiment. The control section was constructed with a conventional SBS-modified mixture. The design for both sections included a 5.5-inch asphalt layer over a 6-inch aggregate base on top of the Test Track subgrade. With this design, bottom-up fatigue cracking is anticipated as the failure mode.

The study was conducted in two phases: Phase I consisted of a laboratory experiment using a dense-graded asphalt mix design. The mixture was designed using the hybrid B2Last®+SBS modified binder and an SBS-modified binder, following a balanced mix design (BMD) approach to evaluate resistance to rutting and cracking. Additionally, the mixtures were characterized to gather information for structural analysis to predict pavement performance at the NCAT Test Track.

Phase II involved the construction of the two test sections for field evaluation on the NCAT Test Track. Each section was instrumented with strain gauges, pressure plates, and temperature probes to monitor its structural health and pavement responses throughout the experiment. The field performance in terms of rutting, cracking, smoothness, and texture were surveyed on a weekly basis. In addition, laboratory testing was conducted on the samples of asphalt mixtures taken during the construction of these test sections to assist the field experiment. The following sections describe the results of the study.

21.3 Hybrid B2Last®+SBS Modified Asphalt Binder

The binders used in both sections were modified from a PG 67-22 binder. The control binder was modified with 2.5% linear SBS to attain a performance grade of PG 76-22. The SBS-modified PG 76-22 binder was further modified with the B2Last® modifier at 2.0%, which had been optimized in a prior laboratory experiment, to achieve a performance grade of PG 82-22.

Formulating the hybrid B2Last®+SBS modified PG 82-22 asphalt binder involved several steps. First, the liquid B2Last® material was slowly injected into the liquid SBS-modified PG 76-22 binder, which was heated to 350°F in an asphalt binder tank using a pump at an asphalt terminal. This slow injection was necessary to ensure proper mixing with the asphalt binder. Once the injection was complete, the blend was left to react for 3 to 4 hours at 350°F with

circulation and tank mixers, ensuring adequate mixing. The B2Last® modifier should react to less than 0.01%, and its activity was verified using FT-IR, as shown in Figure 14. After the material had reacted, an asphalt binder sample was taken to verify the performance grade. This modification process can be conducted at an asphalt terminal or an asphalt mixing plant. It can also be used to modify an asphalt binder in the laboratory to develop a formulation, mix design, and laboratory performance testing.

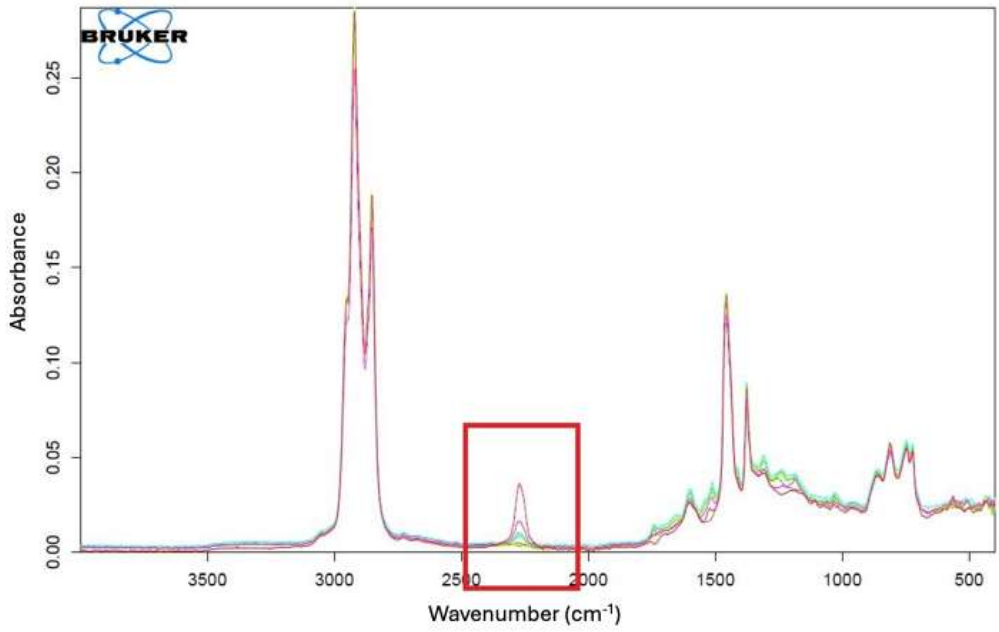

Figure 14. FTIR Verification of B2Last Reactivity

21.4 Phase I Laboratory Experiment

21.4.1 Phase I Experimental Plan

Figure 3 presents the experimental plan of the Phase I study. A 12.5 mm nominal maximum aggregate size (NMAS) dense-graded mix design with 20% reclaimed asphalt pavements (RAP) was used. The design was then modified with a BMD approach to achieve both good rutting and cracking resistance. The BMD approach used was the Performance-Modified Volumetric Design approach per AASHTO PP 105-20, using the Indirect Tensile Asphalt Cracking Test (IDEAL-CT) and Hamburg Wheel Tracking Test (HWTT) for mixture performance evaluation. BMD optimization was conducted on two modified mixes, where the IDEAL-CT and HWTT results were used to select the performance optimum binder content (OBC) of the mixtures. The two polymer-modified mixes were then tested with the Dynamic Modulus (E*) and Cyclic Fatigue tests in an Asphalt Material Performance Tester (AMPT) to determine their stiffness and fatigue resistance characteristics. Finally, theoretical structural analyses were conducted with the anticipated pavement structure of the Additive Group Experiment on the NCAT Test Track to predict the fatigue performance and structural layer coefficients of the two mixes.

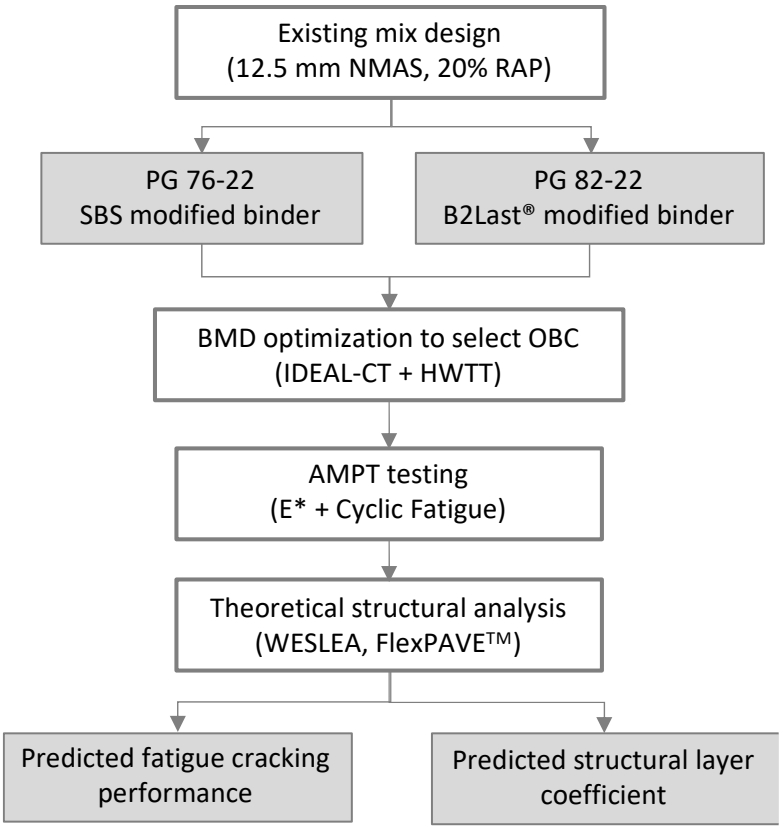

Figure 15. Experimental Plan of the Study

21.4.2 Phase I Materials and BMD Mix Design

The asphalt mixture used in the experiment was based on a 60-gyration 12.5 mm NMAS dense-graded mix design. The mix contained a blend of granite stones, manufactured sand, and 20% RAP. The aggregates were sampled from the East Alabama Paving (EAP) plant in Opelika, Alabama, and the RAP was sampled from the C.W. Matthews plant in Lagrange, Georgia. Baghouse fines were added at 1.0% by weight of aggregate to account for potential aggregate breakdown in production. The RAP had a binder content of 5.7%, and the extracted RAP binder had a high-temperature PG of 100.9°C.

Two asphalt binders were included in the Phase I experiment, including a PG 76-22 SBS modified binder and a PG 82-22 hybrid B2Last®+SBS modified binder. The control PG 76-22 binder was modified with an SBS modifier and a cross-linker. The PG 82-22 hybrid B2Last®+SBS modified binder was formulated by modifying a PG 67-22 binder with 2.5% linear SBS, 2.0% B2Last®, and 0.06% sulfur as crosslinker. Table 11 and Table 12 summarize the PG and Multiple Stress Creep Recovery (MSCR) results, respectively, from the NCAT laboratory. The hybrid B2Last®+SBS modified binder was graded with a true grade of PG 87.0-26.4.

Table 11. Performance Grade Results (AASHTO M320)

Test Properties	PG 76-22 SBS Modified	PG 82-22 Hybrid B2Last®+SBS Modified

Viscosity@135°C (PaS)	1.45	3.84
Original High-temp. Grade (°C)	78.1	87.5
RTFO High-temp. Grade (°C)	78.9	87.0
Intermediate-temp. Grade (°C)	23.9	25.2
Low-temp. Grade (stiffness) (°C)	-25.5	-28.2
Low-temp. Grade (m-value) (°C)	-23.4	-26.4
PAV Delta Tc (°C)	-2.1	-1.8
True Grade (°C)	78.1-23.4	87.0-26.4
Performance Grade (°C)	76-22	82-22

Table 12. MSCR Results at 64°C

Test Properties	PG 64E-22 SBS Modified	PG 64E-22 Hybrid B2Last®+SBS Modified
% Recovery @ 0.1 kPa	70.33	70.46
% Recovery @ 3.2 kPa	69.19	65.60
% Difference, % Recovery	1.62	6.91
J_{nr} @ 0.1 kPa (kPa^{-1})	0.20	0.09
J_{nr} @ 3.2 kPa (kPa^{-1})	0.20	0.10
% Difference, J_{nr} (kPa^{-1})	3.18	15.91

The gradation of the 12.5 mm mix design was developed based on a previous mixture produced at the EAP plant using 20% RAP. The AG mixture design was then optimized to meet the BMD criteria based on the IDEAL-CT per ASTM D8225 and the HWTT per AASHTO T 324. For IDEAL-CT, a cracking tolerance index (CT_{Index}) of 50 was chosen for good cracking resistance based on research conducted at the NCAT Test Track (West et al., 2021). The mix design was initially established with a PG 76-22 SBS modified binder. The performance optimum binder content (OBC) of the mix was 5.6%, with an average CT_{Index} of 54.1 and an average rut depth of 2.5 mm at 20,000 passes with no sign of stripping. IDEAL-CT and HWTT were conducted on short-term specimens aged for 4 hours at 135°C per AASHTO R 30. IDEAL-CT was conducted at 25°C to evaluate intermediate-temperature cracking resistance, while HWTT was conducted at 50°C for rutting evaluation. The gradation and volumetric targets for Phase I, along with the Phase II quality control (QC) values for the plant-produced mixtures, are detailed in Table 13.

Table 13. Phase I Mix Design and Phase II Plant Produced Mixture Quality Control Properties

	N7 SBS Ctrl		S13 B2Last®	
	Target	QC	Target	QC

19 mm (3/4")	100	100	100	100
12.5 mm (1/2")	98	97	98	98
9.5 mm (3/8")	89	84	89	87
4.75 mm (#4)	55	54	55	58
2.36 mm (#8)	41	41	41	44
1.18 mm (#16)	33	32	33	34
0.60 mm (#30)	22	20	22	20
0.30 mm (#50)	12	10	12	10
0.15 mm (#100)	7	6	7	6
0.075 mm (#200)	4.5	4	4.5	3.9
Binder Content (P_b)	5.6	5.7	5.6	5.8
Eff. Binder Content (P_{be})	5	5	5	5.1
Dust-to-Eff. Binder Ratio	0.9	0.8	0.9	0.8
RAP Binder Replacement (%)	21	20	21	19
Rice Gravity (G_{mm})	2.453	2.455	2.453	2.457
Bulk Gravity (G_{mb})	2.344	2.369	2.344	2.347
Air Voids (V_a)	4.4	3.5	4.4	4.5
Aggregate Sp. Gravity (G_{sb})	2.627	2.632	2.627	2.639
VMA (based on G_{sb})	15.8	15.1	15.8	16.2
VFA	72	77	72	72
Avg. Mat Density (% G_{mm})	94.0	95.9	94.0	95.3

21.4.3 Phase I AMPT Testing for Structural Evaluation

Dynamic modulus (E*) testing was conducted using small cylindrical specimens to evaluate the stiffness and viscoelastic characteristics of asphalt mixtures at various temperatures and loading frequencies. The specimens, measuring 38 mm in diameter and 110 mm in height with 7.0 ± 0.5 percent air voids, were prepared as per AASHTO PP 99-19. The testing was performed using an Asphalt Mixture Performance Tester (AMPT) in accordance with AASHTO TP 132-19 at nine temperature-loading frequency combinations, including three temperatures (4, 20, and 40°C) and three loading frequencies (10, 1, and 0.1 Hz).

In addition to the E* test, Cyclic Fatigue testing was conducted to assess the fatigue damage resistance of the asphalt mixtures. This test was also conducted on small-size cylindrical specimens in an AMPT that were prepared in the same manner as for the E* test. The Cyclic Fatigue test was conducted per AASHTO TP 133-19, with testing conducted at a frequency of 10 Hz and a temperature of 21°C, selected based on the climate high-temperature grade requirement of the mix design.

21.4.4 Phase I Analysis to Determine Structural Coefficients

Provisional structural coefficients describing the relative structural capacity of the control SBS modified and hybrid B2Last®+SBS modified mixtures were calculated using two methods. As both methods provided nearly identical results, only the method using FlexPAVE™ percent

damage simulations is presented in this chapter. Additional information about the Phase I analysis of the provisional structural coefficients has been previously published (Timm et al., 2022).

FlexPAVE™ utilizes viscoelastic continuum damage theory to account for the impacts of loading rate and temperature on pavement response and distress mechanisms. It employs three-dimensional finite element analysis with moving loads to evaluate mechanical responses under different traffic loads and incorporates the Enhanced Integrated Climatic Model (EICM) to simulate realistic climatic conditions.

The structural analysis in this study focused on fatigue cracking performance using FlexPAVE™ since it was expected to be the main mode of pavement distress for the experiment at the Test Track. The inputs chosen for the FlexPAVE™ analysis simulated the traffic, climate, and subgrade conditions of the NCAT Test Track and the anticipated pavement structures.

The FlexPAVE™ analysis was conducted for a 2-year design life, with each section modeled as 5.5 inches of AC over 6 inches of granular base to simulate the planned cross-sections. The E* and Cyclic Fatigue FlexMAT™ outputs were used to characterize each asphalt mixture. The moduli of the unbound materials (granular base and subgrade) were derived from the back-calculation of falling weight deflectometer data from previous research cycles at the Test Track (Taylor and Timm, 2009). The loadings were simulated based on the single axles of the Test Track vehicles (18,000 lbs), with a design speed of 45 mph and daily ESAL counts of 13,699.

Simulated percent damage at the pavement design life end was the primary analysis parameter for comparing the fatigue performance of the mixtures tested in Phase I. Iterative FlexPAVE™ simulations with varying asphalt layer thicknesses were conducted to determine equivalent layer thicknesses that had approximately identical simulated percent damage in as the pavement section with 5.5 in of asphalt layer using the PG 76-22 SBS-modified control mixture.

The thicknesses of the layers calculated from the FlexPAVE™ simulations were used to estimate the structural coefficients for the AASHTO 1993 Design Guide of Pavement Structures. The structural coefficient for the asphalt mix in the PG 76-22 control section was assumed to be 0.54, which is the current value used by the Alabama Department of Transportation. Multiplying this value by the asphalt layer thickness of 5.5 inches produced a structural number (SN) of 2.97 for the asphalt layer. Since the other sections were designed to be structurally equivalent (i.e., SN = 2.97) but with different thicknesses, structural coefficients were determined by dividing 2.97 by the corresponding estimated thicknesses from the FlexPAVET™ simulations using Equation 1.

$$a_{1e} = \frac{D_c}{D_e} a_{1c} \qquad \text{Equation 1}$$

Where,

a_{1e} = asphalt structural layer coefficient for the experimental mix.
a_{1c} = asphalt structural layer coefficient for PG 76-22 control mix = 0.54.
D_c = asphalt layer thickness of PG 76-22 control pavement section = 5.5 inches.
D_e = equivalent layer thickness of additive-modified experimental pavement section.

21.4.5 Phase I LMLC BMD Results

In the Phase I laboratory experiment, two mixtures were prepared following the same mix design, with a total asphalt content of 5.6%. The only difference between the mixtures was the virgin binders, each with different base binders and modifiers. Results from the IDEAL-CT and HWTT testing are summarized in Figure 16. The error bars in the IDEAL-CT results represent one standard deviation. The control PG 76-22 SBS mix had an average CT_{Index} of 54.1, while the hybrid B2Last®+SBS mix had an average CT_{Index} of 38.6. Since the IDEAL-CT test was found not sensitive enough to detect differences in cracking resistance provided by polymer modification (Yin et al. 2023a), these IDEAL-CT results should not be used to infer the cracking resistance of these mixtures at the NCAT Test Track. In addition, neither mixture showed any rutting or stripping susceptibility in the HWTT, with a rut depth of 2.5 mm for the PG 76-22 SBS mix and 1.6 mm for the hybrid B2Last®+SBS mix.

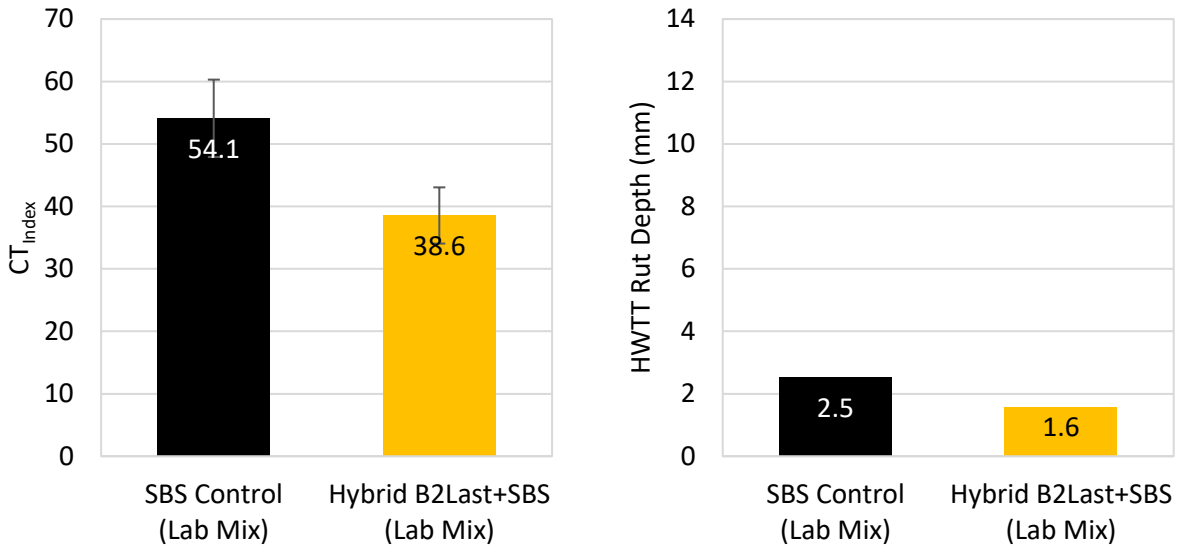

Figure 16. Phase I IDEAL-CT (Left) HWTT Results (Right)

21.4.6 Phase I LMLC AMPT Results

Figure 17 shows the E* master curves for both mixtures on logarithmic and arithmetic scales. The master curves for the two mixtures were similar in the intermediate temperature and frequency range. However, the hybrid B2Last®+SBS modified mixture exhibited a higher E* than the SBS-modified mixture at the high temperature and low loading frequency end (left side) of the master curve. On the other hand, at the low temperature, high loading frequency end (right side) of the master curve, the PG 82-22 B2Last® modified mixture displayed a lower E* than the PG 76-22 SBS modified mixture. This suggests that modification with B2Last® may result in a stiffer mixture that is more resistant to rutting at higher temperatures and less stiff and more flexible at lower temperatures.

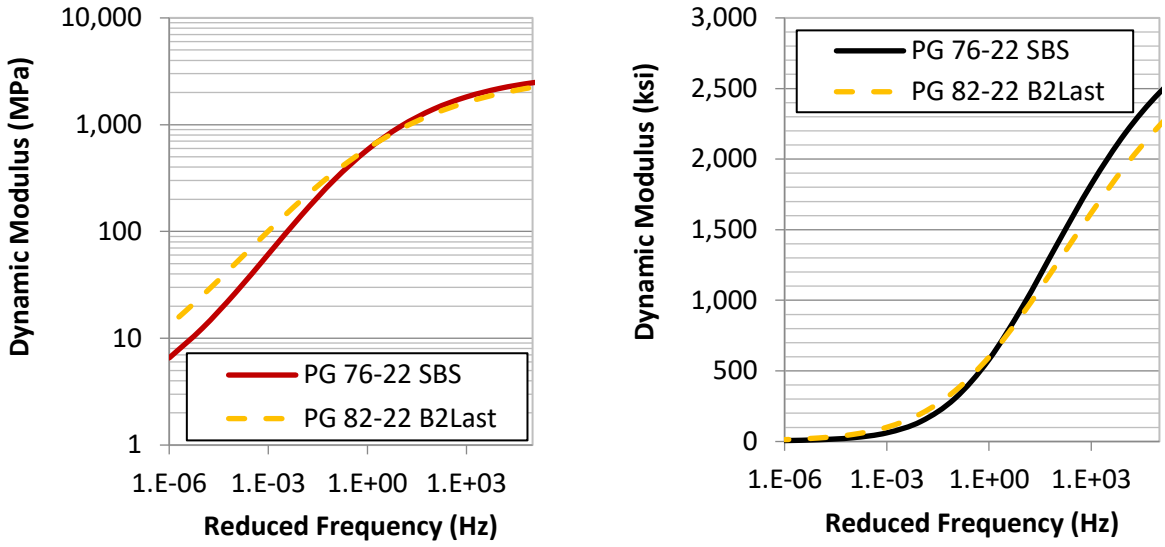

Figure 17. Comparison of E* Master Curves on Logarithmic (left) and Arithmetic (right) Scales

Figure 18 presents the representative S_{app} results and the damage characteristic curves from the Cyclic Fatigue test. Better fatigue damage resistance is indicated by a higher S_{app} and a longer, higher damage characteristic curve. While the control SBS-modified mixture had a higher S_{app}, the hybrid B2Last®+SBS modified mixture showed a longer, higher damage characteristic curve. This suggested that both mixtures would have similar fatigue damage resistance.

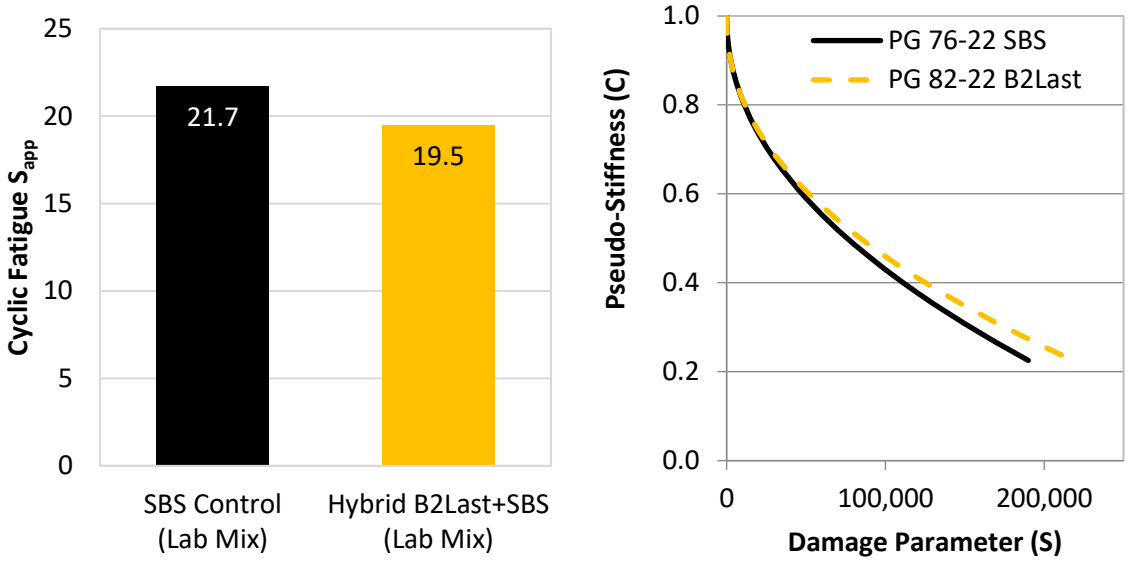

Figure 18. Cyclic Fatigue S_{app} Results (left) and Damage Characteristic Curves (right)

21.4.7 Phase I FlexPAVE™ Analysis

Figure 19 shows the FlexPAVE™ predicted percent damage evolution curves and the structural layer coefficients for two simulated test sections. The analysis demonstrates that the hybrid

B2Last®+SBS modified mixture, when compared to the PG 76-22 SBS modified mix, shows lower predicted fatigue damage over a two-year period with 10 million ESALs. Specifically, the hybrid B2Last®+SBS modified mix section is predicted to have 27% damage, which is approximately 12% lower than the PG 76-22 SBS modified mix section. This suggests that the hybrid B2Last®+SBS modified mix has the potential to enhance the structural pavement capability, allowing for a slightly thinner asphalt pavement structure to maintain the same predicted fatigue cracking performance as the SBS control section. Consequently, it achieves a higher structural layer coefficient of 0.60, compared to the 0.54 coefficient for the SBS control section, while the structural layer coefficient commonly used by state DOTs for asphalt mixture is 0.40 – 0.44.

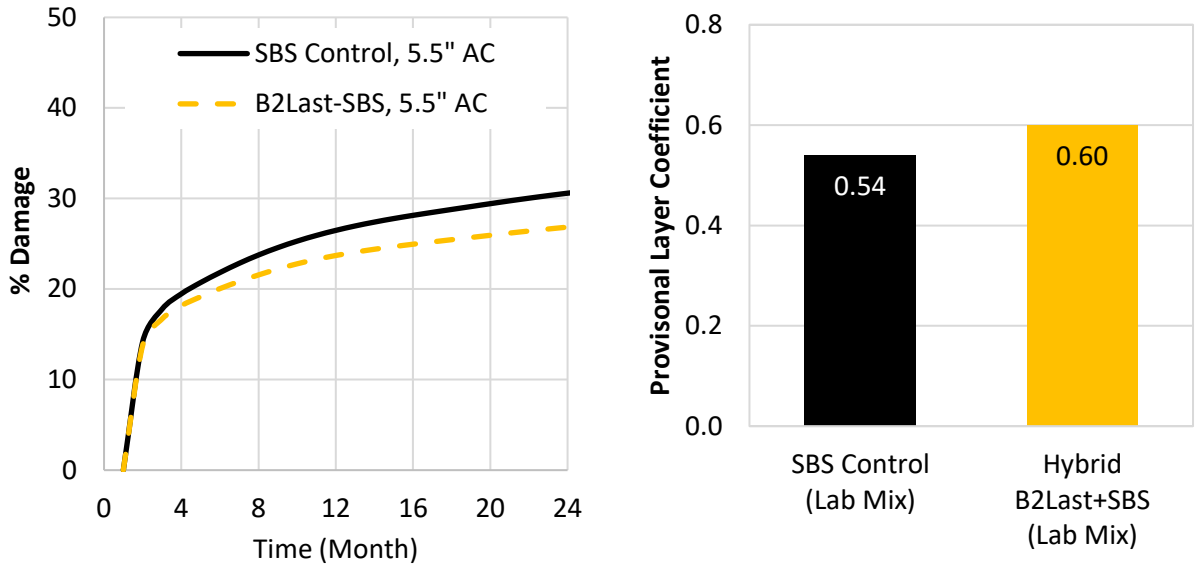

Figure 19. Percent Damage Evolution Curves (left) and Provisional Structural Coefficients (right)

21.5 Phase II Test Track Experimental Plan

Phase II activities included plant production and constructing two full-scale, instrumented test sections. These test sections were then subjected to accelerated traffic application, and their structural and performance characteristics were evaluated weekly. Samples of plant mixtures were collected during construction for a comprehensive laboratory program to support the field evaluation. The following sections provide more information about the Phase II Test Track experimental plan.

21.5.1 Mixture Production and Construction of Test Sections

In Phase II, two 200-foot test sections were built for the two mixtures at the NCAT Test Track. The control SBS-modified mixture was laid in Section N7 on September 3, 2021, while the hybrid B2Last®+SBS modified mixture was placed in Section S13 on September 17, 2021. The production temperature at the plant was approximately 330°F for both mixtures.

Table 13 presents a summary of the mix design for each mixture, along with the results from their quality control testing. The variations observed in Table 13 were deemed to be within the acceptable tolerance for standard construction practices. In-place densities were checked using a nuclear density gauge set in backscatter mode at four random locations and at three offsets (inside, between, and outside the wheelpath). Three field cores were then extracted from the end transition zone of the section to calibrate the density gauge. The resulting average compaction values for the section are also shown in Table 13. Both sections exhibited good, similar densities, with the control SBS modified section recording a density of 95.9% and the hybrid B2Last®+SBS modified section recording a density of 95.3%.

The sections were designed and constructed as 5.5-inch thick-lift pavements. This means the asphalt layer was paved in one lift for both sections to prevent potential slippage failure between lifts. This thick-lift paving was crucial to the design of these sections because the intended mode of failure was bottom-up fatigue cracking. Both mixtures were placed using conventional equipment. Despite its advantages, the thick-lift paving makes it challenging to achieve the required smoothness. Therefore, precision grinding was carried out after paving the two test sections to improve the smoothness and Mean Roughness Index (MRI) of the test sections. Precision grinding has been used in South Carolina and at the Test Track in previous cycles.

Figure 20 shows the as-built cross-sections for both mixtures. The thickness of the control SBS-modified layer deviated from the design thickness of 5.50 inches, which was anticipated due to construction variability and the use of the thick-lift paving method. To ensure a fair comparison of the sections and their respective strain responses, a normalization process was utilized, and this process is described later in this chapter.

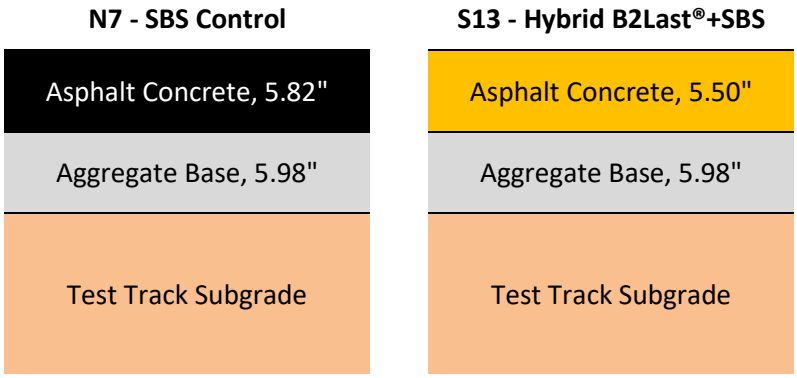

Figure 20. As-Built Cross Sections

21.5.2 Instrumentation of Test Sections

The test sections were instrumented with asphalt strain gauges (ASGs), earth pressure cells (EPCs), and thermocouple temperature probes to monitor the pavement's response to traffic and the environment. ASGs measure the horizontal strain response of the pavement, EPCs measure the vertical pressure that the pavement experiences and thermocouple temperature probes measure the temperature of the pavement. The installation process and instrumentation scheme were in line with previous NCAT Test Track construction cycles. In each

section, twelve ASGs were positioned at the bottom of the asphalt concrete layer. An EPC was placed at the top of the granular base (GB) layer, with another EPC at the top of the subgrade soil to measure the structural response of the pavement sections. A set of thermocouple temperature probes was also installed to measure temperatures at the top, middle, and bottom of the AC layer, as well as 3 inches into the GB layer. These probes were embedded into the sections to capture the temperature gradient through the depth of the pavement.

21.5.3 Test Section Performance Monitoring

Trafficking of the eighth Test Track research cycle began on November 10th, 2021, and concluded on April 5, 2024. During this period, performance data for each test section were collected on a weekly basis, including lane-area and wheelpath cracking percentages, average rut depth, and ride quality (MRI). In addition, falling weight deflectometer (FWD) testing was performed several times monthly to monitor the in-situ moduli of the subgrade, base, and asphalt concrete layers. These performance data collection procedures were consistent with previous research efforts at the NCAT Test Track. Further details regarding mix production, mix sampling, laboratory test specimen production, instrumentation, and data collection procedures can be found in publications by Foshee (2022) and Kmetz (2023).

21.6 Phase II Laboratory Testing Program

21.6.1 Plant-Mixed Lab-Compacted (PMLC) BMD Results

The IDEAL-CT test was conducted on the two mixes following ASTM D8225-19 on specimens conditioned at 25°C, consistent with the BMD testing performed in Phase I. Figure 21 summarizes the IDEAL-CT test results for the two plant-produced mixes at three aging conditions: production PMLC, re-heated (RH) PMLC, and critically aged (CA) PMLC. The production specimens were compacted while the mix was being produced and paved at the Track without re-heating after production. The RH PMLC specimens were prepared by re-heating the 5-gallon buckets of loose mix that were sampled during paving. The critically aged (CA) specimens were compacted from loose mix aged for 8 hours at 135°C, simulating slightly over 5 years of surface field aging at the NCAT Test Track (Chen et al., 2020; Yin et al., 2023b). Each data set represents a minimum of four replicates, and all specimens were compacted to 7.0 ± 0.5 percent air voids at a height of 62 mm in the Superpave Gyratory Compactor (SGC).

In general, the average CT Index for the production specimens was higher than that for the re-heated samples, which was, in turn, greater than that of the critically aged specimens. The hybrid B2Last®+SBS modified mixtures displayed lower average CT index values relative to the control SBS-modified mixture at each of the three aging conditions. It is important to note that these IDEAL-CT results should not be used to conclude that one mixture would have better field cracking performance than the other because the IDEAL-CT test was found to be not sensitive enough to detect differences in cracking resistance provided by polymer modification (Yin et al., 2023a).

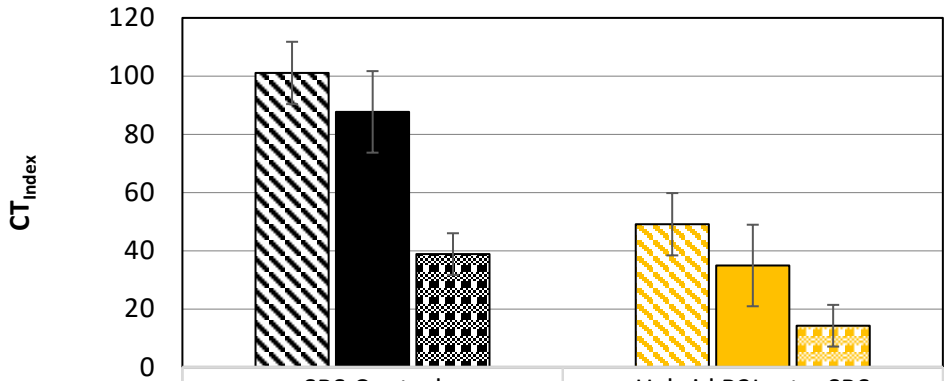

	SBS Control N7-1	Hybrid B2Last + SBS S13-1
Production	101.1	49.2
RH PMLC	87.7	35.0
CA PMLC	38.9	14.3

Figure 21. IDEAL-CT Results for PMLC Mixtures at Multiple Aging Conditions

Rutting resistance of the two mixtures was assessed by the Hamburg Wheel-Tracking Test (HWTT) conducted per AASHTO T 324-22, the high-temperature indirect tension test (HT-IDT) per ALDOT 458, and the IDEAL-RT test per ASTM D8360-22. The HT-IDT and IDEAL-RT tests are evaluated as quicker alternatives to the longer HWTT during mix production. The tests were conducted on re-heated plant-produced mix (RH PMLC) specimens compacted to 7.0 ± 0.5 percent air voids. The HWTT was conducted on four specimens per mix (two wheel-tracks with two specimens per track), while the HT-IDT and IDEAL-RT were each conducted on three replicate specimens. All three rutting tests were conducted on specimens conditioned in water at 50°C.

The RH PMLC HWTT results for the additive group experiment are shown in Figure 22. No stripping was observed in the HWTT for either mixture. The final rut depths after 20,000 passes were 3.06 mm for the control SBS-modified mixture and 1.45 mm for the hybrid B2Last®+SBS modified mixture. These final rut depths are much lower than the common failure criterion in the HWTT for polymer-modified mixes, which is less than 12.5 mm rut depth after 20,000 passes (NAPA, 2024), with the hybrid B2Last®+SBS mixture having better resistance to rutting.

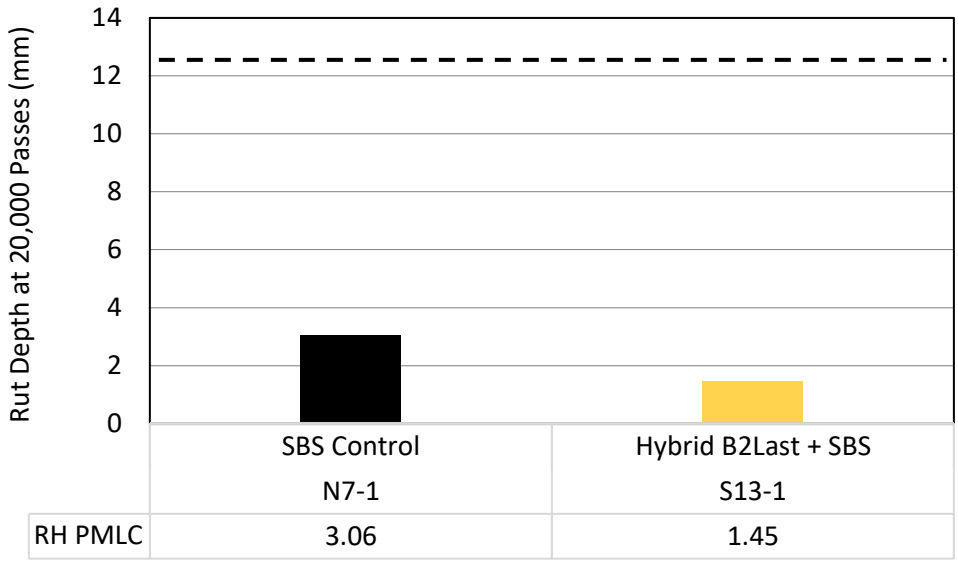

Figure 22. HWTT Results for PMLC RH Mixtures

The RH PMLC HT-IDT and IDEAL-RT results for the additive group experiment are shown in Figure 23 and Figure 24, respectively. For the HT-IDT test, ALDOT recommends a minimum ITS of 20 psi for their BMD special provision for local roads (NAPA, 2024). For the IDEAL-RT, Zhou et al. (2021) recommend a preliminary minimum RT_{Index} of 75 for mixtures with a PG 76-XX base binder or higher. Both mixtures exceeded these recommended preliminary criteria. The hybrid B2Last®+SBS mixture showed higher ITS and RT_{Index}, suggesting better rutting resistance.

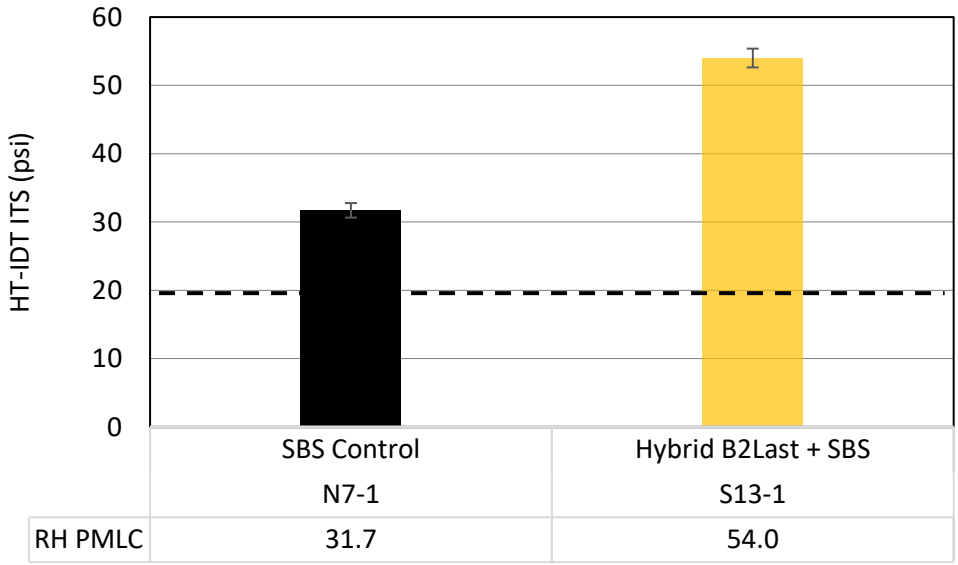

Figure 23. HT-IDT Results for PMLC RH Mixtures

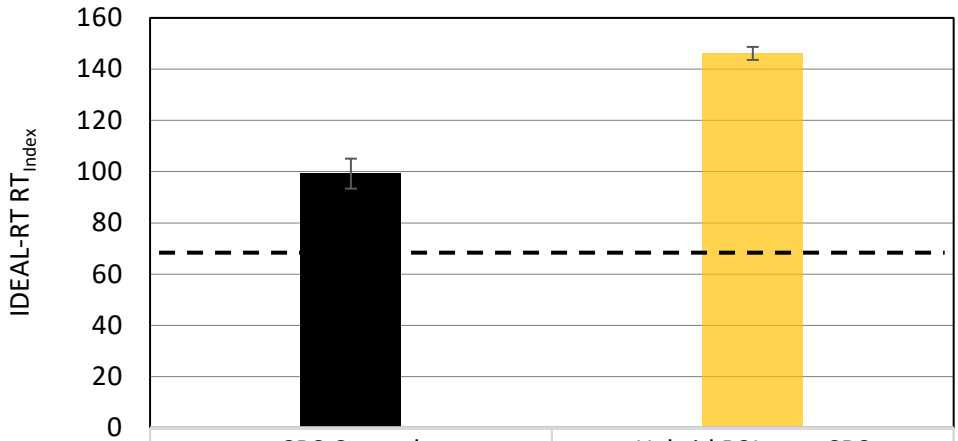

Figure 24. IDEAL-RT Results for PMLC RH Mixtures

21.6.2 PMLC Dynamic Modulus (E) Results*

As for the Phase I study, the E* test was conducted in Phase II following AASHTO TP 132-19, and E* master curves were developed for each mixture using Master Solver for Excel© Version 2.3 according to AASHTO R 84. Testing was conducted with three replicates at temperatures of 4, 20, and 40°C and loading frequencies of 0.1, 1, and 10 Hz. The E* master curve for each mixture was established at a reference temperature of 20°C.

Figure 25 compares the E* master curves developed for the two mixtures. Similar to the E* test results shown in Figure 3, the hybrid B2Last®+SBS modified mixture showed a higher E* than the SBS-modified mixture at high temperatures and low loading frequencies (left side of the master curve). Conversely, at low temperatures and high loading frequencies (right side of the master curve), the PG 82-22 B2Last® modified mixture exhibited a lower E* than the PG 76-22 SBS modified mixture. This indicates that the B2Last® modification may produce a stiffer mixture that is more resistant to rutting at higher temperatures while being less stiff and more flexible at lower temperatures.

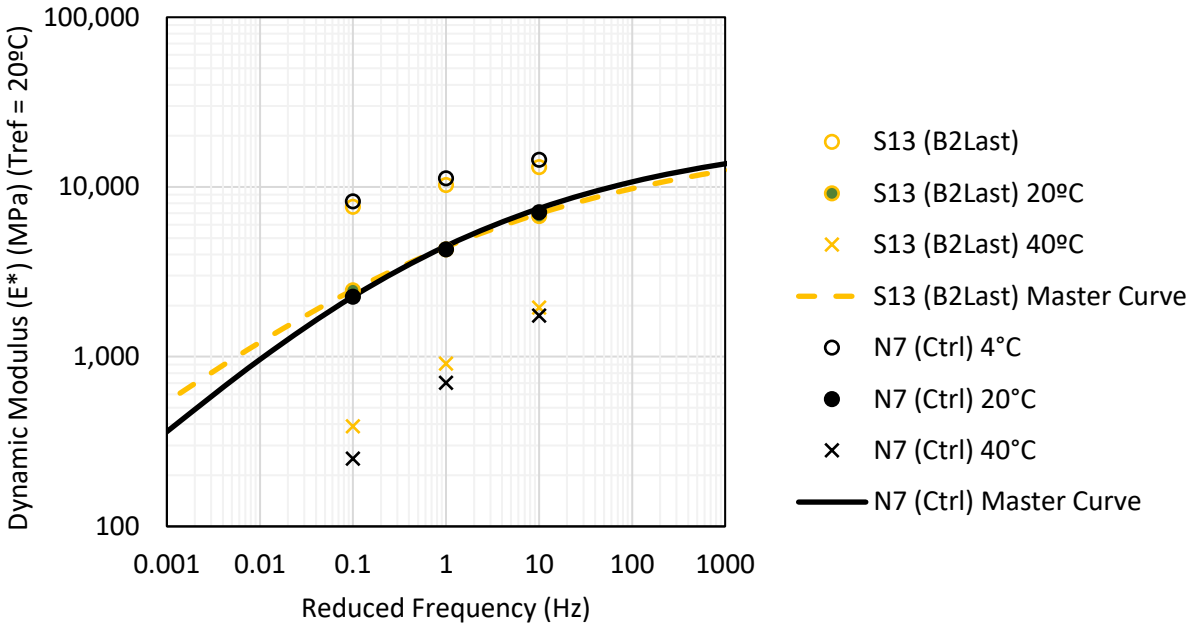

Figure 25. Comparison of E* Master Curves

21.6.3 PMLC Direct Tension Cyclic Fatigue Results

The direct tension cyclic fatigue test was conducted in accordance with AASHTO TP 133-22. All tests were performed at a temperature of 21°C. Initial strain values varied between 450 and 550 microstrain, depending on the stiffness of each mixture. An IPC Global© AMPT Pro was used for testing, and FlexMAT^{TM} Cracking v2.1.1 was used for data processing and analysis. For each mixture, a fitted pseudo stiffness (C) versus damage (S) curve, or "damage characteristic curve", was developed from three or more successful test replicates. Fitted D^R failure criterion values and S_{app} parameters were then calculated for each mixture. S_{app} accounts for the effects of a material's modulus and toughness on its fatigue resistance and is a measure of the amount of fatigue damage the material can tolerate under loading. Higher S_{app} values indicate better fatigue resistance of the mixture.

Figure 26 shows the representative S_{app} parameters for each mixture and the preliminary national thresholds for S_{app} parameters. The preliminary national thresholds categorize mixtures with S_{app} parameters between 8 and 24 as standard (< 10 million ESALs), between 24 and 30 as heavy (between 10 and 30 million ESALs), between 30 and 36 as very heavy (> 30 million ESALs), and greater than 36 as extremely heavy (greater than 30 million ESALs and slow traffic) (FHWA 2019). Both mixtures had similar S_{app} parameters and were in the same heavy traffic category (between 10 and 30 million ESALs). This suggests that the two mixtures would have similar resistance to fatigue cracking.

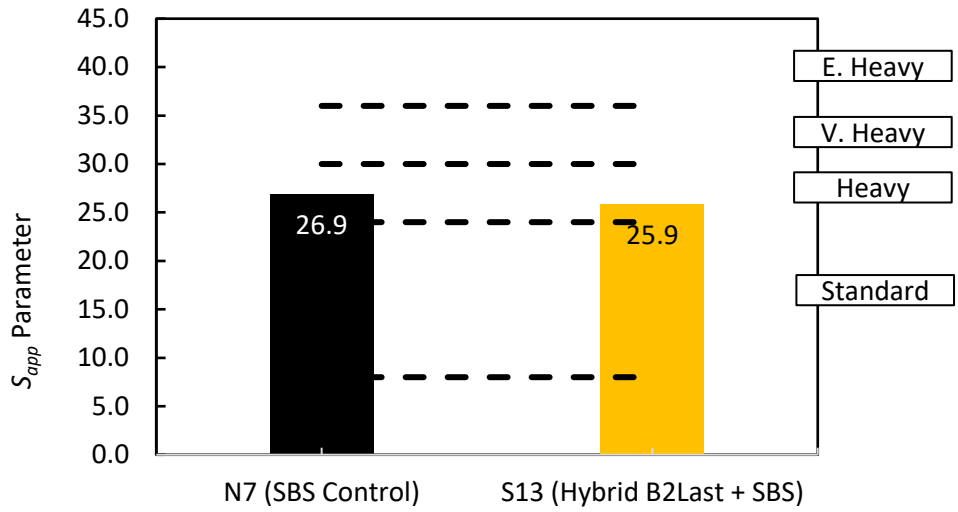

Figure 26. Representative S_{app} Parameters

21.6.4 PMLC Bending Beam Fatigue Results

The bending beam fatigue test (BBFT) was performed in accordance with AASHTO T321-22. An IPC Global© BBFT machine was used for testing. Beam fatigue specimens were tested in a controlled strain configuration at a temperature of 68°F, with a loading frequency of 10 Hz. For each mixture, three strain levels (400, 600, and 800 με) were tested, with three test replicates performed at each strain level. The BBFT data monitoring and recording software produced a raw Excel© output that included the loading cycle, maximum peak-to-peak tensile stress, maximum peak-to-peak tensile strain, specimen flexural stiffness, and flexural stiffness x cycles. This output was used to evaluate the fatigue life and initial stiffness of each mixture. The fatigue failure point was defined as the cycle at which the stiffness times cycles curve reached its peak value.

Fatigue life transfer functions describing the relationship between the applied flexural strain level and the number of cycles to failure (N_f) were developed for each mixture. Figure 27 shows N_f versus strain for the two mixtures with the fitted power regression functions for each mixture in the form of Equation 2.

$$N_f = k_1 \frac{1}{\epsilon}^{k_2} \qquad \text{Equation 2}$$

Where,

N_f = number of cycles to failure
ε = flexural strain
k1 = fitting coefficient 1
k2 = fitting coefficient 2

An ANOVA and subsequent Tukey-Kramer analysis were performed to determine the statistical difference in average N_f values at each strain level, using a significance level of 0.05. The average N_f values of the hybrid B2Last®+SBS mixture did not exhibit statistically significant

differences when compared to the control SBS-modified mixture at all flexural strain levels. This similarity is also reflected in the transfer functions of these mixtures, as they closely resemble each other. These results align with the findings of the cyclic fatigue test, indicating that the two mixtures are likely to have similar resistance to fatigue cracking.

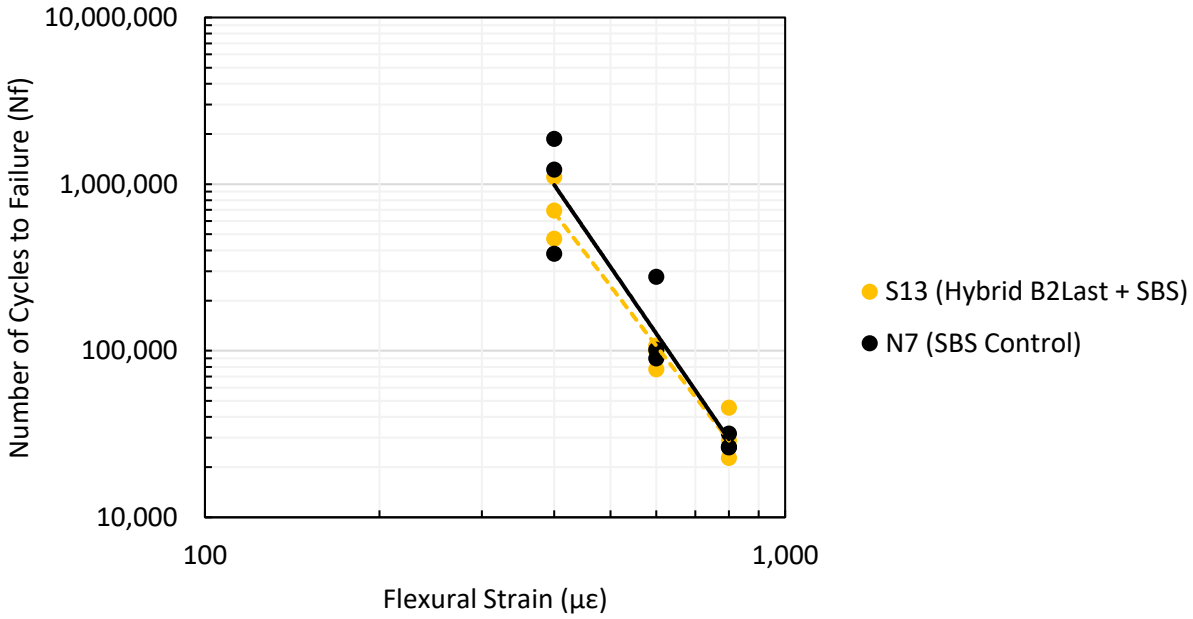

Figure 27. Bending Beam Fatigue Test Results

21.7 Phase II Test Track Performance Data

Performance data, including rut depth, cracking percentage, and ride quality, were collected using a Pathway van for both test sections at the NCAT Test Track. Figure 28 illustrates the ride quality, measured by MRI, in relation to traffic loads for both test sections after around 10 million ESALs (MESALs). It is often not possible to compare the MRI values between the test sections due to variations resulting from short sections, thick-lift paving, and surface grinding processes. Instead, the comparison should be based on changes in MRI over time or with traffic. After 10 million ESALs, no significant changes in MRI were observed for either test section, indicating good ride quality performance.

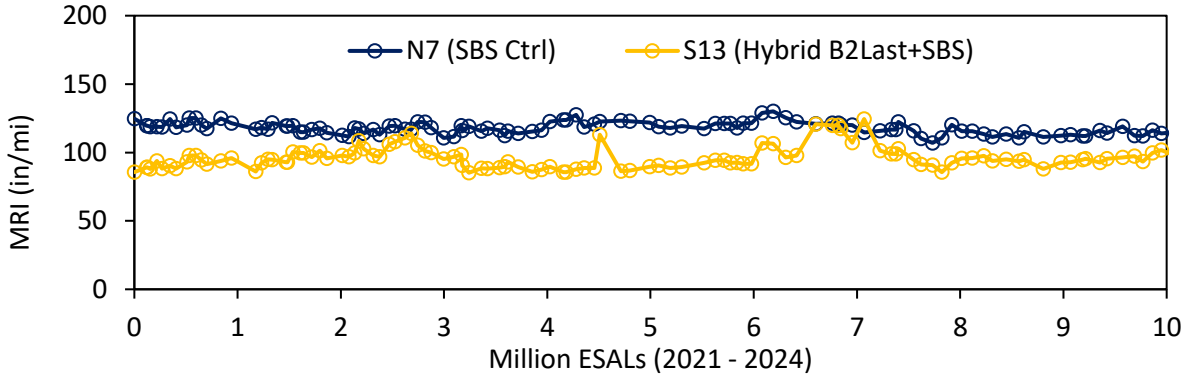

Figure 28. International Roughness Index (MRI)

Figure 29 shows the relationship between average rut depth and traffic for both test sections after approximately 10 MESALs. As anticipated, there has been a slight increase in the average rut depth in each test section due to ongoing traffic. Both test sections show a similar amount of rutting. Notably, the observed level of rutting is well below the failure threshold of 0.50 inches or 12.5 mm, suggesting that both mixtures have exhibited good field rutting performance.

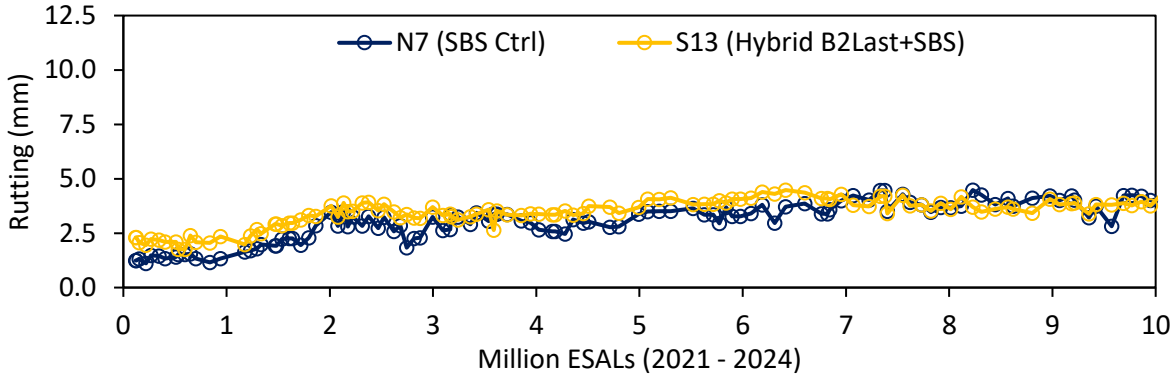

Figure 29. Average Rut Depth

Figure 30 shows the percentage of cracking across the entire lane area for each test section in relation to traffic (MESALs). No cracks were found in Section N7 (SBS Control), but cracking was first observed in Section S13 (hybrid B2Last®+SBS) at 8.31 million ESALs in November 2023. The cracks continued to grow, covering approximately 6.1% of the lane area and 7.2% of the wheelpath area at the end of the research cycle in April 2024. Cores extracted from Section S13 showed that cracking had developed through the full depth of the asphalt layer.

The occurrence of cracking in Section S13 was unexpected, given that the test results from E*, cyclic fatigue, and BBF suggested the cracking resistance of the hybrid B2Last®+SBS mixture should be similar to that of the control SBS mixture at the NCAT Test Track. Consequently, an analysis of the strain and FWD data was conducted to identify the cause of the cracking, as detailed in the following section.

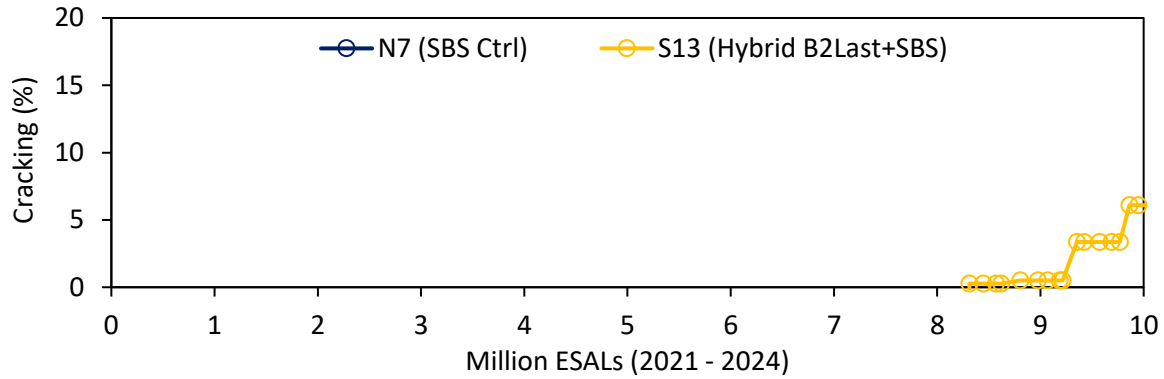

Figure 30. Percentage Lane Area Cracking

21.8 Cause of Cracking in Section S13 (Hybrid B2Last®+SBS)

Both sections were instrumented with asphalt strain gauges (ASGs), earth pressure cells (EPCs), and thermocouple temperature probes to measure and analyze their structural responses. In addition, FWD testing was conducted in the inside and outside wheelpaths, as well as between the wheelpaths, at four random stations within each test section. The FWD test results were then used to back-calculate the moduli of the asphalt concrete (E_{AC}), granular base (E_{GB}), and subgrade ($E_{Subgrade}$) layers. The measured strains and back-calculated moduli were analyzed to determine the cause of the observed cracking in Section S13 (hybrid B2Last®+SBS).

Given that asphalt mixtures can develop cracks due to high tensile strains, the strain data from the ASGs embedded at the bottom of the asphalt layer were first analyzed. Figure 31 shows the measured strains corrected for different thicknesses in Section N7 (SBS Control) and Section S13. To show seasonal variations, the measured strain data were not corrected for temperature. Section S13 experienced higher strains, particularly from March through September. These higher strains may have contributed to the cracking observed in Section S13.

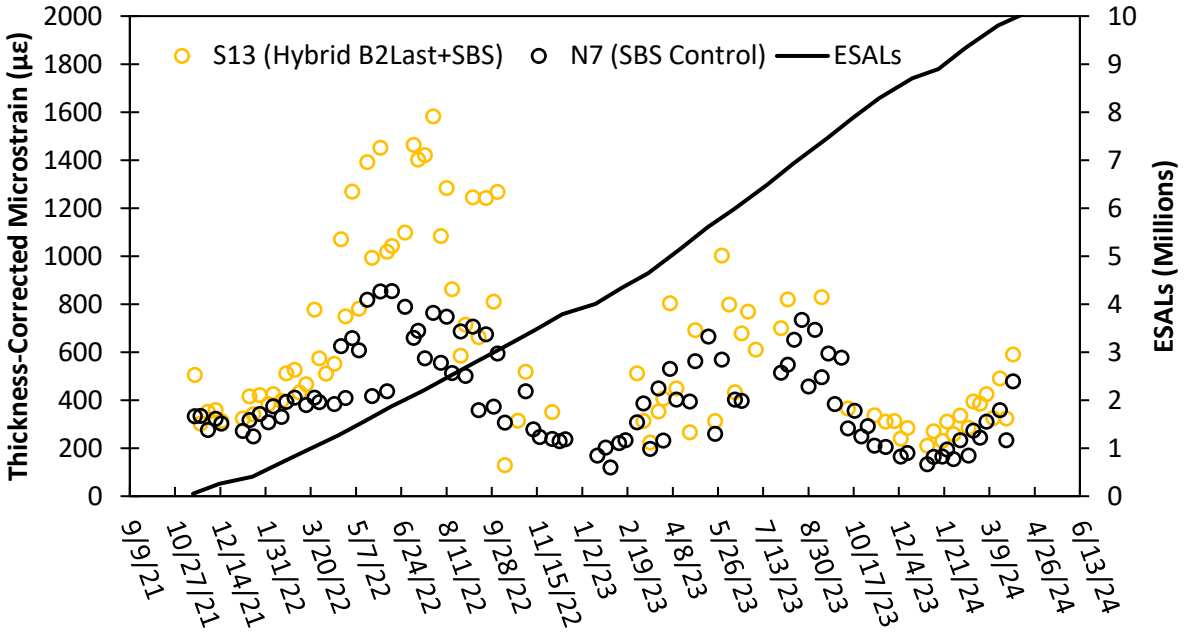

Figure 31. Thickness-Corrected Measured Strains

The back-calculated moduli of the asphalt concrete, granular base, and subgrade layers were then analyzed to determine what led to the high strains at the bottom of the asphalt layer. Figure 32 shows the back-calculated moduli of the asphalt mixture without temperature correction to show seasonal variations. The seasonal high and low moduli shown in Figure 32 correspond to the seasonal low and high measured strains shown in Figure 31. However, as shown in Figure 32, the back-calculated moduli of the two mixtures are similar, and this observation is supported by the E* test results shown in Figure 25. These similar AC moduli should not result in higher strains in Section S13 than in Section N7, as shown in Figure 31.

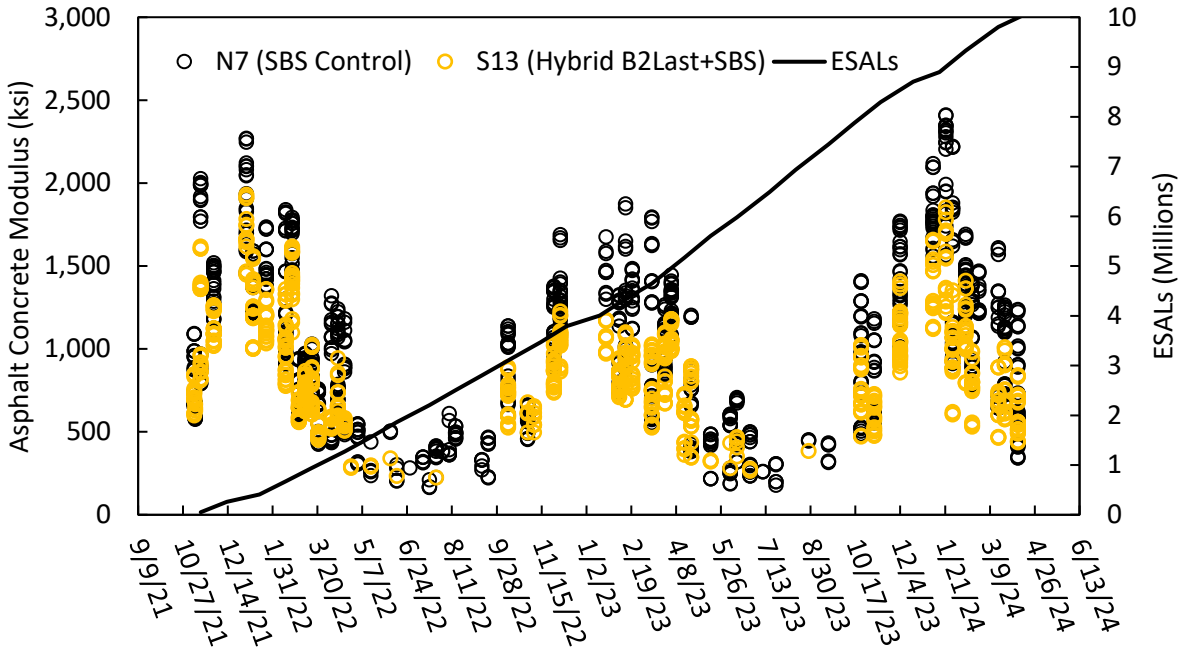

Figure 32. Back-calculated Moduli of Asphalt Concrete

The next step of the analysis involved comparing the back-calculated moduli for the granular base and subgrade layers in the two test sections, as shown in Figure 33 and Figure 34. In both figures, the back-calculated moduli for the granular base and subgrade layers were significantly lower in Section S13 than in Section N7, particularly from March through September. These lower moduli of the base and subgrade layers in Section S13 may have contributed to the higher strains observed in this section. The lower back-calculated moduli of the base and subgrade layers in Section S13 may result from water intrusion through the cold joints around the longitudinal and transverse edges of this section. Water drains slower after rain in Section 13 as it is in the level transition from the south tangent normal crown to the east curve superelevation, increasing the potential for infiltration through the joints.

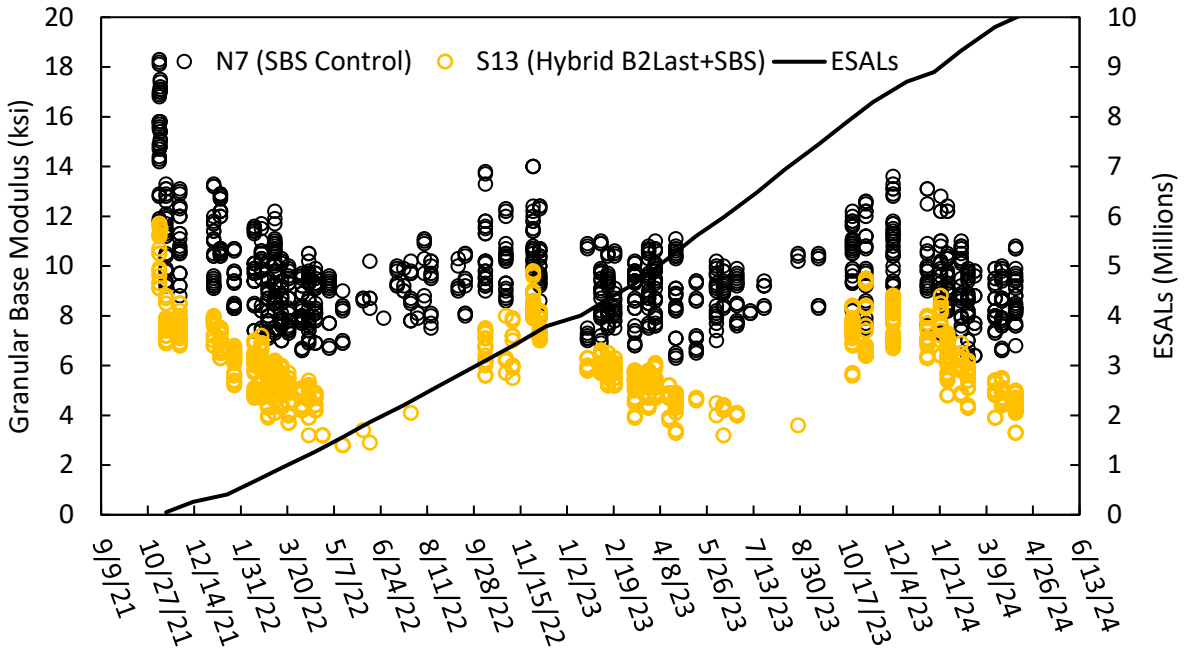

Figure 33. Backcalculated Moduli of Granular Base

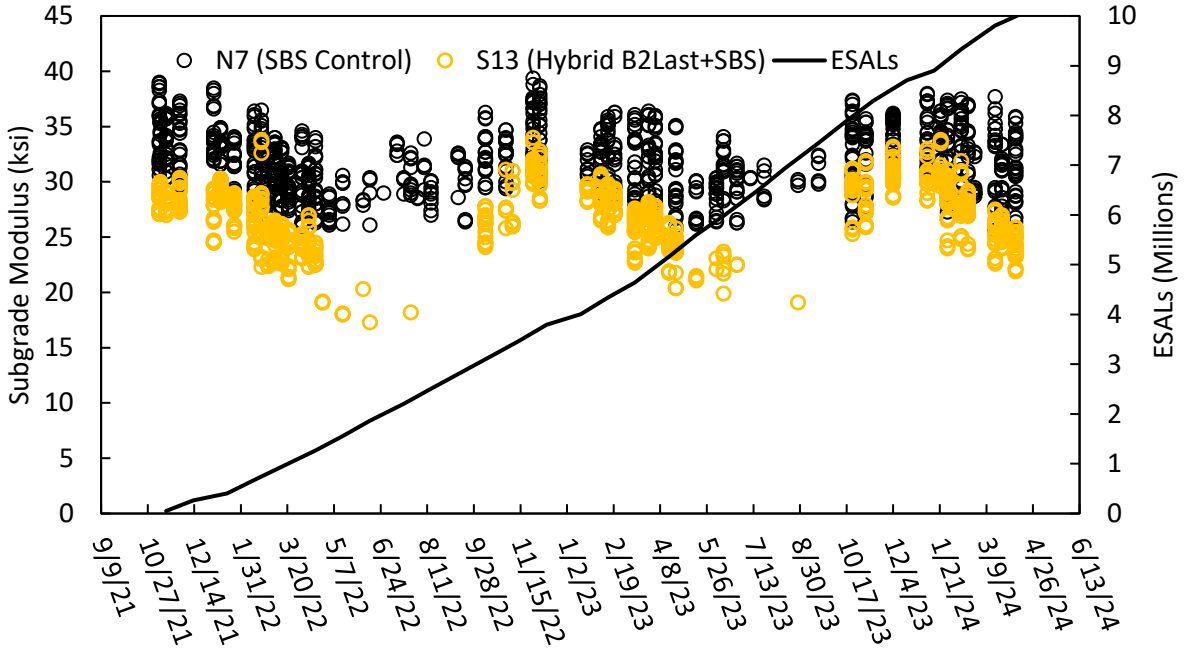

Figure 34. Back-calculated Moduli of Subgrade

To illustrate the impact of reduced back-calculated moduli of the granular base and subgrade layers, the cracking performance of the asphalt layer in Section S13 (hybrid B2Last®+SBS) was assessed through FlexPAVE™ simulations and compared with that of Section N7 (SBS Control). Details on the FlexPAVE™ software and required inputs can be found in Section 21.4.4 of this

report. Two simulations were conducted. The first simulation was based on the average back-calculated moduli of the granular base and subgrade, as well as the average as-built layer thicknesses of Section N7 and Section S13. The second simulation assumed that two asphalt mixtures were constructed on the same foundational support, using the same back-calculated moduli of the granular base and subgrade and as-built thicknesses of Section N7 for both simulated test sections. Additionally, the dynamic and cyclic fatigue data of the plant mix for the control SBS modified and hybrid B2Last®+SBS modified mixtures were utilized for Sections N7 and S13, respectively, in both simulations.

Figure 35 shows the predicted percent damage for the first FlexPAVE™ simulation of Section N7 (SBS Control) and Section S13 (hybrid B2Last®+SBS), using corresponding average in-situ granular base and subgrade moduli, along with average as-built layer thicknesses. An additional analysis was performed using the average support moduli values and layer thicknesses at only Random Location 3 RL3 within Section S13, where foundational support was found to be the weakest, and the most severe distresses were observed. At the end of the two-year simulation period, Section S13 had a higher percent damage than Section N7 and as expected, the inputs for only RL3 led to an increase in percent damage compared to the average inputs for four random locations in Section S13.

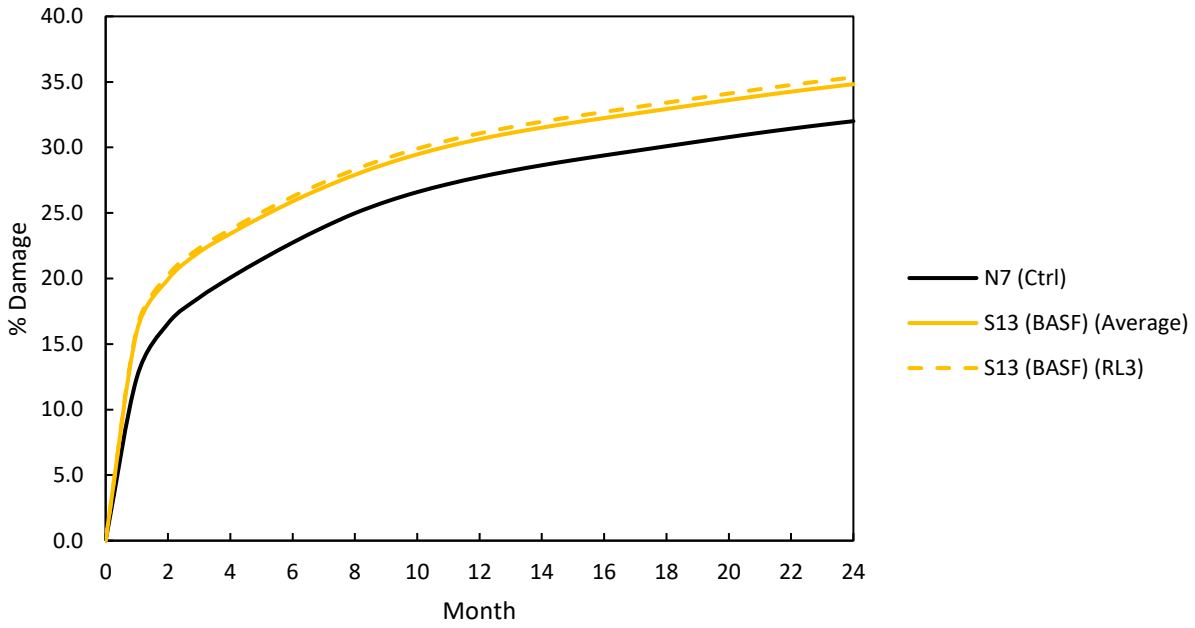

Figure 35. FlexPAVE™ Predicted Percent Damage with In-Situ Input Data

Figure 36 displays the percent damage of the second FlexPAVE™ simulation for Sections N7 and S13, using the same back-calculated moduli of the granular base and subgrade and as-built thicknesses of Section N7 for both simulated sections. In this case, Section S13 was predicted to have a lower percent damage than Section N7 at the end of the two-year period. These FlexPAVE™ simulations highlight the impact of weaker foundational support on the fatigue

performance of Section S13, likely causing the early cracking observed at the NCAT Test Track after 8.31 million ESALs in November 2023.

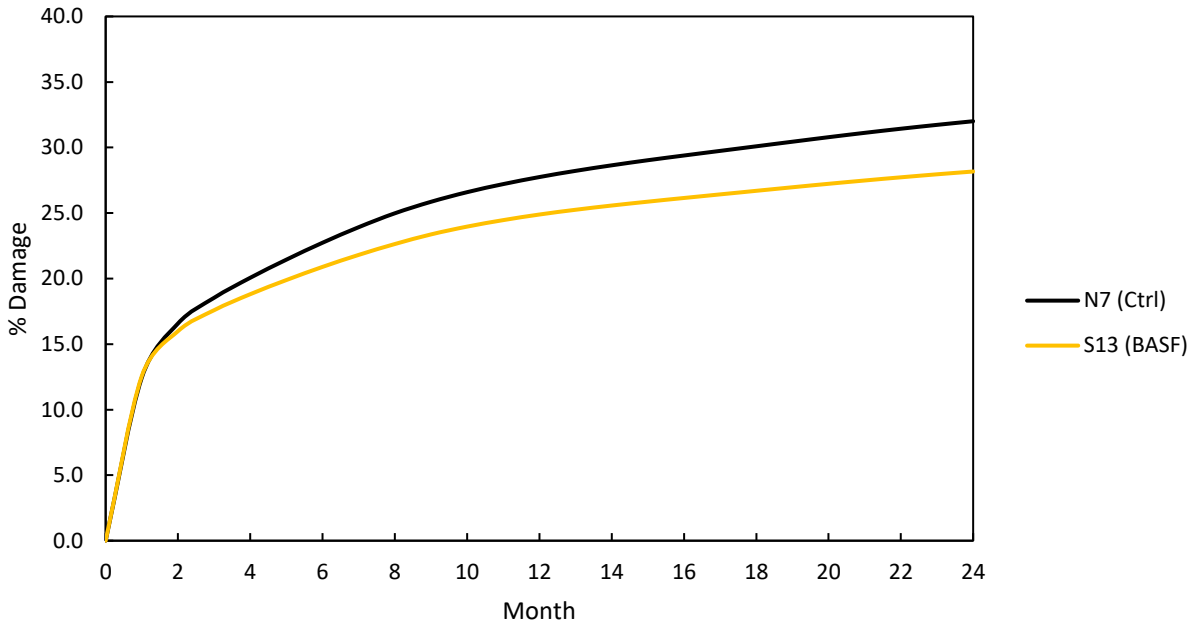

Figure 36. FlexPAVE™ Percent Damage (Identical Support Moduli and Layer Thicknesses)

21.9 Summary and Conclusions

This chapter discusses the evaluation of hybrid B2Last®+SBS modified asphalt mixtures compared to conventional SBS-modified mixtures. The binders used in both sections were modified from a PG 67-22 binder. The control binder was modified with 2.5% SBS to attain a performance grade of PG 76-22. The SBS-modified PG 76-22 binder was further modified with the B2Last® modifier at 2.0% to achieve a performance grade of PG 82-22.

The study involved laboratory testing and full-scale field experiments to assess the performance of these mixtures in terms of fatigue resistance, rutting resistance, and overall structural capacity. The study was conducted in two phases: a laboratory experiment in Phase I and a field performance evaluation at the NCAT Test Track in Phase II.

21.9.1 Phase I Laboratory Experiment

In Phase I, a laboratory experiment was conducted to evaluate the binder and mixture resistance to rutting and cracking and to gather input for structural pavement analysis. A 12.5 mm mix design with 20% RAP was optimized with 6.5% of a PG 76-22 SBS-modified binder to meet the Balanced Mix Design (BMD) criteria, including a minimum CT_{Index} of 50 using the Indirect Tensile Asphalt Cracking Test (IDEAL-CT) and a maximum HWTT rut depth of 12.5 mm after 20,000 passes using the Hamburg Wheel-Tracking Test (HWTT).

Both the control mixture with PG 76-22 SBS binder and the hybrid B2Last®+SBS mixture were prepared with a total asphalt content of 5.6%. The control mixture with PG 76-22 SBS binder had an average CT_{Index} of 54.1, while the hybrid B2Last®+SBS mixture had an average CT_{Index} of

38.6. It is important not to use these IDEAL-CT results to draw conclusions on the cracking resistance of these mixtures at the NCAT Test Track since the IDEAL-CT test was found not sensitive enough to detect differences in cracking resistance provided by polymer modification (Yin et al. 2023). Additionally, both mixtures demonstrated no rutting or stripping susceptibility in the HWTT, with the control mixture achieving a rut depth of 2.5 mm and the hybrid mix yielding a lower rut depth of 1.6 mm.

The dynamic modulus (E*) and cyclic fatigue tests were then conducted using the Asphalt Mixture Performance Tester (AMPT). The E* master curves indicated that the hybrid B2Last®+SBS modified mixture exhibited higher stiffness at high temperatures and low loading frequencies but lower stiffness at low temperatures and high loading frequencies compared to the control SBS-modified mixture. The E* and cyclic fatigue test results were utilized in the FlexPAVE™ simulations, indicating that the hybrid mixture could achieve similar structural performance with a slightly thinner asphalt layer compared to the control mix, resulting in a higher preliminary structural layer coefficient for the hybrid mixture.

21.9.2 Phase II Field Performance Evaluation

Phase II involved the construction of a 200-foot structural experiment section (S13) using the hybrid B2Last®+SBS modified asphalt mixture for field performance evaluation, compared with the control section (N7) using the conventional SBS-modified mixture. The design for both sections included a 5.5-inch asphalt layer over a 6-inch aggregate base on top of the Test Track subgrade. With this design, bottom-up fatigue cracking is anticipated as the failure mode.

Each section was instrumented with strain gauges, pressure plates, and temperature probes to monitor its structural health and pavement responses throughout the experiment. The field performance in terms of rutting, cracking, smoothness, and texture were surveyed on a weekly basis. In addition, laboratory testing was conducted on the samples of asphalt mixtures taken during the construction of these test sections to assist the field experiment.

The laboratory testing program in Phase II included a series of performance tests on plant-mixed, lab-compacted (PMLC) specimens subjected to different aging conditions. These tests included the IDEAL-CT, HWTT, E*, cyclic fatigue, and bending beam fatigue (BBF) to evaluate the cracking and cracking resistance of both mixtures, as well as their contribution to overall structural capacity. The hybrid B2Last®+SBS modified mixtures exhibited lower average CT_{Index} values than the control SBS-modified mixtures under all aging conditions. These CT_{Index} results should not be used solely to assess the cracking resistance of these modified mixtures, as the CT_{Index} was not sensitive enough to detect the effect of polymer modification (Yin et al., 2023). In addition, both mixtures exhibited comparable fatigue resistance based on the cyclic fatigue test results (i.e., S_{app} parameters and C vs. S curve) and BBF test results (cycles to failure at multiple strain levels). The hybrid B2Last®+SBS modified mixture also demonstrated higher E* values at high temperatures and lower E* values at low temperatures compared to the SBS-modified mixture and a lower HWTT final rut depth, indicating improved rutting resistance.

The field performance of the mixtures in two test sections was monitored during the eighth research cycle at the NCAT Test Track from November 2021 to April 2024 after 10 million ESALs. No significant changes in MRI were observed for either test section, indicating good ride

quality. Both test sections showed a slight increase in average rut depth with traffic, but the final field rut depths were well below the failure threshold of 12.5 mm. No cracks were found in Section N7 (SBS Control), but cracking was first observed in Section S13 (hybrid B2Last®+SBS) at 8.31 million ESALs in November 2023, covering approximately 6.1% of the lane area by the end of the study. The occurrence of cracking in Section S13 was unexpected, given that the test results from E*, cyclic fatigue, and BBF suggested the cracking resistance of the hybrid B2Last®+SBS mixture should be similar to that of the control SBS mixture at the NCAT Test Track. Therefore, the strain and FWD data were analyzed to identify the cause of the early cracking in Section S13.

The analysis of the strain and FWD data showed that the early cracking observed in Section S13 was likely caused by higher strains in Section S13 (hybrid B2Last®+SBS) during certain months, corresponding to the weaker foundation support shown in the back-calculated moduli of the granular base and subgrade layers in Section S13, possibly due to water intrusion. The impact of reduced back-calculated moduli of the granular base and subgrade layers on the cracking performance of the asphalt layer in Section S13 was also assessed through FlexPAVE™ simulations and compared with that of Section N7 (SBS Control). The simulations showed that Section S13 had a higher percentage of damage (i.e., it was likely to crack earlier) than Section N7 due to reduced moduli of the as-built granular base and subgrade layers in Section S13. However, when two test sections were simulated based on the same back-calculated moduli of the granular base and subgrade layers, Section S13 was predicted to have a lower percent damage (i.e., not likely to crack earlier) than Section N7. The analysis highlights the impact of weaker foundational support on the fatigue performance of Section S13, likely causing the early cracking observed at the NCAT Test Track after 8.31 million ESALs in November 2023.

Overall, the hybrid B2Last®+SBS modified mixture demonstrated improved rutting resistance and stiffness, with similar fatigue cracking resistance compared to the control SBS-modified mixture. Early cracking in the hybrid mixture at the NCAT Test Track was likely due to weaker foundational support from water intrusion. Both sections will remain in place for continued traffic monitoring, with cracks in the hybrid mixture sealed using B2Last® modified crack seal material. Future plans include milling and resurfacing with an asphalt mixture modified with B2Last® only, similar to the mixture placed on the Test Track exit ramp in 2020.

21.10 References

Becker, Y., M.P. Méndez, Y. Rodríguez (2001). Polymer Modified Asphalt. Vision Tecnologica, Vol. 9, Issue 1, pp. 39-50.

Carrera, V., Garcia-Morales, M., Partal, P., and Gallegos, C. (2010). Novel bitumen/isocyanate-based reactive polymer formulations for the paving industry. Rheologica Acta, 49(6), 563– 572.

Chen, C., Yin, F., Andriescu, A., Moraes, R., Mensching, D., Tran, N., Taylor, A., and West, R. (2020). Preliminary validation of the critical aging procedure for NCAT top-down cracking experiment. Journal of the Association of Asphalt Paving Technologists, 89, 323-362.

Federal Highway Administration (FHWA) (2019). Cyclic Fatigue Index Parameter, S_{app}, for Asphalt Performance Engineered Mixture Design. Tech Brief. FHWA-HIF-19-091. https://www.fhwa.dot.gov/pavement/pub_details.cfm?id=1098.

Foshee, M.M., "Early Characterization and Performance of Flexible Pavements Utilizing Asphalt Additives," MS Thesis, Auburn University, 2022.

Kmetz, M.H., "Laboratory and Field Characterization of Additive-Modified Asphalt Concrete Mixtures," MS Thesis, Auburn University, 2023.

NAPA. (2024). Balanced Mix Design Resource Guide. Retrieved from National Asphalt Pavement Association (NAPA) Website: https://www.asphaltpavement.org/expertise/engineering/resources/bmd-resource-guide.

Taylor, A.J. and D.H. Timm. Mechanistic Characterization of Resilient Moduli for Unbound Pavement Layer Materials. Report No. 09-06, National Center for Asphalt Technology, Auburn University, 2009.

Tran, N., R. Moraes, A. Taylor, and D. Timm (2024). Field Performance of Asphalt Mixture Modified with Reactive Isocyanate Based Modifier. Proceedings of the International Conference on Asphalt Pavement (ISAP2024) Meeting, Montreal, CAN.

Timm, D.H., F. Yin, N. Tran, M.M. Foshee, C. Rodezno, "Comparison of Relative Structural Characterization Methods for Additive-Modified Asphalt Mixtures," Transportation Research Record, Vol. 2676 (11), Transportation Research Board, pp. 676-688, 2022.

West R, Timm D, Powell B, Tran N, Yin F, Bowers B, Rodezno C, Leiva F, Vargas A, Gu F, Moraes R. (2021). Phase VII (2018-2021) NCAT Test Track findings. National Center for Asphalt Technology, Auburn University, AL, USA.

Yin, F., Chen, C., Moraes, R., Hanz, A., Hehir, J., & Knudtson, D. (2023a). Impact of Polymer Modification on IDEAL-CT and I-FIT for Cracking Resistance Evaluation of Asphalt Mixtures. Report No. NRRA202303. Minnesota Department of Transportation, Office of Research & Innovation.

Yin, F., Chen, C., Moraes, R., Sias, J., Dave, E., and Zhou, F. (2023b). Validation of Loose Mix Aging Procedures for Cracking Resistance Evaluation in Balanced Mix Design. MnDOT Report NRRA202308.

Zhou, F., Steger, R., & Mogawer, W. (2021). Development of a coherent framework for balanced mix design and production quality control and quality acceptance. Construction and Building Materials 287.